TOTAL SYNTHESIS OF PYRROLE-ALKALOID-LIKE NATURAL PRODUCTS AND ANALOGUES

By

Grace E. Hubbell

A DISSERTATION

Submitted to
Michigan State University
in partial fulfillment of the requirements
for the degree of

Chemistry – Doctor of Philosophy

2022

ABSTRACT

The pyrrole-alkaloid family of natural products represents a wide range of biological activities, making the synthesis of these types of scaffolds a worthy endeavor. Of particular interest to our lab is the inhibitory activity of some of these natural products towards the human 20S proteasome, a validated target for the treatment of specific cancer including multiple myeloma and mantle cell lymphoma. With this in mind, the synthesis of scaffolds which bear structural similarity to these natural products was endeavored. Herein, the synthesis of pyrrole-alkaloid-like scaffolds is represented in several approaches: small molecule design of bromoindolophakellstatins, methodology development, and total synthesis. The development of a novel Rh(III)-catalyzed C-H activation/annulation between 2-imidazolones and *N*-pivaloyloxybenzohydroxamates is reported, which facilitates access to urea-fused tetrahydroisoquinolone scaffolds which are reminiscent of members of the pyrrole-alkaloid family. Efforts towards the syntheses of bromoindolophakellstatin small molecules is also described. Lastly, route development towards the total syntheses of nagelamide M and the ugibohlin natural products and the particular challenges associated with these approaches are discussed.

ACKNOWLEDGEMENTS

First and foremost, I would like to thank my advisor Dr. Jetze Tepe. Thank you for your patience with my progress throughout my time here and allowing me the opportunity to explore my synthetic interests even if the path was somewhat winding and circuitous. Your willingness to allow me to explore synthetic problems in an independent manner–and ability to reign in my enthusiasm and guide me–have ultimately provided me with the tools to become an independent scientist, and for that I am forever grateful.

I would also like to express my gratitude towards my committee members, Dr. Wulff, Dr. Borhan, and Dr. Huang. Dr. Wulff, it has been a pleasure to learn from you throughout the years and work together on the database project. Thank you for the second cups of coffee and extra windmill cookies on days when I really needed it. Dr. Borhan, thank you for allowing me the opportunity to teach for you and learn from you, it has been an experience for which I am truly grateful. Dr. Huang, thank you for your guidance and honesty throughout the entirety of my graduate career.

There are many others that I would like to thank for their help during my time here. Dr. Karen Draths, thank you for lending an ear and your career advice. I am so grateful to have had you as a mentor early on in my career. I would also like to thank Dr. Dan Holmes and Dr. Li Xie for your help with NMR challenges throughout the years, and Dr. Tony Schilmiller for his help with mass spectrometry.

To my labmates, thank you for providing such a fun, supportive and encouraging atmosphere to work in. Corey and Evert, thank you for your guidance when I first started graduate school and was but a naïve little scientist, and your willingness to provide insight when I truly needed it. Thank you also to my co-workers and friends Katarina, Shafaat, Taylor, Sophie and

Allison, and Konika. Your friendship and support have meant the world to me and made graduate school bearable during the many times that was otherwise difficult. To the younger lab members Charles, Dare, Daniel, Evan, Kyra, Bahareh, Sydney, and Shannon—thank you for your enthusiasm for chemistry and desire to solve problems together. I am grateful to have been able to teach and be taught by all of you and am so excited to see what your futures hold.

Lastly, I would like to thank my family members. To my parents and siblings, thank you for your endless support of me. I would not be where I am today without your love. I would also like to thank my in-laws for their kindness and support. I am grateful to feel accepted into your family and know that I have gained two remarkable parents and supporters.

To my husband, Jurick, thank you for your endless support of me—I know it hasn't always been an easy role to fulfill. From sitting up late with me at the house on Hagadorn as I tried to solve my unknown for CEM 845 first year, to listening to me babble obsessively every night about my chemistry for five years, you have always been my biggest supporter. I could not have gotten through the highs and lows of graduate school without you.

Lastly, to my cats Obie and Stinkie Frankie, thank you for providing me with ample fodder for laughter and joy with your antics. I am so grateful to have you both.

TABLE OF CONTENTS

LIST OF ABBREVIATIONS

Atm	Atmospheric pressure
Boc	Tert-butoxycarbonyl
Bn	Benzyl
BOP	benzotriazole-1-yloxytris(dimethylamino)phosphohexafluorophosphate
BTZ	Bortezomib
Cbz	Benzyl formate
cCP	Constitutive core particle
ChT-L	Chymotrypsin-like
CMD	Concerted metalation deprotonation
°C	Celsius
C-L	Caspase-like
CP	Core particle
$[Cp^*RhCl_2]_2$	Pentamethylcyclopentadienyl rhodium dichloride dimer
DBU	1,8-diazabicyclo[5.4.0]undec-7-ene
DCM	Dichloromethane
DEAD	Diethylazo-dicarboxylate
DG	Directing group
DG^{ox}	Oxidizing directing group
DIBAL-H	di-isobutylaluminum hydride
DIPEA	N,N-diisopropylethylamine
DMAP	4-dimethylaminopyridine
DMDO	dimethyldioxorane

DMF	dimethylformamide
DMSO	dimethylsulfoxide
dppf	1,1,-bis(diphenylphosphino)ferrocene
EC_{50}	50% effective concentration
EDC/EDCI	1-ethyl-3-(3-dimethylaminopropyl)carbodiimide
EtOAc	ethyl acetate
EtOH	ethanol
Equiv.	equivalents
FDA	U.S. Food and Drug Administration
FTIR	Fourier transform infrared
hCP	human core particle
HCT116	Human colorectal carcinoma cell line
HeLa cell	Henrietta Lacks cells
HFIP	hexafluoro-2-propanol
HOBt	hydroxybenzotriazole
IBX	2-iodoxybenzoic acid
IC_{50}	half-maximal inhibitory concentration
iCP	immunocore particle
LUMO	lowest unoccupied molecular orbital
mCPBA	m-chloroperbenzoic acid
MeCN	acetonitrile
Mp	melting point
MTT	3-(4,5-dimethylthiazol-2-yl)-2,5-diphenyl-2*H*-tetrazolium bromide

NBS	N-bromosuccinimide
NIS	N-iodosuccinimide
NMR	nuclear magnetic resonance
OA	oxidative addition
Ph	Phenyl
PIDA	(diacetoxyiodo)benzene
PMB	p-methoxybenzyl
PTSA	*p*-toluenesulfonic acid
RP	Regulatory particle
RT	room temperature
SAR	structure activity relationship
Sat.	saturated
Soln	solution
TBAF	tetrabutylammonium fluoride
TBSCl	tert-butyl-dimethylchlorosilane
Tces	Trichloroethyl sulfonate
TEA	triethylamine
TFA	trifluoroacetic acid
TFE	2,2,2-trifluoroethanol
THF	tetrahydrofuran
T-L	trypsin-like
TLC	thin-layer chromatography
ToF	time of flight

TsCl	*p*-toluenesulfonyl chloride
yCP	yeast core particle

Chapter 1: Natural product scaffolds as inspiration for the design of human 20S proteasome inhibitors[1*]

1.1 Introduction

1.1.1 20S Proteasome

The ubiquitin-proteasome pathway plays an integral role in maintaining homeostasis in eukaryotic cells.[2] The 26S proteasome is a 2.5 MDa threonine protease which is responsible for the degradation of redundant proteins in a cell into oligopeptides for further processing by other pathways (**Figure 1.1**). Ubiquitin-proteasome-mediated degradation has been implicated in the regulation of many signaling proteins including cyclins (involved in cell-cycle progression), p53 (tumor suppressor),[3] and IkBα (inhibitor of transcription factor NF-κB).[4]

Figure 1.1 General diagram of Proteasome system

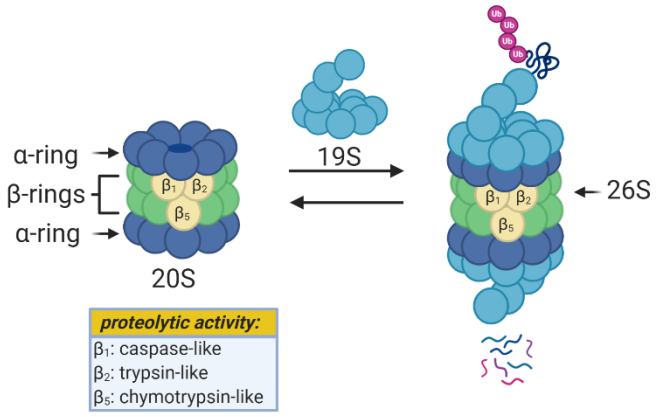

The 26S proteasome is comprised of one or two 19S regulatory particles (RP) which associate with the 700 kDA barrel-like 20S core particle (CP).[5] The 20S core particle is composed of four stacked heptameric rings in an $\alpha_{1\text{-}7}\beta_{1\text{-}7}$ $\beta_{1\text{-}7}$ $\alpha_{1\text{-}7}$ arrangement.[6] The outer α-rings are responsible for recognition of the regulatory particles, and the inner β-rings house the catalytic activity of the protease. The β-rings each consist of seven unique subunits, and three of these subunits (β1, β2, and β5) are responsible for the proteolytic activity of the proteasome. Binding

[*] This chapter reproduced in part from Ref 1. with permission from the Royal Society of Chemistry.

of the 19S caps to the CP facilitates gate-opening, which in turn allows for the proteolytic degradation of polyubiquitinylated proteins. The 19S caps are responsible not only for this gate-opening,[7] but also the recognition of polyubiquitinylated proteins, unravelling of these into linear peptides, and feeding the peptides into the catalytic chamber.[8] Once fed into the chamber, unraveled proteins are cleaved into oligopeptides by the catalytic sites, which all proteolytically cleave the peptide chains with the aid of an *N*-terminal threonine residue (Thr1). Although all three catalytic sites use a nucleophilic threonine to carry out their activity, slight differences between their substrate channels allow for preference towards cleavage of specific peptide residues. The proteasome exhibits caspase-like (C-L, peptidyl-glutamidyl peptide hydrolysing), trypsin-like (T-L) and chymotrypsin-like (ChT-L) activities which are carried out by its β1, β2, and β5 subunits, respectively.[9-11] The first 20S proteasome structure determined by X-ray crystallography was that of the archaebacterium *Thermoplasma acidophilum* in 1995,[6] and many eukaryotic proteasomes have since been characterized. Structural similarity between eukaryotic proteasomes is highly conserved, which has allowed for the use of models such as the yeast 20S proteasome[12] and mammalian 20S proteasome[13, 14] for identification of molecules which exhibit modulatory activity against the proteasome. These models have been especially useful considering that while their X-ray crystal structures were solved throughout the 1990s and early 2000s, which has facilitated inhibitor design greatly, the X-ray crystal structure of the human 20S proteasome was only recently solved in 2015.[15] Two other core particles have also been identified as the immunoproteasome[16] and the thymoproteasome.[17] The differences of selectivity between these are governed by slight differences in the topology within their substrate channels.[18]

1.1.2 Proteasome inhibition for treatment of multiple myeloma

Due to its integral role in maintaining cell homeostasis, modulation of the activity of the 20S proteasome has been considered as a potential way to treat several diseases including cancer,

autoimmune disease, and neurodegeneration.[19-21] Additionally, the proteasome of parasitic species has recently been targeted in the treatment of parasitic diseases.[22] Inhibition of the proteasome has been implicated as a veritable strategy for the treatment of certain cancers, given that inhibition leads to ER stress and apoptosis.[23] The invention of the proteasome-inhibitor Velcade ® (bortezomib) is perhaps the best representation of how targeting the ubiquitin-proteasome pathway can lead to the treatment of some cancers. This dipeptide boronate was approved by the FDA in 2003 as a treatment for multiple myeloma, and its mechanism of action is through direct inhibition of the ChT-L activity of the proteasome.[24] Activation of the proteasome has also been considered for the treatment of neurodegenerative diseases such as Parkinson's and Alzheimer's disease.[25-27]

1.1.3 Conventional Treatment of Multiple Myeloma with peptide-based inhibitors

Following the discovery of the 26S proteasome complex in the 1980s,[28, 29] researchers have since focused upon the development of novel inhibitors of the 20S proteasome for the treatment of oncological diseases.[20, 30-32] In particular, the development of anticancer reagents which act as 20S proteasome inhibitors has been a considerable focus for the treatment of multiple myeloma.[33] The current treatment regimen for multiple myeloma involves the use of several chemotherapeutic agents, and consists of the use of immunomodulatory reagents, steroids and small-molecule proteasome inhibitors simultaneously to combat the disease.[33]

The first synthetic proteasome inhibitors were peptide aldehydes[34] which had been shown to inhibit several types of proteases including serine and cysteine proteases. These peptide aldehydes act as reversible covalent inhibitors of the 20S proteasome, forming a hemiacetal with the nucleophilic threonine residue. Design of more selective inhibitors stemmed from alteration of the electrophilic warhead, leading to the eventual inclusion of boronic acids, vinyl sulfones,[35] and α-ketoaldehydes[36] within the scaffolds of synthetic inhibitors of the 20S proteasome.

Currently, all FDA-approved 20S proteasome inhibitors for treatment of multiple myeloma are built upon peptide-based scaffolds.[30, 31] Peptide-based scaffolds contain optimized amino acid residues to mimic substrates of the 20S proteasome. The residues also participate in hydrogen-bonding and hydrophobic interactions to optimize interaction with the substrate channel.[30] Specific design of the peptide chain has allowed for the generation of subsite-specific inhibitors of the proteasome.[37] The design of such inhibitors is based upon the inherent preference of the C-L, T-L and ChT-L activities towards acidic, basic, and hydrophobic residues, respectively. The installation of hydrophobic sidechains in the peptide-based FDA-approved inhibitors results in its potent inhibition of the ChT-L site. Additionally, these compounds typically contain an electrophilic warhead at their C-terminus which interacts directly with the *N*-terminal threonine hydroxyl residue of proteolytic sites to block their catalytic activity.

Bortezomib (Velcade ®) was the first established 20S proteasome inhibitor to be approved by the FDA for treatment of multiple myeloma.[38] This dipeptidic molecule contains a C-terminal boronic acid which performs a key role in the mechanism of inhibition (**Figure 1.2**).

Figure 1.2 Inhibition of proteasome by bortezomib

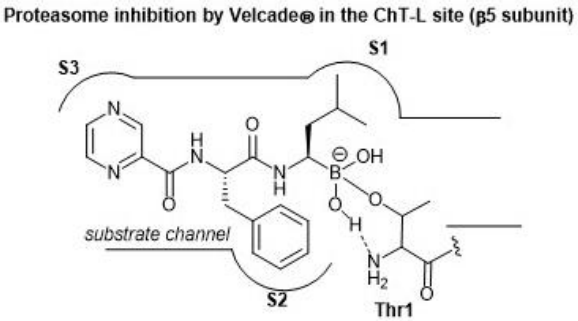

The interaction between covalent inhibitors and the catalytic sites is demonstrated in **Figure 1.2** with bortezomib as an example. The substrate channel accommodates the peptide sidechains of the molecule much like it would a peptide substrate. The electrophilic boronic acid moiety at the terminus of the molecule is susceptible to nucleophilic attack by the Thr1 residue of

the catalytic site. In the case of bortezomib, this electrophile undergoes reversible nucleophilic addition by the amino acid, and the resulting charged species is stabilized through hydrophobic interactions and hydrogen-bonding interactions.[39] The proposed interaction of this molecule was confirmed by X-ray crystallography by the Groll group in 2006.[39] The other FDA approved inhibitors undergo similar mechanisms of inhibition through the formation of covalent bonds with the Thr1 residue and an electrophilic warhead in the form of a boronic acid or α,β-epoxyketone moiety.

Figure 1.3. FDA-approved proteasome inhibitors

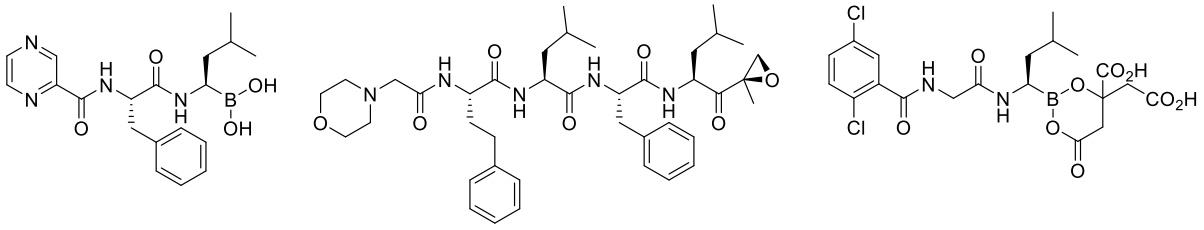

Bortezomib (Velcade ®) Carfilzomib (Kyprolis®) Ixazomib (Ninlaro ®)

Since the discovery of bortezomib, subsequent work has focused on the development of peptide-based inhibitors for the treatment of multiple myeloma in addition to other oncological malignancies (**Figure 1.3**).[40] Carfilzomib (Kyprolis ®) is a peptide-based proteasome inhibitor which was approved in 2012 for the treatment of multiple myeloma. This compound contains an α,β-epoxyketone moiety which undergoes irreversible covalent bond formation with the Thr1 residue to form a morpholine adduct. This molecule was developed from the natural product epoxomicin; discussion of its development is further discussed in a later section of this chapter.

Further development of peptide-based proteasome inhibitors has focused on the development of orally available treatments. Ixazomib (Ninlaro ®) is a bortezomib analog which was the first FDA orally available proteasome inhibitor for the treatment of relapsed or refractory multiple myeloma, approved in 2015.[31] This molecule is administered orally and exists as a

prodrug to afford the active boronic acid species. Several other second-generation inhibitors based upon the bortezomib and carfilzomib are currently in clinical trials for the treatment of various cancer cell types.[31]

1.1.4 Natural products as inhibitors of the 20S proteasome

Nature is an attractive source for the identification of novel proteasome inhibitors: the inherent stereochemical complexity of many natural products may allow researchers insight into unique interactions relative to the established clinically available inhibitors. A variety of methods exist for mining nature for identification of novel proteasome inhibitors including the use of fluorogenic peptide assay, site-specific probes, pathway-specific accumulation assay and NMR spectroscopic assay.[41] These methods have been especially helpful in regard to identification of natural product inhibitors, as some may be utilized with crude mixtures before isolation. Examples of the use of these methods are included in the review. Elucidation of the mechanisms of action by natural products through the methods of X-ray crystallography and computational docking allow for the design of more potent and selective inhibitors based upon the natural product scaffold. The focus of this review is to discuss several classes of natural products which have been identified for their inhibitory activity towards the 20S proteasome, their mechanism of action, and the efforts taken to optimize these scaffolds for potency and selectivity towards human 20S proteasome inhibition.

1.2 Natural product inhibitor scaffolds

1.2.1 Peptide aldehydes

Several families of peptide aldehyde natural products have been identified for their inhibitory activity towards the 20S proteasome (**Scheme 1.1**). The first established natural product-based peptide aldehyde inhibitors tyropeptins A and B are products of the actinomycete microbe *Kitasatospora* sp. MK993-dF2, a strain originally discovered in a soil sample from Kami-gun,

Japan.[42, 43] After extensive spectroscopic analysis, the structures of the tyropeptins A and B were determined as isovaleryl-*L*-tyrosyl-*L*-valyl-*DL*-tyrosinal and n-butyryl-*L*-tyrosyl-*L*-leucyl-*DL*-tyrosinal, respectively. For confirmation of their structures, the total syntheses of the natural products were completed and compared with the isolated samples. The peptide backbone and reactive aldehyde moiety had already been established as a promising proteasome inhibiting scaffold,[44] and therefore the potential biological activities of tyropeptins A and B were of interest to researchers.

Tyropeptin A (**I-1**) competitively inhibits the ChT-L and T-L activities of the 20S proteasome with IC_{50} values of 0.20 μM and 2.9 μM, respectively. Tyropeptin B (**I-2**) is a weaker competitive inhibitor of the 20S proteasome, with IC_{50} values for the ChT-L and T-L sites of 0.39 μM and 7.8 μM, respectively. Tyropeptin A also exhibited cytotoxicity against HeLa S3 human cervical cells and HL-60 promyelocytic leukemia cells with IC_{50} values of 33.2 μM and 8.6 μM, respectively. Derivatives of tyropeptin A were designed by Momose et al. using computational methods.[45, 46] At the time, the crystal structure of the human 20S proteasome had not yet been solved; however, the crystal structure of the bovine 20S proteasome had been determined and was therefore used as a model.[13, 14]

Scheme 1.1 Peptide-aldehyde inhibitors and their analogs

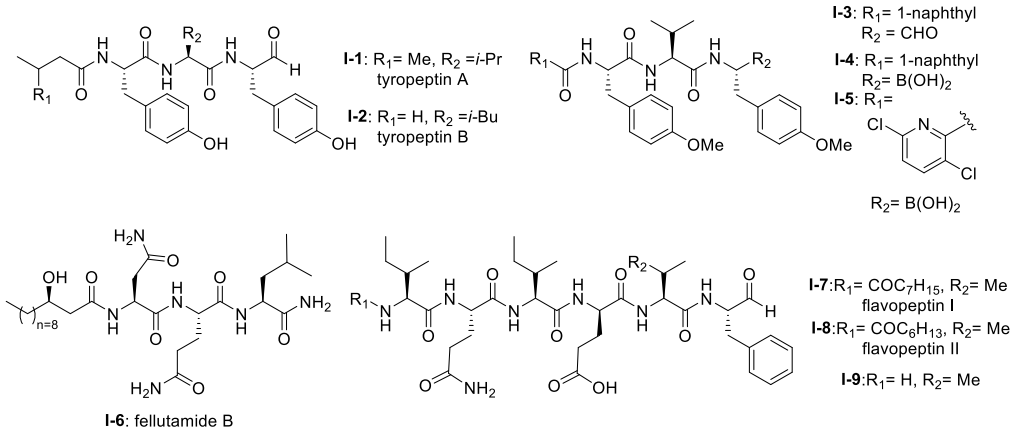

Tyropeptin A was believed to undergo nucleophilic attack by the Thr1O$^{\gamma}$ residue of the active site to form a hemiacetal, and its side chains interact with the subpockets to form an antiparallel β-sheet. Introduction of bulky aromatic groups at the *N*-terminus enhanced inhibitory activity towards the ChT-L site of the proteasome. Optimization led to TP-110 (**I-3**), an *N*-terminal naphthyl derivative with methylated hydroxy positions (IC_{50}: 0.027 μM). TP-110 exhibited improved growth inhibitory activity against cancer cells, likely due to increased hydrophobicity of the molecule to improve cell permeability. In subsequent *in vitro* studies, TP-110 also repressed the chymotrypsin-like activity of the proteasome in human prostate cancer PC-3 cells, inhibiting the proteasome activity by 56% with 0.16 μM.[47] Furthermore, TP-110 induces apoptosis in the prostate cancer cell line. Substitution of the formyl group in TP-110 with boronic acid resulted in enhanced inhibitory potency towards the ChT-L site.[48] Optimization of this scaffold led to boronic acid **I-5**, which bore an *N*-terminal 3,6-dichloro-2-pyridyl substituent and exhibited comparable inhibitory potency towards the chymotrypsin-like activity of the proteasome (IC_{50}: 0.053 μM) to that of bortezomib.[49] Analog **I-5** also displayed good cytotoxic activity towards the RPMI8226 multiple myeloma cells, and was chosen for further *in vitro* and solid tumor studies.[50]

Fellutamide B (**I-6**) was originally isolated from *Penicillium fellutanium*, a fungus which is found in the gastrointestinal tract of the marine fish *Apogon endekataenia*.[51] Fellutamide B demonstrated potent cytotoxicity against murine leukemia P388 (IC_{50}: 0.18 μM) and L1210 (IC_{50}: 1.26 μM) cells, as well as human epidermoid carcinoma KB cells (IC_{50}: 1.26 μM) *in vitro*, though the mechanism of cytotoxicity was not established. The total synthesis of fellutamide B was first achieved by the Crews group.[52] Since then, other groups have also set out to achieve total syntheses of not only fellutamide B, but other members of the fellutamide family as well.[53-55] Fellutamide B potently inhibits the chymotrypsin-like site (IC_{50}: 9.4 ±2.5nM), but the trypsin-like and caspase-

like sites to a lesser extent (IC_{50}: 2.0 ±0.4 μM and 1.2 ±0.8 μM, respectively).[56] *In vitro* studies revealed the ability of the natural product to inhibit the proteasome within cells, as treatment of L-M mouse fibroblasts resulted in accumulation of ubiquitinated proteins.

The flavopeptin class of peptide aldehydes was discovered with the help of proteomics.[57] The Kelleher group utilized the method of Proteomic Investigation of Secondary Metabolism (PrISM) to screen *Streptomyces* species for non-ribosomal peptide synthases (NRPS) responsible for secondary metabolite synthesis. Using the PrISM approach, the group was able to identify a novel NRPS gene cluster from *Streptomyces* sp. NRRL F-6652. With the help of bioinformatics analysis and metabolomics analysis, six flavopeptins were discovered as the products of this gene cluster. Flavopeptins I (**I-7**) and II (**I-8**) were synthesized using solid phase peptide synthesis (SPPS), along with the *N*-terminal amine derivative **I-9**. Due to the similarity of the flavopeptins to other established inhibitors, the natural products were tested for their inhibitory activity towards the ChT-L and C-L sites of the 20S proteasome. Flavopeptins I and II are low micromolar inhibitors of both sites, and the terminal amine derivative **I-9** exhibits submicromolar IC_{50} values for both sites. The flavopeptins were also tested for their cytotoxicity against the multiple myeloma cell lines MM.M1S and FR4, as well as the histiocytic lymphoma cell line, U-937. Flavopeptin I displayed values of IC_{50}: ~35 and 13 μM for the MM cell lines and the lymphoma line, respectively. The *N*-terminal amine derivative **I-9** displayed no cytotoxic activity. The lack of activity is believed to be due to lower cell permeability and stability as compared to flavopeptins I and II.

1.2.2 Syrbactins

Several syrbactin natural products have also been identified for their proteasome inhibition (**Scheme 1.2**). Syrbactins are divided into 3 sub-families: syringolins, glidobactins, and

cepafungins. These compounds are products of plant pathogens, and their similarities include a macrocyclic lactam with an electrophilic α, β-unsaturated carboxamide. Glidobactins (A-H) are natural product syrbactins that are produced by the bacterial strain *Polyangium brachysporum* sp. nov. K481-B101.[58-61] Glidobactins A-C are cytotoxic against melanotic melanoma B16 cells as well as human colon cancer HCT-116 cells, and exhibit potent *in vivo* antitumoral activity towards P388 leukemia in mice.[58] Further modification of the glidobactin A structure by Oka et al. led to the preparation of several derivatives, which were also evaluated for their antitumoral activity.[61] Glidobactin A (**I-10**) was later identified as a nanomolar inhibitor of the ChT-L site of the 20S proteasome, with a K_i value of 49 ±5.4 nM.[62] The compound also inhibited T-L activity of the 20S proteasome, albeit at considerably higher concentrations (2000 ± 600 nM, n=6). The mechanism of inhibition by syrbactins was determined through elucidation of the X-ray crystal structure of the 20S proteasome in complex with glidobactin A and syringolin A. The α,β-unsaturated moiety of glidobactin A undergoes a nucleophilic Michael-type 1,4-addition by the Thr1O$^{\gamma}$ of the chymotrypsin-like and trypsin-like sites of the proteasome. The lipophilic alkyl chain of glidobactin A contributes to its inhibitory activity and served as inspiration in the development of novel syrbactin proteasome inhibitors; the activity of these analogs is discussed in a later section.

Scheme 1.2 Syrbactin natural product inhibitors

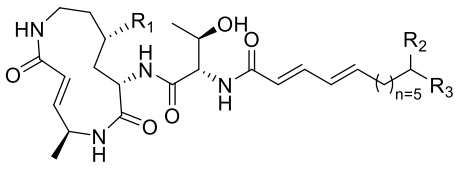

I-10: R_1= H, R_2= H, R_3= Me
glidobactin A
I-11: R_1= OH, R_2= H, R_3= $(CH_2)_2CH_3$
glidobactin C
I-12: R_1= OH, R_2= Me, R_3= Me
cepafungin
I-13: R_1= H, R_2= H, R_3=Me
luminmycin A

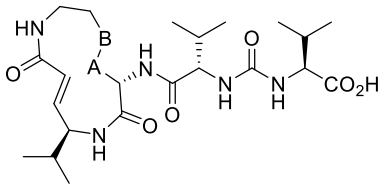

I-14: A-B: HC=CH
syringolin A
I-15: A-B:CH_2-CH_2
syringolin B

Glidobactin C (**I-11**) was recently identified as an inhibitor of the human constitutive and immunoproteasomes through a competitive metabolite profiling technique by the Böttcher group.[63] Glidobactin C exhibited *in vitro* inhibitory activity towards the ChT-L and T-L sites of the human constitutive proteasome (IC_{50}: 2.9 ± 2.2 nM and 2.4 ± 2.8 nM, respectively). The compound also inhibits the human immunoproteasome (ChT-L IC_{50}: 7.1 ± 5.3 nM; T-L IC_{50}: 2.5 ± 2.0 nM). The two additional methylene groups of **I-11** relative to **I-10** are believed to improve its ability to penetrate the cell membrane, resulting in greater activity in cell assays.

The cepafungins were observed as products of the bacteria *Pseudomonas* sp. CB-3 by Shoji et al.[64] Cepafungins I, II, and III were identified as acylpeptide antibiotics which all contain a distinct 12-membered macrolactam ring.[65] The macrolactam ring of all three compounds is comprised of the two amino acids γ-hydroxylysine and 4-amino-2-pentenoic acid, and the distinguishing feature among each is a variable fatty acyl tail at the *N*-terminus of the peptide. Based upon their analysis, the group concluded that the structure of cepafungin II is identical to that of known natural product glidobactin A. The complex of all three compounds displayed a moderate ability to prolong the survival period of mice which bear murine lymphatic leukemia P388 cells. Cepafungin I (**I-12**) was identified as a proteasome inhibitor in later studies: Stein et al. developed an NMR-based proteasome assay to identify natural product inhibitors of the yeast 20S proteasome.[66] Cepafungin I potently inhibits the ChT-L activity of the proteasome (IC_{50}: 4 nM), five times more potent than the known inhibitor glidobactin A (IC_{50}: 19 nM). Cepafungin I also inhibits the T-L activity of the proteasome with an IC_{50} value of 24 nM. The improved inhibitory activity of cepafungin I as compared to glidobactin A is believed to be due to the increased stabilization of the fatty acyl tail through van der Waals interactions.

Luminmycin A (**I-13**) is another natural product of the syrbactin family which has recently

gained attention as a potential proteasome inhibitor. A deoxy derivative of glidobactin A, luminmycin A contains the hallmark 12-membered macrolactam ring responsible for the inhibitory activity of the syrbactin family towards the human 20S proteasome. Luminmycin A was identified as a metabolite of a silenced gene cluster *plu1881-plu1887* of *Photorhabdus luminescens*, and the associated gene cluster was utilized to produce luminmycin A using the method of heterologous expression.[67] The natural product was also observed as a metabolite of crickets following their infection with *Photorhabdus asymbiotica.*[68] Luminmycin A and other natural products belonging to the luminmycin class were successfully isolated following heterologous expression of the same gene cluster, using *E. coli* as host.[69, 70] Recently, luminmycin A was successfully synthesized in the laboratory by Servatius et al.[71] Luminmycin A inhibits the constitutive proteasome (CP) as well as the immunoproteasome (IP), (ChT-L IC_{50}: 0.039 ±0.002 µM (CP), 0.016 ±0.006 µM (IP); T-L 0.026 ±0.008 µM (CP), 0.017 ±0.0016 µM (IP)).[63] The natural product also exhibits cytotoxic activity against human carcinoma HCT-116 cells (IC_{50}: 91.8 nM).

Scheme 1.3 Syringolin-A based proteasome inhibitors

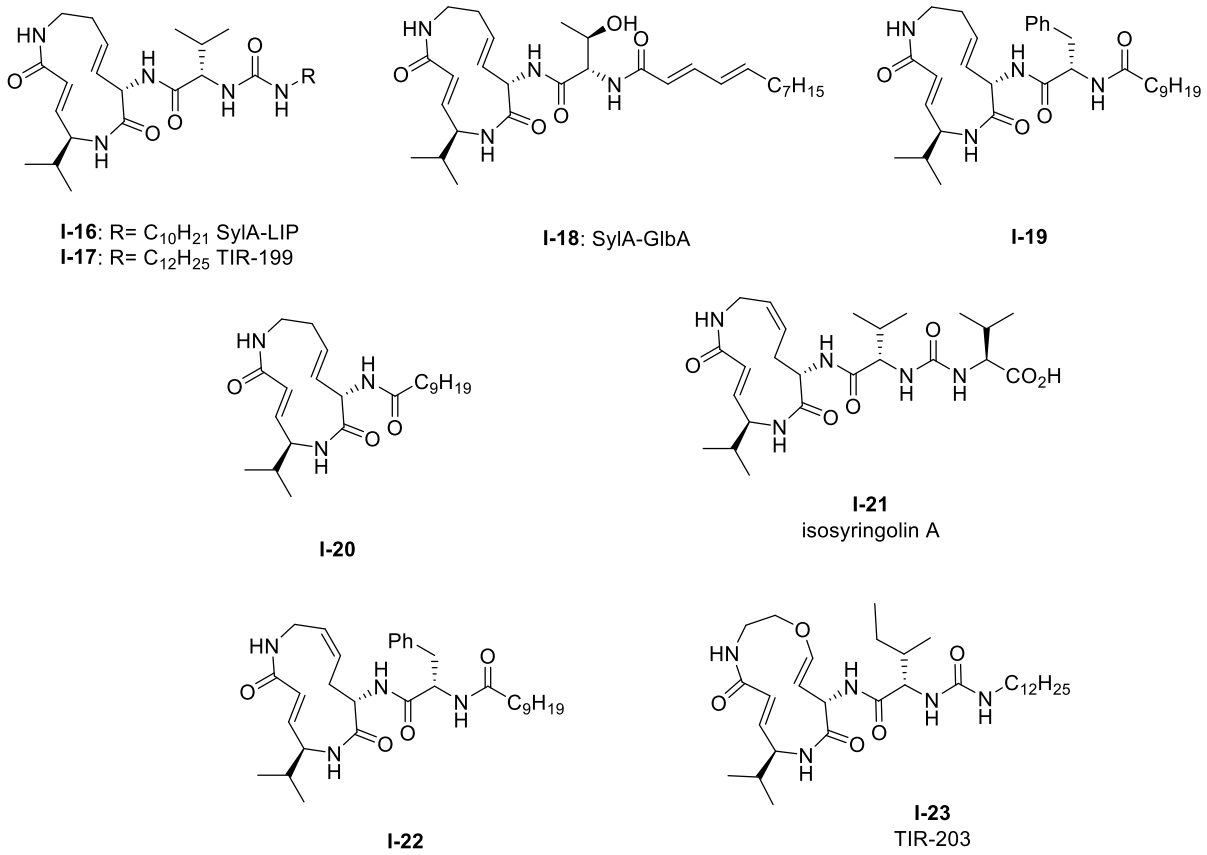

The syringolin family of natural products were identified as secondary metabolites of the pathogen *Pseudomonas syringae* pv. *syringae*, a non-host pathogen of the *Oryza sativa* rice plants.[72, 73] Syringolin A was identified as an inhibitor of the human proteasome in 2008, thus prompting interest in the successful completion of its total synthesis by several research groups. The total syntheses of syringolins A and B were first completed in 2009, with many more syntheses to follow.[74-76] *In vitro* enzymatic assays revealed the inhibitory activities of syringolins A and B toward the 20S proteasome. Syringolin A (**I-14**) inhibits the ChT-L and C-L activities of the 20S proteasome (K_i: 1.1 ± 0.179 μM, and 10.3 ± 1.4 μM, respectively). The macrolactam binds covalently to the 20S proteasome by direct interaction with Thr1O$^{\gamma}$ within the active sites.[62, 77] The α,β-unsaturated carboxamide of syringolin A is rendered especially electrophilic due to the ring

strain of the macrocycle resulting from the presence of two *trans* alkenes; upon 1,4-Michael addition of Thr1O$^{\gamma}$, this ring strain is relieved. In comparison, syringolin B (**I-15**), which lacks one of the *trans* alkenes, is a significantly less potent inhibitor of the 20S proteasome (K_I: 7.7 ± 2.3 μM (ChT-L); 107.8 ± 39.2 μM (T-L).

Additional derivatization of the syringolin A scaffold has been pursued by several groups (**Scheme 1.3**). Alteration of the *N*-terminus of syringolin A from a carboxylic acid to a lipophilic tail led to the production of SylA-LIP **I-16,** which exhibits inhibitory activity towards all three catalytic sites of the proteasome ($K_{i:}$ 8.65 ± 1.33nM (ChT-L); 79.6 ± 29.3 nM (T-L); and 943 ± 100 nM (C-L)).[78] TIR-199 (**I-17**) contains a slightly longer lipophilic tail than SylA-LIP and inhibits the ChT-L (K_i: 18 nM) and T-L (K_i: 194 nM) sites of the human proteasome in *in vitro* enzymatic assays.[79] TIR-199 also inhibits the proteasome in multiple myeloma cell line MM1.RL and neuroblastoma cell line MYCN2 and has demonstrated exciting cytotoxic activity against bortezomib-resistant cell lines (MM1.S BzR and U266 BzR), indicating it can overcome bortezomib resistance *in vivo.*[80] Clerc et. al. further investigated the effects of substitution at the *N*-terminus through the synthesis of a syringolin A-glidobactin A hybrid **I-18.**[81] The inhibitory activity and subsite selectivity of the analogue was tested using competitive activity-based protein profiling (ABPP) in HEK cell lysates and living cells, compared to known syrbactin inhibitors. Further *in vitro* studies revealed that **I-18** inhibits all three catalytic sites of the 20S proteasome (K_i: 12.5± 1.5 nM (ChT-L), 136.9± 12.4 nM (T-L), 3.7 ± 1.2 μM (Casp-L)).[82] Cell culture-based experiments from the same study revealed that the analogue carries out inhibition of the proteasome in several cancer cell lines.

Introduction of hydrophobic sidechains allowed the group to target the S3 subpocket of the β5 subunit for inhibition. Compound **I-19**, which contained a benzyl substituent and lipophilic

side chain, displayed strong inhibitory activity against the ChT-L site of the proteasome (K_i': 0.12 nM) and cytotoxicity towards human RPMI8226 multiple myeloma cells (IC_{50}: 2.2 nM).[76] Further optimization of **I-19** has focused on improving cytotoxicity.[83]

Simplification of the syringolin A scaffold has also been a focus of research by the Ichikawa group. One report focused on analogues that exhibited proteasome inhibition and cytotoxicity against cancer cells by targeting a different intermolecular H-bonding interaction.[84] The *N*-terminal amide of analogue **I-20** is believed to participate in a hydrogen-bonding interaction with Asp114 (β6), similarly to its parent syringolin A. The group hypothesized that removal of the *N*-terminal amide group and replacement with a longer alkyl chain may allow for a switching in the hydrogen-bonding interactions within the β5 subunit and allow for a novel interaction between the substrate and Ala49. The hypothesis was verified through the synthesis of analogue **I-21**, which displayed nanomolar inhibitory activity towards the ChT-L site of the proteasome (IC_{50}: 107 nM). Additionally, analogue **I-21** exhibits nanomolar growth inhibitory activity against several cancer cell lines.

Alteration of the macrocycle structure was also explored. Researchers hypothesized that a more accessible alkene isomer with a similar three-dimensional structure might also be able to carry out inhibitory activity. The group synthesized isosyringolin A (**I-21**) and its analogue **I-22,** which both exhibited inhibition towards the ChT-L site (Ki= 590 nM; 1.53 nM, respectively).[85] Compound **I-22** also exhibited potent cytotoxicity against OPM-2 human myeloma cancer cells (IC_{50}: 6.7nM) and bortezomib-resistant OPM-2 cells (IC_{50}: 60 nM), displaying greater cytotoxicity as compared to bortezomib (IC_{50}: 146 nM). Expansion of the syringolin A ring by Ibarra-Rivera et al. led to oxa-SylA-LIP (**I-23)**, which displays potent cytotoxicity against the MYCN-2 cells (IC_{50}: 0.4 μM) and also inhibits the proteasome in cell-based studies.[86, 87]

Analogue development based upon the syringolin B scaffold has also been investigated by several research groups (**Scheme 1.4**). For example, the SylB-LIP analogue (**I-24**) was developed as a direct comparison to SylA-LIP (**I-16).**[86] Totaro et al. designed more potent syringolin B analogues with greater inhibition towards the β5 subunit based upon the synthesis of syringolin B by Pirrung et al.[75, 88] Introduction of aromatic groups at the P1 and P3 residues in the scaffold led to the discovery of potent inhibitor **I-24** (second order rate-constant(k_{in}/K_i)*:* 4305 $M^{-1}s^{-1}$). The analogue also exhibits potent growth inhibition against various leukemia cell lines.

Scheme 1.4 Syringolin B-based inhibitors

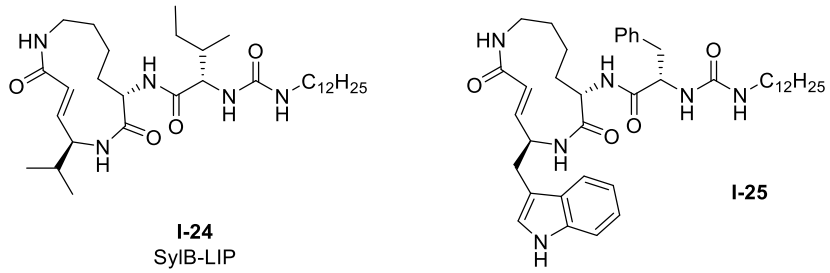

Thiasyrbactin analogues with a sulfur-for-carbon substitution within the macrolactam ring were synthesized with varying levels of sulfur oxidation. These analogues were reported for their activity towards both the constitutive and immunoproteasomes, more selectively inhibiting the T-L site of the immunoproteasome.[89] The biological activity of the analogues was further examined through cytotoxicity experiments with numerous neuroblastoma cell lines. The thiasyrbactin scaffold has established itself as a drug-like starting point for inhibition of the immunoproteasome.

1.2.3 Macrocyclic peptides

Scheme 1.5 TMC-95-based inhibitors

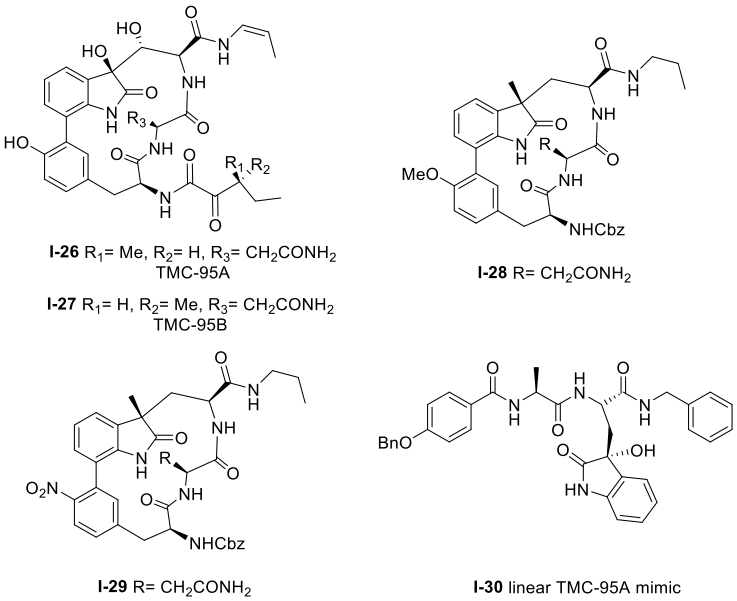

Several classes of macrocyclic peptides have been identified for their inhibitory activity towards the proteasome. Perhaps the most explored class has been the TMC cyclic peptides (**Scheme 1.5**). TMC-95 A, B, C, and D were isolated from the fermentation broth of *Apiospora montagnei* Sacc. TC 1093 by Koguchi et al. while the group was screening for 20S proteasome inhibitors.[90, 91] Among all of the TMC cyclic peptides, TMC-95 A (**I-26**) and B (**I-27**) were identified as specific inhibitors of the 20S proteasome, displaying activity against both the ChT-L (IC_{50}: 5.4 nM (TMC-95 A) and 8.7 nM (TMC-95 B)) and T-L (IC_{50}: 200 nM (TMC-95 A) and 490 nM (TMC-95 B)) subunits. TMC-95A further demonstrated cytotoxic activities against HCT-116 and HL-60 cells with IC_{50} values of 4.4 μM and 9.8 μM, respectively. The X-ray crystal structure of the yCP:TMC-95A complex was later solved by Groll et al. (2.9Å resolution), revealing that the macrocycle reversibly inhibits the 20S CP through non-covalent interactions within the catalytic core.[92] The specificity of the natural product for the chymotrypsin-like site is believed to be due to greater interaction with the S3 specificity pocket.

Due to the biological activity and overall complexity of the TMC-95 natural products, many groups sought to undertake their synthesis.[93-96] The first total syntheses of TMC-95A and B were achieved by Lin and Danishefsky in 2002.[93] The presence of sensitive functional groups in addition to the difficulty in accessing the macrocycle has encouraged subsequent analogue development to be focused on the synthesis of simplified molecules. Kaiser et al. synthesized compound **I-28**, a simplified analogue based upon the minimal requirements for binding as determined from the X-ray crystal structure of TMC-95A/proteasome complex.[97] The analogue exhibited inhibitory activity against the ChT-L site of the 20S human proteasome (IC_{50}: 1.9 μM) as compared to TMC-95A (IC_{50}: 0.012 μM).[98] The same researchers evaluated the effect of additional P' residues at the *C*-terminus of TMC-95A in a separate study.[99] The Danishefsky group established the importance of the enamide moiety at the C-8 position of the molecule;[100] analogues lacking this displayed at least a 1000-fold less potent inhibition towards the ChT-L site as compared to their natural product parent molecule. Furthermore, alteration of the enamide sidechain also affected inhibitory activity; the presence of a propyl substituent in exchange for a propylene or allyl amide sidechain results in diminished activity.

In previous studies, the biaryl moiety of TMC-95A was deemed responsible for the induction and stabilization of a β-type peptide backbone conformation while in complex with the 20S proteasome.[92] Kaiser et al. implemented the substitution of the biaryl heterocycle using a more accessible biaryl ether moiety with the goal of retaining the similar β-type backbone conformation.[101] The biaryl ether analogue **I-29** retains inhibitory potency towards the ChT-L site of the yCP (IC_{50}: 5.5 μM). Later studies revealed that due to the lack of the oxindole, biaryl ether analogues do not adopt the desired stabilized β-type structure while in complex with the 20S proteasome.[102] Wilson et. al later synthesized macrocyclic peptide aldehydes upon the previously

established biaryl ether analogues which are nanomolar inhibitors of the ChT-L site.[103] Further efforts to access simplified analogues of TMC-95A have eliminated synthesis of the challenging macrocycle altogether through the development of linear peptide mimics of the natural product. The Vidal group—in collaboration with many other research groups—has used this linear TMC-95A approach to synthesize effective inhibitors.[104-109] In particular, the linear 3-hydroxyoxindole-containing derivatives exhibited subunit selectivity towards the C-L site).[106] Optimization of the scaffold led to the discovery of potent inhibitor **I-230**, which inhibited the ChT-L of the constitutive and immunoproteasomes (IC_{50}: 7.1 ± 0.2 and 10.2 ± 0.1 nM, respectively).[109] Dimerized linear TMC-95A mimics using the active derivative **I-230** scaffold have also been synthesized to evaluate their ability to inhibit multiple active sites at once. Using either PEG spacers[110] or oligomers of aminohexanoic and adipic acid as spacers,[111] researchers were able to achieve nanomolar inhibition of the ChT-L sites of the 20S proteasome.

Scheme 1.6 Argyrin natural product family of inhibitors

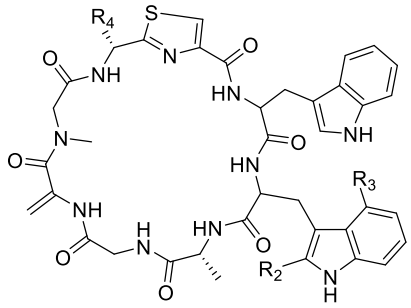

Argyrin A **I-31**: R_1= CH_3, R_2= H, R_3= OCH_3, R_4= CH_3

Argyrin C **I-33** R_1= CH_3, R_2= CH_3, R_3= OCH_3, R_4= CH_3

Argyrin B **I-32** R_1= CH_2CH_3, R_2= H, R_3= OCH_3, R_4= CH_3

Argyrin D **I-34** R_1= CH_2CH_3, R_2= CH_3, R_3= OCH_3, R_4= CH_3

Argyrin F **I-35** R_1= CH_3, R_2= H, R_3= OCH_3, R_4= CH_2OH

Argyrins A-H were isolated from the culture broth of myxobacterium *Archangium gephyra* by the Hofle group in 2002.[112, 113] This group of cyclic octapeptides displayed growth inhibitory

activity against a variety of mammalian cell lines, [112] and became a focus of total synthesis for many groups.[114-116] Argyrins A, B, C, D and F (**I-31 - I-35**) (**Scheme 1.6**) were later identified as low nanomolar inhibitors of the human proteasome.[117, 118] Bulow et al. established that the methoxy group in Trp2 as well as the *exo*-cyclic methylene group are necessary for the ability to inhibit the proteasome.[118] The binding mode of the argyrins was later elucidated through NMR spectroscopy and molecular modeling.[119] Computational inhibition studies using a humanized proteasome model indicated which interactions contributed to argyrin subunit specificity.[120] Using molecular docking, researchers designed novel argyrin A analogues *in silico* which display increased specificity towards the caspase-like site of the 20S humanized proteasome model. The Loizidou group recently reported the specificity of argyrin B towards the immunoproteasome.[121]

Macrocyclic thiopeptides have also been investigated as inhibitors of the human proteasome. Bhat et. al. reported that thiopeptides thiostrepton (**I-36**) and siomycin A (**I-37**) exhibit inhibitory activity against the 20S proteasome, which in turn contributes to the effects observed on the oncogenic transcription factor Fox1 (**Scheme 1.7**).[122, 123] The additional "B-ring" present in thiostrepton and siomycin A contributes to their inhibitory activity towards the 20S proteasome.[124] One avenue of analogue development has focused on targeting the parasite *P. falciparum*, and again illustrated that maintenance of the "B-ring" confers inhibition.[125] Zhang et al. employed the use of an *S. laurentii tsrA* mutant organism to produce Ala2 thiostrepton analogs and additionally evaluated them for their inhibitory activity towards the 20S proteasome.[126]

Scheme 1.7 Macrocyclic thiopeptide inhibitors

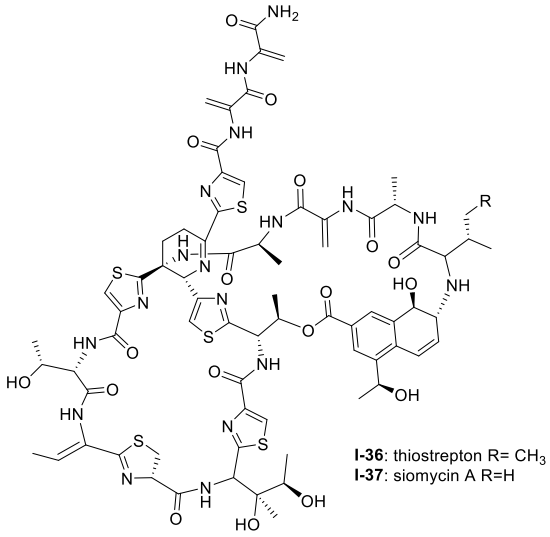

I-36: thiostrepton R= CH_3
I-37: siomycin A R=H

Several macrocyclic peptide scaffolds that have been identified as inhibitors of the proteasome have yet to be further evaluated through SAR studies (**Schemes 1.8** & **1.9**). Among these natural products are the phepropeptins. Phepropeptins A-D (**I-38 - I-41**) are cyclic hexapeptides isolated by Sekizawa et al. from *Streptomyces* sp. MK600-cF7.[127] All four natural products exhibit inhibitory activity against the β5 subunit (IC_{50}: 30.8, 15.3, 17.9, and 10.7 μM, respectively). Because of their stability as cyclic peptides, these natural products were believed to interact with the proteasome through van der Waals and hydrophobic interactions rather than through covalent bond formation.

Scheme 1.8 Phepropeptin inhibitors

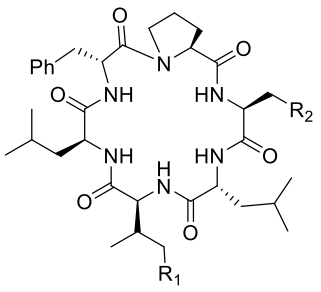

I-38: phepropeptin A R=H, R_2= $CH(CH_3)_2$
I-39: phepropeptin B R=H, R_2= Ph
I-40: phepropeptin C R=CH_3, R_2= $CH(CH_3)_2$
I-41: phepropeptin D R=CH_3, R_2= Ph

Scytonemide A (**I-42**) was isolated from the cultured freshwater cyanobacterium *Scytonema hofmannii* (UTEX 1834).[128] Scytonemide A potently inhibits the ChT-L site of the 20S proteasome (IC_{50}: 96 nM). The presence of an imine moiety within the macrocycle of scytonemide A was hypothesized to be a potential site of attack by the nucleophilic Thr1O$^{\gamma}$ of the active site; however, the X-ray crystal structure of this natural product in complex with the 20S proteasome to validate the hypothesis has not been reported. Recently, the cyclic hexapeptide baceridin (**I-43**) was isolated from the culture broth of an epiphytic *Bacillus* strain and underwent total synthesis by the Kalesse group.[129] Baceridin inhibits all three catalytic sites of the 20S proteasome and inhibits proliferation in several tumor cell lines.

Scheme 1.9 Scytonemide A and baceridin inhibitors

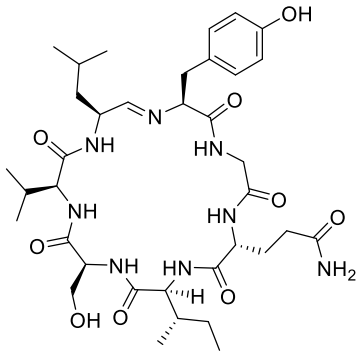

I-42: scytonemide A

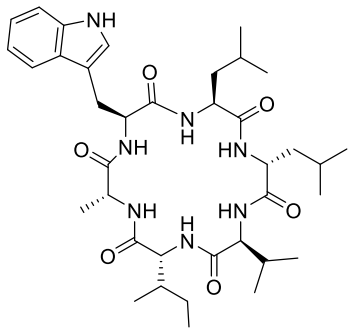

I-43: scytonemide A

1.2.4 β-lactone containing natural products

The β-lactone natural products have also been heavily evaluated for their ability to inhibit the proteasome (**Scheme 1.10**). Lactacystin (**I-44**) was isolated by Omura et al. from *Streptomyces* sp. OM-6519 and displayed biological activity in its initial discovery.[130, 131] In their 1994 study, Fenteany et al. researchers further evaluated lactacystin and analogues including omuralide for their biological activity. Results suggested the contribution of either the *N*-acetyl cysteine or β-lactone moieties towards their ability to affect cell cycle progression in Neuro 2A and MG-63 osteosarcoma cells, although the molecular target of these substrates was unidentified at the

time.[132] A subsequent study indicated that lactacystin inhibits the 20S proteasome.[133] Researchers later determined that rather than acting as an inhibitor towards the 20S proteasome, lactacystin acts as a prodrug of its active β-lactone omuralide (**I-45**).[134, 135] The first total syntheses of lactacystin and omuralide were achieved by the Corey group, and many total syntheses and formal syntheses have been recorded since.[136-138]

In an SAR study of the omuralide scaffold, the Corey group determined that while the hydroxy-isobutyl substituent at C9 is necessary for potent inhibition of 20S bovine proteasome, alteration of the methyl substituent at C7 with larger or bulky alkyl groups improves potency towards the target.[139] Research conducted by Soucy et al. further complemented these results with derivative **I-46,** which contains an *n*-propyl group in place of the methyl substituent at C7. Compound **I-46** as a K_{obs}/[I] which is greater than two-fold more potent than omuralide (K_{obs}/[I]= 46,500 $M^{-1}s^{-1}$).[140] The compact, densely functionalized omuralide scaffold indicated the importance of exploring non-peptidic natural products as potential inhibitors of the 20S proteasome.

Scheme 1.10 β-lactone natural product inhibitors and analogs

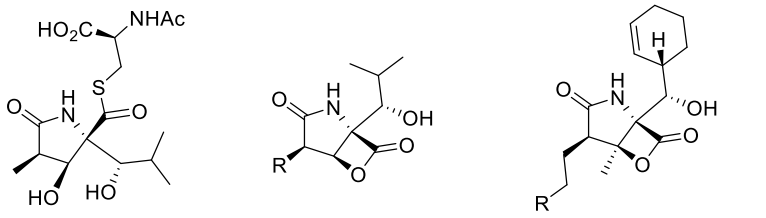

I-44 lactacystin

I-45 omuralide
I-46 R=$(CH_2)_2CH_3$

I-47 salinosporamide R=Cl
I-48 R=OTs
I-49 R=F

Salinosporamide A was first isolated as a product of the ocean sediment-dwelling bacteria *Salinospora* strain CNB-392 and its structure was elucidated by Feling et al.[141] The natural product shares its unique fused γ-lactam-β-lactone fused bicyclic ring scaffold with that of omuralide. Salinosporamide A was tested for its cytotoxicity against HCT-116 human colon carcinoma cells,

displaying an IC_{50} value of 35.1 nM. Due to its structural similarity to omuralide, salinosporamide A (**I-47**) was also tested for its inhibitory activity towards 20S proteasome; it exhibits potent inhibitory activity towards the ChT-L site (IC_{50}: 1.3 nM). Chauhan et al. further investigated the bioactivity of salinosporamide A in *in vitro* and *in vivo* studies.[142] Salinosporamide A inhibits the ChT-L site with an EC_{50} value of 3.5 ± 0.3 nM as well as the C-L and T-L sites with EC_{50} values of 430 ± 34 nM and 28 ±2 nM, respectively. Salinosporamide A also induced apoptosis in multiple myeloma cells which are resistant towards conventional and Bortezomib therapies.

Only a year after its discovery, the Corey group reported the first total synthesis of salinosporamide A;[143] the molecule has since become an attractive target for total synthesis, and many syntheses of salinosporamide A have been reported.[144-158] Exploration of the structure-activity relationship of the salinosporamide scaffold began with Macherla et al,[159] and has since been a focus of several research groups (**Schemes 1.10** & **1.11**). Alteration from the cyclohexenyl ring to other substituted cyclohexanes resulted in lower inhibitory activity towards the 20S proteasome, as well as lower cytotoxicity against multiple myeloma RPMI 8226 cells. Replacement of the chlorine atom with a hydrogen resulted in a 10-fold reduction of its inhibitory activity towards the ChT-L site of the 20S proteasome, as well as a significant reduction of its cytotoxicity towards RPMI 8226 cells. Groll et al. later solved the crystal structure of the yeast proteasome core particle (yCP) in complex with salinosporamide A, implicating the importance of the chloroethyl group in the overall inhibitory activity towards the proteasome.[160] Following transesterification of the β-lactone, the resulting hydroxyl group cyclizes upon the chloro substituent to form a tetrahydrofuran irreversibly.

Manam et. al. synthesized salinosporamide A analogues which replaced the chloro substituents with functionalities of varying leaving group potentials to further probe the

mechanism of inhibition.[161] All analogues potently inhibit the ChT-L site of the 20S proteasome; tosyl analog **I-48** displays inhibitory activity towards the ChT-L site of the 20S proteasome with an IC_{50} value of 2.5 ± 0.4 nM. Qualitative dialysis experiments with the analogues indicated that the presence of a leaving group prolongs the duration of inhibition. The researchers also performed kinetics experiments with salinosporamide A to understand the mechanism of its proteasome inhibition, determining that the natural product is a slow tight binding inhibitor which confers its activity through a multi-step inhibition mechanism. Fluorosalinosporamide **I-49** was later synthesized by Eustáquio and Moore using a combination of genetic engineering and precursor-directed synthesis.[162] Unlike salinosporamide A, **I-49** did not undergo displacement of its halogen to afford an irreversible adduct during inhibition, but rather acts as a reversible inhibitor towards the ChT-L activity of the 20S proteasome with two-fold reduced potency relative to salinosporamide A (IC_{50}: 1.5 ± 0.05 nM). The ability of the fluorine to participate in hydrophobic interactions with the proteasome was cited as a justification of its inhibitory potency.

The Corey group further explored the salinosporamide A and omuralide scaffolds through the synthesis of a γ-lactam-β-lactone hybrid antiprotealide (**I-50**).[163] Antiprotealide—later discovered as a natural product[164]—exhibited 2.5-fold more potent inhibitory activity towards the β5 subunit than omuralide but was less potent than salinosporamide A. Synthesis of the γ-lactam-β-lactone congener (**I-51**) of antiprotealide was also successfully achieved by the Corey group. While the analogue displayed slower inactivation towards the 20S proteasome than salinosporamide A and omuralide, its improved stability under physiologic conditions was an advantageous feature for relevant drug development.

Scheme 1.11 β-lactone-based inhibitors

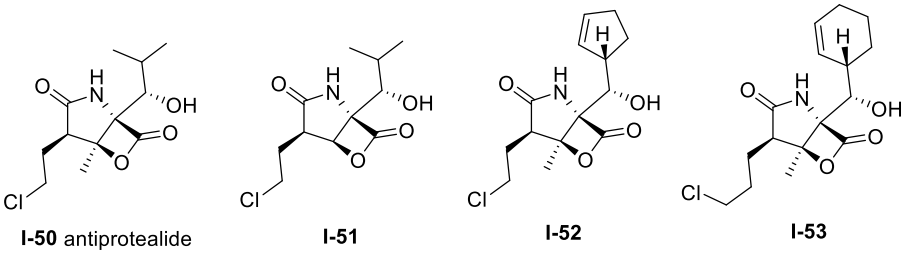

McGlinchey et al. further demonstrated that bulky groups at the C5 position were necessary for *in vitro* inhibition of the β5-subunit.[165] Chemical synthesis and metabolic engineering were also used by this group to synthesize several novel salinosporamide derivatives with varying substituents at the P1 position.[166] The analogue **I-52**—bearing a cyclopentenyl substituent at the P1 position— exhibited equipotent inhibitory potency towards the chymotrypsin-like site of the proteasome in comparison to salinosporamide A, with an IC_{50} value of 2.2±0.1 nM. Analog **I-52** also displays increased cytotoxicity against HCT-116 cells.

The length of the chloroalkyl chain at the C_2 position of the salinosporamide scaffold is also an important feature with regards to its inhibitory potency. Nguyen et al. explored this in their development of an enantioselective route to (—)-salinosporamide A and derivative (—)-homosalinosporamide A.[155] (—)-Homosalinosporamide A varies from (—)-salinosporamide A only through the length of its C_2 sidechain; the compound contains an additional methylene carbon. The researchers proposed that the derivative would behave similarly to salinosporamide A in its mechanism of inhibition towards the human proteasome. (—) homosalinosporamide A (**I-53**) displayed similar inhibitory potency towards the ChT-L activity of the 20S proteasome as compared to (—)-salinosporamide A, with an IC_{50} value of 0.7 ± 0.04 nM (versus 0.8 ±0.08 nM). However, X-ray crystallographic evidence of the hCP: (—)-homosalinosporamide A complex

illustrated that (—)-homosalinosporamide A does not form a tetrahydropyran during its inhibition of the proteasome.[167]

The structurally related cinnabaramides (**Scheme 1.12**) were first isolated from the terrestrial *Streptomycetes* JS360 in 2007 by Stadler et. al.[168] *In vitro* evaluation of the inhibitory potency of the cinnabaramides towards the human 20S proteasome mirrored results of previously established inhibitors of similar structure. For example, cinnabaramide A **(I-54**) (IC_{50}: 1 nM) displayed similar potency as salinosporamide A. Cinnabaramide A is also cytotoxic against colon cancer cell line HCT-116 at a level relative to that of salinosporamide A. Cinnabaramides F (**I-55**) and G (**I-56**) are believed to act as a prodrug to form the reactive *β*-lactone in a manner reminiscent to lactacystin; these natural products display potent inhibition towards the human 20S proteasome with IC_{50} values of 6 nM and 0.6 nM, respectively. *rac*-Cinnabaramide A was later synthesized by the Romo group.[147] In a subsequent study, Rachid et al. accessed chlorinated derivatives of cinnabaramides A-D using mutasynthetic methods.[169] 15-chlorocinnabaramide A (**I-57**) exhibits greater inhibitory activity towards the β5 subunit of the 20S proteasome than its parent compound, with an IC_{50} value of 9.3 ± 5.9 nM (IC_{50} value of cinnabaramide A for this assay was 11.9 ± 7.4 nM). Derivative **I-57** also displays potent cytotoxicity against the HCT-116, RPMI8226, and SW840 cancer cell lines.

Scheme 1.12 Cinnabaramide-based inhibitors

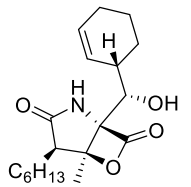

I-54:cinnabaramide A

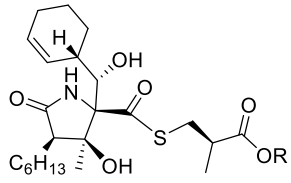

I-55:cinnabaramide F R=H
I-56:cinnabaramide G R=Me

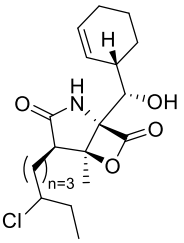

I-57: 15-chloro-cinnabaramide A

Belactosins A and C (**Scheme 1.13**) were first isolated from the culture broth of *Streptomyces* sp. KY11780 by Asai et al.[170] The antiproliferative and antitumor activities of both natural products is attributed to a β-lactone moiety at their C-terminus. Belactosin A contains a cyclopropane ring within its backbone which is absent in that of belactosin C. Belactosin A and C both displayed *in vitro* antiproliferative activity against HeLa S3 cells with IC_{50} values of 51 μM and 200 μM, respectively. Belactosin A further demonstrated the ability to halt cell cycle progression in the G2/M stage in tumor cells. Akai et al. reported the molecular mechanism of action of belactosins A (**I-58**) and C (**I-59**): both demonstrate nanomolar inhibitory activity towards the ChT-L site of the rabbit 20S proteasome, both displaying IC_{50} values of 0.21 μM.[171] Optimization of the belactosin A scaffold was further achieved by benzylation of it carboxylic acid. The first total synthesis of belactosin A was completed by Armstrong and Scutt in 2004.[172] An enantioselective total synthesis of belactosins A, C and its homologue homobelactosin C (**I-60**) was reported shortly thereafter by Larionov and de Meijere.[173] X-ray crystallographic evidence based upon the yCP:homobelactosin complex suggested that the β-lactone moiety undergoes nucleophilic attack by the Thr1O$^{\gamma}$ residue within the catalytic site to form an ester through a covalent, irreversible bond.[174]

Scheme 1.13 Belactosin natural product inhibitors

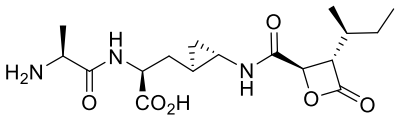

I-58: belactosin A

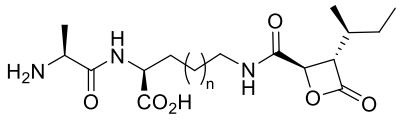

I-59: belactosin C n=1
I-60: homobelactosin C n=2

Exploration of the stereochemistry surrounding the belactosin A cyclopropyl ring indicated its contribution to biological activity (**Scheme 1.14**).[175-177] The (*cis*/*L-anti*) configuration demonstrated promise, as evidenced by compound **I-61**. Compound **I-61** selectively inhibits the ChT-L site of the human 20S proteasome with an IC_{50} value of 5.7± 1.2 nM, comparable to that of bortezomib. Compound **I-61** also inhibits the growth of HCT116 cells with an IC_{50} value of 1.82 μM via the same mechanism as bortezomib (IC_{50} value: 0.01 μM). The X-ray crystal structure of yCP:**I-61** complex (2.8 Å), provided researchers with key interactions that contribute to inhibition. Optimization of the transition-state conformation of **I-61** was subsequently reported.[178] Installation of a methyl group at carbon C1' adjacent to the cyclopropyl group led to analog **I-62**, which is restricted into a predominant *syn* conformation. Derivative **I-62** exhibited lower inhibitory activity towards the ChT-L site relative to the parent compound with an IC_{50} value of 47 ± 2.9 nM. However, when evaluated for its growth inhibitory activity against several tumor cell lines (Hs-Sultan, KB, and HCT-116), compound **I-62** exhibits activity similar to its parent compound.

Scheme 1.14 Belactosin-based inhibitors

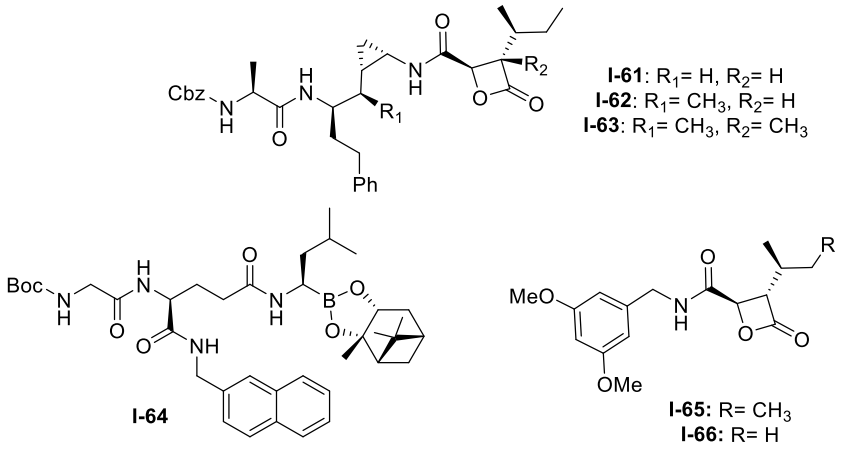

Researchers hypothesized that poor performance of belactosin analogues under biological conditions and in cell studies may be due to chemical or enzymatic hydrolysis of the reactive β-lactone moiety,[178] and thus sought to improve stability by increasing steric hindrance surrounding

the β-lactone ring.[179] Analogue **I-63** not only contains an additional methyl group at the α-position of the lactone carbonyl carbon, but also retains the same methyl group at the C1' carbon adjacent to the cyclopropyl ring to lock it into the *syn* conformation. While analogue **I-63** displays lower activity towards the ChT-L site of the proteasome as compared to parent compound **I-61** (IC_{50}: 1.3 μM and 0.0057 μM, respectively), **I-63** exhibited comparable growth inhibitory activity towards HCT-116 cells relative to the established inhibitor (IC_{50}: 4.0 μM (**I-63**); 1.8 μM (**I-61**)). These results provided a novel belactosin analogue with improved biological stability.

Flexible achiral nonpeptidic analogues with a β-lactone moiety and aromatic tails were synthesized by Kawamura et al. using a topology-based scaffold hopping approach.[180] These synthetically accessible inhibitors represent novel scaffolds with improved drug-likeness in comparison to past belactosin analogues. Simplified nonpeptidic belactosin scaffolds were further explored through synthesis of hybridized bortezomib and epoxomicin analogs.[180, 181] Divergence from the β-lactone moiety of the belactosin scaffold stemmed from an interest to incorporate more stable electrophilic warheads.

Nakamura et al. first sought to optimize the belactosin C scaffold in 2009 through the introduction of a boronate moiety like that of bortezomib.[182] Compound **I-64** was identified as a potent inhibitor of the ChT-L (β5) site of the 20S proteasome (IC_{50}: 0.28 ±0.04 μM) and also exhibited submicromolar growth inhibitory activity against HeLa cells (IC_{50}: 0.35 ±0.02 μM) in an MTT assay. The de Meijere group expanded their previous synthetic endeavors of belactosin scaffolds through the synthesis of novel belactosin C-based proteasome inhibitors.[183] A subsequent report by the same group elected to divert from the dipeptide scaffold of belactosin C to investigate more easily accessible analogues.[184] Analogues containing the *N*-(3,5-dimethoxy)benzyl amido side chain displayed especially potent inhibitory activity towards the β5 subunit. This scaffold was

later altered to produce a minimal β-lactone scaffold for selective inhibition of either the β5c or β5i of the human 20S proteasome.[185] Analogue **I-65** contains a pseudo-isoleucine P1 side chain, whereas **I-66** contains a smaller pseudo valine moiety. This difference in size of the P1 side chain resulted in selective inhibition. Compound **I-65** exhibited preference towards the β5i site (IC_{50}: 14.37 nM) over the β5c (IC_{50}: 21.35 nM), whereas **I-66** preferentially inhibits the β5c (IC_{50}: 26.87nM) over the β5i (IC_{50}: 83.62 nM).

Scheme 1.15 Cystargolide-based inhibitors

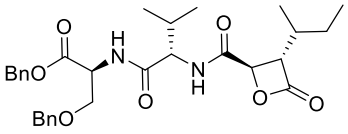

I-67: cystargolide A R_1=H, R_2=CH_2CH_3
I-68: cystargolide B R_1=H, R_2=CH_3
I-69: R_1=Bn, R_2=CH_2CH_3
I-70: R_1=Bn, R_2=CH_3

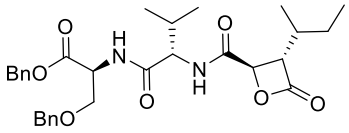

I-71

Another class of β-lactone containing natural products which display intriguing activity towards the proteasome are cystargolides A and B (**Scheme 1.15**). Originally isolated by the Kerr group in 2015 from the actinomycete *Kitasatospora cystarginea* NRRLB16505, these natural products contain a dipeptide backbone with a β-lactone moiety.[186] Cystargolides A (**I-67**) and B (**I-68**) exhibited inhibition towards the ChT-L site of the 20S proteasome with IC_{50} values of 0.36 ± 0.017 μM and 0.93 ± 0.032 μM, respectively. The total syntheses and absolute stereochemistry of cystargolides A and B were later successfully achieved by Tello-Aburto et al.[187] Wolf et al. were also able to access the cystargolides and belactosins using biosynthetic methods. The stereochemistry of these natural products is integral to inhibitory activity: maintaining the (*2R,3S*) absolute stereochemistry contributes to potency of inhibitors.[188] Benzylation of the *N*-terminus also improved inhibitory potency 100-fold, as evidenced by analogues **I-69** (IC_{50}: 9.2 ± 0.59 nM) and **I-70** (IC_{50}: 9.0 ± 1.4 nM).[187] Subsequent optimization of the cystargolide scaffold was

achieved in 2018: benzyl ether **I-71** inhibits the hβ5 subunit of Jurkat cell lysate with an IC_{50} value of 3.1 ± 0.2 nM as compared to cystargolide B (IC_{50}: 0.90 ± 0.11 μM), and is also cytotoxic against MCF-7 and RPMI-8226 cells.[189]

1.2.5 α,β-epoxyketones

The epoxy-ketone containing natural products have become a specific focus to researchers due to their ability to inhibit the 20S proteasome (**Scheme 1.16).** Eponemycin is a dipeptide natural product which features a lipophilic tail at its *N*-terminus and an electrophilic α, β-epoxyketone moiety at its C-terminus. The natural product was isolated from the fermentation broth of the soil-dwelling *Streptomyces hygroscopicus* No. P247-71 (ATCC 53709).[190] Eponemycin (**I-72**) and its derivative dihydroeponemycin (**I-73**) exhibit potent *in vitro* toxicity against B16-F10 and HCT-116 cells. The natural product also demonstrated itself as an inhibitor of angiogenesis.[191] The cellular target of its antitumor activity was later identified by the Crews group as the proteasome with biotinylated eponemycin analogs.[192] Dihydroeponemycin inhibits the proteasome in a competitive and irreversible manner, with the highest rate of inhibition towards the ChT-L site (k_{assoc}: 66.4 ± 8.9 $M^{-1}s^{-1}$). Kim et al. further explored the structure-activity relationship of dihydroeponemycin and analogues to improve understanding of subunit selectivity within the 20S proteasome.[193] The ability of dihydroeponemycin to interact with the immunoproteasome was attributed to its lipophilic C-terminus.

Scheme 1.16 Epoxyketone natural product inhibitors

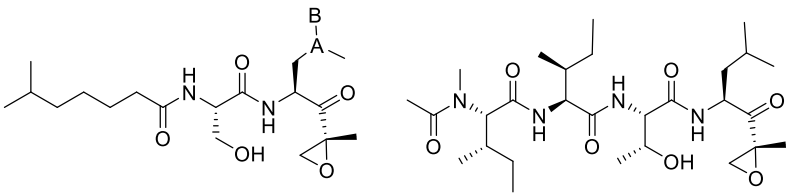

I-72 eponemycin A=B C=CH_2
I-73 dihydroeponemycin A=B CH-CH_2

I-74 epoxomicin

The natural product epoxomicin (**I-74**) was isolated from a soil-dwelling actinomycete No. Q996-17[194] and is comprised of a tetrapeptide skeleton with a C-terminal α,β-epoxyketone. Epoxomicin exhibited strong *in vitro* cytotoxicities against various cancer cell lines including HCT-116 (IC_{50}: 9.0 nM), and additionally exhibits antitumor activity against B16 melanoma. The total synthesis of epoxomicin was first reported by the Crews group in 1999.[195] Due to previous reports that indicated peptide α,β-epoxyketones as inhibitors of the proteasome,[196] epoxomicin was evaluated for this activity. Epoxomicin selectively inhibits the chymotrypsin-like site of the 20S proteasome (k_{assoc}: 35,400 $M^{-1}s^{-1}$). The *N*-terminal P3 and P4 residues play a major role in the potency of inhibition towards the proteasome.[193] As compared to dihydroeponemycin, epoxomicin and its analogues display greater inhibitory potency. The X-ray crystal structure of the yCP:epoxomicin complex was solved by Groll et al. (2.25 Å resolution),[197] revealing the basis for its selectivity towards the ChT-L site. The α,β-epoxyketone was initially believed to undergo a reversible nucleophilic addition by the Thr1O^{γ} to produce a hemiacetal; subsequent attack of the epoxide by Thr1N forms a morpholino adduct irreversibly. Recently, the mechanism of proteasome inhibition by epoxyketones was revised based on X-ray crystallographic data by Schrader et al.[198] Instead of forming a morpholino adduct, epoxyketones are believed to react with the Thr1 residue of the catalytic site to form a 1,4-oxepane ring.

Further optimization of the epoxomicin scaffold has been achieved by several groups (**Scheme 1.17**). The Crews group set out to improve upon this natural product to access more potent and selective analogues, leading to the development of the tetrapeptide epoxyketone YU-101 (**I-75**).[199] *In vitro* studies indicate that YU-101 selectively inhibits the ChT-L site of the 20S proteasome with a k_{assoc} value of 166,000 (5-12 nM), greater than that of epoxomicin and bortezomib. Further optimization of this analogue led to carfilzomib (Kyprolis®, **I-76**) by the

biotech company Proteolix.[200] Carfilzomib exhibits selective, potent inhibitory activity towards the ChT-L site of the proteasome, with an IC_{50} value of 6 nM; the compound also performed well in *in vivo* studies. In 2012 carfilzomib was approved by the FDA for the treatment of refractory multiple myeloma;[201] further alteration of this compound led to the orally available oprozomib (**I-77**).[202] Subsequent optimization of the epoxyketone scaffold has focused on developing analogues which can overcome bortezomib and carfilzomib-resistant multiple myeloma. Kim et al. recently reported a novel epoxyketone **I-78**, which not only inhibits the ChT-L activity of proteasome from RPMI8226 cell lysates (IC_{50}: 2.1 ± 0.9 nM), but also inhibits proteasome activity (ChT-L) nearly three-fold more potently in RPMI8226-Cfz resistant cells than carfilzomib itself (IC_{50}: 106.2 ± 28.9 nM).[203] Other recent advances of the epoxyketone moeity include the design of selective inhibitors for the β1i,[204, 205] β2i,[206, 207] and β5i subunits.[208]

Scheme 1.17 Epoxomicin-based inhibitors

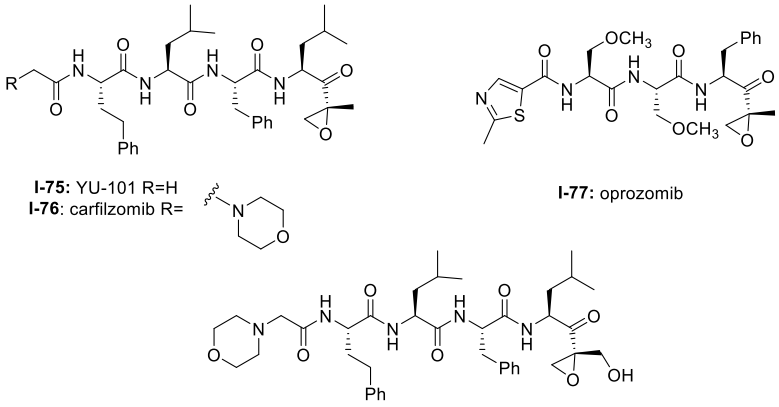

The epoxyketone-containing natural products carmaphycin A and B were isolated from marine cyanobacterium *Symploca* sp.[209] These tripeptides contain a lipophilic *N*-acylated tail at their *N*-terminus and a leucine-derived epoxyketone at their C-terminus. A scalable total synthesis of both carmaphycins was also conducted and both were evaluated for their ability to inhibit the yeast 20S proteasome. Carmaphycins A (**I-79**) and B (**I-80**) (**Scheme 1.18**) exhibited potent

inhibitory activity towards the ChT-L site with IC_{50} values of 2.5 ±0.3 nM and 2.6 ±0.9 nM, respectively. The natural products also displayed cytotoxic activity towards H-460 and HCT-116 cancer cell lines. Structural investigation implicated the importance of the sulfoxide/sulfone moieties in the methionine-derived residue in the interaction with the target; this interaction represents a distinctive binding mode for the carmaphycins relative to previously discovered α, β-epoxyketone inhibitors. Replacement of the α,β-epoxyketone moiety with an enone led to the identification of analogue **I-81,** which is a selective nanomolar inhibitor towards the ChT-L site of the 20S yeast proteasome.[210] Analogue **I-81** interacts through a unique two-step hydroamination mechanism with the catalytic site to form a morpholine adduct. Most recently, carmaphycin-based proteasome inhibitors have been designed for use as antibody drug conjugates as potential cancer treatments.[211]

Scheme 1.18 Carmaphycin-based inhibitors

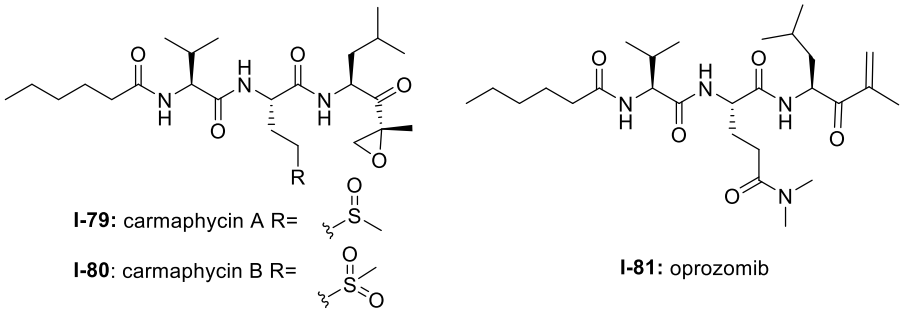

Several other epoxyketone natural products were also isolated and evaluated for their ability to inhibit the proteasome (**Scheme 1.19**). TMC-86A (**I-82**) and B (**I-83**) are isolated from the fermentation broth of *Streptomyces* sp. TC 1084.[212, 213] Both display similar inhibitory potency towards the ChT-L site with IC_{50} values of 5.1 μM and 1.1 μM, respectively. TMC-86A and B also exhibited nanomolar cytotoxicity against various tumor cell lines. TMC-96 (**I-84**) was isolated from the fermentation broth of *Saccharothrix* sp. TC 1094,[212, 213] and contains a branched *N*-acylated terminus and a leucine-derived α,β-epoxyketone moiety similar to dihydroeponemycin.

TMC-96 exhibits inhibitory activity towards the ChT-L and C-L sites of the 20S proteasome (IC_{50}: 2.9μM and 3.5 μM, respectively), and additionally displays nanomolar cytotoxic activity against a variety of tumor cell lines. TMC-89A (**I-85**) and B (**I-86**) are α,β-epoxyketone-containing tripeptides which were isolated from the fermentation broth of *Streptomyces* sp. TC 1087 by Koguchi et al. in their search for new proteasome inhibitors of bacterial origin.[214] When tested for their proteasome inhibitory activity, both displayed equipotent micromolar activity towards the ChT-L site of the 20S proteasome, with IC_{50}: 1.1μM. TMC-89A and B also exhibit slight selectivity towards the T-L site of the 20S proteasome, with IC_{50} values of 390 nM and 510 nM, respectively. *In vitro* cytotoxicity studies reveal that in comparison to many other α, β-epoxyketones, TMC-89A and B are not remarkably cytotoxic against tumor cell lines. Subsequent optimization of these natural products has not been reported but may benefit from the addition of *N*-terminal lipophilic residues to improve cell permeability.

Scheme 1.19 Epoxyketone natural product inhibitors- continued

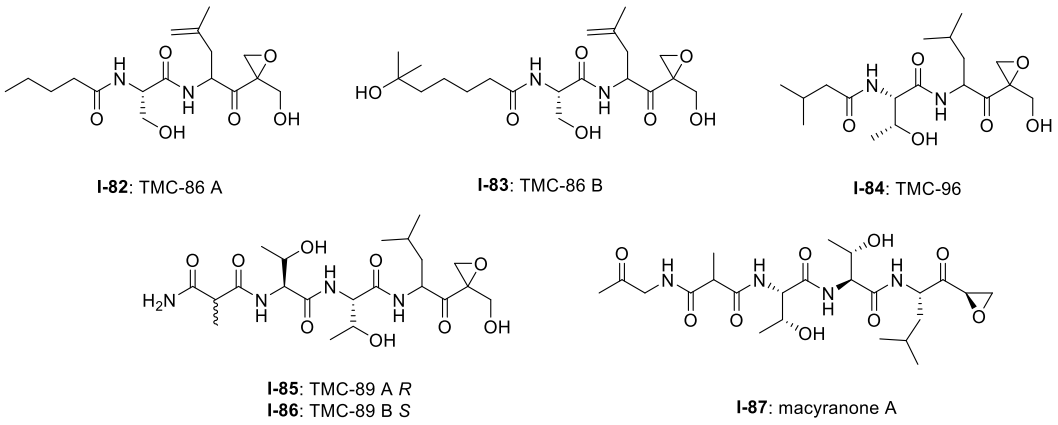

The macyranones are a group of six linear peptides which were produced by the myxobacteria *Cystobacter fuscus* MCy9118.[215] Macryanone A (**I-87**) contains an α,β-epoxyketone moiety which made it an intriguing compound to test for proteasome inhibition. Macyranone A inhibits the ChT-L activity of the yCP (IC_{50}: 5.9 nM) and the human constitutive proteasome and

immunoproteasome, with IC_{50} values of 21 nM and 15 nM, respectively. X-ray crystallographic analysis of the yCP: macyranone complex (2.8 Å resolution) revealed that it reacts irreversibly with the catalytic sites of the proteasome in a similar mechanism to epoxomicin. Despite its promising performance in *in vitro* enzymatic testing, macyranone A displayed poor cytotoxicity against mammalian cell lines including HCT-116, THP-1 and HL-60 cancer cell lines.

Scheme 1.20 Clarepoxcin & landepoxcin inhibitors

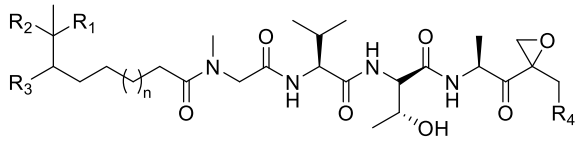

I-88: clarepoxcin A R_1=OH, R_2=CH_3, R_3=H, R_4=H, n=2
I-89: clarepoxcin B R_1=H, R_2=OH, R_3=CH_3, R_4=H, n=3
I-90: clarepoxcin C R_1=H, R_2=CH_3, R_3=H, R_4=OH, n=1
I-91: clarepoxcin D R_1=H, R_2=CH_3, R_3=H, R_4=H, n=1

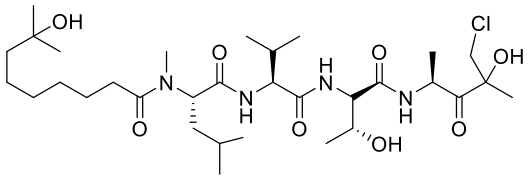

I-92: clarepoxcin E

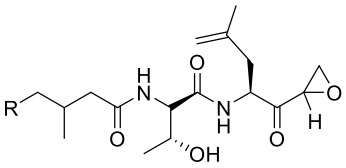

I-93: landepoxcin A R=H
I-94: landepoxcin B R=CH_3

The most recently discovered epoxyketone natural product inhibitors were reported by Owen et al. The group utilized molecular evolutionary analyses of complex metagenomes to target and isolate the previously unidentified clarepoxcin and landepoxcin natural products (**Scheme 1.20**).[216] Clarepoxcins A-E (**I-88 – I-92**) were produced by *S. albus:AR456*, while landepoxcins A (**I-93**) and B (**I-94**) were produced by *S. albus:AR412*. Clarepoxcins A-D are potent low nanomolar inhibitors of the human 20S proteasome, with an IC_{50}~6.9-15.1 nM (ChT-L). The clarepoxcins also exhibited potent cytotoxic activity against HCT-116 cells. While clarepoxcin E did not display inhibitory activity towards the 20S human proteasome, it did exhibit potent cytotoxicity against HCT-116. The authors proposed that in cells, clarepoxcin E acts as a prodrug to form the reactive α, β-epoxyketone moiety. Landepoxcins A and B displayed higher nanomolar inhibitory activity

towards the human 20S proteasome, however landepoxcin A did exhibit impressive cytotoxicity against HCT-116 cells.

1.2.6 Terpenoids

Terpenoids represent a vast class of natural products that have been reported for their biological activities. For example, the agosterols were evaluated by the Tsukamoto group for their ability to inhibit the proteasome. Among the many tested, agosterol C demonstrated the most potent activity against the ChT-L site, with an IC_{50} value of 19.8 μM.[217] Epoxyphomalins A and B were first isolated as products of the marine-derived fungus *Phoma* sp. by Mohamed et al.[218] Epoxyphomalin A displayed cytotoxicity towards several human tumor cell lines. The intracellular target of epoxyphomalins A and B was later identified as the 20S proteasome;[219] both epoxyphomalins A (**I-95**) and B (**I-96**) exhibit dose-dependent inhibition of the 20S human proteasome subunits (**Scheme 1.21**). Epoxyphomalin A demonstrated equipotent inhibition against all three catalytic sites, whereas epoxyphomalin B preferentially inhibits the ChT-L site.

Scheme 1.21 Epoxophomalin inhibitors

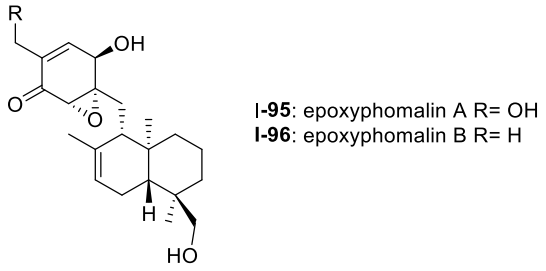

Noda et al. isolated a variety of stronglyphorines from marine sponge *Petrosia corticata* in 2015.[220] The structure-activity relationship of the strongylophorines with their inhibitory activity revealed that the presence of a hemiacetal in addition to a hydroquinone moiety contributes significantly towards the potency of the proteasome inhibitors. Strongylophorines 13/14 (**I-97**) and

strongylophorines 15/16 (**I-98**) exhibited the most potent inhibitory activity towards the ChT-L site of the 20S proteasome with an IC_{50} of 2.1 μM and 3.6 μM, respectively (**Scheme 1.22**).

Scheme 1.22 Strongylophorine inhibitors

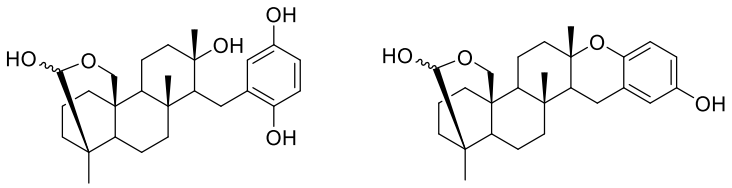

I-**97**: strongylophorines 13/14 I-**98**: strongylophorines 15/16

Petrosaspongiolide M (**I-99**) was isolated from the New Caledonian marine sponge *Petrosaspongi nigra* among the other petrosaspongiolides A-R. The petrosaspongiolides are sesterterpenes all containing a cheilantane skeleton, and were first identified as inhibitors of the preparation of phospholipase A_2.[221] Petrosaspongiolide M was later identified by Margarucci et al. as a proteasome inhibitor using chemical proteomics.[222] The natural product inhibited the C-L and ChT-L activity of the proteasome in a cell-based assay with IC_{50} values of 0.85±0.15 μM and 0.64 ±0.15 μM, respectively. Petrosaspongiolide M was later reported to exhibit potent inhibitory activity towards the ChT-L and C-L activities of the proteasome with submicromolar values in an *in vitro* fluorometric enzyme assay.[223] Optimization led to analogues **I-100** and **I-101,** which both feature a benzothiophen-2-yl substituent at the C4 position of the butenolide ring. Analogue **I-100** exhibited potent inhibitory activity against the ChT-L and C-L site of the 20S proteasome, with IC_{50} values of 0.06 ± 0.009 and 0.22 ±0.03 nM, respectively. The desbrominated analogue **I-101** also displayed potent inhibitory activity towards the ChT-L and C-L sites, with IC_{50} values of 0.07 ± 0.01 nM for both sites (**Scheme 1.23**).

Several other terpenoid natural products have also been identified as inhibitors of the 20S proteasome. The merosesterterpene acanthosulfate (**I-102**) was identified by West and Faulkner as a metabolite of the marine sponge *Acanthodendrilla* sp. in 2008.[224] Acanthosulfate (**Scheme 1.24**)

exhibited inhibition towards the proteasome (IC_{50}: 4.5 μM) but lacked selectivity and potency when tested for activity against the BMS Oncology Diverse Cell Panel (ODCA).

Scheme 1.23 Petrosospongiolide M-based inhibitors

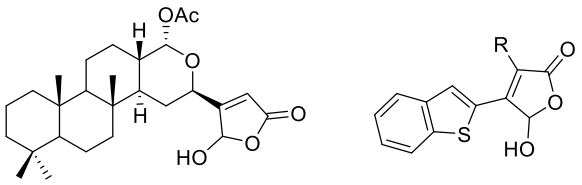

I-99: petrosospongiolide M

I-100: R= Br
I-101: R= H

Celastrol (**I-103**) is a quinone methide triterpene which is extracted from the "Thunder God Vine" (*Tripterygium wilfordii* Hook F.) and has been recognized for its biological activity. Dou et al. discovered the inhibitory activity of celastrol towards the 20S proteasome in 2006.[225] Celastrol selectively inhibits the ChT-L activity of the proteasome with an IC_{50} value of 2.5 μM. The compound also demonstrated the ability to inhibit the proteasome of prostate cancer cells in a cell-based assay at 1-5 μM. Celastrol further demonstrated antitumor activity in an *in vivo* study. Researchers reported that treatment of PC-3 containing mice with the natural product resulted in tumor reduction. Because celastrol has many intracellular targets,[226] focus on optimization of the celastrol scaffold has involved improving its solubility and physiological properties. Recently, celastrol has been reported as cytotoxic against human multiple myeloma cells.[227] Further investigation of compounds from the extract of the "Thunder God Vine" (*Tripterygium wilfordii* Hook F.) focused on the diterpene tri-epoxide lactone triptolide (**I-104**). Originally discovered in 1972, researchers reported its antileukemic activity thus providing impetus for further biological evaluaton.[228, 229] Although triptolide does not inhibit the ChT-L site of purified 20S proteasome, it was able to inhibit proteasomal activity within cancer cells. This interesting result suggests that triptolide acts as a prodrug, and one of its metabolites—perhaps an oxidized ketone—acts instead as the biologically active molecule.

Tiedemann et al. further demonstrated the inhibitory potential of the celastrol scaffold through the investigation of its natural product relative pristimerin and the mechanisms of its biological activity.[230] Pristimerin (**I-105**) contains an identical scaffold to that of celastrol except for the carboxylic acid moiety, which is instead replaced by a methyl ester. Pristimerin selectively inhibits the ChT-L activity of the 20S proteasome with an EC_{50} value of less than 125 nM. Researchers further indicated in a cell-based experiment that pristimerin suppresses NF-KB activity through proteasome dependent and independent pathways. Pristimerin also demonstrated promising activities in cytotoxicity and *in vivo* studies.

Scheme 1.24 Terpenoid natural product inhibitors

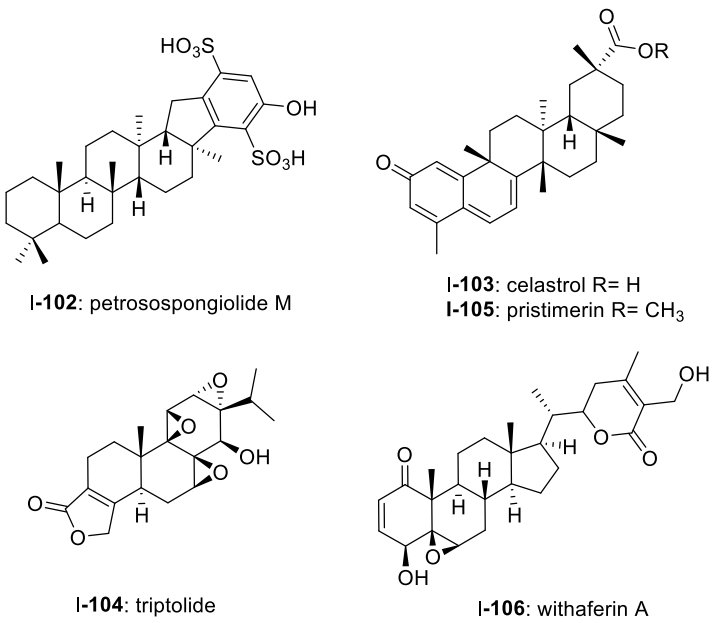

The steroidal lactone withaferin A (**I-106**) is a natural product which was isolated from the Indian Winter Cherry *Withania somnifera* Dunal, a plant which is popular for its use in Ayurvedic medicine.[231] The steroid contains two conjugated ketones and bears structural similarity to celastrol. Withaferin A had previously been recognized for its various biological activities, though the mechanism of action by the natural product had not been elucidated. Dou et al.

identified the 20S proteasome as an intracellular target of withaferin A.[232] Withaferin A inhibits the ChT-L activity of the 20S proteasome with an IC_{50} value of 4.5 μM and also exhibits proteasomal inhibition within PC-3 cells. The natural product also performed well in *in vivo* tumor studies conducted on mice. *In silico* docking studies in addition to kinetic studies suggested that the conjugated ketone moieties of withaferin A may interact covalently with the Thr1O$^{\gamma}$ within the β5 active site to confer inhibition of the 20S proteasome.

Scheme 1.25 Neomacrophorin natural product inhibitors

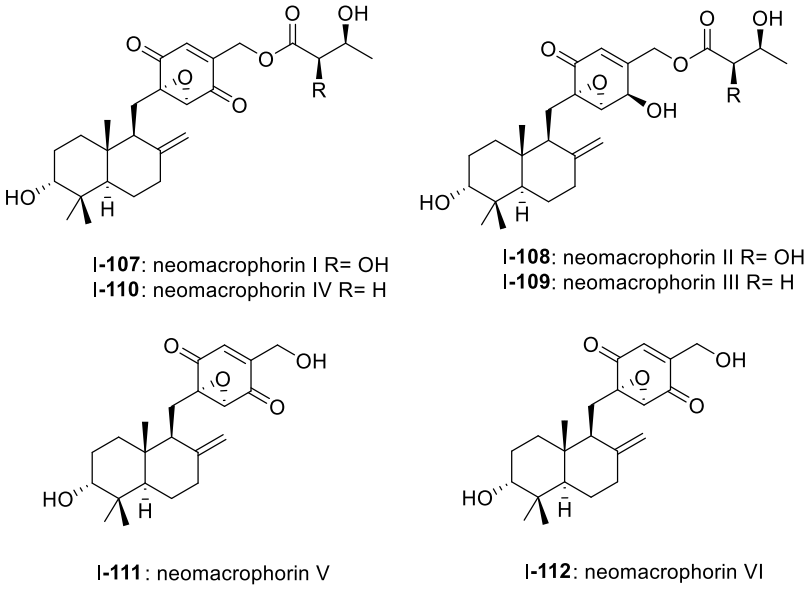

The neomacrophorins (**Scheme 1.25**) were identified as products of soil-dwelling *Trichoderma* sp. 1212-03, and have recently been evaluated for their biological activities[233].[234, 235] Neomacrophorin I demonstrated cytotoxicity against human colorectal cancer COLO 201 cells, though its mode of action for this cytotoxicity was initially unclear. An MTT assay of the neomacrophorins with promyelocytic leukemia HL60 cells revealed that neomacrophorins I-VI (**I-107 – I-112**) inhibit growth of the HL60 cells. The molecules were also responsible for inducing apoptotic cell death in HL60 cells, and further demonstrated *in vitro* inhibitory activity towards the 20S proteasome. Neomacrophorins I and IV demonstrated the most potent inhibitory activity

towards the ChT-L site as compared to the other neomacrophorins, with IC_{50} values of 5.7 ± 1.0 and 5.3 ± 1.2 μM, respectively. The quinone moiety was deemed an important feature for the inhibitory proteasome activity and cytotoxicity.

1.2.7 Alkaloids

Various alkaloids have also been identified as inhibitors of the proteasome. Tsukamoto et al. isolated the aaptamine natural products (**Scheme 1.26**) from the marine sponge *Aaptos suberitoides* as part of their efforts to identify novel proteasome inhibitors from marine invertebrate extracts and marine-derived fungi cultures. Aaptamine (**I-113**), isoaaptamine (**I-114**) and demethylaaptamine (**I-115**) inhibit the ChT-L and C-L sites for both rat and human 20S proteasomes (IC_{50}:7.0-20.2 μM). When tested for cytotoxicity against HeLa cells, the aaptamines did not exhibit a correlation between cytotoxicity and proteasome inhibition.

Scheme 1.26 Aaptamine and salsinol natural product inhibitors

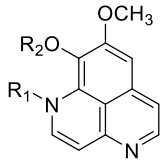

I-113: aaptamine R_1= H, R_2= CH_3
I-114: aaptamine R_1= CH_3, R_2= H
I-115: demethylaaptamine R_1,R_2= H

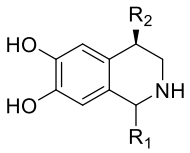

I-116: salsolinol R_1= CH_3, R_2= H
I-117: norsalsolinol R_1=R_2= H

The tetrahydroisoquinoline salsolinol alkaloids were later isolated from the marine sponge *Xestospongia* cf. *vansoesti* and evaluated for their proteasome inhibitory activity.[236] Salsolinol (**I-116**) and its derivative norsalsolinol (**I-117**) inhibit the ChT-L site with IC_{50} values of 279.0 and 193.7 μM, respectively. Cytotoxicity studies indicated that salsolinol is cytotoxic against several cell lines; norsalsolinol displayed cytotoxicity against HeLa cells (IC_{50}: 42.4 μM) but was not tested against other cell lines.

Specific manzamines have been identified as inhibitors of the 20S proteasome by Tsukamoto et al (**Scheme 1.27**).[237, 238] Following their isolation from the marine sponge *Acanthostrongylophora ingens* and structural identification, several were evaluated for their cytotoxicity and proteasome inhibitory activity. Manzamine A (**I-118**), *neo*-kauluamine (**I-119**) and pre-*neo*-kauluamine (**I-120**) exhibit potent inhibitory activity towards the ChT-L site of the 20S proteasome with IC_{50} values of 2.0, 0.13 and 0.34 μM, respectively. Acanthomanzamine D (**I-121**) also exhibits nanomolar inhibitory activity towards the chymotrypsin-like site of the 20S proteasome (IC_{50}: 630 nM), albeit with less potency than the kauluamines. The presence of the eight-membered ring in addition to the β-carboline appeared to be necessary for proteasome inhibition.

Scheme 1.27 Manzamine natural product inhibitors

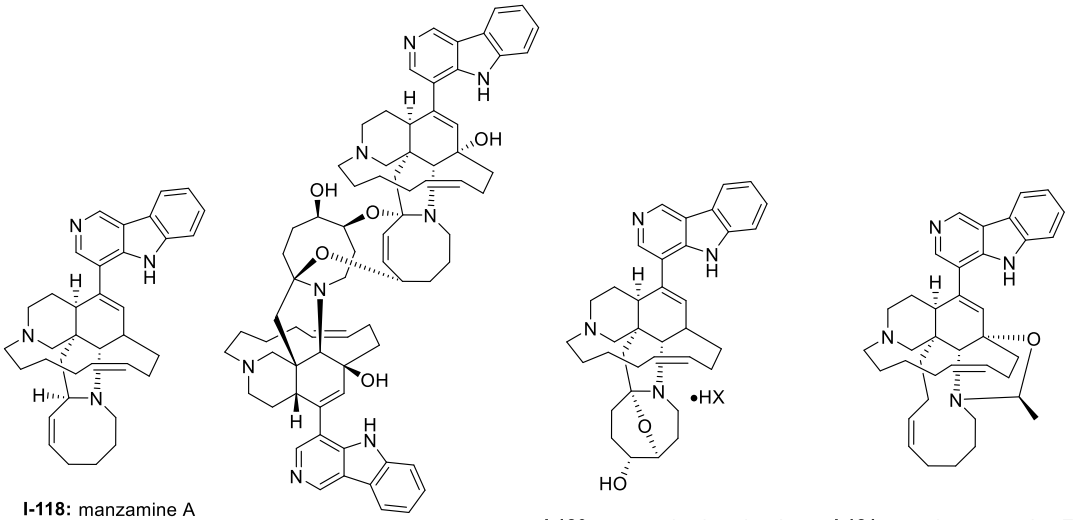

The Tsukamoto group also isolated two halicyclamines from *Acanthostrongylophora ingens* and evaluated them for their biological activity (**Scheme 1.28**).[239] Halicyclamine B (**I-122**) and tetradehydrohalicylamine B (**I-123**) differ only in their level of unsaturation; whereas the latter contains the aforementioned pyridinium ring, the former contains a substituted tetrahydropyridine ring. The halicyclamines were tested for cytotoxic activities against HeLa cells which showed that

tetradehydrohalicyclamine B exhibited low micromolar cytotoxicity (IC_{50}: 12 μM), whereas halicyclamine B is not cytotoxic. Halicyclamine B and tetradehydrohalicyclamine B demonstrated inhibitory activity towards both the cCP and iCP.

Scheme 1.28 Halicyclamine natural product inhibitors

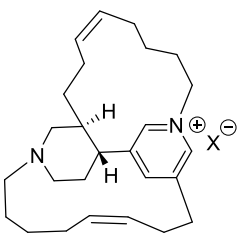

I-122: halicyclamine B

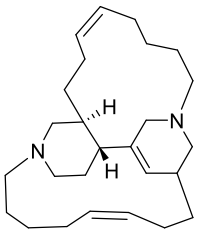

I-123: tetrahydrohalicyclamine B

Cerpegin (**I-124**) and its analogs (**Scheme 1.29**) have been investigated as novel proteasome inhibitors in recent years. Cerpegin itself exhibits selective micromolar inhibition against the C-L activity of the 20S proteasome, with an IC_{50} value of 10.4 ± 0.5μM.[240] Optimization of the N^5 position led to the identification of selective micromolar (IC_{50}: ~5 μM) inhibitors of the caspase-like activity of the 20S proteasome. *In silico* docking suggested an interaction of the N^5 substituents with a Tyr residue (Tyr114, β2 subunit) for their selectivity. Introduction of a large, flexible hydrophobic residue at the C1 position led to the discovery of sixteen derivatives with micromolar (IC_{50}: 2-5 μM) activity towards the β1 subunit.[241] *In silico* docking indicated that these hydrophobic moieties bind within the primed substrate binding channel of the β1 active site to confer selectivity. Replacement of the carbonyl at C4 with a benzylamino moiety further improved the inhibitory activity of the scaffold to lead to β1-selective nanomolar inhibitor (**I-125**) (IC_{50}: 600 nM).[242]

Scheme 1.29 Cerpegin-based inhibitors

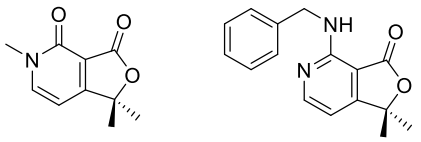

I-124: cerpegin **I-125**

Pyrrole-imidazole alkaloids have also been investigated for their ability to inhibit the proteasome (**Scheme 1.30**). Pyrrole-imidazole alkaloids encompass a large group of heterocyclic natural products isolated from marine sponges.[243] Perhaps one of the most famous pyrrole-imidazole alkaloids is palau'amine (**I-126**). Discovered by Scheuer et. al. in 1993,[244] researchers reported that palau 'amine displayed cytotoxic activity. The first total synthesis of (±)-palau'amine was achieved by the Baran group in 2010,[245] followed by an enantioselective synthesis of (—)-palau'amine shortly thereafter.[246] Due to its reported cytotoxicity, palau'amine and its relatives (±)dibromophakellin (**I-127**) and (±)-dibromophakellstatin (**I-128**) were evaluated as inhibitors of the ChT-L activity of the cCP and iCP.[247] (—)-Palau'amine displayed 2-fold improved inhibitory activity towards the constitutive human 20S proteasome relative to its racemate (IC_{50}: 2.5 (±0.7) vs. 5.5 (±1.5) μM, respectively), indicating that the (—) enantiomer is responsible for inhibitory activity towards the proteasome. The presence of a cyclic urea or guanidine ring is integral to inhibitory activity. Researchers synthesized several indole analogs[248] as potential inhibitors based on the (±)-dibromophakellin scaffold using the same strategy as Hewlett and Tepe in their total synthesis.[249] (±)-Indolophakellin analog **I-130** exhibited potent and specific inhibitory activity towards the β5c of the 20S proteasome (IC_{50}: 3.5 ±0.7 μM) at a comparable potency to (±)-palau'amine. An X-ray crystal structure of the yCP:**I-130** complex (2.5Å resolution) revealed that the analogue confers its inhibition through solely non-covalent interactions with the S3 subpocket of the β5 subunit, including H-bonding and halogen bonding interactions. Since this study, newly discovered pyrrole-imidazole alkaloids have frequently been tested for their proteasomal

inhibitory activity. For example, 5-bromopalau'amine (**I-129**) was recently isolated among several bromopyrrole alkaloids from the *Dictyonella* sp. marine sponge and exhibited inhibition towards the ChT-L site of the 20S proteasome (IC_{50}: 9.2 ± 3.2 μM).[250]

Scheme 1.30 Pyrrole-alkaloid natural product-based inhibitors

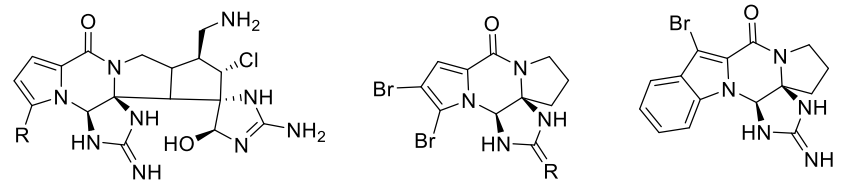

1.2.8 Flavonoids

Many flavonoids have been isolated and evaluated for their ability to inhibit the 20S proteasome based upon their intriguing bioactivities. The green tea-derived catechin polyphenols have been among these flavonoids of interest and include epigallocatechin-3-gallate ((—)-EGCG), epicatechin ((—)-EC), epigallocatechin ((—)-EGC), gallocatechin-gallate ((—)-GCG), and catechin gallate. The ester moiety present in of some of these flavonoids was thought to contribute to proteasome inhibition, as the ester-containing catechins (—)-EGCG (**I-131**), (—)-ECG (**I-132**), (—)-GCG (**I-133**) and (—)-CG (**I-134**) (**Scheme 1.31**) inhibit the chymotrypsin-like activity of the 20S proteasome in a range of IC_{50} values 86-194 nM, (—)-EGCG being the potent among them.[251] Catechins lacking the ester moiety do not display this same inhibitory potency. Subsequent cell-based studies using (—)-EGCG demonstrated the compound's ability to inhibit the 26S proteasome in Jurkat T cells; 10 μM (—)-EGCG inhibited ~70% of the proteasomal ChT-L activity. EGCG also inhibits the ChT-L activity in breast (MCF-7) and prostate (PC-3 and LNCaP) cancer cells. Enantiomeric analogues of natural catechins, (+)-EGCG and (+)-GCG inhibit the ChT-L activity of the proteasome in both *in vitro* and *in vivo* studies to a similar potency

of the natural catechins. However, global protection of the hydroxy groups of (+)-EGCG with benzyl moieties renders the compound inactive, implicating that the presence of at least one hydroxyl group is necessary for inhibitory activity.[252] The mechanism of proteasome inhibition by catechins was later postulated by Smith et al.[253] (—)-EGCG irreversibly inhibits the ChT-L activity of the 20S proteasome in a time-dependent manner, indicative of covalent bond formation within the active site. Docking studies carried out using AutoDock indicated this potential interaction. When docked with the ChT-L site, the ester carbonyl of (—)-EGCG is within 3.18 Å of Thr1O$^{\gamma}$ for nucleophilic attack. The hydrophobic A ring of (—)-EGCG also sits within the S1 subpocket of the ChT-L site to confer selectivity between subunits. Due to instability of (—)-EGCG under biological conditions, subsequent studies of the tea polyphenols for proteasome inhibition focused upon improving analogue stability under physiologically-relevant conditions. Several studies by the Dou group have been conducted to generate bioactive analogues of (—)-EGCG: examples of these include peracetate esters[254, 255] and fluorinated analogues. [256]

Scheme 1.31 Tea polyphenol natural product inhibitors

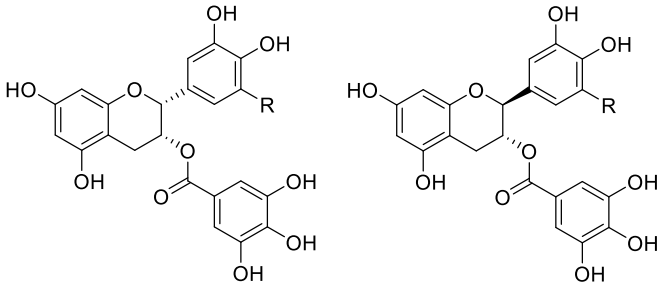

I-131 (–)-EGCG R= OH
I-132 (–)-ECG R= H

I-133 (–)-GCG R= OH
I-134 (–)-CG R= H

In addition to the tea polyphenols, several other flavonoids have been identified for their ability to inhibit the proteasome (**Schemes 1.32-1.37**). Specific features of the flavonoids contribute to the interactions between the compounds and target active sites. The soy isoflavone genistein (**I-135**) was first reported in 2003 by Kazi et. al. for its inhibitory activity towards the

ChT-L site of the 20S proteasome in a cell-free assay with an IC_{50} value of 26 μM.[257] Docking studies suggested that unlike tea polyphenol (—)-EGCG, genistein does not covalently interact with the Thr1 residue of the active site. Genistein was also isolated in addition to proteasome inhibitors isoliquiritigenin (**I-136**) and 7-hydroxyflavanone (**I-137**) from the plant *Spatholobus suberectus*.[258] The three compounds exhibited low micromolar inhibition towards the β5-site of the 20S proteasome, with IC_{50} values ranging from 4.88 (±1.55) to 9.26 (±1.2) μM.

Scheme 1.32 Flavonoid natural product inhibitors

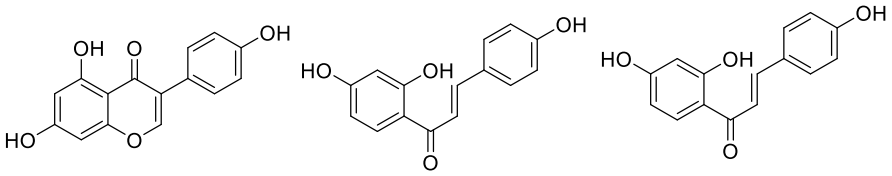

I-135 genistein **I-136** isoliquiritigenin **I-137** 7-hydroxyflavanone

Apigenin (**I-138**), quercetin (**I-141**), kaempferol (**I-142**) and myricetin (**I-143**) were later evaluated by Chen et al. for their ability to inhibit the 20S proteasome.[259] All four compounds inhibited the ChT-L site of the 20S proteasome in a cell-free assay, with apigenin displaying the most potent activity (IC_{50}: 1.8 ± 0.03 μM). The compounds displayed similar inhibitory activity towards the 26S proteasome in intact Jurkat cells. Apigenin was still the most potent of the four compounds. *In silico* docking studies suggested that the carbonyl at C-4 is the site of nucleophilic attack by the Thr1O^{γ} residue of the active site. Additionally, the hydroxyl group at C-3 was believed to interfere with binding of the flavonoids to the active site.

Scheme 1.33 Flavone, flavonol, and flavonoid-based natural product inhibitors

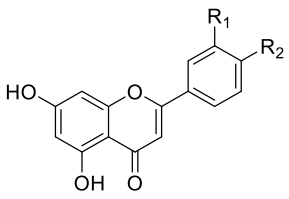

I-138 apigenin R_1= H, R_2= OH
I-139 chrysin R_1,R_2= H
I-140 luteolin R_1= H, R_2= OH

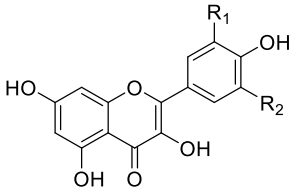

I-141 quercetin R_1= OH, R_2= H
I-142 kaempferol R_1,R_2= H
I-143 myricetin R_1= H, R_2= OH

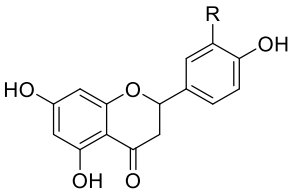

I-144 naringenin R= H
I-145 eriodictyol R= OH

Further studies by the same group evaluated the structure-proteasome-inhibitory activity relationship of flavonoids chrysin (**I-139**), luteolin (**I-143**), naringenin (**I-144**), and eriodictyol (**I-145**) in comparison to apigenin.[260] The 2,3 double-bond featured within the flavanones chrysin, apigenin and luteolin was deemed necessary for of inhibition towards the ChT-L site of the proteasome. A subsequent study by Wu and Fang reported that the inhibition of chrysin, apigenin and luteolin is selective for ChT-L and T-L catalytic activities of the proteasome within tumor cells.[260]

Scheme 1.34 Flavanone-containing natural product inhibitors

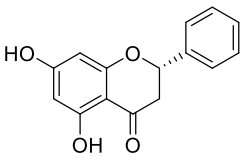

I-146 pinocembrin

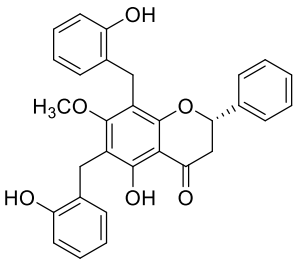

I-147 7-methoxydichamanetin

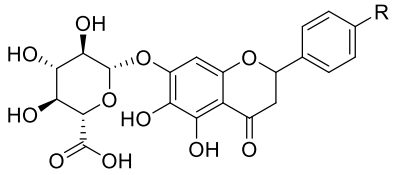

I-148 baicalin R= H
I-149 scutellarin R= OH

Pinocembrin (**I-146**) and 7-methoxydichamanetin (**I-147**) were recently isolated in a bioassay-guided fractionation of the *Piper sarmentosum* plant by Pan et al.[261] These flavanones exhibited inhibitory activities toward the ChT-L site of the human 20S proteasome, with IC_{50} values of 2.87 ± 0.26 and 3.45 ± 0.18 μM, respectively. The flavonoid glycosides baicalin (**I-148**) and scutellarin (**I-149**) were isolated from the Chinese herbal medicines *Scutellaria baicalensis*

and *Erigeron breviscapus* (Vant.) Hand-Mazz by Wu et al. These compounds exhibited the ability to preferentially inhibit ChT-L activity in A549 and HL60 cancer cells.[262] The biflavonoids morelloflavone (**I-150**) and talbotaflavone (**I-151**) were isolated from the stem bark of *Garcinia lateriflora* by Ren et al., and exhibited inhibition against the ChT-L site of the 20S proteasome, with IC_{50} values of 1.3 μM and 4.4 μM, respectively.[263] The prenylated flavonoid sanggenon C was also reported as an inhibitor of the 20S proteasome.[264] Huang et al. indicated that the natural product inhibits the ChT-L activity of the 20S proteasome in enzymatic studies and also in H22 cell lysate in a dose-dependent manner.

Scheme 1.35 Biflavonoid-containing natural product inhibitors

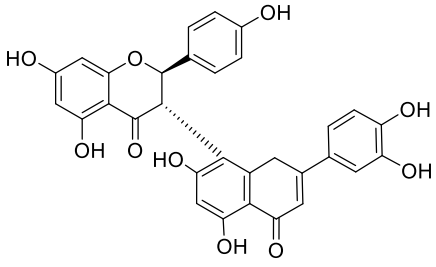

I-150 morelloflavone

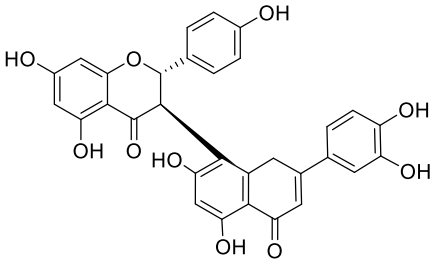

I-151 talbotaflavone

The promiscuous active agent curcumin (**I-152**) is a symmetric polyphenol which was also reported as a proteasome inhibitor through *in vitro* and *in vivo* studies.[265, 266] Curcumin inhibits the ChT-L activity of the 20S mammalian proteasome with an IC_{50} value of 1.85 μM, demonstrates the ability to inhibit the 26S proteasome in human colon cancer HCT-116 and SW480 cell lines, and also induces apoptosis. *In silico* docking studies suggests that the ketone moieties are susceptible to nucleophilic attack by the Thr1O$^{\gamma}$ of the chymotrypsin-like site. A recent study by Zhang et al. introduced an α-aminoboronic acid electrophile to the scaffold to improve potency.[267] These compounds displayed impressive growth inhibitory activity against HCT-116 cells.

Scheme 1.36 Diketone flavonoid natural product inhibitors

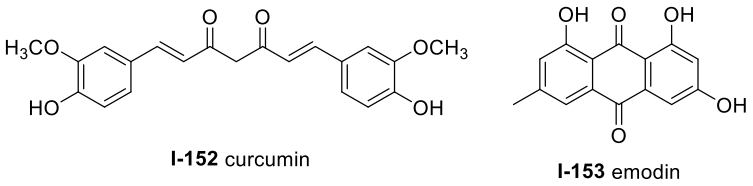

I-152 curcumin **I-153** emodin

Emodin (**I-153**) was recently identified as an inhibitor of the 26S proteasome in the HEK293A-luciferase-cODC cell line. Emodin inhibited luciferase-ODC degradation with an EC_{50} of 6.33 μM and also exhibited inhibitory activity against the ChT-L and C-L sites of the proteasome, with IC_{50} values of 1.22 and 0.24 μM, respectively[268]. *In silico* docking with the catalytic sites of the proteasome indicated that the carbonyls are susceptible to nucleophilic attack by the Thr1O$^{\gamma}$ much like the other carbonyl-containing flavonoids.

1.2.9 Polyketides

Polyketides represent another class of natural products which have been scrutinized for their biological activity. The naphthoquinone shikonin (**I-154**) was isolated from the traditional Chinese medicine *Zi Cao (gromwell)* and reported as an inhibitor of ChT-L activity of 20S rabbit proteasome (IC_{50}: 12.5 μM).[269] The natural product also demonstrates inhibitory activity towards the 26S proteasome in cell studies (PC-3 and murine hepatoma H22). A later study by Wada et al. complemented these results, demonstrating the ability of shikonin to induce apoptosis in various multiple myeloma cells including bortezomib resistant cells KMS11/BTZ (SHK at 2.5-5μM).[270] *In silico* docking studies suggest that the quinone carbonyls interact with the ChT-L site in such a way that they became highly susceptible to the catalytic site's nucleophilic Thr1 residue.

Recently, the cytotoxic macrocycle kendomycin (**I-155**) was identified as a weak inhibitor of the proteasome.[271] Kendomycin exhibited the ability to weakly inhibit the activity of the ChT-L site of the proteasome (IC_{50}: 67.9 μM). X-ray crystallographic analysis of the yCP: kendomycin

complex indicates that it does not interact with the inner chamber of the core particle, but rather covalently attaches to β2-H141N$^{\gamma}$ along the outside of the 20S proteasome. Kendomycin sits within the surface-exposed pocket formed by the interface of the β2-β7' subunits.

Scheme 1.37 Polyketide natural product inhibitors

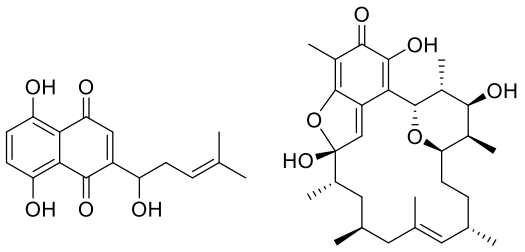

I-154: shikonin **I-155**: kendomycin

1.2.10 Macrolides

Secomycalolide A (**I-156**) was isolated alongside known mycalolide A (**I-157**) and 30-hydroxymycalolide A (**I-158**) from a marine sponge of the genus *Mycale* (**Scheme 1.38**). The mycalolides had previously been reported for their cytotoxicity towards B-16 melanoma cells. *In vitro* studies indicated that these compounds inhibit the ChT-L activity of the proteasome, with IC_{50} values of 11.5, 33.0 and 49.4 μM, respectively.[272] These results suggested that the intact macrocycle is not necessary for inhibitory activity, which could allow for the design of simplified analogues in future studies.

Scheme 1.38 Mycalolide natural product inhibitors

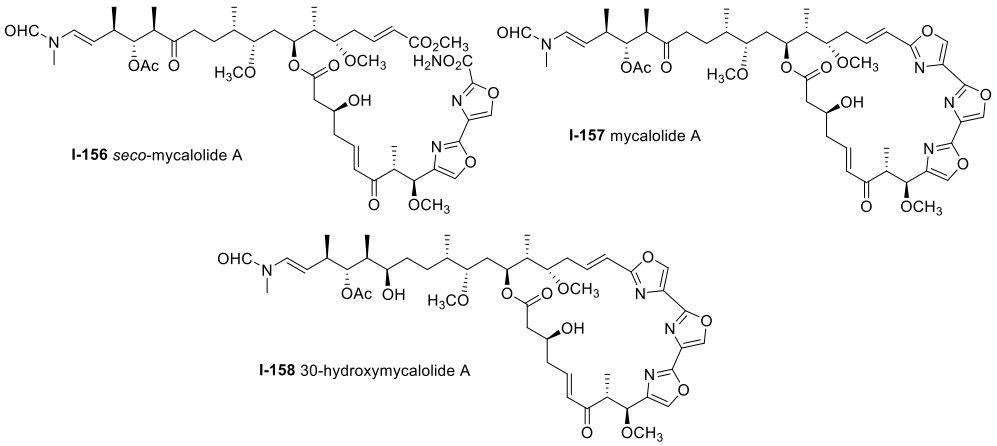

Several macrocyclic cylindrocyclophanes were also reported as proteasome inhibitors by Chlipala et al.[273] The compounds were isolated from the extract of the terrestrial cyanobacteria *Nostoc* species (UIC 10022A) which was collected from a Chicago city parkway. The most potent cylindrocyclophanes A_4-A_2 (**I-159–I-161**) inhibit the ChT-L activity at low micromolar concentrations (IC_{50}: 3.93 ± 0.18, 2.75 ± 0.31, and 2.55 ±0.11 μM, respectively). Cylindrocyclophanes A_4-A_2 also display potent cytotoxicity against HT-29 cells, with EC_{50} values of 2.0, 0.5 and 1.7 μM, respectively. Researchers suggested that in addition to a dichloromethyl moiety, the presence of hydroxyl group at C14 was also important for inhibitory activity. However, the inhibitory potency results did not correlate to cytotoxicity results, suggesting that the main reason for cytotoxicity was not due to proteasome inhibition.

Scheme 1.39 Cylindrocyclophane natural product inhibitors

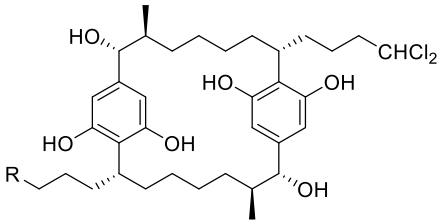

I-159 cylindrocyclophane-A_4 R=$CHCl_2$
I-160: cylindrocyclophane-A_3 R=CH_2Cl
I-161: cylindrocyclophane-A_2 R=CH_3

The macrolide rapamycin (**I-162**), its analogues, and its acyclic analog *seco*-rapamycin (**I-163**) have also been identified as allosteric inhibitors of the 20S proteasome by Osmulski and Gaczynksa.[274] Rather than bind competitively within the catalytic sites of the 20S proteasome, these compounds bind to specific grooves on the α-ring to confer inhibition. Rapamycin inhibits the ChT-L and T-L activities of the 20S proteasome in a reversible manner, with IC_{50} values of 1.9 and 0.4 μM, respectively. Identification of a minimal binding pharmacophore led researchers to the discovery of analog **I-164**, a pipecolic ester carbamate which inhibits the ChT-L site of the 20S proteasome (IC_{50} value of 2.0 μM).[275]

Scheme 1.40 Rapamycin-based inhibitors

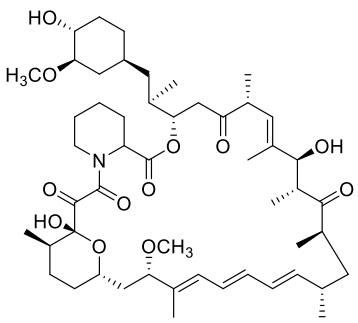

I-162: rapamycin

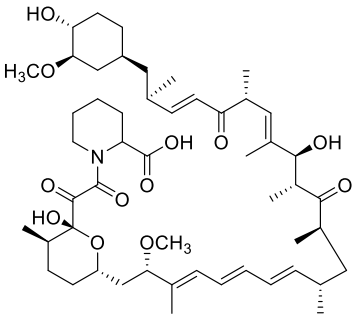

I-163: *seco*-rapamycin

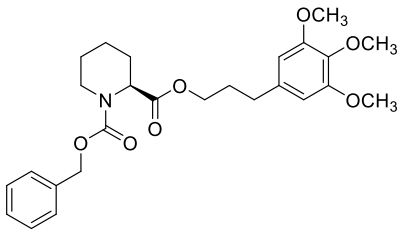

I-164

1.3 Conclusion

Modulation of the 20S proteasome is a valuable strategy for the treatment of many diseases. Several natural product classes have been identified as proteasome inhibitors, making them intriguing starting points in the search of drug leads. Not only do these scaffolds provide opportunity for inhibition by allosteric and competitive modes, but the complex structures have also facilitated extensive structure-activity relationship studies to better understand their mechanism of interaction with the 20S proteasome. Inherent challenges associated with the use of natural product-based inhibitors include product isolation from crude mixtures and subsequent synthesis of the complex substrates, as exemplified in the case of some natural product-based inhibitors. However, the use of X-ray crystallography and computational docking have been integral in the determination of their mechanisms of inhibition. These methods allow for the strategic synthesis of novel (often simplified) scaffolds, which retain the key components of their parent molecule. Modification of natural product scaffolds by researchers has led to more potent, physiologically relevant, and selective inhibitors as starting points for the treatment of disease. Thus far, the clinical impact of proteasome inhibitors has been significant with several agents currently clinically used to treat multiple myeloma and mantle cell lymphoma.

In our continued efforts to discover novel inhibitors of the 20S proteasome, we sought to further investigate the pyrrole-alkaloid scaffolds for inhibitory activity. The work described in this thesis includes the efforts to access potential inhibitors through small molecule synthesis, methodology development, and total syntheses of natural products of this family. Chapter 2 entails synthetic efforts towards the bromoindolophakellstatin analogs for evaluation as 20S proteasome inhibitors. Chapter 3 describes the development of a novel Rh(III)-catalyzed C-H activation/annulation to access urea-fused tetrahydroisoquinolone scaffolds which are reminiscent of the active pyrrole-alkaloid inhibitors. Chapter 4 describes the efforts towards the total syntheses of several natural products belonging to the pyrrole-alkaloid family.

REFERENCES

1. Hubbell, G. E.; Tepe, J. J., *RSC Chem. Biol.*, **2020**, *1*, 305-332.

2. Hershko, A.; Ciechanover, A., *Annu. Rev. Biochem.*, **1998**, *67*, 425-479.

3. Ciechanover, A.; DiGiuseppe, J. A.; Schwartz, A. L.; Brodeur, G. M., *Prog. Clin. Biol. Res.*, **1991**, *366*, 37-43.

4. Chen, Z.; Hagler, J.; Palombella, V. J.; Melandri, F.; Scherer, D.; Ballard, D.; Maniatis, T., *Genes Dev.*, **1995**, *9*, 1586-1597.

5. Peters, J. M.; Cejka, Z.; Harris, J. R.; Kleinschmidt, J. A.; Baumeister, W., *J. Mol. Biol.*, **1993**, *234*, 932-937.

6. Lowe, J.; Stock, D.; Jap, B.; Zwickl, P.; Baumeister, W.; Huber, R., *Science*, **1995**, *268*, 533-539.

7. Da Fonseca, P. C. A.; Morris, E. P., *J. Biol. Chem.*, **2008**, *283*, 23305-23314.

8. Orlowski, M.; Wilk, S., *Arch. Biochem.*, **2000**, *383*, 1-16.

9. Tanaka, K.; Yoshimura, T.; Kumatori, A.; Ichihara, A.; Ikai, A.; Nishigai, M.; Kameyama, K.; Takagi, T., *J. Biol. Chem.*, **1988**, *263*, 16209-16217.

10. Groll, M.; Heinemeyer, W.; Jäger, S.; Ullrich, T.; Bochtler, M.; Wolf, D. H.; Huber, R., *Proc. Natl. Acad. Sci. U.S.A.*, **1999**, *96*, 10976-10983.

11. Groll, M.; Bochtler, M.; Brandstetter, H.; Clausen, T.; Huber, R., *ChemBioChem.*, **2005**, *6*, 222-256.

12. Groll, M.; Ditzel, L.; Löwe, J.; Stock, D.; Bochtler, M.; Bartunik, H. D.; Huber, R., *Nature*, **1997**, *386*, 463-471.

13. Unno, M.; Mizushima, T.; Morimoto, Y.; Tomisugi, Y.; Tanaka, K.; Yasuoka, N.; Tsukihara, T., *J. Biochem.*, **2002**, *131*, 171-173.

14. Unno, M.; Mizushima, T.; Morimoto, Y.; Tomisugi, Y.; Tanaka, K.; Yasuoka, N.; Tsukihara, T., *Structure*, **2002**, *10*, 609-618.

15. Harshbarger, W. D.; Miller, C.; Diedrich, C.; Sacchettini, J. C., *Structure*, **2015**, *23*, 418.

16. Aki, M.; Shimbara, N.; Takashina, M.; Akiyama, K.; Kagawa, S.; Tamura, T.; Tanahashi, N.; Yoshimura, T.; Tanaka, K.; Ichihara, A., *J. Biochem.*, **1994**, *115*, 257-269.

17. Murata, S.; Sasaki, K.; Kishimoto, T.; Niwa, S. I.; Hayashi, H.; Takahama, Y.; Tanaka, K., *Science*, **2007**, *316*, 1349-1353.

18. Huber, E. M.; Basler, M.; Schwab, R.; Heinemeyer, W.; Kirk, C. J.; Groettrup, M.; Groll, M., *Cell*, **2012**, *148*, 727-738.

19. Huber, E. M.; Groll, M., *Angew. Chem., Int. Ed. Engl.*, **2012**, *51*, 8708-8720.

20. Teicher, B. A.; Ara, G.; Herbst, R.; Palombella, V. J.; Adams, J., *Clin. Cancer Res.*, **1999**, *5*, 2638-2645.

21. Gillessen, S.; Groettrup, M.; Cerny, T., *Onkologie*, **2002**, *25*, 534-539.

22. Xie, S. C.; Dick, L. R.; Gould, A.; Brand, S.; Tilley, L., *Expert Opin. Ther. Targets*, **2019**, *23*, 903-914.

23. Pereira, D. M.; Valentao, P.; Correia-da-Silva, G.; Teixeira, N.; Andrade, P. B., *Nat. Prod. Rep.*, **2015**, *32*, 705.

24. Kane, R. C.; Bross, P. F.; Farrell, A. T.; Pazdur, R., *Oncologist*, **2003**, *8*, 508-513.

25. Njomen, E.; Tepe, J. J., *J. Med. Chem.*, **2019**, *62*, 6469-6481.

26. Jones, C. L.; Njomen, E.; Sjogren, B.; Dexheimer, T. S.; Tepe, J. J., *ACS Chem. Biol.*, **2017**, *15*, 2240-2247.

27. Jones, C. L.; Tepe, J. J., *Molecules*, **2019**, *24*, 2841-2868.

28. Hough, R.; Pratt, G.; Rechsteiner, M., *J. Biol. Chem.*, **1986**, *261*, 2400-2408.

29. Hough, R.; Pratt, G.; Rechsteiner, M., *J. Biol. Chem.*, **1987,** *262*, 8303-8313.

30. Micale, N.; Scarbaci, K.; Troiano, V.; Ettari, R.; Grasso, S.; Zappala, M., *Med. Res. Rev.*, **2014,** *34*, 1001-1069.

31. Park, J.-E.; Miller, Z.; Jun, Y.; Lee, W.; Kim, K. B., *Transl. Res.*, **2018,** *198*, 1-16.

32. Adams, J.; Palombella, V. J.; Sausville, E. A.; Johnson, J.; Destree, A.; Lazarus, D. D.; Maas, J.; Pien, C. S.; Prakash, S.; Elliot, P. J., *Cancer Res.*, **1999,** *59*, 2615-2622.

33. Rajkumar, S. V., *Am. J. Hematol.*, **2020,** *95*, 548-567.

34. Rock, K. L.; Gramm, C.; Rothstein, L.; Clark, K.; Stein, R.; Dick, L.; Hwang, D.; Goldberg, A. L., *Cell*, **1994**, *78*, 761-771.

35. Bogyo, M.; McMaster, J. S.; Gaczynska, M.; Tortorella, D.; Goldberg, A. L.; Ploegh, H., *Proc. Natl. Acad. Sci. U.S.A.*, **1997**, *94*, 6629-6634.

36. Lynas, J. F.; Harriott, P.; Healy, A.; McKervey, M. A.; Walker, B., *Bioorganic Med.Chem. Lett.*, **1998**, *8*, 373-378.

37. Adams, J., *Oncologist*, **2004,** *7*, 9-16.

38. Field-Smith, A.; Morgan, G. J.; Davies, F. E., *Ther. Clin. Risk. Manag.*, **2006,** *2*, 271-279.

39. Groll, M.; Berkers, C.; Ploegh, H.; Ovaa, H., *Structure,* **2006**, *14*, 451-456.

40. Herndon, T. M.; Deisseroth, A.; Kaminskas, E.; Kane, R. C.; Koti, K. M.; Rothmann, M. D.; Habtermariam, B.; Bullock, J.; Bray, J. D.; Hawes, J.; Palmby, T. R.; Jee, J.; Adams, W.; Mahayni, H.; Brown, J.; Dorantes, A.; Sridhara, R.; Farrel, A. T.; Pazdur, R., *Clin. Cancer Res.*, **2013,** *19*, 4559-4563.

41. Stein, M. L.; Groll, M., *Biochim. Biophys. Acta – Mol. Cell Res.*, **2014**, *1843*, 26-38.

42. Momose, I.; Sekizawa, R.; Hashizume, H.; Kinoshita, N.; Homma, Y.; Hamada, M.; Iinuma, H.; Takeuchi, T. T., *J. Antibiot.*, **2001**, *54*, 997-1003.

43. Momose, I.; Sekizawa, R.; Hirosawa, S.; Ikeda, D.; Naganawa, H.; Inuma, H.; Takeuchi, T., *J. Antibiot.*, **2001**, *54*, 1004-1012.

44. Shinohara, K.; Tomioka, M.; Nakano, H.; Toné, S.; Ito, H.; Kawashima, S., *Biochem. J.*, **1996**, *317*, 385-388.

45. Momose, I.; Umezawa, Y.; Hirosawa, S.; Iijima, M.; Iinuma, H.; Ikeda, D., *Biosci. Biotech. Biochem.*, **2005**, *69*, 1733-1742.

46. Momose, I.; Umezawa, Y.; Hirosawa, S.; Iinuma, H.; Ikeda, D., *Bioorg. Med. Chem. Lett.*, **2005**, *15*, 1867-1871.

47. Momose, I.; Iijima, M.; Kawada, M.; Ikeda, D., *Biosci. Biotech. Biochem.*, **2007**, *71*, 1036-1043.

48. Watanabe, T.; Momose, I.; Abe, M.; Abe, H.; Sawa, R.; Umezawa, Y.; Ikeda, D.; Takahashi, Y.; Akamatsu, Y., *Bioorg. Med. Chem. Lett.*, **2009**, *19*, 2343-2345.

49. Watanabe, T.; Abe, H.; Momose, I.; Takahashi, Y.; Ikeda, D.; Akamatsu, Y., *Bioorg. Med. Chem. Lett.*, **2010**, *20*, 5839-5842.

50. Momose, I.; Abe, H.; Watanabe, T.; Ohba, S.I.; Yamazaki, K.; Dan, S.; Yamori, T.; Masuda, T.; Nomoto, A., *Cancer Sci.*, **2014**, *105*, 1609-1615.

51. Shigemori, H.; Wakuri, S.; Yazawa, K.; Nakamura, T.; Sasaki, T.; Kobayashi, J. I., *Tetrahedron*, **1991**, *47*, 8529-8534.

52. Schneekloth, J. S.; Sanders, J. L.; Hines, J.; Crews, C. M., *Bioorg. Med. Chem. Lett.*, **2006**, *16*, 3855-3858.

53. Giltrap, A. M.; Cergol, K. M.; Pang, A.; Britton, W. J.; Payne, R. J., *Mar. Drugs*, **2013**, *11*, 2382-2397.

54. Yadav, J. S.; Dachavaram, S. S.; Grée, R.; Das, S., *Tetrahedron Lett.* **2015**, *56*, 3999-4001.

55. Pirrung, M. C.; Zhang, F.; Ambadi, S.; Gangadhara Rao, Y., *Org. Biomol. Chem.*, **2016**, *14*, 8367-8375.

56. Hines, J.; Groll, M.; Fahnestock, M.; Crews, C. M., *Chem. Biol.* **2008**, *15*, 501-512.

57. Chen, Y.; McClure, R. A.; Zheng, Y.; Thomson, R. J.; Kelleher, N. L., *J. Am. Chem.Soc.*, **2013**, *135*, 10449-10456.

58. Oka, M.; Nishiyama, Y. ; Ohta, S.; Kamei, H.; Konishi, M.; Miyaki, T.; Oki, T.; Kawaguchi, H., *J. Antibiot*., **1988**, *10*, 1331-1337.

59. Oka, M.; Ohkuma, H.; Kamei, H.; Konishi, M.; Oki, T.; Kawaguchi, H., *J. Antibiot*., **1988**, *41*, 1906-1909.

60. Oka, M.; Yaginuma, K.; Numata, K.; Konishi, M.; Oki, T.; Kawaguchi, H., *J. Antibiot*., **1988**, *41*, 1338-1350.

61. Oka, M.; Numata, K. i.; Nishiyama, Y.; Kamei, H.; Konishi, M.; Oki, T.; Kawaguchi, H., *J. Antibiot*., **1988**, 1812-1822.

62. Groll, M.; Schellenberg, B.; Bachmann, A. S.; Archer, C. R.; Huber, R.; Powell, T. K.; Lindow, S.; Kaiser, M.; Dudler, R., *Nature*, **2008**, *452*, 755-758.

63. Pawar, A.; Basler, M.; Goebel, H.; Alvarez Salinas, G. O.; Groettrup, M.; Böttcher, T., *ACS Cent. Sci.*, **2020**, *6*, 241-246.

64. Shoji, J. i.; Hinoo, H.; Kato, T.; Hattori, T.; Hirooka, K.; Tawara, K.; Shiratori, O.; Terui, Y., *J. Antibiot*., **1990**, *43*, 783-787.

65. Terui, Y.; Nishikawa, J.; Hinoo, H.; Kato, T.; Shoji, J. I., *J. Antibiot*., **1990**, *43*, 788-795.

66. Stein, M. L.; Beck, P.; Kaiser, M.; Dudler, R.; Becker, C. F. W.; Groll, M., *Proc. Natl. Acad. Sci. U.S.A.*, **2012**, *109*, 18367-18371.

67. Fu, J.; Bian, X.; Hu, S.; Wang, H.; Huang, F.; Seibert, P. M.; Plaza, A.; Xia, L.; Müller, R.; Stewart, A. F.; Zhang, Y., *Nat. Biotechnol.,* **2012,** *30,* 440-446.

68. Theodore, C. M.; King, J. B.; You, J.; Cichewicz, R. H., *J. Nat. Prod.* **2012**, *75*, 2007-2011.

69. Bian, X.; Plaza, A.; Zhang, Y.; Müller, R., *J. Nat. Prod.* **2012**, *75*, 1652-1655.

70. Bian, X.; Huang, F.; Wang, H.; Klefisch, T.; Müller, R.; Zhang, Y., *Chembiochem.,* **2014,** *15*, 2221-2224.

71. Servatius, P.; Stach, T.; Kazmaier, U., *Eur. J. Org.Chem.,* **2019**, *2019*, 3163-3168.

72. Wäspi, U.; Blanc, D.; Winkler, T.; Rüedi, P.; Dudler, R., *Mol. Plant Microbe Interact.,* **1998**, *11*, 727-733.

73. Waspi, U.; Hassa, P.; Staempfli, A. A.; Molleyres, L. P.; Winkler, T.; Dudler, R., *Microbiol. Res.*, **1999**, *154*, 89-93.

74. Dai, C.; Stephenson, C. R. J., *Org. Lett.*, **2010**, *12*, 3453-3455.

75. Pirrung, M. C.; Biswas, G.; Ibarra-Rivera, T. R., *Org. Lett.* **2010**, *12*, 2402-2405.

76. Chiba, T.; Hosono, H.; Nakagawa, K.; Asaka, M.; Takeda, H.; Matsuda, A.; Ichikawa, S., *Angew. Chem., Int. Ed. Engl.,* **2014**, *53*, 4836-4839.

77. Clerc, J.; Groll, M.; Illich, D. J.; Bachmann, A. S.; Huber, R.; Schellenberg, B.; Dudler, R.; Kaiser, M., *Proc. Natl. Acad. Sci. U.S.A.*, **2009**, *106*, 6507-6512.

78. Archer, C. R.; Koomoa, D. L. T.; Mitsunaga, E. M.; Clerc, J.; Shimizu, M.; Kaiser, M.; Schellenberg, B.; Dudler, R.; Bachmann, A. S., *Biochem. Pharmacol.,* **2010**, *80*, 170-178.

79. Bachmann, A. S.; Opoku-Ansah, J.; Ibarra-Rivera, T. R.; Yco, L. P.; Ambadi, S.; Roberts, C. C.; Chang, C. A.; Pirrung, M. C., *J. Biol. Chem.* **2016**, *291*, 8350-8362.

80. Pierce, M. R.; Robinson, R. M.; Ibarra-Rivera, T. R.; Pirrung, M. C.; Dolloff, N. G.; Bachmann, A. S., *Leuk. Res.*, **2020**, *88*.

81. Clerc, J.; Li, N.; Krahn, D.; Groll, M.; Bachmann, A. S.; Florea, B. I.; Overkleeft, H. S.; Kaiser, M., *Chem. Comm.,* **2011**, *47*, 385-387.

82. Archer, C. R.; Groll, M.; Stein, M. L.; Schellenberg, B.; Clerc, J.; Kaiser, M.; Kondratyuk, T. P.; Pezzuto, J. M.; Dudler, R.; Bachmann, A. S., *Biochemistry,* **2012**, *51*, 6880-6888.

83. Chiba, T.; Matsuda, A.; Ichikawa, S., *Bioorg. Med. Chem. Lett.*, **2015**, *25*, 4872-4877.

84. Chiba, T.; Kitahata, S.; Matsuda, A.; Ichikawa, S., *Chem. Pharm. Bull.* **2016**, *64*, 811-816.

85. Kitahata, S.; Chiba, T.; Yoshida, T.; Ri, M.; Iida, S.; Matsuda, A.; Ichikawa, S., *Org. Lett.*, **2016**, *18*, 2312-2315.

86. Ibarra-Rivera, T. R.; Opoku-Ansah, J.; Ambadi, S.; Bachmann, A. S.; Pirrung, M. C., , **2011**, *67*, 9950-9956.

87. Opoku-Ansah, J.; Ibarra-Rivera, T. R.; Pirrung, M. C.; Bachmann, A. S., *Pharm. Biol.*, **2012**, *50*, 25-29.

88. Totaro, K. A.; Barthelme, D.; Simpson, P. T.; Sauer, R. T.; Sello, J. K., *Bioorg. Med. Chem.*, **2015**, *23*, 6218-6222.

89. Bakas, N. A.; Schultz, C. R.; Yco, L. P.; Roberts, C. C.; Chang, C. e. A.; Bachmann, A. S.; Pirrung, M. C., *Bioorg. Med. Chem.*, **2018,** *26*, 401-412.

90. Koguchi, Y.; Kohno, J.; Nishio, M.; Takahashi, K.; Okuda, T.; Ohnuki, T.; Komatsubara, S., *J. Antibiot.* **2000,** *53*, 105-109.

91. Kohno, J.; Koguchi, Y.; Nishio, M.; Nakao, K.; Kuroda, M.; Shimizu, R.; Ohnuki, T.; Komatsubara, S., *J. Org. Chem.*, **2000**, *65*, 990-995.

92. Groll, M.; Koguchi, Y.; Huber, R.; Kohno, J., *J. Mol. Biol.*, **2001**, *311*, 543-548.

93. Lin, S.; Danishefsky, S. J., *Angew. Chem., Int. Ed. Engl.*, **2002**, *41*, 512-515.

94. Albrecht, B. K.; Williams, R. M., *Org. Lett.*, **2003**, *5*, 197-200.

95. Inoue, M.; Sakazaki, H.; Furuyama, H.; Hirama, M., *Angew. Chem., Int. Ed. Engl.*, **2003**, *42*, 2654-2657.

96. Lin, S.; Yang, Z. Q.; Kwok, B. H. B.; Koldobskiy, M.; Crews, C. M.; Danishefsky, S. J., *J. Am. Chem. Soc.*, **2004,** *126*, 6347-6355.

97. Kaiser, M.; Groll, M.; Renner, C.; Huber, R.; Moroder, L., *Angew. Chem., Int. Ed. Engl.*, **2002**, *41*, 780-783.

98. Kaiser, M.; Groll, M.; Siciliano, C.; Assfalg-Machleidt, I.; Weyher, E.; Kohno, J.; Milbradt, A. G.; Renner, C.; Huber, R.; Moroder, L., *ChemBioChem*, **2004**, *5*, 1256-1266.

99. Kaiser, M.; Siciliano, C.; Assfalg-Machleidt, I.; Groll, M.; Milbradt, A. G.; Moroder, L., *Org. Lett.*, **2003,** *5*, 3435-3437.

100. Yang, Z. Q.; Kwok, B. H. B.; Lin, S.; Koldobskiy, M. A.; Crews, C. M.; Danishefsky, S. J., *ChemBioChem*, **2003**, *4*, 508-513.

101. Kaiser, M.; Milbradt, A. G.; Siciliano, C.; Assfalg-Machleidt, I.; Machleidt, W.; Groll, M.; Renner, C.; Moroder, L., *Chem. Biodivers.*, **2004**, *1*, 161-173.

102. Groll, M.; Götz, M.; Kaiser, M.; Weyher, E.; Moroder, L., *Chem. Biol.*, **2006**, *13*, 607-614.

103. Wilson, D. L.; Meininger, I.; Strater, Z.; Steiner, S.; Tomlin, F.; Wu, J.; Jamali, H.; Krappmann, D.; Götz, M. G., *ACS Med. Chem. Lett.*, **2016**, *7*, 250-255.

104. Berthelot, A.; Piguel, S.; Le Dour, G.; Vidal, J., *J. Org. Chem.* **2003,** *68*, 9835-9838.

105. Basse, N.; Piguel, S.; Papapostolou, D.; Ferrier-Berthelot, A.; Richy, N.; Pagano, M.; Sarthou, P.; Sobczak-Thépot, J.; Reboud-Ravaux, M.; Vidal, J., *J. Med. Chem.*, **2007,** *50*, 2842-2850.

106. Groll, M.; Gallastegui, N.; Maréchal, X.; Le Ravalec, V.; Basse, N.; Richy, N.; Genin, E.; Huber, R.; Moroder, L.; Vidal, J.; Reboud-Ravaux, M., *ChemMedChem*, **2010**, *5*, 1701-1705.

107. Desvergne, A.; Cheng, Y.; Grosay-Gaudrel, S.; Maréchal, X.; Reboud-Ravaux, M.; Genin, E.; Vidal, J., *J. Med. Chem*., **2014**, *57*, 9211-9217.

108. Xu, K.; Wang, K.; Yang, Y.; Yan, D. A.; Huang, L.; Chen, C. H.; Xiao, Z., *Eur. J. Med. Chem.*, **2015**, *98*, 61-68.

109. Richy, N.; Sarraf, D.; Maréchal, X.; Janmamode, N.; Le Guével, R.; Genin, E.; Reboud-Ravaux, M.; Vidal, J., *Eur. J. Med. Chem.*, **2018**, *145*, 570-587.

110. Maréchal, X.; Pujol, A.; Richy, N.; Genin, E.; Basse, N.; Reboud-Ravaux, M.; Vidal, J., *Eur. J. Med. Chem.*, **2012**, *52*, 322-327.

111. Desvergne, A.; Genin, E.; Maréchal, X.; Gallastegui, N.; Dufau, L.; Richy, N.; Groll, M.; Vidal, J.; Reboud-Ravaux, M., *J. Med. Chem.*, **2013**, *56*, 3367-3378.

112. Sasse, F.; Steinmetz, H.; Schupp, T.; Petersen, F.; Memmert, K.; Hofmann, H.; Heusser, C.; Brinkmann, V.; von Matt, P.; Höfle, G.; Reichenbach, H., *J. Antibiot.*, **2002**, *55*, 543-551.

113. Vollbrecht, L.; Steinmetz, H.; Höfle, G., *J. Antibiot.*, **2002**, *55*, 715-721.

114. Ley, S. V.; Prieur, A.; Heusser, C., *Org. Lett.*, **2002**, *4*, 711-714.

115. Wu, W.; Li, Z.; Zhou, G.; Jiang, S., *Tetrahedron Lett.*, **2011**, *52*, 2488-2491.

116. Pogorevc, D.; Tang, Y.; Hoffmann, M.; Zipf, G.; Bernauer, H. S.; Popoff, A.; Steinmetz, H.; Wenzel, S. C., *ACS Synth.Biol.*, **2019**, *8*, 1121-1133.

117. Nickeleit, I.; Zender, S.; Sasse, F.; Geffers, R.; Brandes, G.; Sörensen, I.; Steinmetz, H.; Kubicka, S.; Carlomagno, T.; Menche, D.; Gütgemann, I.; Buer, J.; Gossler, A.; Manns, M. P.; Kalesse, M.; Frank, R.; Malek, N. P., *Cancer Cell*, **2008,** *14*, 23-35.

118. Bülow, L.; Nickeleit, I.; Girbig, A. K.; Brodmann, T.; Rentsch, A.; Eggert, U.; Sasse, F.; Steinmetz, H.; Frank, R.; Carlomagno, T.; Malek, N. P.; Kalesse, M., *ChemMedChem* **2010,** *5*, 832-836.

119. Stauch, B.; Simon, B.; Basile, T.; Schneider, G.; Malek, N. P.; Kalesse, M.; Carlomagno, T., *Angew. Chem., Int. Ed. Engl.*, **2010**, *49*, 3934-3938.

120. Loizidou, E. Z.; Zeinalipour-Yazdi, C. D., *Chem. Biol. Drug Des.*, **2014**, *84*, 99-107.

121. Allardyce, D. J.; Bell, C. M.; Loizidou, E. Z., *Chem. Biol. Drug Des* **., 2019**, *94*, 1556-1567.

122. Bhat, U. G.; Zipfel, P. A.; Tyler, D. S.; Gartel, A. L., *Cell Cycle*, **2008**, *7*, 1851-1855.

123. Bhat, U. G.; Halasi, M.; Gartel, A. L., *PLoS One*, **2009**, *4*, 1-5.

124. Pandit, B.; Bhat, U.; Gartel, A. L., *Cancer Biol. Ther.*, **2011**, *11*, 43-47.

125. Schoof, S.; Pradel, G.; Aminake, M. N.; Ellinger, B.; Baumann, S.; Potowski, M.; Najajreh, Y.; Kirschner, M.; Arndt, H. D., *Angew. Chem., Int. Ed. Engl.*, **2010**, *49*, 3317-3321.

126. Zhang, F.; Li, C.; Kelly, W. L., *ACS Chem. Biol.* **2016**, *11*, 415-424.

127. Sekizawa, R.; Momose, I.; Kinoshita, N.; Naganawa, H.; Hamada, M.; Muraoka, Y.; Iinuma, H.; Takeuchi, T., *J. Antibiot.*, **2001**, *54*, 874-881.

128. Krunic, A.; Vallat, A.; Mo, S.; Lantvit, D. D.; Swanson, S. M.; Orjala, J., *J. Nat. Prod.*, **2010,** *73*, 1927-1932.

129. Niggemann, J.; Bozko, P.; Bruns, N.; Wodtke, A.; Gieseler, M. T.; Thomas, K.; Jahns, C.; Nimtz, M.; Reupke, I.; Brüser, T.; Auling, G.; Malek, N.; Kalesse, M., *ChemBioChem*, **2014**, *15*, 1021-1029.

130. Ōmura, S.; Matsuzaki, K.; Fujimoto, T.; Kosuge, K.; Furuya, T.; Fujita, S.; Nakagawa, A., *J. Antibiot.*, **1991**, *44*, 117-118.

131. Ōmura, S.; Fujimoto, T.; Otoguro, K.; Matsuzaki, K.; Moriguchi, R.; Tanaka, H.; Sasaki, Y., *J. Antibiot.,* **1991**, *44*, 113-116.

132. Fenteany, G.; Standaert, R. F.; Reichard, G. A.; Corey, E. J.; Schreiber, S. L., *Proc. Natl. Acad. Sci. U.S.A.,* **1994**, *91*, 3358-3362.

133. Fenteany, G.; Standaert, R. F.; Lane, W. S.; Choi, S.; Corey, E. J.; Schreiber, S. L., *Science,* **1995**, *268*, 726-731.

134. Craiu, A.; Gaczynska, M.; Akopian, T.; Gramm, C. F.; Fenteany, G.; Goldberg, A. L.; Rock, K. L., *J. Biol. Chem.,* **1997**, *272*, 13437-13445.

135. Dick, L. R.; Cruikshank, A. A.; Destree, A. T.; Grenier, L.; McCormack, T. A.; Melandri, F. D.; Nunes, S. L.; Palombella, V. J.; Parent, L. A.; Plamondon, L.; Stein, R. L., *J. Biol. Chem.,* **1997,** *272*, 182-188.

136. Corey, E. J.; Reichard, G. A., *J. Am. Chem. Soc*., **1992**, *114*, 10677-10678.

137. Corey, E. J.; Li, W.; Reichard, G. A., *J. Am. Chem. Soc*., **1998**, *120*, 2330-2336.

138. Corey, E. J.; Li, W.-D. Z., *Chem. Pharm. Bull.,* **1999**, *47*, 1-10.

139. Corey, E. J.; Li, W. D. Z.; Nagamitsu, T.; Fenteany, G., *Tetrahedron,* **1999**, *55*, 3305-3316.

140. Soucy, F.; Grenier, L.; Behnke, M. L.; Destree, A. T.; McCormack, T. A.; Adams, J.; Plamondon, L., *J. Am. Chem. Soc*., **1999**, *121*, 9967-9976.

141. Feling, R. H.; Buchanan, G. O.; Mincer, T. J.; Kauffman, C. A.; Jensen, P. R.; Fenical, W.; John, D., *Angew. Chem., Int. Ed. Engl.,* **2003**, *42*, 355-357.

142. Chauhan, D.; Catley, L.; Li, G.; Podar, K.; Hideshima, T.; Velankar, M.; Mitsiades, C.; Mitsiades, N.; Yasui, H.; Letai, A.; Ovaa, H.; Berkers, C.; Nicholson, B.; Chao, T. H.; Neuteboom, S. T. C.; Richardson, P.; Palladino, M. A.; Anderson, K. C., *Cancer Cell*, **2005**, *8*, 407-419.

143. Reddy, L. R.; Saravanan, P.; Corey, E. J., *J. Am. Chem. Soc*., **2004**, *126*, 6230-6231.

144. Reddy, L. R.; Fournier, J. F.; Subba Reddy, B. V.; Corey, E. J., *Org. Lett.,* **2005**, *7*, 2699-2701.

145. Endo, A.; Danishefsky, S. J., *J. Am. Chem. Soc*., **2005**, *127*, 8298-8299.

146. Mulholland, N. P.; Pattenden, G.; Walters, I. A. S., *Org. Biomol. Chem.,* **2006**, *4*, 2845-2846.

147. Gil, M.; Henry, N.; Romo, D., *Org.Lett.,* **2007**, *9*, 2143-2146.

148. Ling, T.; Macherla, V. R.; Manam, R. R.; McArthur, K. A.; Potts, B. C., *Org. Lett.,* **2007,** *9*, 2289-2292.

149. Mulholland, N. P.; Pattenden, G.; Walters, I. A. S., *Org. Biomol. Chem.,* **2008**, *6*, 2782-2789.

150. Fukuda, T.; Sugiyama, K.; Arima, S.; Harigaya, Y.; Tohru, N.; Omura, S., *Org. Lett.,* **2008,** *10*, 4239-4242.

151. Takahashi, K.; Midori, M.; Kawano, K.; Ishihara, J.; Hatakeyame, S., *Angew. Chem., Int. Ed. Engl.,* **2008**, *47*, 6244-6246.

152. Mosey, R. A.; Tepe, J. J., *Tetrahedron Lett.* **2009**, *50*, 295-297.

153. Nguyen, H.; Ma, G.; Romo, D., *Chem. Comm.* **2010**, *46*, 4803-4805.

154. Kaiya, Y.; Hasegawa, J.-i.; Momose, T.; Sata, T.; Chida, N., *Chem. Asian J.,* **2010**, *6*, 209-219.

155. Nguyen, H.; Ma, G.; Gladysheva, T.; Fremgen, T.; Romo, D., *J. Org. Chem.,* **2011**, *76*, 2-12.

156. Satoh, N.; Yokoshima, S.; Fukuyama, T., *Org. Lett.,* **2011**, *13*, 3028-3031.

157. Marx, L. B.; Burton, J. W., A *Chem. Eur. J.,* **2018**, *24*, 6747-6754.

158. Gholami, H.; Kulshrestha, A.; Favor, O. K.; Staples, R. J.; Borhan, B., *Angew. Chem., Int. Ed. Engl.,* **2019**, *58*, 10110-10113.

159. Macherla, V. R.; Mitchell, S. S.; Manam, R. R.; Reed, K. A.; Chao, T. H.; Nicholson, B.; Deyanat-Yazdi, G.; Mai, B.; Jensen, P. R.; Fenical, W. F.; Neuteboom, S. T. C.; Lam, K. S.; Palladino, M. A.; Potts, B. C. M., *J. Med. Chem.,* **2005**, *48*, 3684-3687.

160. Groll, M.; Huber, R.; Potts, B. C. M., *J. Am. Chem. Soc*., **2006**, *128*, 5136-5141.

161. Manam, R. R.; McArthur, K. A.; Chao, T. H.; Weiss, J.; Ali, J. A.; Palombella, V. J.; Groll, M.; Lloyd, G. K.; Palladino, M. A.; Neuteboom, S. T. C.; Macherla, V. R.; Potts, B. C. M., *J. Med. Chem.,* **2008**, *51*, 6711-6724.

162. Eustáquio, A. S.; Moore, B. S., *Angew. Chem., Int. Ed. Engl.,* **2008**, *47*, 3936-3938.

163. Reddy, L. R.; Fournier, J. F.; Reddy, B. V. S.; Corey, E. J., *J. Am. Chem. Soc*., **2005**, *127*, 8974-8976.

164. Manam, R. R.; Macherla, V. R.; Tsueng, G.; Dring, C. W.; Weiss, J.; Neuteboom, S. T. C.; Lam, K. S.; Potts, B. C., *J. Nat. Prod.*, **2009**, *72*, 295-297.

165. McGlinchey, R. P.; Nett, M.; Eustáquio, A. S.; Asolkar, R. N.; Fenical, W.; Moore, B. S., *J. Am. Chem. Soc*., **2008**, *130*, 7822-7823.

166. Nett, M.; Gulder, T. A. M.; Kale, A. J.; Hughes, C. C.; Moore, B. S., *J. Med. Chem.*, **2009,** *52*, 6163-6167.

167. Groll, M.; Nguyen, H.; Vellalath, S.; Romo, D., *Mar. Drugs*, **2018**, *16*, 1-9.

168. Stadler, M.; Bitzer, J.; Mayer-Bartschmid, A.; Müller, H.; Benet-Buchholz, J.; Gantner, F.; Tichy, H. V.; Reinemer, P.; Bacon, K. B., *J. Nat. Prod.*, **2007**, *70*, 246-252.

169. Rachid, S.; Huo, L.; Herrmann, J.; Stadler, M.; Köpcke, B.; Bitzer, J.; Müller, R., *ChemBioChem*, **2011**, *12*, 922-931.

170. Asai, A.; Hasegawa, A.; Ochiai, K.; Yamashita, Y.; Mizukami, T., *J. Antibiot.*, **2000**, *53*, 81-83.

171. Asai, A.; Tsujita, T.; Sharma, S. V.; Yamashita, Y.; Akinaga, S.; Funakoshi, M.; Kobayashi, H.; Mizukami, T., *Biochem. Pharmacol.*, **2004**, *67*, 227-234.

172. Armstrong, A.; Scutt, J. N., *ChemComm.*, **2004**, 510-511.

173. Larionov, O. V.; De Meijere, A., *Org. Lett.*, **2004**, *6*, 2153-2156.

174. Groll, M.; Larionov, O. V.; Huber, R.; De Meijere, A., *Proc. Natl. Acad. Sci. U.S.A.*, **2006**, *103*, 4576-4579.

175. Yoshida, K.; Yamaguchi, K.; Sone, T.; Unno, Y.; Asai, A.; Yokosawa, H.; Matsuda, A.; Arisawa, M.; Shuto, S., *Org. Lett.*, **2008**, *10*, 3571-3574.

176. Yoshida, K.; Yamaguchi, K.; Mizuno, A.; Unno, Y.; Asai, A.; Sone, T.; Yokosawa, H.; Matsuda, A.; Arisawa, M.; Shuto, S., *Org. Biomol. Chem.*, **2009**, *7*, 1868-1877.

177. Kawamura, S.; Unno, Y.; List, A.; Mizuno, A.; Tanaka, M.; Sasaki, T.; Arisawa, M.; Asai, A.; Groll, M.; Shuto, S., *J. Med. Chem.*, **2013**, *56*, 3689-3700.

178. Kawamura, S.; Unno, Y.; Tanaka, M.; Sasaki, T.; Yamano, A.; Hirokawa, T.; Kameda, T.; Asai, A.; Arisawa, M.; Shuto, S., *J. Med. Chem.*, **2013**, *56*, 5829-5842.

179. Kawamura, S.; Unno, Y.; Asai, A.; Arisawa, M.; Shuto, S., *Org. Biomol. Chem.*, **2013**, *11*, 6615-6622.

180. Kawamura, S.; Unno, Y.; Hirokawa, T.; Asai, A.; Arisawa, M.; Shuto, S., *ChemComm.*, **2014**, *50*, 2445-2447.

181. Kawamura, S.; Unno, Y.; Asai, A.; Arisawa, M.; Shuto, S., *Bioorg. Med. Chem.*, **2014,** *22*, 3091-3095.

182. Nakamura, H.; Watanabe, M.; Ban, H. S.; Nabeyama, W.; Asai, A., *Bioorg. Med. Chem. Lett.*, **2009**, *19*, 3220-3224.

183. Korotkov, V. S.; Ludwig, A.; Larionov, O. V.; Lygin, A. V.; Groll, M.; De Meijere, A., *Org. Biomol. Chem.*, **2011**, *9*, 7791-7798.

184. De Meijere, A.; Korotkov, V. S.; Lygin, A. V.; Larionov, O. V.; Sokolov, V. V.; Graef, T.; Es-Sayed, M., *Org. Biomol. Chem.*, **2012**, *10*, 6363-6374.

185. Groll, M.; Korotkov, V. S.; Huber, E. M.; De Meijere, A.; Ludwig, A., *Angew. Chem., Int. Ed. Engl.*, **2015**, *54*, 7810-7814.

186. Gill, K. A.; Berrué, F.; Arens, J. C.; Carr, G.; Kerr, R. G., *J. Nat. Prod.*, **2015,** *78*, 822-826.

187. Tello-Aburto, R.; Hallada, L. P.; Niroula, D.; Rogelj, S., *Org. Biomol. Chem.*, **2015**, *1 3*, 10127-10130.

188. Wolf, F.; Bauer, J. S.; Bendel, T. M.; Kulik, A.; Kalinowski, J.; Gross, H.; Kaysser, L., *Angew. Chem., Int. Ed. Engl.*, **2017**, *56*, 6665-6668.

189. Niroula, D.; Hallada, L. P.; Le Chapelain, C.; Ganegamage, S. K.; Dotson, D.; Rogelj, S.; Groll, M.; Tello-Aburto, R., *Eur. J. Med. Chem.* **2018**, *157*, 962-977.

190. Sugawara, K.; Hatori, M.; Nishiyama, Y.; Tomita, K.; Kamei, H.; Konishi, M.; Oki, T., *J. Antibiot.*, **1990**, *43*, 8-18.

191. Oikawa, T.; Hasegawa, M.; Shimamura, M.; Ashino, H.; Murota, S.-i.; Morita, I., *Biochem .Biophys. Res. Comm.*, **1991**, *181*, 1070-1076.

192. Meng, L.; Kwok, B. H. B.; Sin, N.; Crews, C. M., *Cancer Res.*, **1999**, *59*, 2798-2801.

193. Kyung, B. K.; Myung, J.; Sin, N.; Crews, C. M., *Bioorg. Med. Chem. Lett.* **1999**, *9*, 3335-3340.

194. Hanada, M.; Sugawara, K.; Kaneta, K.; Toda, S.; Nishiyama, Y.; Tomita, K.; Yamamoto, H.; Konishi, M.; Oki, T., *J. Antibiot.*, **1992**, *45*, 1746-1752.

195. Sin, N.; Kyung, B. K.; Elofsson, M.; Meng, L.; Auth, H.; Kwok, B. H. B.; Crews, C. M., *Bioorg. Med. Chem. Lett.*, **1999**, *9*, 2283-2288.

196. Spaltenstein, A.; Leban, J. J.; Huang, J. J.; Reinhardt, K. R.; Viveros, O. H.; Sigafoos, J.; Crouch, R., *Tetrahedron Lett.*, **1996**, *37*, 1343-1346.

197. Groll, M.; Kim, K. B.; Kairies, N.; Huber, R.; Crews, C. M., *J. Am. Chem. Soc.* **2000**, *122*, 1237-1238.

198. Schrader, J.; Henneberg, F.; Mata, R. A.; Tittmann, K.; Schneider, T. R.; Stark, H.; Bourenkov, G.; Chari, A., *Science*, **2016**, *353*, 1-6.

199. Elofsson, M.; Splittgerber, U.; Myung, J.; Mohan, R.; Crews, C. M., *Chem. Biol.* **1 999**, *6*, 811-822.

200. Demo, S. D.; Kirk, C. J.; Aujay, M. A.; Buchholz, T. J.; Dajee, M.; Ho, M. N.; Jiang, J.; Laidig, G. J.; Lewis, E. R.; Parlati, F.; Shenk, K. D.; Smyth, M. S.; Sun, C. M.; Vallone, M. K.; Woo, T. M.; Molineaux, C. J.; Bennett, M. K., *Cancer Res.*, **2007**, *67*, 6383-6391.

201. McCormack, P. L., *Drugs* **2012**, *72*, 2023-2032.

202. Zhou, H. J.; Aujay, M. A.; Bennett, M. K.; Dajee, M.; Demo, S. D.; Fang, Y.; Ho, M. N.; Jiang, J.; Kirk, C. J.; Laidig, G. J.; Lewis, E. R.; Lu, Y.; Muchamuel, T.; Parlati, F.; Ring, E.; Shenk, K. D.; Shields, J.; Shwonek, P. J.; Stanton, T.; Sun, C. M.; Sylvain, C.; Woo, T. M.; Yang, J., *J. Med. Chem.*, **2009**, *52*, 3028-3038.

203. Lee, M. J.; Bhattarai, D.; Yoo, J.; Miller, Z.; Park, J. E.; Lee, S.; Lee, W.; Driscoll, J. J.; Kim, K. B., *J. Med. Chem.*, **2019**, *62*, 4444-4455.

204. Britton, M.; Lucas, M. M.; Downey, S. L.; Screen, M.; Pletnev, A. A.; Verdoes, M.; Tokhunts, R. A.; Amir, O.; Goddard, A. L.; Pelphrey, P. M.; Wright, D. L.; Overkleeft, H. S.; Kisselev, A. F., *Chem. Biol.*, **2009**, *16*, 1278-1289.

205. De Bruin, G.; Huber, E. M.; Xin, B. T.; Van Rooden, E. J.; Al-Ayed, K.; Kim, K. B.; Kisselev, A. F.; Driessen, C.; Van Der Stelt, M.; Van Der Marel, G. A.; Groll, M.; Overkleeft, H. S., *J. Med. Chem.*, **2014**, *57*, 6197-6209.

206. DeBruin, G.; Xin, B. T.; Kraus, M.; Van Der Stelt, M.; Van Der Marel, G. A.; Kisselev, A. F.; Driessen, C.; Florea, B. I.; Overkleeft, H. S., *Angew. Chem., Int. Ed. Engl.*, **2016**, *55*, 4199-4203.

207. Xin, B. T.; Huber, E. M.; De Bruin, G.; Heinemeyer, W.; Maurits, E.; Espinal, C.; Du, Y.; Janssens, M.; Weyburne, E. S.; Kisselev, A. F.; Florea, B. I.; Driessen, C.; Van Der Marel, G. A.; Groll, M.; Overkleeft, H. S., *J. Med. Chem.*, **2019**, *62*, 1626-1642.

208. Muchamuel, T.; Basler, M.; Aujay, M. A.; Suzuki, E.; Kalim, K. W.; Lauer, C.; Sylvain, C.; Ring, E. R.; Shields, J.; Jiang, J.; Shwonek, P.; Parlati, F.; Demo, S. D.; Bennett, M. K.; Kirk, C. J.; Groettrup, M., *Nat. Med.*, **2009**, *15*, 781-787.

209. Pereira, A. R.; Kale, A. J.; Fenley, A. T.; Byrum, T.; Debonsi, H. M.; Gilson, M. K.; Valeriote, F. A.; Moore, B. S.; Gerwick, W. H., *ChemBioChem*, **2012**, *13*, 810-817.

210. Trivella, D. B. B.; Pereira, A. R.; Stein, M. L.; Kasai, Y.; Byrum, T.; Valeriote, F. A.; Tantillo, D. J.; Groll, M.; Gerwick, W. H.; Moore, B. S., *Chem. Biol.*, **2014**, *21*, 782-791.

211. Almaliti, J.; Miller, B.; Pietraszkiewicz, H.; Glukhov, E.; Naman, C. B.; Kline, T.; Hanson, J.; Li, X.; Zhou, S.; Valeriote, F. A.; Gerwick, W. H., *Eur. J. Med. Chem.*, **2019**, *161*, 416-432.

212. Koguchi, Y.; Nishio, M.; Suzuki, S. I.; Takahashi, K.; Ohnuki, T.; Komatsubara, S., *J. Antibiot.*, **1999,** *52*, 1069-1076.

213. Koguchi, Y.; Kohno, J.; Suzuki, S. I.; Nishio, M.; Takahashi, K.; Ohnuki, T.; Komatsubara, S., *J. Antibiot.*, **1999,** *53*, 63-65.

214. Koguchi, Y.; Nishio, M.; Suzuki, S.-i.; Takahashi, K.; Ohnuki, T., *J. Antibiot.*, **2000**, *53*, 967-972.

215. Keller, L.; Plaza, A.; Dubiella, C.; Groll, M.; Kaiser, M.; Müller, R., *J. Am. Chem. Soc.*, **2015**, *137*, 8121-8130.

216. Owen, J. G.; Charlop-Powers, Z.; Smith, A. G.; Ternei, M. A.; Calle, P. Y.; Reddy, B. V. B.; Montiel, D.; Brady, S. F., *Proc. Natl. Acad. Sci. U.S.A.*, **2015**, *112*, 4221-4226.

217. Tsukamoto, S.; Tatsuno, M.; Van Soest, R. W. M.; Yokosawa, H.; Ohta, T., *J. Nat. Prod.*, **2003,** *66*, 1181-1185.

218. Mohamed, L. E.; Gross, H.; Pontius, A.; Kehraus, S.; Krick, A.; Kelter, G.; Maier, A.; Fiebig, H. H.; König, G. M., *Org. Lett.*, **2009**, *11*, 5014-5017.

219. Mohamed, I. E.; Kehraus, S.; Krick, A.; König, G. M.; Kelter, G.; Maier, A.; Fiebig, H. H.; Kalesse, M.; Malek, N. P.; Gross, H., *J. Nat. Prod.*, **2010**, *73*, 2053-2056.

220. Noda, A.; Sakai, E.; Kato, H.; Losung, F.; Mangindaan, R. E. P.; De Voogd, N. J.; Yokosawa, H.; Tsukamoto, S., *Bioorg. Med. Chem. Lett.*, **2015**, *25*, 2650-2653.

221. Randazzo, A.; Debitus, C.; Minale, L.; Pastor, P. G.; Alcaraz, M. J.; Payá, M.; Gomez-Paloma, L., *J. Nat. Prod.*, **1998**, *61*, 571-575.

222. Margarucci, L.; Monti, M. C.; Tosco, A.; Riccio, R.; Casapullo, A., *Angew. Chem., Int. Ed. Engl.*, **2010**, *49*, 3960-3963.

223. Margarucci, L.; Tosco, A.; De Simone, R.; Riccio, R.; Monti, M. C.; Casapullo, A., *ChemBioChem*, **2012**, *13*, 982-986.

224. West, L. M.; Faulkner, D. J., *J. Nat. Prod.,* **2008**, *71*, 269-271.

225. Yang, H.; Chen, D.; Qiuzhi, C. C.; Yuan, X.; Dou, Q. P., *Cancer Res.,* **2006**, *66*, 4758-4765.

226. Kannaiyan, R.; Shanmugam, M. K.; Sethi, G., *Cancer Lett.,* **2011**, *303*, 9-20.

227. Zhong, Y. l.; Xu, G. j.; Huang, S.; Zhao, L.; Zeng, Y.; Xiao, X. f.; An, J. l.; Liu, J.; Yang, T., *Eur. J. Pharmacol.,* **2019**, *853*, 184-192.

228. Kupchan, S. M.; Court, W. A.; Dailey, R. G.; Gilmore, C. J.; Bryan, R. F., *J. Am. Chem. Soc.,* **1972**, *94*, 7194-7195.

229. Lu, L.; Kanwar, J.; Schmitt, S.; Cui, Q. C.; Zhang, C.; Zhao, C.; Dou, Q. P., *Anticancer Res.,* **2011**, *31*, 1-10.

230. Tiedemann, R. E.; Schmidt, J.; Keats, J. J.; Shi, C. X.; Yuan, X. Z.; Palmer, S. E.; Mao, X.; Schimmer, A. D.; Stewart, A. K., *Blood,* **2009**, *113*, 4027-4037.

231. Mishra, L. C.; Singh, B. B.; Dagenais, S., *Altern. Med. Rev.,* **2000**, *5*, 334-346.

232. Yang, H.; Shi, G.; Dou, Q. P., *Mol. Pharmacol.,* **2007**, *71*, 426-247.

233. Tsukamoto, S.; Yamanokuchi, R.; Yoshitomi, M.; Sato, K.; Ikeda, T.; Rotinsulu, H.; Mangindaan, R. E. P.; de Voogd, N. J.; van Soest, R. W. M.; Yokosawa, H., *Bioorg. Med. Chem. Lett.,* **2010**, *20*, 3341-3343.

234. Hirose, A.; Maeda, H.; Tonouchi, A.; Nehira, T.; Hashimoto, M., *Tetrahedron,* **2014**, *70*, 1458-1463.

235. Uesugi, S.; Honmura, Y.; Nishiyama, M.; Kusakabe, K.; Tonouchi, A.; Yamashita, T.; Hashimoto, M.; Kimura, K. I., *Bioorg. Med. Chem. Lett.,* **2019**, *27*, 115161-115161.

236. Nagasawa, Y.; Ueoka, R.; Yamanokuchi, R.; Horiuchi, N.; Ikeda, T.; Rotinsulu, H.; Mangindaan, R. E. P.; Ukai, K.; Kobayashi, H.; Namikoshi, M.; Hirota, H.; Yokosawa, H.; Tsukamoto, S., *Chem. Pharm. Bull.,* **2011**, *59*, 287-290.

237. El-Desoky, A. H.; Kato, H.; Eguchi, K.; Kawabata, T.; Fujiwara, Y.; Losung, F.; Mangindaan, R. E. P.; De Voogd, N. J.; Takeya, M.; Yokosawa, H.; Tsukamoto, S., *J. Nat. Prod.,* **2014**, *77*, 1536-1540.

238. Furusato, A.; Kato, H.; Nehira, T.; Eguchi, K.; Kawabata, T.; Fujiwara, Y.; Losung, F.; Mangindaan, R. E. P.; De Voogd, N. J.; Takeya, M.; Yokosawa, H.; Tsukamoto, S., *Org. Lett.,* **2014**, *16*, 3888-3891.

239. Kato, H.; El-Desoky, A. H.; Takeishi, Y.; Nehira, T.; Angkouw, E. D.; Mangindaan, R. E. P.; de Voogd, N. J.; Tsukamoto, S., *Bioorg. Med. Chem. Lett.*, **2019**, *29*, 8-10.

240. Pham, T. H.; Hovhannisyan, A.; Bouvier, D.; Tian, L.; Reboud-Ravaux, M.; Melikyan, G.; Bouvier-Durand, M., *Bioorg. Med. Chem. Lett.*, **2012**, *22*, 3822-3827.

241. Hovhannisyan, A.; Pham, T. H.; Bouvier, D.; Qin, L.; Melikyan, G.; Reboud-Ravaux, M.; Bouvier-Durand, M., *Bioorg. Med. Chem. Lett.*, **2013**, *23*, 2696-2703.

242. Hovhannisyan, A.; Pham, T. H.; Bouvier, D.; Piroyan, A.; Dufau, L.; Qin, L.; Cheng, Y.; Melikyan, G.; Reboud-Ravaux, M.; Bouvier-Durand, M., *Bioorg. Med. Chem. Lett.*, **2014**, *24*, 1571-1580.

243. Lindel, T., Chemistry and Biology of the Pyrrole–Imidazole Alkaloids. *Alkaloids Chem. Biol.* **2017**, *77*, 117-219.

244. Kinnel, R. B.; Gehrken, H. P.; Scheuer, P. J., *J. Am. Chem. Soc.*, **1993**, *115*, 3376-3377.

245. Seiple, I. B.; Su, S.; Young, I. S.; Lewis, C. A.; Yamaguchi, J.; Baran, P. S., *Angew. Chem., Int. Ed. Engl.*, **2010**, *49*, 1095-1098.

246. Seiple, I. B.; Su, S.; Young, I. S.; Nakamura, A.; Yamaguchi, J.; Jørgensen, L.; Rodriguez, R. A.; Ömalley, D. P.; Gaich, T.; Köck, M.; Baran, P. S., *J. Am. Chem. Soc.*, **2011,** *133*, 14710-14726.

247. Lansdell, T. A.; Hewlett, N. M.; Skoumbourdis, A. P.; Fodor, M. D.; Seiple, I. B.; Su, S.; Baran, P. S.; Feldman, K. S.; Tepe, J. J., *J. Nat. Prod.*, **2012**, *75*, 980-985.

248. Beck, P.; Lansdell, T. A.; Hewlett, N. M.; Tepe, J. J.; Groll, M., *Angew. Chem., Int. Ed. Engl.*, **2015**, *54*, 2830-2833.

249. Hewlett, N. M.; Tepe, J. J., *Org. Lett.* **2011**, *13*, 4550-4553.

250. De Souza, R. T. M. P.; Freire, V. F.; Gubiani, J. R.; Ferreira, R. O.; Trivella, D. B. B.; Moraes, F. C.; Paradas, W. C.; Salgado, L. T.; Pereira, R. C.; Amado Filho, G. M.; Ferreira, A. G.; Williams, D. E.; Andersen, R. J.; Molinski, T. F.; Berlinck, R. G. S., *J. Nat. Prod.*, **2018**, *81*, 2296-2300.

251. Nam, S.; Smith, D. M.; Dou, Q. P., *J. Biol. Chem.*, **2001**, *276*, 13322-13330.

252. Smith, D. M.; Wang, Z.; Kazi, A.; Li, L. H.; Chan, T. H.; Dou, Q. P., *Mol. Med.*, **2002**, *8*, 382-392.

253. Smith, D. M.; Daniel, K. G.; Wang, Z.; Guida, W. C.; Chan, T. H.; Dou, Q. P., *Proteins: Struct.*, **2004**, *54*, 58-70.

254. Lam, W. H.; Kazi, A.; Kuhn, D. J.; Chow, L. M. C.; Chan, A. S. C.; Ping Dou, Q.; Chan, T. H., *Bioorg. Med. Chem.,* **2004**, *12*, 5587-5593.

255. Landis-Piwowar, K. R.; Huo, C.; Chen, D.; Milacic, V.; Shi, G.; Tak, H. C.; Dou, Q. P., *Cancer Res.*, **2007**, *67*, 4303-4310.

256. Yang, H.; Sun, D. K.; Chen, D.; Cui, Q. C.; Gu, Y. Y.; Jiang, T.; Chen, W.; Wan, S. B.; Dou, Q. P., *Cancer Lett.*,**2010**, *292*, 48-53.

257. Kazi, A.; Daniel, K. G.; Smith, D. M.; Kumar, N. B.; Dou, Q. P., *Biochem. Pharmacol.*, **2003,** *66*, 965-976.

258. Shim, S. H., 20S proteasome inhibitory activity of flavonoids isolated from Spatholobus suberectus. *Phytother. Res.,* **2011**, *25*, 615-618.

259. Chen, D.; Daniel, K. G.; Chen, M. S.; Kuhn, D. J.; Landis-Piwowar, K. R.; Dou, Q. P., *Biochem. Pharmacol.,* **2005**, *69*, 1421-1432.

260. Wu, Y. X.; Fang, X., *Planta Med.*, **2010**, *76*, 128-132.

261. Pan, L.; Matthew, S.; Lantvit, D. D.; Zhang, X.; Ninh, T. N.; Chai, H.; Carcache De Blanco, E. J.; Soejarto, D. D.; Swanson, S. M.; Kinghorn, A. D., *J. Nat. Prod.,* **2011**, *74*, 2193-2199.

262. Wu, Y. X.; Sato, E.; Kimura, W.; Miura, N., *Phytother. Res.*, **2013**, *27*, 1362-1367.

263. Ren, Y.; Lantvit, D. D.; De Blanco, E. J. C.; Kardono, L. B. S.; Riswan, S.; Chai, H.; Cottrell, C. E.; Farnsworth, N. R.; Swanson, S. M.; Ding, Y.; Li, X. C.; Marais, J. P. J.; Ferreira, D.; Kinghorn, A. D., *Tetrahedron*, **2010**, *66*, 5311-5320.

264. Huang, H.; Liu, N.; Zhao, K.; Zhu, C.; Lu, X.; Li, S.; Lian, W.; Zhou, P.; Dong, X.; Zhao, C.; Guo, H.; Change Zhang; Yang, C.; Wen, G.; Lu, L.; Li, X.; Guan, L.; Liu, C.; Wang, X.; Dou, Q. P.; Liu, J., *Front. Biosci.,* **2011,** *3*, 1315-1325.

265. Jana, N. R.; Dikshit, P.; Goswami, A.; Nukina, N., *J. Biol.Chem,* **2004**, *279*, 11680-11685.

266. Milacic, V.; Banerjee, S.; Landis-Piwowar, K. R.; Sarkar, F. H.; Majumdar, A. P. N.; Dou, Q. P., *Cancer Res.*, **2008**, *68*, 7283-7292.

267. Zhang, W.; Bai, H.; Han, L.; Zhang, H.; Xu, B.; Cui, J.; Wang, X.; Ge, Z.; Li, R., *Bioorg. Med. Chem. Lett.*, **2018**, *28*, 2459-2464.

268. He, Y.; Huang, J.; Wang, P.; Shen, X.; Li, S.; Yang, L.; Liu, W.; Suksamrarn, A.; Zhang, G.; Wang, F., *Oncotarget,* **2016,** *7*, 4664-4679.

269. Yang, H.; Zhou, P.; Huang, H.; Chen, D.; Ma, N.; Cui, Q. C.; Shen, S.; Dong, W.; Zhang, X.; Lian, W.; Wang, X.; Dou, Q. P.; Liu, J., *Int. J. Cancer*, **2009**, *124*, 2450-2459.

270. Wada, N.; Kawano, Y.; Fujiwara, S.; Kikukawa, Y.; Okuno, Y.; Tasaki, M.; Ueda, M.; Ando, Y.; Yoshinaga, K.; Ri, M.; Iida, S.; Nakashima, T.; Shiotsu, Y.; Mitsuya, H.; Hata, H., *Int. J. Oncol.*, **2015**, *46*, 963-972.

271. Beck, P.; Heinemeyer, W.; Späth, A. L.; Elnakady, Y.; Müller, R.; Groll, M., *Journal of Mol. Biol.*, **2014**, *426*, 3108-3117.

272. Tsukamoto, S.; Koimaru, K.; Ohta, T., *Mar. Drugs*, **2005**, *3*, 29-35.

273. Chlipala, G. E.; Sturdy, M.; Krunic, A.; Lantvit, D. D.; Shen, Q.; Porter, K.; Swanson, S. M.; Orjala, J., *J. Nat. Prod.*, **2010**, *73*, 1529-1537.

274. Osmulski, P. A.; Gaczynska, M., *Mol. Pharmacol.*, **2013**, *84*, 104-113.

275. Giletto, M. B.; Osmulski, P. A.; Jones, C. L.; Gaczynska, M. E.; Tepe, J. J.,. *Org. Biomol. Chem.*, **2019**, *17*, 2734-2746.

Chapter 2: Efforts towards the synthesis of bromoindolophakellstatin analogs for 20S proteasome inhibition

2.1 Introduction & Background

The Tepe group has been focused on the synthesis of small molecules and natural products and their analogs as potential inhibitors of the 20S human proteasome (core particle: CP).[1-3] The oroidin alkaloids have been of particular interest to the Tepe group due to the abundance of biological activities reported for some of these scaffolds, including reports of cytotoxicity towards cancer cells.[4-7] With these activities in mind, some of these natural products and their analogs were evaluated by our lab for their inhibitory activity towards the 20S proteasome. An overview of this work is shown below (**Figure 2.1**).

Figure 2.1 *In vitro* inhibitory activity of pyrrole-alkaloids towards the 20S human proteasome

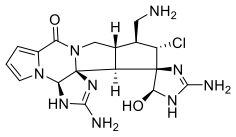

Palau'amine (1)

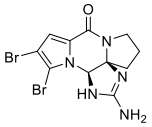

Dibromophakellin (2)

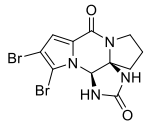

Dibromophakellstatin (3)

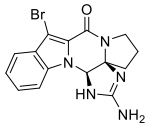

Bromo-indolo-phakellin (4)

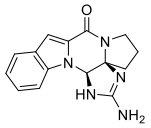

Indolo-phakellin (5)

Compound	IC_{50} (μM)		
	CT-L	Casp-L[c]	T-L[b]
(±)-1	5.5 ± 1.5[a]	3.0	>100
(–)-1	2.5 ± 0.7[a]	1.6	>100
(±)-2	25.3 ± 4.4[a]	27.1	>100
(±)-3	11.9 ± 0.7[a]	16.1	>100
4	3.5 ± 0.7[c]	--	--
5	25 ± 2.5[c]	--	--

[a] n=4 [b] n=2 [c] n=3

In 2012, several pyrrole alkaloids were evaluated (**Figure 2.1**, compounds **1-3**) as inhibitors of the 20S proteasome.[8] The compounds were tested for their inhibitory activity towards the different catalytic sites of the proteasome using an *in vitro* fluorescent peptide assay. The first molecule tested was palau'amine (**II-1**), a complex scaffold belonging to the family of natural products. When racemic palau'amine was tested, it demonstrated inhibitory activity towards both the CT-L and C-L sites of the 20S proteasome. Intriguingly, the (–)-enantiomer of palau'amine appeared to be the active molecule in the racemic mixture, given the lower IC_{50} when tested

towards the different catalytic sites. The more synthetically accessible natural products (±)-dibromophakellin (**II-2**) and (±)-dibromophakellstatin (**II-3**) were also tested for their inhibitory activity towards the catalytic sites and demonstrated moderate activity towards the CT-L and C-L sites of the 20S proteasome. Palau'amine was shown to inhibit the proteasome irreversibly by kinetics and washing studies. When the alkene precursor of **II-2** and **II-3** was tested, no inhibition was observed, indicating the importance of the fused urea or guanidine scaffold to confer activity.

This initial work inspired further development of the (±)-bromoindolophakellin scaffold (**II-4**) for evaluation as a proteasome inhibitor.[9] (±)-Bromoindolophakellin was tested for its activity towards the CT-L site of the 20S proteasome (IC_{50} = 3.5 μM ±0.7) and demonstrated greater potency than the (–)-palau'amine scaffold. Lack of the bromine atom at the C_3-position of the indole scaffold resulted in a diminished inhibitory activity.

In collaboration with the Groll group, the X-ray crystal structure of **II-4** and the yeast 20S proteasome was successfully obtained (**Figure 2.2 A,** PDB: 4RUR, 2.5 Å). The interactions between **II-4** and the β5 chymotrypsin-like catalytic subunit are demonstrated in **Figure 2.2 B**. Key functional group requirements for interaction with the proteasome include the amino-imidazoline moiety, the carbonyl of the carboxamide and the brominated indole heterocycle. These functionalities participate in noncovalent interactions with the specific residues within the S_3 subpocket of the chymotrypsin-like catalytic site (β5 subunit) of the 20S human proteasome. The indole core is believed to interact with residues in the S_3 subpocket (His108) through van der Waals interactions. Further inspection of the crystal structure also indicated the importance of the fused guanidine scaffold: the geometry of the (–)-enantiomer contributes to the interaction with a hydrogen-bonding network with several residues within the S_3 subpocket (Ser124, Arg137, Glu134). A halogen binding interaction between the bromine atom of **II-4** and the carbonyl of

Thr21 was also observed within the crystal structure and was believed to be a key contributor towards the inhibitory potency observed for this molecule when compared to the non-brominated analog **II-5**. While the pyrrolidinyl ring sits in proximity with Val31 interact through a van der Waals interaction, substitution of this ring was not previously believed to be advantageous due to the size constraints within the S_3 subpocket. Notably, these inhibitors do not interact with the Thr1 residue responsible for proteolysis, and they therefore represent a novel class of inhibitors which interact with the human proteasome in a unique mechanism.

Figure 2.2 X-ray crystal structure of 4 with the yCP at 2.5 Å and diagram of interactions

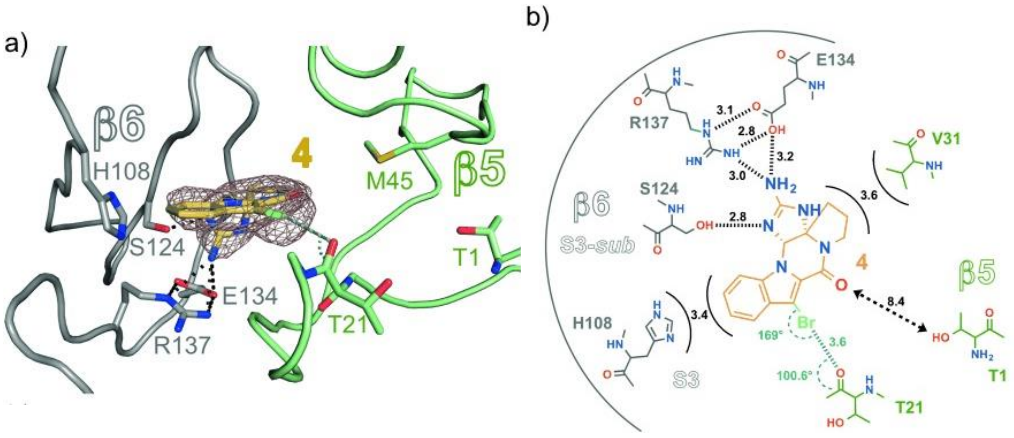

The non-covalent inhibitory activity of the dibromophakellin and dibromophakellstatin natural products and their analogs remained a point of interest in our lab. When comparing the inhibitory activities of (**II-2**) and (**II-3**), the greater inhibitory activity of the **II-3** indicated the importance of further exploration of the dibromophakellstatin scaffold and its analogs for their inhibitory activities. We proposed that development of an approach to bromoindolophakellstatin analogs may provide access to novel 20S proteasome inhibitors that may build upon the desired potencies of the dibromophakellstatin and bromoindolophakellin scaffolds. In addition to accessing the bromoindolophakellstatin analog **II-6**, we also envisioned this work could explore alteration of the scaffold such that other functional groups could be installed in place of the

pyrrolodinyl cycle originally located in the natural product (**Scheme 2.1**). While others have explored functionalization of the pyrrolodinyl cycle of dibromophakellstatin as a function of its cytotoxicity,[6] no research has been reported on exploring the constraints of size on this location of the dibromophakellstatin ring where the pyrrolodinyl cycle is altogether absent from the scaffold.

Scheme 2.1 Proposed bromoindolophakellstatin analogs based upon previous inhibitors

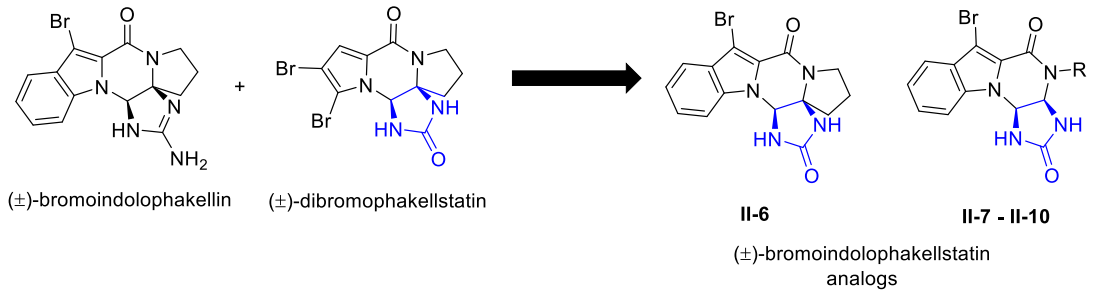

Our original findings resulting from the X-ray crystal structure obtained with the yCP:**II-4** suggested that functionalization of the pyrrolidine cycle may be constrained by the S_3 pocket of the β_5 subunit. However, we envisioned that while functionalization may not confer additional interactions within the S_3 pocket, additional interactions could be targeted through synthesis of molecules which could extend further towards the S_1 subpocket. Previously, the Groll group established the ability of the hydroxyurea scaffold to act as non-covalent inhibitor of the 20S proteasome.[10] The group designed and synthesized the **HU-10** (IC_{50} (CT-L)= 0.34 ± 0.04 μM) as a CT-L specific inhibitor which binds solely through non-covalent, reversible interactions.

The X-ray crystal structure of yCP:**HU-10** was obtained (PDB: 3SHJ) and provided insight into the interactions of the HU-10 within the β_5 pocket. Analysis of the crystal structure indicated that the 1-adamantyloxy moiety may have hydrophobic interactions with residues in the S_3 subpocket. The phenyl ring extends into the S_1 subpocket and interacts through van der Waals interactions with several residues (Ala49, Val31, Met45). The hydroxyurea moiety extends further

towards the catalytic site (Thr1) but does not appear to interact through a covalent mechanism with the residue. Instead, the hydroxyurea interacts through hydrogen-bonding with several residues within the S_1 pocket.

Figure 2.3 Structural super-position of **II-4** and **HU-10** in β_5 site

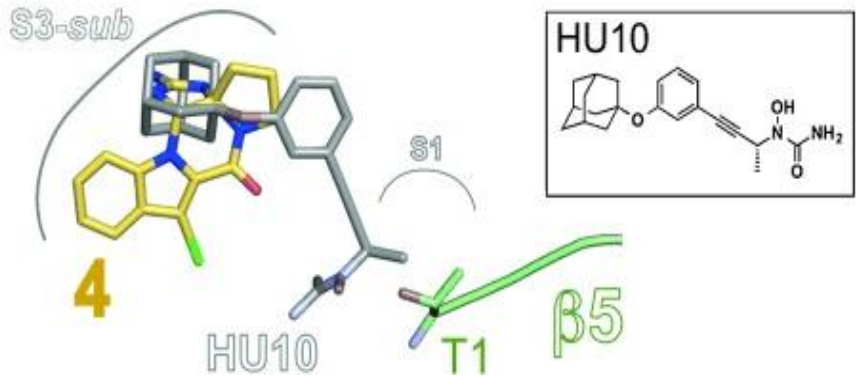

The interaction of the phenyl ring with the S_1 subpocket was a point of intrigue due to the observation that a structural superposition of the **HU-10** and **II-4** within the β_5 binding channel indicated the potential to install the phenyl ring off the amide of the bromoindophakellin core (**Figure 2.3**).[9] Based upon these observations, a small number of molecules were designed to explore the utility of the bromoindolophakellstatin core and its *N*-functionalized analogs with the goal being to determine whether modification from the pyrrolidine ring would pose any benefits (**Scheme 2.2**).

Scheme 2.2 Desired preliminary bromoindolophakellstatin analogs

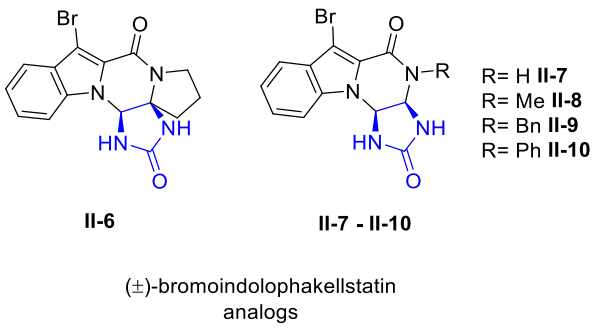

The following section describes the synthetic efforts towards the bromoindolophakellstatins through multiple approaches.

2.2 Results & Discussion

2.2.1 Attempted construction of indolopiperazinone core by intermolecular oxidative cyclization

The cyclic guanidine moiety is a common feature in marine sponge alkaloids, especially those which are derived from oroidin and clathrodin. In our synthesis of proteasome inhibitors, we have established the importance of the cyclic guanidine and urea functionalities for activity. [8]

In the total synthesis for dibromophakellin by former lab member Dr. Nicole Hewlett, the cyclic guanidine is accessed by NBS-mediated guanidine cyclization of the core. [11] Access to these polycyclic guanidine-containing natural products and analogs is also approached using the 2-aminoimidazole or 1,3-dihydro-*2H*-imidazol-2-one as a reactive unit which is ambiphilic in nature depending upon the circumstances. These functionalities are rendered electrophilic using an oxidative strategy such as bromination or use of an oxidative reagent like dimethyldioxirane or an oxaziridine.[12-15] Cyclization is afforded by intramolecular nucleophilic attack upon the activated imine species. The Büchi group utilized this type of strategy in their total synthesis of dibromophakellin;[16] milder conditions were presented by the Horne group in their synthesis of dibromophakellstatin.[17] Horne's group utilized a brominating reagent (NBS) in the presence of a strong acid (TFA), followed by quenching with triethylamine to afford the natural product in 45% yield (**Scheme 2.3**). While these strategies have often been utilized in total synthesis in an intramolecular approach, we considered whether they could be applicable to a general intermolecular strategy to access the urea-fused piperazinone core.

Scheme 2.3 Horne's construction of urea-fused piperazinone core of dibromophakellstatin

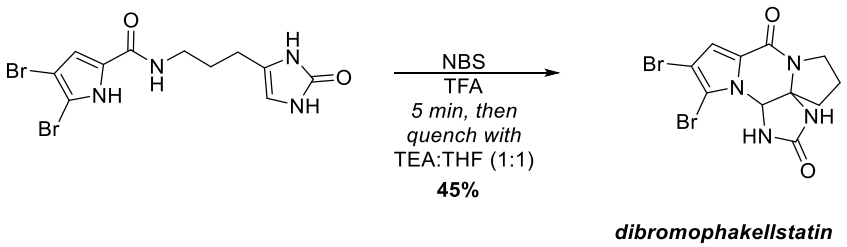

The proposed mechanism of the formation of the urea-fused piperazinone core is shown below in S**cheme 2.4**. First, bromination imidazolone renders it electrophilic and prone to attack by the nucleophilic amide nitrogen to afford the spirocyclic intermediate **II-11**. Subsequent nucleophilic attack by the pyrrole nitrogen leads to construction of the desired piperazinone core to achieve the desired tetracyclic scaffold. We envisioned that in an intermolecular approach, the reaction mechanism could occur by the same means.

Scheme 2.4 Proposed mechanism of urea-fused piperazinone formation

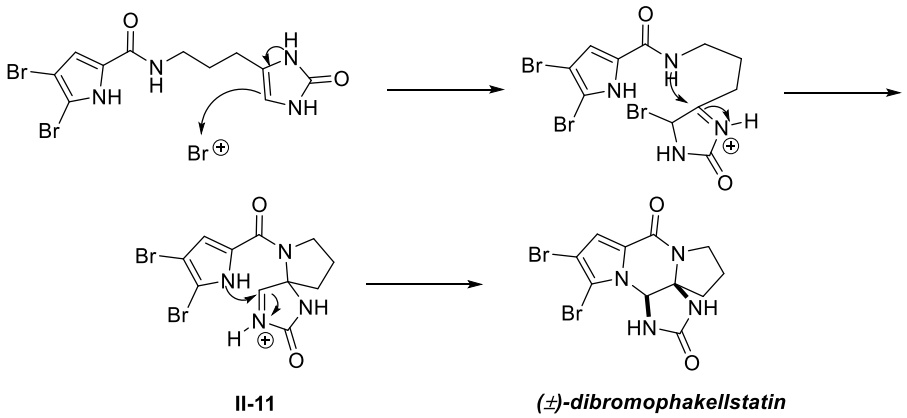

To begin the investigation of this proposed intermolecular cyclization, model pyrrole **II-12** and indole **II-13** were used with 1,3-dihydro-2-imidazolone under brominative conditions. Pyrrole **II-12** was synthesized through 4,5-dibromo-2-trichloroacetylpyrrole, the synthesis of which is provided in Chapter 4 of this dissertation. Indole **II-13** was synthesized in one step from

1*H*-indole-2-carboxylic acid. The syntheses of both starting materials are shown below in **Scheme 2.5**.

Scheme 2.5 Syntheses of model pyrrole **II-12** and indole **II-13**

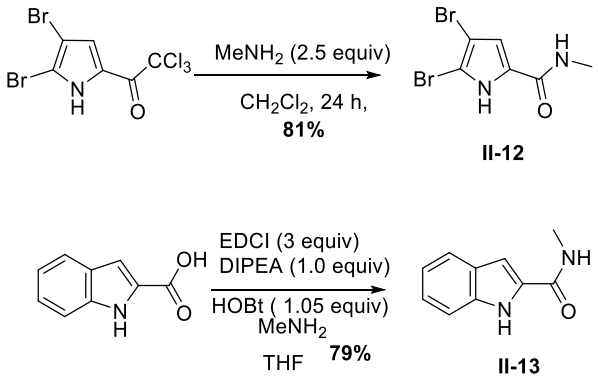

Attempted oxidative cyclization under brominative conditions using 1,3-dihydro-2-imidazolone as the activated alkene are summarized in **Table 2.1.** Initial attempts utilized dichloromethane as solvent of choice, due to its common use with *N*-bromosuccinimide. The first reaction carried out was that with the model pyrrole substrate **II-12** (Table 2.1, entry 1). Using one equivalent of brominating agent, no cyclization was observed. Rather, preferential bromination at the C_3 position of the pyrrole occurs to afford complete substitution of the pyrrole ring. No cyclization was observed from this reaction, and the tri-brominated pyrrole carboxamide species was isolated from this reaction in 75% yield. Use of excess NBS was proposed to potentially afford the cyclized product, which would also be brominated at the C_3 position of the pyrrole **II-12** (Table 2.1, entry 2). Unfortunately, no cyclized product was observed by crude NMR or HRMS.

Table 2.1 Attempts at cyclization with *N*-bromosuccinimide and 2-imidazolone

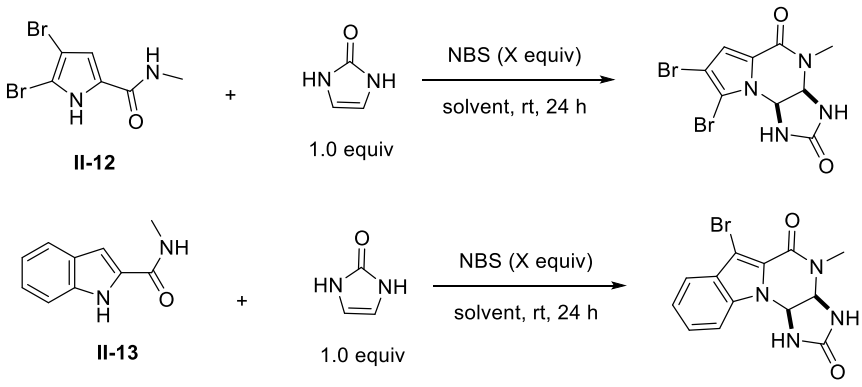

Entry	Conditions	Result[a]
1	Pyrrole **II-12**, NBS (1.0 equiv), 2-imidazolone, CH_2Cl_2, rt	No cyclization observed; bromination of pyrrole occurs preferentially
2	Pyrrole **II-12**, NBS (2.0 equiv), 2-imidazolone, CH_2Cl_2, rt	No cyclization observed; bromination of pyrrole occurs preferentially
3	Indole **II-13**, NBS (2.0 equiv), 2-imidazolone, CH_2Cl_2, rt	No cyclization observed; Indole bromination occurs preferentially
4	Indole **II-13**, NBS (2.0 equiv), 2-imidazolone, MeCN, rt	No cyclization observed; bromination of indole occurs preferentially
5	Indole **II-13**, NBS (4.0 equiv), 2-imidazolone, MeCN, rt	No cyclization observed; bromination of indole occurs preferentially

[a]Products were observed by high-resolution mass spectrometry and NMR. Starting material and brominated products were observed; no evidence suggests cyclized product formation.

This same strategy was attempted with indole **II-13** (**Table 2.1**, entry 3), under the same prediction that the C_3 position would become brominated, and that cyclization may occur from the additional oxidant. Instead, dibromination of the indole carboxamide occurs so that the C_3 and C_5 positions of the molecule become substituted by electrophilic aromatic substitution.

Due to the insolubility of the 2-imidazolone, the more polar solvent acetonitrile was chosen for subsequent reaction. While the use of acetonitrile as solvent does improve solubility of the starting material in the reaction, preferential mono- and di-bromination of the model indole

carboxamide still occurs, and no cyclization is observed by NMR or HRMS (**Table 2.1**, entries 4 and 5).

To improve solubility issues experienced with the 2-imidazolone starting material, the compound was diacylated to afford the protected 2-imidazolone species. The synthesis of this species is provided in Chapter 3 of this dissertation. The results of the reactions using the diacylated substrate are detailed in **Table 2.2**.

Bromination at the C_5 position of an indole is not considered to occur readily, and so it was thought that if the indole carboxamide model substrate is deliberately mono-brominated at the C_3 position, it would be advantageous to determine if any cyclization can occur with lower equivalents of brominating reagent. The synthesis of the indole **II-14** is detailed in **Scheme 2.6** below.

Scheme 2.6 Synthesis of the brominated indole model substrate **II-14**

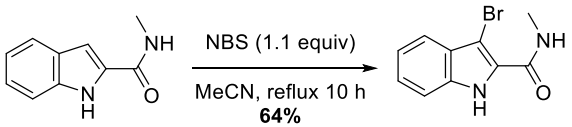

II-13 **II-14**

Using the *N,N'*-diacylated imidazolone under the same brominative conditions affords the same outcome. Electrophilic aromatic bromination of the indole species occurs over oxidative cyclization. Even though the C_5 position of the indole is considerably less nucleophilic than the C_3 position, dibromination occurs readily in these systems rather than the intermolecular cyclization process.

Table 2.2 Attempts at cyclization with *N*-bromosuccinimide and *N,N'*diacyl-2-imidazolone

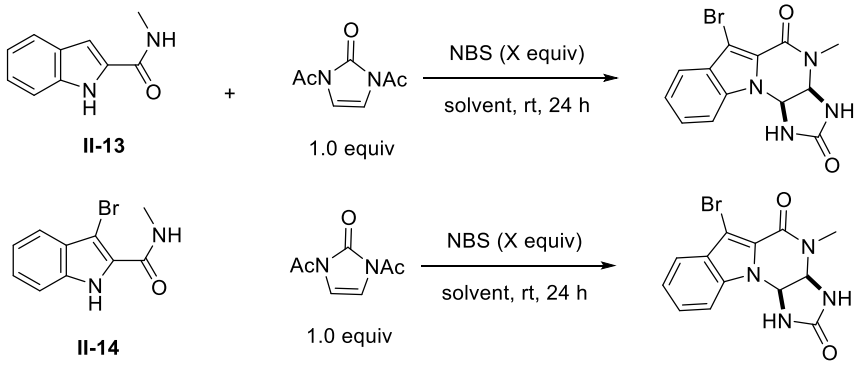

Entry	Conditions	Result[a]
1	Indole **II-13**, NBS (2.0 equiv), *N,N'*-diacyl-2-imidazolone, CH_2Cl_2 rt	No cyclization observed; bromination of indole occurs preferentially
2	Indole **II-13**, NBS (2.0 equiv), *N,N'*-diacyl-2-imidazolone, MeCN rt	No cyclization observed; bromination of indole occurs preferentially
3	Indole **II-13**, NBS (4.0 equiv), *N,N'*-diacyl-2-imidazolone, MeCN rt	No cyclization observed; bromination of indole occurs preferentially
4	Indole **II-14**, NBS (1.1 equiv), *N,N'*-diacyl-2-imidazolone, MeCN rt	No cyclization observed; bromination of indole occurs preferentially
5	Indole **11-14**, NBS (1.1 equiv), *N,N'*-diacyl-2-imidazolone, MeCN rt	No cyclization observed; bromination of indole occurs preferentially

[a]Products were observed by high-resolution mass spectrometry and NMR. Starting material and brominated products were observed; no evidence suggests cyclized product formation.

This same oxidative cyclization under brominative conditions was attempted with 2-aminoimidazole. These results are summarized in **Table 2.3**. In comparison to the 2-imidazolone and *N,N'*-diacetyl-2-imidazolone substrates, the 2-aminoimidazole was considered as a potential substrate of interest to outcompete the pyrrole and indole substrates due to its increased nucleophilicity. The amino group at the 2-position acts as an electron donating group, rendering the heterocycle more nucleophilic and electron dense than the imidazolone substrates previously utilized. I proposed that the use of 2-aminoimidazole could afford the desired cyclization by a

slightly altered mechanism which involved reaction between 2-aminoimidazole and the brominating reagent to afford a reactive α-bromoiminium intermediate which would be reactive towards nucleophilic attack (**Scheme 2.7**).

Scheme 2.7 Proposed mechanism of intermolecular NBS-mediated cyclization

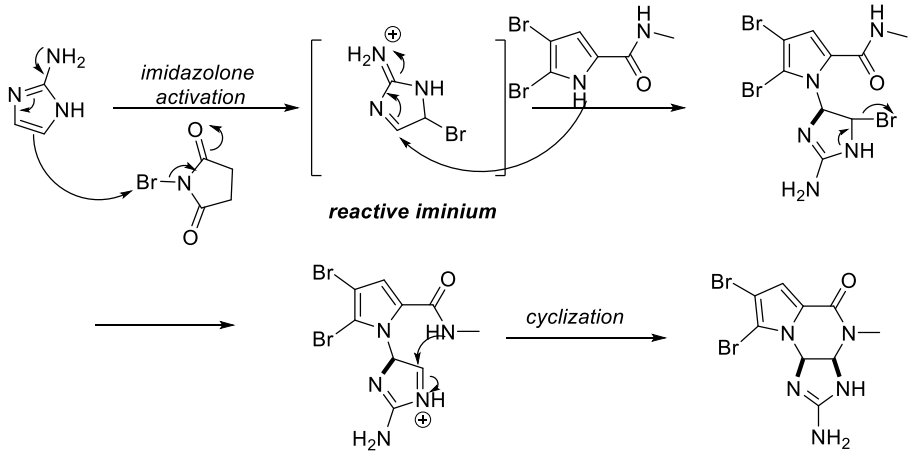

Using the pyrrole and indole substrates, classic conditions for bromination were attempted using NBS. Changing solvent from dichloromethane to trifluoroacetic acid was a deliberate attempt to further activate NBS towards nucleophilic attack. Again, rather than affording the desired cyclized product, bromination of the pyrrole and indole substrates rather occurs under these conditions.

Table 2.3 Attempts at NBS-mediated cyclization with 2-aminoimidazole

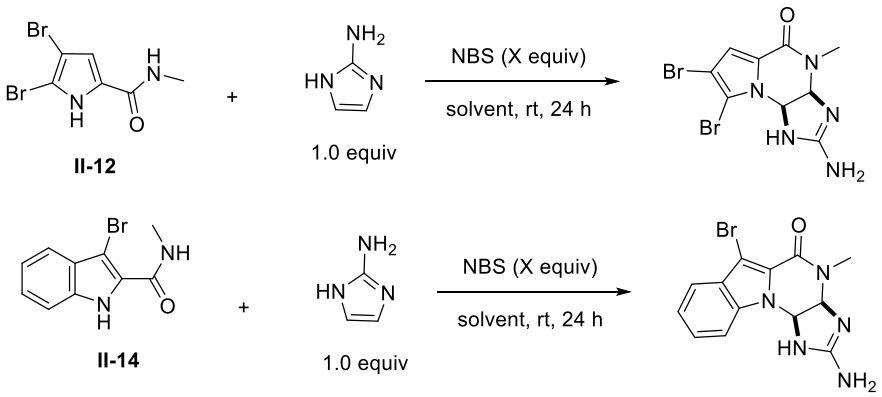

Entry	Conditions	Result[a]
1	Pyrrole **II-12**, NBS (1.0 equiv), 2-aminoimidazole, CH_2Cl_2, rt	No cyclization observed; bromination of pyrrole occurs preferentially
2	Pyrrole **II-12**, NBS (1.0 equiv), 2-aminoimidazole, TFA, 0 °C to rt	No cyclization observed; bromination of pyrrole occurs preferentially
3	Indole **II-14**, NBS (1.0 equiv), 2-aminoimidazole, TFA, 0 °C to rt	No cyclization observed; bromination of indole occurs preferentially

[a]Products were observed by high-resolution mass spectrometry. Starting material and brominated products were observed; no evidence suggests cyclized product formation.

Following extensive exploration of brominative conditions to facilitate the oxidative cyclization in question, it became obvious that a different route to the cyclized product may be necessary. Unfortunately, the reaction favors electrophilic aromatic substitution of the heterocyclic model pyrrole and indole substrates but does not facilitate oxidative cyclization at all.

In the Chen group's synthesis of dibromophakellstatin, the group utilizes a hypervalent iodine species to facilitate an intramolecular diamination/cyclization to afford the natural product (**Scheme 2.8**). This reaction system uses specifically (*bis*-acetoxy)-iodobenzene (PIDA) and excess sodium carbonate base in an alcoholic solvent to produce the desired tricycle. The mechanism of this reaction is similar to that which was proposed in **Scheme 2.4**.

Scheme 2.8 Chen's ultimate step to afford the natural product dibromophakellstatin

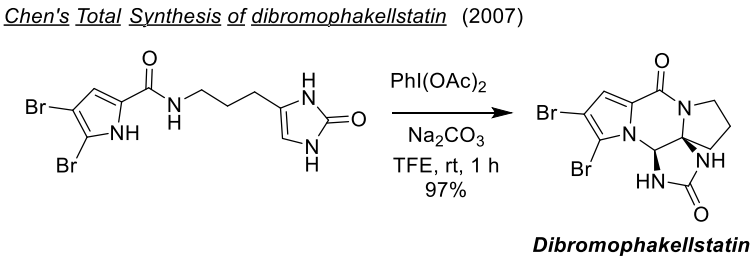

Using these same conditions in an intermolecular approach, several reactions were attempted, and their conditions and results are summarized in **Table 2.4** It appears that even at refluxing temperatures, no reaction occurs to afford the cyclization product. Unfortunately, there was no indication of any reaction between PIDA and the indole or pyrrole substrates.

Table 2.4 Attempted hypervalent iodine-mediated oxidative cyclization reactions

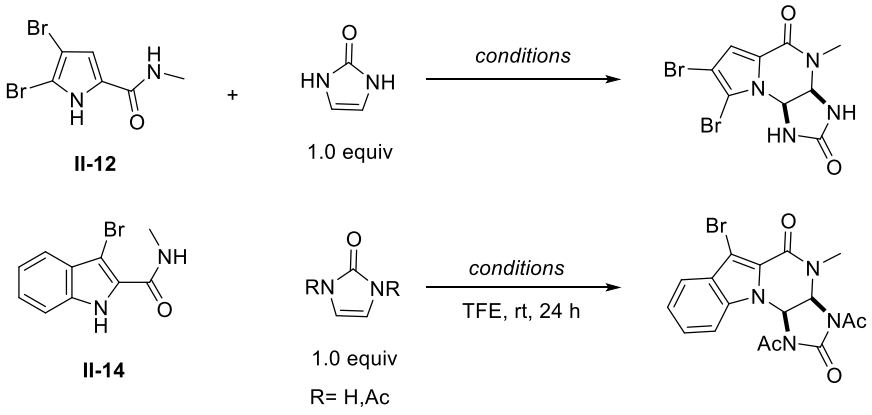

Entry	Conditions	Result
1	Indole **II-14**, 2-imidazolone (1.0 equiv), PIDA (1.0 equiv), Na_2CO_3 (10 equiv), TFE, rt	No cyclization observed; starting material observed by TLC/crude NMR/HRMS
2	Indole **II-14**, N,N'-diacetyl-2-imidazolone (1.0 equiv), PIDA (1.0 equiv), Na_2CO_3 (10 equiv), TFE, rt	No cyclization observed; starting material observed by TLC/crude NMR/HRMS
3	Pyrrole **II-12**, 2-imidazolone (1.0 equiv), PIDA (1.0 equiv), Na_2CO_3 (10 equiv), TFE, rt to reflux	No cyclization observed; starting material observed by TLC/crude NMR/HMRS

Following repeated failures in applying the halogen-mediated intramolecular approaches to an intermolecular system, the focus of this work was shifted to instead apply a multi-step approach to access the indolophakellstatin core. This work is summarized in the next section.

2.2.2 Multi-step approach to access indolophakellstatin cores

After failure to access the indolophakellstatin core through an expeditious approach, synthesis of these scaffolds was next attempted through a multi-step approach. This approach closely mirrored the synthetic routes developed in the synthesis of the indolophakellins analogs and our synthesis of dibromophakellstatin. The retrosynthesis of this approach is provided below (**Scheme 2.9**). Synthesis of the desired urea-fused piperazinone scaffolds would be achieved following deprotection of a urea synthon, which would be utilized in an NBS-mediated approach to access the fused core from an alkene scaffold. The alkene scaffold would be constructed by synthetic manipulation of an indole carboxamide. An analogous route was envisioned for the tricyclic scaffolds.

Scheme 2.9 Retrosynthetic analysis of bromoindolophakellstatin **II-6**

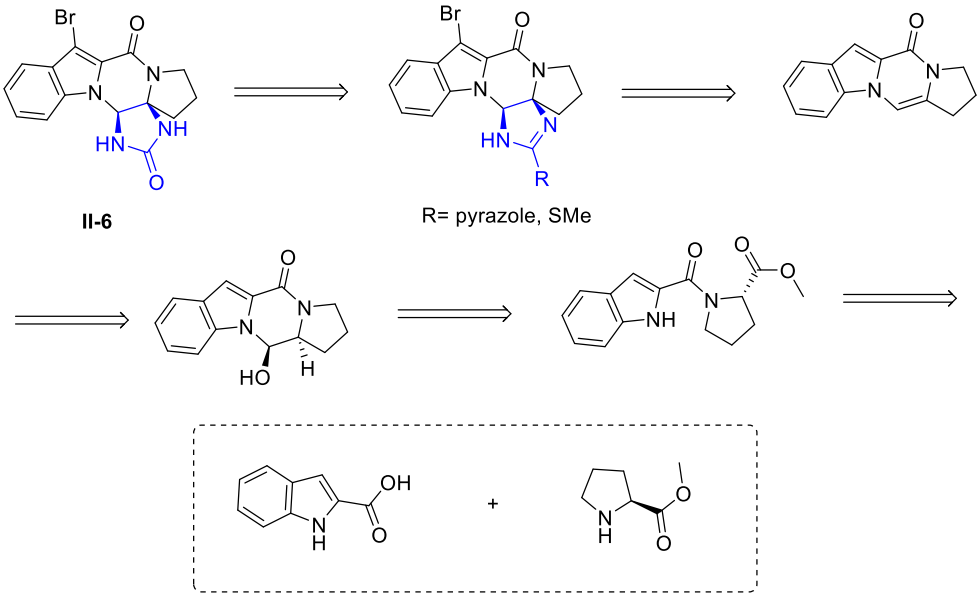

Following the synthetic approach described in our previous report,[11] the indole carboxamide (**II-15**) was synthesized by EDCI coupling with indole-2-carboxylic acid and *L*-proline methyl ester hydrochloride. Subsequent reductive cyclization with sodium borohydride afforded the tetracyclic alcohol **II-16** in 55 % yield. The tetracyclic alkene scaffold **II-17** was next accessed by an acid-mediated elimination of the alcohol with methanesulfonic acid (**Scheme 2.10**). With the desired alkene in hand, construction of the urea-scaffold became the next synthetic focus.

Unlike construction of the guanidine-fused piperazinone core, access to the urea-fused core was expected to be more complicated based upon past results and efforts reported by our lab. While a protected guanidine could be used in the NBS-mediated approach to access dibromophakellin, use of urea to access dibromophakellstatin resulted in the formation of the undesired *O*-cyclized product. A suitable urea synthon which could only undergo *N*-cyclization was thus necessary. In the total synthesis of dibromophakellstatin, pyrazole carboxamidine was utilized as urea synthon.[18]

Scheme 2.10 Synthetic access to tetracyclic alkene **II-17**

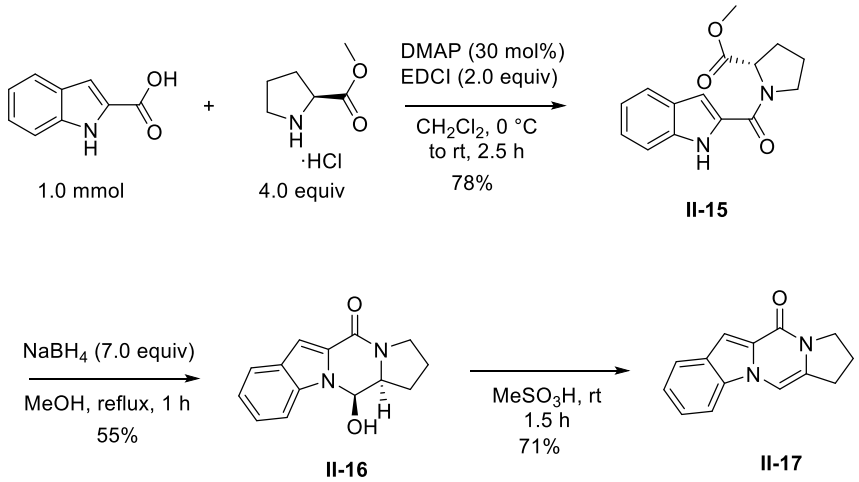

NBS-mediated cyclization from alkene **II-17** was thus carried out using this synthon, however this led to several products which were difficult to isolate by column chromatography. HRMS indicated that a dibrominated cyclic product predominates in the crude reaction mixture;

the location of this bromine was expected to be located on the pyrazole ring and occur due to the required excess of NBS necessary for the cyclization. The challenges of purification using pyrazole carboxamidine as urea synthon led to the decision to instead use S-methyl thiourea as urea precursor. Similar to the pyrazole substrate, this reagent was expected to result in preferential N-cyclization to access the desired tetracyclic core that could be subsequently undergo modification to afford the desired molecule **II-6**. Gratifyingly, the use of *S*-methylurea under optimized conditions resulted in complete conversion of the tetracyclic alkene to access the semi-crude tetracycle **II-18**. The identity of **II-18** was supported by crude NMR and HRMS of this semi-pure product.

Scheme 2.11 Attempts towards **II-18** with urea synthons

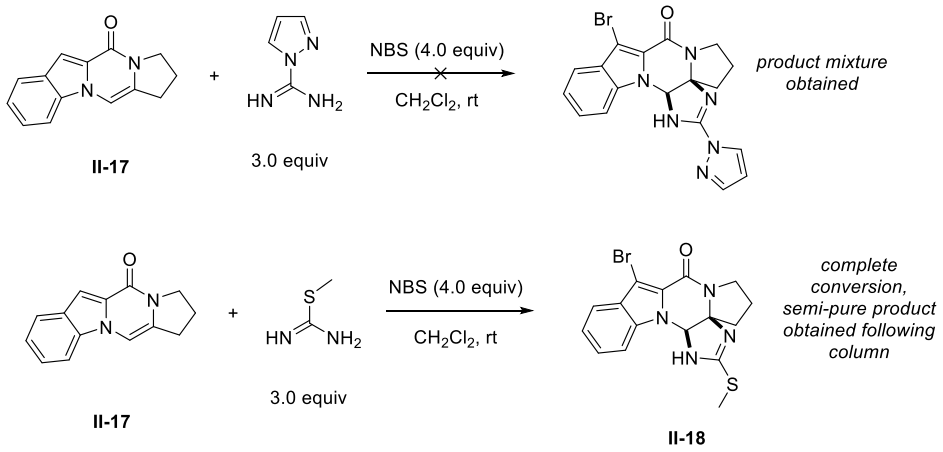

The last focus in this work was access to the desired bromoindolophakellstatin analog **II-6**. Common methods exist for conversion of *S*-methyl ureas to urea including acid-mediated[19] and use of oxidative approaches to facilitate displacement of the thio group.[20] The acid-mediated hydrolysis was first attempted with the tetracyclic and tricyclic species, however several attempts failed to afford the desired ureas even after several days of heating. Oxidative conditions are next planned to access the desired urea (**Scheme 2.12**). If successful, these conditions are expected to be applicable towards the synthesis of other substrates.

Scheme 2.12 Attempted hydrolysis of **II-18** and proposed future approach

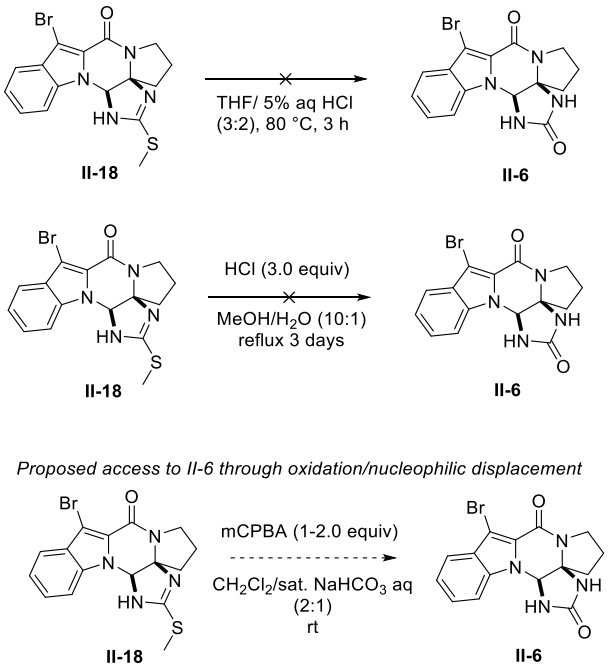

While the tetracyclic core was synthesized, a simultaneous synthesis of the tricyclic cores was undertaken (**Scheme 2.13**). The desired tricyclic alkene was accessible through a two-step process. First, indole-2-carboxylic acid was subjected to BOP-mediated coupling to access the dimethoxy acetal **II-19**. Subsequent acid-mediated cyclization afforded the desired alkene **II-20**, which was separable from its *C*-cyclized regioisomer.

Scheme 2.13 Synthesis of tricyclic alkene core **II-20**

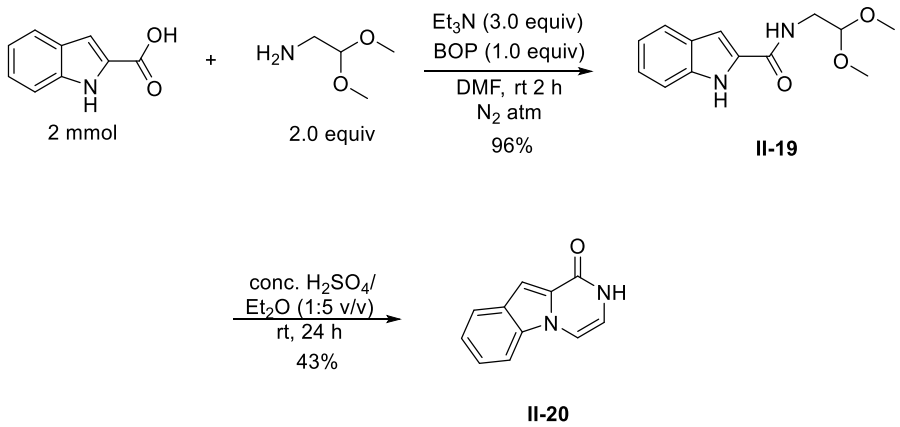

Functionalization of the tricyclic alkene afforded the desired *N*-substituted alkenes in moderate to excellent yields (**Scheme 2.14**). Alkylation and benzylation using suitable halides and sodium hydride afforded the *N*-methyl alkene (**II-21**) and *N*-benzylated alkene (**II-22**), respectively. The *N*-phenyl scaffold **II-23** was accessed through and Chan-Lam coupling approach.[21]

Scheme 2.14 *N*-functionalization of tricyclic alkene **II-20**

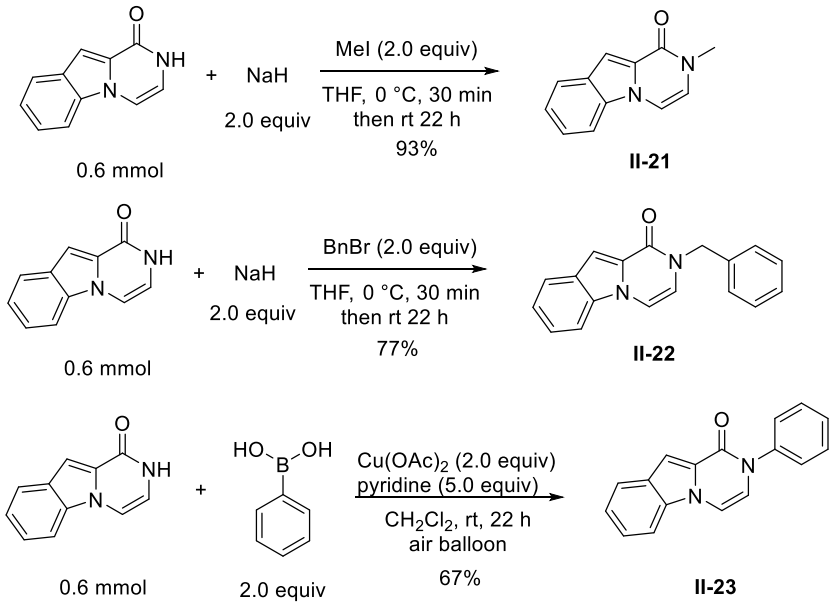

With the *N*-functionalized alkenes in hand, application of the NBS-mediated thiourea cyclization was next attempted. The reaction conditions were first applied to access to the unsubstituted product **II-24** from the alkene **II-19** (**Scheme 2.15**) as a semi-pure product as determined by NMR and HRMS. Initial attempts were made to access the *N*-substituted tricyclic thiourea substrates as well, and while the reaction did appear to be successful in the case of the *N*-methyl analog, conversion in the case of the *N*-benzyl and *N*-phenyl analogs was poor. The reason for this failure to convert efficiently to the desired products is not well-understood at this time.

Scheme 2.15 NBS-mediated synthesis of cyclic thiourea **II-24**

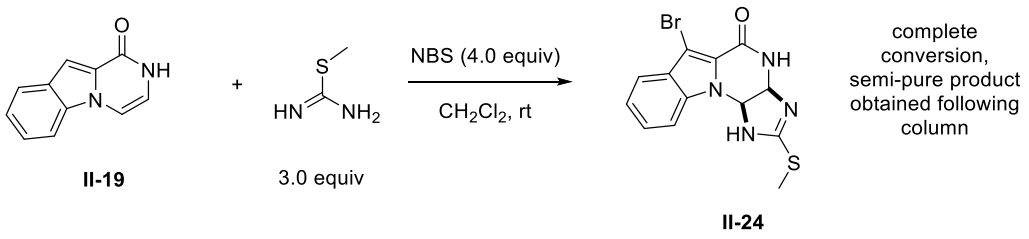

2.3 Conclusion & Future Directions

An altered synthetic approach is envisioned to access the *N*-substituted alkene scaffolds by late-stage functionalization of the amide moiety (**Scheme 2.16**). Instead of the use of the S-methylthiourea as urea synthon, this approach would utilize *N*-Boc-*S*-methylthiourea as starting material so that selective functionalization could be attempted on the penultimate step. This approach would facilitate a later divergence in the synthesis of the small molecules. Subsequent conversion to the urea and deprotection would afford the desired products for evaluation as 20S proteasome inhibitors.

Scheme 2.16 Proposed alternative route to *N*-functionalized scaffolds

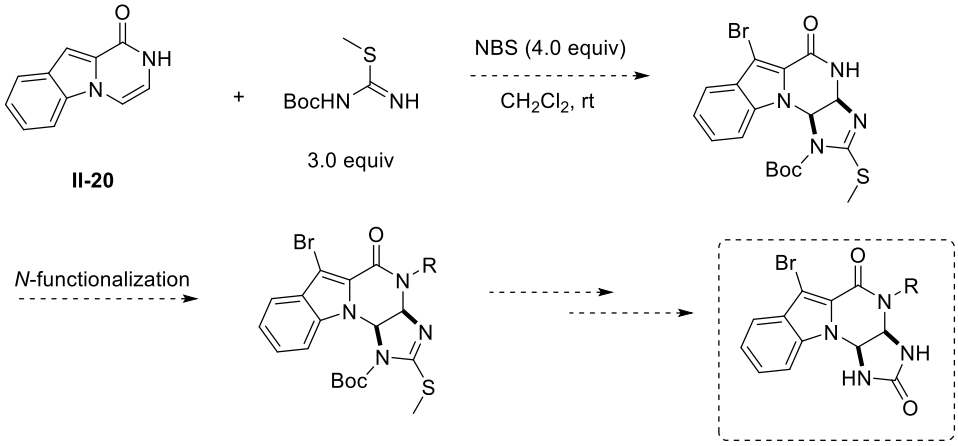

This chapter signifies the progression of synthesis of the bromoindolophakellstatins from early expeditious approaches to a reliable multi-step synthesis to access the penultimate step in the synthesis. While early attempts at expeditious routes failed to access the urea- and guanidine-fused

piperazinone cores due to competing halogenation, the multi-step approach facilitates access to the thiourea-fused piperazinone core. Future work will focus on access to the urea-fused core through an oxidative approach. These molecules will be subsequently evaluated for their inhibitory activity towards the 20S proteasome. Early challenges associated with a lack of appropriate methodology to access the urea-fused scaffolds through an expeditious route served as inspiration for the development of a novel methodology which is the focus of discussion in Chapter 3 of this thesis.

2.4 Experimental

4,5-dibromo-*N*-methyl-1*H*-pyrrole-2-carboxamide (II-12)

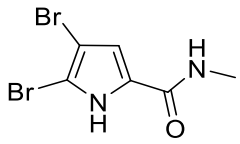

2,2,2-trichloro-1-(4,5-dibromo-1*H*-pyrrol-2-yl)ethan-1-one (0.9956 g, 2.60 mmol) was dissolved in 26 mL CH_2Cl_2. The flask was sealed, and methylamine (3.26 mL, 2.0 M in THF, 6.52 mmol) was added via syringe. The reaction stirred at rt for 5.5 hours under N_2 atm until all starting material was consumed, as observed by thin-layer chromatography. Volatiles were evaporated *in vacuo* to yield a crude beige solid. The crude solid was purified by automated CombiFlash chromatography (EtOAc/Hexane) to yield a white solid (0.6146 g, 81%). mp: 197-198 °C. ^{1}H NMR (500 MHz, DMSO-d_6) δ 12.67 (s, 1H), 8.10 (q, J = 4.3 Hz, 1H), 6.84 (s, 1H), 2.70 (d, J = 4.6 Hz, 3H). ^{13}C{^{1}H} NMR (126 MHz, DMSO-d_6) δ 159.4, 128.3, 112.2, 104.4, 97.8, 25.6. FTIR (cm^{-1}): 3426, 3133, 3109, 2934, 1641. HRMS-ESI (m/z) calcd for $C_6H_5Br_2N_2O$[M-H]- 278.8774. Mass not found.

N-methyl-1*H*-indole-2-carboxamide (II-13)

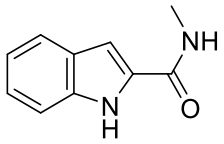

1*H*-indole-2-carboxylic acid (2.09 g, 13.0 mmol), was dissolved in dry THF (80 mL) in round-bottom flask equipped with stir bar. To the flask was added DIPEA (2.26 mL, 12.97 mmol) by syringe. HOBt-hydrate (2.10 g, 13.7 mmol) was next added in one portion, followed finally by introduction of methylamine (7.78 mL, 15.6 mmol) by syringe. EDCI-HCl (7.50 g, 39.1 mmol) was added to the reaction flask in one portion. The reaction was stirred at rt under N_2 atm for 14.5 hours. The reaction mixture was concentrated by rotary evaporator to remove all solvent. The

reaction was purified by automated CombiFlash chromatography (EtOAc/Hexane) to yield a white solid (2.27 g, 79%). mp: 208-210 °C. ^{1}H NMR (500 MHz, DMSO-d_6) δ 11.57 (s, 1H), 8.46 (q, *J* = 4.9 Hz, 1H), 7.61 (d, *J* = 7.7 Hz, 1H), 7.43 (d, *J* = 7.9 Hz, 1H), 7.18 (t, *J* = 7.5 Hz, 1H), 7.06 (s, 1H), 7.00 (t, *J* = 7.5 Hz), 2.80 (d, *J* = 4.5 Hz, 3H). ^{13}C{^{1}H} NMR (126 MHz, DMSO-d_6) δ 161.6, 136.3, 131.9, 127.1, 123.1, 121.4, 119.7, 112.3, 102.0, 25.8. FTIR (cm^{-1}): 3413 (sharp), 3257 (br), 2930, 1625. HRMS-ESI (m/z) calcd for $C_{10}H_{11}N_2O$[M+H]+ 175.0871. Found 175.0932.

3-bromo-*N*-methyl-1*H*-indole-2-carboxamide (II-14)

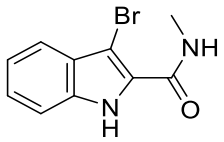

N-methyl-1*H*-indole-2-carboxamide **II-13** (0.254 g, 1.46 mmol) was dissolved in 20 mL dry acetonitrile. To the reaction flask was added *N*-bromosuccinimide (0.288 g, 1.61 mmol), and the reaction was heated at reflux for 10 hours under N_2 atm. The reaction was subsequently removed from heat and allowed to cool to rt. Volatiles were removed by rotary evaporation to yield a crude white solid. This crude material was recrystallized with ethanol, to yield a fluffy white solid (0.369 g, 64%). mp: 199-201 °C. ^{1}H NMR (500 MHz, DMSO-d_6) δ 11.98 (s, 1H), 7.91 (q, *J* = 4.6 Hz, 1H), 7.48 (d, *J* = 8.0 Hz, 1H), 7.45 (d, *J* = 8.2 Hz, 1H), 7.29 (t, *J* = 7.3 Hz, 1H), 7.17 (t, *J* = 7.6 Hz, 1H), 2.87 (d, *J* = 4.6 Hz, 3H). ^{13}C{^{1}H} NMR (126 MHz, DMSO-d_6) δ 160.6, 134.9, 128.8, 126.6, 124.6, 120.8, 119.4, 112.7, 89.8, 26.3. FTIR (cm^{-1}): 3405 (sharp), 3247, st, br), 3058, 2933, 1632. HRMS-ESI (m/z) calcd for $C_{10}H_{10}N_2O$[M+H]+ 254.0055. Found 253.9913.

methyl (1*H*-indole-2-carbonyl)-*L*-prolinate (II-15)

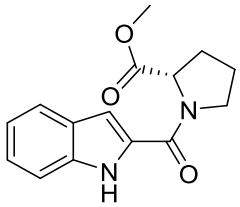

1*H*-indole-2-carboxylic acid (0.484 g, 3.0 mmol) was suspended in dry CH_2Cl_2 in a round bottom flask equipped with stir bar. The reaction was cooled to 0 °C; *L*-proline methyl ester hydrochloride (1.56 g, 12.0 mmol) was added in one portion. DMAP (0.111 g, 0.91 mmol) was added to the mixture, followed by addition of EDCI-HCl (0.934 g, 6.0 mmol). The reaction stirred at 0 °C for 30 min, then at rt for 2 h under N_2 atm. The reaction was subsequently transferred to a separatory funnel and washed once with water. The organic layer was separated, dried over Na_2SO_4, filtered and concentrated to afford the crude product. The desired product was purified by automated CombiFlash chromatography (EtOAc/Hexane) to afford a white foam (0.638 g, 78%). Mp: 131-133 °C ^{1}H NMR (500 MHz, $CDCl_3$) δ 9.80 (s, 1H), 7.69 (d, *J* = 8.2 Hz, 1H), 7.48 (d, *J* = 8.4 Hz, 1H), 7.30 (t, *J* = 7.5 Hz, 1H), 7.14 (t, *J* = 7.1 Hz, 1H), 6.98 (s, 1H), 4.80-4.77 (m, 1H), 4.15-3.99 (m, 2H), 3.77 (s, 3H), 2.33-2.05 (m, 4H). ^{13}C{^{1}H} NMR (126 MHz, $CDCl_3$) δ 172.8, 161.3, 135.9, 129.9, 128.0, 124.9, 122.3, 120.6, 112.1, 106.2, 60.5, 52.5, 48.9, 28.9, 25.6. FTIR (cm^{-1}): 3268, 3058, 2952, 1737, 1591. HRMS-ESI (m/z) calcd for $C_{15}H_{17}N_2O_3$[M+H]+ 273.1239, found 273.1248.

(12*R*,12a*S*)-12-hydroxy-2,3,12,12a-tetrahydro-1*H*,5*H*-pyrrolo[1',2':4,5]pyrazino[1,2-a]indol-5-one (II-16)

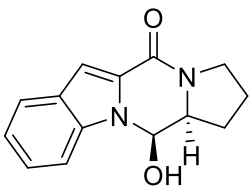

Methyl (1*H*-indole-2-carbonyl)-*L*-prolinate (**II-15**) (0.135 g, 0.5 mmol) was combined in a dry round bottom flask with dry methanol (4.5 mL) and stir bar. To the flask was added sodium borohydride (0.132 g, 3.5 mmol), and the reaction mixture was heated to reflux by sand bath under N_2 atm for 1 h. The reaction was removed and cooled to rt prior to transfer to freezer to facilitate precipitation of the desired product. The resulting white precipitate was collected by vacuum filtration and washed with cold methanol. The product was isolated as a white solid (0.066 g, 55%) as ~20:1 mixture of diastereomers as determined by ^{1}H-NMR. Mp: 205-207 °C. ^{1}H NMR (500 MHz, DMSO-d_6) (major diastereomer peaks reported) δ 7.67 (d, J = 8.0 Hz, 1H), 7.61 (d, J = 8.4 Hz, 1H), 7.33 (t, J = 7.4 Hz, 1H), 7.15 (t, J = 7.5 Hz, 1H), 7.02 (s, 1H), 6.72 (br s, 1H), 6.07 (d, J = 2.5 Hz, 1H), 4.15-4.11 (m, 1H), 3.65-3.60 (m, 1H), 3.47-3.42 (m, 1H), 2.14-2.00 (m, 3H), 1.93-1.83 (m, 1H). ^{13}C{^{1}H} NMR (126 MHz, DMSO-d_6) (major diastereomer peaks reported) δ 156.9, 129.6, 127.4, 123.9, 121.9, 120.7, 111.0, 104.1, 72.4, 61.0, 44.4, 27.1, 22.7. FTIR (cm^{-1}): 3120, 2950, 2873, 1605, 1095. HRMS-ESI (m/z) calcd for $C_{14}H_{15}N_2O_2$[M+H]+ 243.1134, found 243.1143.

2,3-dihydro-1*H*,5*H*-pyrrolo[1',2':4,5]pyrazino[1,2-a]indol-5-one (II-17)

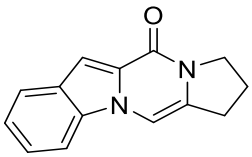

(12*R*,12a*S*)-12-hydroxy-2,3,12,12a-tetrahydro-1*H*,5*H*-pyrrolo[1',2':4,5]pyrazino[1,2-a]indol-5-one (**II-16**) (0.350 g, 1.4 mmol) was added to a dry round bottom flask containing stir bar and methanesulfonic acid (6 mL). The resulting reaction mixture was stirred at rt under N_2 atm for 1.5 h. After the requisite time period, the reaction was cooled to 0 °C, and water (13 mL) was added. The aqueous layer was transferred to a separatory funnel and extracted with CH_2Cl_2 (3x 10 mL). The combined organic layers were dried over anh. Na_2SO_4, filtered and concentrated to afford an

oily green residue. The reaction was purified by automated CombiFlash chromatography (EtOAc/Hexane) to afford the desired product as a pale-yellow microcrystalline solid (0.231 g, 71%). Mp: 175 °C (decomp). ^{1}H NMR (500 MHz, DMSO-d_6) δ 8.00 (d, J = 8.4 Hz, 1H), 7.89 (s, 1H), 7.79 (d, J = 8.2 Hz, 1H), 7.36 (t, J = 7.6 Hz, 1H), 7.25 (t, J = 7.6 Hz, 1H), 7.18 (s, 1H), 3.95 (t, J = 7.0 Hz, 2H), 3.01 (td, J = 7.6, 1.3 Hz, 2H), 2.13 (p, J = 7.4 Hz, 2H). ^{13}C{^{1}H} NMR (126 MHz, DMSO-d_6) δ 154.9, 131.6, 128.3, 127.5, 127.5, 127.1, 122.1, 122.0, 111.6, 100.6, 99.9, 46.4, 27.7, 22.5. FTIR (cm^{-1}): 306, 3049, 2957, 1627. HRMS-ESI (m/z) calcd for $C_{14}H_{13}N_2O$[M+H]+ 225.1028, found 225.1037.

***N*-(2,2-dimethoxyethyl)-1*H*-indole-2-carboxamide (II-19)**

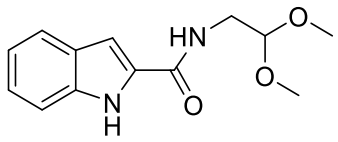

1*H*-indole-2-carboxylic acid (0.322 g, 2.0 mmol) was added to a dry round bottom flask equipped with stir bar. To the flask was added anhydrous DMF (5 mL). Aminoacetaldehyde dimethylacetal (0.44 mL, 4.0 mmol) was added to the flask by syringe, followed by addition of triethylamine (0.84 mL, 6.0 mmol). Benzotriazole-1-yl-oxy-tris-(dimethylamino)-phosphonium hexafluorophosphate (0.885 g, 2.0 mmol) was finally added to the reaction mixture, and this stirred for 2 h at rt under N_2 atm. The reaction mixture was then diluted in water (20 mL) and extracted three times with EtOAc (20 mL ea). The pooled organic layers were washed with brine (3 x 20 mL), then dried over anh. Na_2SO_4, filtered and concentrated to afford a crude reaction mixture. The reaction was purified by automated CombiFlash chromatography (EtOAc/Hexane) to afford the desired product as a pale-yellow solid (0.475 g, 96%). Mp: 124-126 °C. ^{1}H NMR (500 MHz, $CDCl_3$) δ 10.25 (s, 1H), 7.67 (d, J = 8.0 Hz, 1H), 7.49 (d, J = 8.2 Hz, 1H), 7.29 (t, J = 7.9 Hz, 1H), 7.14 (t, J = 7.8 Hz, 1H), 6.96 (s, 1H), 6.76 (t, J = 5.4 Hz, 1H), 4.57 (t, J = 5.3 Hz,

1H), 3.72 (t, *J* = 5.6 Hz, 2H), 3.48 (s, 6H). $^{13}C\{^{1}H\}$ NMR (126 MHz, $CDCl_3$) δ 162.2, 136.8, 130.6, 127.7, 124.6, 122.0, 120.6, 112.2, 103.0, 102.7, 54.9, 41.4. FTIR (cm^{-1}): 3297, 3233, 2937, 1629, 1552. HRMS-ESI (m/z) calcd for $C_{13}H_{17}N_2O_3$[M+H]+ 249.1239, found 249.1260, 217.0987 (-CH_4O).

pyrazino[1,2-a]indol-1(2*H*)-one (II-20)

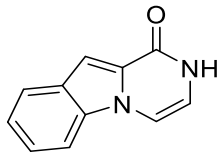

A 1:5 v/v solution of conc. H_2SO_4/Et_2O (1.25 mL:6.2 mL) was prepared in a dry round bottom flask equipped with stir bar. The solution was cooled to 0 °C, then to the stirring solution was added acetal **II-19** (0.124 g, 0.5 mmol) in one portion. The reaction mixture was allowed to proceed at rt under N_2 atm for 24 h. After 24 h, the pH of the solution was adjusted to ~ 8-9 by addition of sat. aq. $NaHCO_3$ solution. The basified mixture was then transferred to a separatory funnel and was extracted three times with EtOAc (100 mL ea.). The organic layers were combined, dried over anh Na_2SO_4, filtered and concentrated to afford a crude reaction mixture. The sample was dissolved in a minimal amount of CH_2Cl_2/MeOH and adsorbed onto silica gel. The reaction was purified by automated CombiFlash chromatography (EtOAc/Hexane) to afford a white solid (0.040 g, 43%). Mp: 255 °C (decomp). ^{1}H NMR (500 MHz, DMSO-d_6) δ 10.75 (s, 1H), 8.07 (d, *J* = 8.3 Hz, 1H), 7.84 (d, *J* = 5.9 Hz, 1H), 7.82 (d, *J* = 8.0 Hz, 1H), 7.39 (t, *J* = 7.4 Hz, 1H, 7.29 (t, *J* = 7.8 Hz, 1H), 7.23 (s, 1H), 6.66 (t, *J* = 5.6 Hz, 1H). $^{13}C\{^{1}H\}$ NMR (126 MHz, DMSO-d_6) δ 157.0, 132.0, 128.2, 126.8, 123.6, 122.3, 122.1, 112.3, 111.8, 106.0, 101.2. FTIR (cm^{-1}): 3120, 3043, 1625, 1369. HRMS-ESI (m/z) calcd for $C_{11}H_9N_2O$[M+H]+ 185.0715, found 185.0723.

2-methylpyrazino[1,2-a]indol-1(2*H*)-one (II-21)

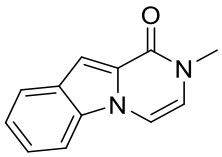

Alkene **II-20** (0.111 g, 0.6 mmol) was added to a dry round bottom flask equipped with stir bar. To the flask was added dry THF (5 mL). The reaction flask was cooled to 0 °C and sodium hydride (0.050 g, 1.2 mmol, 60 wt% in mineral oil suspension) was added in one portion. The reaction was stirred at 0 °C for 30 min under N_2 atm. Methyl iodide (0.08 mL, 1.2 mmol) was added to the flask by syringe, and the reaction was removed from ice bath. The resulting reaction mixture stirred at rt under N_2 atm for 22 h. After 22 h, the reaction was cooled to 0 °C, and the pH of the solution was adjusted to ~6 by slow addition of sat. NH_4Cl solution. The reaction was further diluted in water (5 mL) and transferred to a separatory funnel. The aqueous layer was extracted twice with EtOAc (50 mL ea). The organic layers were pooled, dried over anh. Na_2SO_4, filtered and concentrated to afford a crude solid. The reaction was purified by automated CombiFlash chromatography (CH_2Cl_2/MeOH) and afforded the desired product as a yellow amorphous solid (0.112 g, 93%). Mp: 144-146 °C. ^{1}H NMR (500 MHz, DMSO-d_6) δ 8.06 (d, J = 8.6 Hz, 1H), 7.93 (d, J = 6.0 Hz, 1H), 7.82 (d, J = 8.1 Hz, 1H), 7.39 (t, J = 7.3 Hz, 1H, 7.29 (t, J = 7.7 Hz, 1H), 7.23 (s, 1H), 6.91 (d, J = 5.8 Hz, 1H), 3.42 (s, 3H). ^{13}C{^{1}H} NMR (126 MHz, DMSO-d_6) δ 156.3, 131.8, 127.7, 123.6, 122.4, 122.1, 117.2, 111.7, 106.1, 101.0, 34.5. FTIR (cm^{-1}): 3105, 3045, 2937, 1667, 1629. HRMS-ESI (m/z) calcd for $C_{12}H_{11}N_2O$[M+H]+ 199.0871, found 199.0888.

2-benzylpyrazino[1,2-a]indol-1(2*H*)-one (II-22)

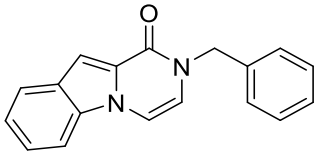

Alkene **II-20** (0.110 g, 0.6 mmol) was added to a dry round bottom flask equipped with stir bar. To the flask was added dry THF (5 mL). The reaction flask was cooled to 0 °C and sodium hydride (0.053 g, 1.2 mmol, 60 wt% in mineral oil suspension) was added in one portion. The reaction was stirred at 0 °C for 30 min under N_2 atm. Benzyl bromide (0.15 mL, 1.2 mmol) was added to the flask by syringe, and the reaction was removed from ice bath. The resulting reaction mixture stirred at rt under N_2 atm for 22 h. After 22 h, the reaction was cooled to 0 °C, and the pH of the solution was adjusted to ~6 by slow addition of sat. NH_4Cl solution. The reaction was further diluted in water (5 mL) and transferred to a separatory funnel. The aqueous layer was extracted twice with EtOAc (50 mL ea). The organic layers were pooled, dried over anh. Na_2SO_4, filtered and concentrated to afford a crude solid. The reaction was purified by automated CombiFlash chromatography (EtOAc/Hexane) and afforded the desired product as a beige solid (0.126 g, 77%). Mp: 140-142 °C. ^{1}H NMR (500 MHz, DMSO-d_6) δ 8.06 (d, J = 8.2 Hz, 1H), 7.96 (d, J = 5.9 Hz, 1H), 7.84 (d, J = 8.1 Hz, 7.40 (t, J = 7.6Hz, 1H), 7.39-7.27 (m, 7 H), 5.10 (s, 2H). ^{13}C{^{1}H} NMR (126 MHz, DMSO-d_6) δ156.0, 137.5, 132.0, 128.6, 127.6, 127.5, 127.0, 123.8, 122.4, 122.1, 116.4, 111.7, 106.7, 101.9, 49.3. HRMS-ESI (m/z) calcd for $C_{18}H_{15}N_2O$[M+H]+ 275.1184, found 275.1190.

2-phenylpyrazino[1,2-a]indol-1(2H)-one (II-23)

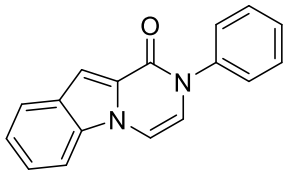

Alkene **II-20** (0.112 g, 0.6 mmol) was dissolved in dry CH_2Cl_2 in a round-bottom flask equipped with stir bar. Phenylboronic acid (0.148 g, 1.2 mmol) was added to the reaction flask, followed by addition of copper (II) acetate (0.240 g, 1.2 mmol), pyridine (0.24 mL), and 4 Å molecular sieves.

An air balloon was attached to the reaction flask, the this stirred at rt for 24 h. After 24 h, the reaction mixture was diluted in CH_2Cl_2 and filtered through celite plug. The resulting filtrate was concentrated to afford a crude residue. The crude residue was dissolved in a minimal amount of CH_2Cl_2/MeOH and adsorbed onto silica gel. The reaction was purified by automated CombiFlash chromatography (CH_2Cl_2/MeOH) and afforded the desired product as a pale-yellow microcrystalline solid (0.106 g, 67%). Mp: 241-251 °C ^{1}H NMR (500 MHz, DMSO-d_6) δ 8.14 (d, J = 8.4 Hz, 1H), 8.04 (d, J = Hz, 1H), 7.86 (d, J = 7.9 Hz, 1H), 7.56-7.51 (m, 4H), 7.46-7.43 (m, 2H), 7.36 (s, 1H), 7.33 (t, J = 7.4 Hz, 1H), 6.99 (d, J = 6.1 Hz, 1H). ^{13}C{^{1}H} NMR (126 MHz, DMSO-d_6) δ 155.6, 139.9, 132.2, 129.1, 127.8, 127.5, 127.1, 126.9, 124.1, 122.5, 122.2, 116.8, 111.9, 106.7, 102.9. FTIR (cm^{-1}): 3105, 3045, 2937, 1667, 1629. HRMS-ESI (m/z) calcd for $C_{17}H_{13}N_2O$[M+H]+ 261.1028, found 261.1040.

REFERENCES

1. Azevedo, L. M.; Lansdell, T. A.; Ludwig, J. R.; Mosey, R. A.; Woloch, D. K.; Cogan, D. P.; Patten, G. P.; Kuszpit, M. R.; Fisk, J. S.; Tepe, J. J., *J. Med. Chem.*, **2013**, *56*, 5974.

2. McDaniel, T. J.; Lansdell, T. A.; Dissanayake, A. A.; Azevedo, L. M.; Claes, J.; Odom, A. L., *Bioorg. Med. Chem.*, **2016**, *24*, 2441.

3. Giletto, M. B.; Osmulski, P. A.; Jones, C. L.; Gaczynska, M. E.; Tepe, J. J., *Org. Biomol. Chem.*, **2019**, *17*, 2734-2746.

4. Kinnel, R. B.; Gehrken, H. P.; Scheuer, P. J., J. Am. Chem. Soc., **1993**, *115*, 3376-3377.

5. Kinnel, R. B.; Gehrken, H.-P.; Swali, R.; Skoropowski, G.; Scheuer, P. J., *J. Org. Chem.*, **1998**, *63*, 3281-3286.

6. R.P., M.; Zollinger, M.; Jones, P. G.; Kelter, G.; Fiebig, H.-H.; Lindel, T., *Eur. J. Org. Chem.*, **2012,** 685-698.

7. Lindel, T., *Alkaloids Chem. Biol.*, **2017,** *77*, 117-219.

8. Lansdell, T. A.; Hewlett, N. M.; Skoumbourdis, A. P.; Fodor, M. D.; Seiple, I. B.; Su, S.; Baran, P. S.; Feldman, K. S.; Tepe, J. J., *J. Nat. Prod.*, **2012**, *75*, 980-985.

9. Beck, P.; Lansdell, T. A.; Hewlett, N. M.; Tepe, J. J.; Groll, M., *Angew. Chem., Int. Ed. Engl.*, **2015,** *54*, 2830-2833.

10. Gallastegui, N.; Beck, P.; Arciniega, M.; Huber, R.; Hillebrand, S.; Groll, M., *Angew. Chem., Int. Ed. Engl.*, **2012**, *51*, 247-249.

11. Hewlett, N. M.; Tepe, J. J., *Org. Lett.* **2011**, *13*, 4550-4553.

12. Feldman, K. S.; Fodor, M. D., *J. Am. Chem. Soc.*, **2008**, *130*, 14964-14965.

13. Picon, S.; Dau, E. T. T.; Martin, M.-T.; Retallieau, P.; Zaparucha, A.; Al-Mourabit, A., *Org. Lett.*, **2009**, *11*, 2523-2526.

14. Su, S.; Rodriguez, R. A.; Baran, P. S., *J. Am. Chem. Soc.*, **2011**, *133*, 13922-13925.

15. Ding, H.; Roberts, A. G.; Harran, P. G., *Angew. Chem., Int. Ed. Engl.*, **2012**, *51*, 4340-4343.

16. Foley, L. H.; Buchi, G., *J. Am. Chem. Soc.* **1982**, *104*, 1776-1777.

17. Weise, K. J.; Yakushijin, K.; Horne, D. A., *Tetrahedron Lett.* **2002**, *43*, 5135-5136.

18. Hewlett, N. M., **2014**. *New methodology to access small molecule proteasome inhibitors - including the total synthesis of dibromophakellin, dibromophakellstatin, and analogs*. Michigan State University.

19. Gazieva, G. A.; Anikina, L. V.; Nechaeva, T. V.; Pukhov, S. A.; Karpova, T. B.; Popkov, S. V.; Nelyubina, Y. V.; Kolotyrkina, N. G.; Kravechenko, A. N., *Eur. J. Med. Chem.*, **2017,** *140*, 141-154.

20. Imaoka, T.; Akimoto, T.; Iwamoto, O.; Nagasawa, K., *Chem. Asian J.*, **2010**, *5*, 1810-1816.

21. Su, W.-G.; Dai, G.; Xiao, K.; Jia, H.; Venable, J. D.; Bembenek, S. D. Novel heteroaryl and heterocycle compounds, compositions and methods. WO2014015675A1, 01/30/2014, 2014.

APPENDIX

Figure 2.4 ^{1}H and $^{13}C\{^{1}H\}$ NMR spectra of compound **II-12**

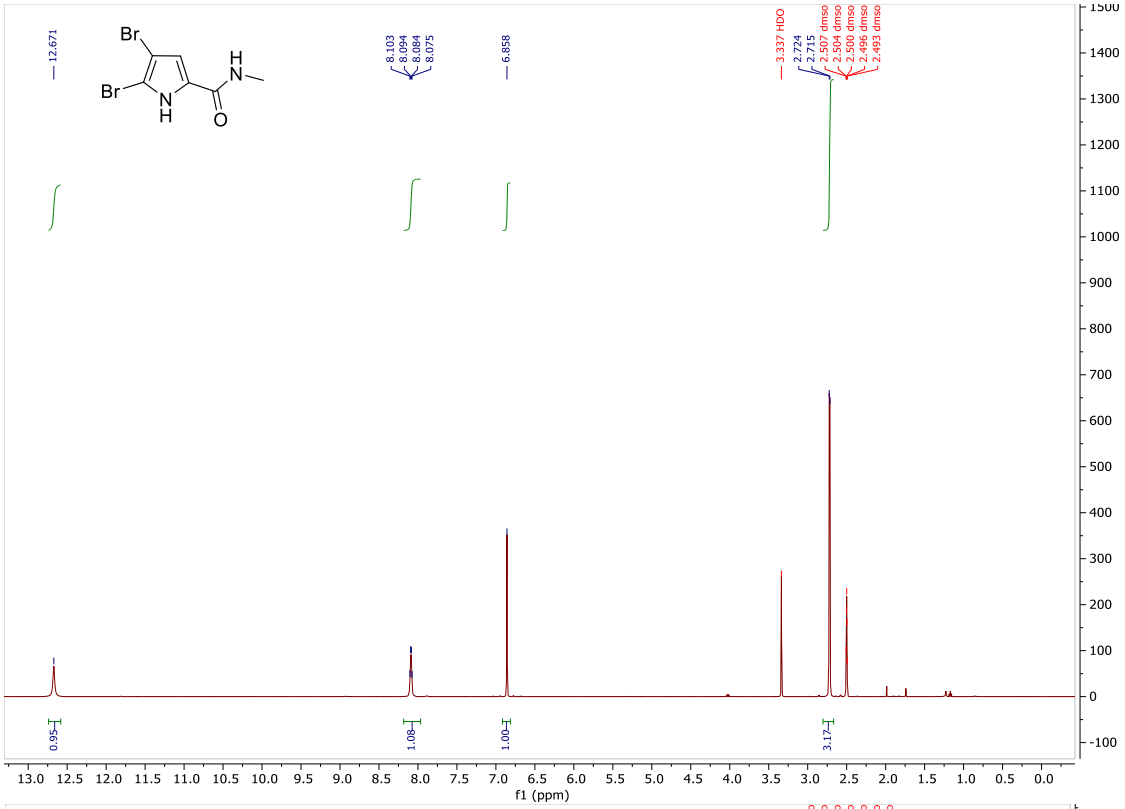

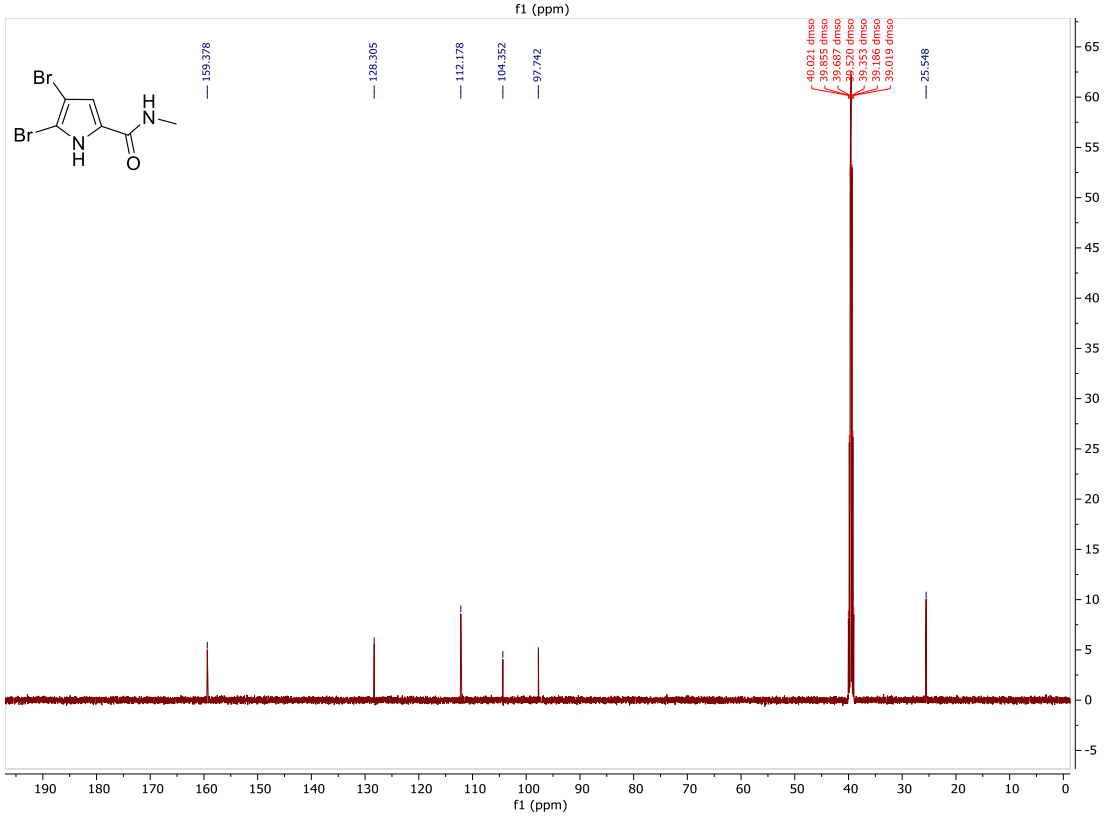

Figure 2.5 ^{1}H and $^{13}C\{^{1}H\}$ NMR spectra of compound **II-13**

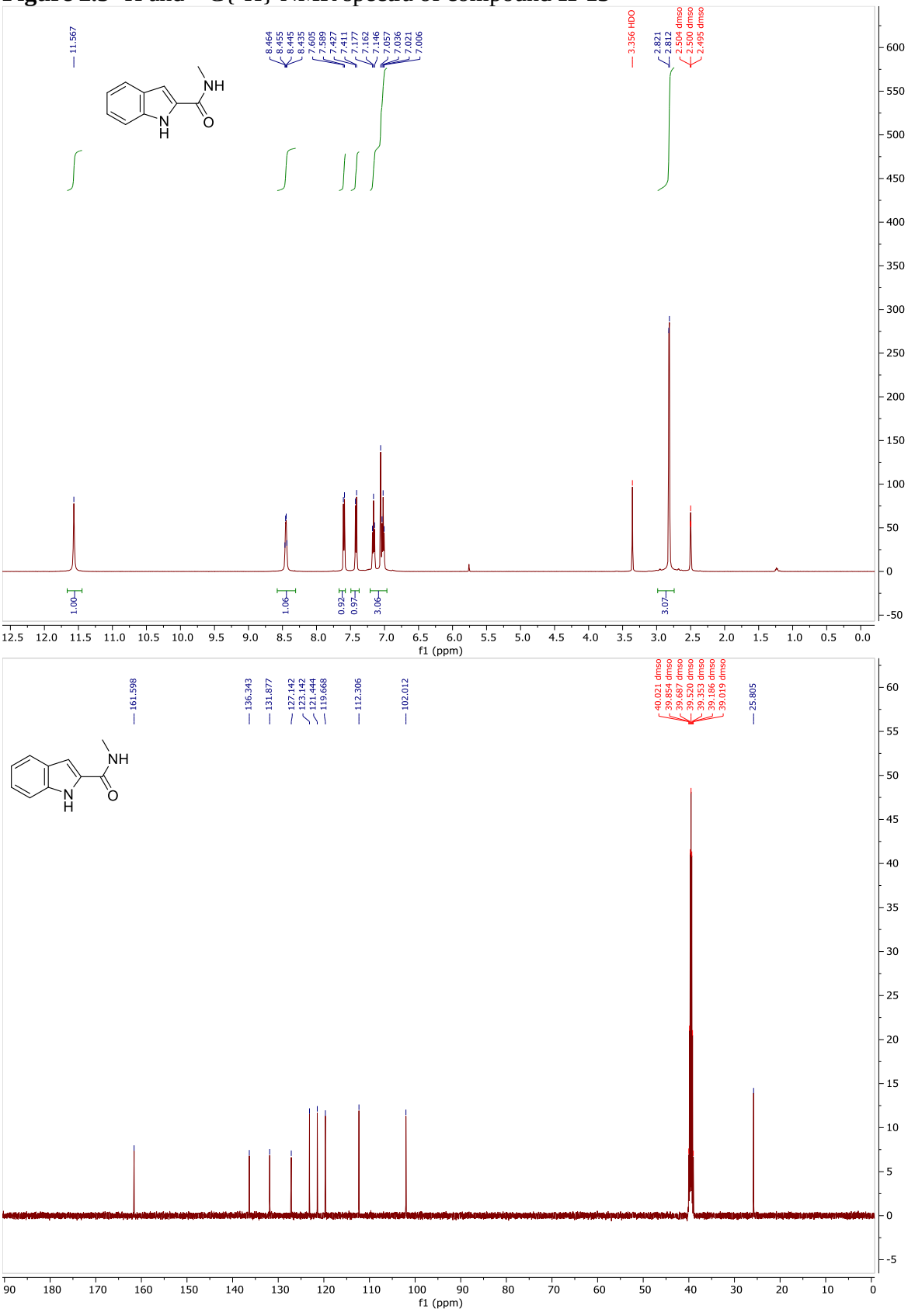

Figure 2.6 ^{1}H and $^{13}C\{^{1}H\}$ NMR spectra of compound **II-14**

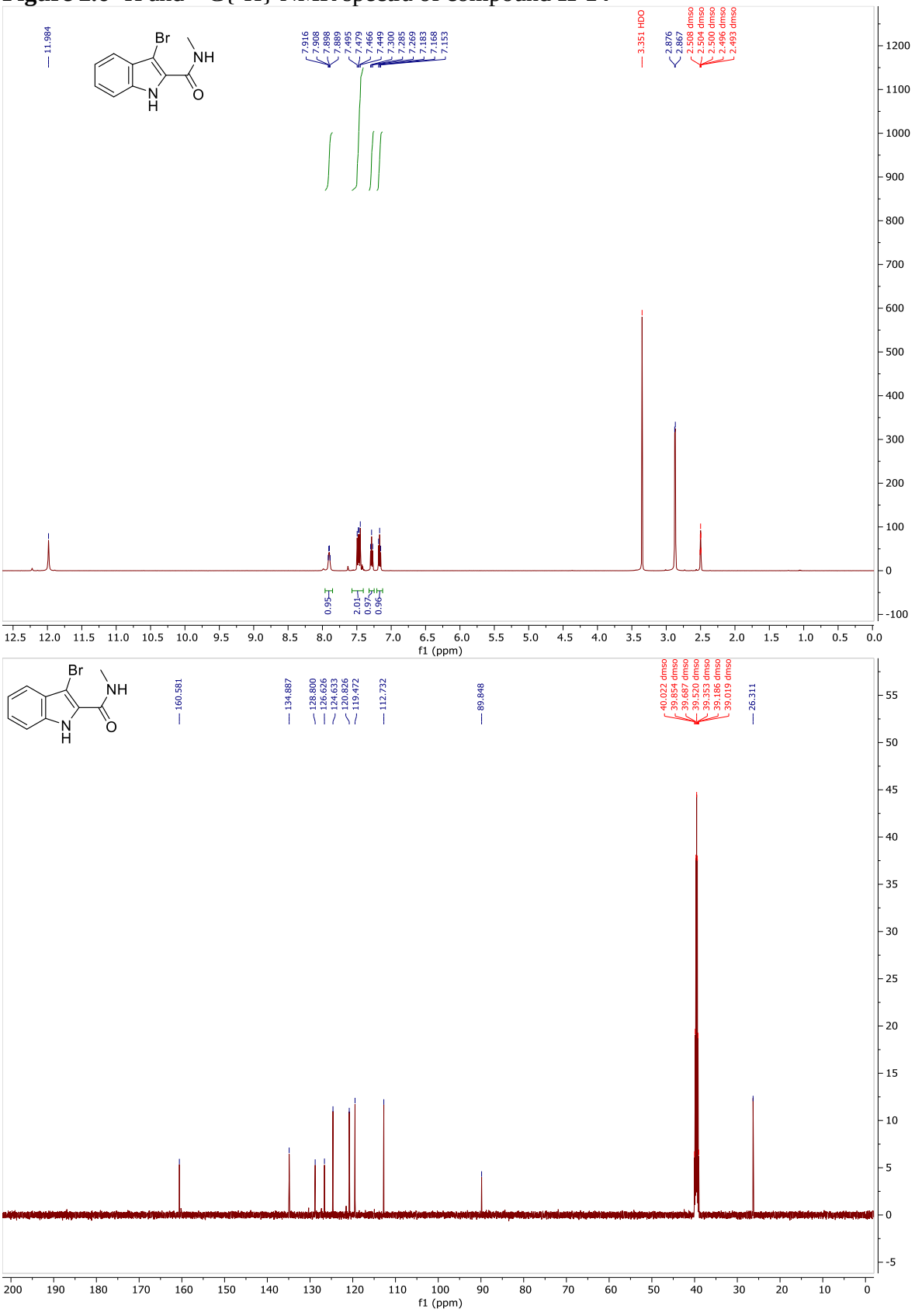

Figure 2.7 ^{1}H and $^{13}C\{^{1}H\}$ NMR spectra of compound **II-15**

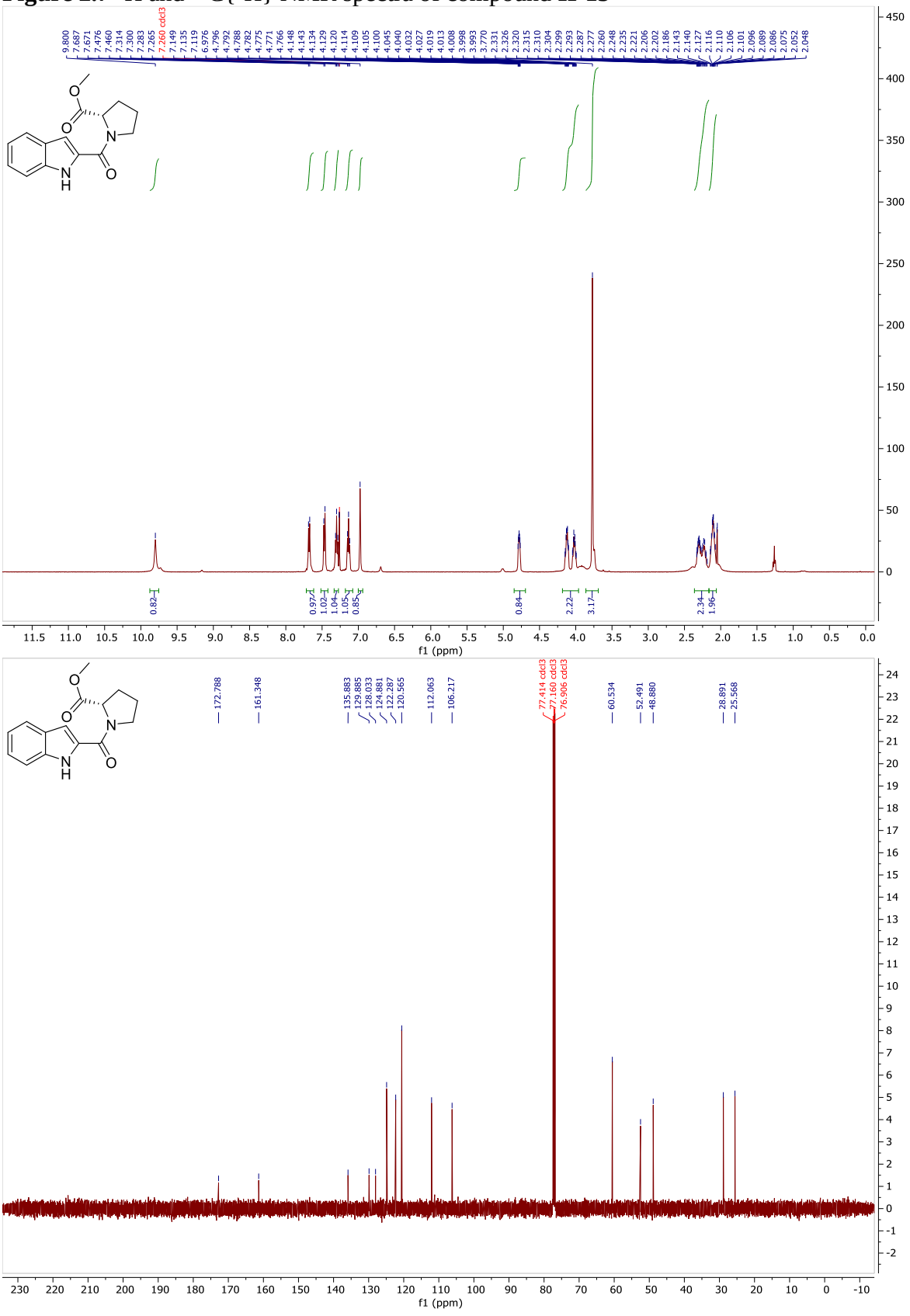

Figure 2.8 ^{1}H and $^{13}C\{^{1}H\}$ NMR spectra of compound **II-16**

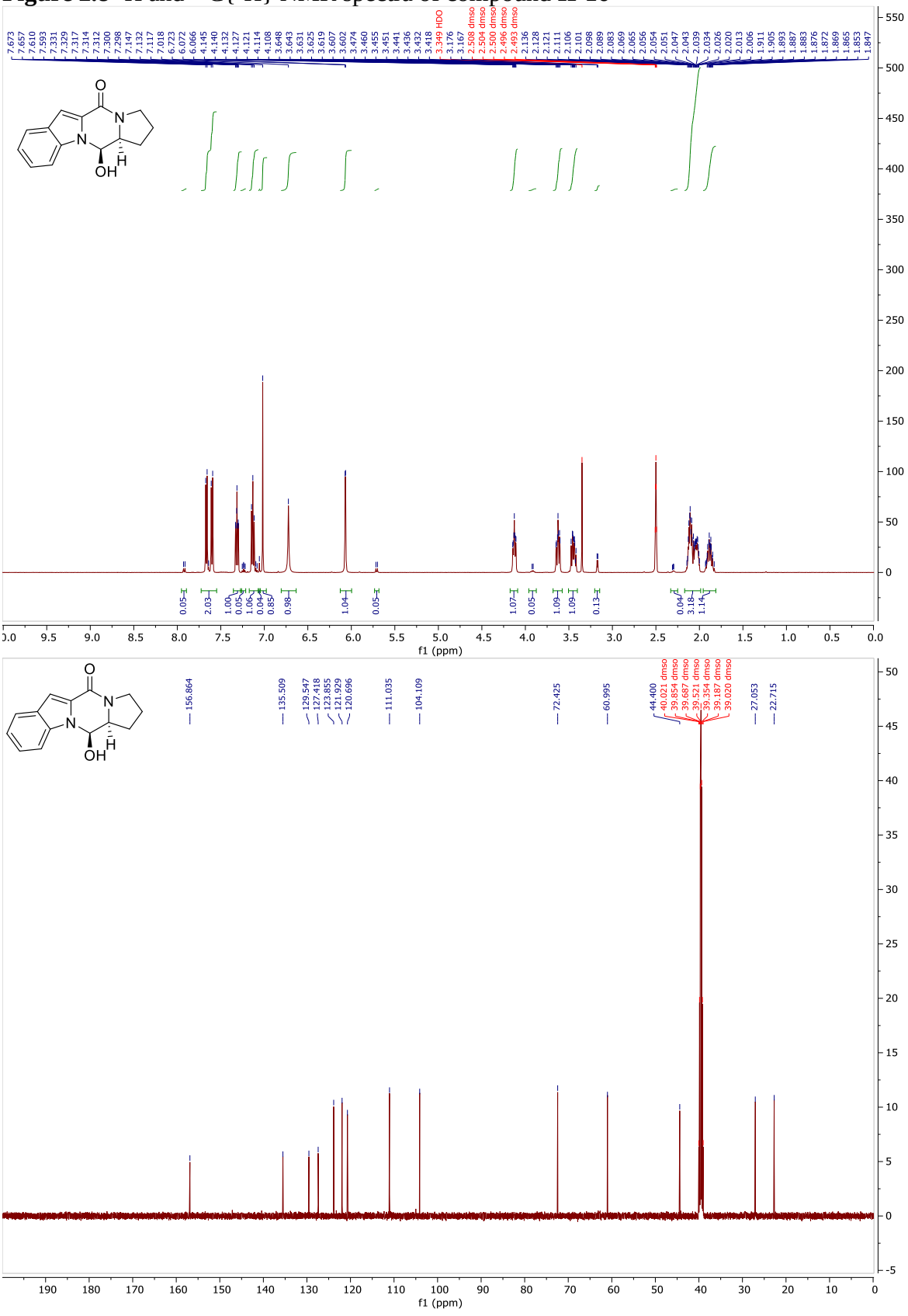

Figure 2.9 ^{1}H and $^{13}C\{^{1}H\}$ NMR spectra of compound **II-17**

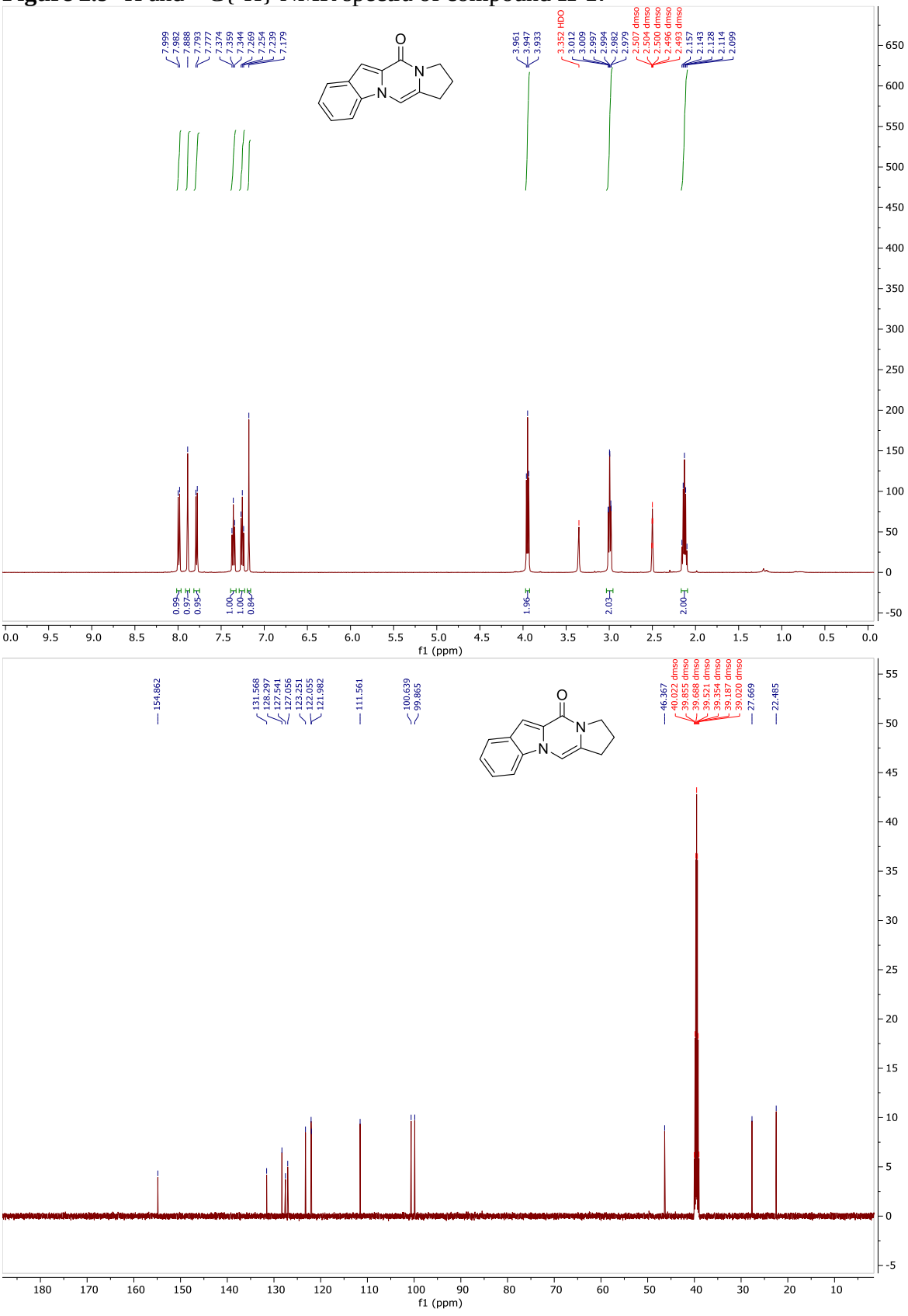

Figure 2.10 ^{1}H and $^{13}C\{^{1}H\}$ NMR spectra of compound **II-19**

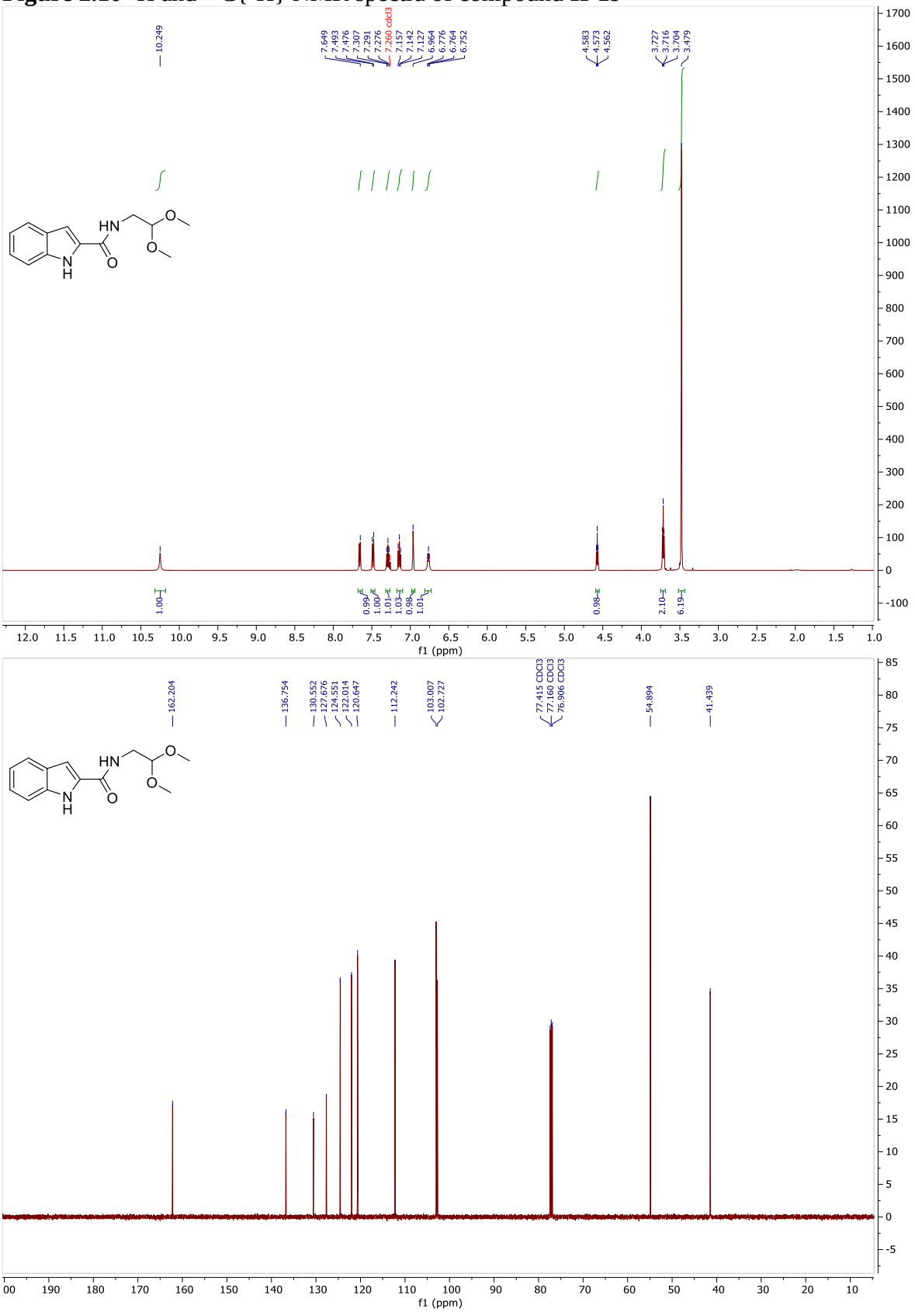

Figure 2.11 ^{1}H and $^{13}C\{^{1}H\}$ NMR spectra of compound **II-20**

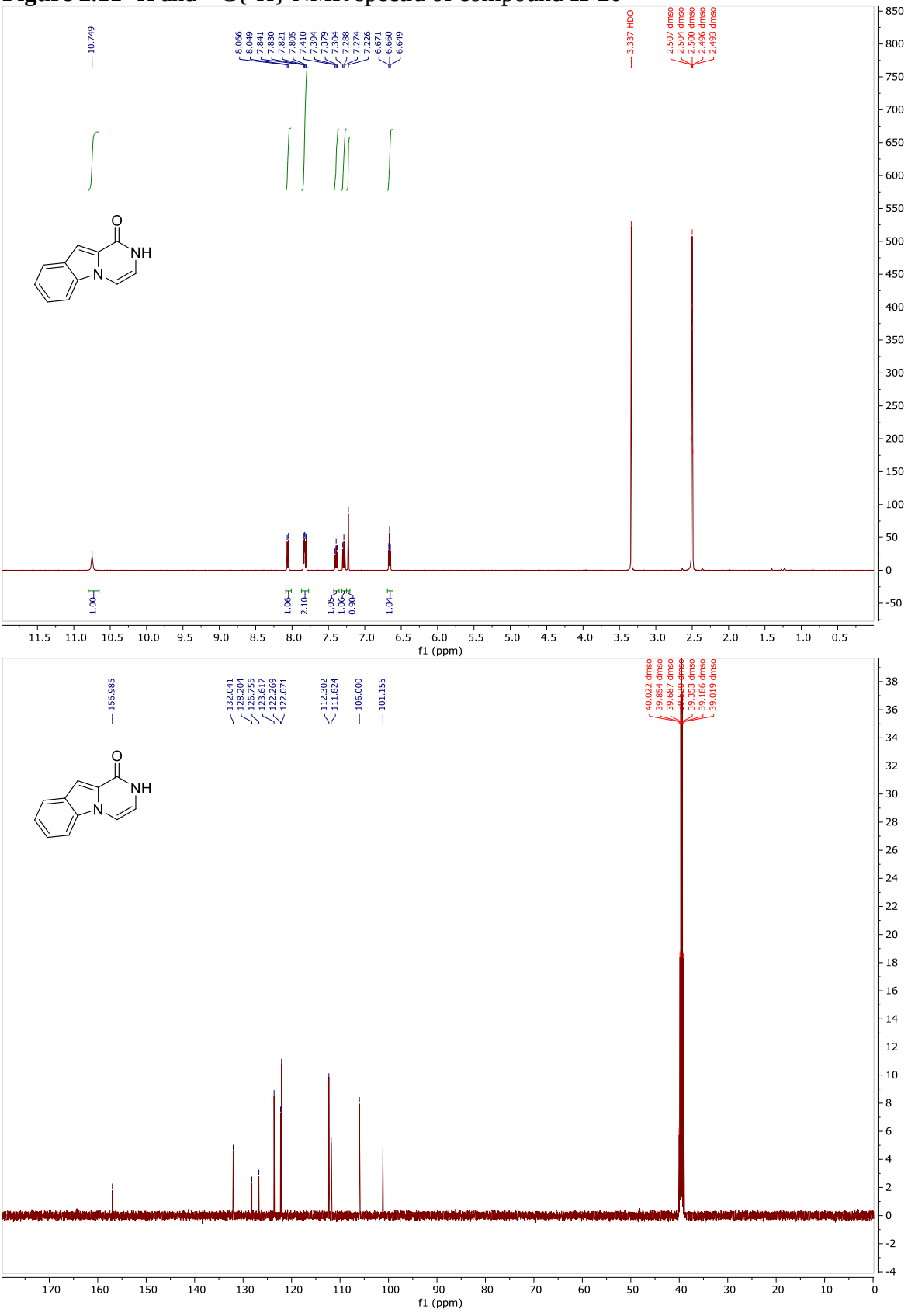

Figure 2.12 ^{1}H and $^{13}C\{^{1}H\}$ NMR spectra of compound **II-21**

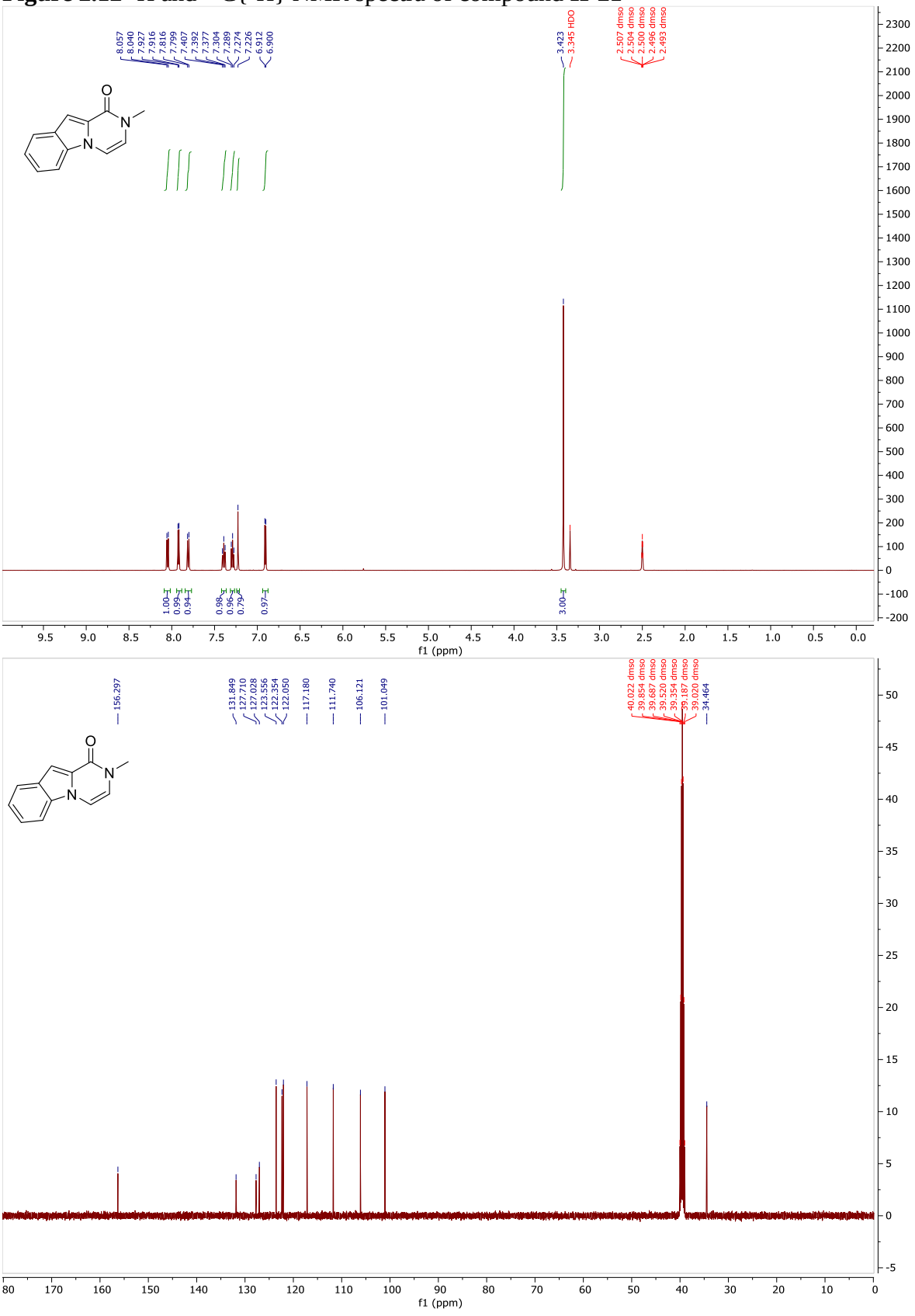

Figure 2.13 ^{1}H and $^{13}C\{^{1}H\}$ NMR spectra of compound **II-22**

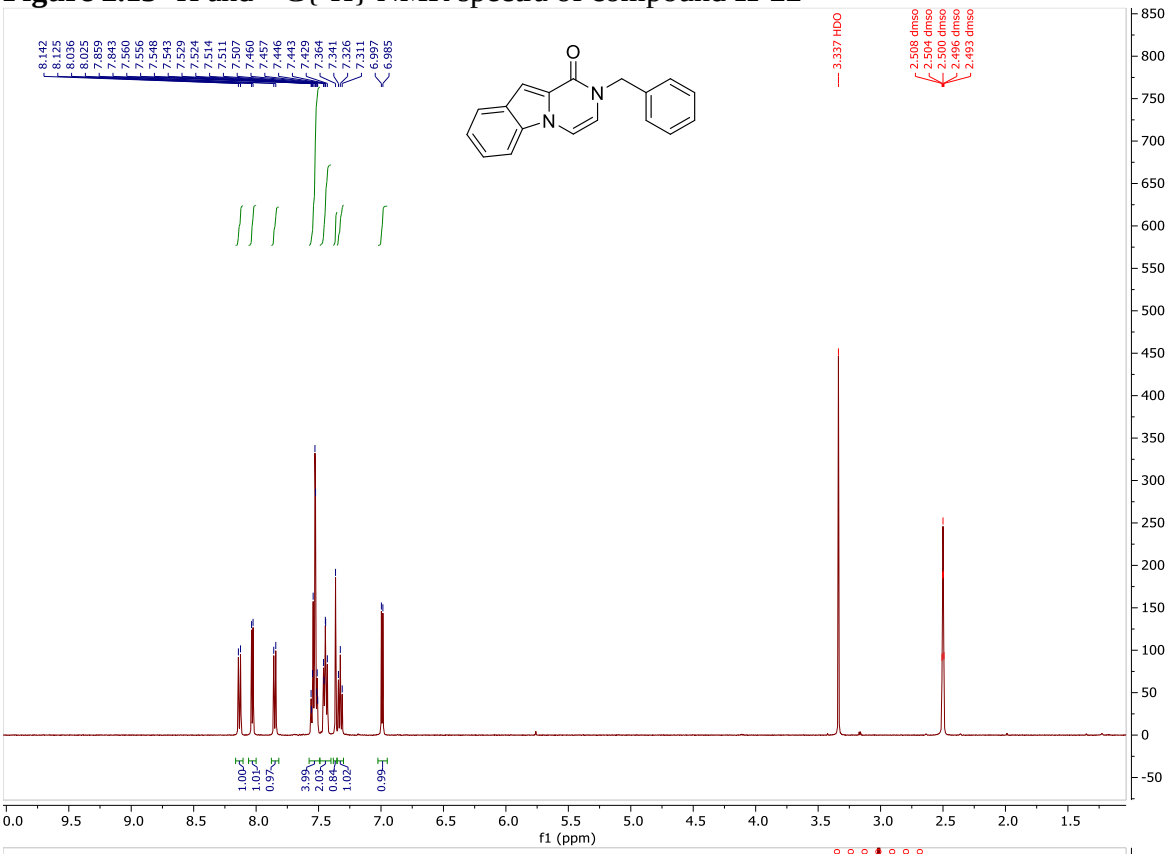

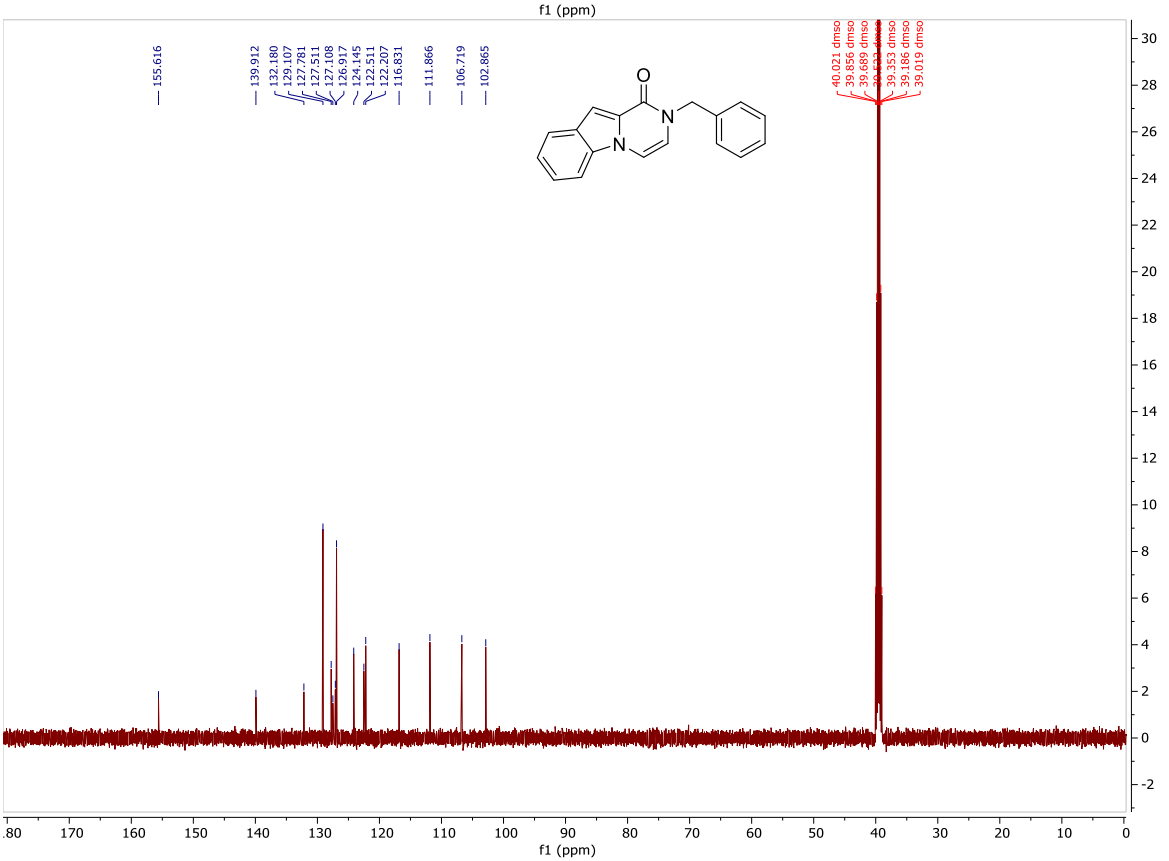

Figure 2.14 ^{1}H and $^{13}C\{^{1}H\}$ NMR spectra of compound **II-23**

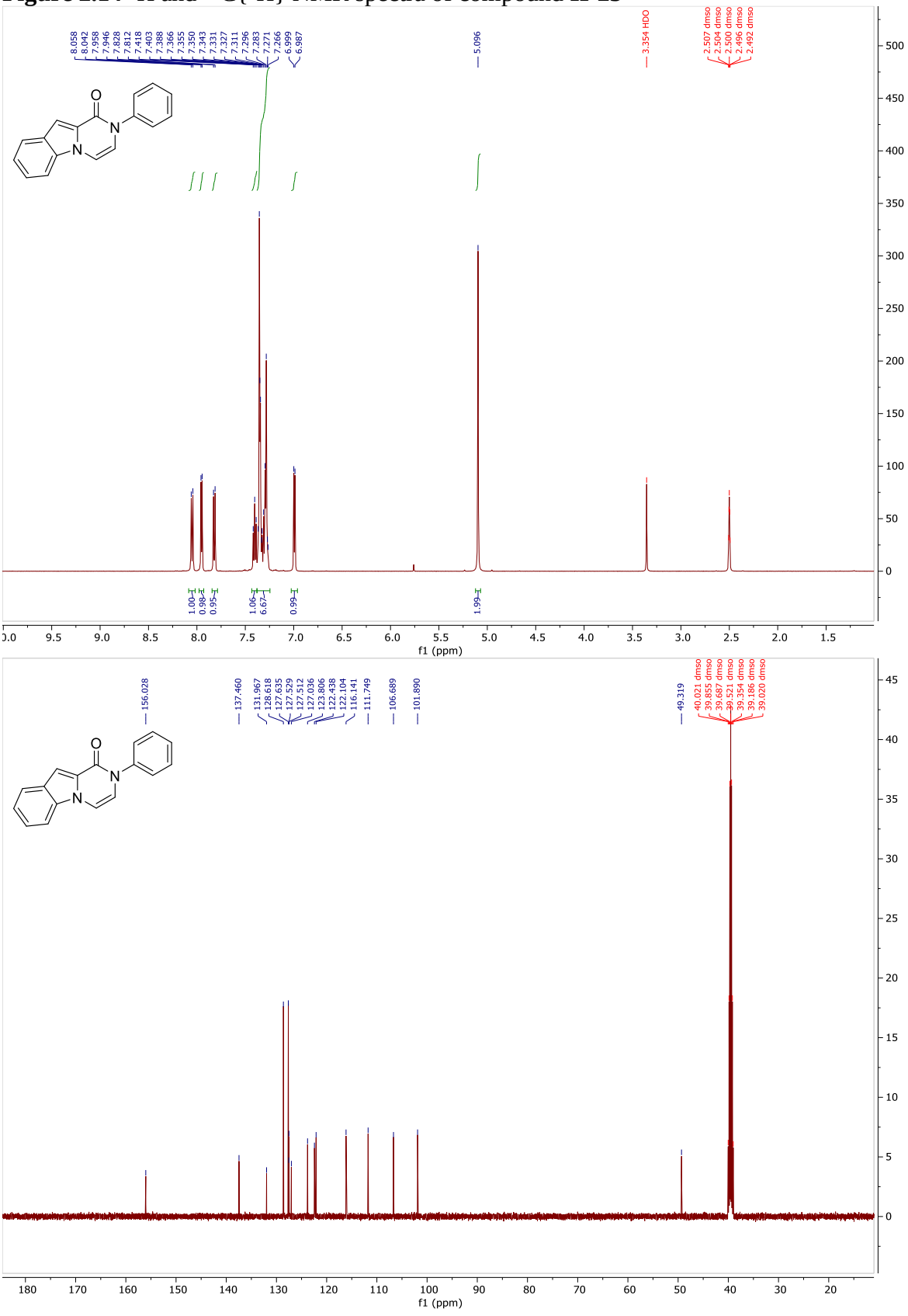

Chapter 3: Rh(III)-catalyzed C-H activation/annulation to access urea-fused isoquinolones[1†]

3.1 Introduction & Background

The urea- and guanidine-fused -piperazinone and -pyridinone bicyclic scaffold is a common feature among the pyrrole-imidazole alkaloid family of natural products (**Figure 3.1**). This core has been highlighted as a necessary component that contributes to the biological activities of the natural products and analogs;[2-4] thus, expeditious access to this bicyclic core would be advantageous to further explore natural product mimics of this family.

Figure 3.1 Examples of pyrrole alkaloids bearing urea- and guanidine-fused pyridone and piperazinone cores

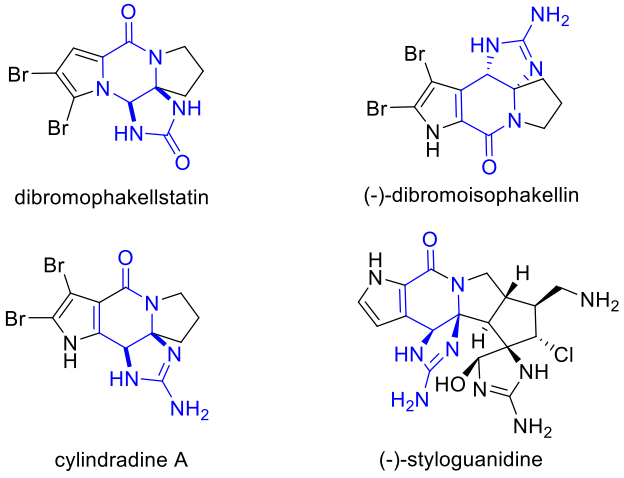

A variety of methods exist for the construction of the urea- or guanidine-fused piperazinone core including intramolecular diamination upon imidazole species[5-10] or elaboration of the central piperazinone ring.[11, 12] Conversely, access to the fused dihydropyridone core is underrepresented in literature. Typical access to the bicyclic ring occurs through isomerization of the isomeric natural products[6] and functionalization of pyridone core.[13, 14] The notable challenge associated

† This chapter is reproduced in part with permission from reference 1. Copyright 2022 American Chemical Society.

with construction of this scaffold has been a considerable obstacle toward the synthesis of complex pyrrole-alkaloids such as the styloguanidines, which have yet to be the subject of total synthesis.

One approach which allows expeditious access to annulated heterocyclic scaffolds is C-H activation using transition metal catalysts. While cross-coupling approaches rely on the use of prefunctionalized materials, directed oxidative approaches utilize an internal directing group which can coordinate to the metal center and facilitate functionalization at the *ortho*-position relative to the directing group (**Scheme 3.1**). This approach also requires the use of external oxidants in the form of copper or silver salts to regenerate the active metal species.

Scheme 3.1 General directed C-H annulation using a directing group

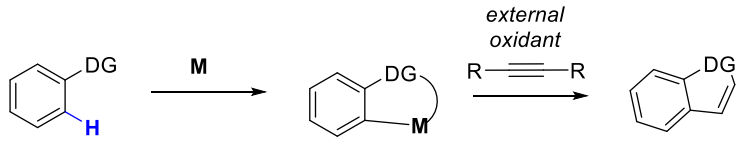

In 2007, Satoh & Miura reported the use of a Rh(I)/Rh(III) cycle for the annulation of benzoic acids with internal alkynes to access isocoumarin scaffolds.[15, 16] It was in this initial study that the specific precatalyst $[RhCp^*Cl_2]_2$ was reported as a superior rhodium species for this type of transformation. Several other Rh species including $RhCl_3•H_2O$, $Rh(acac)_3$, $[RhCl(cod)]_2$, and $[RhCl(C_2H_4)_4]_2$ were also evaluated but failed to provide more than trace amounts of the isocoumarin product.[15] The reaction required the use of external oxidant $Cu(OAc)_2•H_2O$, which could be used catalytically when an ambient atmosphere was applied to the system. Under these conditions, the formation of naphthalene byproducts were observed due to a decarboxylative route and introduction of multiple alkyne species.

Scheme 3.2 Satoh & Miura's Rh-catalyzed access to isocoumarins under oxidative conditions

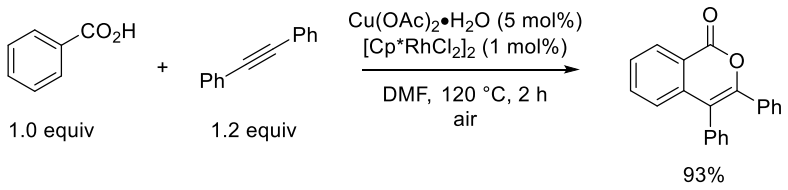

In addition to benzoic acids, many other coordinating groups have been reported which are capable of undergoing similar transformations including phenols, imines, heterocycles such as phenylazoles or pyridines, and amides as well as many others. These approaches have allowed access to a number of different heterocyclic products including isoquinolone and pyridinone cores through [4+2] annulations. Some of the implicit drawbacks associated with the initial work in this realm were the requirement of high temperatures and external oxidants to access the desired products. These challenges led to subsequent work towards developing alternative oxidative conditions for annulation to take place.

One approach which has arisen is the use of an internal oxidizing directing group ($DG^{ox)}$ which could afford a redox-neutral environment by which reactions would take place. This group would not only retain the ability to coordinate to the metal center and direct C-H activation towards the ortho position, but it would also be responsible for re-oxidizing the metal catalyst to its active oxidation state in the system. Typically, the use of these groups allowed for the reaction to take place under milder conditions relative to the previous oxidative approaches. Pioneering work by Gerfaud et al.,[17] Cui and Wu *et al.*[18] and the Hartwig group[19] demonstrated the utility of N−O bonds as a form of internal oxidant/directing group in the presence of palladium catalysts. While the work by Gerfaud et al and the Hartwig appears to undergo an oxidative addition of Pd(0) to the N-O bond directly, in the report by Cui and Wu et al., the N-O bond in the quinoline-*N*-oxide

substrates acts as terminal oxidant to regenerate the active Pd(II) catalyst in the system (**Scheme 3.3**).

Scheme 3.3 Cui and Wu's use of quinoline-*N*-oxides as DG^{ox}

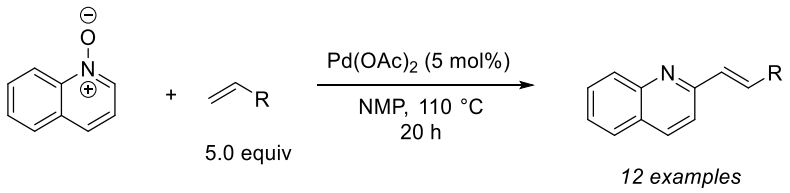

The Fagnou[20, 21] and Glorius[22] groups subsequently introduced benzoyl hydroxamates as substrates for Rh(III)-catalyzed annulations to access isoquinolones and 3,4-dihydroisoquinolones using alkenes and alkynes as coupling partners (**Scheme 3.4**). The choice of internal oxidant was key in achieving the formation of annulated products; *N*-pivaloyloxy benzohydroxamates were identified as the optimum partners in these reactions to afford the ring-closed annulation product. The use of alkoxy benzohydroxamates did not provide the annulation products, but rather underwent a Fujiwara-Moritani "oxidative Heck"-type reaction to afford *ortho*-alkenylated products when alkenes were used as coupling partners.

Scheme 3.4 Seminal work by Fagnou and Glorius

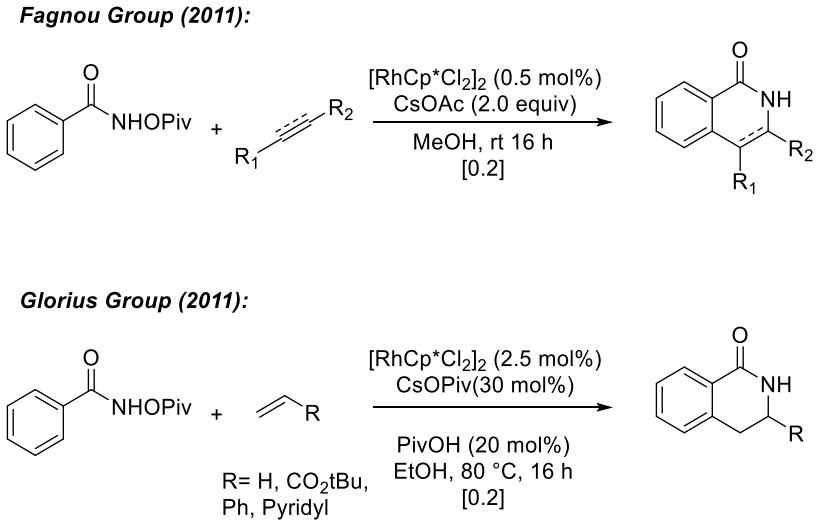

Following the discoveries by Fagnou and Glorius, computational studies by Xu *et al*[23] investigated the possible effects of internal oxidizing groups and differing outcomes in this type of reaction. The use of non-coordinating alkoxy hydroxamate was reported to produce Heck-like products resulting from β-hydride elimination. However, the coordinative ability of the pivaloyl group contributes directly to the alternative product outcome in this reaction.

The general mechanism of the Rh(III)-catalyzed C-H activation/annulation of alkenes and *N*-pivaloyloxy benzohydroxamates as reported from computational studies by Xu *et al.* is shown in **Scheme 3.5** below. In the first step, *N*-pivaloyloxy benzohydroxamate undergoes N-activation to form intermediate **II**. Subsequent C-H activation takes place to afford the 5-membered rhodacycle **III**. Coordination and migratory insertion of the olefin moiety affords the 7-membered intermediate **IV**. The coordination of the pivaloyl group with the Rh-center affords a coordinatively saturated species which is stabilized and circumvents the formation of the Heck-like product via a β-hydride elimination pathway. Acyl migration of the pivaloyl group to the Rh-center affords the reactive Rh(V) nitrene intermediate **V**. This intermediate then undergoes reductive elimination to form the sp^3-sp^3 C-N bond and afford the cyclic intermediate **VI**. This finally undergoes protonation with the generated acetic acid equivalents in the reaction medium to afford the annulated product.

Scheme 3.5 General mechanism of Rh(III)-cat C-H activation/annulation

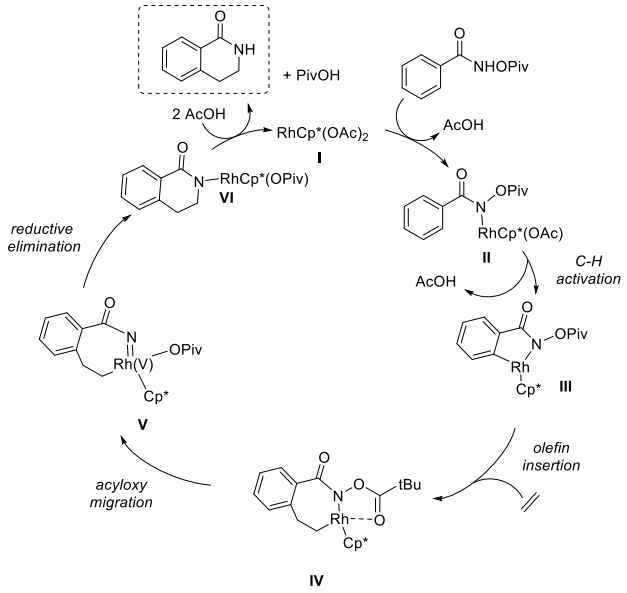

There are several proposed reaction modes for Rh-mediated C-H bond cleavage: concerted metalation deprotonation (CMD), oxidative addition (OA), Friedel-Crafts type electrophilic aromatic substitution (S_EAr), and σ-complex assisted metathesis (σ-CAM). A general scheme of these modes is shown below (**Scheme 3.6**).[24] In their seminal papers, Fagnou and co-workers implicated the CMD mechanism as the mode of C-H activation based upon computational studies.[21] This mode of C-H bond cleavage has been since considered as the general mode by which Rh(III)-catalyzed C-H annulations take place. In this mode, the formation of the Rh-C bond and deprotonation by the acetate ligand occur simultaneously. Acetic acid is then liberated after this step, and the 5-membered rhodacycle is formed.

Scheme 3.6 Proposed modes of Rh-mediated C-H bond cleavage

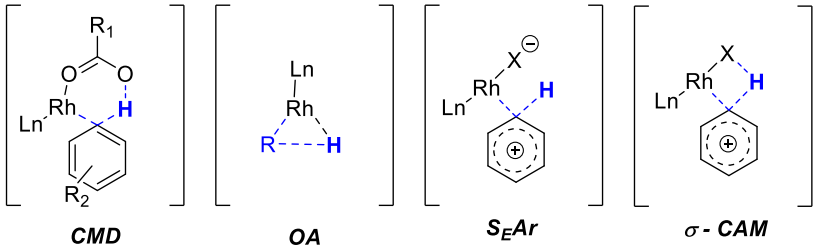

The seminal studies by Fagnou and Glorius have since led to the development of myriad methods to access isoquinolones and substituted 3,4-dihydroisoquinolone scaffolds and other heterocycles.[25-43] Regioselectivity in these reactions with respect to unsymmetrically substituted alkene coupling partners is often governed by several factors, however the Rovis group has investigated modification of the cyclopentadienyl ligands to alter reaction outcomes.[31] For example, introduction of a sterically hindered di-*tert*-butyl cyclopentadienyl ligand afforded high regioselectivity when simple monoalkylated alkene substrates were utilized. This work demonstrated the use of ligand control in the system to improve regioselective outcomes.

Further alteration of the cyclopentadienyl ligand has included the development of asymmetric conditions to afford enantioselective C-H annulations. The Rovis and Cramer groups both developed asymmetric conditions to access enantioselective transformations.[44, 45] Ward and Rovis reported the generation of a chiral environment by developing an artificial metalloenzyme which contained the Rh-species bound through a biotin linker.[44] The Cramer group has focused on development of chiral cyclopentadienyl ligands to afford enantioselectivity in these reactions.[45]

The identity of the alkene and alkyne coupling partner has varied greatly, however it has been largely designated towards electron-neutral and electron-deficient substrates. One exception of note is that conducted by Webb *et al* in 2014 (**Scheme 3.7**).[46] In this study, researchers sought to evaluate the utility of electron-dense alkene substrates which are noticeably absent from

previous literature approaches with the exception of one example presented by the Fagnou group. Vinyl acetate was identified as a viable acetylene equivalent in this study to access a variety of substituted isoquinolone scaffolds in low to excellent yields (48 - 99%). Other electron-dense alkenes including *n*-butyl vinyl ether, dihydrofuran, and *N*-Boc protected dihydropyrrole were also identified in this study as viable coupling partners to access tetrahydroisoquinolone, and dihydroisoquinolone scaffolds. This work represents a unique example in which electron-dense alkenes are utilized in the annulations.

Scheme 3.7 Methodology by Webb *et al* with electron-dense alkene substrates

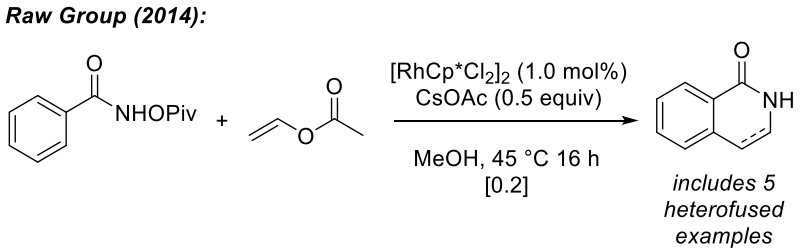

In our continued efforts to further explore the biological activity of the pyrrole-alkaloid natural products and their small molecule analogs,[2, 3, 12, 47-50] the development of novel methods to access scaffolds reminiscent of the pyrrole-alkaloid scaffolds is an ever-present need. As discussed in the previous chapter, expeditious access to the desired urea- and guanidine-fused scaffolds is challenging. In particular, application of established methods used to construct the fused piperidone scaffolds typically fail when access to the fused pyridone core is instead desired.

The previous literature examples of Rh(III)-catalyzed C-H activation/annulations served as initial inspiration in the subsequent methodology, which sought to explore the use of heterocyclic diazole substrates as alkene partners to access urea- and guanidine-fused dihydroisoquinolone scaffolds (**Scheme 3.8**). Heterocyclic diazoles are notably missing in previous literature with regards to Rh(III)-catalyzed C-H activation/annulations.

Scheme 3.8 Proposed methodology

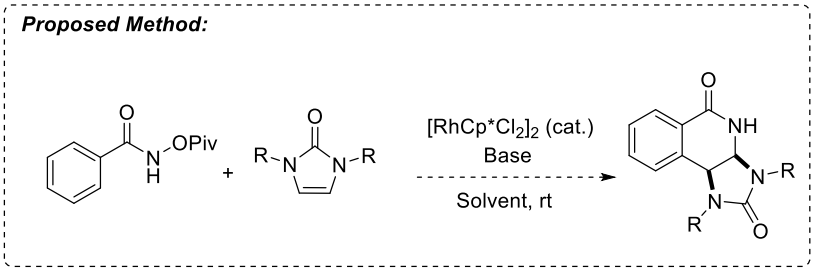

The overall goal of this work would be to facilitate access to the urea-fused tetrahydroisoquinolone scaffolds in an expeditious route. Given their structural similarity to the urea- and guanidine-fused pyrrole alkaloid natural products, we believe that access to these substrates may provide opportunities in the future for the development of biologically active molecules. The development of this methodology is discussed herein.

3.2 Methodology Optimization

3.2.1 Initial Annulation Attempts

Initial explorations of the use of heterocyclic diazoles began with the utilization of imidazo[1,2-*a*]pyrimidine as alkene equivalent and masked 2-aminoimidazoline (**Table 3.1**). However, after several attempts, the desired annulated product was never observed.

Table 3.1 Initial Annulation attempts using imidazo[1,2-*a*]pyrimidine as alkene partner

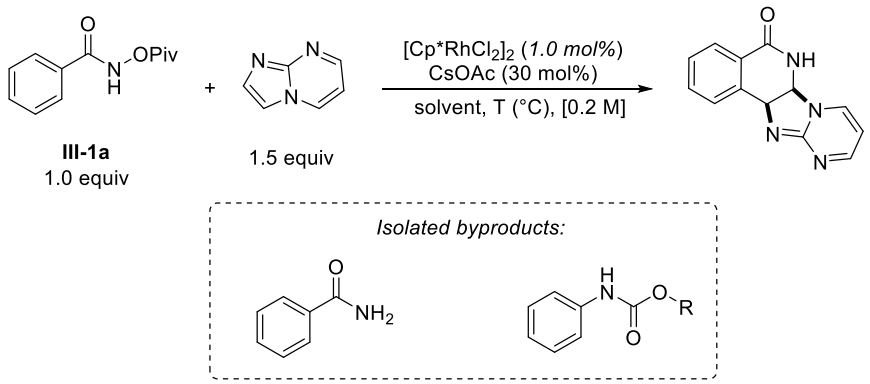

Entry	Solvent	Temp (°C)	Time (h)	Results[a]
1	MeOH	rt	>72	85% **III-1a**; no product
2	MeOH	45	48	64% **III-1a**; 9% benzamide
3	MeOH	65	48	21% **III-1a**; 18% benzamide; 27% Lossen
4	HFIP	45	48	49% **III-1a**; 35% benzamide
5	TFE	45	48	51% **III-1a**; benzamide
6[b]	TFE	rt-50	66	26% benzamide

[a] Isolated yield. [b] $[RhCp^*Cl_2]_2$ (5.0 mol%), CsOAc (50 mol%), [0.4 M], 22 h at rt, then 44 h at 45-50 °C.

The major isolated products from the reactions resulted from degradation of the benzohydroxamate substrate under these conditions. The formation of the benzamide byproduct occurs by N-O bond reduction. The alkoxy carbamate is believed to arise from a metal-assisted Lossen rearrangement; this type of rearrangement was previously reported by Jašíková *et al.* using zinc and potassium bases and benzohydroxamic acids.[51] Formation of the carbamate via Lossen rearrangement was proposed by Webb *et al*. in their previous studies.[46, 52] This specific rearrangement has since been exploited in subsequent Rh(III)-catalyzed methods to access various substrates including indoles, pyrroles,[53] and pyridone[54] scaffolds.

A general mechanism of metal-assisted Lossen rearrangement is shown below (**Scheme 3.9)**. Base first deprotonates the amide nitrogen, resulting in production of the anionic species **I**.

Coordination of the amide carbonyl and the oxygen to the metal facilitates rearrangement to extrude the pivalate and afford the isocyanate **II**. This is subsequently trapped as the carbamate **III** in the presence of alcoholic solvents.

Scheme 3.9 Proposed mechanism of metal-assisted Lossen rearrangement

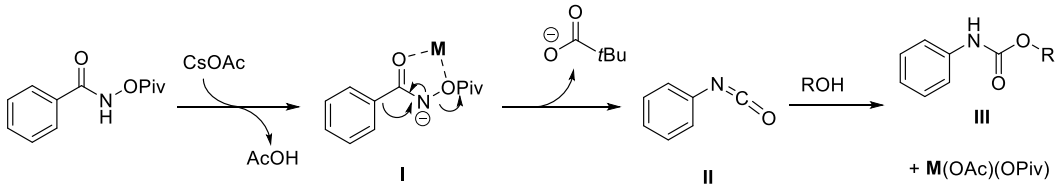

An alternative diazole substrate was thus elected for future studies to instead access the urea-fused scaffolds: *N*,*N*-diacylimidazolone **III-2a**. An initial attempt was made, resulting in the isolation of the monoacylated annulation product **III-3a** in 24% yield (**Scheme 3.10**).

Scheme 3.10 Initial attempt at C-H annulation with **III-2a**

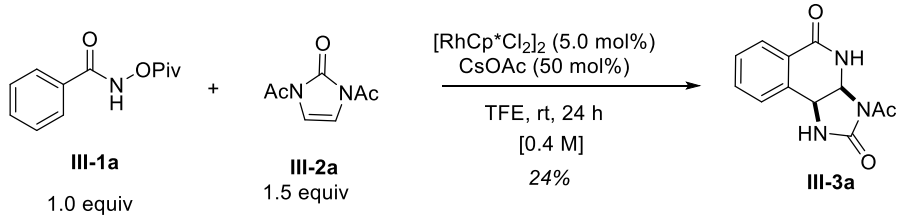

The product identity was elucidated by 2D-NMR experiments and later confirmed by X-ray crystallography whereby the acyl group is located distal to the phenyl ring (**Figure 3.2**). With this promising initial result in hand, the next focus became optimization of the methodology.

Figure 3.2 X-ray crystal structure of monoacylated annulation product **III-3a**

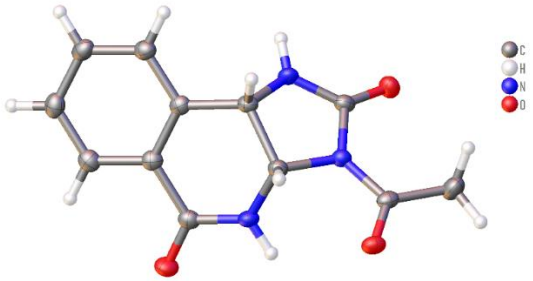

Early optimization studies focused upon the reaction of *N*-(pivaloyloxy)benzamide **III-1a** with *N*,*N*-diacylated imidazolone **III-2a**. A solvent screen was first conducted utilizing various solvents (**Table 3.2**, entries 1-6). As previous studies had indicated the superior performance of alcoholic solvents in this approach relative to aprotic solvents, various alcohols were screened. These initial attempts resulted in the formation of a distribution of mono- and diacylated annulation products in moderate yields as determined by ^{1}H-NMR utilizing 1,3,5-trimethoxybenzene as internal standard. Further evaluation of product distribution relative to alcoholic solvents suggests that a base-catalyzed deacylation of the diacylated imidazolone occurs *in situ* to afford the mono and diacylated products; the formation of the monoacylated product increases with increased acidity of the alcoholic solvent. To avoid deacylation, polar aprotic solvent MeCN was assessed, however yield of the reaction was a mere 20% yield.

Table 3.2 Initial reaction screening with imidazolone **III-2a**

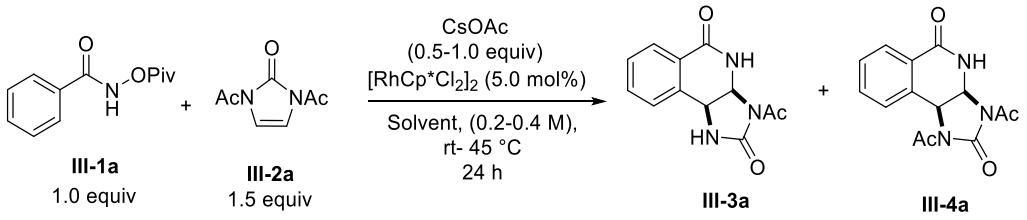

III-1a 1.0 equiv + **III-2a** 1.5 equiv → **III-3a** + **III-4a**

Entry	Solvent	Conc	Temp	Equiv CsOAc	SM Recovery	^{1}H-NMR Yield*
1	MeOH	0.4 M	rt	0.5	10%	28% **III-3a**, 23% **III-4a**
2	EtOH	0.4 M	rt	0.5	5%	8% **III-3a**, 55% **III-4a**
3	i-PrOH	0.4 M	rt	0.5	43%	46% **III-4a**
4	TFE	0.4 M	rt	0.5	47%	43% **III-3a**
5	HFIP	0.4 M	rt	0.5	quant	trace pdt
6	MeCN	0.4 M	rt	0.5	40%	20% **III-4a**
7	EtOH	0.4 M	45	0.5	0%	9% **III-3a**, 22% **III-4a**
8	EtOH	0.2 M	rt	0.5	11%	7% **III-3a**, 60% **III-4a**
9	EtOH	0.2 M	rt	1.0	trace	25% **III-3a**, 49% **III-4a**
10**	EtOH	0.2 M	rt	1.0	0%	2% **III-3a**, 44% **III-4a**
11***	EtOH	0.2 M	rt	1.0	5%	7% **III-3a**, 43% **III-4a**

*[1] H-NMR yield determined utilizing 1,3,5-trimethoxybenzene as standard. **NaOAc screened as base. ***KOAc screened as base.

As EtOH initially provided the greatest yield in initial screening, this solvent was explored in subsequent studies (**Table 3.2**, entries 7-11). The temperature of the reaction was increased from room temperature to 45 °C (entry 7) but resulted in lower yield of the products. Diminished yield in this entry was believed to occur due to increased rate of deacylation of the imidazol-2-one substrate. The product resulting from the fully deacylated imidazolone was never observed in crude mixtures by NMR. Therefore, increasing temperature at this time was not a feasible solution.

Further optimization focused upon the base in this reaction. Acetate and carbonate bases are suitable choices due to their ability to coordinate efficiently to the Rh-center, however the choice of base was limited to acetate bases in this study to avoid rapid deacylation of the imidazole-2-one substrate. The optimized yield was achieved by utilization of a stoichiometric amount of cesium acetate (entry 9). Sodium and potassium acetate were also evaluated, however resulted in diminished yields (entries 10 and 11). Further attempts to optimize the overall yield of the reaction using EtOH did not result in improved yields.

It should be noted that this reaction was not initially carried out under conventional conditions: conflicting NMR studies of the reaction resulted in the realization that the reaction occurred only under higher reaction concentrations relative to many previous studies. **Figure 3.3** below depicts the general reaction approach for the initial reaction studies (see experimental section for a detailed reaction procedure). An initial reaction mixture was stirred at room temperature for 24 hours prior to concentration *in vacuo* to afford a crude oil. This concentrated reaction mixture then sat under vacuum pump for 2 hours prior to analysis and quantification by NMR. Based upon the results of NMR studies, it is believed that at the lower reaction concentration, no annulation takes place. The observed product distribution results from the deacylation of the imidazol-2-one substrate in the initial 24-hour time period.

Figure 3.3 Image depiction of reaction protocol with respect to concentration

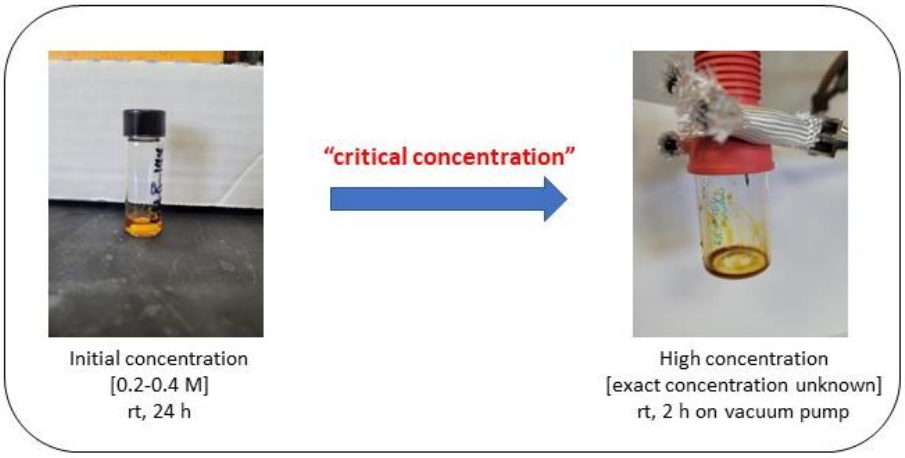

While these results were initially promising, challenges quickly arose which needed to be addressed before moving forward: a distribution of products was nonideal for isolation purposes and attempts to isolate the diacylated annulation product were complicated by co-elution with not only the monoacylated imidazolone byproduct **III-2b**, but also the observed byproduct benzamide. Other *N*-substituted imidazolones were briefly evaluated that were more resilient under these conditions including benzyl, Troc, Ethoc, Moc groups. However, these all resulted in low yields and were thus abandoned as alternatives to the *N*,*N*-diacylated imidazolone substrate.

These challenges prompted a re-evaluation of the initial reaction conditions with respect to productive conversion of the benzohydroxamate starting material. While EtOH did provide an optimized overall yield of 74%, complete conversion of the starting material to other aromatic byproducts hindered further optimization using this solvent. In contrast, while reactions conducted with fluorinated solvents (entries 4 and 5) resulted in lower yields of product, the mass balance for these reactions between starting material and products were 90-100%. Because HFIP appeared to cause excessive deacylation of the imidazolone scaffold under these conditions, the less acidic solvent TFE was the focus of subsequent studies.

Based upon the known necessity of high concentration on this reaction, vacuum pump studies were initiated to determine the maximum conversion to the desired product using TFE as solvent (**Table 3.3**). Under the same conditions as previously described, the reactions were placed under vacuum upon concentration for varying times (2, 9.5, >12 h). Gratifyingly, the formation of the monoacylated substrate increased as the reaction mixture sat as an oil for increased time periods, with a nearly quantitative yield of product after sitting overnight (entry 3).

Table 3.3 Vacuum-pump studies of reaction using TFE as solvent

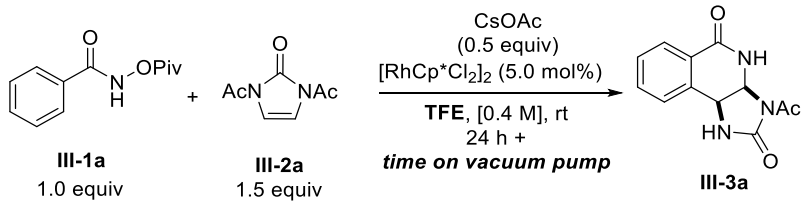

III-1a 1.0 equiv

III-2a 1.5 equiv

III-3a

Entry	Conc	Equiv CsOAc	Time on vacuum pump	SM Recovery	^{1}H-NMR Yield*
1**	0.4 M	0.5	2 h	47%	43% **III-3a**
2	0.4 M	0.5	9.5 h	12%	83% **III-3a**
3	0.4 M	0.5	> 12 h	0%	95% **III-3a**

*^{1}H-NMR yield determined utilizing 1,3,5-trimethoxybenzene as standard.
** Table 3.2, entry 4.

While these results were encouraging, the reaction only appeared to occur upon achievement of a "critical" concentration and thus the formation of the monoacylated imidazolone *in situ* was all that was optimized in a 24 h period. The next mode of action was to determine the optimal time frame to access the monoacylated imidazolone **III-2b** such that the reaction time could be lowered. Monitoring the base-catalyzed deacylation of the imidazolone starting material revealed that the diacylated substrate is completely converted to monoacylated substrate or free imidazolone within 4 h. Subsequent addition of the pivalate and catalyst, followed by concentration under standard conditions leads to the desired product in 85% by ^{1}H-NMR (**Scheme 3.11**).

Scheme 3.11 Determination of optimal time for *in situ* monodeacylation of **III-2a**

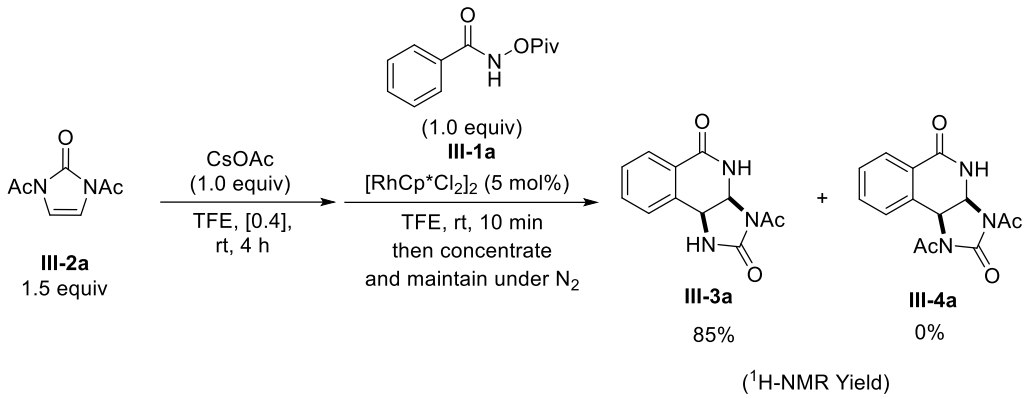

These initial optimization studies provided answers regarding the optimal solvent TFE for use in this reaction. However, the experimental protocol for this approach was complicated by the necessary access to a "critical concentration" at which the reaction takes place, which was only accessible by concentration *in vacuo* to a crude oil. This became a cause of concern for creating a robust protocol for future use. In the next section, optimization of the reaction using monoacylated imidazolone **III-2b** sought to determine this "critical concentration" resulting in a more operational protocol.

3.2.2 Optimization utilizing *N*-acylimidazol-2-one as coupling partner

As discussed in the previous section, the deacylation of imidazolone **III-2a** occurred under alcoholic conditions at 0.4 M concentration which resulted in the initially observed product distributions. Due to the acidity of TFE, the product distribution favored the monoacylated annulation product, whereby an optimal amount of monoacylated imidazolone was generated at 0.4 M concentration prior to achieving the "critical concentration" at which annulation takes place. However, this initial approach was complication by the requirement that the monoacylated imidazolone **III-2b** be generated *in situ* prior to achieving this critical concentration. To circumvent this issue and allow for exploration of reaction concentration, monoacylated

imidazolone **III-2b** was selected as alkene substrate for subsequent studies. The monoacylated imidazolone is accessible in two steps from commercially available 1,3-dihydroimidazol-2-one (**Scheme 3.12**). Monodeacylation was achieved by base-catalyzed alcoholysis of **III-2a** in methanol.

Scheme 3.12 Two-step synthesis of *N*-acylimidazolone **III-2b**

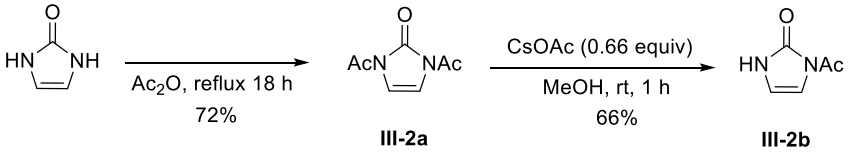

Initial attempts toward optimization with **III-2b** focused upon determining the effect of the reaction concentration on yield. Increasing the concentration of the reaction from 1.0 to 3.0 M (**Table 3.4**, entries 1−4) proved beneficial, affording the desired monoacylated substrate **III-3a** in 76% yield as quantified by ^{1}H-NMR. The other regioisomer was never observed in crude reaction mixtures, nor was there evidence of the deacylated annulation product in either crude H-NMR or HRMS.

While a higher reaction concentration was beneficial, incomplete conversion of **III-1a** in the 24 h period prompted further optimization. Extending the reaction time to 36 h increased the yield of the desired product (entry 5, 87%). When the temperature was increased to 45 °C, there was a comparable improvement (entry 6, 86%) in only 18 h. Optimized conditions were achieved by increasing the equivalents of **III-2b** from 1.5 to 2.5 equiv (entry 7, 92%). Catalyst loading was also explored; decreased catalyst loading at 2.5 mol % resulted in a slightly diminished yield (entry 8). The use of polar aprotic solvent MeCN also resulted in diminished yields (entry 9).

Table 3.4 Optimization attempts with *N*-acylimidazolone **III-2b**

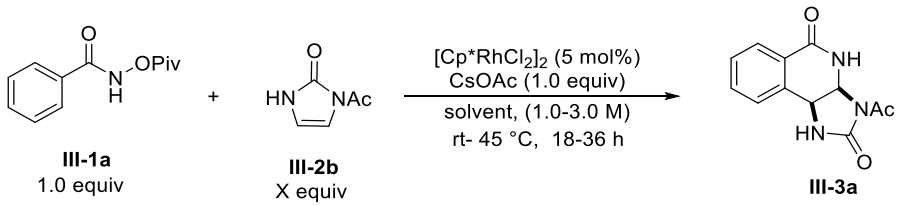

III-1a 1.0 equiv + **III-2b** X equiv → **III-3a**

Entry	Solvent	Conc	Temp	Time	Equiv **III-2b**	^{1}H-NMR Yield* **III-3a**
1	TFE	1.0 M	rt	24 h	1.5	35%
2	TFE	2.0 M	rt	24 h	1.5	59%
3	TFE	2.5 M	rt	24 h	1.5	68%
4	TFE	3.0 M	rt	24 h	1.5	76%
5	TFE	3.0 M	rt	36 h	1.5	87%
6	TFE	3.0 M	45 °C	18 h	1.5	86%
7	**TFE**	**3.0 M**	**45 °C**	**18 h**	**2.5**	**92%**
8**	TFE	3.0 M	45 °C	18 h	2.5	85%
9	MeCN	3.0 M	45 °C	18 h	2.5	67%

*^{1}H-NMR yield determined utilizing 1,3,5-trimethoxybenzene as standard.
**Catalyst loading: 2.5 mol%.

With optimized conditions in hand, we sought next to establish the scope of this methodology. The results of scope evaluation are discussed in the following section.

3.3 Scope Evaluation

3.3.1 Carbocycle Scope: Electronic Effects at the *p*-position

With optimized conditions in hand, we sought next to establish the scope of this methodology. The *N*-pivaloyloxybenzohydroxamates and heterocycles were synthesized from known procedures, and the syntheses of these molecules is detailed in the experimental section of this chapter. In total, 18 substrates were synthesized for evaluation of this methodology. Following synthesis of the starting materials, scope evaluation was focused first on annulation with para-substituted *N*-(pivaloyloxy)benzamides (**Scheme 3.13**).

Scheme 3.13 Scope Evaluation for *p*-substituted carbocycles[a]

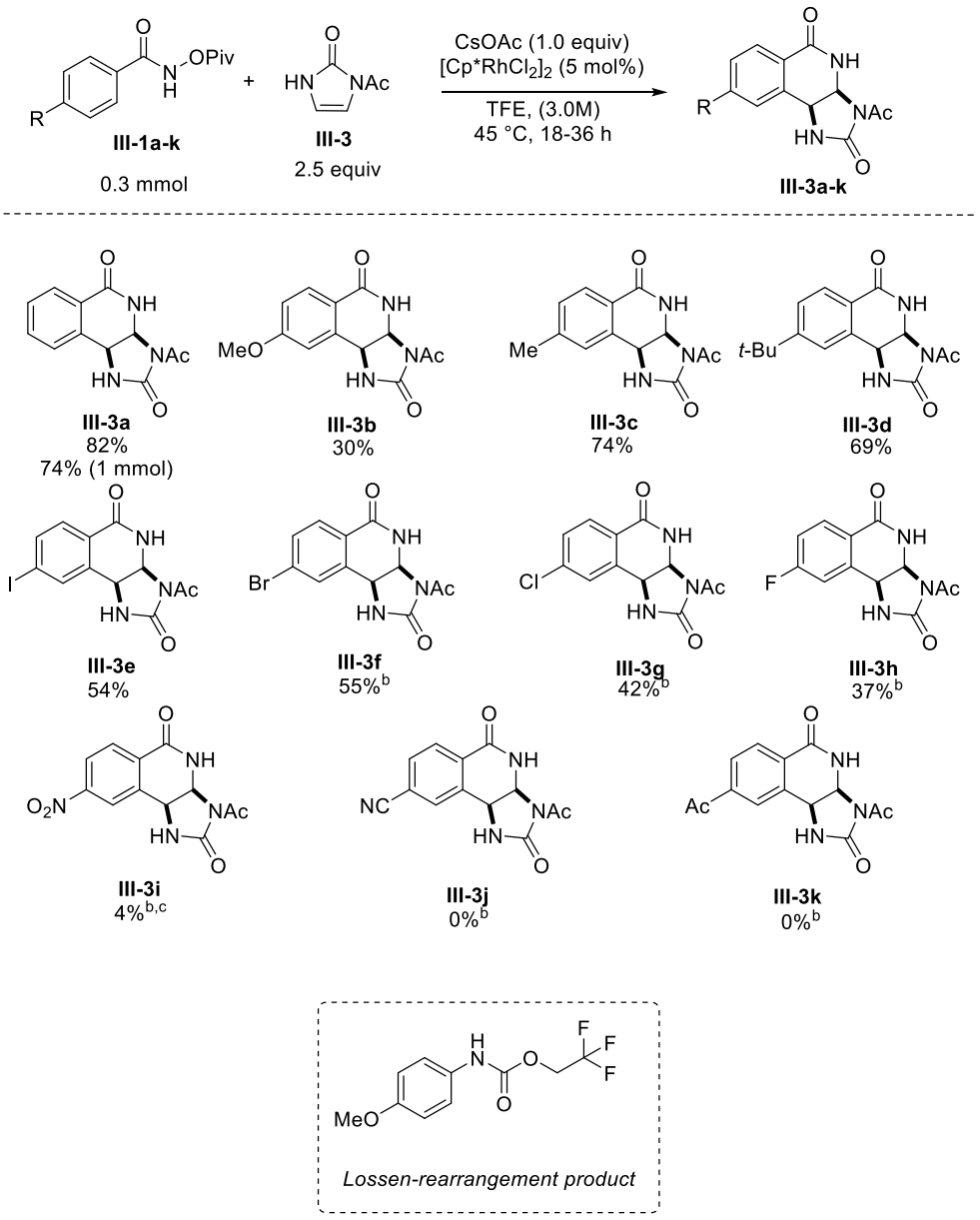

[a] Isolated yield. [b] Reaction conducted using 3.5 equiv **III-2b**, 45 °C, 36 h. [c] Reaction conducted at 0.53 mmol scale.

The reaction with model substrate **III-1a** furnished the desired annulated product **III-3a** in an isolated yield of 82% at 0.3 mmol scale. The reaction was also successful at a 1 mmol scale, resulting in an isolated yield of 74%. Alkyl substituents bore little influence on the reaction, affording the desired annulation substrates in reasonable yields (**III-3c** and **III-3d**). Electron-donating and -withdrawing substituents were tolerated; however, electron-withdrawing groups

slowed reaction progression. For example, when halogenated substrates **III-1e-h** required modified conditions (36 h, 3.5 equiv **III-2b**) to afford the desired products. Reactions with electron-donating groups occurred faster than electron-withdrawing substitutions, suggestive of an electrophilic C−H activation mechanism. The yields of the para substituted halogenated substrates decreased in order of increased inductive withdrawal (**III-3f−3h**). Attempts to improve the yield of *p*-iodo benzohydroxamate **III-3e** by applying the modified reaction conditions were unsuccessful due to difficulty in separating the annulation product from unreacted imidazolone **III-2b**. Reactions with several strongly electron withdrawing groups were attempted (*p*-Ac, *p*-CN, *p*-NO_2); however, conversion was poor, and isolation complicated by formation of benzamide byproducts resulting from N−O bond reduction. A similar N-O reduction byproduct was previously reported in a recent methodology developed by Saiegh *et al*.[40] The nitro-substituted annulation product **III-3i** was isolated in 4% yield only after several attempts and scale-up.

Introduction of the electron-rich *p*-MeO group resulted in low isolated yield of 30% of **III-3b** due in part to detrimental Lossen-rearrangement to afford the carbamate byproduct in 26% yield at this temperature. The electron-donating capability of the methoxy group facilitates rapid Lossen rearrangement relative to the unsubstituted phenyl ring or electron-deficient rings. This same issue was reported by Webb *et al*.,[46] and authors described that lowering temperature of the reaction facilitated greater product with the *p*-MeO substrate. While this was not attempted at this time, it may be a solution to the low observed yield under current conditions.

3.3.2 Carbocycle Scope: Regioselectivity at the *m*-position

Regiochemical effects were next investigated using meta-substituted unsymmetric substrates. The results of these studies are shown below in **Scheme 3.14**.

Scheme 3.14 Scope evaluation of *m*-substituted carbocycles[a]

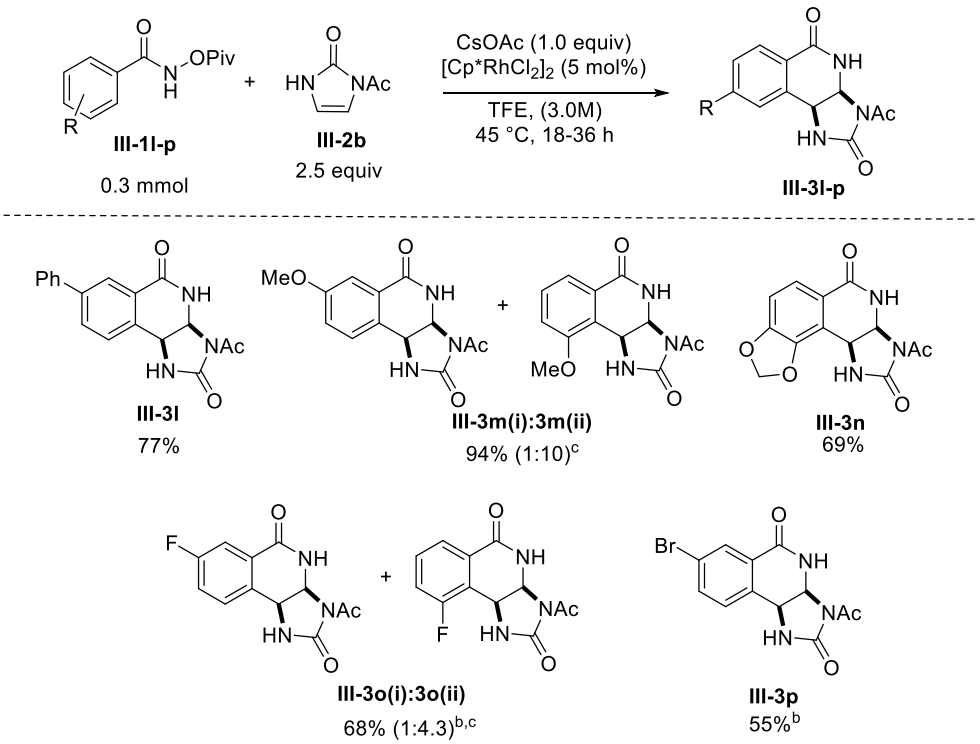

[a] Isolated yield. [b] Reaction conducted with 3.5 equiv **III-2b** for 36 h. [c] Product ratio determined by ^{1}H-NMR.

Regioselectivity was sensitive toward steric effects as evidenced by the formation of m-Ph derivative **III-3l** in 77% yield as a single regioisomer. However, the reaction with the m-MeO-substituted derivative provided a 94% yield of a 1:10 mixture of regioisomers **III-3m(i):3m(ii)** with a regiochemical preference for the contiguously substituted annulation product. Though some previous reports in similar methods have indicated marginal regioselectivity for this type of substitution,[55-57] there is little precedence for this level of regioselectivity toward the more sterically hindered species. This is believed to be taking place under kinetic preference. The site of greatest electron-density appears to direct this regioselectivity: the most electron-dense carbon which is capable of C-H activation is that which is located ortho- to both the methoxy substituent and the pivaloyloxyhydroxamate moiety.

The less sterically hindered piperonylic acid derivative **III-1n** also provided the contiguously substituted product **III-3n** in 69% yield, consistent with previous literature reports for similar methods.[41, 46, 57-59] When the *m*-F substituted derivative was subjected to reaction conditions, 68% yield of a 1:4.3 mixture of regioisomers **III-3o(i):3o(ii)** was isolated. This outcome can be rationalized by the commonly observed "ortho-fluorine effect", whereby C−H activation takes place ortho to a C−F bond, which has also been observed in similar methods.[60, 61] By comparison, the *m*-Br substituted derivative provided 55% yield of the annulated product **III-3p** as a single regioisomer, resulting from C−H activation at the less sterically hindered site.

3.3.3 Heterocycle Scope

Substrate scope was also explored using heterocyclic hydroxamates (**Scheme 3.15**). The results of this investigation are provided below.

Scheme 3.15 Scope evaluation of heterocyclic pivaloyloxyhydroxamates[a]

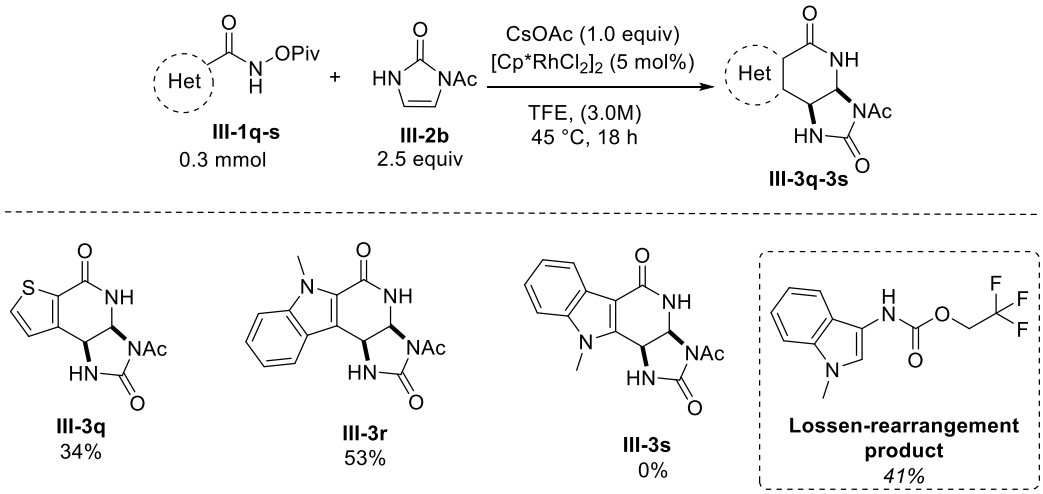

[a] Isolated yield.

While the annulated products were formed for the thiophene derivative **III-1q** and C-2 substituted indole derivative **III-1r** in low to moderate yields, no product was isolated when C-3 substituted indole **III-1s** was subjected to reaction conditions. The electron-donating behavior of

the indole results in detrimental Lossen rearrangement to afford the carbamate in 41% yield. The less successful access to these fused heterocyclic species may arise from the reported variance in rates of reactions for certain heterocyclic substrates in comparison to carbocycles.[46, 62] Further optimization with these derivatives was not pursued at this time.

3.4 Mechanistic Studies & Discussion

3.4.1 Reversibility of C-H Activation

The C−H activation step was deemed reversible under the optimized conditions as determined by ESI-MS and in a reversibility experiment using deuterated TFE (**Scheme 3.16**). The mono and di-deuterated starting materials were prominent in HRMS, indicating that incorporation of deuterium took place in the process of this reaction. These results suggest that the C-H activation step in this system is reversible in nature.

Scheme 3.16 Reversibility of C-H activation

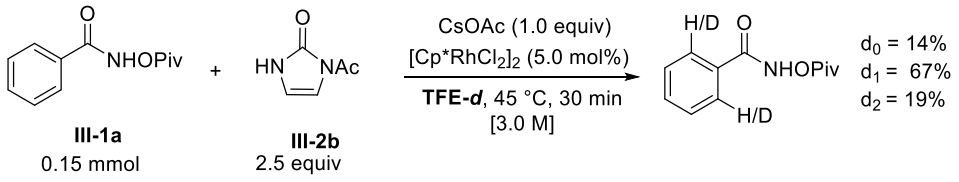

3.4.2 Regioselectivity with respect to Acyl group

We were intrigued by the regioselective formation of monoacylated products with respect to the location of the acyl moiety. The regiochemical preference could be due to steric factors, whereby the acyl moiety is oriented farthest from the phenyl ring. The acyl group may also be acting as a coordinating group, which can form a coordinatively saturated complex to allow access to the monoacylated product in a regioselective manner. Amide and carbamate moieties have been previously reported to coordinate to the Rh-center to afford regiocontrol in similar methods.[46, 63] (**Scheme 3.17**).

Scheme 3.17 Literature precedence of amide and carbamate coordination in Rh(III)-catalyzed C-H activations and annulations

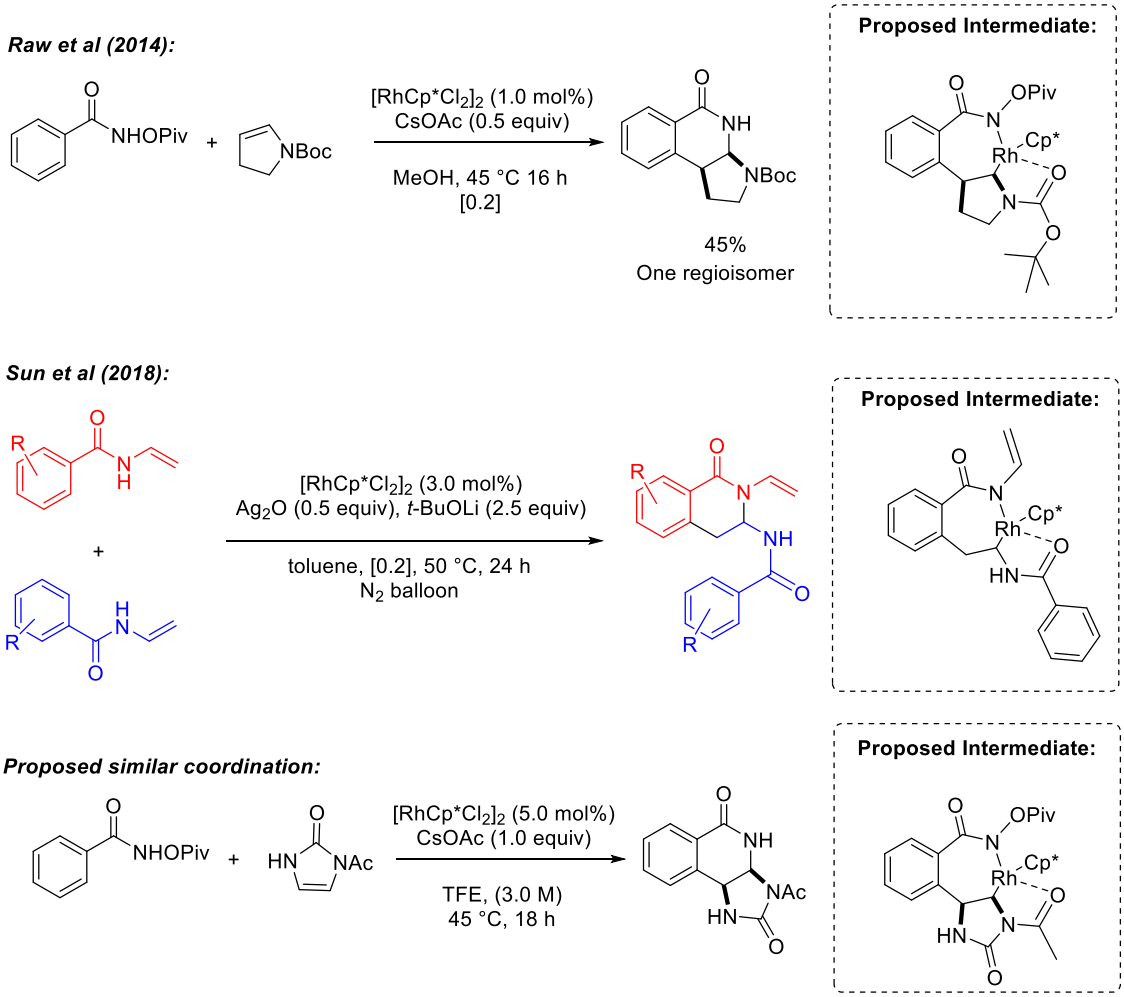

To test the effect of the acyl group on the reaction, 1,3-dihydro-2-imidazolone was utilized as an alkene partner under optimized conditions to afford compound **III-5a**. No annulated product was observed and instead decomposition of the benzohydroxamate **III-1a** occurred. However, **III-5a** was successfully accessed from compound **III-3a** by hydrolysis (**Scheme 3.18**). These results corroborate the previous data, whereby the completely deacylated annulation product was never observed in crude reaction mixtures. Based upon this experiment, the coordination of the acyl group appears necessary to facilitate product formation in this reaction. However, computational experiments may be necessary to further elucidate the exact effect of the acyl group on reaction outcomes.

Scheme 3.18 Effect of Acyl group on reaction

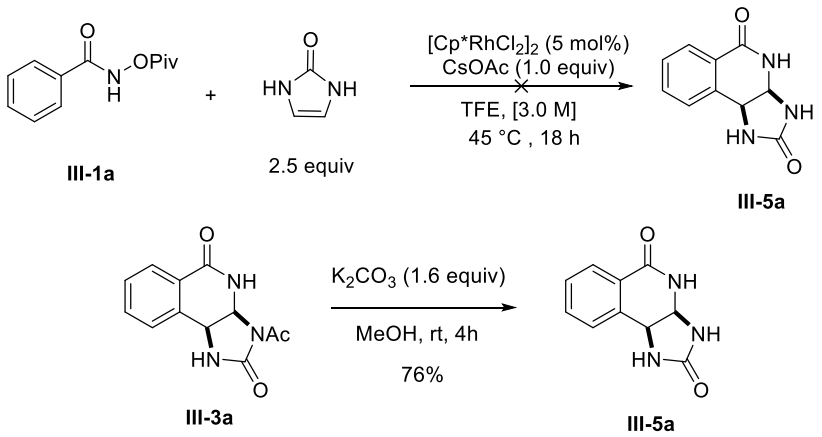

With these results in hand, another protected imidazolone scaffold was evaluated as a substrate under optimized conditions, largely due to the desire to determine whether a more resilient protecting group could be installed on the imidazolone scaffold that could survive the transformation. The desired imidazolone would ideally also be capable of carrying out a similar coordination with the Rh-center, thus a carbamate protecting group was desirable. *N*,*N*-diBoc-protected 2-imidazolone **III-2c** was synthesized and subsequently subjected to optimized reaction conditions to afford the annulated product **III-6** in 39% yield by ^{1}H-NMR (**Scheme 3.19**).

Scheme 3.19 Reaction with *N*,*N*-diBoc-imidazol-2-one **III-2c**

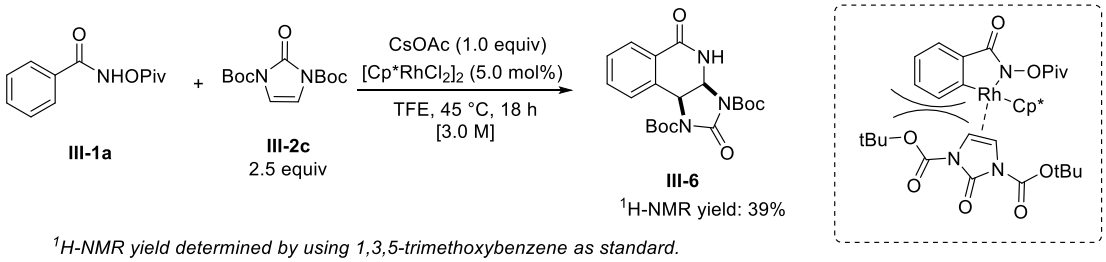

^{1}H-NMR yield determined by using 1,3,5-trimethoxybenzene as standard.

The lowered yield in this reaction may be due to the steric demand of the imidazolone which is not encountered with **III-2b**. This steric clash may hinder efficient coordination of the alkene with the Rh-center, and subsequently affect the insertion of the alkene to proceed forward in the catalytic cycle.

3.4.3 Proposed Mechanism

Based upon previous reports and the results of the control reaction, the proposed mechanism of annulation is provided as follows (**Scheme 3.20**). Active Rh(III) species **I** is first coordinated to *N*-(pivaloyloxy)benzamide **III-1a** to afford intermediate **II**. Subsequent C−H activation occurs to afford five-membered rhodacyclic intermediate **III**. Coordination of the imidazolone substrate followed by insertion results in the 7-membered rhodacycle **IV**, which subsequently undergoes migration of the pivaloyloxy moiety to afford the Rh(V) nitrene intermediate **V**. Subsequent reductive elimination affords 6-membered intermediate **VI**, which finally undergoes protonation to form the annulated product and regenerate **I**.

As was previously mentioned, there are several proposed modes by which C-H bond cleavage may take place in the presence of Rh-centers: concerted metalation deprotonation (CMD), oxidative addition (OA), Friedel-Crafts type electrophilic aromatic substitution (S_EAr), and σ-complex assisted metathesis (σ-CAM). The CMD mechanism has been commonly reported for the Rh(III)-catalyzed C-H annulation strategies, however computational experiments would be beneficial to further investigate these mechanistic possibilities. \

Scheme 3.20 Proposed catalytic cycle of annulation

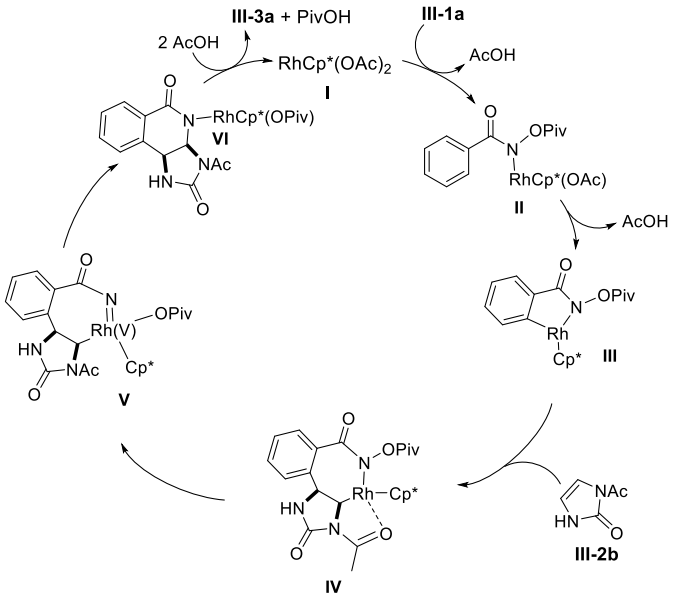

3.5 Conclusion

In conclusion, a mild Rh(III)-catalyzed C−H activation/ annulation has been developed, which facilitates access to urea-fused-dihydroisoquinolone scaffolds. The monoacylated-imidazol-2-one substrate **III-2b** has been identified as an efficient alkene partner in this approach. The method is tolerant toward a variety of functional groups and is applicable to both carbocyclic and heterocyclic hydroxamates. This method allows construction of a complex scaffold in one step and may be beneficial in future studies in the synthesis of small molecule mimics of the pyrrole alkaloid family of natural products for biological evaluation. A potential adaptation of this protocol to access natural products belonging to the pyrrole alkaloids such as dibromoisophakellin and the styloguanidines is also envisioned as a future endeavor in the Tepe Lab.

3.6 Experimental

General Information

Reactions were carried out under a nitrogen atmosphere in flame-dried glassware unless otherwise noted. Solvents and reagents were purchased from commercial suppliers and used without further purification, unless otherwise mentioned. THF and DCM were purified through a column packed with dry alumina and dispensed by a nitrogen pressure delivery system. Acetonitrile and triethylamine were distilled over calcium hydride. 2,2,2-trifluoroethanol was obtained from Sigma-Aldrich and used without further preparation. Magnetic stirring was used for all reactions. Yields refer to chromatographically and spectroscopically pure compounds unless otherwise noted. Column chromatography was performed using a Teledyne ISCO CombiFlash® NextGen system with prepacked columns (RediSep® Normal-phase silica, 20-40 microns) where noted. ^{1}H and $^{13}C\{^{1}H\}$ NMR spectra were recorded on a Varian Unity Plus-500 spectrometer. Chemical shifts are reported relative to the residue peaks of the solvent ($CDCl_3$: 7.26 ppm for ^{1}H and 77.0 ppm for ^{13}C) (DMSO-d_6: 2.50 ppm for ^{1}H and 39.5 ppm for ^{13}C) (CD_3OD: 3.31 ppm for ^{1}H and 47.6 ppm for ^{13}C). The following abbreviations are used to denote the multiplicities: s = singlet, d = doublet, dd = doublet of doublets, td= triplet of doublets, t = triplet, and m = multiplet. The following abbreviation is used to denote a broad signal: br = broad. Coupling constants (*J*) are quoted in Hz. Assignments were made based on chemical shift and coupling data, using 2D-NMR experiments (COSY, HSQCAD, HMBCAD) where necessary. Infrared spectra were recorded on a Jasco Series 6600 FTIR spectrometer, with absorbance reported in wavenumbers (cm^{-1}). High resolution electrospray mass spectra (ESI-MS) were obtained at the Mass Spectrometry Facility of Michigan State University with a Micromass Q-ToF Ultima API LC-MS/MS mass spectrometer.

Preparation of Starting materials:

***O*-pivaloylhydroxylammonium trifluoromethanesulfonate**

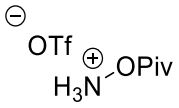

N-Boc-hydroxylamine (4.00 g, 30 mmol) was dissolved in DCM (60 mL) in a dry round bottom flask equipped with stir bar. The resulting solution was cooled by ice bath, and triethylamine (4.19 mL, 30 mmol) was added by syringe. Pivaloyl chloride (30 mmol) was next introduced by syringe. The reaction was removed from ice bath and allowed to stir at rt under N_2 atm for 2 h. The reaction was next transferred to a separatory funnel, and the organic layer was washed with water (30 mL), sat. aq. $NaHCO_3$ solution (30 mL) and finally brine (30 mL). The organic layer was dried over Na_2SO_4, filtered and concentrated to afford the crude product.

The crude product was dissolved in diethyl ether (75 mL) in a round-bottom flask equipped with stir bar. The reaction was cooled by ice bath, and to the flask was added trifluoromethane sulfonic acid (2.65 mL, 30 mmol) via syringe. The reaction was removed from ice bath and stirred under N_2 atm for 1 h. After 1 h, petroleum ether (75 mL) was added to the flask, and a white precipitate crashed out of the solution. This white solid was isolated by vacuum filtration and washed with petroleum ether then dried under vacuum to afford the desired product as a white solid (6.88 g, 86% over two steps) mp: 124-125 °C. This product was used as-is in subsequent reactions. ^{1}H NMR (500 MHz, $CDCl_3$) δ 1.21 (s, 9H). $^{13}C\{^1H\}$ NMR (126 MHz, $CDCl_3$) δ 174.9, 120.7 (q, *J*= 322 Hz), 38.0, 26.5. ^{19}F-NMR ($CDCl_3$) δ -77.8. Spectral data is consistent with the literature.[21]

***N*-(pivaloyloxy)benzamide (III-1a)**

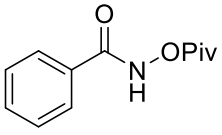

Following a modified procedure from Webb et. al.[46] benzohydroxamic acid (685.4 mg, 5.0 mmol) was dissolved in dry THF (20 mL) in a dry RB flask and cooled to 0 °C. To the flask was added pivaloyl chloride (0.62 mL, 5.0 mmol), followed immediately by triethylamine (0.84 mL, 6.0 mmol). The mixture was removed from ice bath and stirred at rt for two hours under N_2 atm. Upon completion, water was added to the reaction mixture (15 mL), and the mixture was extracted three times with ethyl acetate (3x 20 mL). The organic layers were pooled, dried over Na_2SO_4, filtered and concentrated to yield a crude product. The product was purified by automated CombiFlash chromatography (EtOAc/Hexane) to yield a white solid (996.7 mg, 90%). mp: 108-110 °C. ^{1}H NMR (500 MHz, $CDCl_3$) δ 9.32 (s, 1H), 7.83 (d, *J*= 8.0 Hz, 2H), 7.57 (t, *J*= 7.5 Hz, 1H), 7.47 (t, *J*= 7.8 Hz, 2H), 1.37 (s, 9H). ^{13}C{^{1}H} NMR (126 MHz, $CDCl_3$) δ 177.1, 166.9, 132.8, 131.0, 128.9, 127.6, 38.6, 27.1. FTIR (cm^{-1}): 3222, 3067, 2975, 1779, 1651, 1063. HRMS-ESI (m/z) calcd for $C_{12}H_{16}NO_3$ [M+H]+ 222.1130, found 222.1124.

4-methoxy-*N*-(pivaloyloxy)benzamide (III-1b)

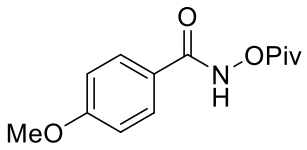

Following a previous literature procedure by Guimond et al,[21] to a flask containing a 2:1 EtOAc/Water mixture (11.25 mL total) was added sodium carbonate (318.4 mg, 1.5 mmol). The flask was cooled to 0 °C, then *O*-pivaloylhydroxylammonium trifluoromethane sulfonate (402.6 mg, 1.51 mmol) was added. 4-methoxybenzoyl chloride was added to the flask in one portion and the reaction stirred for 2 h at 0 °C. The reaction was removed from ice bath and diluted with ethyl acetate (18 mL), then extracted three times with sat. aq. $NaHCO_3$ (3x ~10 mL). The organic layer was dried over Na_2SO_4, filtered and concentrated to afford a crude solid. The solid was purified by automated CombiFlash chromatography (EtOAc/Hexane, 0-20% gradient) to afford a white

solid (313.9 mg, 81%). m.p. 139-141 °C. ^{1}H NMR (500 MHz, $CDCl_3$) δ 9.31 (br s, 1H), 7.79 (d, *J*= 8.9 Hz, 2H), 6.94 (d, *J*= 8.9 Hz, 2 H), 3.85 (s, 3H), 1.36 (s, 9H). $^{13}C\{^{1}H\}$ NMR (126 MHz, $CDCl_3$) δ 177.4, 166.9, 163.3, 129.6, 123.1, 114.2, 55.6, 38.6, 27.2. FTIR (cm^{-1}): 3223, 3050, 2973, 1770, 1645, 1254, 1066. HRMS-ESI (m/z) calcd for $C_{13}H_{17}NO_4$ [M+H]+ 252.1236, found 252.1228.

4-methyl-*N*-(pivaloyloxy)benzamide (III-1c)

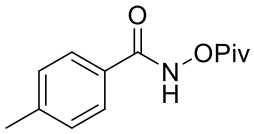

Following a modified procedure by Guimond et al,[21] to a flask containing a 2:1 EtOAc/Water mixture (11.25 mL total) was added sodium carbonate (318.5 g, 3.0 mmol). The flask was cooled to 0 °C, then *O*-pivaloylhydroxylammonium trifluoromethane sulfonate (404.5 mg, 1.51 mmol) was added. 4-methyl-benzoyl chloride (0.20 mL, 1.5 mmol) was added to the flask via syringe and the reaction stirred overnight at rt. The reaction was diluted with ethyl acetate (5 mL), then extracted three times with sat. aq. $NaHCO_3$ (3x ~10 mL). The organic layer was dried over Na_2SO_4, filtered and concentrated to afford a crude solid. The solid was purified by automated CombiFlash chromatography (EtOAc/Hexane, 0-20% gradient) to afford a white solid (250.8 g, 70%). mp: 141-142 °C. ^{1}H NMR (500 MHz, $CDCl_3$) δ 9.30 (br s, 1H), 7.72 (d, *J*= 8.3 Hz, 2H), 7.27-7.25 (m, 2H), 2.41 (s, 3H), 1.36 (s, 9H). $^{13}C\{^{1}H\}$ NMR (126 MHz, $CDCl_3$) δ 177.3, 167.1, 143.6, 129.6, 128.1, 127.6, 38.6, 27.2, 21.8. FTIR (cm^{-1}): 3170, 3040, 2977, 1777, 1645, 1063. HRMS-ESI (m/z) calcd for $C_{13}H_{17}NO_3Na$ [M+Na]+ 258.1106, found 258.1102.

4-(*tert*-butyl)-*N*-(pivaloyloxy)benzamide (III-1d)

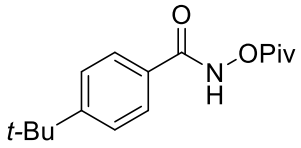

Following a modified procedure by Guimond et al,[21] to a flask containing a 2:1 EtOAc/Water mixture (11.25 mL total) was added sodium carbonate (318.6 mg, 3.0 mmol). The flask was cooled to 0 °C, then *O*-pivaloylhydroxylammonium trifluoromethane sulfonate (408.2 mg, 1.51 mmol) was added. 4-*tert*-butylbenzoyl chloride (0.29 mL, 1.5 mmol) was added to the flask via syringe and the reaction stirred overnight at rt. The reaction was diluted with ethyl acetate (5 mL), then extracted three times with sat. aq. $NaHCO_3$ (3x ~10 mL). The organic layer was dried over Na_2SO_4, filtered and concentrated to afford a crude solid. The solid was purified by automated CombiFlash chromatography (EtOAc/Hexane, 0-20% gradient) to afford a white solid (406.1 mg, 44%). mp: 85-87 °C. ^{1}H NMR (500 MHz, $CDCl_3$) δ 9.33 (br s, 1H), 7.76 (d, *J*= 8.3 Hz, 2H), 7.48 (d, *J*= 8.44 Hz, 2H), 1.36 (s, 9H), 1.34 (s, 9H). $^{13}C\{^1H\}$ NMR (126 MHz, $CDCl_3$) δ 177.3, 167.0, 156.5, 128.1, 127.5, 125.9, 38.6, 35.2, 31.2, 27.2. FTIR (cm^{-1}): 3211, 3054, 2961, 1781, 1647, 1069. HRMS-ESI (m/z) calcd for $C_{16}H_{24}NO_3[M+H]+$ 278.1756, found 278.1750.

4-iodo-*N*-(pivaloyloxy)benzamide (III-1e)

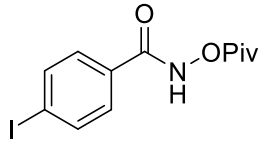

Following a modified procedure by Guimond et al,[21] to a flask containing a 2:1 EtOAc/Water mixture (11.25 mL total) was added sodium carbonate (318.2 mg, 3.0 mmol). The flask was cooled to 0 °C, then *O*-pivaloylhydroxylammonium trifluoromethane sulfonate (402.7 mg, 1.51 mmol) was added. 4-iodobenzoyl chloride (0.3997 g, 1.5 mmol) was added to the flask in one portion,

and the reaction stirred for 6 h at 0 °C. The reaction was removed from ice bath and diluted with ethyl acetate (18 mL), then extracted three times with sat. aq. $NaHCO_3$ (3x ~10 mL). The organic layer was dried over Na_2SO_4, filtered and concentrated to afford a crude solid. The solid was purified by automated CombiFlash chromatography (Petroleum Ether:EtOAc, 0-20% gradient) to afford a white solid (396.3 mg, 76%). mp:147-148 °C. ^{1}H NMR (500 MHz, MeOD-*d*$_4$) δ NH peak missing, 7.90 (d, *J*= 8.4 Hz, 2H), 7.58 (d, *J*= 8.5 Hz, 2H), 1.34 (s, 9H). ^{13}C{^{1}H} NMR (126 MHz, MeOD-*d*$_4$) δ 177.5, 167.1, 139.2, 132.0, 130.1, 100.2, 39.4, 27.5. FTIR (cm^{-1}): 3140, 3001, 2973, 1779, 1654, 1069. HRMS-ESI (m/z) calcd for $C_{12}H_{15}NO_3I$ [M+H]+ 348.0097, found 348.0096.

4-bromo-*N*-(pivaloyloxy)benzamide (III-1f)

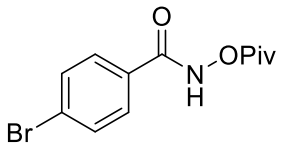

Following a modified procedure by Guimond et al,[21] in a dry flask equipped with stir bar was added 4-bromobenzoic acid (302.2 mg, 1.5 mmol), anhydrous dichloromethane (7.5 mL), and dimethylformamide (3 drops). Oxalyl chloride (0.16 mL, 1.89 mmol) was introduced slowly dropwise via syringe. The reaction was allowed to stir for 2.5 hours at rt under N_2 atmosphere. After 2.5 hours, the reaction mixture was concentrated *in vacuo* to afford the crude acid chloride. The crude acid chloride was suspended in EtOAc (5.5 mL) and added to a flask containing EtOAc/Water (4.0 mL:3.75 mL), sodium carbonate (319.8 mg, 3.02 mmol), *O*-pivaloylhydroxylammonium trifluoromethane sulfonate (405.7 mg, 1.52 mmol) at 0 °C. The reaction stirred at 0 °C under N_2 atmosphere for 2 hours. The reaction was removed from ice bath and diluted with EtOAc (15 mL total) and transferred to separatory funnel. The organic layer was extracted once with sat. aq. $NaHCO_3$ solution (10 mL), once with brine (10 mL), and separated. The organic layer was dried over Na_2SO_4, filtered and concentrated *in vacuo* to yield a crude solid.

The solid was purified by automated CombiFlash chromatography (Petroleum Ether:EtOAc, 0-20% gradient) to afford a white solid (269.9 mg, 60%). m.p. 131-132 °C. ^{1}H NMR (500 MHz, $CDCl_3$) δ 9.35 (br s, 1H), 7.68 (d, *J*= 8.5 Hz, 2H), 7.61 (d, *J*= 8.5 Hz, 2H), 1.36 (s, 9H). $^{13}C\{^{1}H\}$ NMR (126 MHz, $CDCl_3$) δ 177.2, 166.0, 132.2, 129.7, 129.1, 127.7, 38.6, 27.1. FTIR (cm^{-1}): 3142, 3004, 2979, 1779, 1649, 1065. HRMS-ESI (m/z) calcd for $C_{12}H_{15}NO_3Br$ [M+H]+ 300.0235, found 300.0231.

4-chloro-*N*-(pivaloyloxy)benzamide (III-1g)

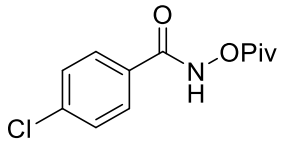

Following a modified procedure by Guimond et al,[21] to a flask containing a 2:1 EtOAc/Water mixture (11.25 mL total) was added sodium carbonate (319.3 mg, 3.0 mmol). The flask was cooled to 0 °C, then *O*-pivaloylhydroxylammonium trifluoromethane sulfonate (403.4 mg, 1.51 mmol) was added. 4-chlorobenzoyl chloride (0.19 mL, 1.5 mmol) was added to the flask in one portion, and the reaction stirred for 3 h at 0 °C. The reaction was removed from ice bath and diluted with ethyl acetate (18 mL), then extracted three times with sat. aq. $NaHCO_3$ (3x ~10 mL). The organic layer was dried over Na_2SO_4, filtered, and concentrated to afford a crude solid. The solid was purified by automated CombiFlash chromatography (Petroleum Ether:EtOAc, 0-20% gradient) to afford a white solid (285.4 mg, 75%). mp:121-123 °C. ^{1}H NMR (500 MHz, $CDCl_3$) δ 9.28 (br s, 1H), 7.76 (d, *J*= 8.5 Hz, 2H), 7.45 (d, *J*= 8.6 Hz, 2H), 1.36 (s, 9H). $^{13}C\{^{1}H\}$ NMR (126 MHz, $CDCl_3$) δ 177.2, 165.9, 139.2, 129.3, 129.26, 129.0, 38.6, 27.1. FTIR (cm^{-1}): 3140, 3001, 2973, 1779, 1654, 1069. HRMS-ESI (m/z) calcd for $C_{12}H_{15}NO_3Cl$ [M+H]+ 256.0740, found 256.0745.

4-fluoro-*N*-(pivaloyloxy)benzamide (III-1h)

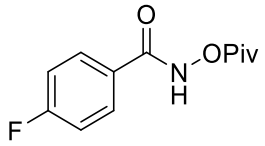

Following a modified procedure by Guimond et al,[21] to a flask containing a 2:1 EtOAc/Water mixture (18 mL total) was added sodium carbonate (317.7 mg, 3.00 mmol). The flask was cooled to 0 °C, then *O*-pivaloylhydroxylammonium trifluoromethane sulfonate (40.18 mg, 1.53 mmol) was added. 4-fluorobenzoyl chloride was added to the flask in one portion, and the reaction stirred for 6 h at 0 °C. The reaction was removed from ice bath and diluted with ethyl acetate (18 mL), then extracted three times with sat. aq. $NaHCO_3$ (3x ~10 mL). The organic layer was dried over Na_2SO_4, filtered and concentrated to afford a crude solid. The solid was purified by automated CombiFlash chromatography (Petroleum Ether:EtOAc, 0-20% gradient) to afford a white solid (255.3 mg, 71%). m.p. 109-110 °C. ^{1}H NMR (500 MHz, $CDCl_3$) δ 9.26 (br s, 1H), 7.86-7.82 (m, 2H), 7.15 (t, *J*= 8.5 Hz, 2 H), 1.36 (s, 3H). ^{13}C{^{1}H} NMR (126 MHz, $CDCl_3$) δ 177.1, 165.9, 165.5 (d, *J*= 254.0 Hz), 130.1 (d, *J*= 9.1 Hz), 127.1 (d, *J*= 3.2 Hz), 116.1 (d, *J*= 19.9 Hz), 38.6, 27.1. FTIR (cm^{-1}): 3155, 3045, 2973, 1779, 1649, 1234, 1072. HRMS-ESI (m/z) calcd for $C_{12}H_{15}NO_3F$ [M+H]+ 240.1036, found 240.1034.

4-nitro-*N*-(pivaloyloxy)benzamide (III-1i)

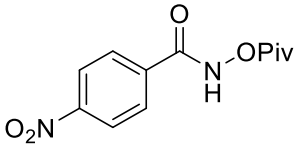

Following a modified procedure by Guimond et al,[21] to a flask containing a 2:1 EtOAc/Water mixture (11.25 mL total) was added sodium carbonate (318.4 mg, 3.0 mmol). The flask was cooled to 0 °C, then *O*-pivaloylhydroxylammonium trifluoromethane sulfonate (406.5 mg, 1.52 mmol)

was added. 4-nitrobenzoyl chloride (278.5 mg, 1.5 mmol) was added to the flask in one portion, and the reaction stirred for 6 h at 0 °C. The reaction was removed from ice bath and diluted with ethyl acetate (18 mL), then extracted three times with sat. aq. $NaHCO_3$ (3x 10 mL). The organic layer was dried over Na_2SO_4, filtered and concentrated to afford a crude solid. The solid was purified by automated CombiFlash chromatography (Petroleum Ether:EtOAc, 0-20% gradient) to afford a white solid (121.6 mg, 30%). m.p. 117-119 °C. ^{1}H NMR (500 MHz, $CDCl_3$) δ 9.35 (br s, 1H), 8.34 (d, *J*= 8.9 Hz, 2H), 8.00 (d, *J*= 8.9 Hz, 2H), 1.37 (s, 9H). $^{13}C\{^1H\}$ NMR (126 MHz, $CDCl_3$) δ 177.0, 164.6, 150.4, 136.5, 128.9, 124.2, 38.6, 27.1. FTIR (cm^{-1}): 3343, 3069, 2970, 1784, 1688, 1065. HRMS-ESI (m/z) calcd for $C_{12}H_{13}N_2O_5$ $[M-H]^-$ 265.0825, found 265.0833.

4-cyano-*N*-(pivaloyloxy)benzamide (III-1j)

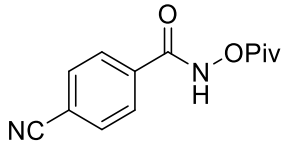

Following a modified procedure by Guimond et al,[21] in a dry flask equipped with stir bar was added 4-cyanobenzoic acid (215.9 mg, 1.5 mmol), anhydrous dichloromethane (7.5 mL), and dimethylformamide (3 drops). Oxalyl chloride (0.16 mL, 1.9 mmol) was introduced slowly dropwise via syringe. The reaction was allowed to stir for 3 hours at rt under N_2 atmosphere After 3 hours, the reaction mixture was concentrated *in vacuo* to afford a crude solid. The solid was purified by automated CombiFlash chromatography (EtOAc/Hexane) to afford a waxy white solid (92.9 mg, 26%). mp: 102-103°C. ^{1}H NMR (500 MHz, $CDCl_3$) 9.41 (br s, 1H), 7.92 (d, *J*= 8.08 Hz, 2H) 7.78 (d, *J*= 8.09 Hz, 2H), 1.36 (s, 9H). $^{13}C\{^1H\}$ NMR (126 MHz, $CDCl_3$) δ 177.0, 165.0, 134.9, 132.8, 128.3, 117.8, 116.4, 38.6, 27.1. FTIR (cm^{-1}): 3208, 2985, 2233, 1784, 1651, 1078. HRMS-ESI (m/z) calcd for $C_{13}H_{13}N_2O_3$ $[M-H]^-$ 245.0926, found 245.0932.

4-acetyl-*N*-(pivaloyloxy)benzamide (III-1k)

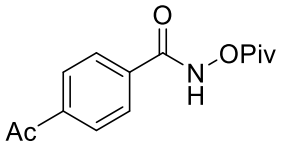

Following a modified procedure by Guimond et al,[21] in a dry flask equipped with stir bar was added 4-acetylbenzoic acid (571.4 mg, 3.5 mmol), anhydrous dichloromethane (17.5 mL), and dimethylformamide (5 drops). Oxalyl chloride (0.37 mL, 4.4 mmol) was introduced slowly dropwise via syringe. The reaction was allowed to stir for 22 hours at rt under N_2 atmosphere. After 22 hours, the reaction mixture was concentrated *in vacuo* to afford the crude acid chloride. The crude acid chloride was suspended in EtOAc (8.7 mL) and added to a flask containing EtOAc:Water (11.7 mL:5.8 mL), potassium carbonate (0.9694g, 7.01 mmol), *O*-pivaloylhydroxylammonium trifluoromethane sulfonate (1.026 g, 3.84 mmol) at 0 °C. The reaction was allowed to slowly warm to rt while stirring under N_2 atmosphere for 2 hours. The reaction was removed from ice bath and diluted with EtOAc and transferred to separatory funnel. The organic layer was extracted once with sat. aq. $NaHCO_3$ solution, once with brine, and separated. The organic layer was dried over Na_2SO_4, filtered, and concentrated *in vacuo* to yield a crude oil. The crude was purified by automated CombiFlash chromatography (EtOAc/Hexane) to afford a pale-yellow solid (359.9 mg, 39%). mp: 127-128 °C. ^{1}H NMR (500 MHz, $CDCl_3$) δ 9.67 (br s, 1H), 7.98 (d, *J*= 8.46 Hz, 2H), 7.88 (d, *J*= 8.4 Hz, 2H), 2.62 (s, 3H), 1.34 (s, 9H). $^{13}C\{^1H\}$ NMR (126 MHz, $CDCl_3$) δ 197.4, 177.1, 165.8, 140.2, 134.9, 128.8, 128.0, 38.6, 27.2, 27.0. FTIR (cm^{-1}): 3184, 2975, 1781, 1685, 1660, 1069. HRMS-ESI (m/z) calcd for $C_{14}H_{18}NO_4$ [M+H]+ 264.1236, found 264.1216.

***N*-(pivaloyloxy)-[1,1'-biphenyl]-3-carboxamide (III-1l)**

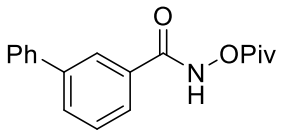

Following a modified procedure by Guimond et al,[21] in a dry flask equipped with stir bar was added [1,1'-biphenyl]-3-carboxylic acid (294.1 mg, 1.5 mmol), anhydrous dichloromethane (7.5 mL), and dimethylformamide (3 drops). Oxalyl chloride (0.16 mL, 1.89 mmol) was introduced slowly dropwise via syringe. The reaction was allowed to stir for 2.5 hours at rt under N_2 atmosphere. After 2.5 hours, the reaction mixture was concentrated *in vacuo* to afford the crude acid chloride. The crude acid chloride was suspended in EtOAc (5.5 mL) and added to a flask containing EtOAc:Water (4.0 mL:3.75 mL), sodium carbonate (313.8 mg, 2.96 mmol), and *O*-pivaloylhydroxylammonium trifluoromethane sulfonate (405.6 mg, 1.52 mmol) at 0 °C. The reaction stirred at 0 °C under N_2 atmosphere for 2 hours. The reaction was removed from ice bath and diluted with EtOAc (15 mL total) and transferred to separatory funnel. The organic layer was extracted once with sat. aq. $NaHCO_3$ solution (10 mL), once with brine (10 mL), and separated. The organic layer was dried over Na_2SO_4, filtered and concentrated *in vacuo* to yield a crude solid. The solid was purified by automated CombiFlash chromatography (Petroleum Ether:EtOAc, 0-20% gradient) to afford a white solid (263.6 mg, 60%). mp: 123-124 °C. ^{1}H NMR (500 MHz, $CDCl_3$) δ 9.40 (br s, 1H), 8.05 (s, 1 H), 7.80-7.76 (m, 2H), 7.61-7.59 (m, 2H), 7.55-7.51 (m, 1 H), 7.48-7.45 (m, 2H), 7.41-7.37 (m, 1H), 1.38 (s, 9H). ^{13}C{^{1}H} NMR (126 MHz, $CDCl_3$) δ 177.2, 167.0, 142.1, 139.9, 131.6, 131.5, 129.4, 129.1, 128.1, 127.3, 126.4, 126.2, 38.6, 27.2. FTIR (cm^{-1}): 3184, 3007, 2979, 1784, 1654, 1066. HRMS-ESI (m/z) calcd for $C_{18}H_{20}NO_3$ [M+H]+ 298.1443, found 298.1443.

3-methoxy-*N*-(pivaloyloxy)benzamide (III-1m)

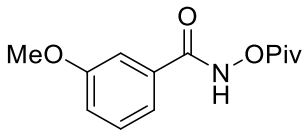

Following a modified procedure by Guimond et al,[21] to a flask containing a 2:1 EtOAc/Water water (11.25 mL total) was added sodium carbonate (318.3 mg, 3.00 mmol). The flask was cooled to 0 °C, then *O*-pivaloylhydroxylammonium trifluoromethane sulfonate (402.5 mg, 1.51 mmol) was added. 3-methoxybenzoyl chloride was added to the flask in one portion, and the reaction stirred for 6 h at 0 °C. The reaction was removed from ice bath and diluted with ethyl acetate (18 mL), then extracted three times with sat. aq. $NaHCO_3$ (3x ~10 mL). The organic layer was dried over Na_2SO_4, filtered and concentrated to afford a crude solid. The solid was purified by automated CombiFlash chromatography (Petroleum Ether:EtOAc, 0-20% gradient) to afford a white solid (301.1 mg, 80%). m.p. 57-59 °C ^{1}H NMR (500 MHz, $CDCl_3$) δ 9.49 (br s, 1H), 7.35-7.30 (m, 3H), 7.08-7.06 (m, 1 H), 3.82 (s, 3H), 1.35 (s, 9H). $^{13}C\{^1H\}$ NMR (126 MHz, $CDCl_3$) δ 177.1, 166.7, 160.0, 132.2, 129.9, 119.4, 119.3, 112.5, 55.6, 38.6, 27.1. FTIR (cm^{-1}): 3193, 3007, 2979, 1781, 1660, 1065. HRMS-ESI (m/z) calcd for $C_{13}H_{17}NO_4$ [M+H]+ 252.1236, found 252.1232.

***N*-(pivaloyloxy)benzo[d][1,3]dioxole-5-carboxamide (III-1n)**

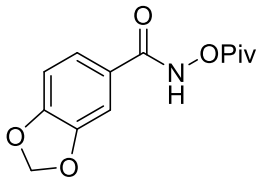

Following a modified procedure by Guimond et al,[21] in a dry flask equipped with stir bar was added piperonylic acid (249.4 mg, 1.5 mmol), anhydrous dichloromethane (7.5 mL), and dimethylformamide (3 drops). Oxalyl chloride (0.16 mL, 1.89 mmol) was introduced slowly dropwise via syringe. The reaction was allowed to stir for 3 hours at rt under N_2 atmosphere. After

3 hours, the reaction mixture was concentrated *in vacuo* to afford the crude acid chloride. The crude acid chloride was suspended in EtOAc (5.5 mL) and added to a flask containing EtOAc:Water (4.0mL:3.75 mL), sodium carbonate (321.9 mg, 3.02 mmol), *O*-pivaloylhydroxylammonium trifluoromethane sulfonate (407.7 mg, 1.52 mmol) at 0 °C. The reaction stirred at rt under N_2 atmosphere for 2 hours. The reaction was diluted with ethyl acetate (10 mL), then extracted with sat. aq. $NaHCO_3$, and brine (10 mL ea). The organic layer was dried over Na_2SO_4, filtered and concentrated to afford a crude solid. The solid was purified by automated CombiFlash chromatography (EtOAc/Hexane, 0-20% gradient) to afford a clear oil. The resulting oil was triturated in hexane to afford the desired product as a powdery white solid (320.9 mg, 81%). mp: 134-135 °C ^{1}H NMR (500 MHz, $CDCl_3$) δ 9.25 (br s, 1H), 7.39 (dd, *J*= 8.1, 1.5 Hz, 1H), 7.28 (d, *J*= 1.8 Hz, 1 H), 6.85 (d, *J*= 8.2 Hz, 1H), 6.04 (s, 2H), 1.35 (s, 9H). ^{13}C{^{1}H} NMR (126 MHz, $CDCl_3$)δ 177.4, 166.5, 151.6, 148.3, 124.9, 122.8, 108.5, 108.0, 102.0, 38.6, 27.2. FTIR (cm^{-1}): 3204, 3021, 2979, 1768, 1645, 1069. HRMS-ESI (m/z) calcd for $C_{13}H_{15}NO_5Na$ [M+Na]+ 288.0848, found 288.0840.

3-fluoro-*N*-(pivaloyloxy)benzamide (III-1o)

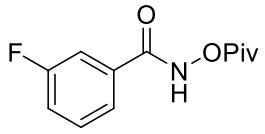

Following a modified procedure by Guimond et al,[21] in a dry flask equipped with stir bar was added 3-fluorobenzoic acid (209.2 mg, 1.5 mmol), anhydrous dichloromethane (7.5 mL), and dimethylformamide (3 drops). Oxalyl chloride (0.16 mL, 1.9 mmol) was introduced slowly dropwise via syringe. The reaction was allowed to stir for 2.5 hours at rt under N_2 atmosphere. After 2.5 hours, the reaction mixture was concentrated *in vacuo* to afford the crude acid chloride. The crude acid chloride was suspended in EtOAc (5.5 mL) and added to a flask containing

EtOAc:Water (4.0 mL:3.75 mL), sodium carbonate (313.8 mg, 3.0 mmol), *O*-pivaloylhydroxylammonium trifluoromethane sulfonate (405.6 mg, 1.52 mmol) at 0 °C. The reaction was allowed to slowly warm to rt while stirring under N_2 atmosphere for 2 hours. The reaction was removed from ice bath and diluted with EtOAc (15 mL total) and transferred to separatory funnel. The organic layer was extracted once with sat. aq. $NaHCO_3$ solution (10 mL), once with brine (10 mL), and separated. The organic layer was dried over Na_2SO_4, filtered and concentrated *in vacuo* to yield a crude solid. The solid was purified by automated CombiFlash chromatography (EtOAc/Hexane) to afford a white solid (238.1 mg, 67%). mp: 98-99 °C. ^{1}H NMR (500 MHz, $CDCl_3$) δ 9.40 (br s, 1H), 7.58-7.56 (m, 1H), 7.52 (dt, *J*= 9.1 Hz, 2.2 Hz, 1H), 7.45-7.41 (m, 1H), 7.28-7.24 (m, 1H), 1.36 (s, 9H). ^{13}C{^{1}H} NMR (126 MHz, $CDCl_3$) δ 177.1, 165.6, 162.8 (d, *J* = 249.1 Hz), 133.1 (d, *J* = 7.05 Hz), 130.8 (d, *J* = 7.82 Hz), 123.1 (d, *J* = 3.14 Hz), 120.0 (d, *J* = 21.27 Hz), 115.0 (d, *J* = 23.21 Hz), 38.6, 27.1. FTIR (cm^{-1}): 3232, 3078, 2981, 1784, 1699, 1221, 1061. HRMS-ESI (m/z) calcd for $C_{12}H_{13}NO_3F$ [M-H]$^-$ 238.0880, found 238.0876.

3-bromo-*N*-(pivaloyloxy)benzamide (III-1p)

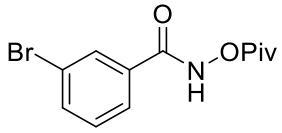

Following a modified procedure by Guimond et al,[21] in a dry flask equipped with stir bar was added 3-bromobenzoic acid (300.5 mg, 1.5 mmol), anhydrous dichloromethane (7.5 mL), and dimethylformamide (3 drops). Oxalyl chloride (0.16 mL, 1.9 mmol) was introduced slowly dropwise via syringe. The reaction was allowed to stir for 2.5 hours at rt under N_2 atmosphere. After 2.5 hours, the reaction mixture was concentrated *in vacuo* to afford the crude acid chloride. The crude acid chloride was suspended in EtOAc (5.5 mL) and added to a flask containing EtOAc:Water (4.0 mL:3.75 mL), sodium carbonate (325.0 mg, 3.1 mmol), *O*-

pivaloylhydroxylammonium trifluoromethane sulfonate (405.8 mg, 1.52 mmol) at 0 °C. The reaction stirred at 0 °C under N_2 atmosphere for 2 hours. The reaction was removed from ice bath and diluted with EtOAc (15 mL total) and transferred to separatory funnel. The organic layer was extracted once with sat. aq. $NaHCO_3$ solution (10 mL), once with brine (10 mL), and separated. The organic layer was dried over Na_2SO_4, filtered and concentrated *in vacuo* to yield a crude solid. The solid was purified by automated CombiFlash chromatography (Petroleum Ether:EtOAc, 0-20% gradient) to afford a white solid (249.3 mg, 55%) mp: 113-115 °C. ^{1}H NMR (500 MHz, $CDCl_3$) δ 9.40 (br s, 1H), 7.94 (t, *J*= 1.73 Hz, 1 H), 7.73-7.67 (m, 2H), 7.33 (t, *J*= 7.8 Hz, 1 H), 1.35 (s, 9H). $^{13}C\{^1H\}$ NMR (126 MHz, $CDCl_3$) δ 177.1, 165.4, 135.8, 132.9, 130.8, 130.5, 126.1, 123.1, 38.6, 27.1. FTIR (cm^{-1}): 3167, 3069, 2968, 1779, 1658, 1066. HRMS-ESI (m/z) calcd for $C_{12}H_{15}NO_3Br$ [M+H]+ 300.0235, found 300.0233.

***N*-(pivaloyloxy)thiophene-2-carboxamide (III-1q)**

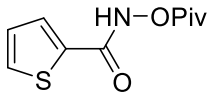

Following a modified procedure by Webb et al,[46] in a dry flask equipped with stir bar was added thiophene-2-carboxylic acid (191.1 mg, 1.5 mmol), anhydrous dichloromethane (7.5 mL), and dimethylformamide (3 drops). Oxalyl chloride (0.16 mL, 1.9 mmol) was introduced slowly dropwise via syringe. The reaction was allowed to stir for 3.5 hours at rt under N_2 atmosphere. After 3.5 hours, the reaction mixture was concentrated *in vacuo* to afford the crude acid chloride. The crude acid chloride was suspended in THF (4.0 mL) and added to a flask containing THF (7.5 mL), triethylamine (0.42 mL, 3.0 mmol), *O*-pivaloylhydroxylammonium trifluoromethane sulfonate (441.5 mg, 1.65 mmol) at 0 °C. The reaction was allowed to slowly warm to rt while stirring under N_2 atmosphere for 2 hours. The reaction was removed from ice bath and concentrated

to afford a crude residue, which was diluted with EtOAc (15 mL total) and transferred to separatory funnel. The organic layer was extracted once with sat. aq. $NaHCO_3$ solution (15 mL), once with brine (15 mL), and separated. The organic layer was dried over Na_2SO_4, filtered, and concentrated *in vacuo* to yield a crude solid. The solid was purified by automated CombiFlash chromatography (EtOAc/Hexane) to afford a white solid (121.8 mg, 36%). mp: 150-151 °C ^{1}H NMR (500 MHz, $CDCl_3$) δ 9.25 (br s, 1H), 7.67 (d, *J*= 3.75 Hz, 1H), 7.59 (d, *J*= 5.0 Hz, 1H), 7.12 (t, *J*= 4.3 Hz, 1H), 1.36 (s, 9H). $^{13}C\{^1H\}$ NMR (126 MHz, $CDCl_3$) δ 177.2, 162.0, 133.8, 131.9, 130.6, 128.0, 38.6, 27.2. FTIR (cm^{-1}): 3184, 3050, 2975, 1784, 1637, 1063. HRMS-ESI (m/z) calcd for $C_{10}H_{14}NO_3S$ [M+H]+ 228.0694, found 228.0684.

1-methyl-*N*-(pivaloyloxy)-1*H*-indole-2-carboxamide (III-1r)

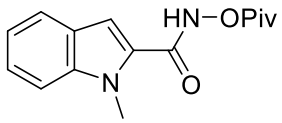

Following a modified procedure by Webb et al,[46] in a dry flask equipped with stir bar was added 1-methyl-*1H*-indole-2-carboxylic acid (260.5 mg, 1.5 mmol), anhydrous dichloromethane (7.5 mL), and dimethylformamide (3 drops). Oxalyl chloride (0.16 mL, 1.9 mmol) was introduced slowly dropwise via syringe. The reaction was allowed to stir for 3 hours at rt under N_2 atmosphere. After 3 hours, the reaction mixture was concentrated *in vacuo* to afford the crude acid chloride. The crude acid chloride was suspended in THF (4.0 mL) and added to a flask containing THF (7.5 mL), triethylamine (0.42 mL, 3.0 mmol), *O*-pivaloylhydroxylammonium trifluoromethane sulfonate (441.6 mg, 1.65 mmol) at 0 °C. The reaction was allowed to slowly warm to rt while stirring under N_2 atmosphere for 2 hours. The reaction was removed from ice bath and concentrated to afford a crude residue, which was diluted with EtOAc (15 mL total) and transferred to separatory funnel. The organic layer was extracted once with sat. aq. $NaHCO_3$ solution (15 mL), once with

brine (15 mL), and separated. The organic layer was dried over Na_2SO_4, filtered, and concentrated *in vacuo* to yield a crude solid. The solid was purified by automated CombiFlash chromatography (EtOAc/Hexane) to afford a beige solid (287.5 mg, 68%). mp: 124-125 °C ^{1}H NMR (500 MHz, $CDCl_3$) δ 9.30 (br s, 1H), 7.67 (d, *J*= 8.3 Hz, 1H), 7.40-7.35 (m, 2H), 7.19-7.16 (m, 1H), 7.07 (s, 1H), 4.01 (s, 3H), 1.39 (s, 9H). ^{13}C{^{1}H} NMR (126 MHz, $CDCl_3$) δ 177.3, 162.2, 139.6, 127.4, 126.0, 125.2, 122.5, 121.0, 110.4, 106.3, 38.6, 31.6, 27.2. FTIR (cm^{-1}): 3246, 3050, 2970, 1779, 1654, 1066. HRMS-ESI (m/z) calcd for $C_{15}H_{19}N2O_3$ [M+H]+ 275.1396, found 275.1391.

1-methyl-*N*-(pivaloyloxy)-1*H*-indole-3-carboxamide (III-1s)

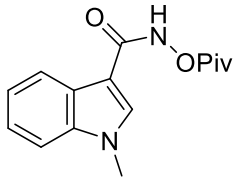

Following a modified procedure by Webb et al,[46] in a dry flask equipped with stir bar was added 1-methyl-*1H*-indole-3-carboxylic acid (263.0 mg, 1.5 mmol), anhydrous dichloromethane (7.5 mL), and dimethylformamide (3 drops). Oxalyl chloride (0.16 mL, 1.9 mmol) was introduced slowly dropwise via syringe. The reaction was allowed to stir for 3 hours at rt under N_2 atmosphere. After 3 hours, the reaction mixture was concentrated *in vacuo* to afford the crude acid chloride. The crude acid chloride was suspended in THF (4.0 mL) and added to a flask containing THF (7.5 mL), triethylamine (0.42 mL, 3.0 mmol), *O*-pivaloylhydroxylammonium trifluoromethane sulfonate (441.6 mg, 1.65 mmol) at 0 °C. The reaction was allowed to slowly warm to rt while stirring under N_2 atmosphere for 2 hours. The reaction was removed from ice bath and concentrated to afford a crude residue, which was diluted with EtOAc (15 mL total) and transferred to separatory funnel. The organic layer was extracted once with sat. aq. $NaHCO_3$ solution (15 mL), once with brine (15 mL), and separated. The organic layer was dried over Na_2SO_4, filtered, and concentrated

in vacuo to yield a crude solid. The solid was purified by automated CombiFlash chromatography (EtOAc/Hexane) to afford a white solid (151.9 mg, 37%). mp: 137-138 °C ^{1}H NMR (500 MHz, $CDCl_3$) δ 9.21 (br s, 1H), 8.07-8.05 (m, 1H), 7.73 (s, 1H), 7.36-7.27 (m, 3H), 3.79 (s, 3H), 1.38 (s, 9H). $^{13}C\{^{1}H\}$ NMR (126 MHz, $CDCl_3$) δ 177.8, 165.8, 137.2, 133.5, 125.6, 123.2, 122.2, 121.2, 110.2, 106.8, 38.6, 33.6, 27.3. FTIR (cm^{-1}): 3211, 3060, 2975, 1772, 1640, 1082. HRMS-ESI (m/z) calcd for $C_{15}H_{19}N2O_3$ [M+H]+ 275.1396, found 275.1399.

1,1'-(2-oxo-1*H*-imidazole-1,3(2*H*)-diyl)bis(ethan-1-one) (III-2a)

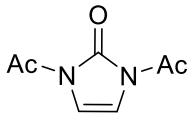

Following a modified procedure by Perrotta et al.,[64] 1,3-dihydro-2-imidazolone (4.02 g, 47.8 mmol) was suspended in acetic anhydride (60 mL) in a round bottom flask equipped with stir bar. The reaction was attached to reflux condenser and heated to reflux by sandbath under N_2 atm for 19 h. The flask was removed from heat and allowed to cool; the volatiles were removed under rotary evaporation. Residual acetic acid was removed by azeotropic distillation with toluene over several times. The resulting crude solid was purified by silica plug (CH_2Cl_2 as eluent) to afford a white solid (5.79 g, 72%). mp: 99-101 °C ^{1}H NMR (500 MHz, $CDCl_3$) δ 7.07 (s, 2H), 2.64 (s, 6H). $^{13}C\{^{1}H\}$ NMR (126 MHz, $CDCl_3$) δ 167.8, 149.6, 109.6, 24.3. FTIR (cm^{-1}): 3127, 2939, 1707 (br, s). HRMS-ESI (m/z) calcd for $C_7H_8N_2O_3Na$ [M+Na]+ 191.0433, found 191.0449.

1-acetyl-1,3-dihydro-2*H*-imidazol-2-one (III-2b)

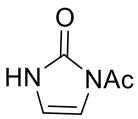

1,1'-(2-oxo-1*H*-imidazole-1,3(2*H*)-diyl)bis(ethan-1-one) **III-2a** (1.010 g, 6 mmol) was suspended in MeOH (15 mL) in a dry round-bottom flask equipped with stir bar. To the flask was added

cesium acetate (755.6 mg, 0.66 equiv) in one portion. The reaction was stirred at rt under N_2 atm for 1 h. The crude reaction mixture was diluted in brine (10 mL) and then promptly extracted with ethyl acetate (3 x 60 mL). The organic layers were pooled, dried over Na_2SO_4, filtered and concentrated to afford a crude solid. The solid was purified by automated CombiFlash chromatography (EtOAc/Hexane) to afford a white crystalline solid (501.7 mg, 66%). M.p.: 138-140 °C. ^{1}H NMR (500 MHz, DMSO-*d*$_6$) δ 10.48 (br s, 1H), 6.83 (d, *J*= 3.3 Hz, 1H), 6.63 (d, *J*= 3.3 Hz, 1H), 2.49 (s, 3H). ^{13}C{^{1}H} NMR (126 MHz, DMSO-*d*$_6$) δ 168.1, 152.0, 112.4, 106.6, 23.5. FTIR (cm^{-1}): 3202, 3144, 2930, 1689 (br, s). HRMS-ESI (m/z) calcd for $C_5H_6N_2O_2Na$ [M+Na]+ 149.0327, found 149.0308.

di-*tert*-butyl-2-oxo-*1H*-imidazole-1,3(2*H*)-dicarboxylate (III-2c)

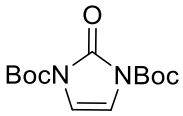

1,3-dihydro-2-imidazolone (501.1 mg, 6.00 mmol) was dissolved in dry acetonitrile (17 mL) in a round bottom flask equipped with stir bar. The reaction was cooled to 0 °C by ice bath. To the flask was added 4-dimethylaminopyridine (150.7 mg, 1.23 mmol), followed by addition of di-tert-butyl decarbonate (3.27 g, 15.0 mmol). The reaction stirred at 0 °C for 2.5 h and was then allowed to stir at rt under N_2 atm for 18 h. The crude reaction was transferred to a separatory funnel and diluted with ethyl acetate (30 mL). The organic layer was washed once with brine (30 mL) and separated. The organic layer was dried over Na_2SO_4, filtered, and concentrated *in vacuo* to yield a crude solid. The solid was purified by automated CombiFlash chromatography (EtOAc/Hexane) to afford a white solid (1.30 g, 76%). mp: 145-146 °C ^{1}H NMR (500 MHz, $CDCl_3$) δ 6.69 (s, 2H), 1.58 (2, 18H). ^{13}C{^{1}H} NMR (126 MHz, $CDCl_3$) δ 147.6, 146.6, 109.7, 85.1, 28.0. FTIR (cm^{-1}):

3165, 2983, 1803 (br, s). HRMS-ESI (m/z) calcd for $C_{13}H_{21}N_2O_5$ [M+H]+ 285.1451, found 285.1447.

Scope Evaluation: Annulation Products

3-acetyl-1,3a,4,9b-tetrahydro-2*H*-imidazo[4,5-c]isoquinoline-2,5(3*H*)-dione. (III-3a)

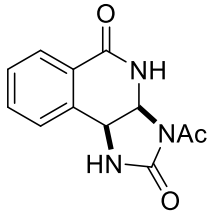

Without particular precautions to exclude air or moisture, *N*-(pivaloyloxy)benzamide **III-1a** (66.4 mg, 0.30 mmol), imidazolone **III-2b** (94.6 mg, 0.75 mmol), $[Cp^*RhCl_2]_2$ (9.20 mg, 5 mol %), and cesium acetate (57.6 mg, 0.30 mmol) were added into a one-dram vial (15 x 45 mm) equipped with stir bar. Lastly, 2,2,2-trifluoroethanol (0.10 mL, 3.0 M reaction mixture) was added to the vial by syringe, and the reaction vial was sealed with cap and PTFE tape. The reaction was stirred briefly at rt (<2 minutes) to afford an equilibrated orange suspension, then heated to 45 °C and stirred for 18 h. Following heating for 18 h, the reaction was removed from heat. The crude mixture was diluted in dichloromethane/methanol (1:1, < 5 mL) and transferred to scintillation vial and concentrated *in vacuo* to afford a crude mixture. The resulting mixture was adsorbed onto silica, then subjected to flash chromatography (EtOAc/Hexane, gradient 50%-100% EtOAc) to afford the desired monoacylated annulated product as a beige solid (60.0 mg, 82%). mp: 253°C (decomp). ^{1}H NMR (500 MHz, DMSO-d_6) δ 8.51 (s, 1H), 7.96-7.93 (m, 2H), 7.64 (t, *J*= 7.6 Hz 1H), 7.52 (t, *J*= 7.6 Hz, 1H), 7.47 (d, *J*= 7.6 Hz, 1H), 6.00 (d, *J*= 7.1 Hz, 1H), 5.00 (d, *J*= 7.1 Hz, 1 H), 2.37 (s, 3H). ^{13}C {^{1}H} NMR (126 MHz, DMSO-d_6) δ 169.9, 161.3, 154.3, 134.2, 132.8, 129.1, 129.0, 127.2, 126.0, 63.3, 47.0, 23.4. FTIR (cm^{-1}): 3215, 3102, 3049, 2926, 1733, 1702, 1678. HRMS-ESI (m/z) calcd for $C_{12}H_{12}N_3O_3$ [M+H]+ 246.0879, found 246.0873.

1 mmol scale reaction to afford III-3a:

Into a dry 5 mL round bottom flask equipped with stir bar was added *N*-(pivaloyloxy)benzamide **III-1a** (221.2 mg, 1.0 mmol), imidazolone **III-2b** (315.8 mg, 2.5 mmol), $[Cp^*RhCl_2]_2$ (30.8 mg, 5 mol %), and cesium acetate (191.9 mg, 1.0 mmol). To the flask was added 2,2,2-trifluoroethanol (0.33 mL, 3.0 M reaction mixture). The reaction flask was sealed with rubber septum and PTFE tape and stirred briefly at rt (<2 minutes) to afford an equilibrated orange suspension, then heated to 45 °C and stirred for 18 h. Following heating for 18 h, the reaction was removed from heat. The crude mixture was diluted in dichloromethane/methanol (1:1, <10 mL) and transferred to scintillation vial and concentrated *in vacuo* to afford a crude mixture. The resulting mixture was adsorbed onto silica then purified by automated CombiFlash chromatography (EtOAc/Hexane, gradient 50%-100% EtOAc). The resulting solid was triturated in CH_2Cl_2/Hexane and isolated by vacuum filtration to afford a beige solid (182.5 mg, 74%).

3-acetyl-8-methoxy-1,3a,4,9b-tetrahydro-2*H*-imidazo[4,5-c]isoquinoline-2,5(3*H*)-dione (III-3b)

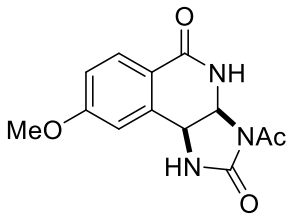

Without particular precautions to exclude air or moisture, 4-methoxy-*N*-(pivaloyloxy)benzamide **III-1b** (75.6 mg, 0.30 mmol), imidazolone **III-2b** (94.8 mg, 0.75 mmol), $[Cp^*RhCl_2]_2$ (9.20 mg, 5 mol %), and cesium acetate (57.6 mg, 0.30 mmol) were added into a one-dram vial (15 x 45 mm) equipped with stir bar. Lastly, 2,2,2-trifluoroethanol (0.10 mL, 3.0 M reaction mixture) was added to the vial by syringe, and the reaction vial was sealed with cap and PTFE tape. The reaction was stirred briefly at rt (<2 minutes) to afford an equilibrated orange suspension, then heated to 45 °C and stirred for 18 h. Following heating for 18 h, the reaction was removed from heat. The crude

mixture was diluted in dichloromethane/methanol (1:1, < 5 mL) and transferred to scintillation vial and concentrated *in vacuo* to afford a crude mixture. The resulting mixture was adsorbed onto silica, then subjected to flash chromatography (EtOAc/Hexane) to afford the desired monoacylated annulated product as a light beige solid (24.8 mg, 30%). mp: 275°C (decomp). ^{1}H NMR (500 MHz, DMSO-d_6) δ 8.48 (s, 1H), 7.89 (d, *J*= 8.5 Hz, 1H), 7.69 (s, 1H), 7.06-7.02 (m, 2H), 5.95 (d, *J*= 7.4 Hz, 1H), 4.97 (d, *J*= 7.5 Hz, 1H), 3.84 (s, 3H), 2.35 (s, 3H). ^{13}C{^{1}H} NMR (126 MHz, DMSO-d_6) δ 170.2, 162.6, 161.2, 154.2, 136.6, 129.4, 118.5, 114.8, 113.5, 63.5, 55.7, 46.9, 23.5. FTIR (cm^{-1}): 3261, 3170, 3083, 2974, 1744, 1664, 1270. HRMS-ESI (m/z) calcd for $C_{13}H_{14}N_3O_4$ [M+H]+ 276.0984, found 276.0987.

3-acetyl-8-methyl-1,3a,4,9b-tetrahydro-2*H*-imidazo[4,5-c]isoquinoline-2,5(3*H*)-dione (III-3c)

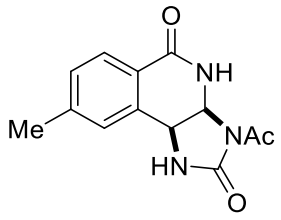

Without particular precautions to exclude air or moisture, 4-methyl-*N*-(pivaloyloxy)benzamide **III-1c** (70.6 mg, 0.30 mmol), imidazolone **III-2b** (94.7 mg, 0.75 mmol), [Cp*RhCl$_2$]$_2$ (9.20 mg, 5 mol %), and cesium acetate (57.8 mg, 0.30 mmol) were added into a one-dram vial (15 x 45 mm) equipped with stir bar. Lastly, 2,2,2-trifluoroethanol (0.10 mL, 3.0 M reaction mixture) was added to the vial by syringe, and the reaction vial was sealed with cap and PTFE tape. The reaction was stirred briefly at rt (<2 minutes) to afford an equilibrated orange suspension, then heated to 45 °C and stirred for 18 h. Following heating for 18 h, the reaction was removed from heat. The crude mixture was diluted in dichloromethane/methanol (1:1, < 5 mL) and transferred to scintillation vial and concentrated *in vacuo* to afford a crude mixture. The resulting mixture was adsorbed onto silica, then purified by automated CombiFlash chromatography (EtOAc/Hexane) to afford the

desired monoacylated annulated product which was further triturated in a minimal amount of dichloromethane/hexane to afford a beige solid (57.8 mg, 74%). mp: 277°C (decomp). ^{1}H NMR (500 MHz, DMSO-d_6) δ 8.46 (s, 1H), 7.84-7.82 (m, 2H), 7.33 (d, *J*= 8.0 Hz, 1H), 7.28 (s, 1H), 5.97 (dd *J*= 7.5, 1.3 Hz, 1H), 4.94 (d, *J*= 7.2 Hz, 1H), 2.38 (s, 3H), 2.36 (s, 3H). ^{13}C{^{1}H} NMR (126 MHz, DMSO-d_6) δ 170.0, 161.4, 154.2, 142.9, 134.2, 129.7, 129.4, 127.3, 123.5, 63.4, 47.0, 23.4, 21.2. FTIR (cm^{-1}): 3303, 3180, 3047, 2924, 1755, 1660. HRMS-ESI (m/z) calcd for $C_{13}H_{14}N_3O_3$ [M+H]+ 260.1035, found 260.1032.

3-acetyl-8-(*tert*-butyl)-1,3a,4,9b-tetrahydro-2*H*-imidazo[4,5-c]isoquinoline-2,5(3*H*)-dione (III-3d)

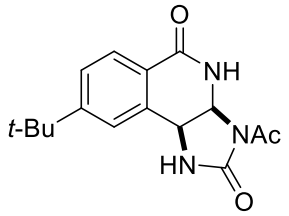

Without particular precautions to exclude air or moisture, 4-(*tert*-butyl)-*N*-(pivaloyloxy)benzamide **III-1d** (83.6 mg, 0.30 mmol), imidazolone **III-2b** (94.7 mg, 0.75 mmol), $[Cp^*RhCl_2]_2$ (9.40 mg, 5 mol %), and cesium acetate (57.9 mg, 0.30 mmol) were added into a one-dram vial (15 x 45 mm) equipped with stir bar. Lastly, 2,2,2-trifluoroethanol (0.10 mL, 3.0 M reaction mixture) was added to the vial by syringe, and the reaction vial was sealed with cap and PTFE tape. The reaction was stirred briefly at rt (<2 minutes) to afford an equilibrated orange suspension, then heated to 45 °C and stirred for 18 h. Following heating for 18 h, the reaction was removed from heat. The crude mixture was diluted in dichloromethane/methanol (1:1, < 5 mL) and transferred to scintillation vial and concentrated *in vacuo* to afford a crude mixture. The resulting mixture was adsorbed onto silica, then purified by automated CombiFlash chromatography (EtOAc/Hexane) to afford the desired monoacylated annulated product as a white solid (62.6 mg, 69%). mp: 269 °C (decomp). ^{1}H NMR (500 MHz, DMSO-d_6) δ 8.53 (s, 1H), 7.88

(d, *J*= 8.2 Hz, 1H), 7.80 (s, 1H), 7.55 (dd, *J*= 8.1, 1.6 Hz, 1H), 7.49 (d, *J*= 1.4 Hz, 1H), 5.98 (dd, *J*= 7.4, 1.5 Hz, 1H), 5.00 (d, *J*= 7.4 Hz, 1H), 2.36 (s, 3H), 1.31 (s, 9H). $^{13}C\{^{1}H\}$ NMR (126 MHz, DMSO-d_6) δ 170.2, 161.4, 155.9, 154.2, 134.2, 127.0, 125.9, 125.8, 123.3, 63.5, 47.0, 35.0, 30.9, 23.5. FTIR (cm^{-1}): 3413, 3153, 3036, 2981, 1753, 1642. HRMS-ESI (m/z) calcd for $C_{16}H_{20}N_3O_3$ [M+H]+ 302.1505, found 302.1505.

3-acetyl-8-iodo-1,3a,4,9b-tetrahydro-2*H*-imidazo[4,5-c]isoquinoline-2,5(3*H*)-dione (III-3e)

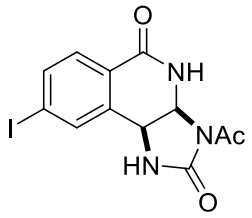

Without particular precautions to exclude air or moisture, 4-iodo-*N*-(pivaloyloxy)benzamide **III-1e** (104.8 mg, 0.30 mmol), imidazolone **III-2b** (94.6 mg, 0.75 mmol), $[Cp^*RhCl_2]_2$ (9.20 mg, 5 mol %), and cesium acetate (57.5 mg, 0.30 mmol) were added into a one-dram vial (15 x 45 mm) equipped with stir bar. Lastly, 2,2,2-trifluoroethanol (0.10 mL, 3.0 M reaction mixture) was added to the vial by syringe, and the reaction vial was sealed with cap and PTFE tape. The reaction was stirred briefly at rt (<2 minutes) to afford an equilibrated orange suspension, then heated to 45 °C and stirred for 18 h. Following heating for 18 h, the reaction was removed from heat. The crude mixture was diluted in dichloromethane/methanol (1:1, < 5 mL) and transferred to scintillation vial and concentrated *in vacuo* to afford a crude mixture. The resulting mixture was adsorbed onto silica, then purified by automated CombiFlash chromatography (EtOAc/Hexane) to afford the desired monoacylated annulated product as a tan amorphous solid (61.1 mg, 54%). 318 °C (decomp). ^{1}H NMR (500 MHz, DMSO-d_6) δ 8.47 (s, 1H), 8.06 (s, 1H), 7.91-7.89 (m, 2H), 7.69 (d, *J*= 8.5 Hz, 1H), 5.97 (dd, *J*= 7.2, 1.6 Hz, 1H), 4.97 (d, *J*= 7.3 Hz, 1H), 2.35 (s, 3H). $^{13}C\{^{1}H\}$ NMR (126 MHz, DMSO-d_6) δ 170.0, 161.0, 154.1, 137.9, 137.5, 136.2, 129.0, 125.5, 100.6, 63.3,

46.3, 23.5. FTIR (cm^{-1}): 3217, 3122, 3083, 2983, 1738, 1691, 1662. HRMS-ESI (m/z) calcd for $C_{12}H_{10}N_3O_3I$ [M+H]+ 371.9845, found 371.9847.

3-acetyl-8-bromo-1,3a,4,9b-tetrahydro-2*H*-imidazo[4,5-c]isoquinoline-2,5(3*H*)-dione (III-3f)

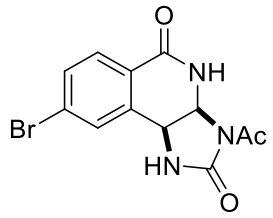

Without particular precautions to exclude air or moisture, 4-bromo-*N*-(pivaloyloxy)benzamide **III-1f** (90.0 mg, 0.30 mmol), imidazolone **III-2b** (132.8 mg, 1.05 mmol), $[Cp^*RhCl_2]_2$ (9.10 mg, 5 mol %), and cesium acetate (57.9 mg, 0.30 mmol) were added into a one-dram vial (15 x 45 mm) equipped with stir bar. Lastly, 2,2,2-trifluoroethanol (0.10 mL, 3.0 M reaction mixture) was added to the vial by syringe, and the reaction vial was sealed with cap and PTFE tape. The reaction was stirred briefly at rt (<2 minutes) to afford an equilibrated orange suspension, then heated to 45 °C and stirred for 36 h. Following heating for 36 h, the reaction was removed from heat. The crude mixture was diluted in dichloromethane/methanol (1:1, < 5 mL) and transferred to scintillation vial and concentrated *in vacuo* to afford a crude mixture. The resulting mixture was adsorbed onto silica, then purified by automated CombiFlash chromatography (EtOAc/Hexane) to afford the desired monoacylated annulated product as a white solid (53.5 mg, 55%). mp: 310 °C (decomp). ^1H NMR (500 MHz, DMSO-d_6) δ 8.49 (s, 1H), 8.10 (s, 1H), 7.87 (d, *J*= 8.2 Hz, 1H), 7.74–7.71 (m, 2H), 5.98 (d, *J*= 7.1 Hz, 1H), 5.01 (d, *J*= 7.1 Hz, 1H), 2.35 (s, 3H). $^{13}C\{^1H\}$ NMR (126 MHz, DMSO-d_6) δ 170.0, 160.7, 154.1, 136.6, 132.1, 131.7, 129.4, 126.3, 125.2, 63.4, 46.5, 23.5. FTIR (cm^{-1}): 3211, 3122, 3081, 2904, 1738, 1698, 1662. HRMS-ESI (m/z) calcd for $C_{12}H_{11}N_3O_3Br$ [M+H]+ 323.9984, found 323.9983.

3-acetyl-8-chloro-1,3a,4,9b-tetrahydro-2*H*-imidazo[4,5-c]isoquinoline-2,5(3*H*)-dione (III-3g)

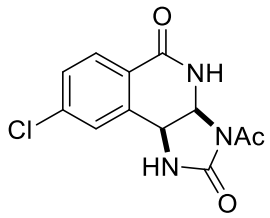

Without particular precautions to exclude air or moisture, 4-chloro-*N*-(pivaloyloxy)benzamide **III-1g** (77.2 mg, 0.30 mmol), imidazolone **III-2b** (132.3 mg, 1.05 mmol), $[Cp^*RhCl_2]_2$ (9.20 mg, 5 mol %), and cesium acetate (57.9 mg, 0.30 mmol) were added into a one-dram vial (15 x 45 mm) equipped with stir bar. Lastly, 2,2,2-trifluoroethanol (0.10 mL, 3.0 M reaction mixture) was added to the vial by syringe, and the reaction vial was sealed with cap and PTFE tape. The reaction was stirred briefly at rt (<2 minutes) to afford an equilibrated orange suspension, then heated to 45 °C and stirred for 36 h. Following heating for 36 h, the reaction was removed from heat. The crude mixture was diluted in dichloromethane/methanol (1:1, < 5 mL) and transferred to scintillation vial and concentrated *in vacuo* to afford a crude mixture. The resulting mixture was adsorbed onto silica, then purified by automated CombiFlash chromatography (EtOAc/Hexane) to afford the desired monoacylated annulated product as a white solid (35.5 mg, 42%). mp: 298 °C (decomp). ^{1}H NMR (500 MHz, DMSO-d_6) δ 8.49 (s, 1H), 8.09 (s, 1H), 7.95 (d, *J*= 8.2 Hz, 1H), 7.60-7.57 (m, 2H), 5.99 (dd, *J*= 7.2, 1.7 Hz, 1H), 5.01 (d, *J*= 7.4 Hz, 1H), 2.35 (s, 3H). ^{13}C{^{1}H} NMR (126 MHz, DMSO-d_6) δ 170.0, 160.5, 154.1, 137.3, 136.5, 129.3, 129.1, 128.8, 124.9, 63.4, 46.5, 23.5. FTIR (cm^{-1}): 3259, 3177, 3087, 2917, 1746, 1666. HRMS-ESI (m/z) calcd for $C_{12}H_{11}N_3O_3Cl$ [M+H]+ 280.0489, found 280.0489.

3-acetyl-8-fluoro-1,3a,4,9b-tetrahydro-2*H*-imidazo[4,5-c]isoquinoline-2,5(3*H*)-dione (III-3h)

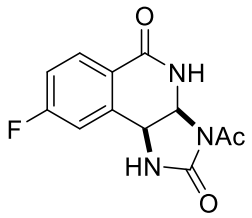

Without particular precautions to exclude air or moisture, 4-fluoro-*N*-(pivaloyloxy)benzamide **III-1h** (71.8 mg, 0.30 mmol), imidazolone **III-2b** (132.3 mg, 1.05 mmol), $[Cp^*RhCl_2]_2$ (9.30 mg, 5 mol %), and cesium acetate (58.4 mg, 0.30 mmol) were added into a one-dram vial (15 x 45 mm) equipped with stir bar. Lastly, 2,2,2-trifluoroethanol (0.10 mL, 3.0 M reaction mixture) was added to the vial by syringe, and the reaction vial was sealed with cap and PTFE tape. The reaction was stirred briefly at rt (<2 minutes) to afford an equilibrated orange suspension, then heated to 45 °C and stirred for 36 h. Following heating for 36 h, the reaction was removed from heat. The crude mixture was diluted in dichloromethane/methanol (1:1, < 5 mL) and transferred to scintillation vial and concentrated *in vacuo* to afford a crude mixture. The resulting mixture was adsorbed onto silica, then purified by automated CombiFlash chromatography (EtOAc/Hexane) to afford the desired monoacylated annulated product as a beige solid (29.1 mg, 37%). mp: 308 °C (decomp). ^{1}H NMR (500 MHz, DMSO-d_6) δ 8.51 (s, 1H), 8.02-7.99 (m, 2H), 7.38-7.34 (m, 2H), 5.99 (dd, *J*= 7.3, 1.3 Hz, 1H), 5.02 (d, *J*= 7.3 Hz, 1H), 2.35 (s, 3H). ^{13}C{^{1}H} NMR (126 MHz, DMSO-d_6) δ 170.0, 164.4 (d, *J*= 250.6 Hz), 160.5, 154.2, 137.5 (d, *J*= 9.1 Hz), 130.4 (d, *J*= 9.6 Hz), 122.67 (d, *J*= 2.6 Hz), 116.3 (d, *J*= 22.0 Hz), 115.6 (d, *J*= 22.9 Hz), 63.4, 46.7, 23.5. FTIR (cm^{-1}): 3259, 3191, 3087, 2922, 1739, 1671. HRMS-ESI (m/z) calcd for $C_{12}H_{11}N_3O_3F$ [M+H]+ 264.0784, found 264.0783.

3-acetyl-8-nitro-1,3a,4,9b-tetrahydro-2*H*-imidazo[4,5-c]isoquinoline-2,5(3*H*)-dione (III-3i)

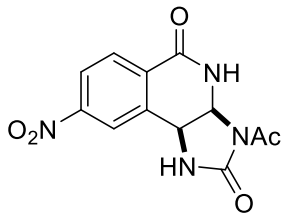

Without particular precautions to exclude air or moisture, 4-nitro-*N*-(pivaloyloxy)benzamide **III-1i** (143.0 mg, 0.54 mmol), imidazolone **III-2b** (236.7 mg, 1.89 mmol), $[Cp^*RhCl_2]_2$ (16.7 mg, 5 mol %), and cesium acetate (103.7 mg, 0.30 mmol) were added into a one-dram vial (15 x 45 mm) equipped with stir bar. Lastly, 2,2,2-trifluoroethanol (0.10 mL, 3.0 M reaction mixture) was added to the vial by syringe, and the reaction vial was sealed with cap and PTFE tape. The reaction was stirred briefly at rt (<2 minutes) to afford an equilibrated orange suspension, then heated to 45 °C and stirred for 36 h. Following heating for 36 h, the reaction was removed from heat. The crude mixture was diluted in dichloromethane/methanol (1:1, < 5 mL) and transferred to scintillation vial and concentrated *in vacuo* to afford a crude mixture. The resulting mixture was adsorbed onto silica, then purified by manual flash chromatography (EtOAc/Hexane) to afford the desired monoacylated annulated product as an off-white solid. The product was obtained following precipitation from a minimal amount of CH_2Cl_2/Hexane/MeOH to afford a white amorphous solid (6.3 mg, 4%). mp: 318 °C (decomp). ^{1}H NMR (500 MHz, DMSO-d_6) δ 8.60 (s, 1H), 8.44-8.43 (m, 2H), 8.34 (d, *J*= 8.3 Hz, 1H), 8.20 (d, *J*= 8.5 Hz, 1H), 6.04 (d, *J*= 7.3 Hz, 1H), 5.16 (d, *J*= 7.2 Hz, 1H), 2.36 (s, 3H). ^{13}C{^{1}H} NMR (126 MHz, DMSO-d_6) δ 170.0, 159.8, 154.1, 149.7, 136.4, 131.2, 129.1, 124.2, 123.8, 63.3, 46.5, 23.5. FTIR (cm^{-1}): 3239, 3175, 3081, 2915, 1757, 1671, 1340. HRMS-ESI (m/z) calcd for $C_{12}H_{10}N_4O_5$ [M+H]+ 291.0729, found 291.0731.

3-acetyl-7-phenyl-1,3a,4,9b-tetrahydro-2*H*-imidazo[4,5-c]isoquinoline-2,5(3*H*)-dione (III-3l)

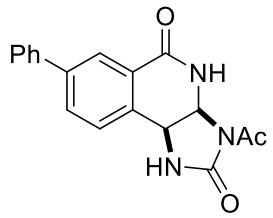

Without particular precautions to exclude air or moisture, *N*-(pivaloyloxy)-[1,1'-biphenyl]-3-carboxamide **III-1l** (89.2 mg, 0.30 mmol), imidazolone **III-2b** (94.4 mg, 0.75 mmol), $[Cp^*RhCl_2]_2$ (9.20 mg, 5 mol %), and cesium acetate (57.9 mg, 0.30 mmol) were added into a one-dram vial (15 x 45 mm) equipped with stir bar. Lastly, 2,2,2-trifluoroethanol (0.10 mL, 3.0 M reaction mixture) was added to the vial by syringe, and the reaction vial was sealed with cap and PTFE tape. The reaction was stirred briefly at rt (<2 minutes) to afford an equilibrated orange suspension, then heated to 45 °C and stirred for 18 h. Following heating for 18 h, the reaction was removed from heat. The crude mixture was diluted in dichloromethane/methanol (1:1, < 5 mL) and transferred to scintillation vial and concentrated *in vacuo* to afford a crude mixture. The resulting mixture was adsorbed onto silica, then subjected to manual column chromatography (EtOAc/Hexane) to afford the desired monoacylated annulated product as a tan solid (73.9 mg, 77%). mp: 284 °C (decomp). ^{1}H NMR (500 MHz, DMSO-d_6) δ 8.55 (s, 1H), 8.19 (d, *J*= 1.85 Hz, 1H), 8.05 (s, 1H), 7.97 (dd, *J*= 8.0, 1.9 Hz, 1H), 7.72 (d, *J*= 7.6 Hz, 2H), 7.58 (d, *J*= 8.0 Hz, 1H), 7.51 (t, *J*= 7.6 Hz, 2H), 7.42 (t, *J*= 7.4 Hz, 1H), 6.02 (dd, *J*= 7.2, 1.2 Hz, 1H), 5.05 (d, *J*= 7.2 Hz, 1H), 2.37 (s, 3H). ^{13}C{^{1}H} NMR (126 MHz, DMSO-d_6) δ 170.0, 161.3, 154.3, 140.8, 138.9, 133.2, 130.9, 129.9, 129.2, 128.1, 126.8, 126.6, 125.0, 63.4, 46.8, 23.5. FTIR (cm^{-1}): 3230, 3115, 3036 (w), 2924, 1741, 1683. HRMS-ESI (m/z) calcd for $C_{18}H_{16}N_3O_3$ [M+H]+ 322.1192, found 322.1188.

3-acetyl-7-methoxy-1,3a,4,9b-tetrahydro-2*H*-imidazo[4,5-c]isoquinoline-2,5(3*H*)-dione (3m(i)) *and* 3-acetyl-9-methoxy-1,3a,4,9b-tetrahydro-2*H*-imidazo[4,5-c]isoquinoline-2,5(3*H*)-dione (3m(ii))

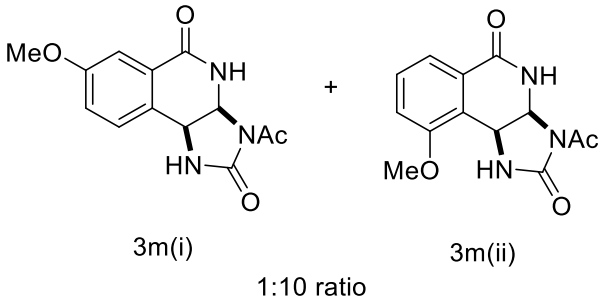

3m(i) 3m(ii)

1:10 ratio

Without particular precautions to exclude air or moisture, 3-methoxy-*N*-(pivaloyloxy)benzamide **III-1m** (75.6 mg, 0.30 mmol), imidazolone **III-2b** (94.6 mg, 0.75 mmol), $[Cp^*RhCl_2]_2$ (9.10 mg, 5 mol %), and cesium acetate (57.9 mg, 0.30 mmol) were added into a one-dram vial (15 x 45 mm) equipped with stir bar. Lastly, 2,2,2-trifluoroethanol (0.10 mL, 3.0 M reaction mixture) was added to the vial by syringe, and the reaction vial was sealed with cap and PTFE tape. The reaction was stirred briefly at rt (<2 minutes) to afford an equilibrated orange suspension, then heated to 45 °C and stirred for 18 h. Following heating for 18 h, the reaction was removed from heat. The crude mixture was diluted in dichloromethane/methanol (1:1, < 5 mL) and transferred to scintillation vial and concentrated *in vacuo* to afford a crude mixture. The resulting mixture was adsorbed onto silica, then purified by manual column chromatography (EtOAc/Hexane) to afford the desired monoacylated annulated products as a mixture of inseparable regioisomers (1:10, 3m(i):3m(ii)) as a white solid (77.6 mg, 94%). FTIR (cm^{-1}): 3362, 3257, 2932, 1722, 1678, 1254. HRMS-ESI (m/z) calcd for $C_{13}H_{14}N_3O_4$ [M+H]+ 276.0984, found 276.0983.

III-3m(i)

^{1}H NMR (500 MHz, DMSO-d_6) δ 8.43 (s, 1H), 7.95 (s, 1H), 7.44 (d, *J*= 2.8 Hz, 1H), 7.39 (d, *J*= 8.4 Hz, 1H), 7.22 (dd, *J*= 8.4 Hz, 2.8 Hz, 1H), 5.97 (d, *J*= 6.8 Hz, 1H), 4.94 (d, *J*= 7.2 Hz, 1H),

3.82 (s, 3H), 2.36 (s, 3H). $^{13}C\{^{1}H\}$ NMR (126 MHz, DMSO-d_6) δ 169.9, 159.7, 154.27, 130.6, 127.5, 126.1, 119.3, 110.9, 63.4, 55.5, 46.6, 23.4. *One quaternary carbon is missing or hidden*

III-3m(ii)

^{1}H NMR (500 MHz, DMSO-d_6) δ 8.27 (s, 1H), 7.84 (s, 1H), 7.56 (d, *J*= 7.7 Hz, 1H), 7.49 (t, *J*= 8.0 Hz, 1H), 7.30 (d, *J*= 8.2 Hz, 1H), 5.99 (d, *J*= 7.3 Hz, 1H), 5.06 (d, *J*= 7.3 Hz, 1H), 3.85 (s, 3H), 2.37 (s, 3H). $^{13}C\{^{1}H\}$ NMR (126 MHz, DMSO-d_6) δ 169.7, 161.3, 157.0, 154.29, 129.9, 127.2, 121.6, 118.8, 114.8, 63.0, 56.1, 42.5, 23.3.

3-acetyl-1,3a,4,10c-tetrahydro-*2H*-[1,3]dioxolo[4,5-f]imidazo[4,5-c]isoquinoline-2,5(*3H*)-dione (III-3n)

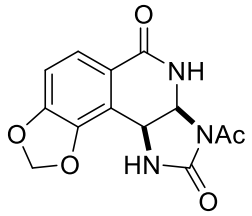

Without particular precautions to exclude air or moisture, *N*-(pivaloyloxy)benzo[d][1,3]dioxole-5-carboxamide **III-1n** (79.8 mg, 0.30 mmol), imidazolone **III-2b** (94.4 mg, 0.75 mmol), $[Cp^*RhCl_2]_2$ (9.20 mg, 5 mol %), and cesium acetate (57.9 mg, 0.30 mmol) were added into a one-dram vial (15 x 45 mm) equipped with stir bar. Lastly, 2,2,2-trifluoroethanol (0.10 mL, 3.0 M reaction mixture) was added to the vial by syringe, and the reaction vial was sealed with cap and PTFE tape. The reaction was stirred briefly at rt (<2 minutes) to afford an equilibrated orange suspension, then heated to 45 °C and stirred for 18 h. Following heating for 18 h, the reaction was removed from heat. The crude mixture was diluted in dichloromethane/methanol (1:1, < 5 mL) and transferred to scintillation vial and concentrated *in vacuo* to afford a crude mixture. The resulting mixture was adsorbed onto silica, then subjected to column chromatography (EtOAc/Hexane) to afford the desired monoacylated annulated product as a white solid (60.0 mg, 69%). mp: 302 °C (decomp). ^{1}H NMR (500 MHz, DMSO-d_6) δ 8.45 (s, 1H), 7.72 (s, 1H), 7.55

(d, *J*= 8.2 Hz, 1H), 7.07 (d, *J*= 8.2 Hz, 1H), 6.21 (d, *J*= 0.7 Hz, 1H), 6.16 (d, *J*= 0.7 Hz, 1H), 5.99 (d, *J*= 6.9 Hz, 1H), 4.99 (d, *J*= 6.8 Hz, 1 H), 2.36 (s, 3H). $^{13}C\{^{1}H\}$ NMR (126 MHz, DMSO-d_6) δ 169.5, 160.8, 154.2, 150.7, 145.6, 122.6, 120.2, 114.5, 108.7, 102.8, 63.3, 42.5, 23.3. FTIR (cm^{-1}): 3297, 3228, 3120, 2913, 1731, 1673, 1254. HRMS-ESI (m/z) calcd for $C_{13}H_{12}N_3O_5$ [M+H]+ 290.0777, found 290.0775.

3-acetyl-7-fluoro-1,3a,4,9b-tetrahydro-2*H*-imidazo[4,5-c]isoquinoline-2,5(3*H*)-dione (III-3o(i)) *and* 3-acetyl-9-fluoro-1,3a,4,9b-tetrahydro-2*H*-imidazo[4,5-c]isoquinoline-2,5(3*H*)-dione (III-3o(ii))

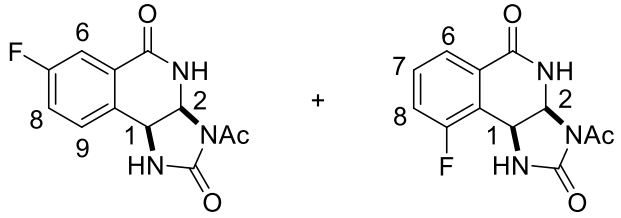

3o(i) 3o(ii)

1:4.3 ratio

Without particular precautions to exclude air or moisture, 3-fluoro-*N*-(pivaloyloxy)benzamide **III-1o** (72.0 mg, 0.30 mmol), imidazolone **III-2b** (132.5 mg, 1.05 mmol), $[Cp^*RhCl_2]_2$ (9.20 mg, 5 mol %), and cesium acetate (57.5 mg, 0.30 mmol) were added into a one-dram vial (15 x 45 mm) equipped with stir bar. Lastly, 2,2,2-trifluoroethanol (0.10 mL, 3.0 M reaction mixture) was added to the vial by syringe, and the reaction vial was sealed with cap and PTFE tape. The reaction was stirred briefly at rt (<2 minutes) to afford an equilibrated orange suspension, then heated to 45 °C and stirred for 36 h. Following heating for 36 h, the reaction was removed from heat. The crude mixture was diluted in dichloromethane/methanol (1:1, < 5 mL) and transferred to scintillation vial and concentrated *in vacuo* to afford a crude mixture. The resulting mixture was adsorbed onto silica, then purified by automated CombiFlash chromatography (EtOAc/Hexane) to afford the desired compounds as an inseparable mixture of regioisomers (1:4.3 3o(i):3o(ii)), as a white

powder (53.9 mg, 68%). FTIR (cm^{-1}): 3217 (br), 3107, 2970, 1744, 1666, 1246. HRMS-ESI (m/z) calcd for $C_{12}H_{11}N_3O_3F$ [M+H]+ 264.0784, found 264.0783.

III-3o(i)

^{1}H NMR (500 MHz, DMSO-d_6) δ 8.49 (s, 1H), 8.17 (s, 1H), 7.65 (d, *J*= 8.9 Hz, 1H), 7.61-7.52 (m, 2H)), coalesces with signals of 3m (ii)), 6.00 (d, *J*= 7.1 Hz, H_2), 5.00 (d, *J*= 7.2 Hz, H_1), 2.36 (s, 3H). ^{13}C{^{1}H} NMR (126 MHz, DMSO-d_6) δ 169.8 (C_q), 162.2 (d, *J*= 246.0 Hz, C-F), 160.3 (C_q), 154.21 (C_q), 131.8 (d, *J*= 7.5 Hz, C_9), 130.4 (d, *J*= 3.0 Hz, C_q), 128.5 (d, *J*= 7.7 Hz, C_q), 119.9 (d, *J*= 21.9 Hz, C_6/C_8), 113.4 (d, *J*= 23.2 Hz, C_6/C_8), 63.3 (C_2), 46.5 (C_1), 23.4.

III-3o(ii)

^{1}H NMR (500 MHz, DMSO-d_6) δ 8.54 (s, 1H), 8.09 (s, 1H), 7.82 (d, *J*= 7.5 Hz), 7.61-7.52 (m, 2H), coalesces with signals of 3m (i)), 6.05 (d, *J*= 6.8 Hz, H_2), 5.13 (d, *J*= 6.7 Hz, H_1), 2.37 (s, 3H). ^{13}C{^{1}H} NMR (126 MHz, DMSO-d_6) δ 169.4 (C_q), 160.3 (C_q), 160.1 (d, *J*= 248.8 Hz, C-F), 154.26 (C_q), 130.8 (d, *J*= 2.9 Hz, C_7), 128.4 (d, *J*= 2.9 Hz, C_q), 123.3 (d, *J*= 3.0 Hz, C_6), 120.7 (d, *J*= 16.1 Hz, C_q), 119.4 (d, *J*= 20.6 Hz, C_8), 63.1 (C_2), 41.7 (d, *J*= 3.6 Hz, C_1), 23.3.

3-acetyl-7-bromo-1,3a,4,9b-tetrahydro-2*H*-imidazo[4,5-c]isoquinoline-2,5(3*H*)-dione (III-3p)

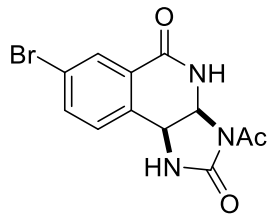

Without particular precautions to exclude air or moisture, 3-bromo-*N*-(pivaloyloxy)benzamide **III-1p** (90.1 mg, 0.30 mmol), imidazolone **III-2b** (132.7 mg, 1.05 mmol), $[Cp^*RhCl_2]_2$ (9.10 mg, 5 mol %), and cesium acetate (57.1 mg, 0.30 mmol) were added into a one-dram vial (15 x 45 mm) equipped with stir bar. Lastly, 2,2,2-trifluoroethanol (0.10 mL, 3.0 M reaction mixture) was added to the vial by syringe, and the reaction vial was sealed with cap and PTFE tape. The reaction was

stirred briefly at rt (<2 minutes) to afford an equilibrated orange suspension, then heated to 45 °C and stirred for 36 h. Following heating for 36 h, the reaction was removed from heat. The crude mixture was diluted in dichloromethane/methanol (1:1, < 5 mL) and transferred to scintillation vial and concentrated *in vacuo* to afford a crude mixture. The resulting mixture was adsorbed onto silica, then purified by automated CombiFlash chromatography (EtOAc/Hexane) to afford the desired monoacylated annulated product as a beige solid (53.7 mg, 55%). mp: 262 °C (decomp). ^{1}H NMR (500 MHz, DMSO-d_6) δ 8.52 (s, 1H), 8.18 (s, 1H), 8.02 (s, 1H), 7.88 (d, *J*= 8.0 Hz), 7.45 (d, *J*= 8.2 Hz, 1H), 5.99 (d, *J*= 7.1 Hz, 1H), 4.98 (d, *J*= 7.2 Hz, 1H), 2.36 (s, 3H). ^{13}C{^{1}H} NMR (126 MHz, DMSO-d_6) δ 169.9, 160.1, 154.2, 135.5, 133.4, 131.5, 129.6, 128.1, 122.2, 63.2, 46.5, 23.4. FTIR (cm^{-1}): 3167, 3078, 2973, 1753, 1664. HRMS-ESI (m/z) calcd for $C_{12}H_{11}N_3O_3Br$ [M+H]+ 323.9984, found 323.9983.

3-acetyl-1,3a,4,8b-tetrahydro-2*H*-imidazo[4,5-b]thieno[3,2-d]pyridine-2,5(3*H*)-dione (III-3q)

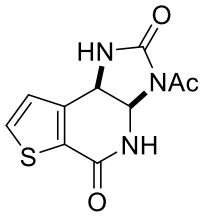

Without particular precautions to exclude air or moisture, *N*-(pivaloyloxy)thiophene-2-carboxamide **III-1q** (68.8 mg, 0.30 mmol), imidazolone **III-2b** (94.7mg, 0.75 mmol), $[Cp^*RhCl_2]_2$ (9.30 mg, 5 mol %), and cesium acetate (58.0 mg, 0.30 mmol) were added into a one-dram vial (15 x 45 mm) equipped with stir bar. Lastly, 2,2,2-trifluoroethanol (0.10 mL, 3.0 M reaction mixture) was added to the vial by syringe, and the reaction vial was sealed with cap and PTFE tape. The reaction was stirred briefly at rt (<2 minutes) to afford an equilibrated orange suspension, then heated to 45 °C and stirred for 18 h. Following heating for 18 h, the reaction was removed from heat. The crude mixture was diluted in dichloromethane/methanol (1:1, < 5 mL) and

transferred to scintillation vial and concentrated *in vacuo* to afford a crude mixture. The resulting mixture was adsorbed onto silica, then purified by manual column chromatography (EtOAc/Hexane) to afford the desired monoacylated annulated product as a light orange solid (26.1 mg, 34%). mp: 272 °C (decomp). ^{1}H NMR (500 MHz, DMSO-d_6) δ 8.55 (s, 1H), 7.93 (d, *J*= 4.7 Hz, 1H), 7.84 (s, 1H), 7.20 (d, *J*= 5.0 Hz), 5.98 (dd, *J*= 8.2, 2.0 Hz, 1H), 5.06 (d, *J*= 8.1Hz, 1H), 2.35 (s, 3H). ^{13}C{^{1}H} NMR (126 MHz, DMSO-d_6) δ 170.6, 158.3, 154.2, 141.1, 133.2, 129.8, 127.7, 65.2, 44.8, 23.6. FTIR (cm^{-1}): 3213 (b), 3083, 2924, 1738, 1673. HRMS-ESI (m/z) calcd for $C_{10}H_{1o}N_3O_3S$ [M+H]+ 252.0443, found 252.0441.

3-acetyl-6-methyl-3a,4,6,10c-tetrahydroimidazo[4',5':5,6]pyrido[3,4-*b*]indole-2,5(1*H*,3*H*)-dione (III-3r)

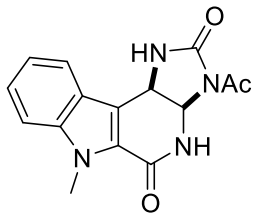

Without particular precautions to exclude air or moisture, 1-methyl-*N*-(pivaloyloxy)-*1H*-indole-2-carboxamide **III-1r** (82.2 mg, 0.30 mmol), imidazolone **III-2b** (94.7 mg, 0.75 mmol), $[Cp^*RhCl_2]_2$ (9.10 mg, 5 mol %), and cesium acetate (0.0576 mg, 0.30 mmol) were added into a one-dram vial (15 x 45 mm) equipped with stir bar. Lastly, 2,2,2-trifluoroethanol (0.10 mL, 3.0 M reaction mixture) was added to the vial by syringe, and the reaction vial was sealed with cap and PTFE tape. The reaction was stirred briefly at rt (<2 minutes) to afford an equilibrated orange suspension, then heated to 45 °C and stirred for 18 h. Following heating for 18 h, the reaction was removed from heat. The crude mixture was diluted in dichloromethane/methanol (1:1, < 5 mL) and transferred to scintillation vial and concentrated *in vacuo* to afford a crude mixture. The resulting mixture was adsorbed onto silica, then purified by manual column chromatography (EtOAc/Hexane) to afford the desired monoacylated annulated product as a dark pink-red solid

(47.7 mg, 53%). mp: 296 °C (decomp). ^{1}H NMR (500 MHz, DMSO-d_6) δ 8.65 (s, 1H), 7.80 (d, *J*= 7.8 Hz, 1H), 7.63 (s, 1H), 7.60 (d, *J*= 8.4 Hz, 1H), 7.38 (t, *J*= 7.5 Hz, 1H), 7.19 (t, *J*= 7.6 Hz, 1H), 6.06 (dd, *J*= 7.7, 1.3 Hz, 1H), 5.30 (d, *J*= 7.6 Hz, 1H), 4.06 (s, 3H), 2.38 (s, 3H). ^{13}C{^{1}H} NMR (126 MHz, DMSO-d_6) δ 170.3, 158.6, 154.5, 138.7, 125.1, 123.55, 123.52, 120.7, 120.6, 114.2, 110.9, 65.1, 43.4, 31.2, 23.5. FTIR (cm^{-1}): 3201, 3109, 2932, 1731, 1669. HRMS-ESI (m/z) calcd for $C_{15}H_{15}N_4O_3$ [M+H]+ 299.1144, found 299.1142.

1,3a,4,9b-tetrahydro-2*H*-imidazo[4,5-*c*]isoquinoline-2,5(3*H*)-dione. (III-5)

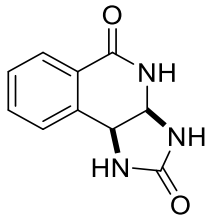

3-acetyl-1,3a,4,9b-tetrahydro-2*H*-imidazo[4,5-c]isoquinoline-2,5(3*H*)-dione **III-3a** (65.2 mg, 0.27 mmol) was dissolved in methanol (13 mL) in a dry round bottom flask equipped with stir bar. Potassium carbonate (57.5 mg, 0.42 mmol) was added in one portion and the reaction stirred under N_2 atm for 4 h. After 4 h, the pH of the solution was neutralized with 10% aqueous HCl solution. The crude mixture was then concentrated *in vacuo*. The desired product was then purified by automated CombiFlash chromatography (CH_2Cl_2/MeOH) and isolated as a white crystalline solid (41.1 mg, 76%). mp: 280 °C (decomp). ^{1}H NMR (500 MHz, DMSO-d_6) δ 8.18 (d, *J*= 2.4 Hz, 1H), 7.92 (dd, *J*= 7.7, 1.1 Hz, 1H), 7.62 (td, *J*= 7.5, 1.4 Hz, 1H), 7.50 (d, *J*= 7.5 Hz, 1H), 7.47 (td, *J*= 7.5, 1.1 Hz, 1H), 7.36 (s, 1H), 6.92 (s, 1H), 5.30-5.28 (m, *J*= 7.2, 2.8, 1.5 Hz, 1H), 4.85 (d, *J*= 7.3 Hz, 1H). ^{13}C{^{1}H} NMR (126 MHz, DMSO-d_6) δ 161.9, 161.3, 136.8, 132.6, 128.3, 128.1, 126.7, 126.2, 62.5, 50.0. FTIR (cm-1): 3278, 3208, 3129, 2906, 1673, 1647. HRMS-ESI (m/z) calcd for $C_{10}H_{10}N_3O$ [M+H]+ 203.0773, found: 203.0773.

Control Reaction: Effect of Protecting Group

Effect of the Acyl group

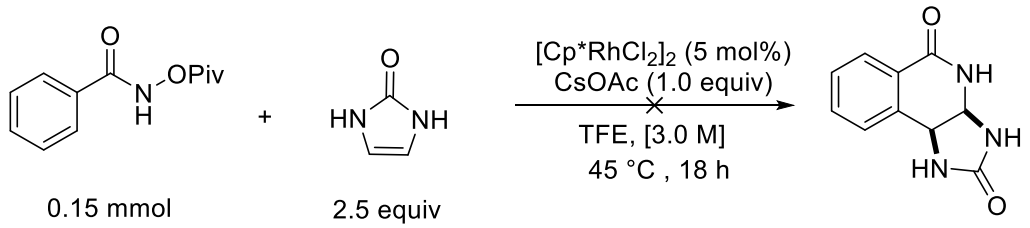

Without particular precautions to exclude air or moisture, *N*-(pivaloyloxy)benzamide **III-1a** (33.2 mg, 0.15 mmol), 1,3-dihydroimidazol-2-one (31.8 mg, 0.38 mmol), $[Cp^*RhCl_2]_2$ (4.60 mg, 5 mol %), and cesium acetate (28.8 mg, 0.15 mmol) were added into a one-dram vial (15 x 45 mm) equipped with stir bar. Lastly, 2,2,2-trifluoroethanol (0.05 mL, 3.0 M reaction mixture) was added to the vial by syringe, and the reaction vial was sealed with cap and PTFE tape. The reaction was stirred briefly at rt (<2 minutes) to afford an equilibrated orange suspension, then heated to 45 °C and stirred for 18 h. Following heating for 18 h, the reaction was removed from heat. The crude mixture was diluted in dichloromethane/methanol (1:1, < 5 mL) and transferred to scintillation vial and concentrated *in vacuo* to afford a crude mixture. Immediately following concentration, 1,3,5-trimethoxybenzene (25.3 mg, 0.15 mmol) was added to the reaction mixture, and this was diluted with DMSO-d_6 (1.0 mL). The reaction mixture was allowed to dissolve completely prior to transfer to an NMR tube. The presence of annulation product **III-5a** was not detected when the sample was subjected to ^{1}H-NMR experimental analysis.

Effect of the DiBoc group

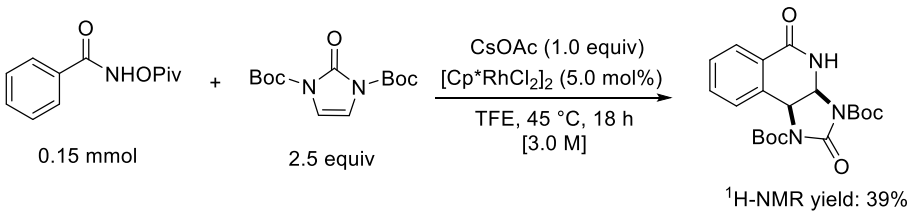

[1]H-NMR yield determined by using 1,3,5-trimethoxybenzene as standard.

Without particular precautions to exclude air or moisture, *N*-(pivaloyloxy)benzamide **III-1a** (33.2 mg, 0.15 mmol), di-tert-butyl 2-oxo-1*H*-imidazole-1,3(2*H*)-dicarboxylate **III-2c** (106.6 mg, 0.38 mmol), $[Cp^*RhCl_2]_2$ (4.6 mg, 5 mol %), and cesium acetate (28.4 mg, 0.15mmol) were added into a one dram vial (15 x 45 mm) equipped with stir bar. Lastly, 2,2,2-trifluoroethanol (0.5 mL, 3.0 M reaction mixture) was added to the vial by syringe, and the reaction vial was sealed with cap and PTFE tape. The reaction was stirred briefly at rt (<2 minutes) to afford an equilibrated orange suspension, then heated to 45 °C and stirred for 18 h. Following heating for 18 h, the reaction was removed from heat. The crude mixture was diluted in dichloromethane/methanol (1:1, < 5 mL) and transferred to scintillation vial and concentrated *in vacuo* to afford a crude mixture. Immediately following concentration, 1,3,5-trimethoxybenzene (25.2 mg, 0.15 mmol) was added to the reaction mixture, and this was diluted with DMSO-d_6 (1.0 mL). The reaction mixture was allowed to dissolve completely prior to transfer to an NMR tube. The presence of annulation product was observed in 39% yield when the sample was subjected to ^{1}H-NMR experimental analysis, using 1,3,5-trimethoxybenzene as internal control.

Reversibility of reaction in presence of monoacylated imidazolone III-2b

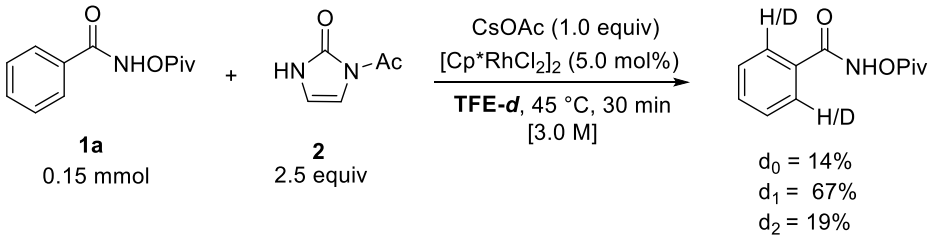

Without particular precautions to exclude air or moisture, *N*-(pivaloyloxy)benzamide **III-1a** (66.8 mg, 0.30 mmol), imidazolone **III-2b** (94.4 mg, 0.75 mmol), $[Cp^*RhCl_2]_2$ (9.2 mg, 5 mol %), and cesium acetate (57.8 mg, 0.30 mmol) were added into a one-dram vial (15 x 45 mm) equipped with stir bar. Lastly, deuterated 2,2,2-trifluoroethanol (0.1 mL, 3.0 M reaction mixture) was added to the vial by syringe, and the reaction vial was sealed with cap and PTFE tape. The reaction was stirred briefly at rt (<2 minutes) to afford an equilibrated orange suspension, then heated to 45 °C and stirred for 30 minutes. The reaction was then removed from heat and diluted in dichloromethane (< 5 mL) and transferred to scintillation vial. To the vial was added silica, and the crude product was subsequently adsorbed onto the silica gel following evaporation *in vacuo*. The crude reaction mixture was then purified to recover the benzohydroxamate (32.3 mg, 48%) which was then subjected to ESI-MS to determine deuterium incorporation. Significant deuterium incorporation was observed. The results of this study are tabulated in the table below.

Table 3.5 Percent deuterium incorporation (HRMS-ESI+)

Percent Deuterium Incorporation (HRMS- ESI+)						
Identity	m/z	Intensity	Adj. Intensity	Calculated M+2 Contribution	Fraction of Total	%D Incorp.
d_0	222.1125	5508	5508	716.04	0.137174433	13.72%
d_1	223.1223	27683	26966.96	3505.7048	0.671600842	67.16%
d_2	224.1275	11184	7678.2952	998.178376	0.191224725	19.12%
		Sum	Sum			
		44375	40153.2552			

Reaction Optimization Studies

Initial Optimization Studies

N-(Pivaloyloxy)benzamide **III-1a** (33.1 mg, 0.15 mmol), $[Cp^*RhCl_2]_2$ (4.6 mg, 5 mol%) and acetate base (0.07 mmol, or 0.15 mmol) were combined in a one-dram vial (15 x 45 mm) equipped with stir bar. To the vial was added solvent (0.38 mL, 0.40 M or 0.76 mL, 0.20 M); the reaction was stirred briefly prior to addition of N,N'-diacylimidazolone **III-2a** (37.8 mg, 0.23 mmol) in one portion. The resulting reaction was sealed with cap and PTFE tape and allowed to stir (rt or 45 °C) for 24 h. The crude mixture was then diluted in dichloromethane (~5 mL) and transferred to a scintillation vial prior to rotary evaporation (700 mmHg, 45 °C) to afford a crude viscous oil. The oil was placed under vacuum for an additional 2 hours at rt. The crude reaction was then diluted in 1.0 mL DMSO-d_6, and 1,3,5-trimethoxybenzene (25.2 mg, 0.15 mmol) was added to the crude. The resulting solution was transferred to NMR tube and subjected to ^{1}H-NMR analysis to calculate yield.

Table 3.2 Initial reaction screening with imidazolone **III-2a**

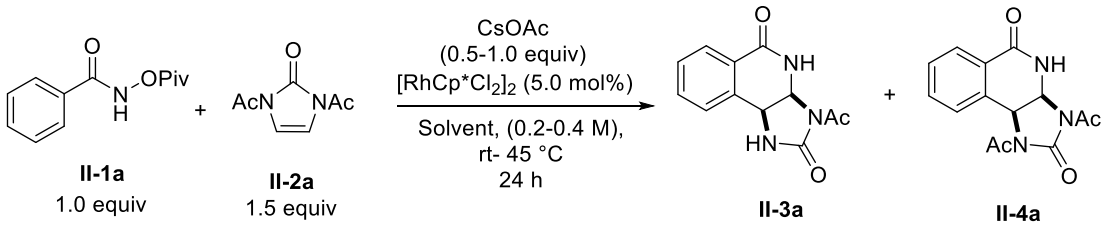

II-1a 1.0 equiv + **II-2a** 1.5 equiv → **II-3a** + **II-4a**

Entry	Solvent	Conc	Temp	Equiv CsOAc	SM Recovery	^{1}H-NMR Yield*
1	MeOH	0.4 M	rt	0.5	10%	28% **III-3a**, 23% **III-4a**
2	EtOH	0.4 M	rt	0.5	5%	8% **III-3a**, 55% **III-4a**
3	i-PrOH	0.4 M	rt	0.5	43%	46% **III-4a**
4	TFE	0.4 M	rt	0.5	47%	43% **III-3a**
5	HFIP	0.4 M	rt	0.5	quant	trace pdt
6	MeCN	0.4 M	rt	0.5	40%	20% **III-4a**
7	EtOH	0.4 M	45	0.5	0%	9% **III-3a**, 22% **III-4a**
8	EtOH	0.2 M	rt	0.5	11%	7% **III-3a**, 60% **III-4a**

Table 3.2 (cont'd)

9	EtOH	0.2 M	rt	1.0	trace	25% **III-3a**, 49% **III-4a**
10**	EtOH	0.2 M	rt	1.0	0%	2% **III-3a**, 44% **III-4a**
11***	EtOH	0.2 M	rt	1.0	5%	7% **III-3a**, 43% **III-4a**

*^{1}H-NMR yield determined utilizing 1,3,5-trimethoxybenzene as standard. **NaOAc screened as base. ***KOAc screened as base.

While reaction conditions were initially optimized using EtOH as solvent (entry 9), difficulties associated with purification and the formation of other aromatic byproducts under these conditions prompted us to reinvestigate 2,2,2-trifluoroethanol as solvent. Vacuum pump studies were thus initiated using TFE to determine whether higher yields were accessible when the reaction sat as a crude oil (see below).

Vacuum-pump studies utilizing TFE as solvent

N-(Pivaloyloxy)benzamide **III-1a** (33.1 mg, 0.15 mmol), $[Cp^*RhCl_2]_2$ (4.6 mg, 5 mol%) and CsOAc (28.7 mg, 0.15 mmol) were combined in a one-dram vial (15 x 45 mm) equipped with stir bar. To the vial was added 2,2,2-trifluoroethanol (0.38 mL, 0.40 M); the reaction was stirred briefly prior to addition of N,N'-diacylimidazolone **III-2b** (37.8 mg, 0.23 mmol) in one portion. The resulting reaction was sealed with cap and PTFE tape and allowed to stir at rt for 24 h. The crude mixture was then diluted in dichloromethane (~5 mL) and transferred to a scintillation vial prior to rotary evaporation (700 mmHg, 45 °C) to afford a crude viscous oil. The oil was placed under vacuum for an additional time period at rt. The crude reaction was then diluted in 1.0 mL DMSO-d_6, and 1,3,5-trimethoxybenzene (25.2 mg, 0.15 mmol) was added to the crude. The resulting solution was transferred to NMR tube and subjected to ^{1}H-NMR analysis to calculate yield.

Table 3.3 Vacuum pump studies of reaction utilizing TFE as solvent

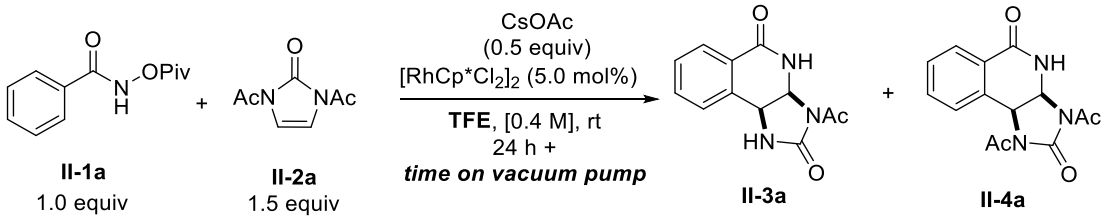

Entry	Conc	Equiv CsOAc	Time on vacuum pump	SM Recovery	^{1}H-NMR Yield*
1**	0.4 M	0.5	2 h	47%	43% **III-3a**
2	0.4 M	0.5	9.5 h	12%	83% **III-3a**
3	0.4 M	0.5	> 12 h	0%	95% **III-3a**

*^{1}H-NMR yield determined utilizing 1,3,5-trimethoxybenzene as standard.

These results prompted the further investigation of reaction yield as a function of constant concentration as discussed in the manuscript (see below).

Concentration studies utilizing TFE as solvent

Without particular precautions to exclude air or moisture, *N*-(pivaloyloxy)benzamide **III-1a** (33.2 mg, 0.15 mmol), imidazolone **III-2b** (28.6 mg, 0.23 mmol or 47.3 mg, 0.38 mmol), $[Cp^*RhCl_2]_2$ (4.6 mg, 5 mol % or 2.3 mg, 2.5 mol%), and cesium acetate (28.8 mg, 0.15 mmol) were added into a one-dram vial (15 x 45 mm) equipped with stir bar. Lastly, 2,2,2-trifluoroethanol (0.15 to 0.05 mL, 1.0-3.0 M) was added to the vial by syringe, and the reaction vial was sealed with cap and PTFE tape. The reaction was stirred briefly at rt (<2 minutes) to afford an equilibrated orange suspension, then stirred (rt to 45 °C) for the determined time period (18-24 h). The resulting crude mixture was diluted in dichloromethane/methanol (1:1, < 5 mL) and transferred to scintillation vial and concentrated *in vacuo* to afford a crude mixture. The crude mixture was immediately diluted in 1.0 mL DMSO-d_6, and to the vial was added 1,3,5-trimethoxybenezene (25.2 mg, 0.15 mmol).

The resulting crude solution was transferred to an NMR tube and subjected to ^{1}H-NMR analysis to calculate yield.

Table 3.4 Final optimization studies using imidazolone **III-2b**

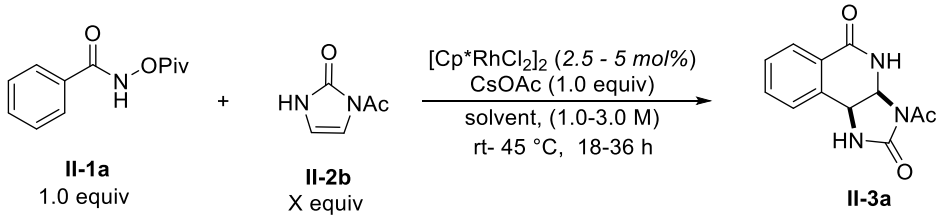

II-1a
1.0 equiv

II-2b
X equiv

II-3a

Entry	Solvent	Conc	Temp	Time	Equiv III-2b	^{1}H-NMR Yield* **III-3a**
1	TFE	1.0 M	rt	24 h	1.5	35%
2	TFE	2.0 M	rt	24 h	1.5	59%
3	TFE	2.5 M	rt	24 h	1.5	68%
4	TFE	3.0 M	rt	24 h	1.5	76%
5	TFE	3.0 M	rt	36 h	1.5	87%
6	TFE	3.0 M	45 °C	18 h	1.5	86%
7	**TFE**	**3.0 M**	**45 °C**	**18 h**	**2.5**	**92%**
8**	TFE	3.0 M	45 °C	18 h	2.5	85%
9	MeCN	3.0 M	45 °C	18 h	2.5	67%

*^{1}H-NMR yield determined utilizing 1,3,5-trimethoxybenzene as standard.
**Catalyst loading: 2.5 mol%.

REFERENCES

1. Hubbell, G. E.; Tepe, J. J., *Org. Lett.,* **2022**, *24*, 6740-6744.

2. Lansdell, T. A.; Hewlett, N. M.; Skoumbourdis, A. P.; Fodor, M. D.; Seiple, I. B.; Su, S.; Baran, P. S.; Feldman, K. S.; Tepe, J. J., *J. Nat. Prod.* **2012**, *75*, 980-985.

3. Beck, P.; Lansdell, T. A.; Hewlett, N. M.; Tepe, J. J.; Groll, M., *Angew. Chem., Int. Ed. Engl.,* **2015**, *54*, 2830-2833.

4. De Souza, R. T. M. P.; Freire, V. F.; Gubiani, J. R.; Ferreira, R. O.; Trivella, D. B. B.; Moraes, F. C.; Paradas, W. C.; Salgado, L. T.; Pereira, R. C.; Amado Filho, G. M.; Ferreira, A. G.; Williams, D. E.; Andersen, R. J.; Molinski, T. F.; Berlinck, R. G. S., *J. Nat. Prod.,* **2018**, *81*, 2296-2300.

5. Foley, L. H.; Buchi, G., *J. Am. Chem. Soc.,* **1982**, *104*, 1776-1777.

6. Weise, K. J.; Yakushijin, K.; Horne, D. A., *Tetrahedron Lett.,* **2002**, *43*, 5135-5136.

7. Lu, J.; Tan, X.; Chen, C., *J. Am. Chem. Soc.,* **2007**, *129*, 7768-7769.

8. Feldman, K. S.; Skoumbourdis, A., *Org. Lett.,* **2005**, *7*, 929-931.

9. Feldman, K. S.; Skoumbourdis, A. P.; Fodor, M. D., *J. Org. Chem.,* **2007**, *72*, 8076-8086.

10. Feldman, K. S.; Nuriye, A. Y.; Li, J., *J. Org. Chem.,* **2011**, *76*, 5042-5060.

11. Chung, R.; Yu, E.; Incarvito, C. D.; Austin, D. J., *Org. Lett.,* **2004**, *6*, 3881-3884.

12. Hewlett, N. M.; Tepe, J. J., *Org. Lett.,* **2011**, *13*, 4550-4553.

13. Iwata, M.; Kanoh, K.; Imaoka, T.; Nagasawa, K., *ChemComm.,* **2014**, *50*, 6991-6994.

14. Iwata, M.; Kamijoh, Y.; Yamamoto, E.; Yamanaka, M.; Nagasawa, K., *Org. Lett,.* **2017**, *19*, 420-423.

15. Ueura, K.; Satoh, T.; Miura, M., *Org. Lett.,* **2007**, *9*, 1407-1409.

16. Ueura, K.; Satoh, T.; Miura, M., *J. Org. Chem.,* **2007**, *72*, 5362-5367.

17. Gerfaud, T.; Neuville, L.; Zhu, J., *Angew. Chem., Int. Ed. Engl.,* **2009**, *48*.

18. Wu, J.; Cui, X.; Chen, L.; Jiang, G.; Wu, Y.,. *J. Am. Chem. Soc.,* **2009**, *131*, 13888-13889.

19. Tan, Y.; Hartwig, J. F., *J. Am. Chem. Soc.,* **2010**, *132*, 3676-3677.

20. Guimond, N.; Gouliaras, C.; Fagnou, K., *J. Am. Chem. Soc.,* **2010**, *132*, 6908-6909.

21. Guimond, N.; Gorelsky, S. I.; Fagnou, K., *J. Am. Chem. Soc.* **2011**, *133*, 6449-6457.

22. Rakshit, S.; Grohmann, C.; Besset, T.; Glorius, F., *J. Am. Chem. Soc.*, **2011**, *133*, 2350-2 353.

23. Xu, L.; Zhu, Q.; Huang, G.; Cheng, B.; Xia, Y., *J. Org. Chem.*, **2012**, *77*, 3017-24.

24. Qi, X.; Li, Y.; Bai, R.; Lan, Y., *Acc. Chem. Res.*, **2017**, *50*, 2799.

25. Wang, H.; Grohmann, C.; Nimphius, C.; Glorius, F., *J. Am. Chem. Soc.*, **2012**, *134*, 19592-19595.

26. Wang, H.; Glorius, F., *Angew. Chem., Int. Ed. Engl.*, **2012**, *51*, 7318-7322.

27. Hyster, T. K.; Rovis, T., *Synlett.* **2013**, *24*, 1842-1844.

28. Presset, M.; Oelhrich, D.; Rombouts, F.; Molander, G. A., *Org. Lett.*, **2013**, *15*, 1528-1531.

29. Shi, Z.; Boultadakis-Arapinis; Koester, D. C.; Glorius, F., *ChemComm.*, **2014**, *50*, 2650-2652.

30. Wodrich, M. D.; Ye, B.; Gonthier, J. F.; Corminboeuf, C.; Cramer, N., *Chem. Eur. J.* **2014**, *20*, 15409-18.

31. Hyster, T. K.; Dalton, D. M.; Rovis, T., *Chem. Sci.*, **2015**, *6*, 254-258.

32. Zhu, R. Y.; Farmer, M. E.; Chen, Y. Q.; Yu, J. Q., *Angew. Chem., Int. Ed. Engl.*, **2016**, *55*, 10578-99.

33. Wu, J.-Q.; Zhang, S.-S.; Gao, H.; Zisong, Q.; Zhou, C.-J.; Ji, W.-W.; Liu, Y.; Chen, Y.; Li, Q.; Li, X.; Wang, H., *J. Am. Chem. Soc.*, **2017**, *139*, 3537-3545.

34. Semakul, N.; Jackson, K. E.; Paton, R. S.; Rovis, T., *Chem. Sci.*, **2017**, *8*, 1015-1020.

35. Krieger, J.-P.; Lesuisse, D.; Ricci, G.; Perrin, M.-A.; Meyer, C.; Cossy, J., *Org. Lett.*, **2017**, *19*, 2706-2709.

36. Trifonova, E. A.; Ankudinov, N. M.; Kozlov, M. V.; Sharipov, M. Y.; Nelyubina, Y. V.; Perekalin, D. S., *Chem. Eur. J.*, **2018**, *24*, 16570-16575.

37. Kong, D.-S.; Wang, Y.-F.; Zhao, Y.-S.; Li, Q.-H.; Chen, Y.-X.; Tian, P.; Lin, G.-Q., *Org. Lett.*, **2018**, *20*, 1154-1157.

38. Reddy, C. R.; Mallesh, K., *Org. Lett.*, **2018**, *20*, 150-153.

39. Barber, J. S.; Scales, S.; Tran-Dube, M.; Wang, F.; Sach, N. W.; Bernier, L.; Collins, M. R.; Zhu, J. J.; McAlpine, I. J.; Patman, R. L., *Org. Lett.*, **2019**, *21*, 5689-5693.

40. Saiegh, T. J.; Chetodal, H.; Meyer, C.; Cossy, J., *Org. Lett.*, **2019**, *21*, 8364-8368.

41. Raji Reddy, C.; Mallesh, K.; Bodasu, S.; Donthiri, R. R., *J. Org. Chem.*, **2020**, *85*, 7905-7915.

42. Adhikari, G. K. D.; Chebolu, R.; Ravikumar, P. C., *ACS Omega.*, **2020,** *5*, 24033-24044.

43. Barber, J. S.; Kong, D.; Li, W.; McAlpine, I. J.; Nair, S. K.; Sakata, S. K.; Sun, N.; Patman, R. L., *Synlett.*, **2021**, *32*, 202-206.

44. Hyster, T. K.; Knorr, L.; Ward, T. R.; Rovis, T., *Science*, **2012**, *388*, 500-503.

45. Ye, B.; Cramer, N.,. *Science*, **2012**, *338*, 504-506.

46. Webb, N. J.; Marsden, S. P.; Raw, S. A., *Org. Lett.*, **2014**, *16*, 4718-4721.

47. Nguyen, T. N. T.; Tepe, J. J., *Curr. Med. Chem.*, **2009**, *16*, 3122-3143.

48. Nguyen, T. N. T.; Zaib, R. S.; Luderer, M. J.; Hovde, S.; Henry, R. W.; Tepe, J. J., *ACS Chem. Biol.*, **2012**, *7*, 172-184.

49. Zaib, R. S.; Lansdell, T. A.; Tepe, J. J., *Bioorg. Med. Chem.*, **2012**, *20*, 1475-1481.

50. Zaib, R. S.; Tepe, J. J., *Tetrahedron Lett.*, **2015**, 3011-3013.

51. Jašíková, L.; Hanikýřová, E.; Škríba, A.; Jašík, J.; Roithová, J., *J. Org. Chem.*, **2012**, *77*, 2829-2836.

52. Webb, N. J. Development and application of rhodium(III)-catalysed C-H activation methodologies. University of Leeds, Leeds, England, 2014.

53. Yamada, T.; Shibata, Y.; Kawauchi, S.; Yoshizaki, S.; Tanaka, K., *Chem. Eur. J.*, **2018**, *24*, 5723-5727.

54. Tan, J.-F.; Bormann, C. T.; Severin, K.; Cramer, N.,. *ACS Catal.*, **2020**, *10*, 3790-3796.

55. Umeda, N.; Hirano, K.; Satoh, T.; Shibata, N.; Sato, H.; Miura, M., *J. Org. Chem.*, **2011**, *76*, 13-24.

56. Tan, E.; Quinonero, O.; Elena de Orbe, M.; Echavarren, A. M., *ACS Catal.*, **2018**, *8*, 2166-2172.

57. Webb, N. J.; Raw, S. A.; Marsden, S. P., *Tetrahedron.*, **2018**, *74*, 5200-5205.

58. Zhang, Y.; Wang, D.; Cui, S., *Org. Lett.*, **2015**, *17*, 2494-2947.

59. Mishra, V. K.; Ravikumar, P. C.; Maier, M. E., *Tetrahedron.*, **2016**, *72*, 6499-6509.

60. Selmeczy, A. D.; Jones, W. D., *Organometallics*, **1994**, *13*, 522-532.

61. Li, L.; W.W., B.; Jones, W. D., *Organometallics* **2009,** *28*, 3492-3500.

62. Carr, K. J. T.; Davies, D. L.; Macgregor, S. A.; Singh, K.; Villa-Marcos, B., *Chem. Sci.* **2014**, *5*, 2340.

63. Sun, R.; Yang, X.; Chen, X.; Zhang, C.; Zhao, X.; Wang, X.; Zheng, X.; Yuan, M.; Fu, H.; Li, R.; Chen, H., *Org. Lett.*, **2018**, *20*, 6755-6759.

64. Perrotta, D., Wang, M-M., Waser, J., *Angew. Chem., Int. Ed. Engl.*, **2018**, *57*, 5120-5123.

APPENDIX

Figure 3.4 ^{1}H ,$^{13}C\{^{1}H\}$, and ^{19}F NMR spectra of compound *O*-pivaloylhydroxylammonium trifluoromethanesulfonate

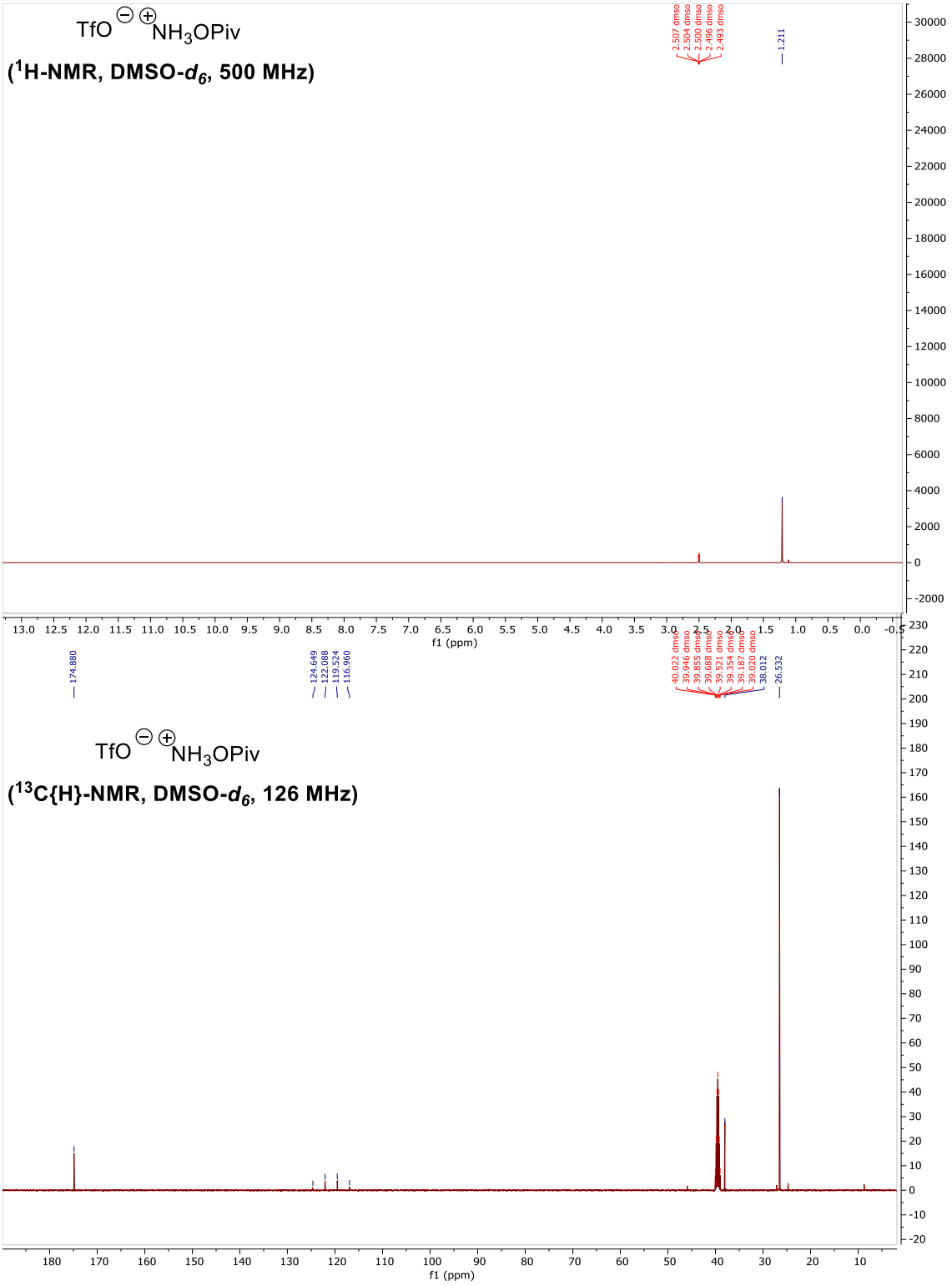

Figure 3.4 (con'td)

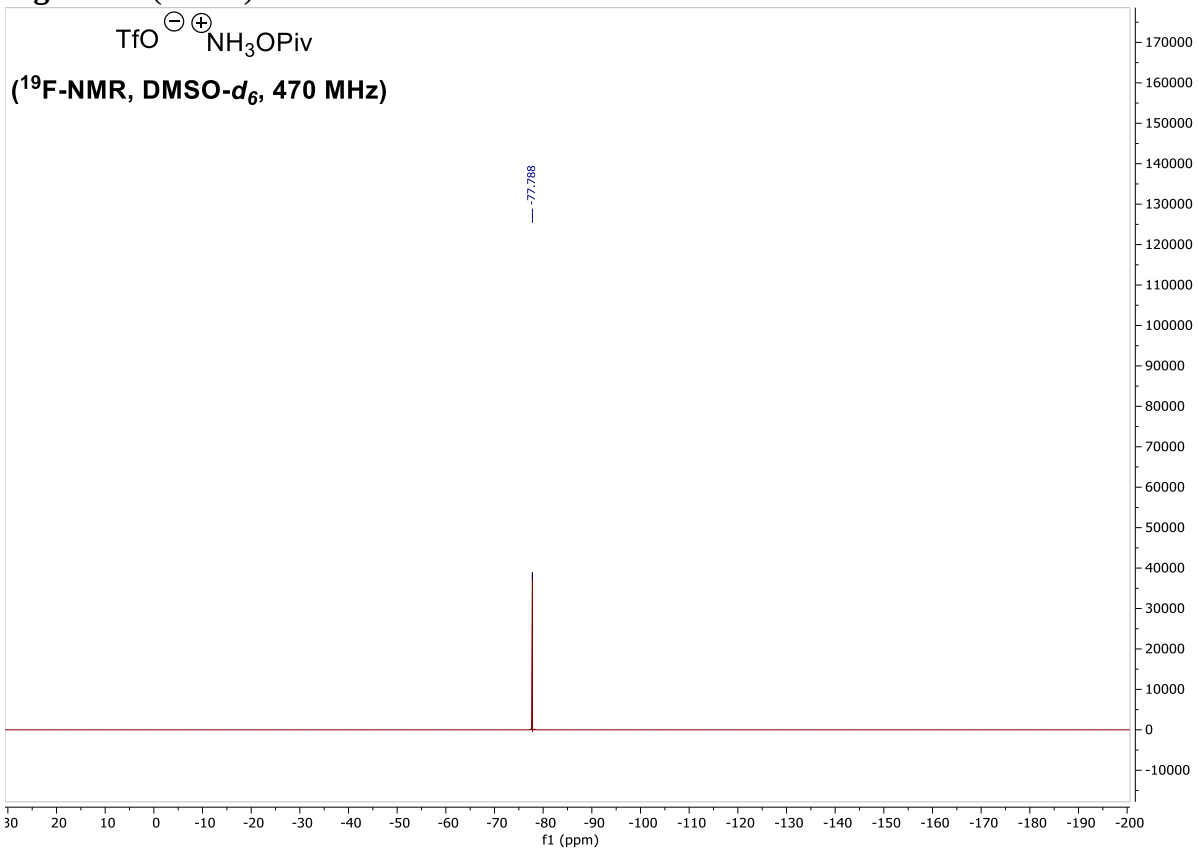

Figure 3.5 ^{1}H and $^{13}C\{^{1}H\}$ NMR spectra of compound **III-1a**

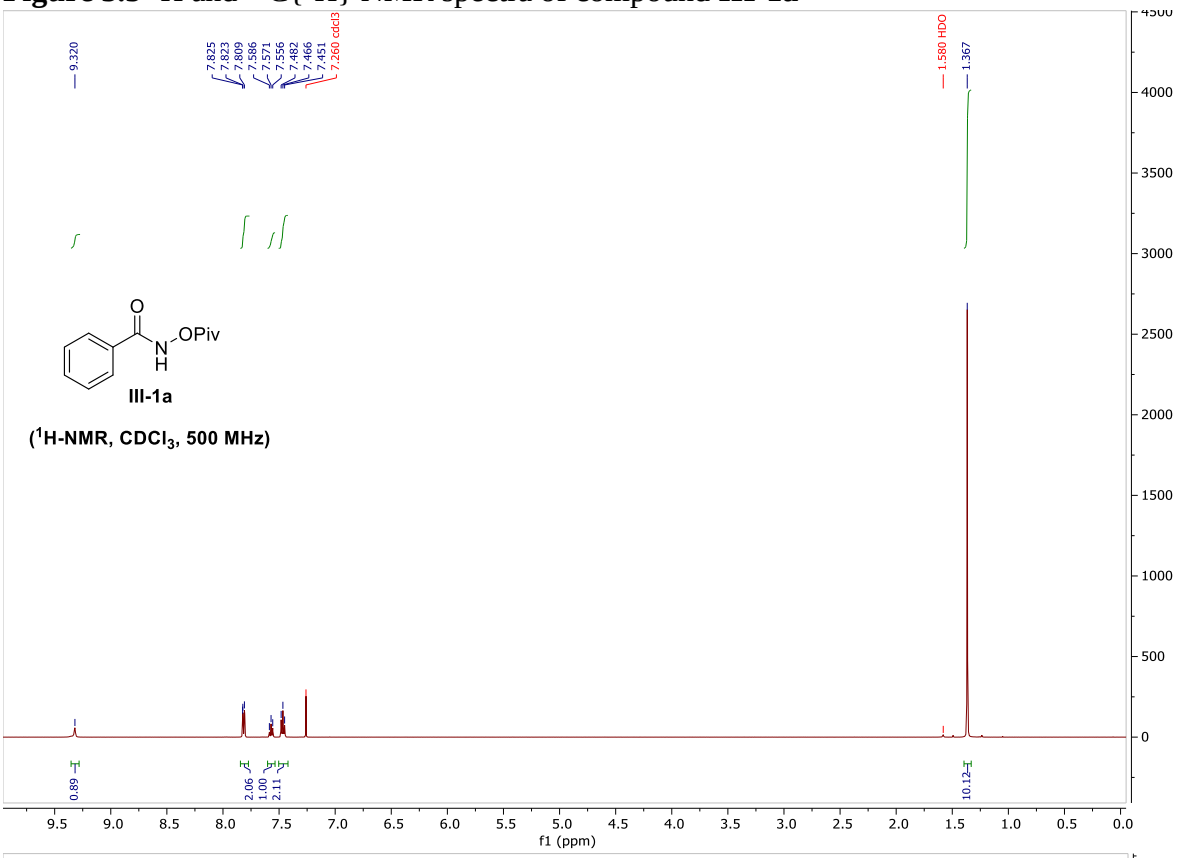

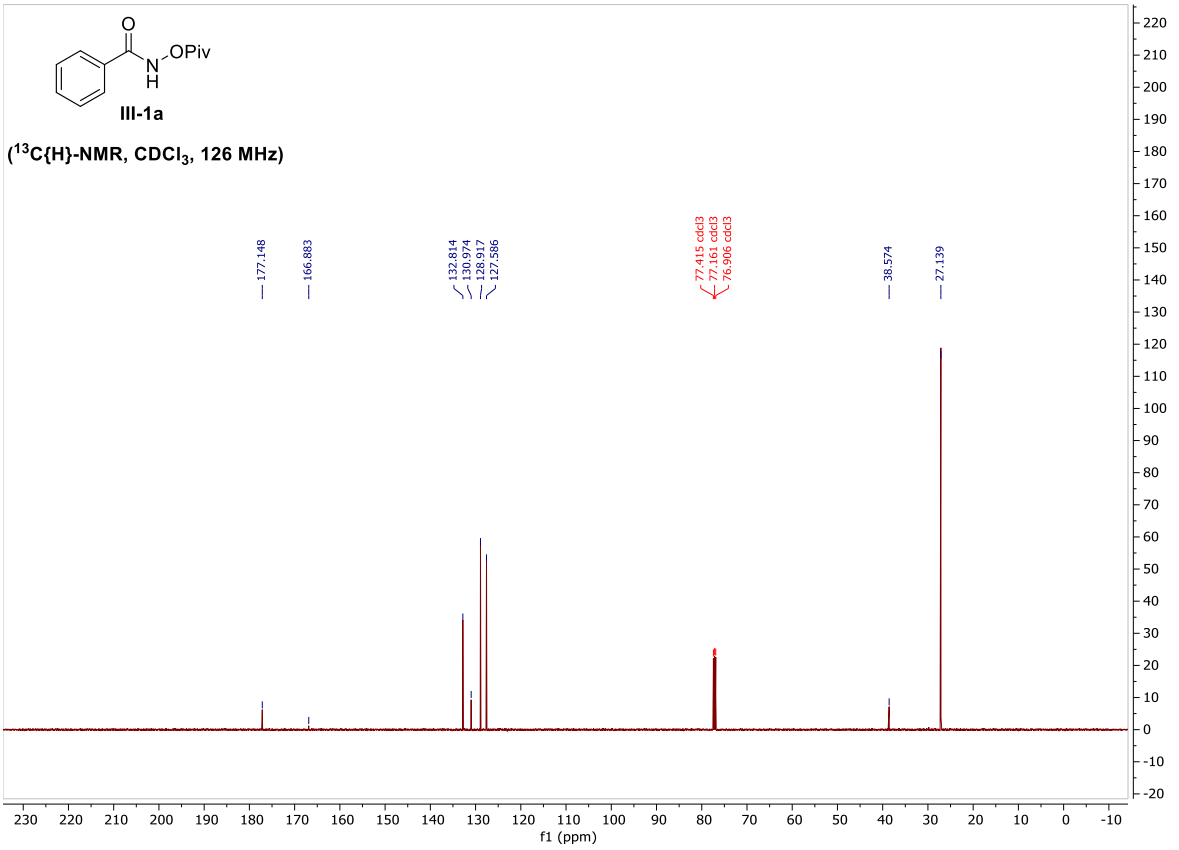

Figure 3.6 ^{1}H and $^{13}C\{^{1}H\}$ NMR spectra of compound **III-1b**

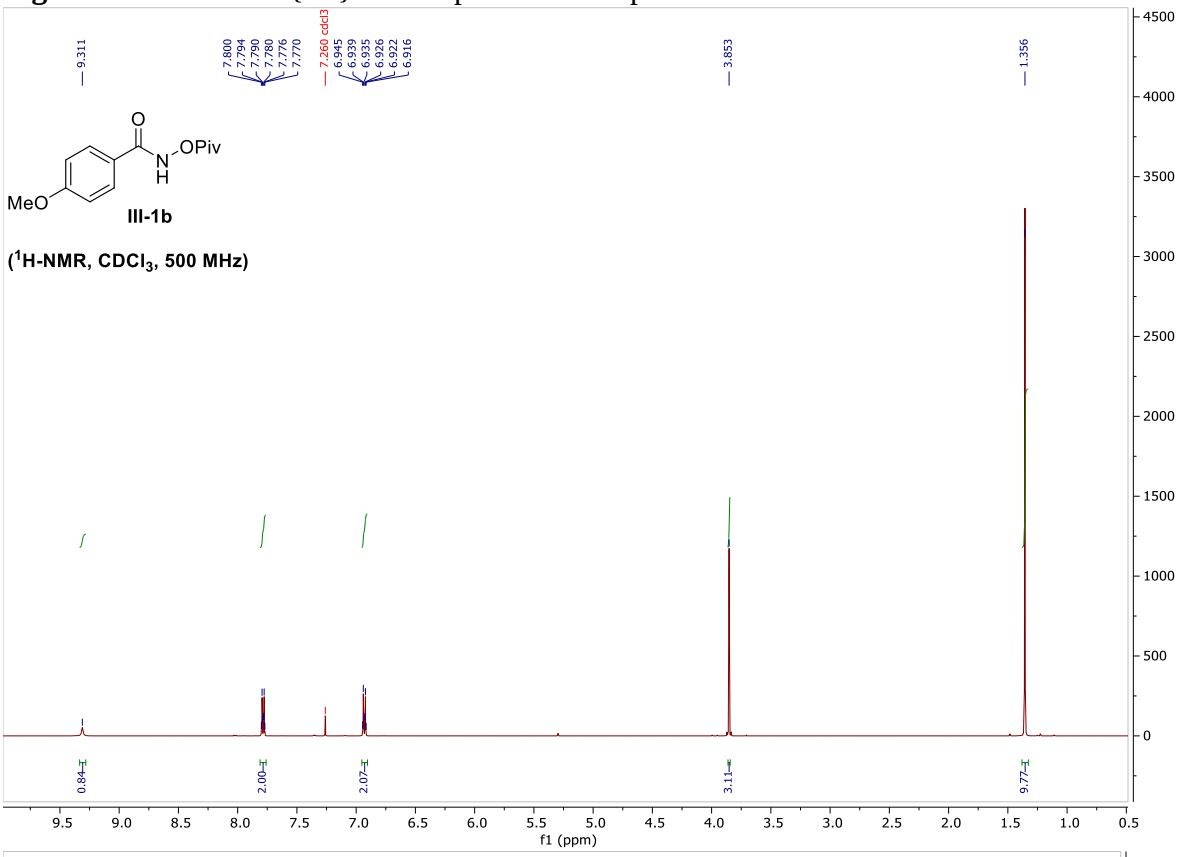

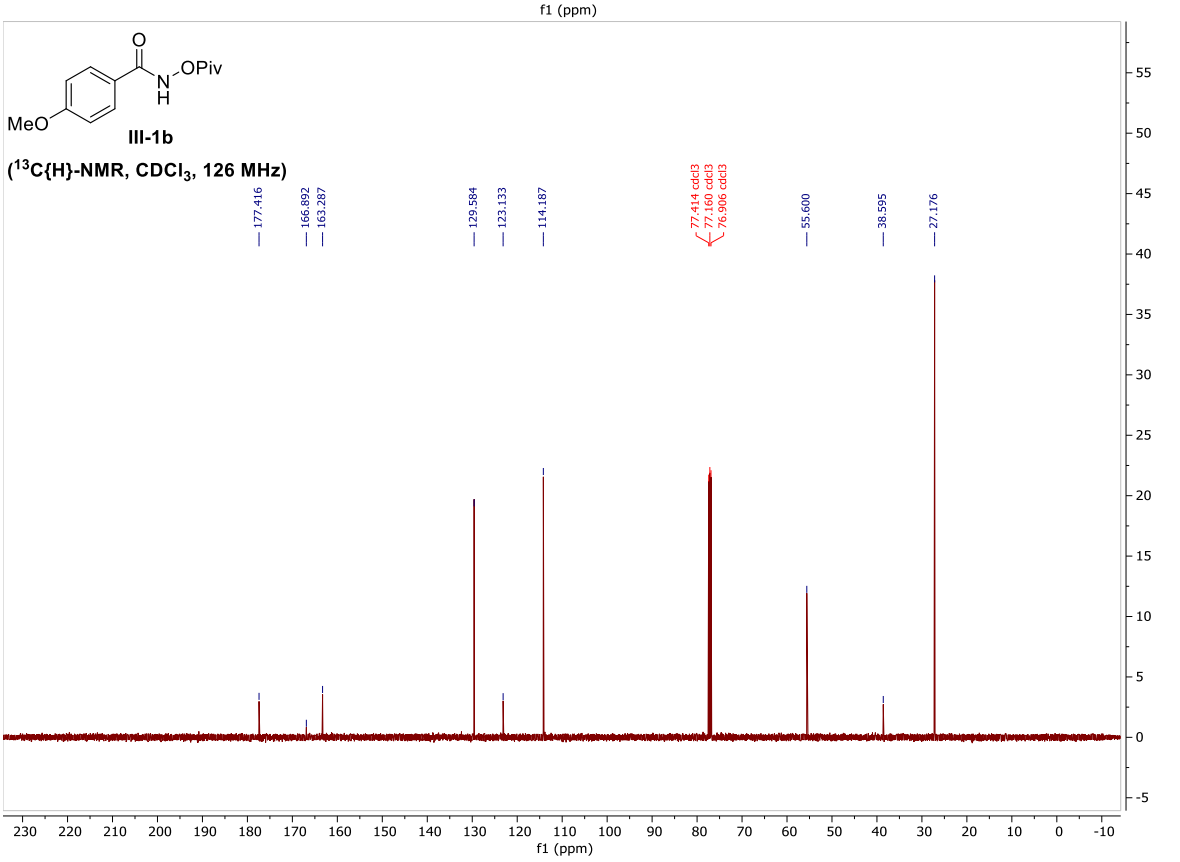

Figure 3.7 ^{1}H and $^{13}C\{^{1}H\}$ NMR spectra of compound **III-1c**

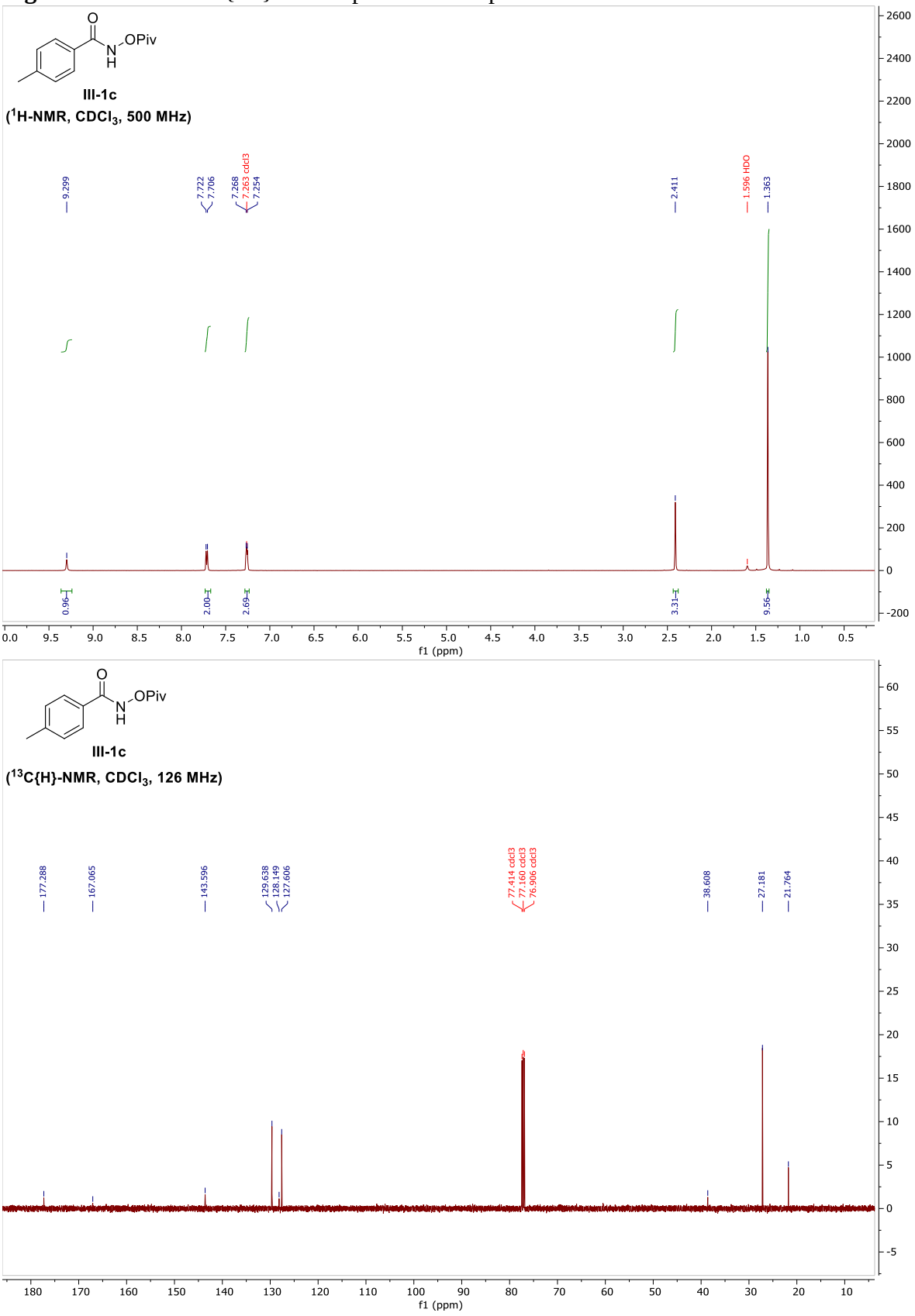

Figure 3.8 ^{1}H and $^{13}C\{^{1}H\}$ NMR spectra of compound **III-1d**

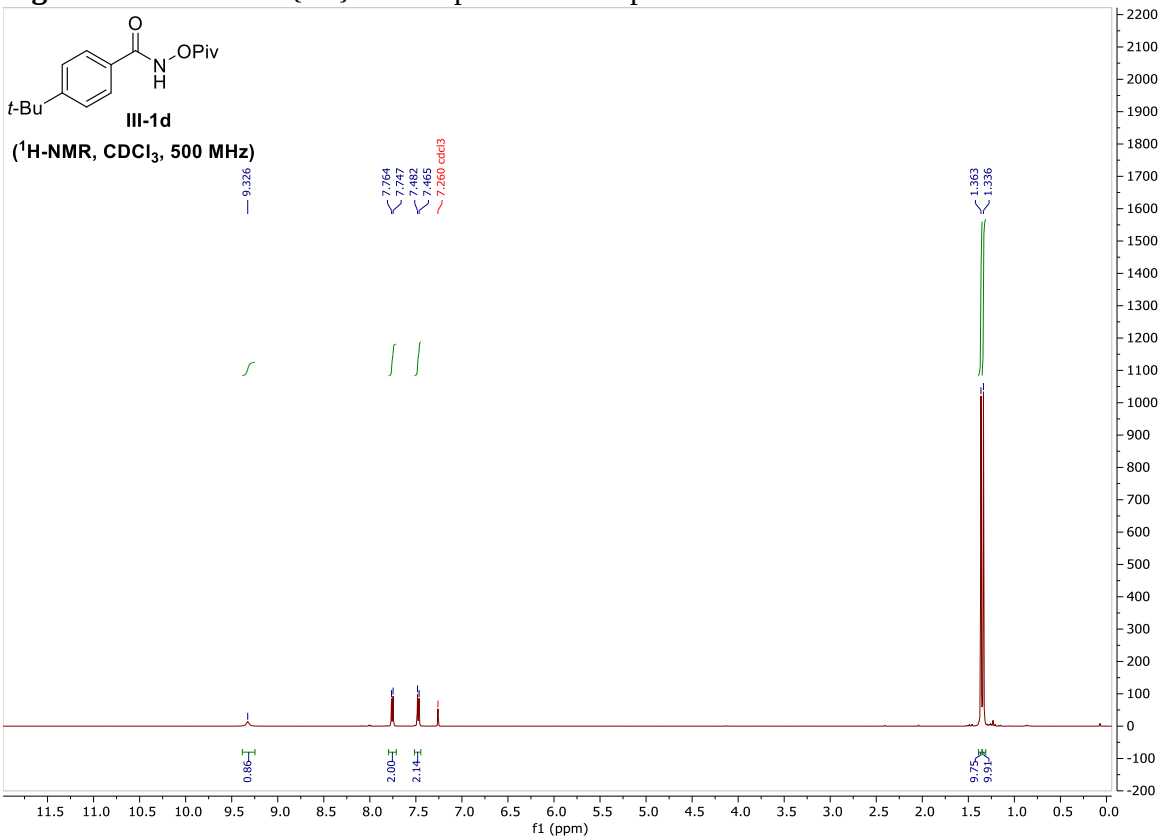

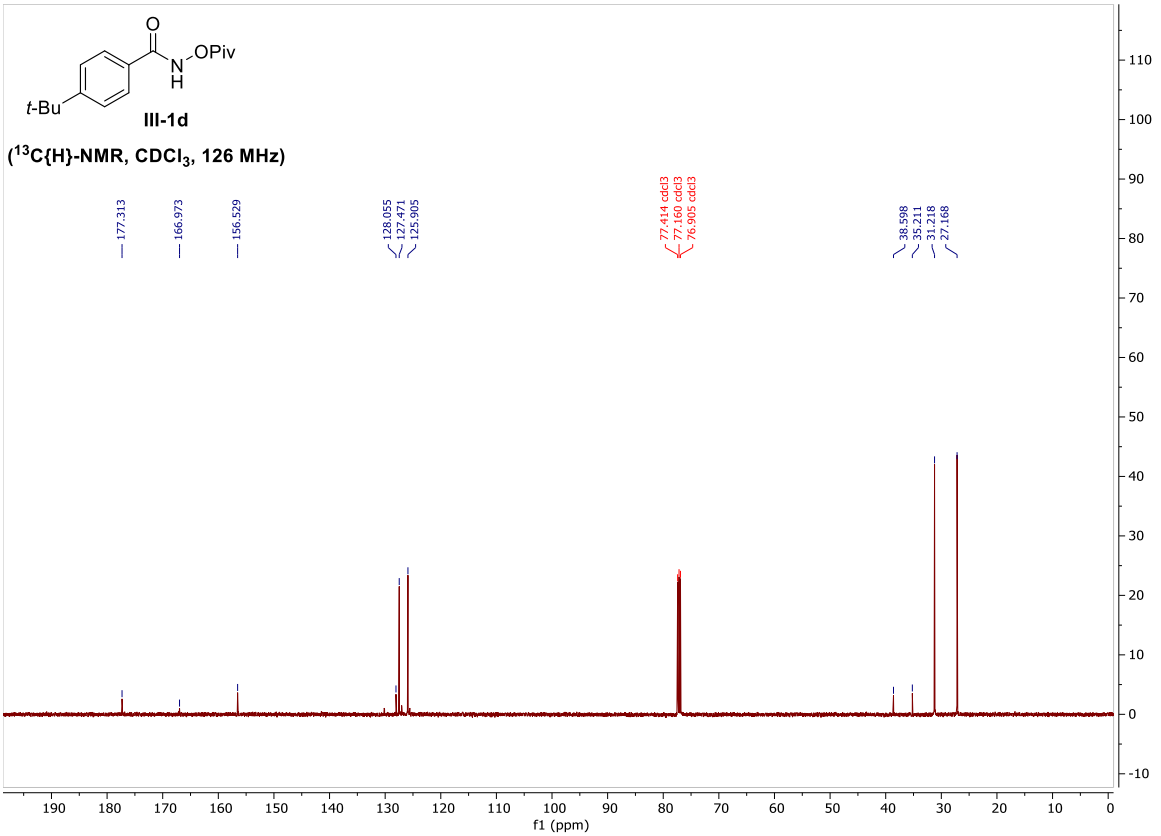

Figure 3.9 ^{1}H and $^{13}C\{^{1}H\}$ NMR spectra of compound **III-1e**

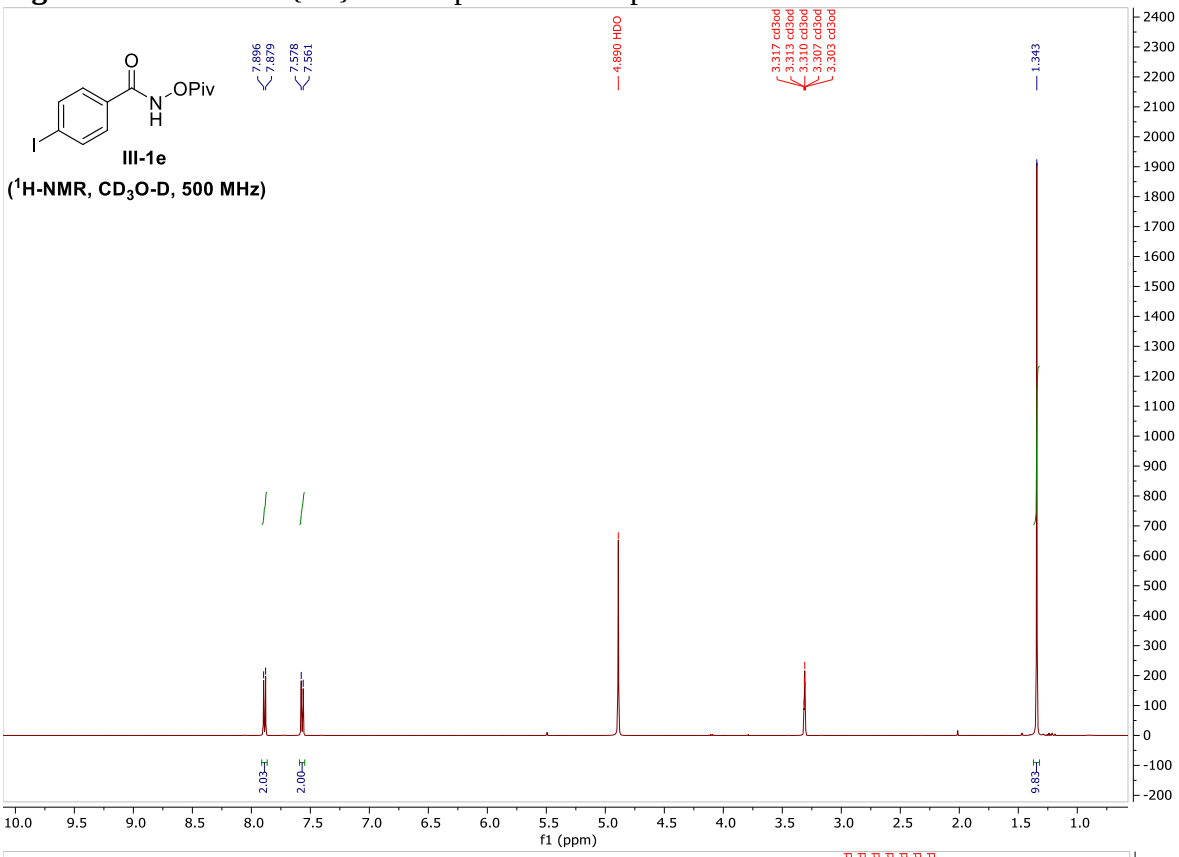

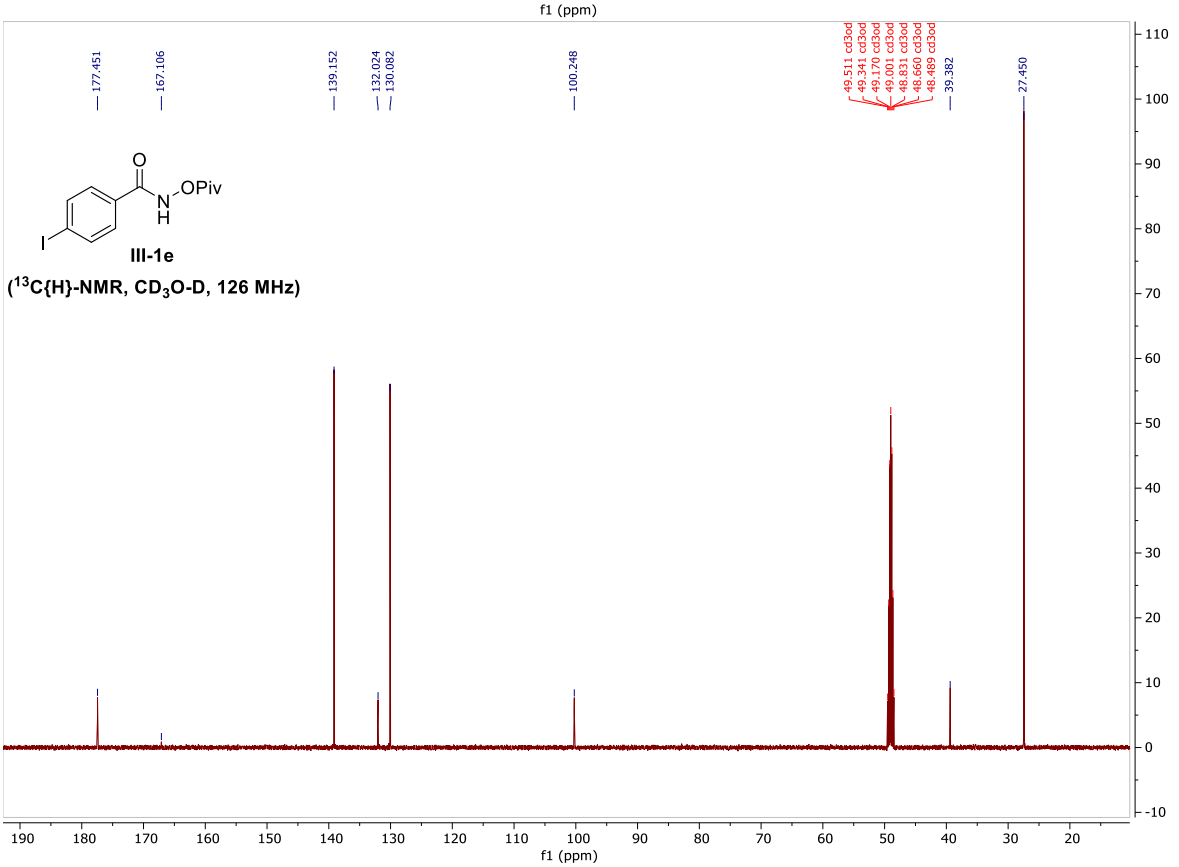

Figure 3.10 ^{1}H and $^{13}C\{^{1}H\}$ NMR spectra of compound **III-1f**

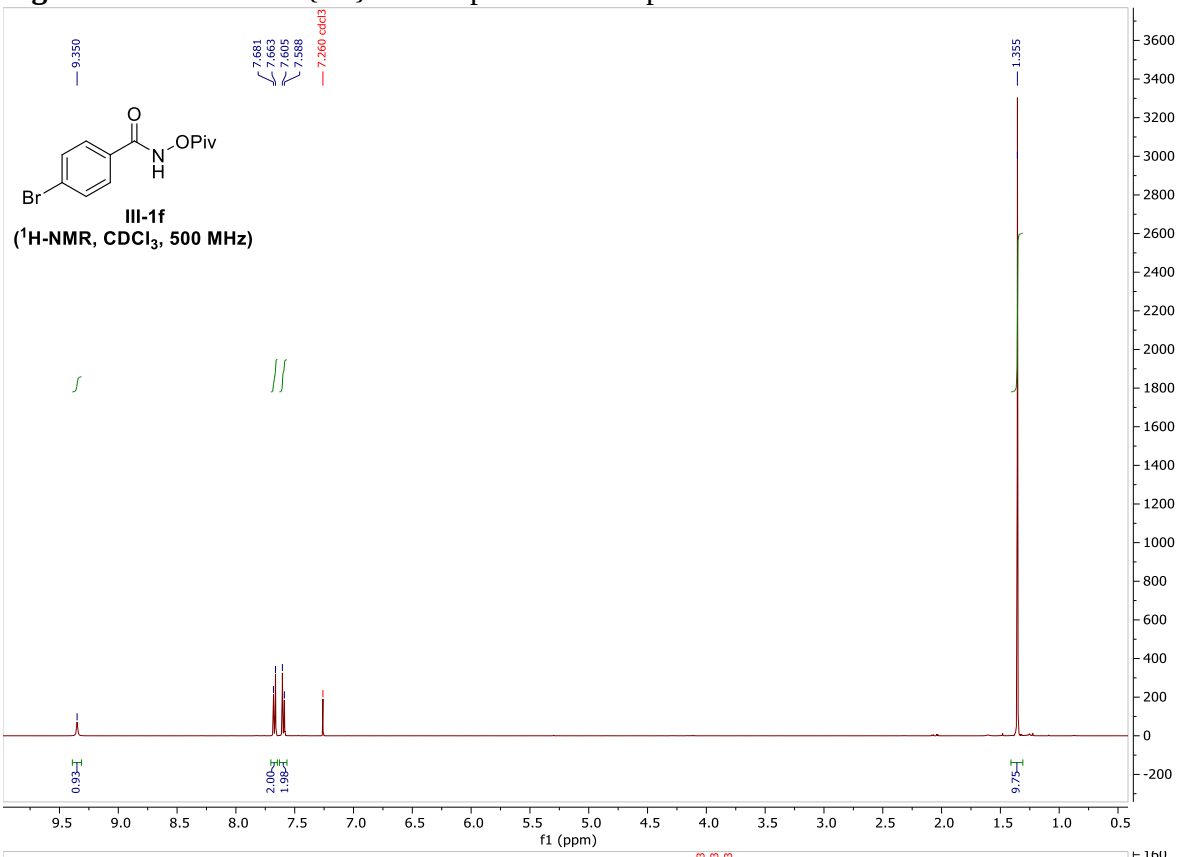

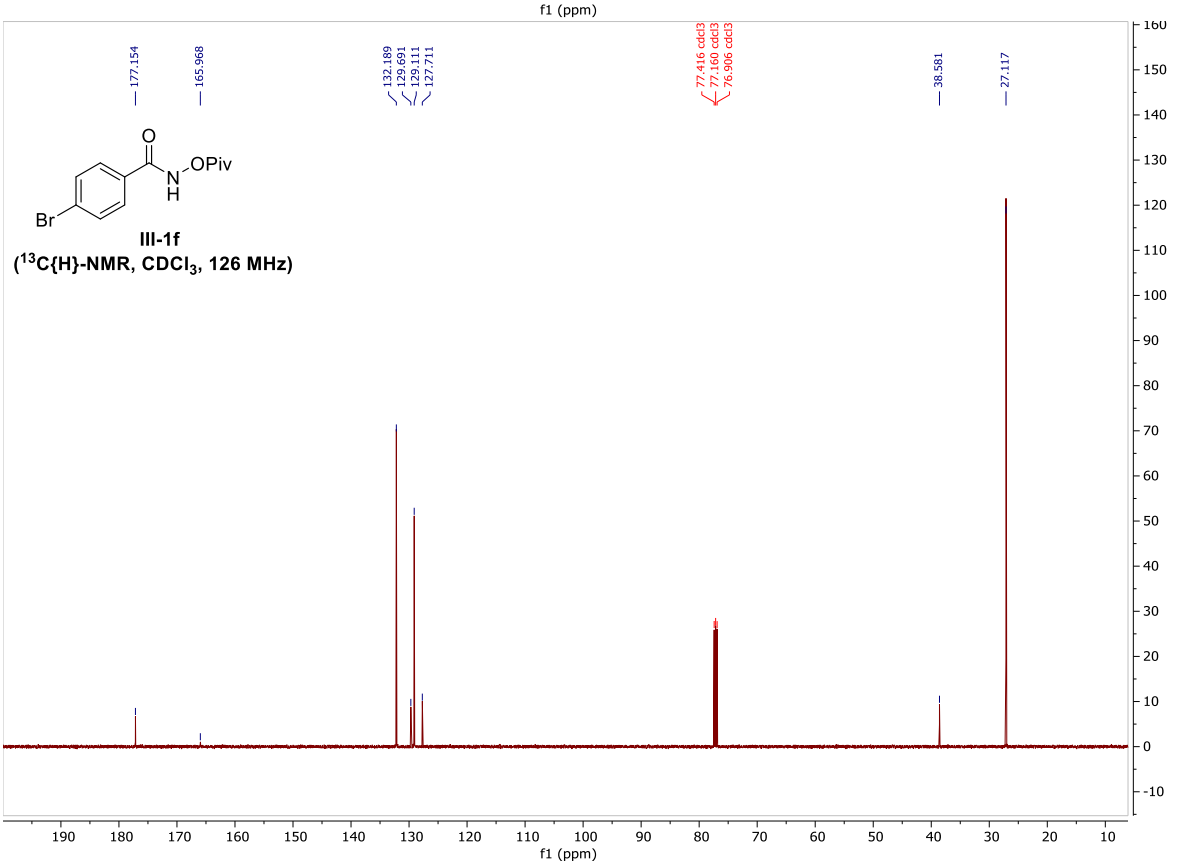

Figure 3.11 ^{1}H and $^{13}C\{^{1}H\}$ NMR spectra of compound **III-1g**

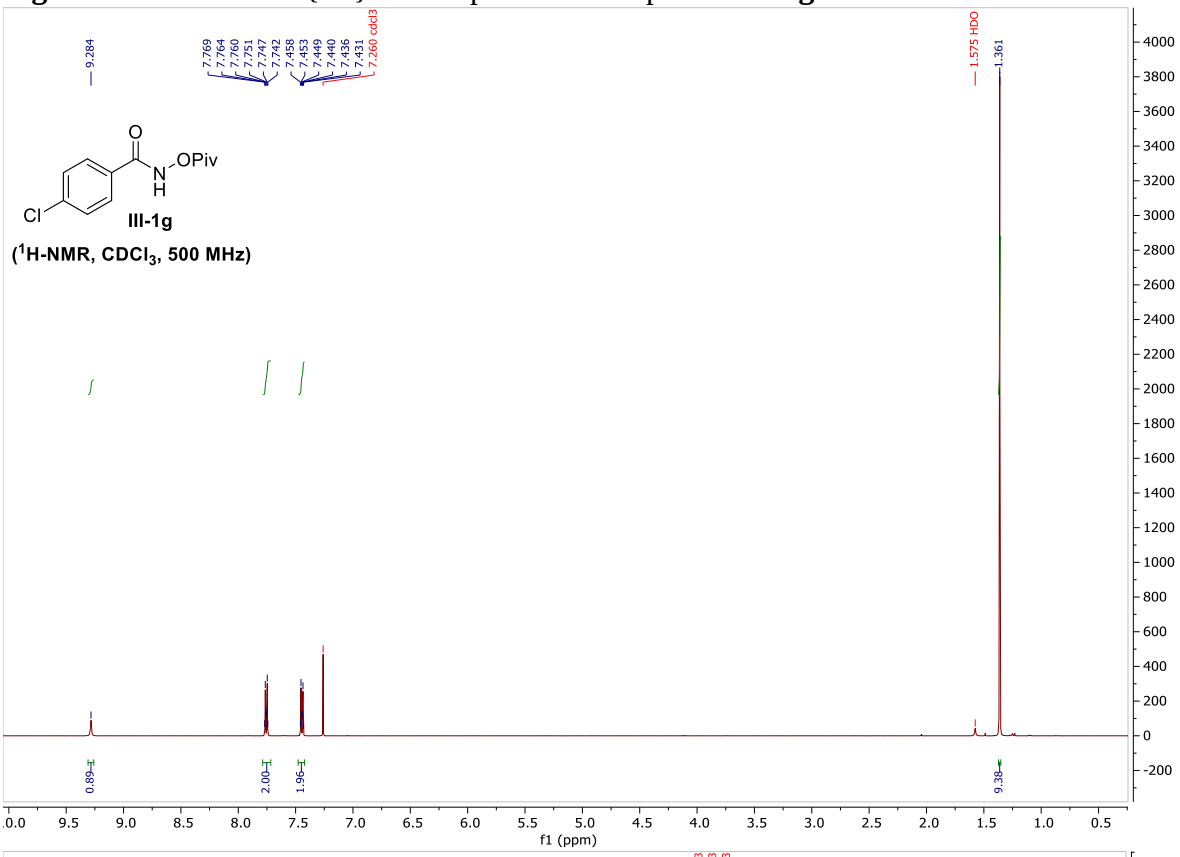

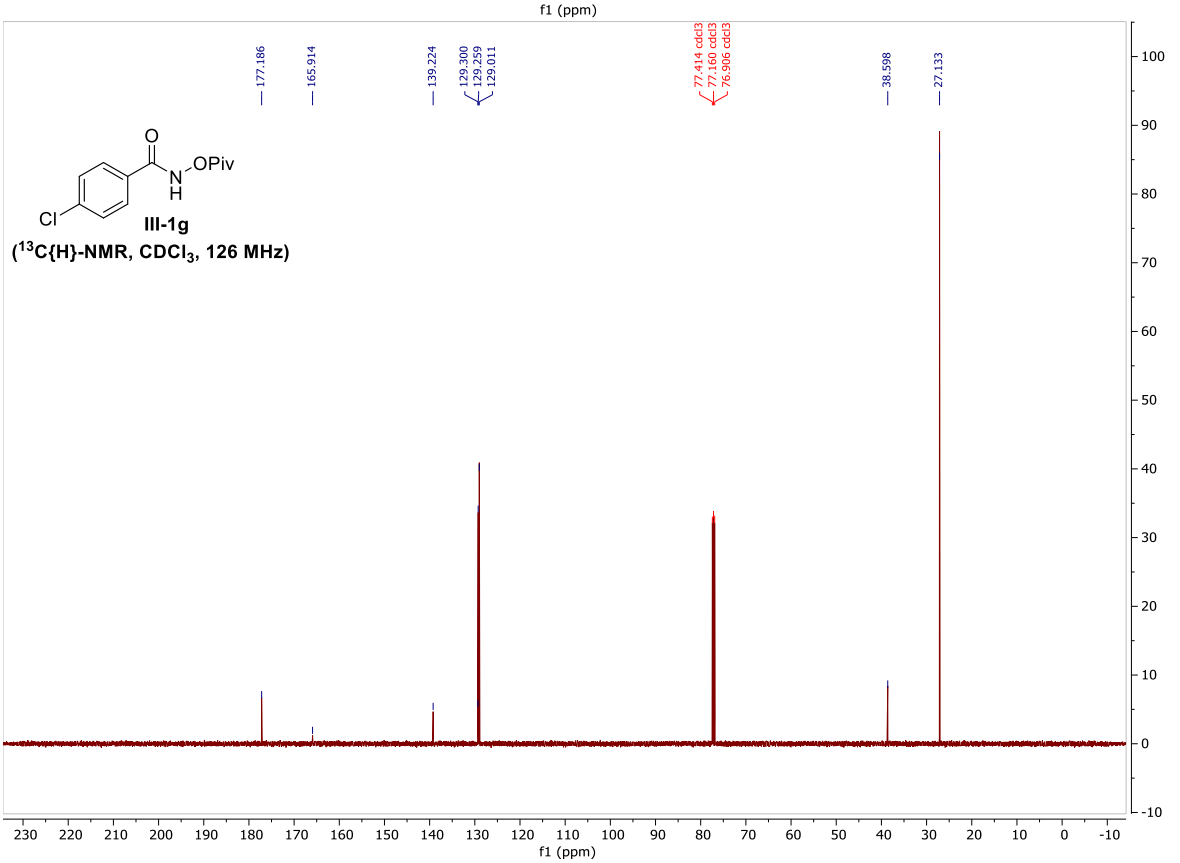

Figure 3.12 ^{1}H and $^{13}C\{^{1}H\}$ NMR spectra of compound **III-1h**

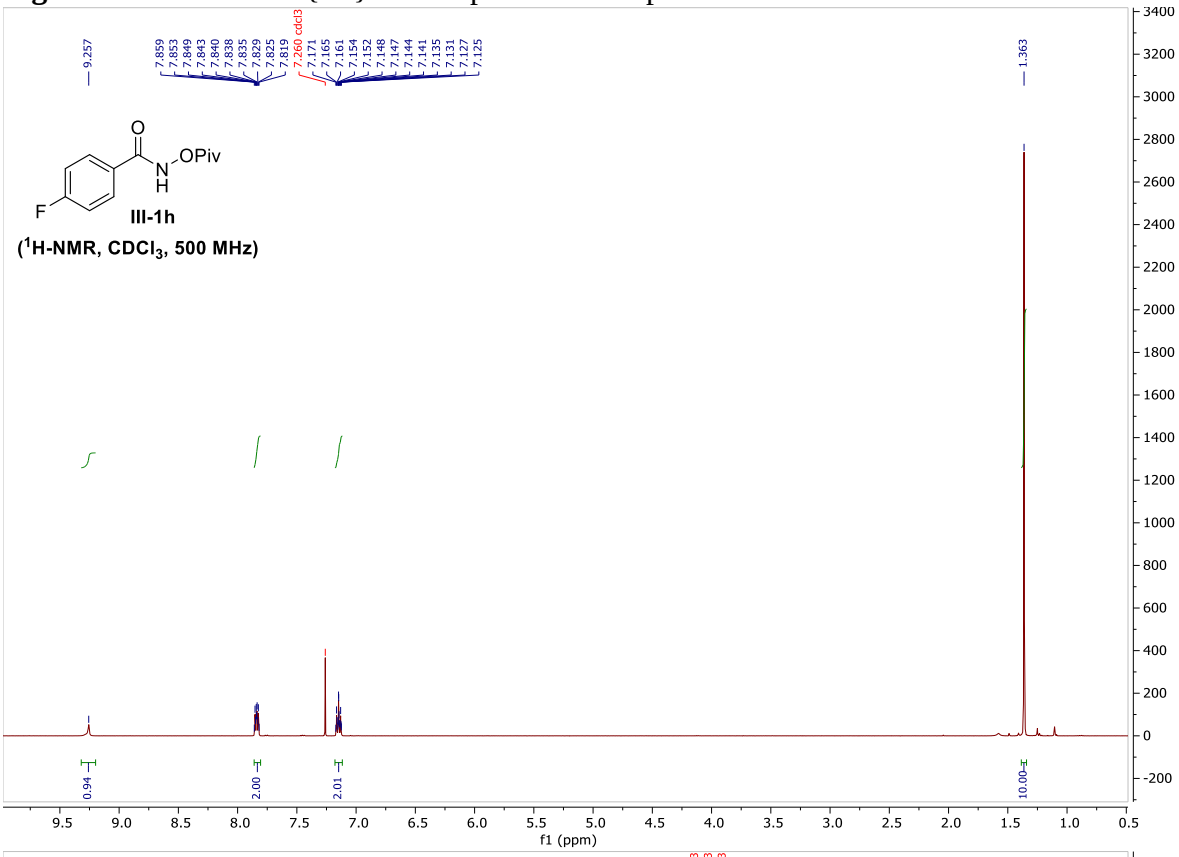

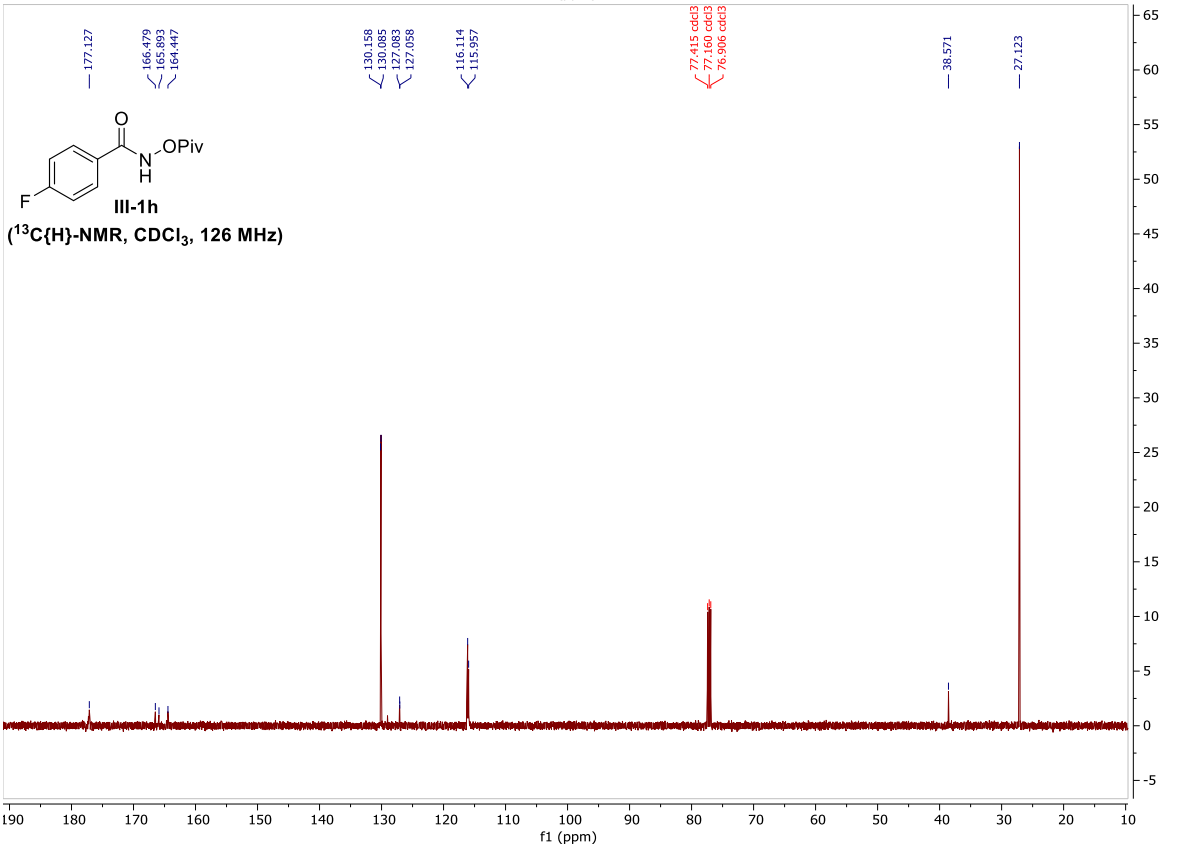

Figure 3.13 ^{1}H and $^{13}C\{^{1}H\}$ NMR spectra of compound **III-1i**

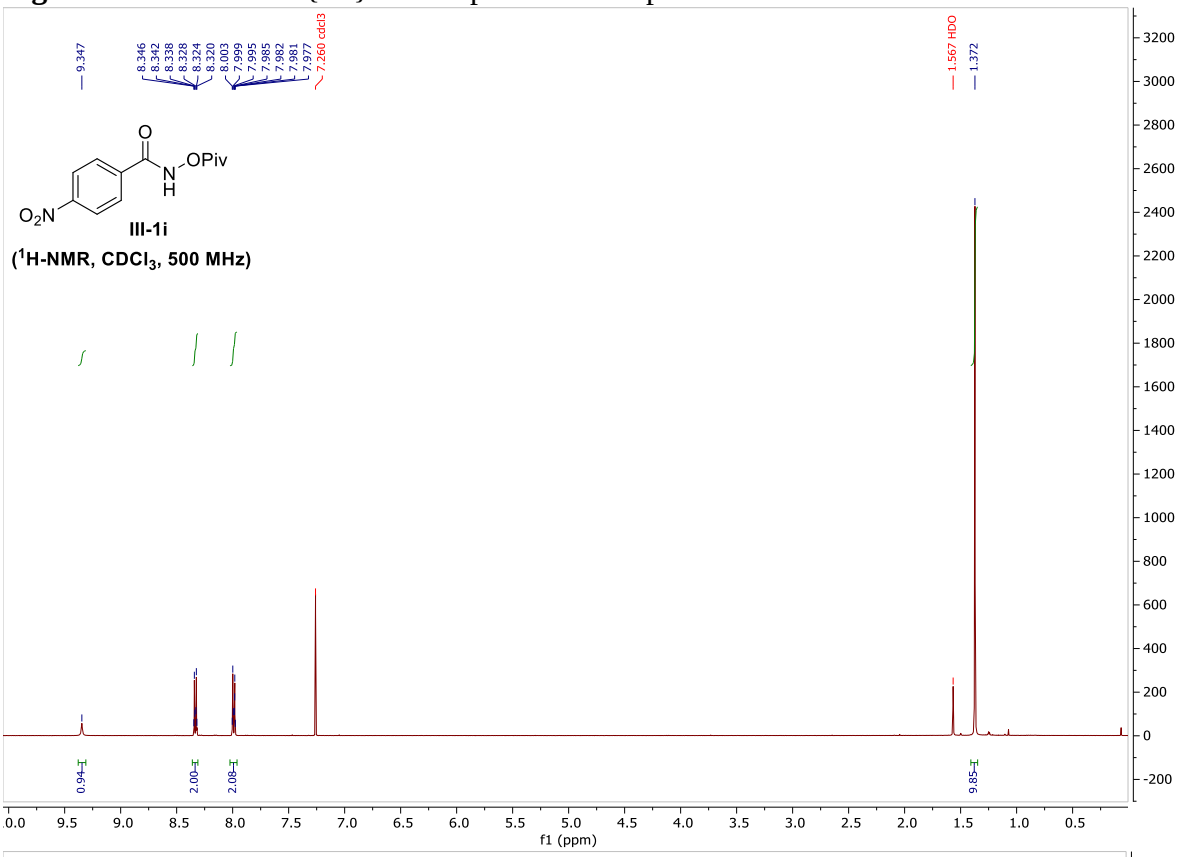

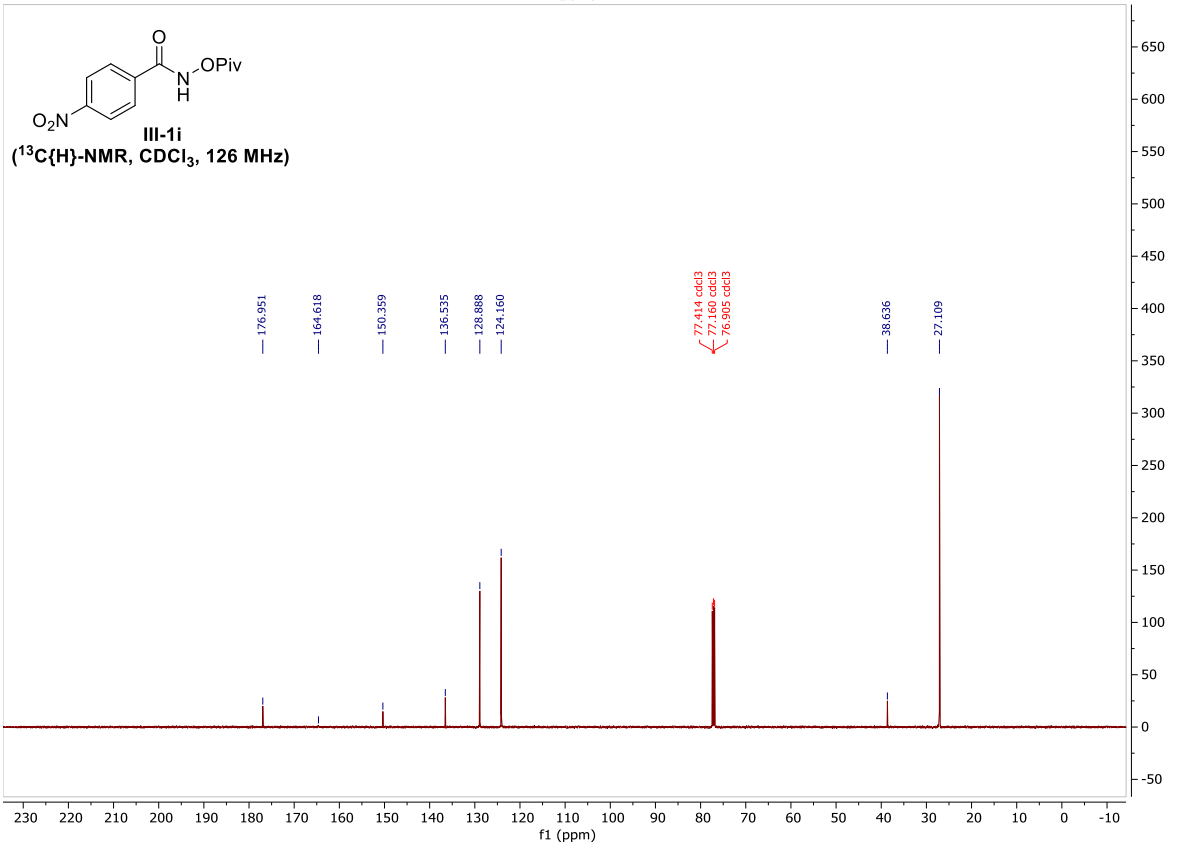

Figure 3.14 ^{1}H and $^{13}C\{^{1}H\}$ NMR spectra of compound **III-1j**

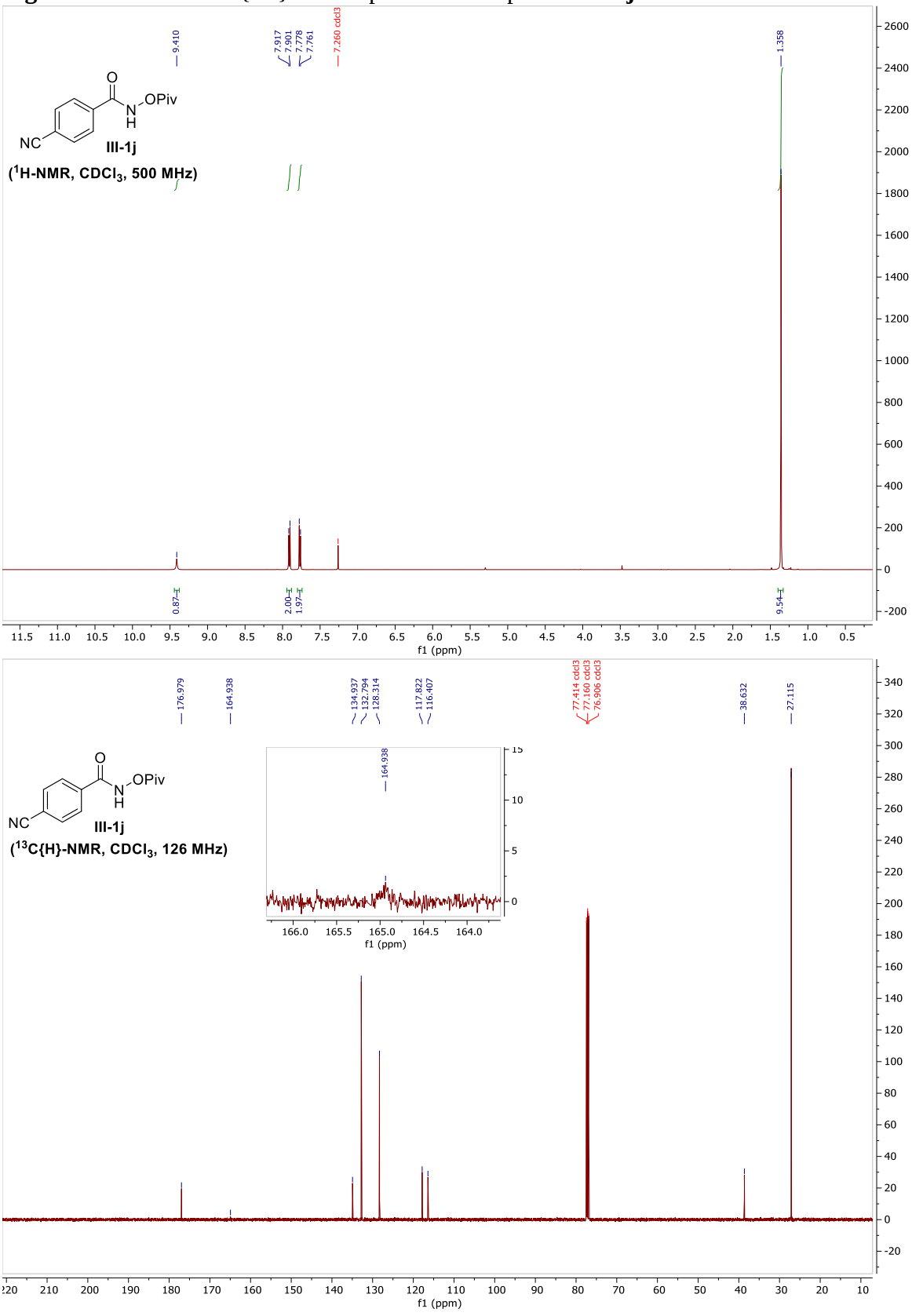

Figure 3.15 ^{1}H and $^{13}C\{^{1}H\}$ NMR spectra of compound **III-1k**

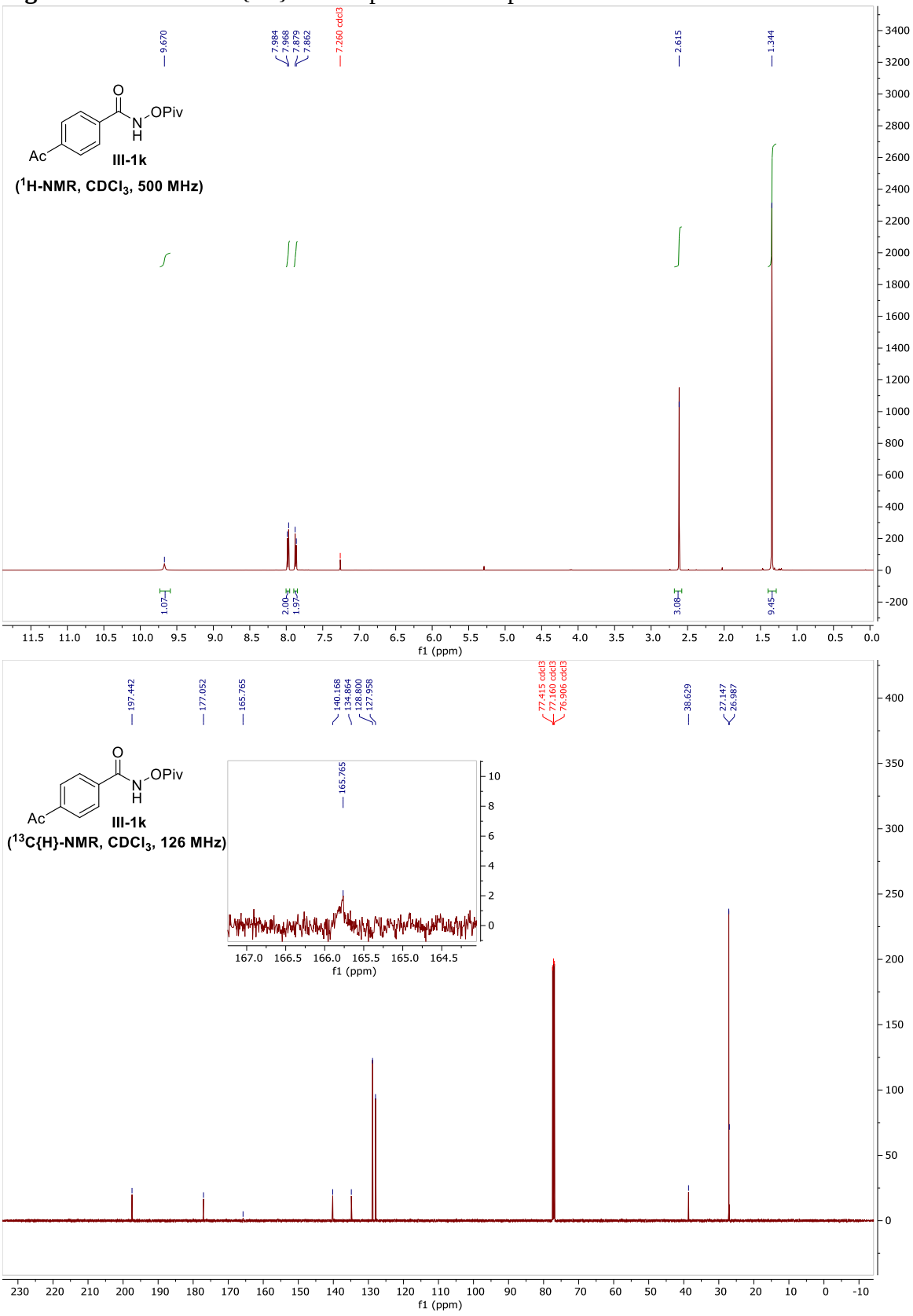

Figure 3.16 ^{1}H and $^{13}C\{^{1}H\}$ NMR spectra of compound **III-1l**

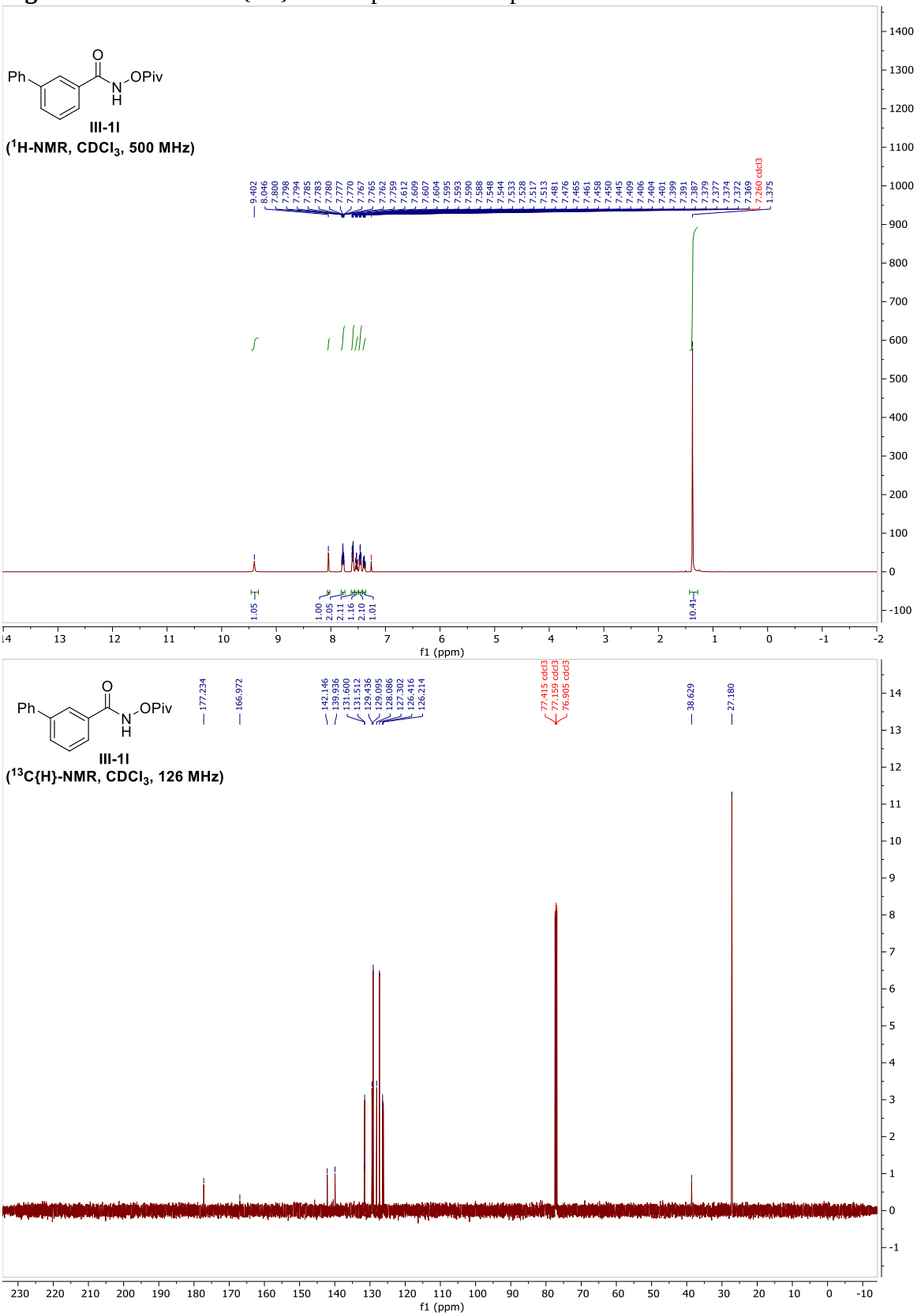

Figure 3.17 ^{1}H and $^{13}C\{^{1}H\}$ NMR spectra of compound **III-1m**

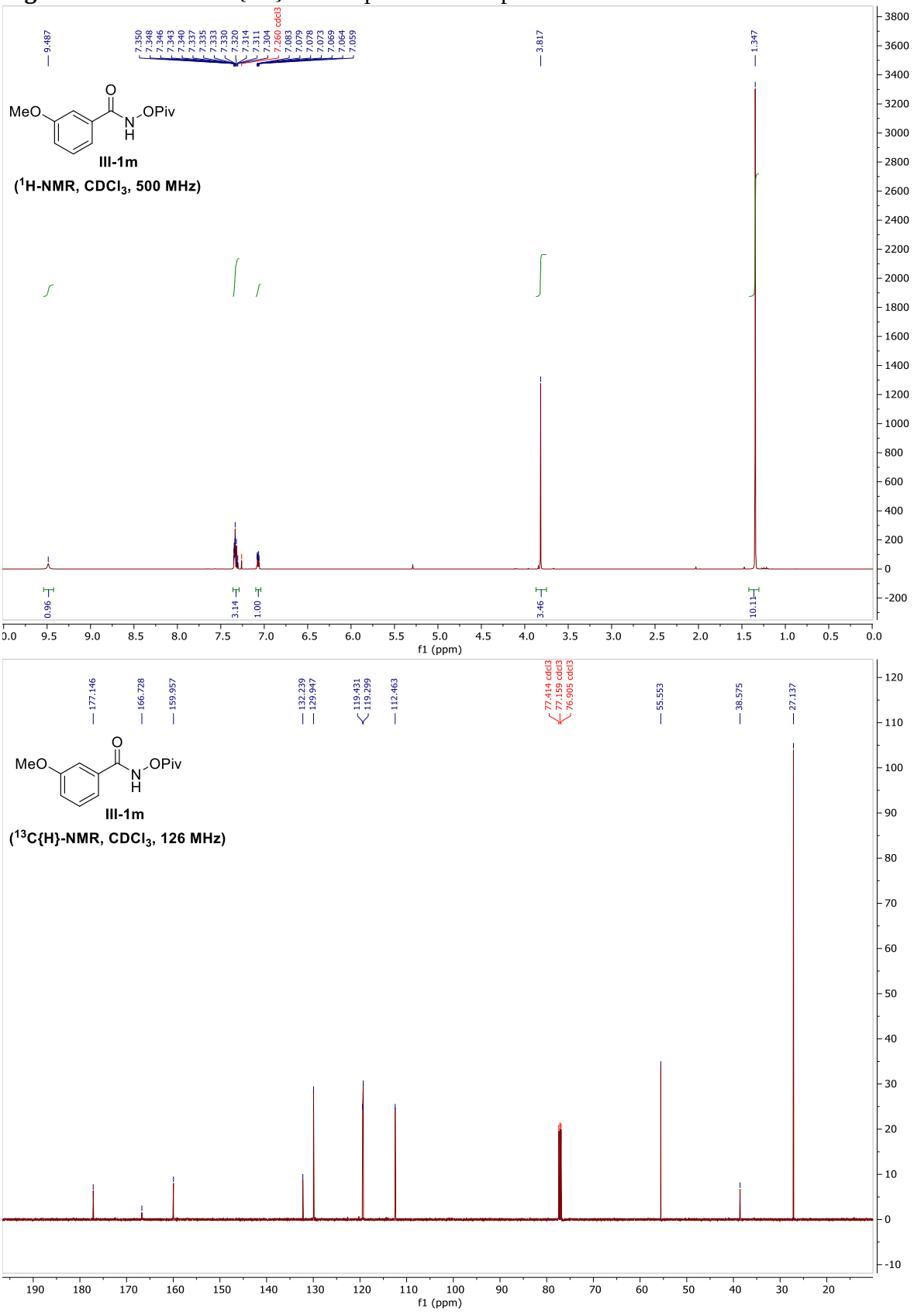

Figure 3.18 ^{1}H and $^{13}C\{^{1}H\}$ NMR spectra of compound **III-1n**

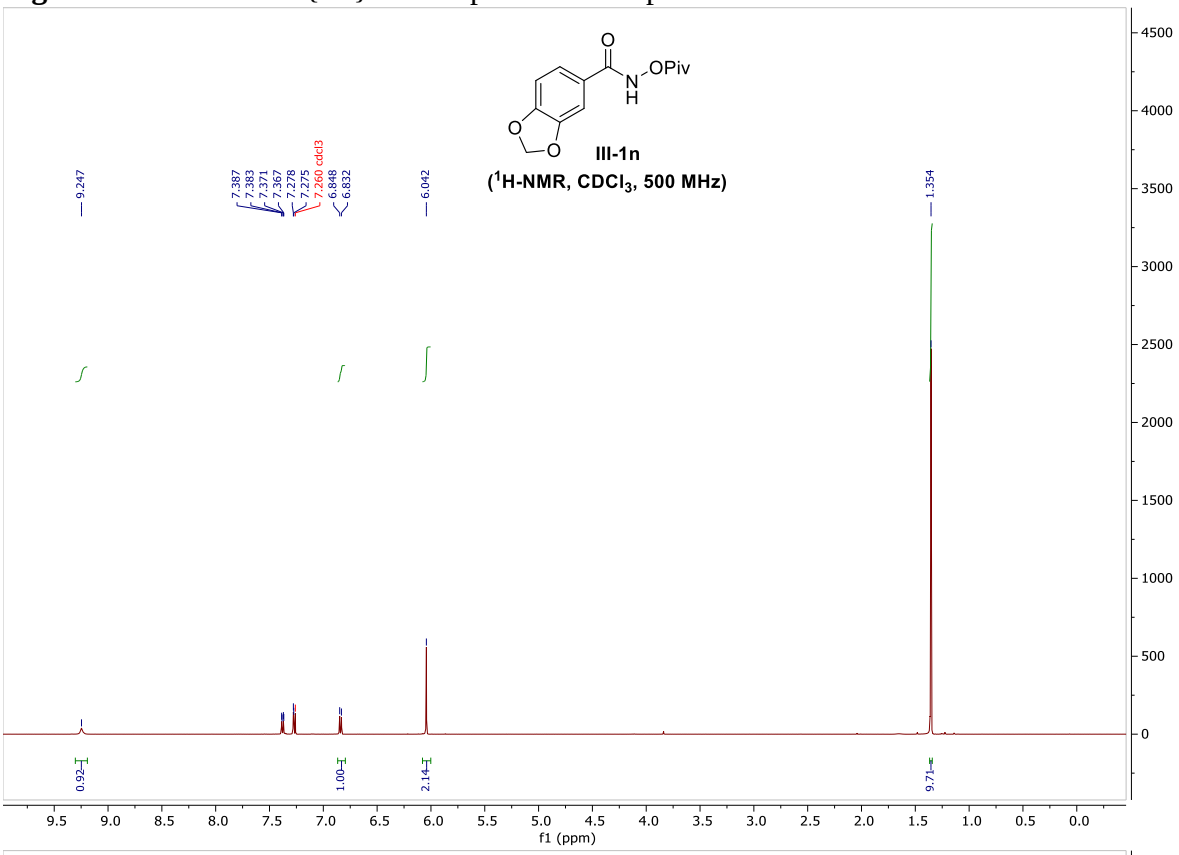

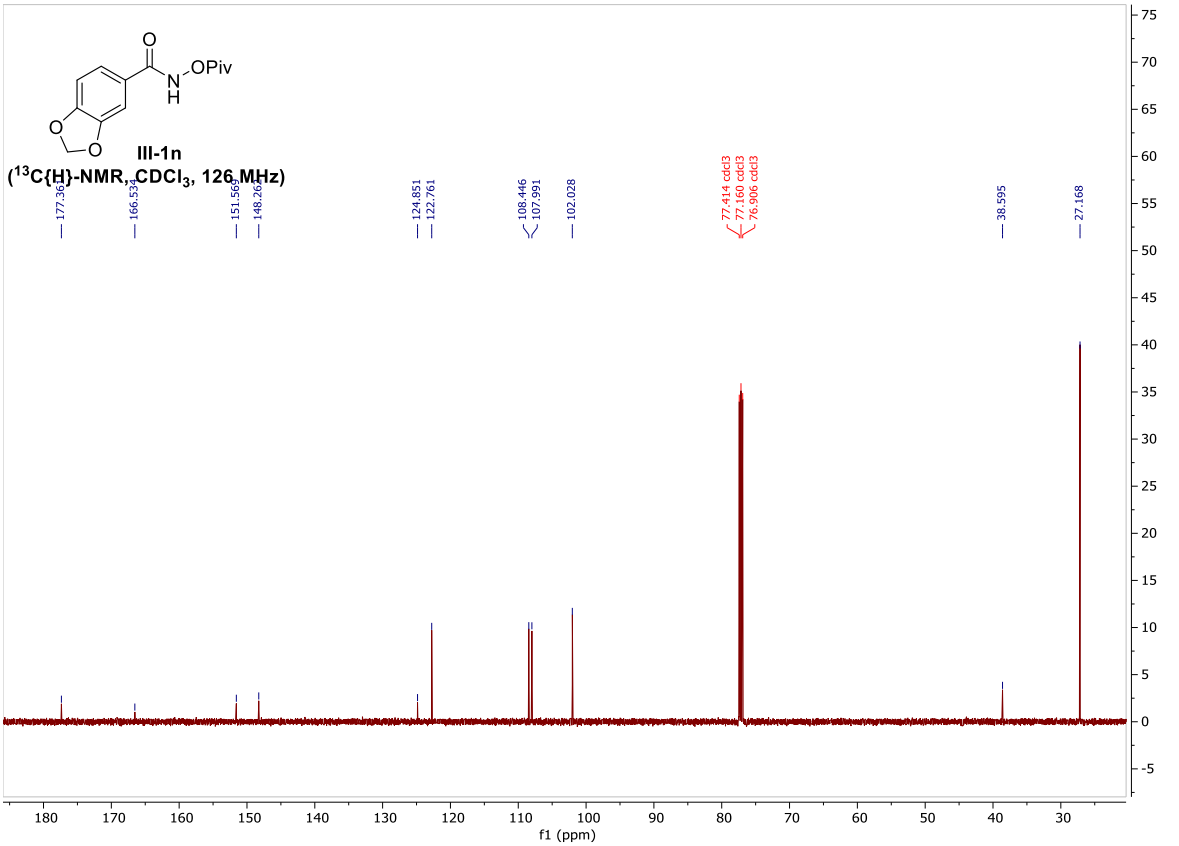

Figure 3.19 ^{1}H and $^{13}C\{^{1}H\}$ NMR spectra of compound **III-1o**

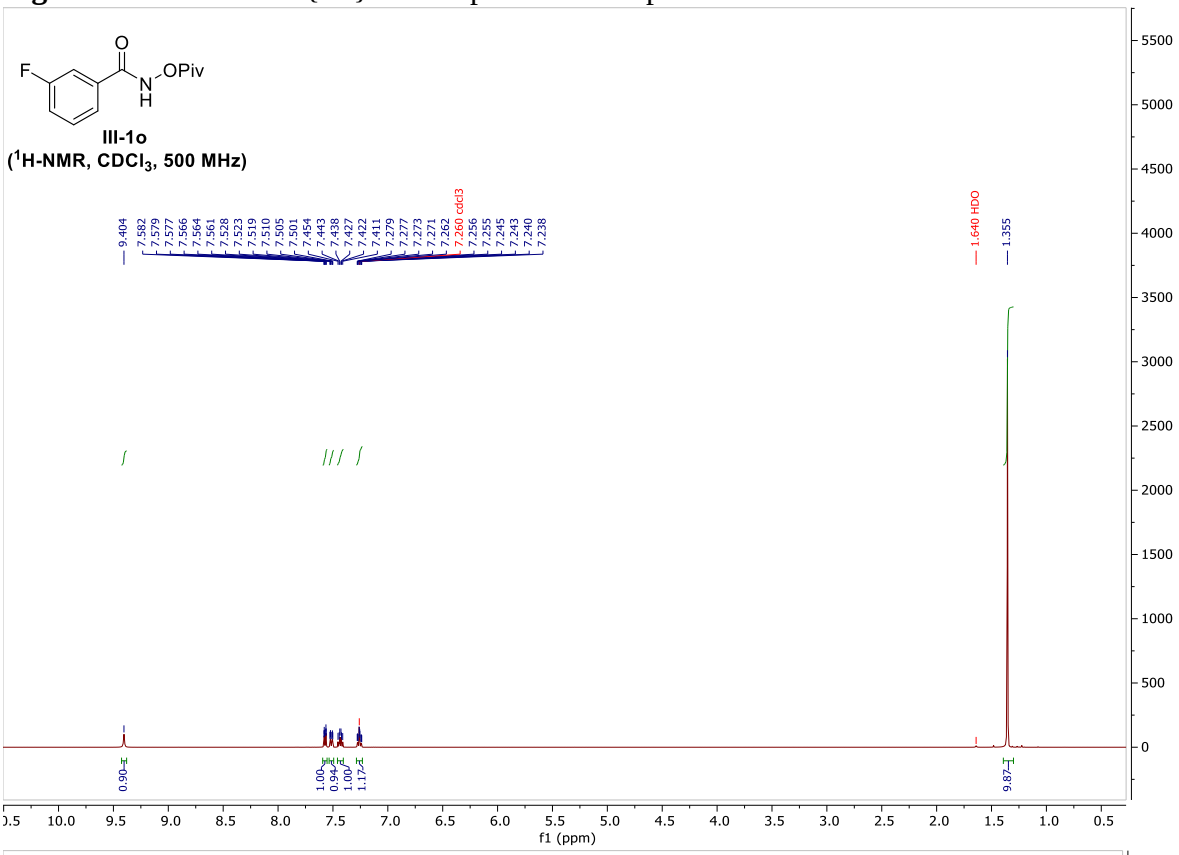

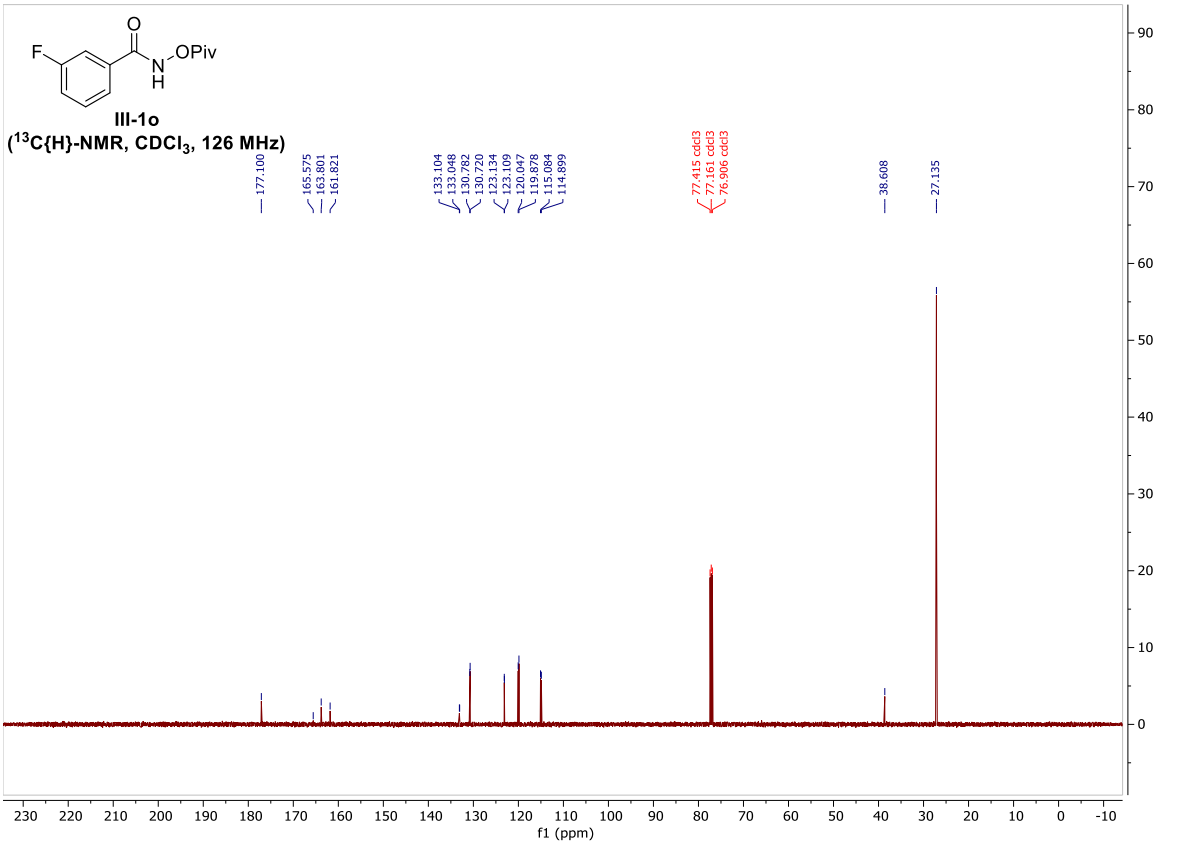

Figure 3.20 ^{1}H and $^{13}C\{^{1}H\}$ NMR spectra of compound **III-1p**

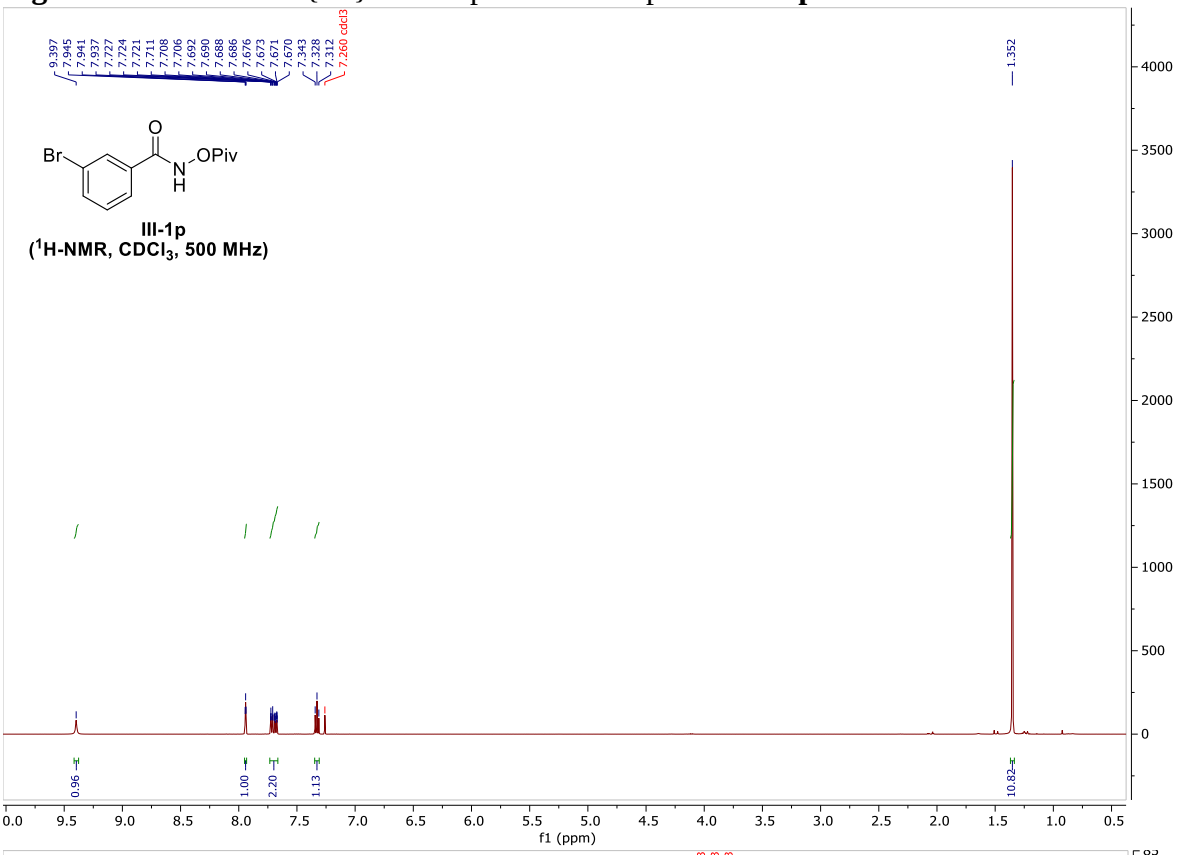

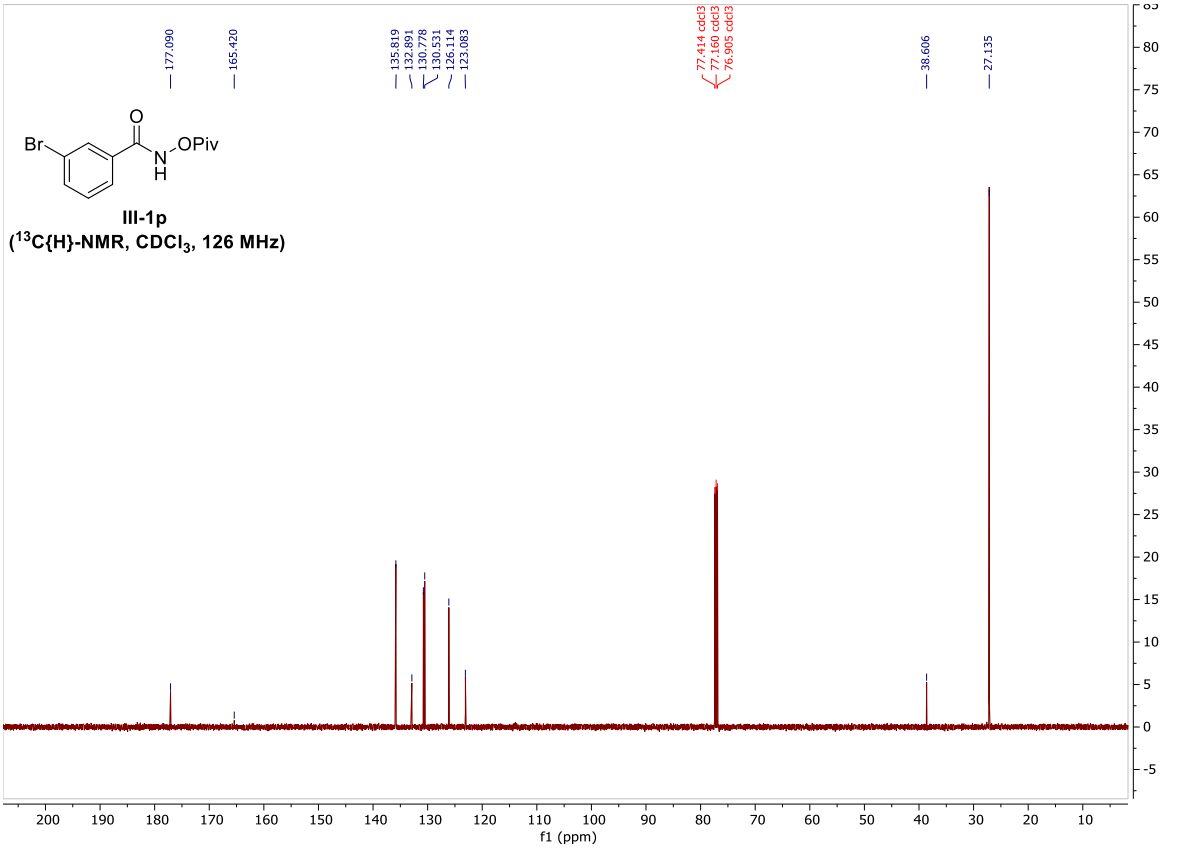

Figure 3.21 ^{1}H and $^{13}C\{^{1}H\}$ NMR spectra of compound **III-1q**

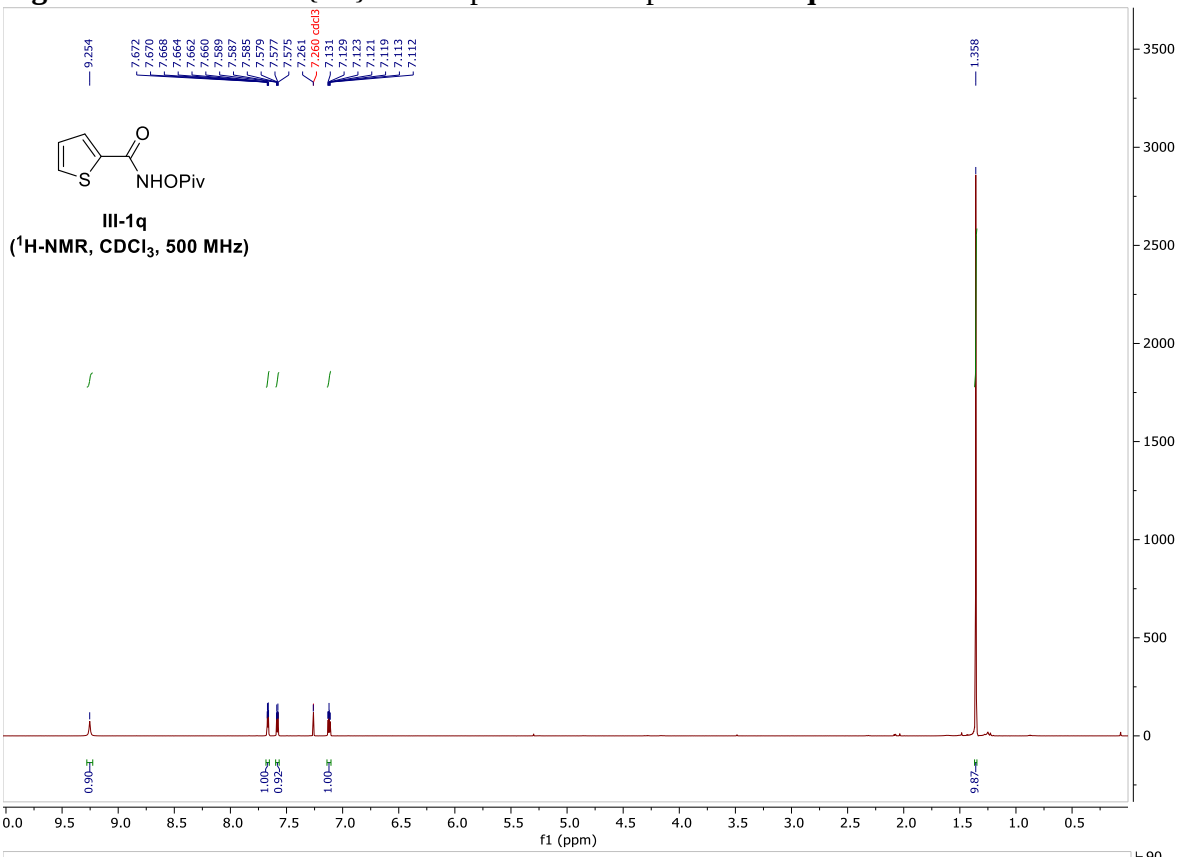

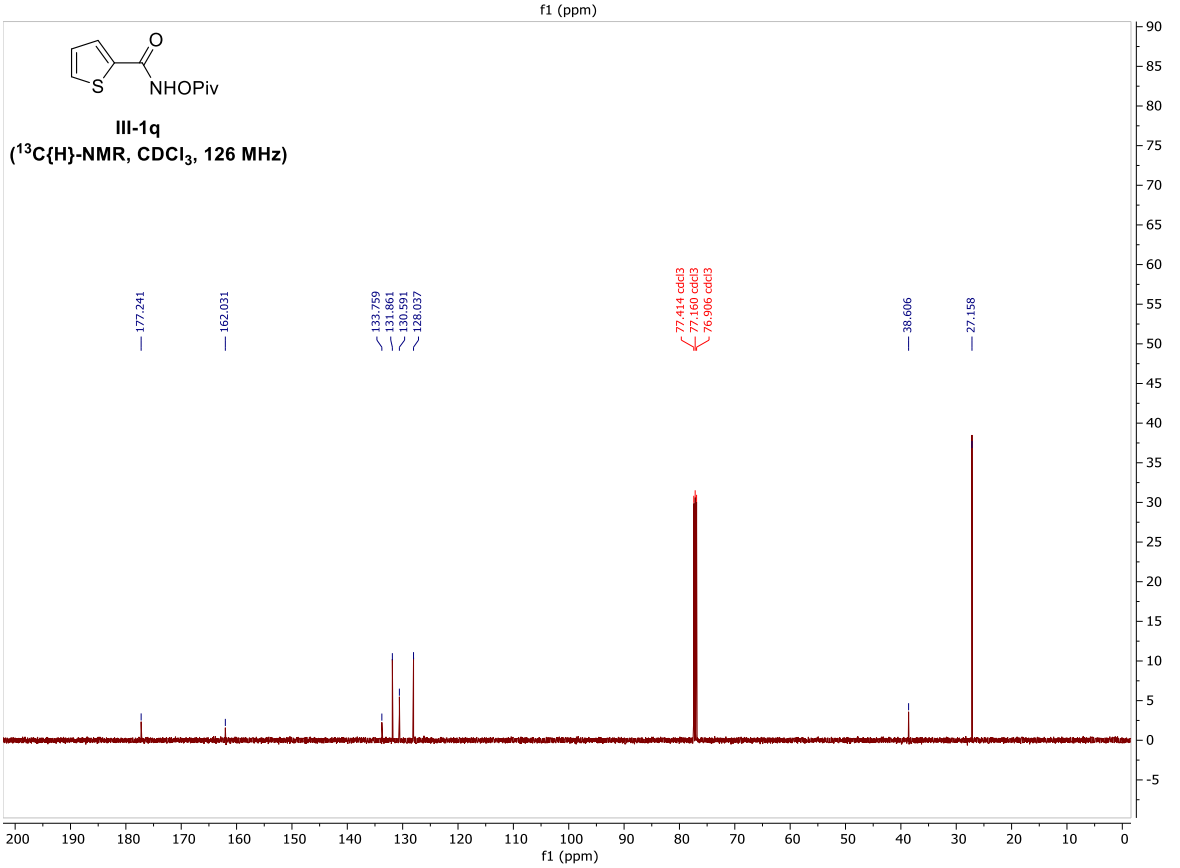

Figure 3.22 ^{1}H and $^{13}C\{^{1}H\}$ NMR spectra of compound **III-1r**

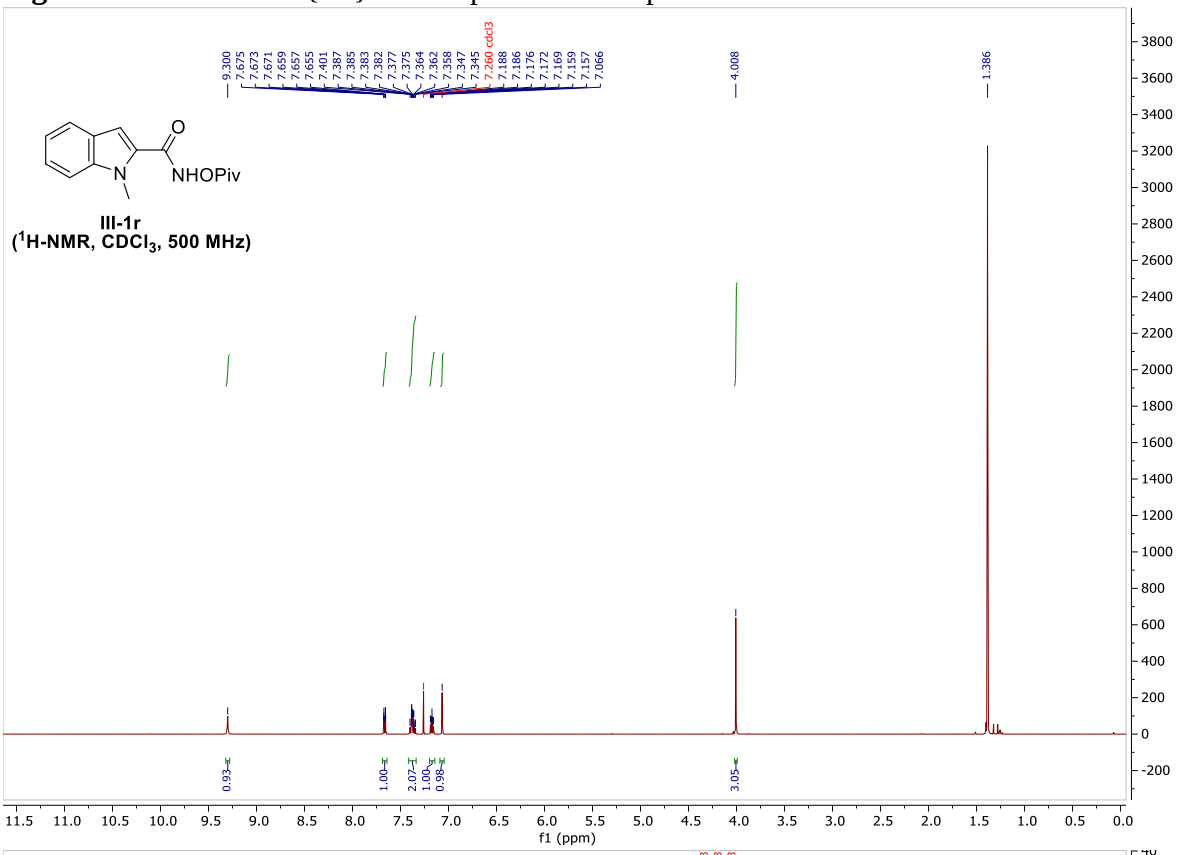

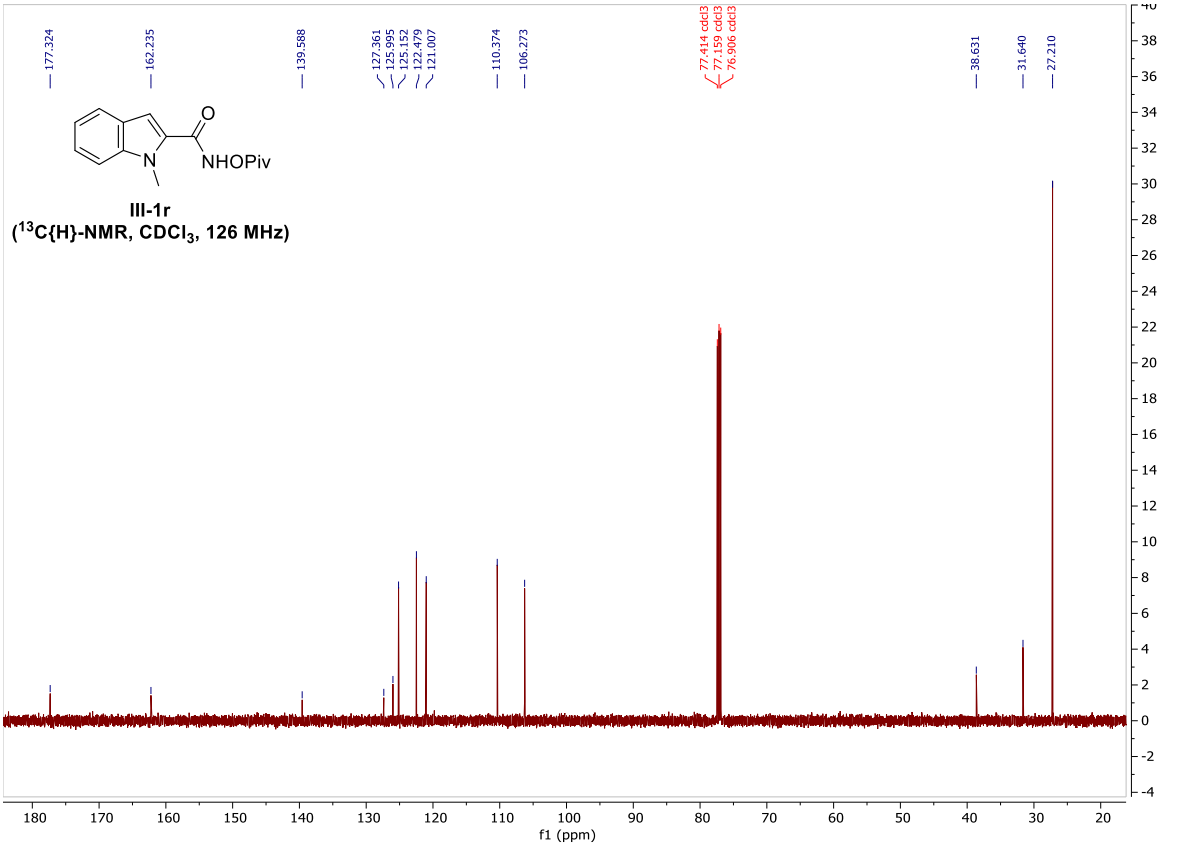

Figure 3.23 ^{1}H and $^{13}C\{^{1}H\}$ NMR spectra of compound **III-1s**

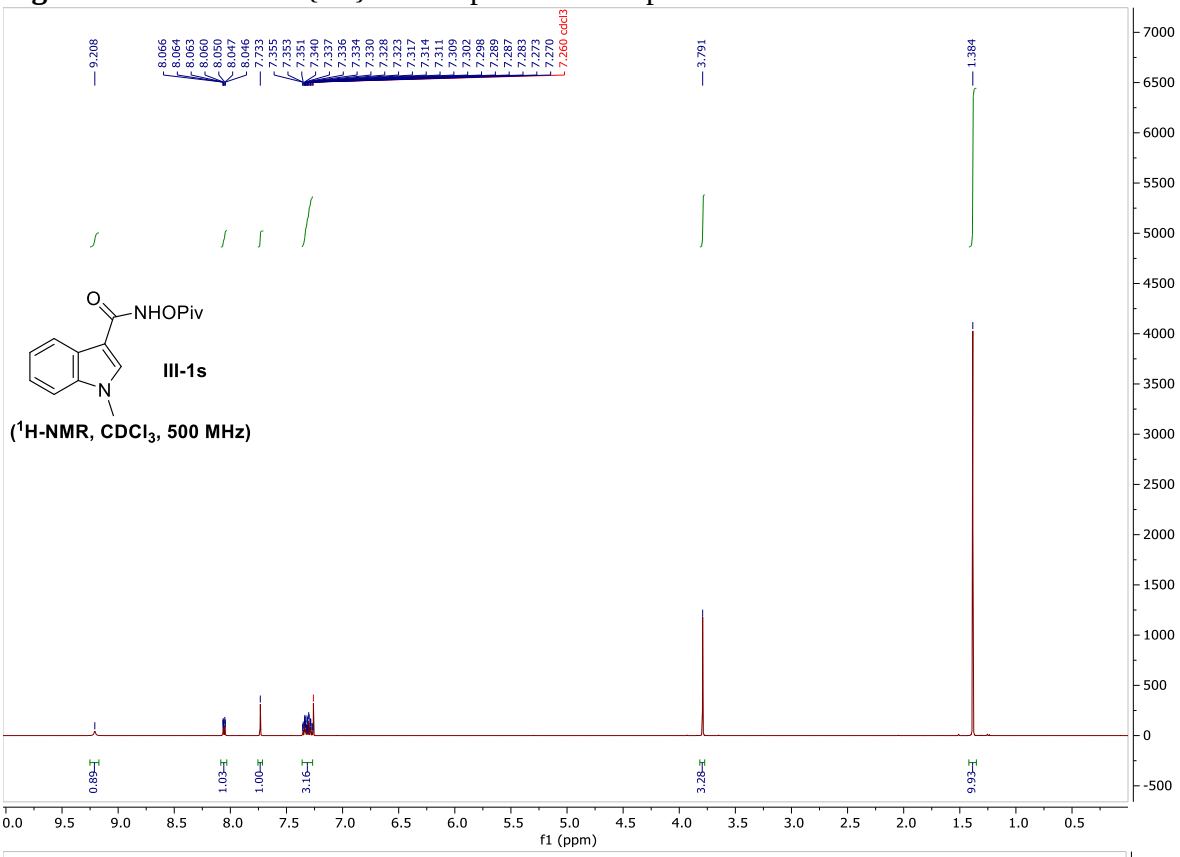

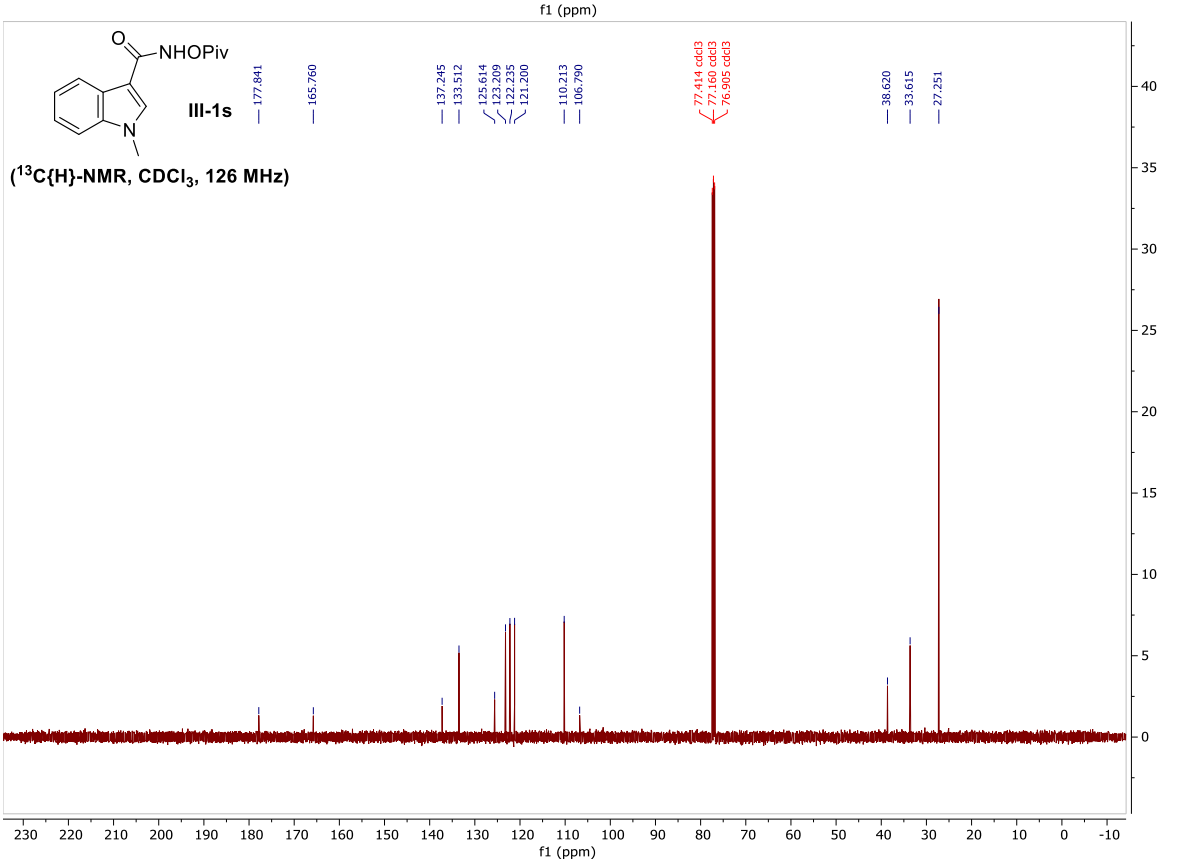

Figure 3.24 ^{1}H and $^{13}C\{^{1}H\}$ NMR spectra of compound **III-2a**

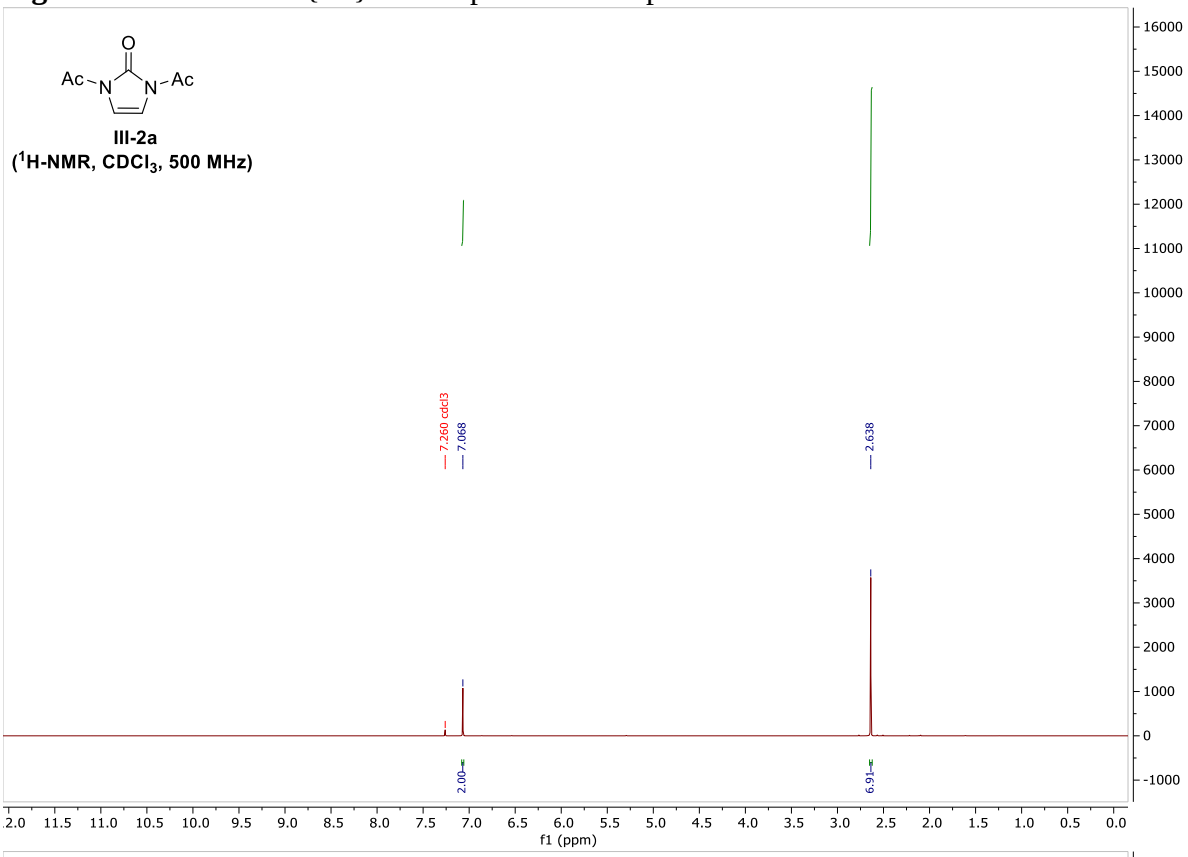

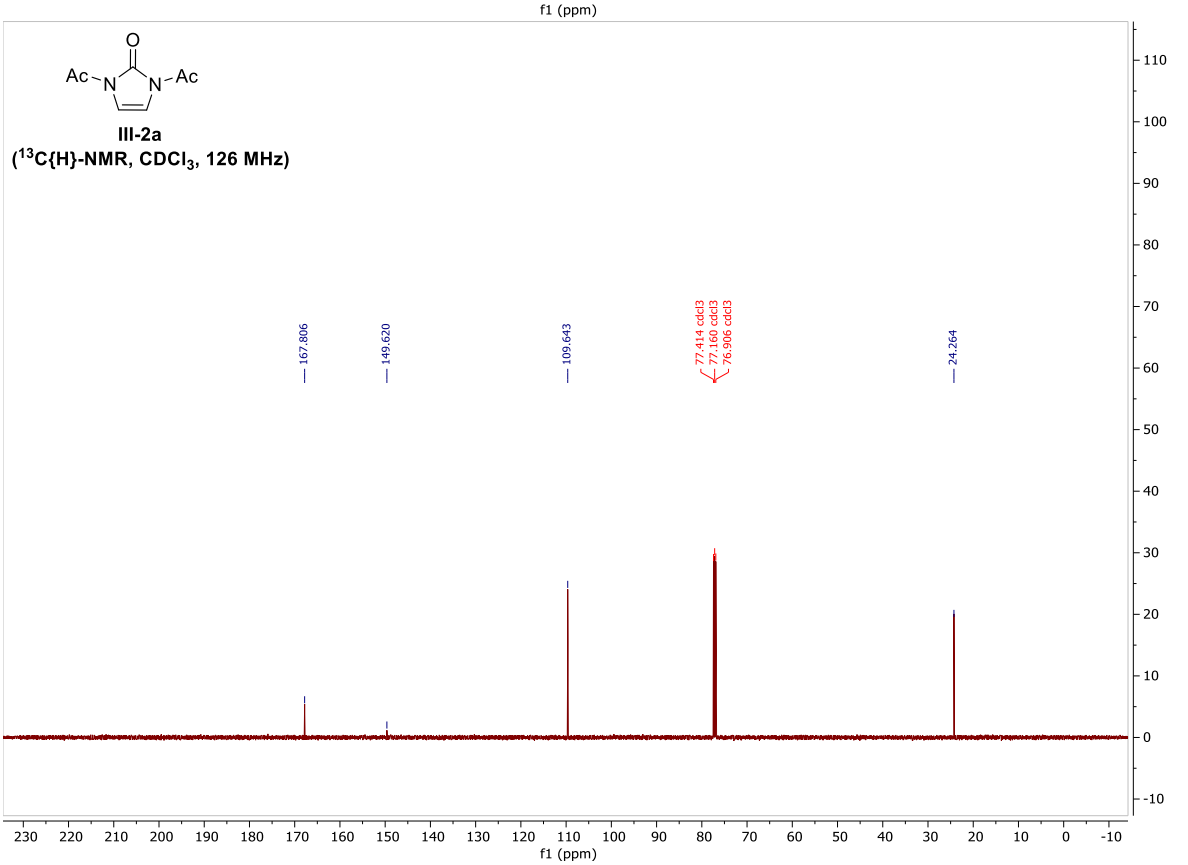

Figure 3.25 ^{1}H and $^{13}C\{^{1}H\}$ NMR spectra of compound **III-2b**

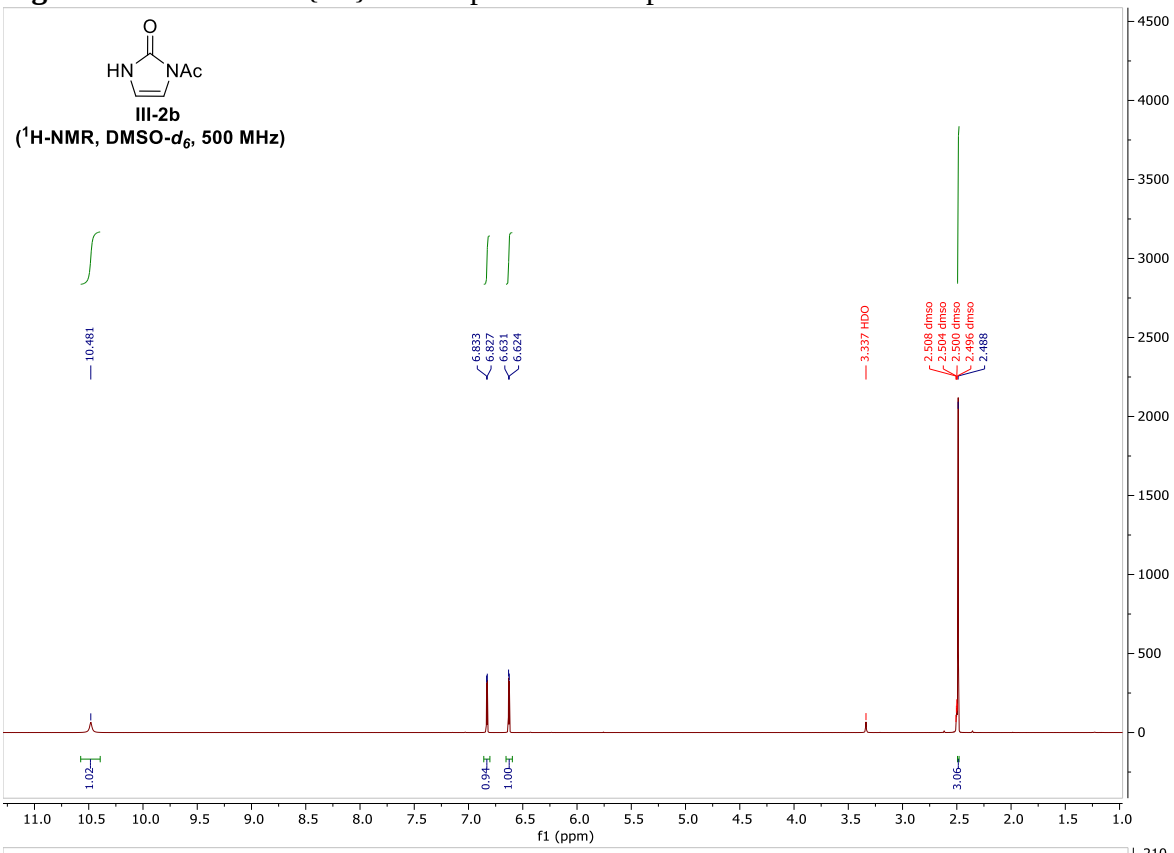

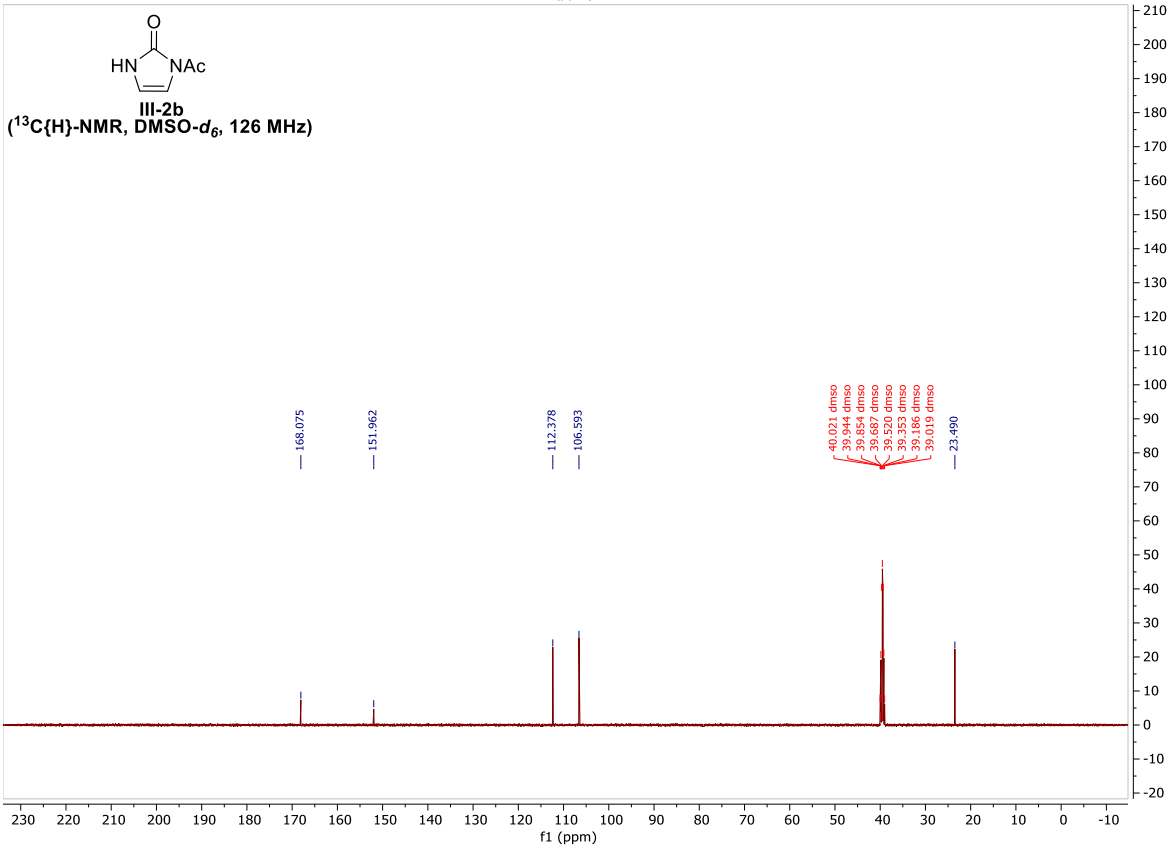

Figure 3.26 ^{1}H and $^{13}C\{^{1}H\}$ NMR spectra of compound **III-2c**

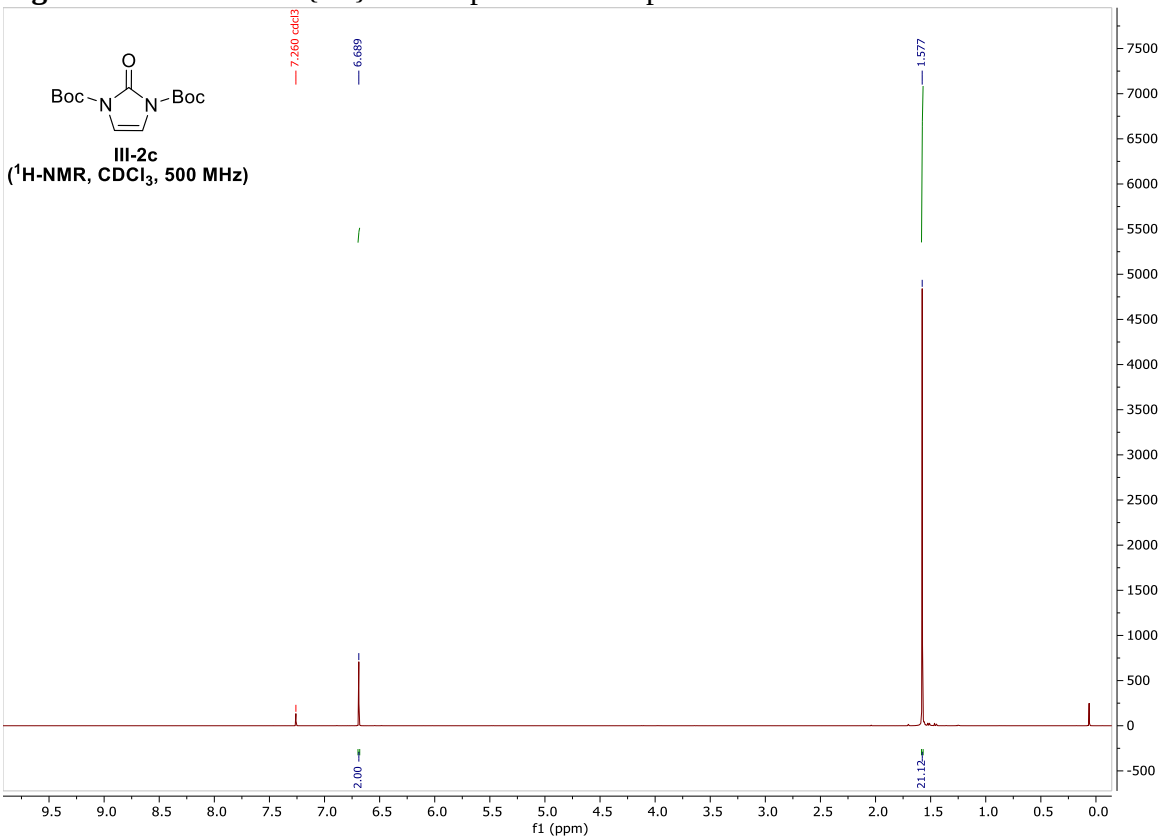

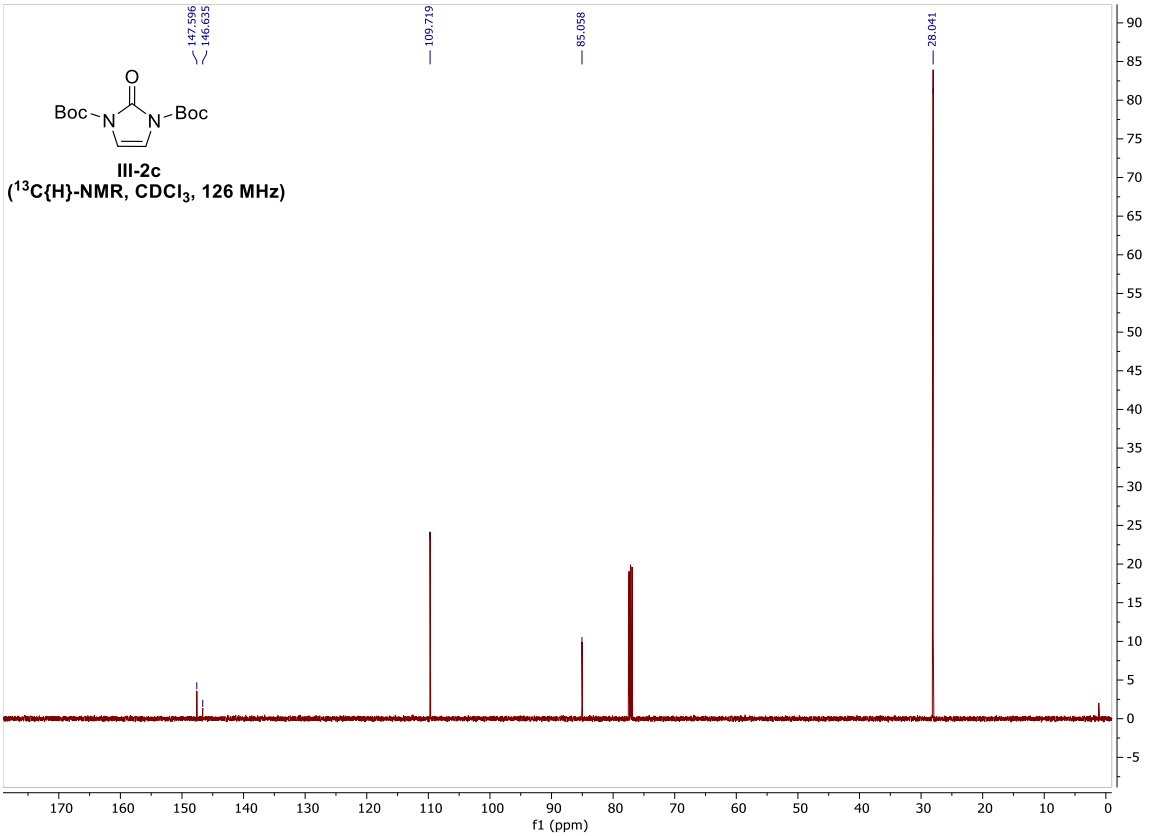

Figure 3.27 ^{1}H and ^{13}C{^{1}H} NMR spectra of compound **III-3a**

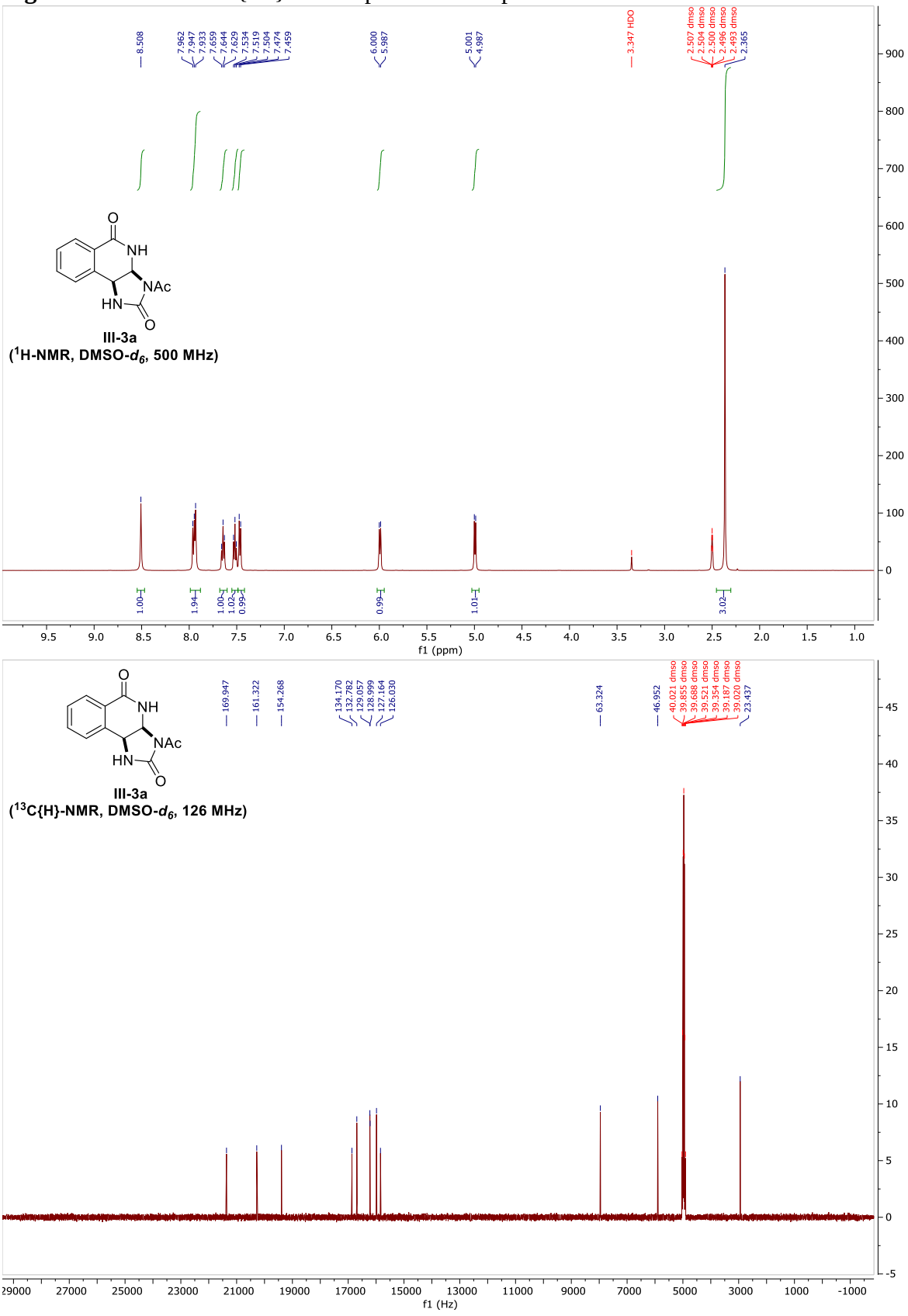

Figure 3.28 ^{1}H and $^{13}C\{^{1}H\}$ NMR spectra of compound **III-3b**

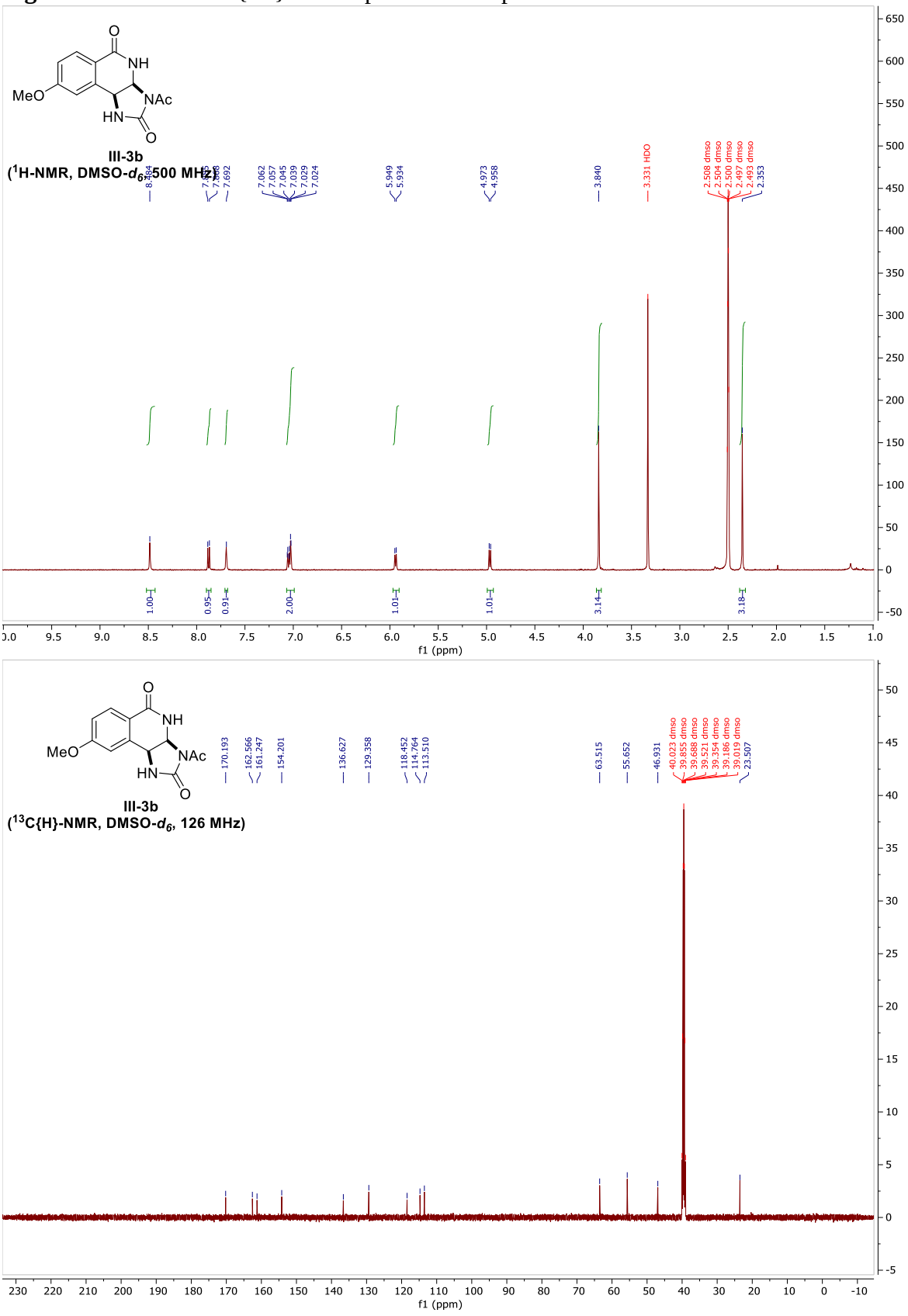

Figure 3.29 ^{1}H and $^{13}C\{^{1}H\}$ NMR spectra of compound **III-3c**

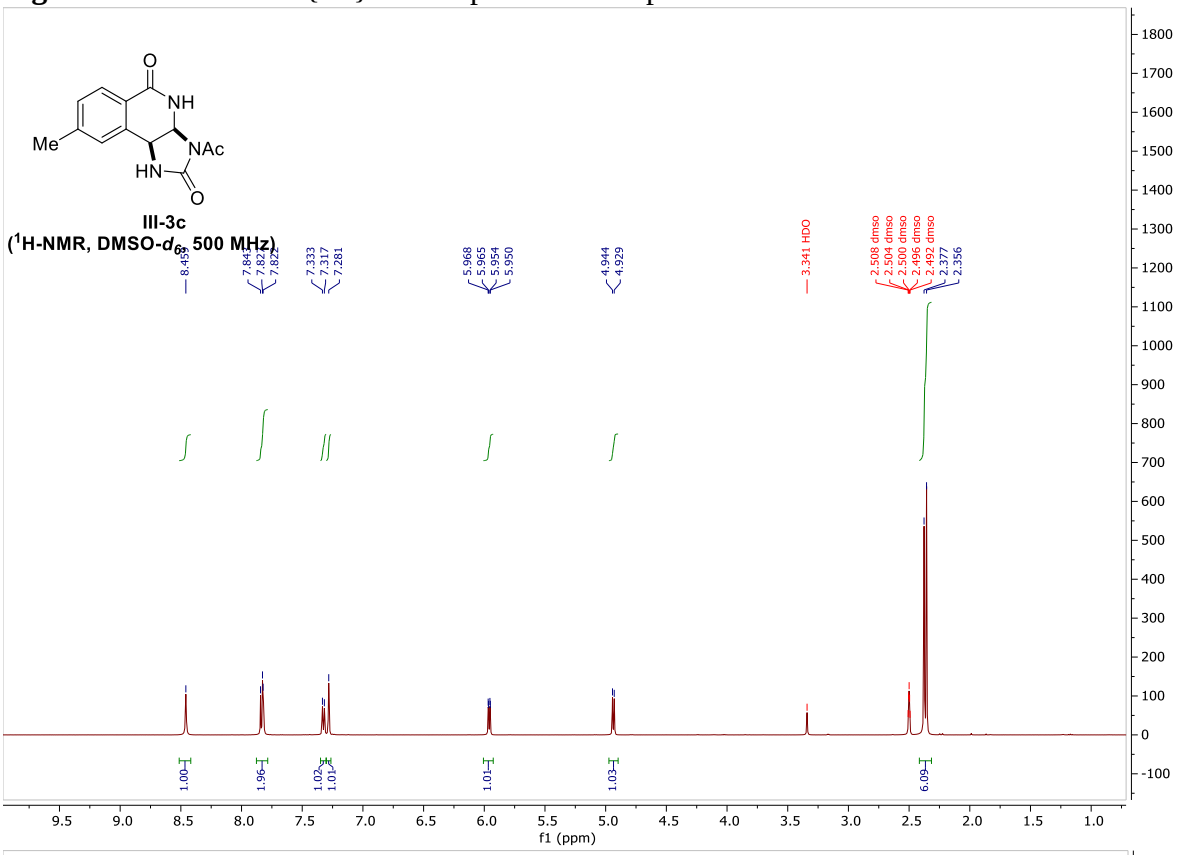

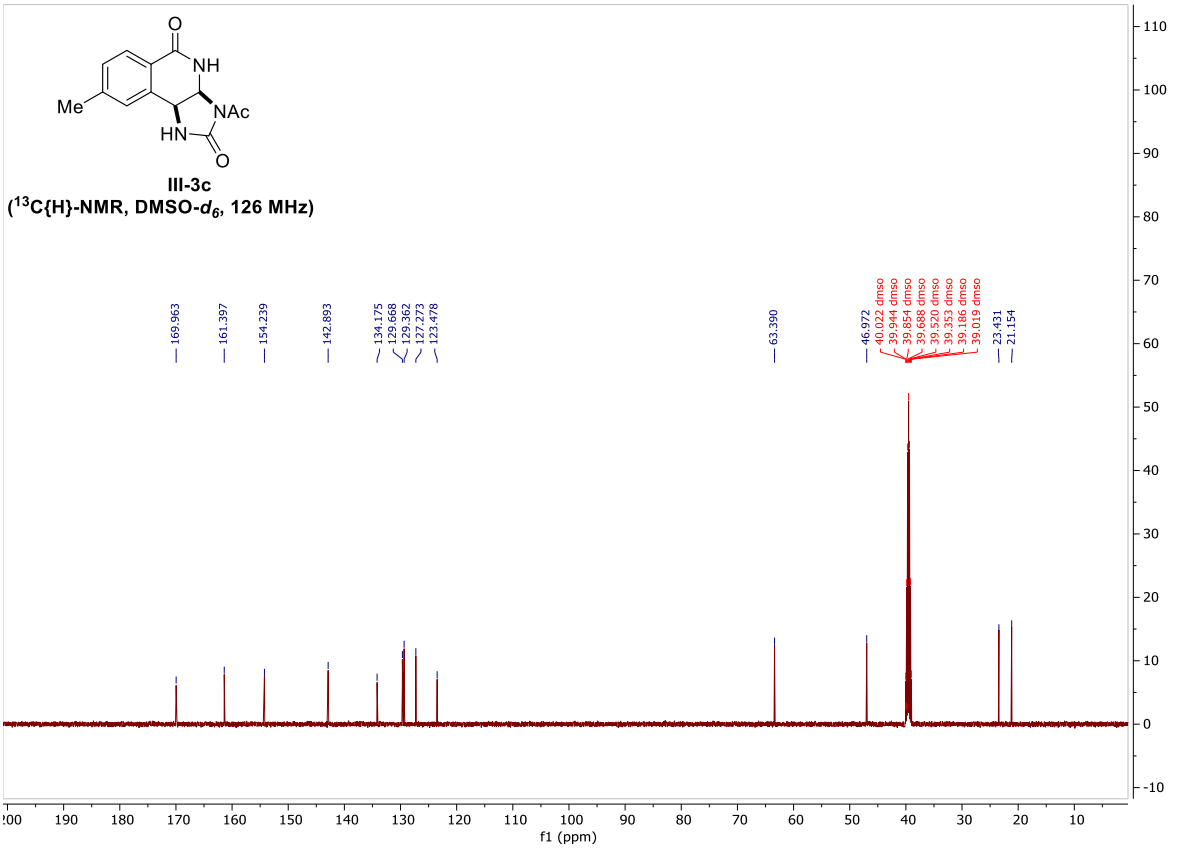

Figure 3.30 ^{1}H and ^{13}C{^{1}H} NMR spectra of compound **III-3d**

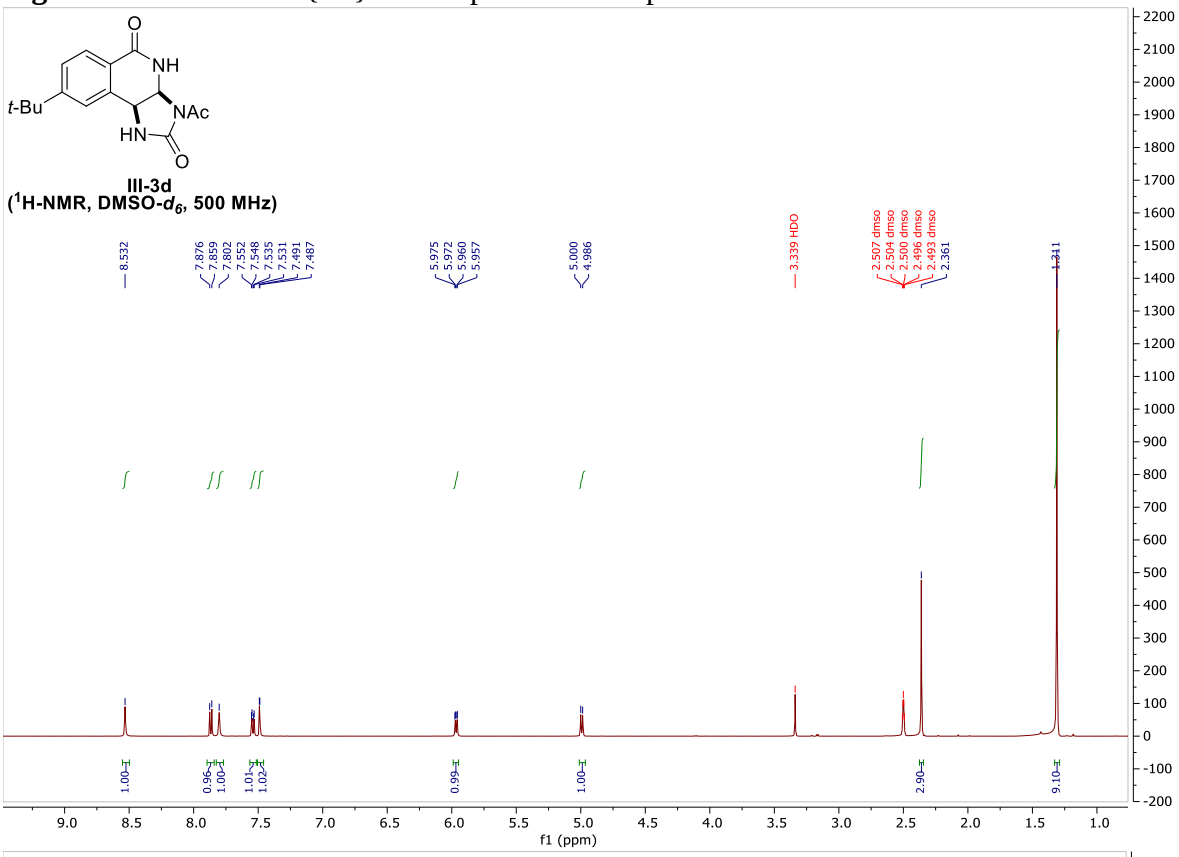

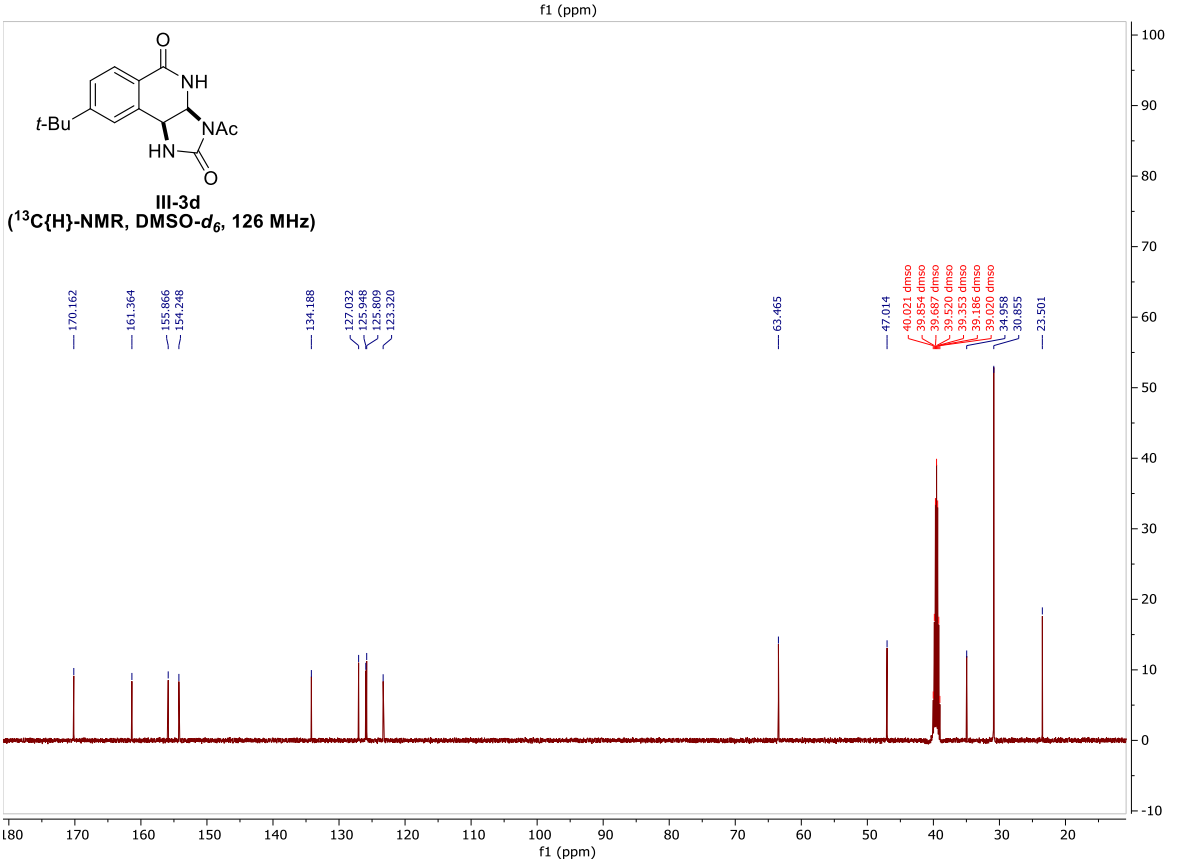

Figure 3.31 ^{1}H and $^{13}C\{^{1}H\}$ NMR spectra of compound **III-3e**

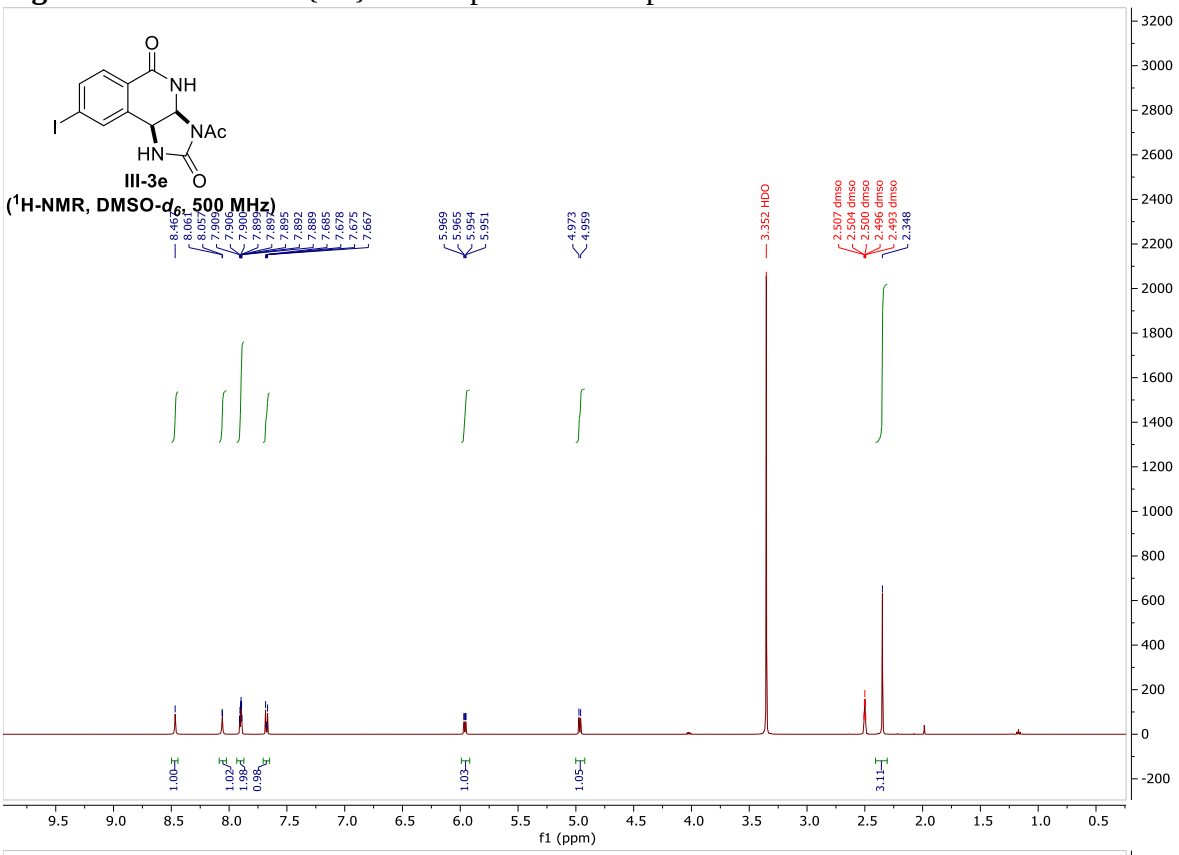

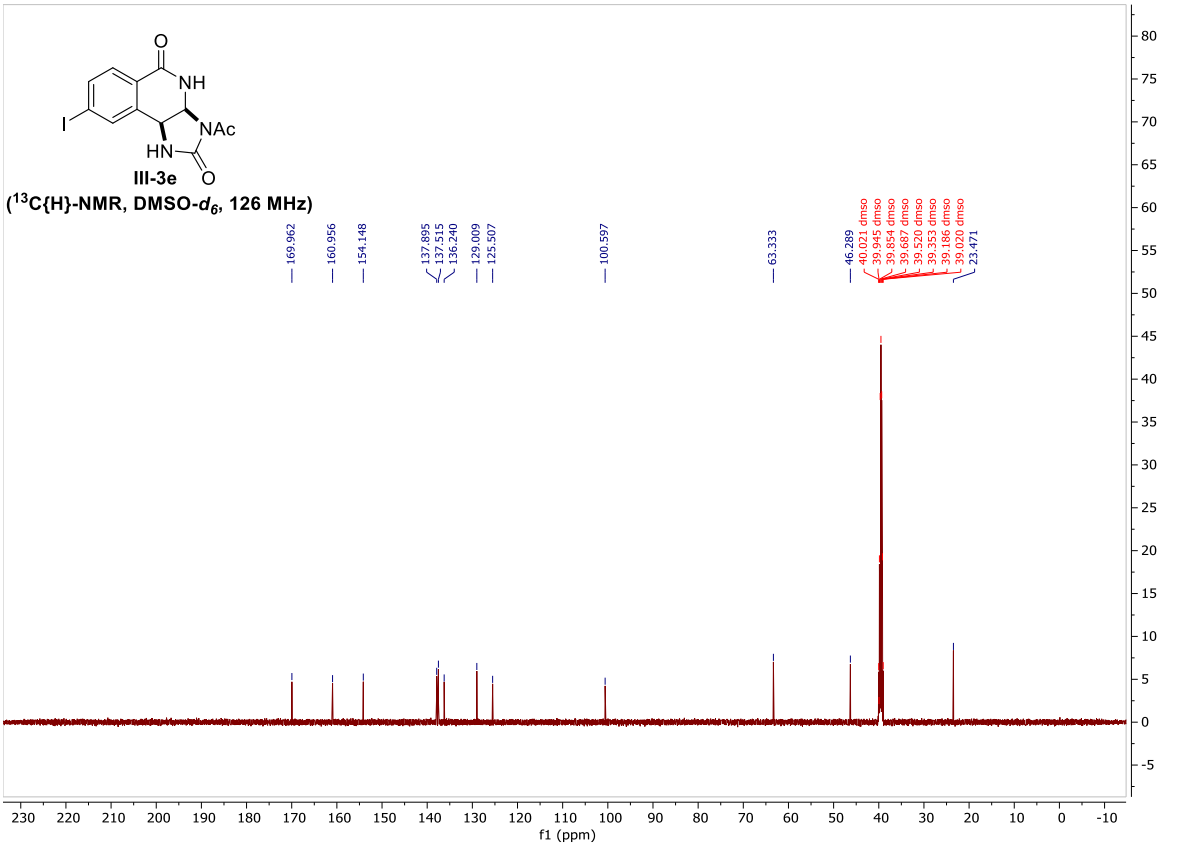

Figure 3.32 ^{1}H and $^{13}C\{^{1}H\}$ NMR spectra of compound **III-3f**

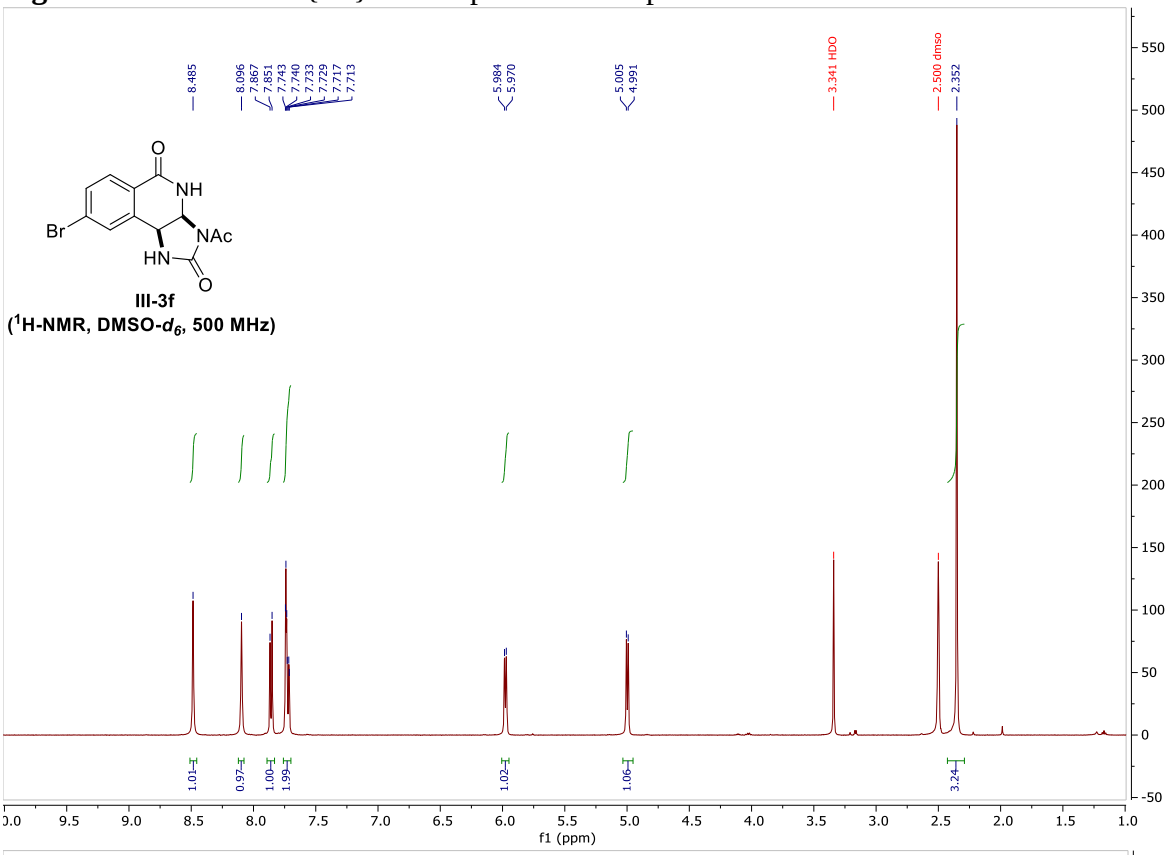

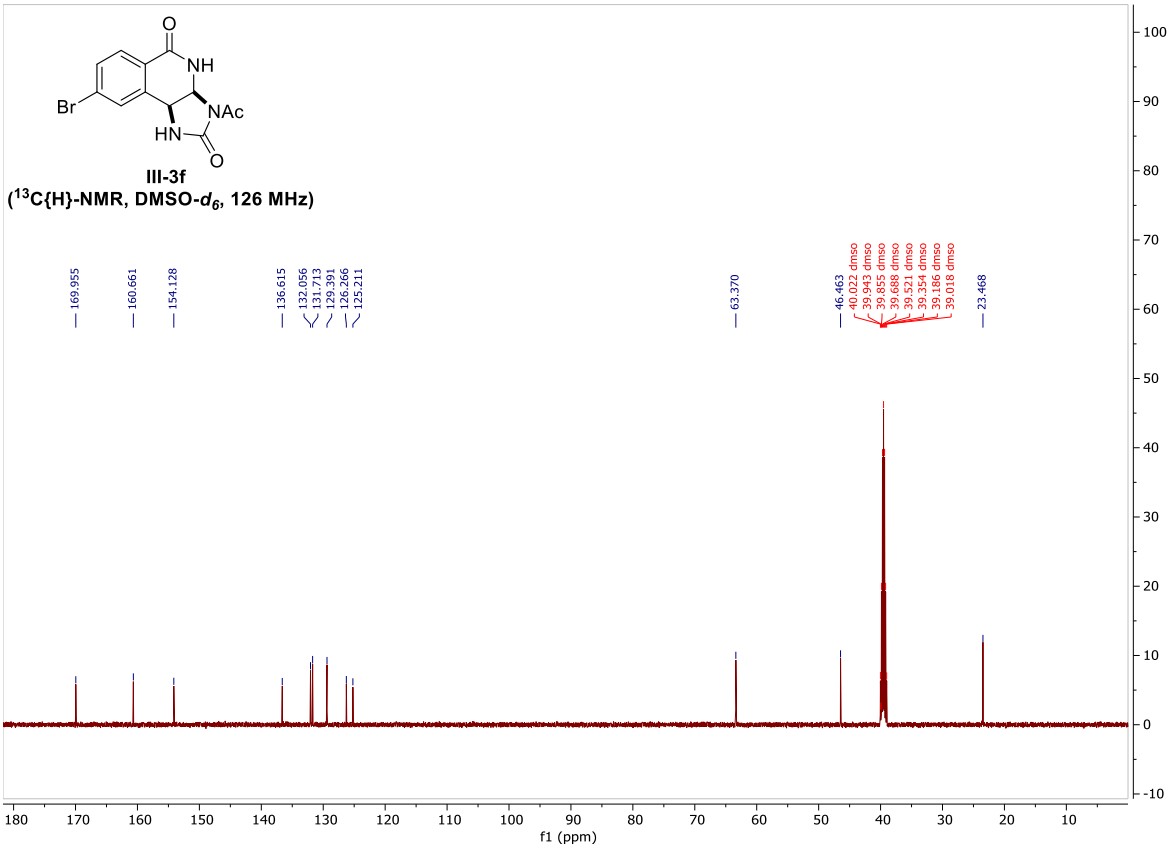

Figure 3.33 ^{1}H and $^{13}C\{^{1}H\}$ NMR spectra of compound **III-3g**

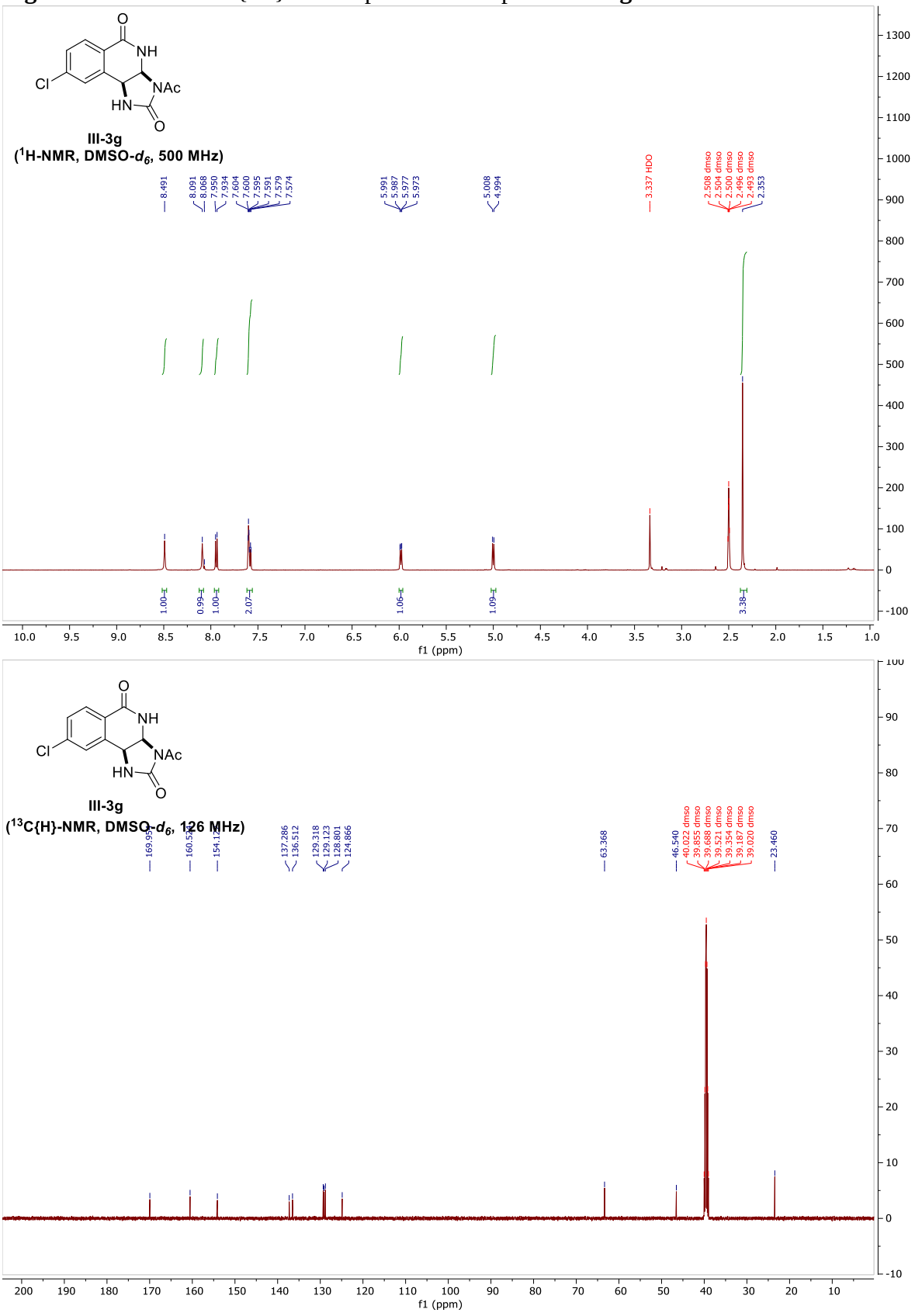

Figure 3.34 ^{1}H and $^{13}C\{^{1}H\}$ NMR spectra of compound **III-3h**

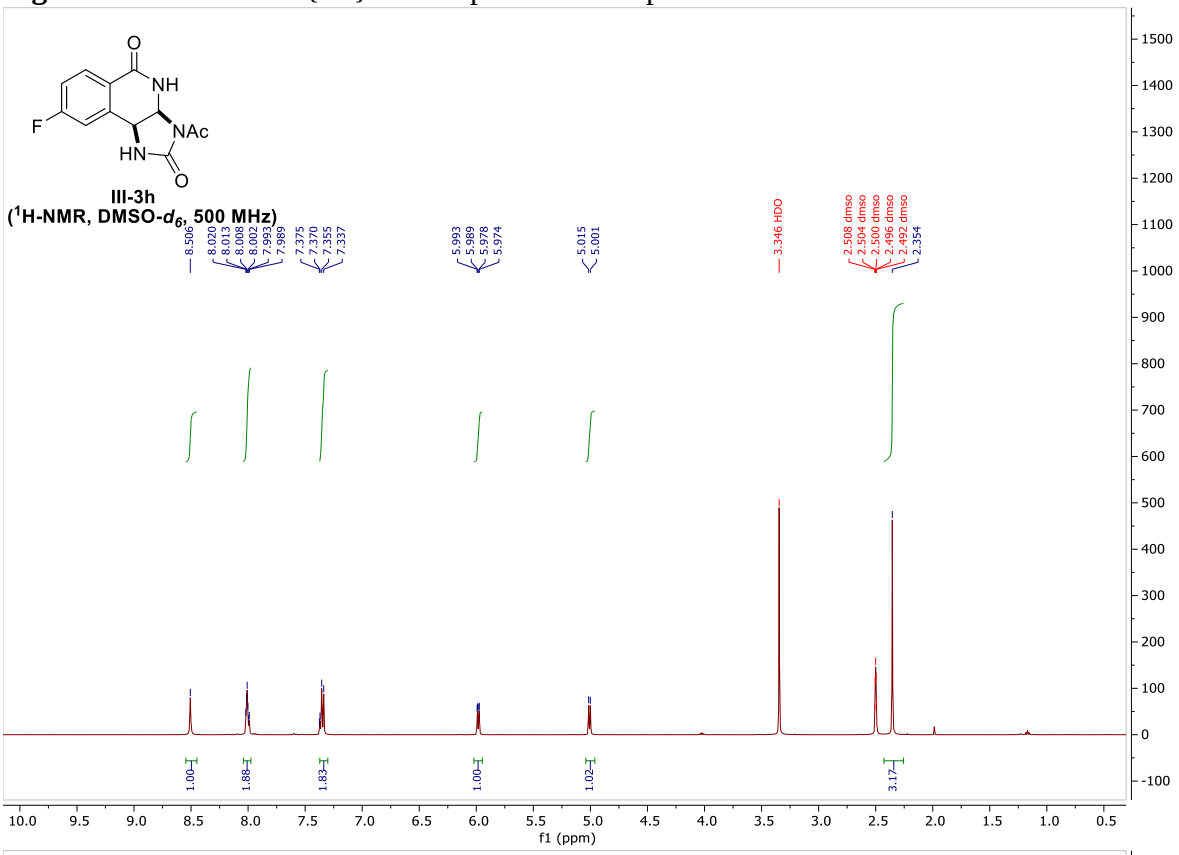

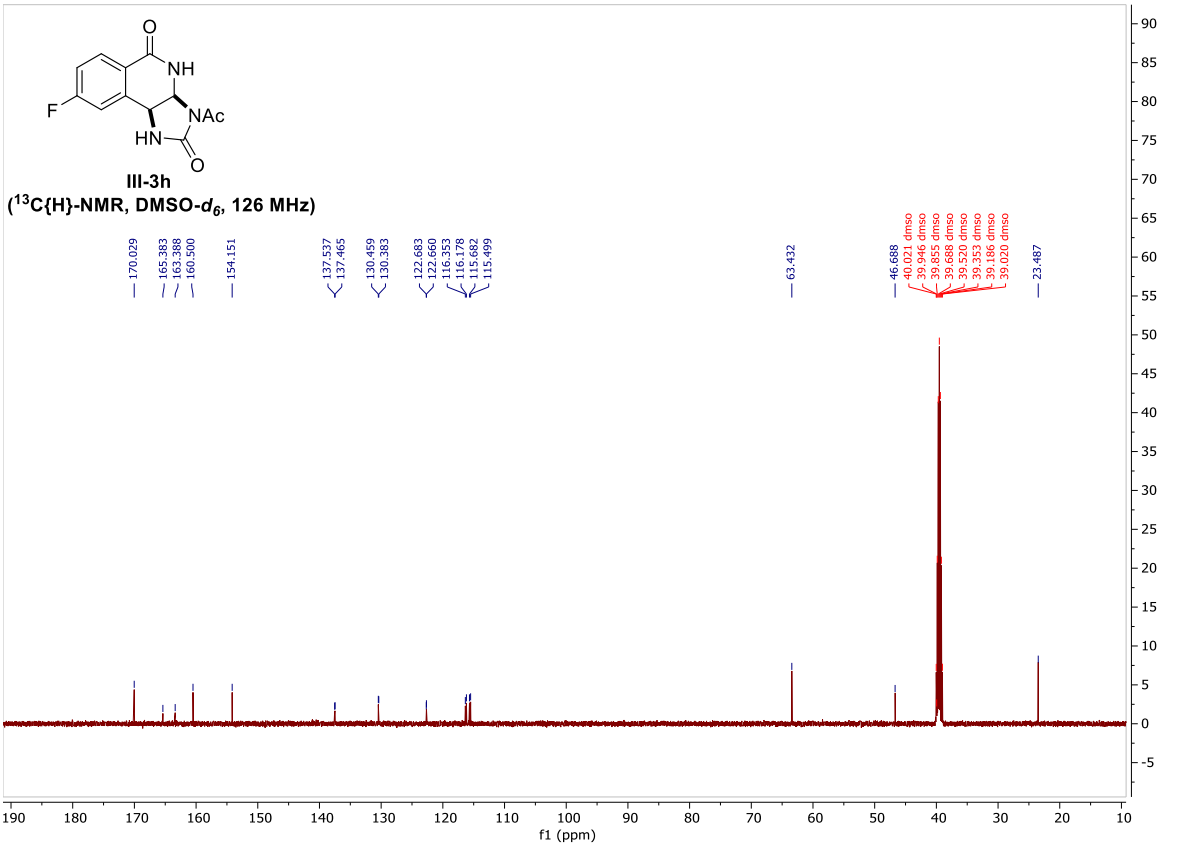

Figure 3.35 ^{1}H and $^{13}C\{^{1}H\}$ NMR spectra of compound **III-3i**

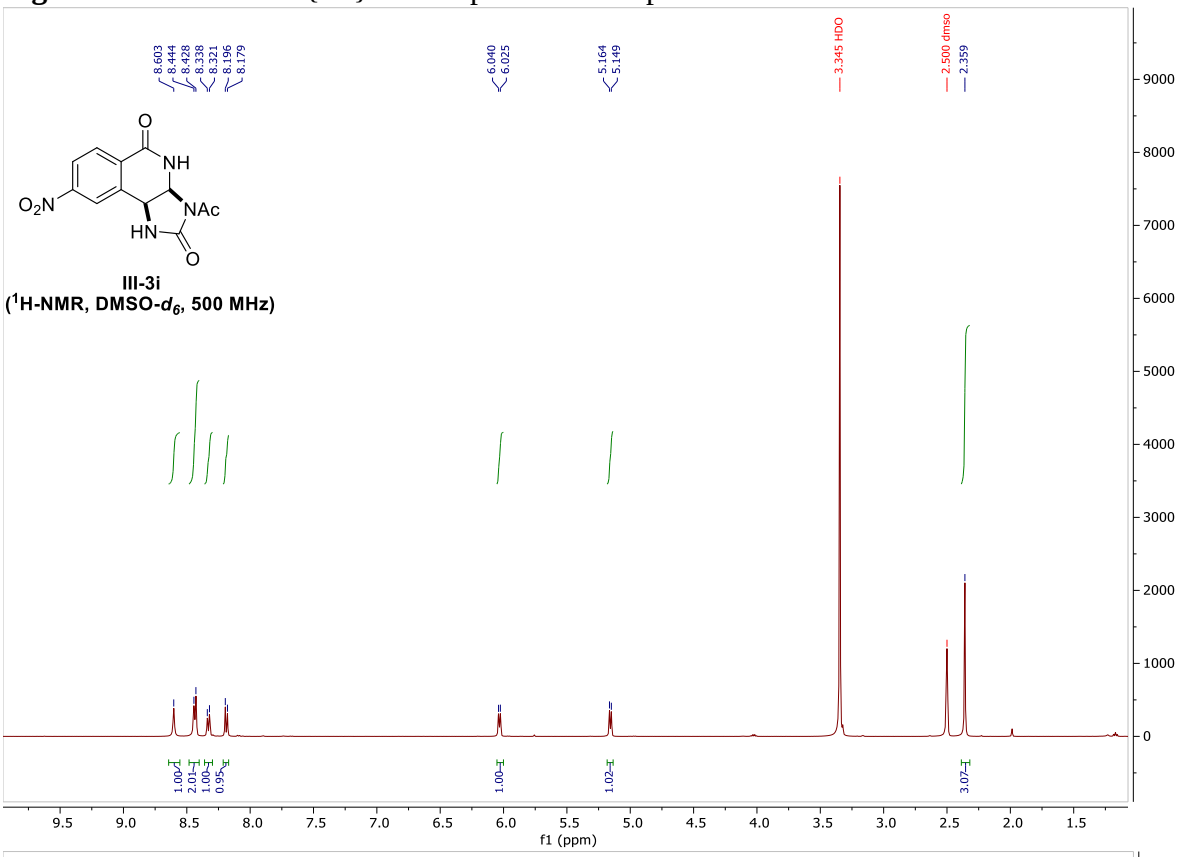

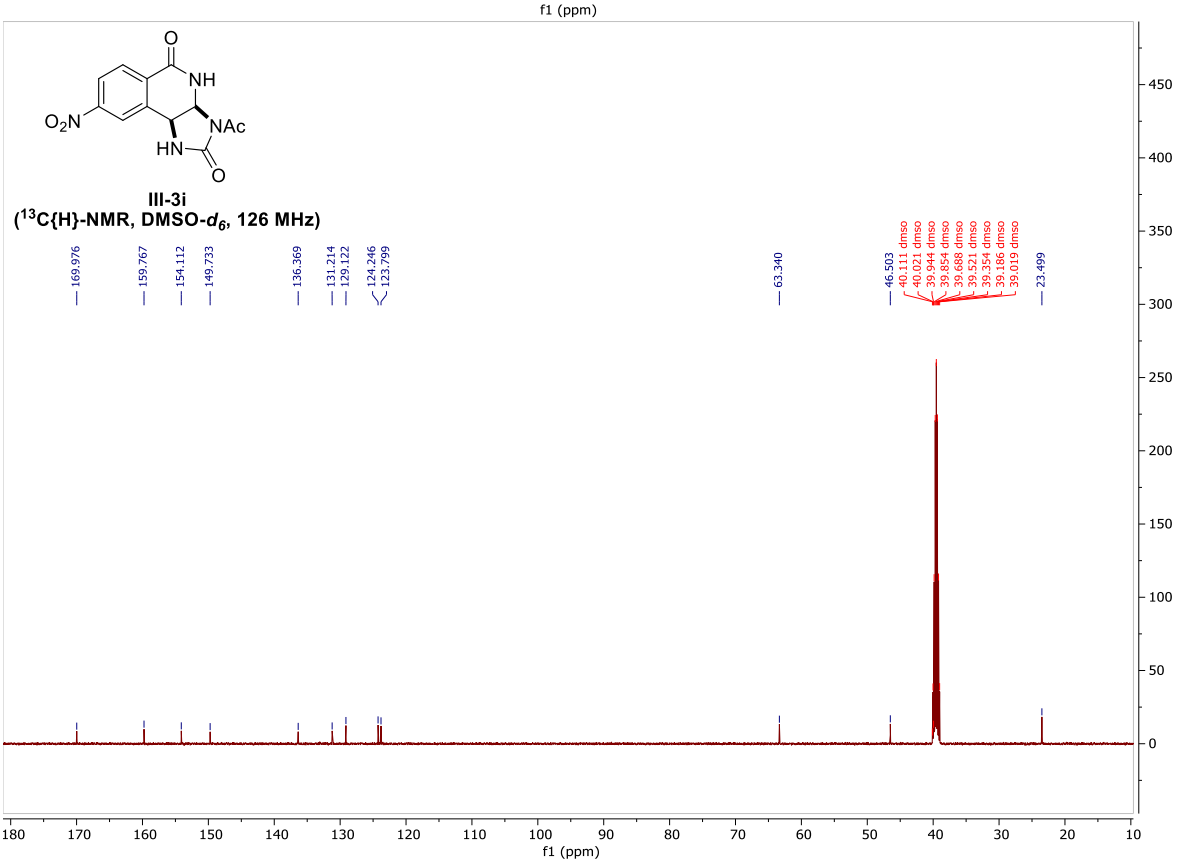

Figure 3.36 ^{1}H and $^{13}C\{^{1}H\}$ NMR spectra of compound **III-3l**

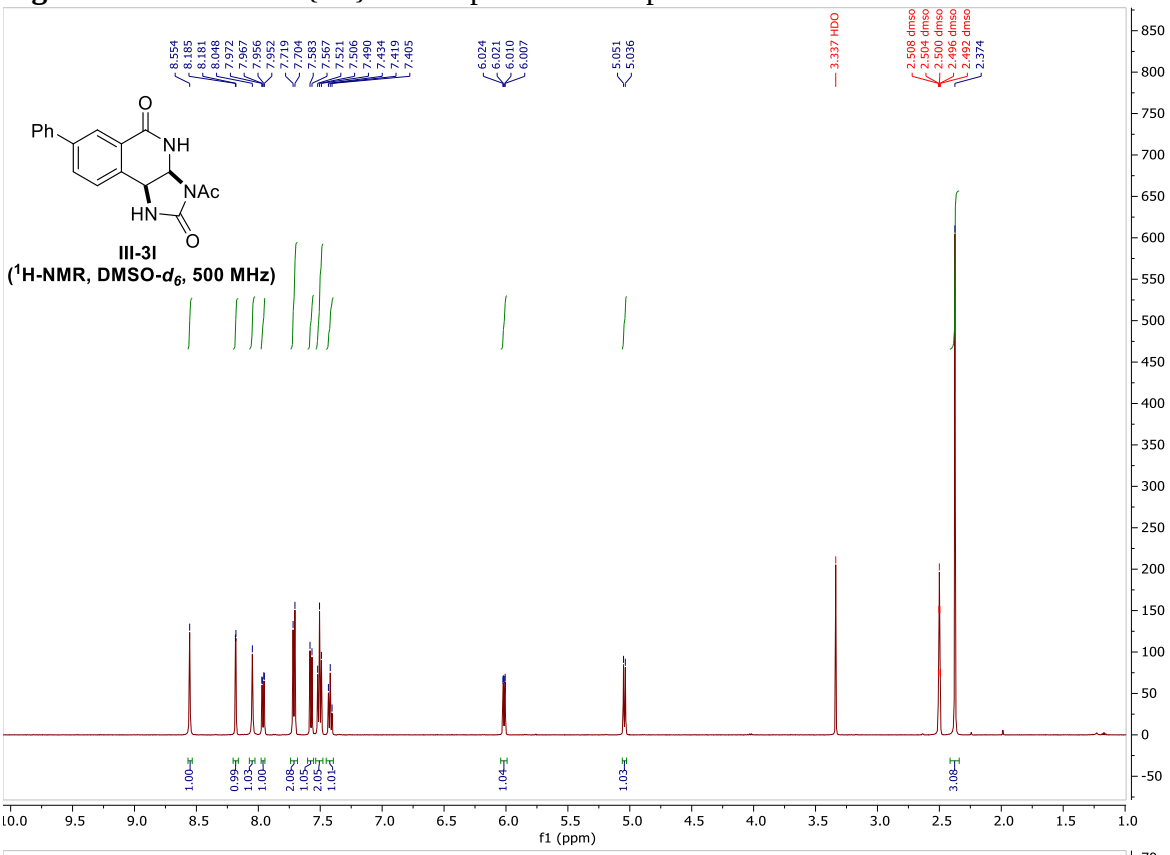

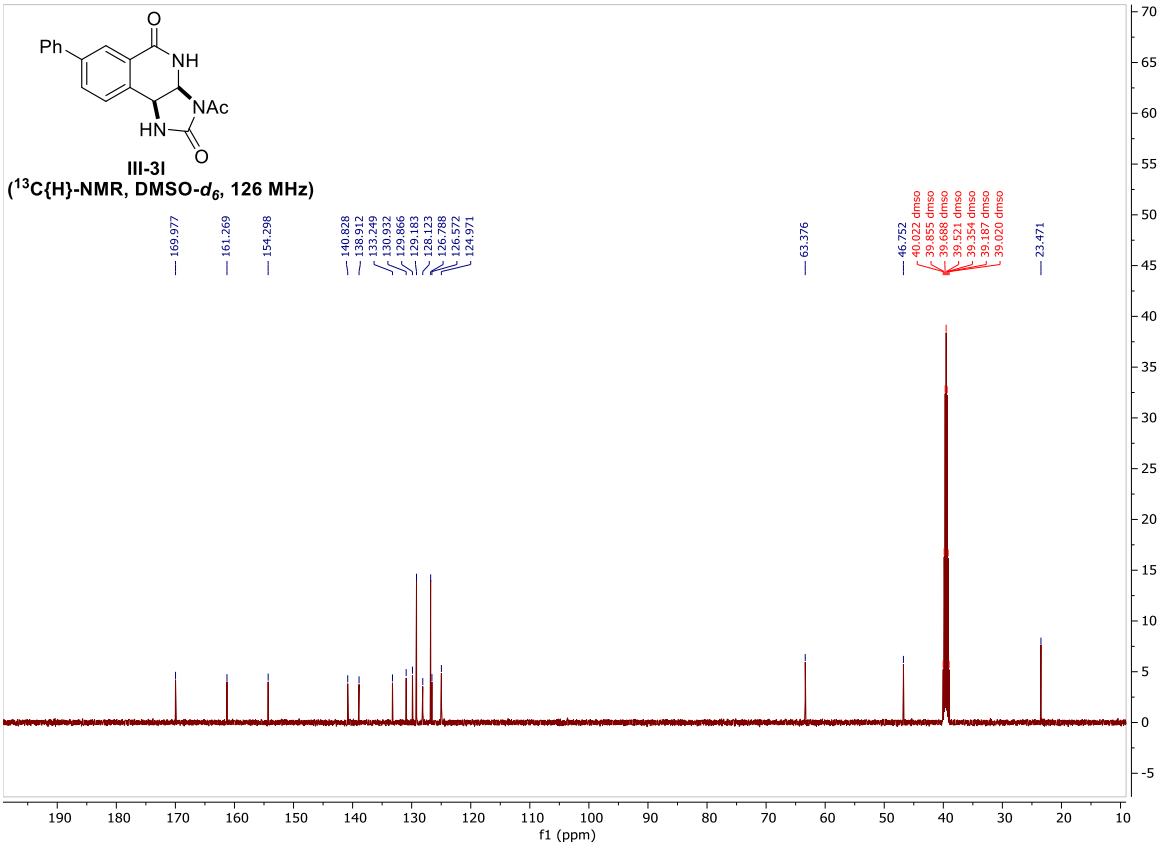

Figure 3.37 ^{1}H and $^{13}C\{^{1}H\}$ NMR spectra of compound **III-3m(i)** and **III-3m(ii)**

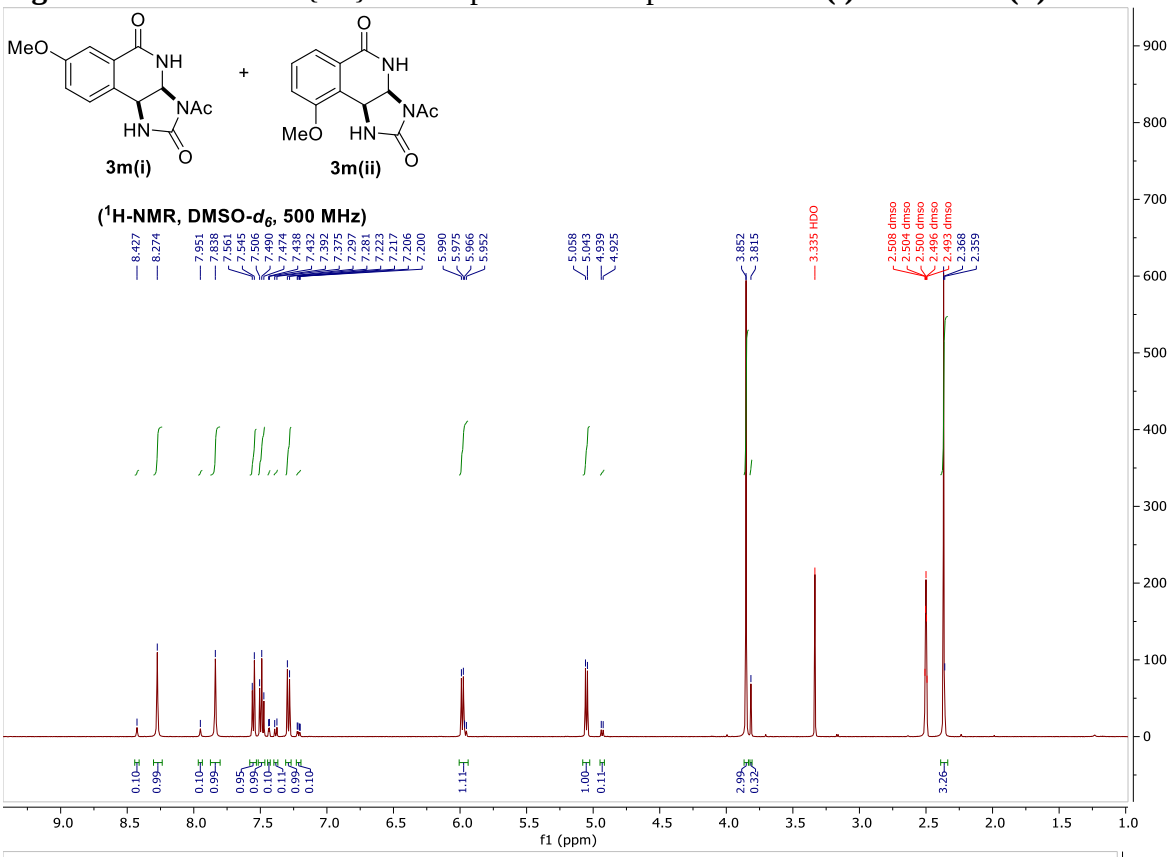

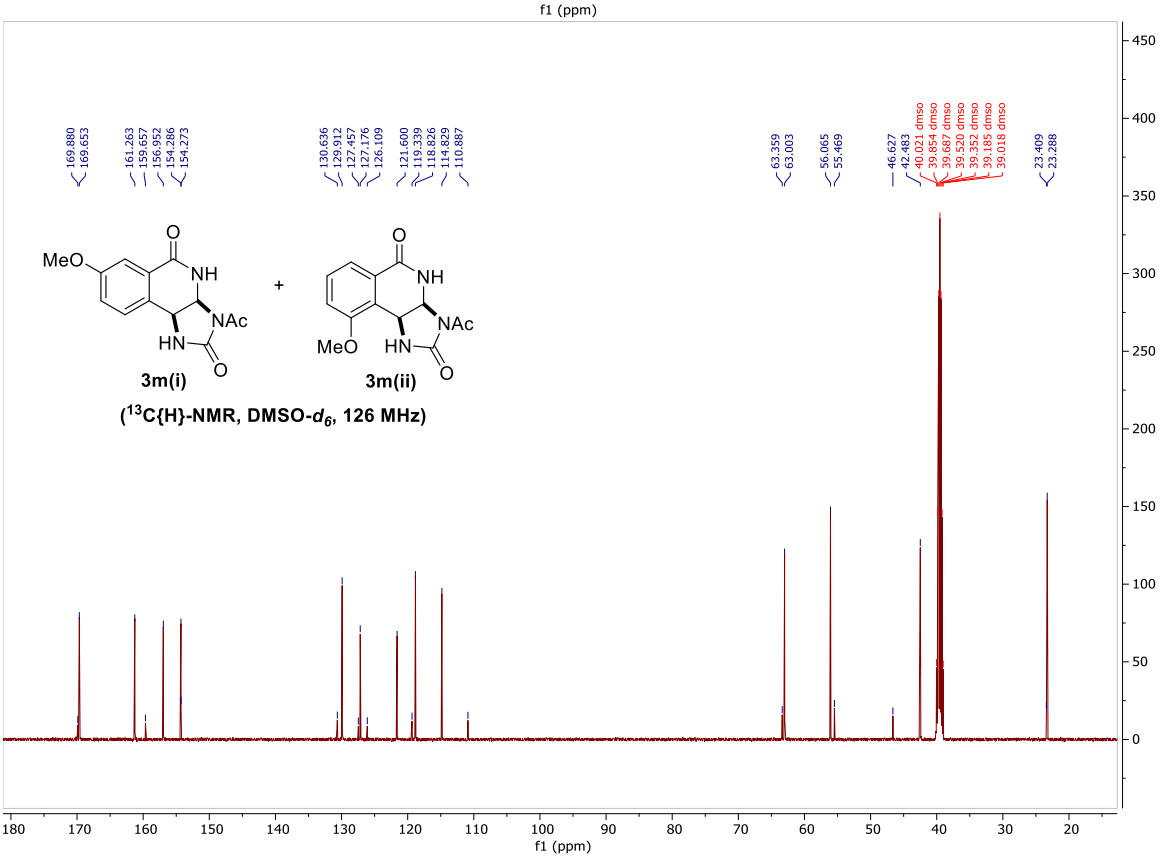

Figure 3.38 ^{1}H and $^{13}C\{^{1}H\}$ NMR spectra of compound **III-3n**

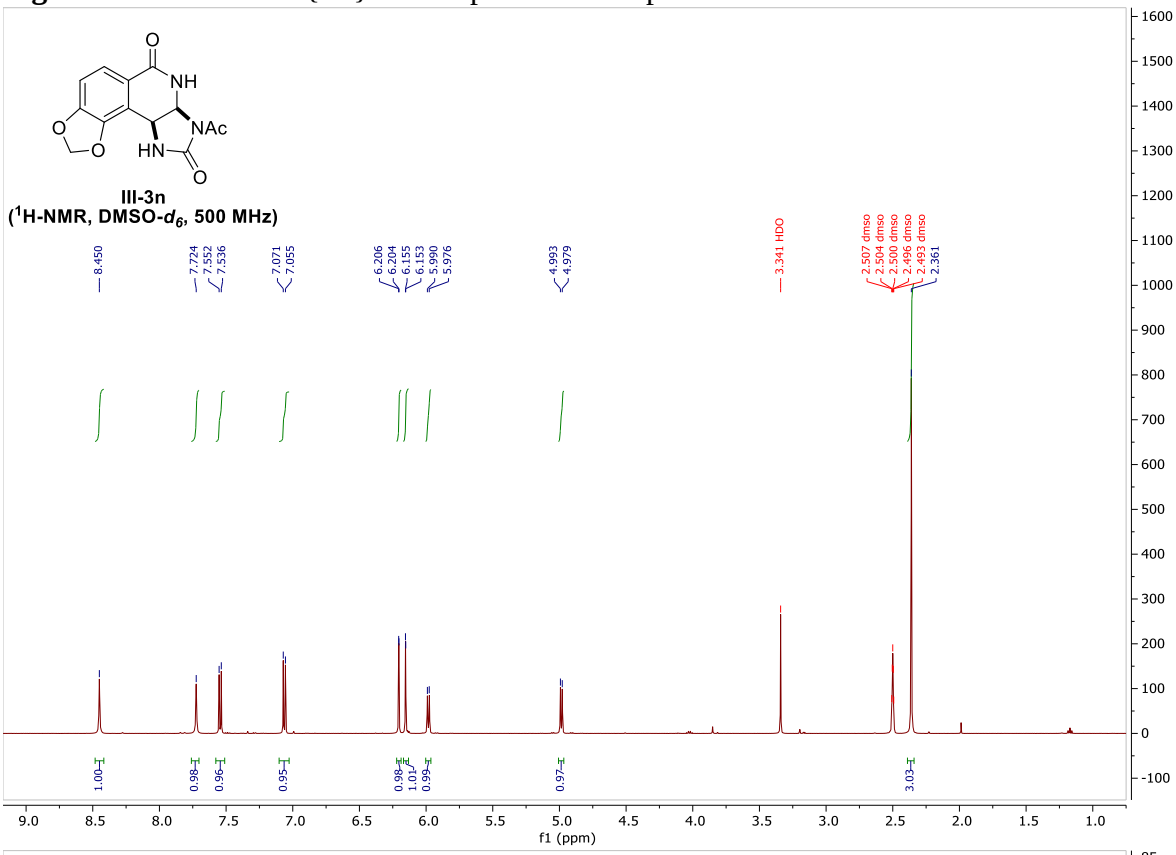

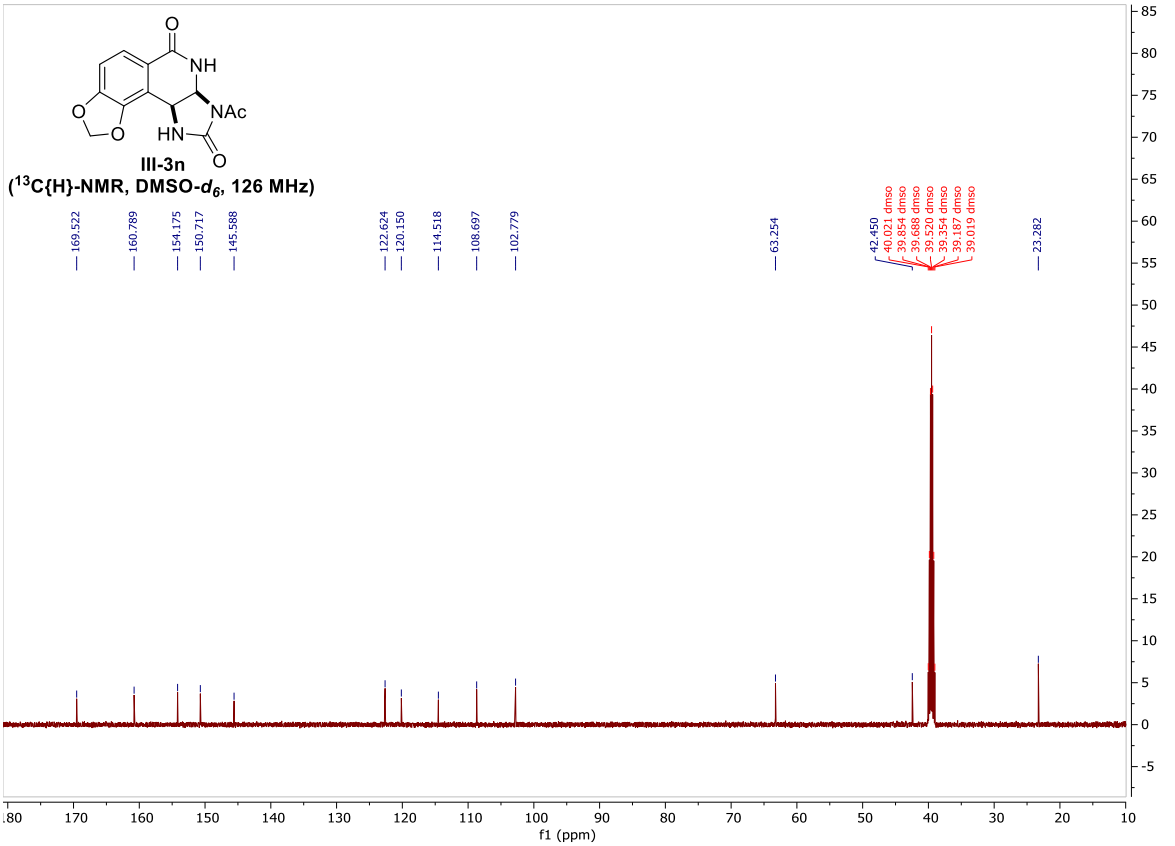

Figure 3.39 ^{1}H and $^{13}C\{^{1}H\}$ NMR spectra of compound **III-3o(i)** and **III-3o(ii)**

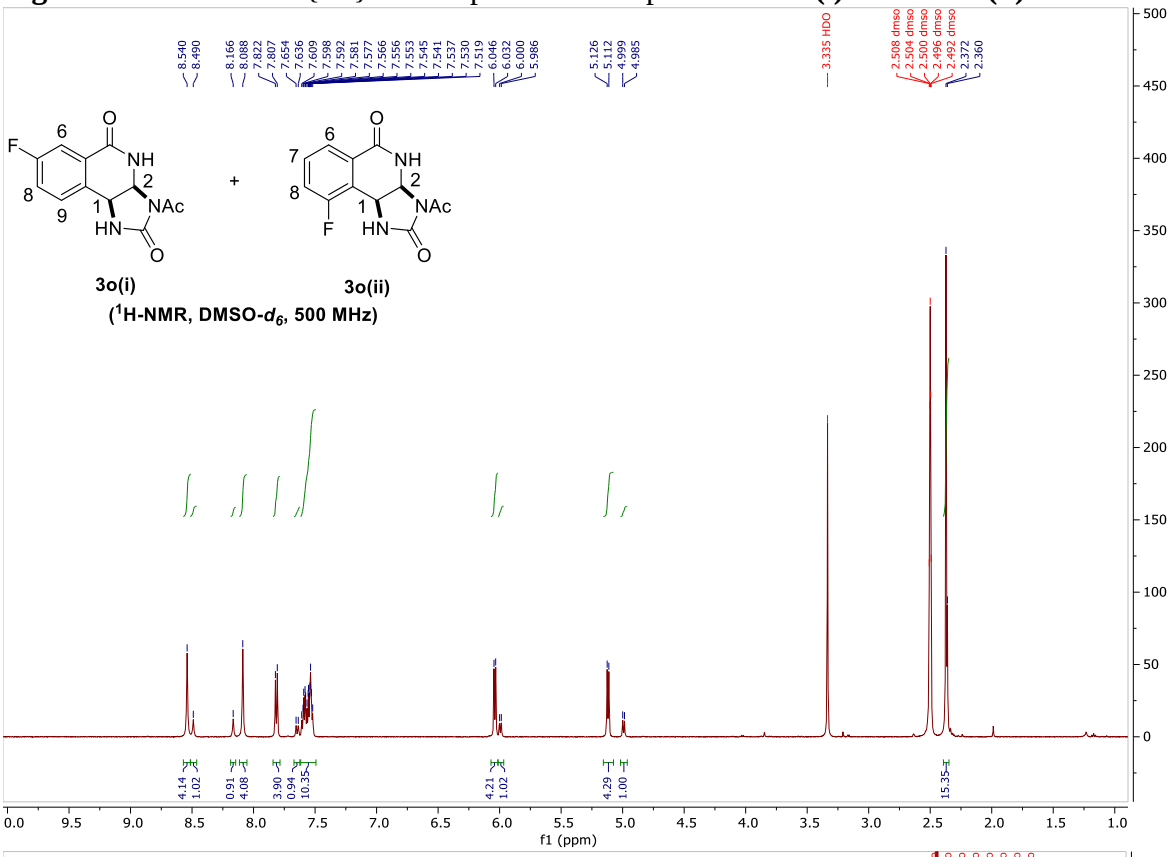

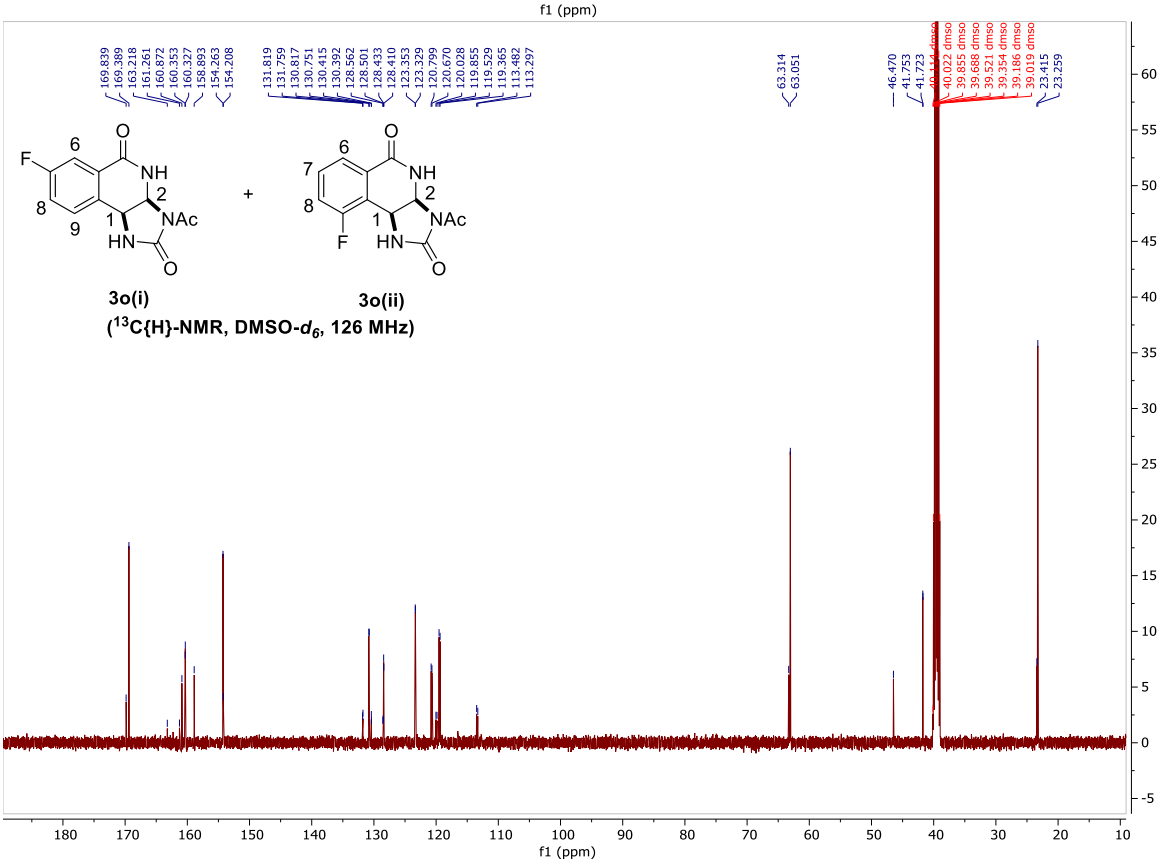

Figure 3.40 ^{1}H and $^{13}C\{^{1}H\}$ NMR spectra of compound **III-3p**

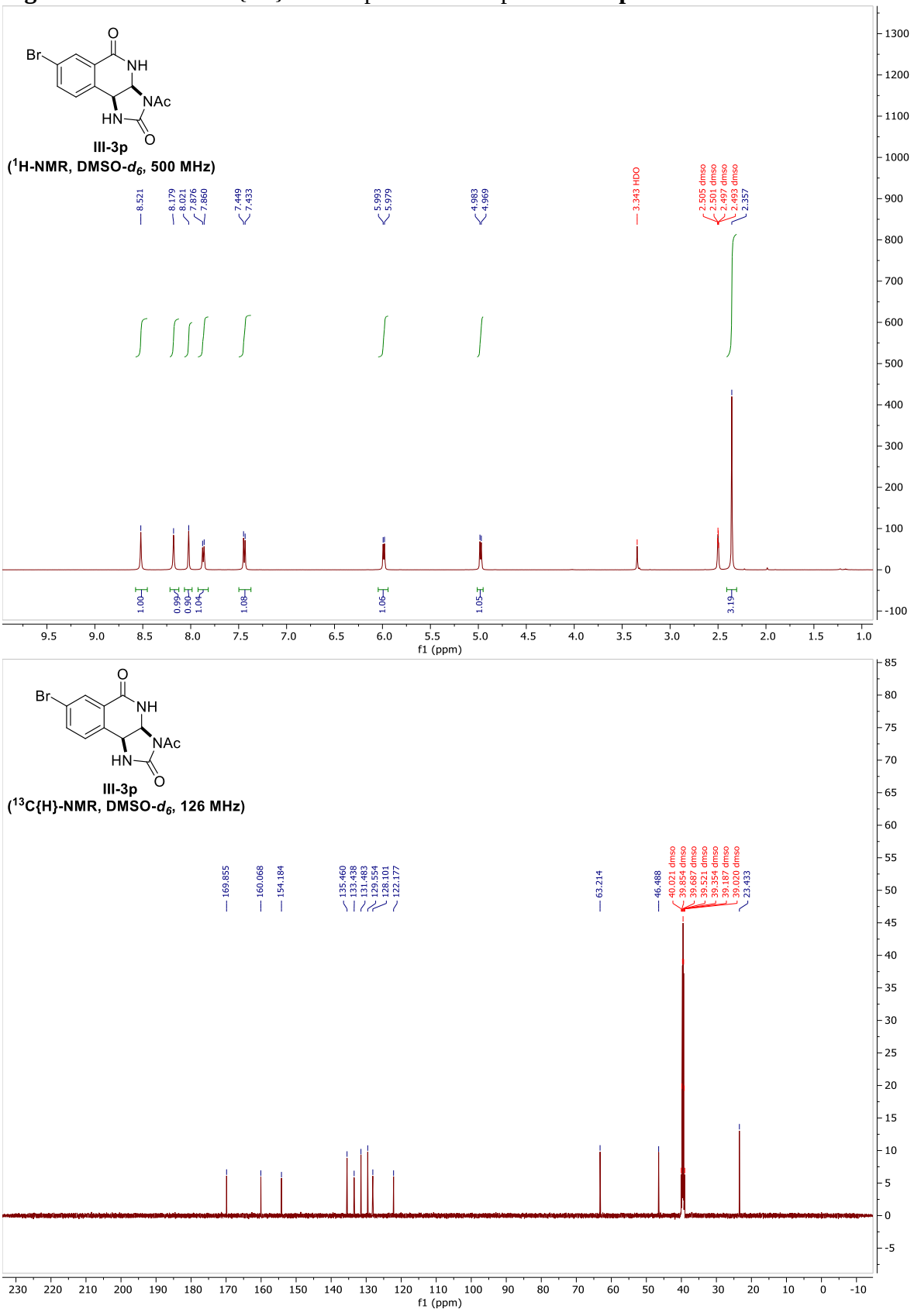

Figure 3.41 ^{1}H and $^{13}C\{^{1}H\}$ NMR spectra of compound **III-3q**

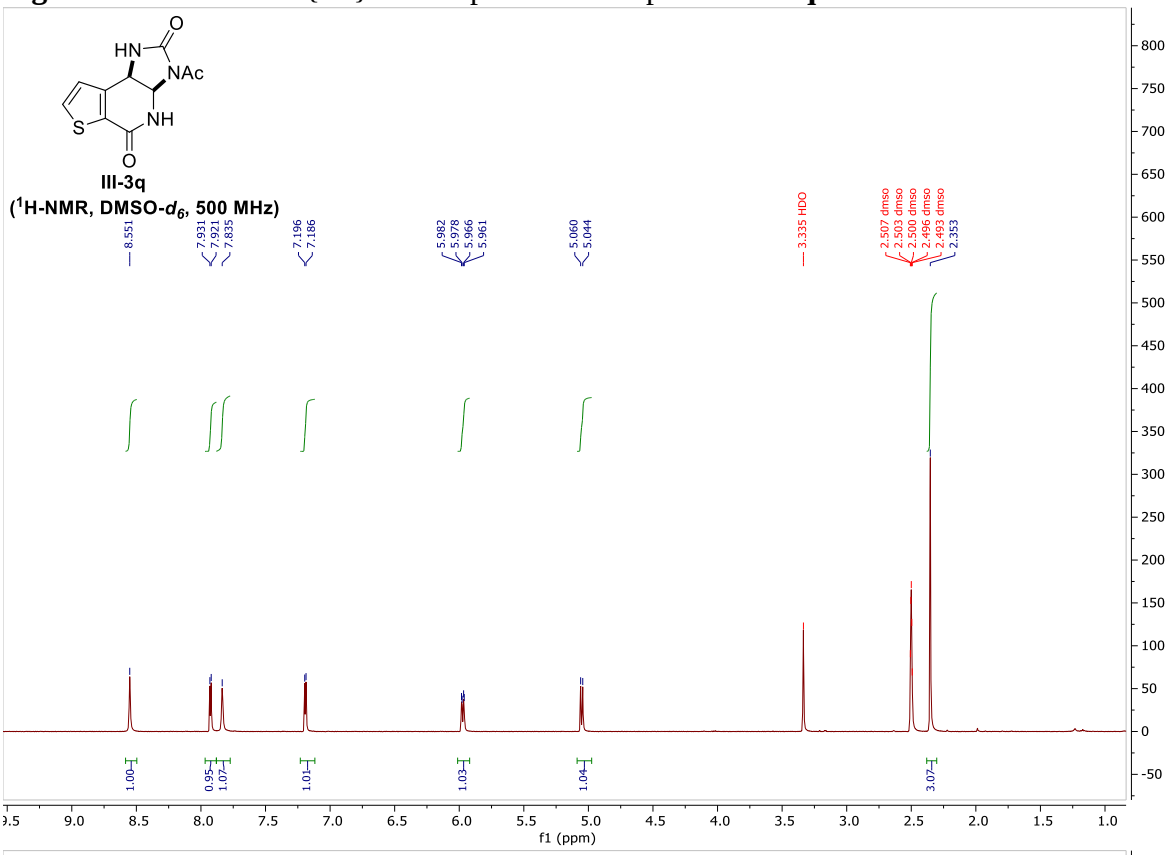

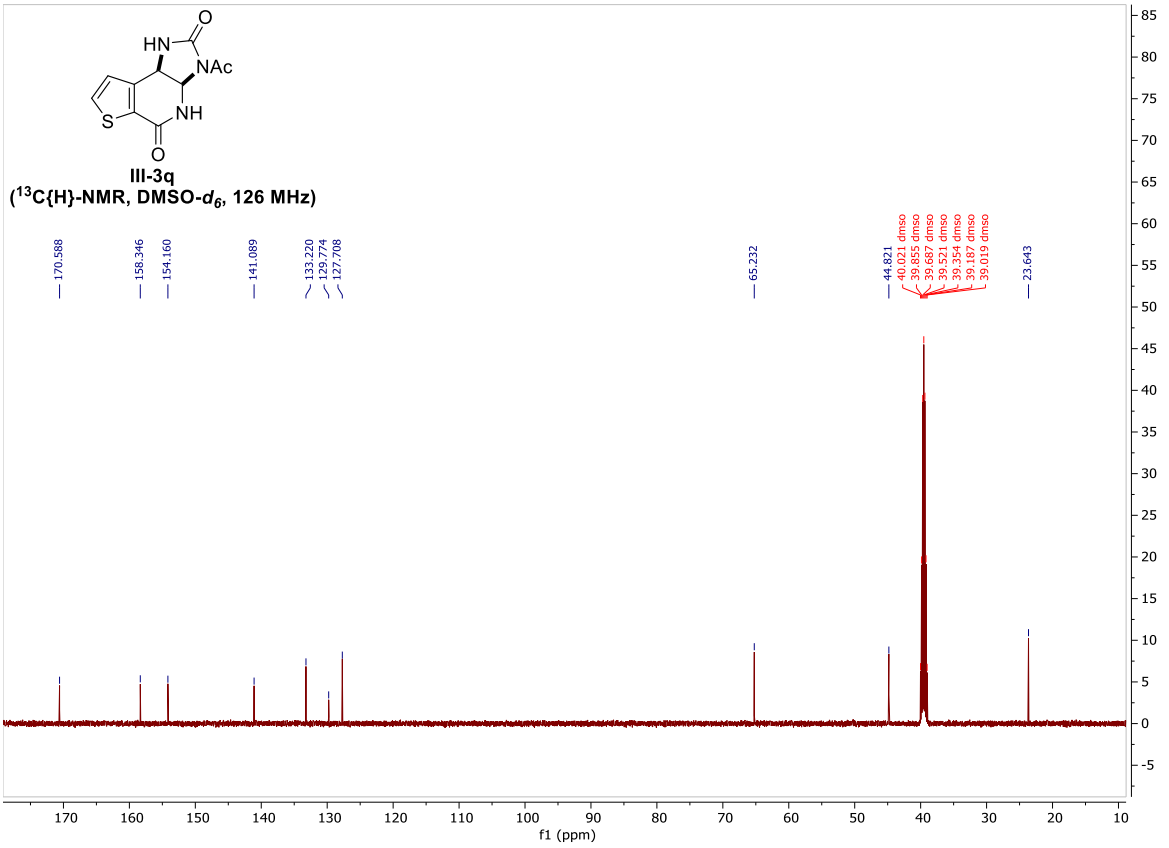

Figure 3.42 ^{1}H and $^{13}C\{^{1}H\}$ NMR spectra of compound **III-3r**

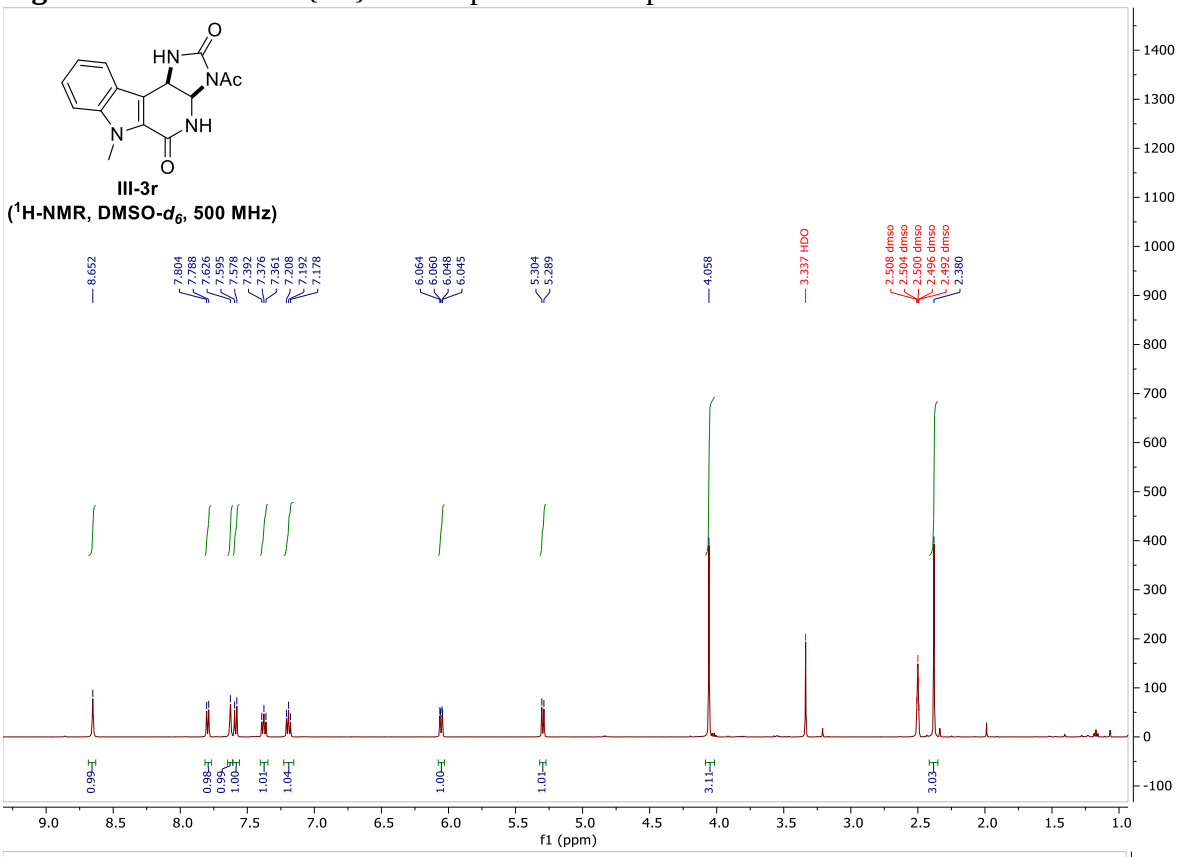

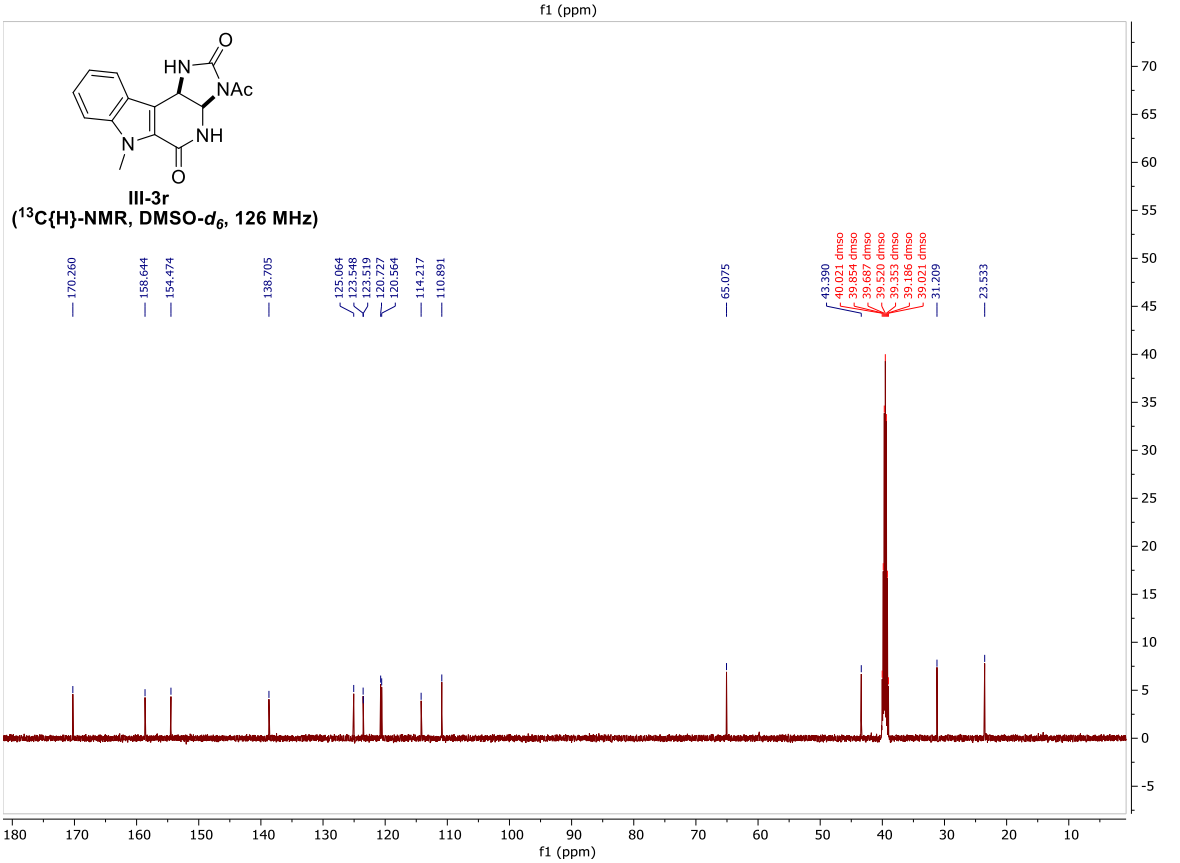

Figure 3.43 ^{1}H and $^{13}C\{^{1}H\}$ NMR spectra of compound **III-5**

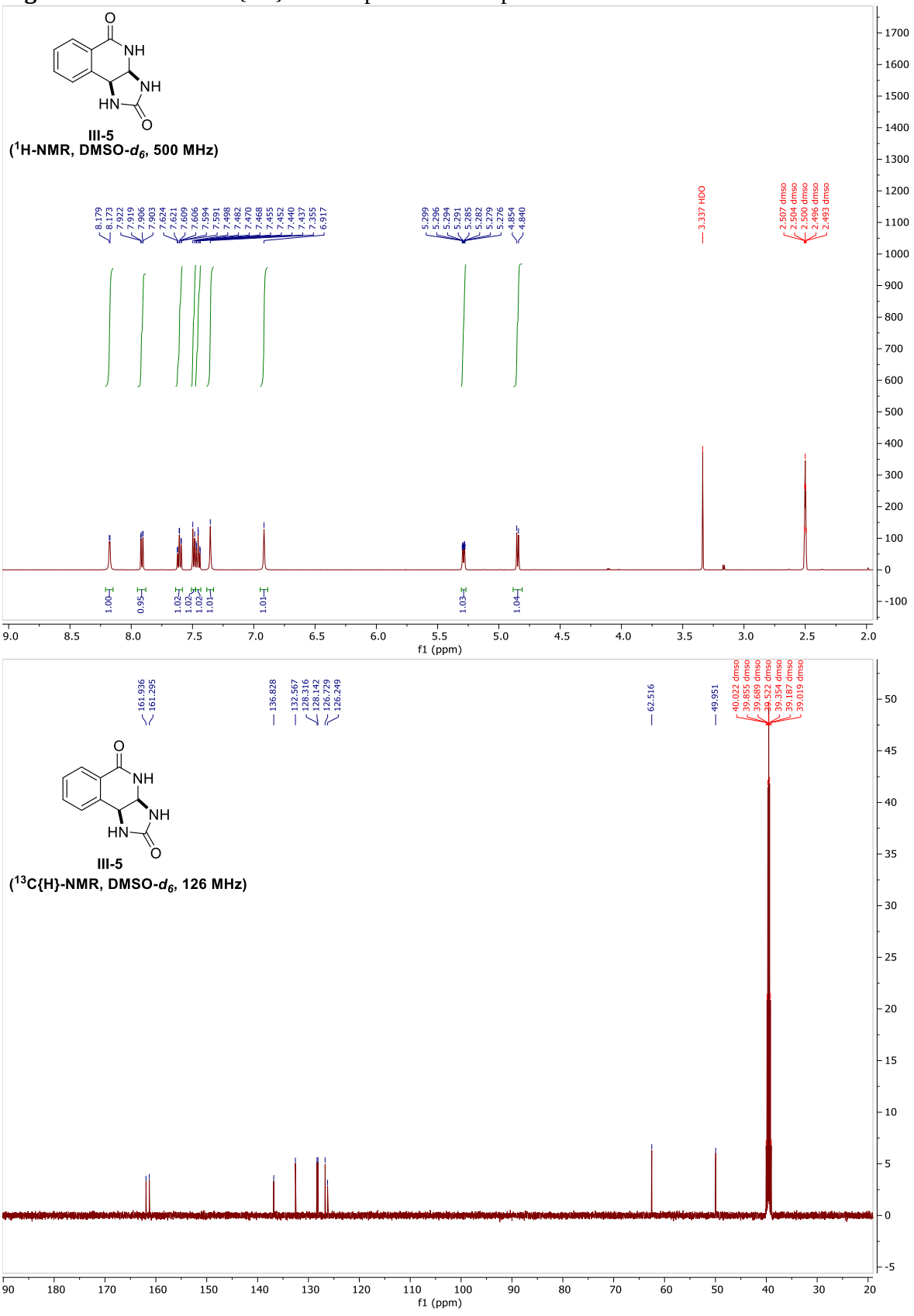

Crystallographic Analysis and Experimental

Hydrogen atoms on the Nitrogen atoms were found and refine isotropically.

X-ray crystallographic analysis was performed by Dr. Richard Staples.

Figure 3.44 X-ray crystal structure of the monoacylated annulation product **III-3a**, thermal ellipsoid shown with 50% probability

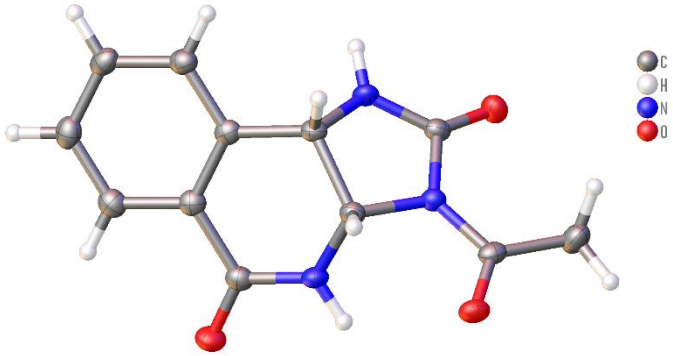

Experimental. Single colourless irregular-shaped crystals of **JJT222A** were recrystallized from methanol by method of slow evaporation over the period of a week. A suitable crystal with dimensions 0.33 × 0.10 × 0.05 mm^3 was selected and mounted on a nylon loop with paratone oil on a XtaLAB Synergy, Dualflex, HyPix diffractometer. The crystal was kept at a steady T = 100.00(10) K during data collection. The structure was solved with the **ShelXT** (Sheldrick, 2015) solution program using dual methods and by using **Olex2** 1.5 (Dolomanov et al., 2009) as the graphical interface. The model was refined with **ShelXL** 2018/3 (Sheldrick, 2015) using full matrix least squares minimization on $\boldsymbol{F^2}$.

Crystal Data. $C_{12}H_{11}N_3O_3$, M_r = 245.24, monoclinic, $P2_1/c$ (No. 14), a = 7.14244(8) Å, b = 8.20227(11) Å, c = 18.7428(2) Å, b = 98.2515(11)°, a = g = 90°, V = 1086.66(2) $Å^3$, T = 100.00(10) K, Z = 4, Z' = 1, m(Cu K_a) = 0.927, 12391 reflections measured, 2187 unique (R_{int} = 0.0335) which were used in all calculations. The final wR_2 was 0.0922 (all data) and R_1 was 0.0338 (I≥2 s(I)).

Table 3.6 Crystal Data

Compound	**JJT222A**
Formula	$C_{12}H_{11}N_3O_3$
CCDC	2151168
$D_{calc.}$/ g cm^{-3}	1.499
m/mm^{-1}	0.927
Formula Weight	245.24
Color	colourless
Shape	irregular-shaped
Size/mm^3	0.33×0.10×0.05
T/K	100.00(10)
Crystal System	monoclinic
Space Group	$P2_1/c$
a/Å	7.14244(8)
b/Å	8.20227(11)
c/Å	18.7428(2)
a/°	90
b/°	98.2515(11)
g/°	90
V/Å^3	1086.66(2)
Z	4
Z'	1
Wavelength/Å	1.54184
Radiation type	Cu K$_a$
Q_{min}/°	4.768

Table 3.6 (cont'd)

$Q_{max}/^{\circ}$	76.930
Measured Refl's.	12391
Indep't Refl's	2187
Refl's I≥2 *s*(I)	2018
R_{int}	0.0335
Parameters	172
Restraints	0
Largest Peak	0.272
Deepest Hole	-0.222
GooF	1.063
wR_2 (all data)	0.0922
wR_2	0.0902
R_1 (all data)	0.0360
R_1	0.0338

Structure Quality Indicators

Reflections: d min (Cu\a) 2Θ=154.4° 0.79 | I/σ(I) 43.6 | Rint 3.35% | Full 135.4° 95% to 154.4° 100

Refinement: Shift 0.000 | Max Peak 0.3 | Min Peak -0.2 | GooF 1.063

A colourless irregular-shaped-shaped crystal with dimensions 0.33×0.10×0.05 mm^3 was mounted on a nylon loop with paratone oil. Data were collected using a XtaLAB Synergy, Dualflex, HyPix diffractometer equipped with an Oxford Cryosystems low-temperature device, operating at T = 100.00(10) K.

MSU Data were measured using *w* scans using Cu K_a radiation (micro-focus sealed X-ray tube, 50 kV, 1 mA). The total number of runs and images was based on the strategy calculation from the program CrysAlisPro 1.171.41.123a (Rigaku OD, 2022). The achieved resolution was Q =

76.930.

Cell parameters were retrieved using the CrysAlisPro 1.171.41.123a (Rigaku OD, 2022) software and refined using CrysAlisPro 1.171.41.123a (Rigaku OD, 2022) on 7653 reflections, 62 % of the observed reflections. Data reduction was performed using the CrysAlisPro 1.171.41.123a (Rigaku OD, 2022) software which corrects for Lorentz polarization. The final completeness is 100.00 out to 76.930 in *Q* CrysAlisPro 1.171.41.123a (Rigaku Oxford Diffraction, 2022) Numerical absorption correction based on gaussian integration over a multifaceted crystal model Empirical absorption correction using spherical harmonics, implemented in SCALE3 ABSPACK scaling algorithm.

The structure was solved in the space group $P2_1/c$ (# 14) by using dual methods using the ShelXT (Sheldrick, 2015) structure solution program. The structure was refined by Least Squares ShelXL incorporated in Olex2 software program. All non-hydrogen atoms were refined anisotropically. Hydrogen atom positions were calculated geometrically and refined using the riding model, except for the hydrogen atom on the non-carbon atom(s) which were found by difference Fourier methods and refined isotropically when data permits.

CCDC 2151168 contains the supplementary crystallographic data for this paper. The data can be obtained free of charge from The Cambridge Crystallographic Data Centre via www.ccdc.cam.ac.uk/structures.

There is a single molecule in the asymmetric unit, which is represented by the reported sum formula. In other words: Z is 4 and Z' is 1.

Figure 3.45 The following hydrogen bonding interactions with a maximum D-D distance of 3.1 Å and a minimum angle of 110 ° are present in **JJT222A**: N2–O3_*1: 2.816 Å*, *N3–O1*_2: 2.995 Å, N3–O3: 3.014 Å., thermal ellipsoids shown with 50% probability

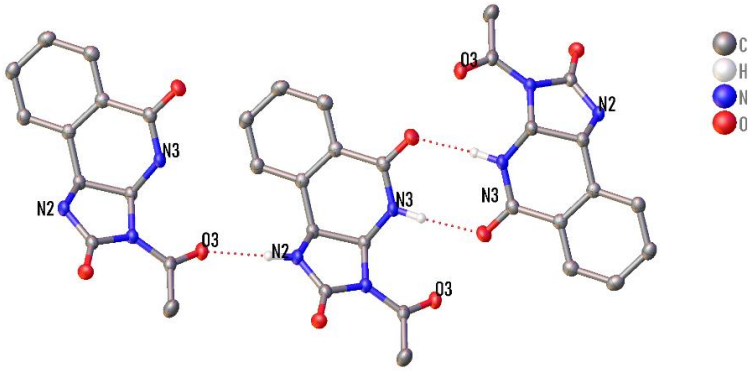

Figure 3.46 Packing diagram of JJT222A, thermal ellipsoids shown with 50% probability

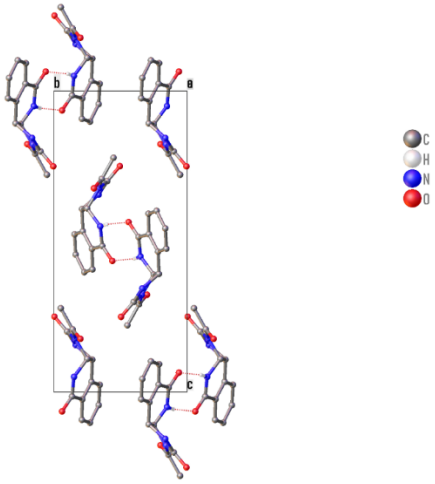

Figure 3.47 Diffraction Data

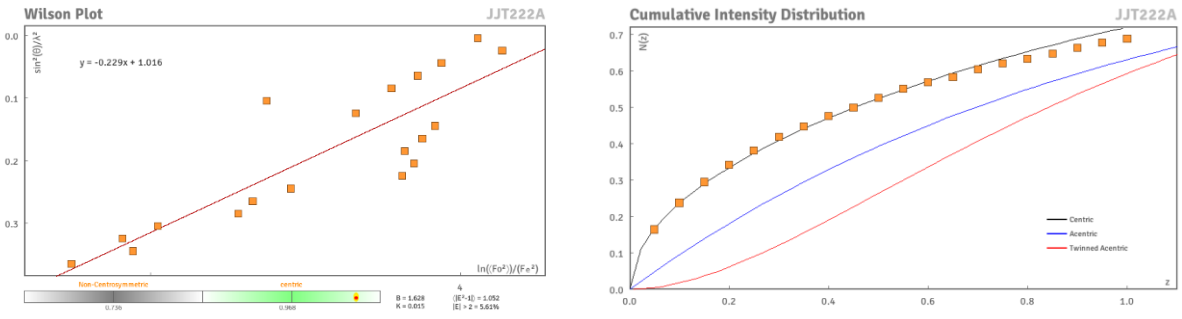

Figure 3.47 (cont'd)

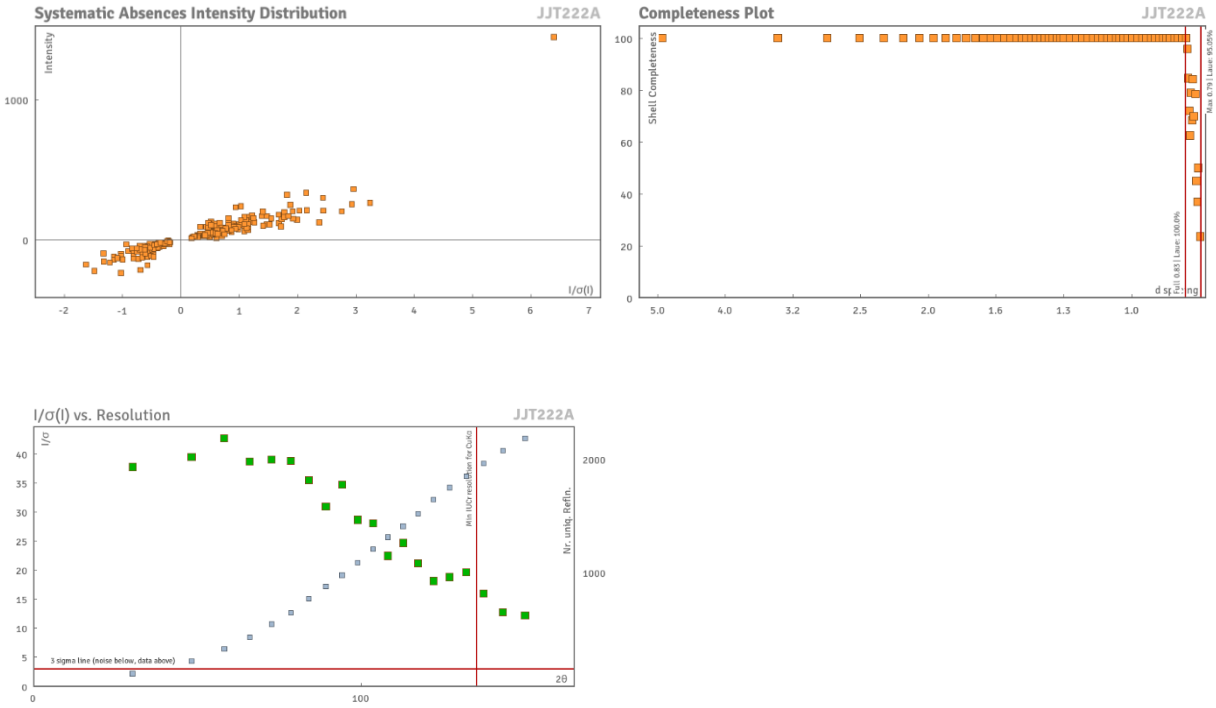

Figure 3.48 Refinement and Data

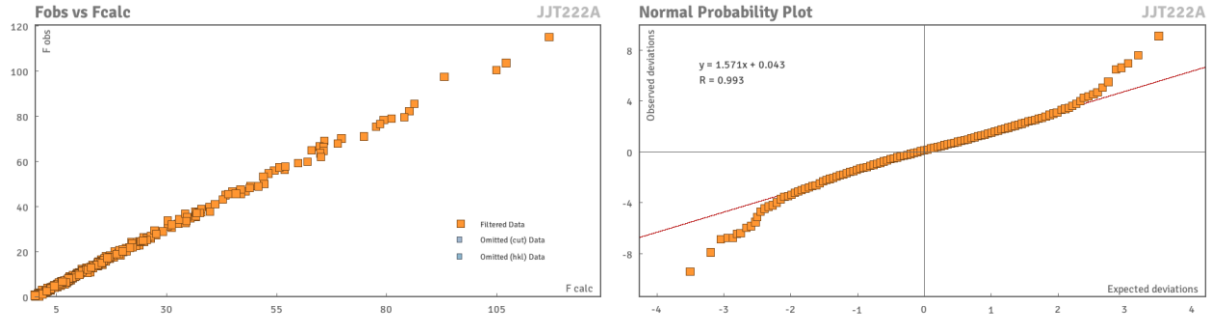

Table 3.7 Fractional Atomic Coordinates ($\times 10^4$) and Equivalent Isotropic Displacement Parameters ($Å^2 \times 10^3$) for **JJT222A**. U_{eq} is defined as 1/3 of the trace of the orthogonalised U_{ij}

Atom	x	y	z	U_{eq}
O1	3518.6(12)	5611.1(11)	5645.0(5)	26.3(2)
O2	-123.5(11)	5043.2(12)	2496.8(4)	25.3(2)
O3	5259.2(11)	6992.1(11)	3232.3(5)	23.7(2)
N1	2174.9(13)	6592.0(12)	3225.2(5)	18.7(2)
N2	-778.3(13)	6635.7(13)	3440.7(5)	20.8(2)
N3	3144.1(14)	6513.2(12)	4496.8(5)	20.8(2)
C1	2254.3(15)	7503.3(14)	3899.1(6)	18.6(2)
C2	158.7(15)	7879.4(14)	3922.7(6)	18.8(2)
C3	-439.1(16)	7823.2(14)	4661.3(6)	19.0(2)
C4	-2197.3(16)	8442.0(14)	4760.6(7)	22.5(3)
C5	-2792.9(17)	8363.7(15)	5434.3(7)	24.4(3)
C6	-1607.2(18)	7714.0(15)	6018.7(7)	25.7(3)
C7	149.9(17)	7104.0(15)	5924.3(7)	23.3(3)
C8	728.6(16)	7134.7(14)	5243.1(6)	19.6(2)
C9	2571.9(16)	6363.1(14)	5149.2(6)	20.2(2)
C10	320.4(15)	5991.2(14)	2991.6(6)	19.4(2)
C11	3793.7(16)	6403.5(14)	2917.6(6)	20.3(3)
C12	3706.7(18)	5519.6(18)	2217.1(7)	31.0(3)

Table 3.8 Anisotropic Displacement Parameters ($\times 10^4$) for **JJT222A**. The anisotropic displacement factor exponent takes the form: $-2p^2[h^2a^{*2} \times U_{11} + ... + 2hka^* \times b^* \times U_{12}]$

Atom	U_{11}	U_{22}	U_{33}	U_{23}	U_{13}	U_{12}
O1	23.8(4)	29.5(5)	24.6(4)	5.8(4)	0.1(3)	5.2(3)
O2	21.7(4)	31.3(5)	22.2(4)	-6.0(3)	1.3(3)	-4.2(3)
O3	14.9(4)	26.9(5)	28.8(4)	2.0(3)	1.5(3)	-0.3(3)
N1	15.4(5)	20.5(5)	19.7(5)	-1.4(4)	0.6(4)	0.0(3)
N2	12.6(5)	27.2(5)	21.8(5)	-3.1(4)	0.3(4)	-1.1(4)
N3	15.1(5)	24.7(5)	22.0(5)	0.8(4)	0.4(4)	3.9(4)
C1	16.4(5)	19.0(5)	19.7(5)	-0.9(4)	0.3(4)	-0.4(4)
C2	16.5(5)	17.7(6)	21.3(5)	-0.2(4)	-0.2(4)	0.9(4)
C3	18.3(5)	15.5(5)	22.9(6)	-2.8(4)	2.0(4)	-2.1(4)
C4	20.2(6)	21.2(6)	25.3(6)	-3.8(5)	0.2(4)	0.5(4)
C5	20.1(6)	23.2(6)	30.4(6)	-7.5(5)	5.3(5)	-0.8(4)
C6	29.3(6)	23.6(6)	25.2(6)	-5.4(5)	7.7(5)	-3.9(5)
C7	25.7(6)	19.9(6)	23.6(6)	-1.0(5)	1.4(4)	-2.5(4)
C8	20.0(5)	15.8(5)	22.9(6)	-1.1(4)	1.9(4)	-2.4(4)
C9	18.5(5)	18.5(6)	22.7(6)	-0.3(4)	0.0(4)	-2.0(4)
C10	16.1(5)	21.9(6)	19.5(5)	1.4(4)	0.2(4)	-0.8(4)
C11	16.3(5)	19.9(6)	24.6(6)	3.6(4)	2.7(4)	2.4(4)
C12	22.7(6)	38.5(7)	32.7(7)	-8.9(6)	7.6(5)	1.3(5)

Table 3.9 Bond Lengths in Å for **JJT222A**

Atom	Atom	Length/Å
O1	C9	1.2332(15)
O2	C10	1.2169(15)
O3	C11	1.2245(14)
N1	C1	1.4617(14)
N1	C10	1.4221(14)
N1	C11	1.3728(14)
N2	C2	1.4599(15)
N2	C10	1.3391(15)
N3	C1	1.4540(14)
N3	C9	1.3494(15)
C1	C2	1.5351(15)
C2	C3	1.5067(15)
C3	C4	1.3915(16)
C3	C8	1.3938(16)
C4	C5	1.3905(17)
C5	C6	1.3910(19)
C6	C7	1.3858(18)
C7	C8	1.3975(16)
C8	C9	1.4937(16)
C11	C12	1.4932(17)

Table 3.10 Bond Angles in ° for **JJT222A**

Atom	**Atom**	**Atom**	**Angle/°**
C10	N1	C1	111.23(9)
C11	N1	C1	119.33(9)
C11	N1	C10	129.43(10)
C10	N2	C2	114.01(9)
C9	N3	C1	126.40(10)
N1	C1	C2	102.16(8)
N3	C1	N1	109.79(9)
N3	C1	C2	114.22(9)
N2	C2	C1	101.77(9)
N2	C2	C3	112.46(9)
C3	C2	C1	115.24(9)
C4	C3	C2	119.47(10)
C4	C3	C8	119.56(11)
C8	C3	C2	120.96(10)
C5	C4	C3	120.28(11)
C4	C5	C6	120.12(11)
C7	C6	C5	119.86(11)
C6	C7	C8	120.15(11)
C3	C8	C7	119.99(11)
C3	C8	C9	121.21(10)
C7	C8	C9	118.76(10)

Table 3.10 (cont'd)

O1	C9	N3	121.59(11)
O1	C9	C8	121.36(11)
N3	C9	C8	117.05(10)
O2	C10	N1	125.83(10)
O2	C10	N2	128.25(10)
N2	C10	N1	105.88(10)
O3	C11	N1	117.81(11)
O3	C11	C12	122.67(10)
N1	C11	C12	119.51(10)

Table 3.11 Torsion Angles in ° for **JJT222A**

Atom	**Atom**	**Atom**	**Atom**	**Angle/°**
N1	C1	C2	N2	21.15(11)
N1	C1	C2	C3	143.13(9)
N2	C2	C3	C4	-76.15(13)
N2	C2	C3	C8	102.70(12)
N3	C1	C2	N2	-97.32(11)
N3	C1	C2	C3	24.66(14)
C1	N1	C10	O2	-171.19(11)
C1	N1	C10	N2	6.68(13)
C1	N1	C11	O3	1.22(16)
C1	N1	C11	C12	-178.04(11)

Table 3.11 (cont'd)

C1	N3	C9	O1	-173.23(11)
C1	N3	C9	C8	7.37(17)
C1	C2	C3	C4	167.82(10)
C1	C2	C3	C8	-13.33(15)
C2	N2	C10	O2	-173.27(12)
C2	N2	C10	N1	8.93(13)
C2	C3	C4	C5	178.39(10)
C2	C3	C8	C7	179.64(10)
C2	C3	C8	C9	-2.74(16)
C3	C4	C5	C6	2.11(18)
C3	C8	C9	O1	-172.67(11)
C3	C8	C9	N3	6.73(16)
C4	C3	C8	C7	-1.51(17)
C4	C3	C8	C9	176.10(10)
C4	C5	C6	C7	-1.74(18)
C5	C6	C7	C8	-0.25(18)
C6	C7	C8	C3	1.88(17)
C6	C7	C8	C9	-175.79(11)
C7	C8	C9	O1	4.97(17)
C7	C8	C9	N3	-175.63(10)
C8	C3	C4	C5	-0.47(17)
C9	N3	C1	N1	-137.26(11)

Table 3.11 (cont'd)

C9	N3	C1	C2	-23.22(16)
C10	N1	C1	N3	103.57(10)
C10	N1	C1	C2	-17.99(12)
C10	N1	C11	O3	-177.56(11)
C10	N1	C11	C12	3.18(18)
C10	N2	C2	C1	-19.64(12)
C10	N2	C2	C3	-143.52(10)
C11	N1	C1	N3	-75.41(12)
C11	N1	C1	C2	163.02(10)
C11	N1	C10	O2	7.66(19)
C11	N1	C10	N2	-174.47(11)

Table 3.12 Hydrogen Fractional Atomic Coordinates ($\times 10^4$) and Equivalent Isotropic Displacement Parameters ($Å^2 \times 10^3$) for **JJT222A**. U_{eq} is defined as 1/3 of the trace of the orthogonalised U_{ij}

Atom	**x**	**y**	**z**	U_{eq}
H2	-2010(20)	6543(19)	3365(8)	29(4)
H3	4220(30)	6040(20)	4431(9)	36(4)
H1	2977.59	8539.36	3870.28	22
H2A	-145.85	8979.29	3706.61	23
H4	-2994.11	8919.84	4366.49	27
H5	-4011.72	8754.63	5495.49	29
H6	-2001.02	7688.46	6481.67	31
H7	962.81	6663.93	6323.45	28

Table 3.12 (cont'd)

H12A	3262.69	4402.66	2272.91	46
H12B	4969.64	5492.18	2070.81	46
H12C	2830.63	6083.98	1847.9	46

Table 3.13 Hydrogen Bond information for **JJT222A**

D	H	A	d(D-H)/Å	d(H-A)/Å	d(D-A)/Å	D-H-A/deg
N2	H2	O3[1]	0.875(17)	1.964(17)	2.8162(13)	164.1(15)
N3	H3	O1[2]	0.884(18)	2.128(18)	2.9950(13)	166.5(15)
N3	H3	O3	0.884(18)	2.589(16)	3.0135(13)	110.4(13)

[1]-1+x,+y,+z; [2]1-x,1-y,1-z

Citations

CrysAlisPro (Rigaku, V1.171.41.123a, 2022)

O.V. Dolomanov and L.J. Bourhis and R.J. Gildea and J.A.K. Howard and H. Puschmann, Olex2: A complete structure solution, refinement and analysis program, *J. Appl. Cryst.*, (2009), **42**, 339-341.

Sheldrick, G.M., Crystal structure refinement with ShelXL, *Acta Cryst.*, (2015), **C71**, 3-8.

Sheldrick, G.M., ShelXT-Integrated space-group and crystal-structure determination, *Acta Cryst.*, (2015), **A71**, 3-8.

The Rikagu Synergy S Diffractometer was purchased with support from the MRI program by the National Science Foundation under Grant No. 1919565.

Figure 3.49 Thermal ellipsoid plot for annulated product **3a**, shown with 50% probability

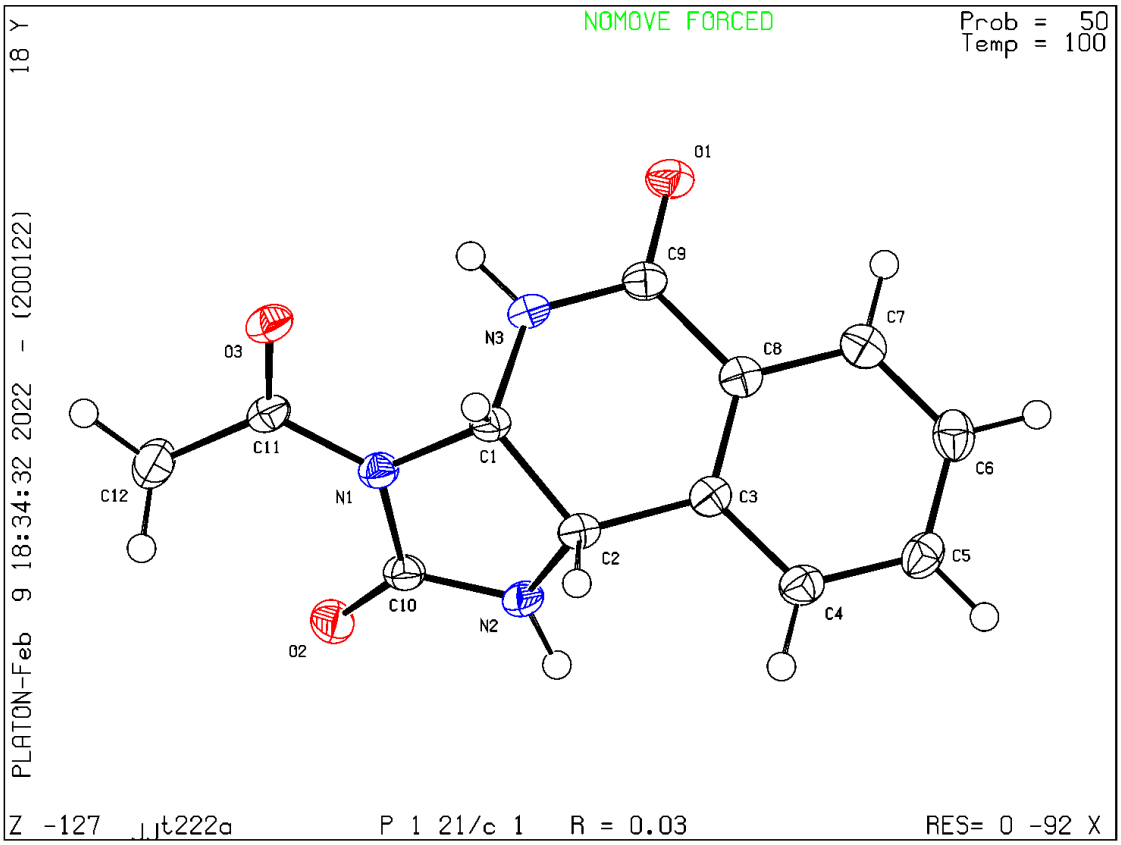

Chapter 4: Efforts towards the total syntheses of pyrrole-alkaloid natural products

4.1 Nagelamide M

4.1.1 Introduction

The genus of marine sponge *Agelas* have been recognized as common source of pyrrole alkaloid natural products as secondary metabolites.[1] Nagelamide M (**Figure 4.1**) was isolated in 2008 by the Kobayashi group from the marine sponge *Agelas sp.* (SS-1134) off the coast of Okinawa, Japan.[2] Nagelamide M (**IV-1**) belongs to a rare family of pyrrole-alkaloid products which contain a taurine moiety.[1] The product demonstrated antimicrobial activity when tested against *Aspergillus niger* (MIC, 33.3 μg/mL) in initial studies, however no further biological activity has since been reported.

Figure 4.1 nagelamide M

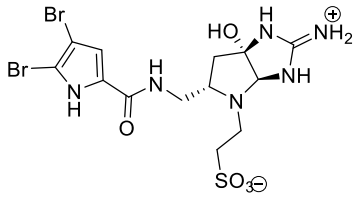

nagelamide M

Similarly to many natural products of the pyrrole-alkaloid family, nagelamide M consists of a dibromopyrrole-carboxamide moiety which is connected to a diversified imidazole core. Nagelamide M is unique among the pyrrole-alkaloid natural products, as it contains a 2-aminooctahydropyrrolo[2,3-*d*]imidazole ring which has not been reported in other isolated natural products from this family. Access to this specific core represents a synthetic challenge which would we sought to endeavor.

The motivation of accessing the 2-aminooctahydropyrrolo[2,3-*d*]imidazole was also due to our desire to further explore the pyrrole alkaloids as potential proteasome inhibitors: a structural

overlay of the core with the S3 subpocket of the ChT-L site of the proteasome revealed that this bicycle may not only potentially interact in a similar fashion to the previous indolophakellstatin inhibitors, but also undergo an additional hydrogen-bonding interaction with its hydroxyl group. Thus, embarking on the first total synthesis of nagelamide M would be not only of synthetic significance, but also biological significance to our group. The results of these efforts are described in Chapter 4-Part 1 of this dissertation.

Figure 4.2 *In silico* structural overlay of nagelamide M core in S3 subpocket of ChT-L site

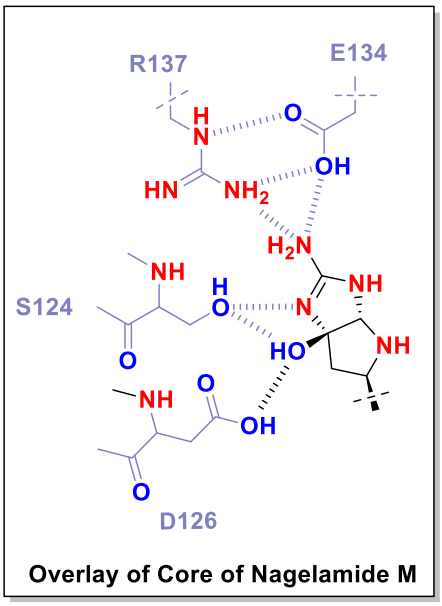

4.1.2 Results & Discussion

When considering potential approaches to the first total synthesis of nagelamide M, specific attention towards the synthesis of the 2-aminooctahydropyrrolo[2,3-*d*]imidazole scaffold must be paid. In the literature, similar scaffolds can be found in the structures of oroidin alkaloids such as axinellamine A, axinellamine B, nagelamide O, and dibromoagelaspongin (**Figure 4.3**).

Figure 4.3 Natural product scaffolds with similar [5.5] or [5.6] fused cores

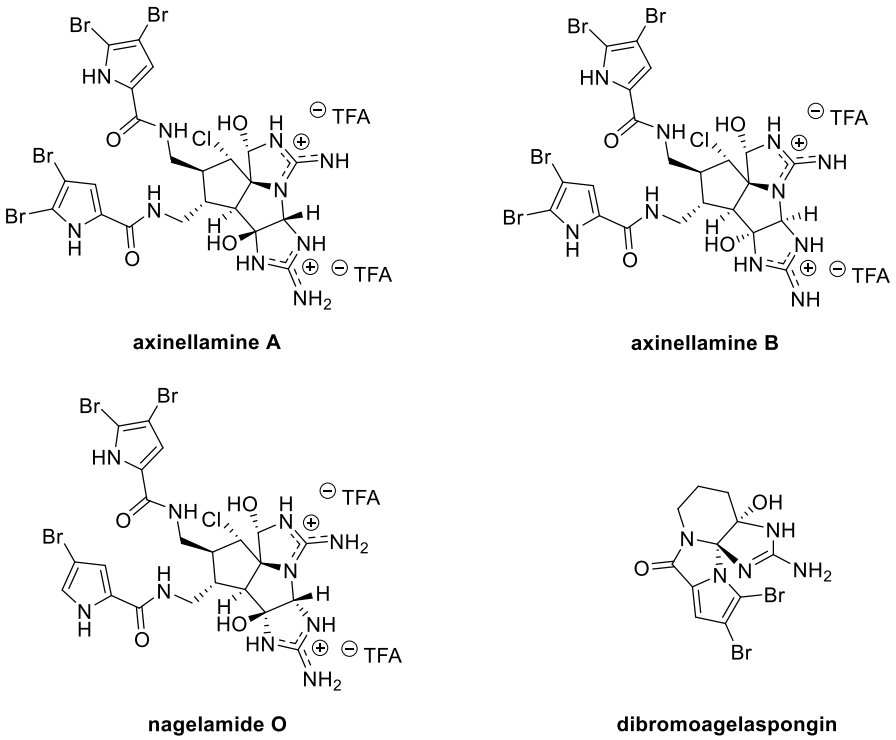

Formation of this scaffold has been approached most often from alteration of the 2-aminoimidazole structure via intramolecular oxidative cyclization pathway. The general mechanism of the oxidative approach is provided in **Scheme 4.1** below. In these approaches, a suitable oxidant is used to first oxidize the 2-aminoimidazole moiety and generate a reactive intermediate. This intermediate is subsequently attacked nucleophilically by an intramolecular nucleophile to access the desired cyclized product.

Scheme 4.1 General mechanism of oxidative cyclization upon 2-aminoimidazole

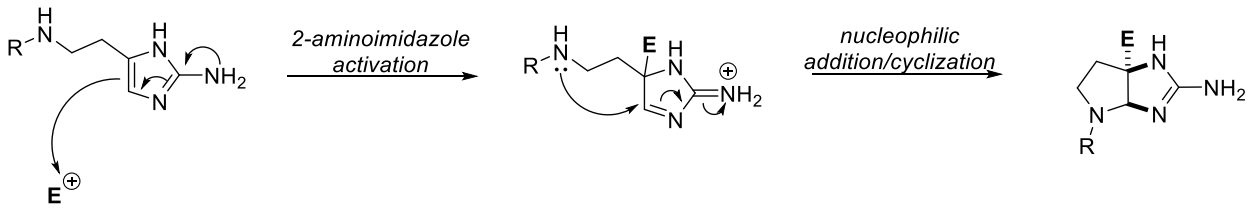

Specific examples of oxidative approaches from literature are detailed in **Scheme 4.2**. The Feldman group has investigated Pummerer-mediated oxidative cyclization to contribute to the synthesis of (±)-dibromoagelaspongin.[3] *N*-chlorosuccinimide was utilized to activate the aminoimidazole towards nucleophilic attack and construct the [5.6] fused core. The desired hydroxyl group was installed through five additional steps. Direct access to the hydroxylated [5.6]-core of (±)-dibromoagelaspongin was reported by the Al-Mourabit group using a dimethyl dioxirane-mediated oxidative cyclization in their biomimetically inspired synthesis of the (±)-dibromoagelaspongin core.[4] In the total synthesis of (±)-axinellamine A and (±)-axinellamine B, the Baran group also utilized the dimethyldioxirane-mediated oxidation of a 2-aminoimidazole to generate a reactive intermediate.[5] Nucleophilic attack upon this intermediate affords the desired ring closure. The Harran group has also utilized oxidation of the 2-aminoimidazole followed by intramolecular nucleophilic capture to afford the desired bicycle in their synthesis of halogen-deficient axinellamines.[6] The group opted to utilize oxaziridine-mediated oxidation with a Davis reagent analog to afford the desired bicycle.

In the case of nagelamide M, a similar oxidative cyclization may be difficult to achieve given the challenging synthesis associated with its necessary precursor. Instead, we sought to construct nagelamide M through an alternative approach which would use readily available starting materials. The initial retrosynthesis of nagelamide M is provided in **Scheme 4.3**. The natural product could be afforded from installation of the taurine moiety upon a 2-aminooctahydropyrrolo[2,3-*d*] imidazole core. In the attempt of generating this scaffold from a simple method which does not come from oxidative cyclization upon the preexisting appended 2-amino-imidazole, the proposed retrosynthetic analysis of nagelamide M may suggest a late-stage cyclization upon a reactive α-keto imine electrophilic intermediate to yield the desired bicycle.

Scheme 4.2 Representative approaches to core via oxidative approaches

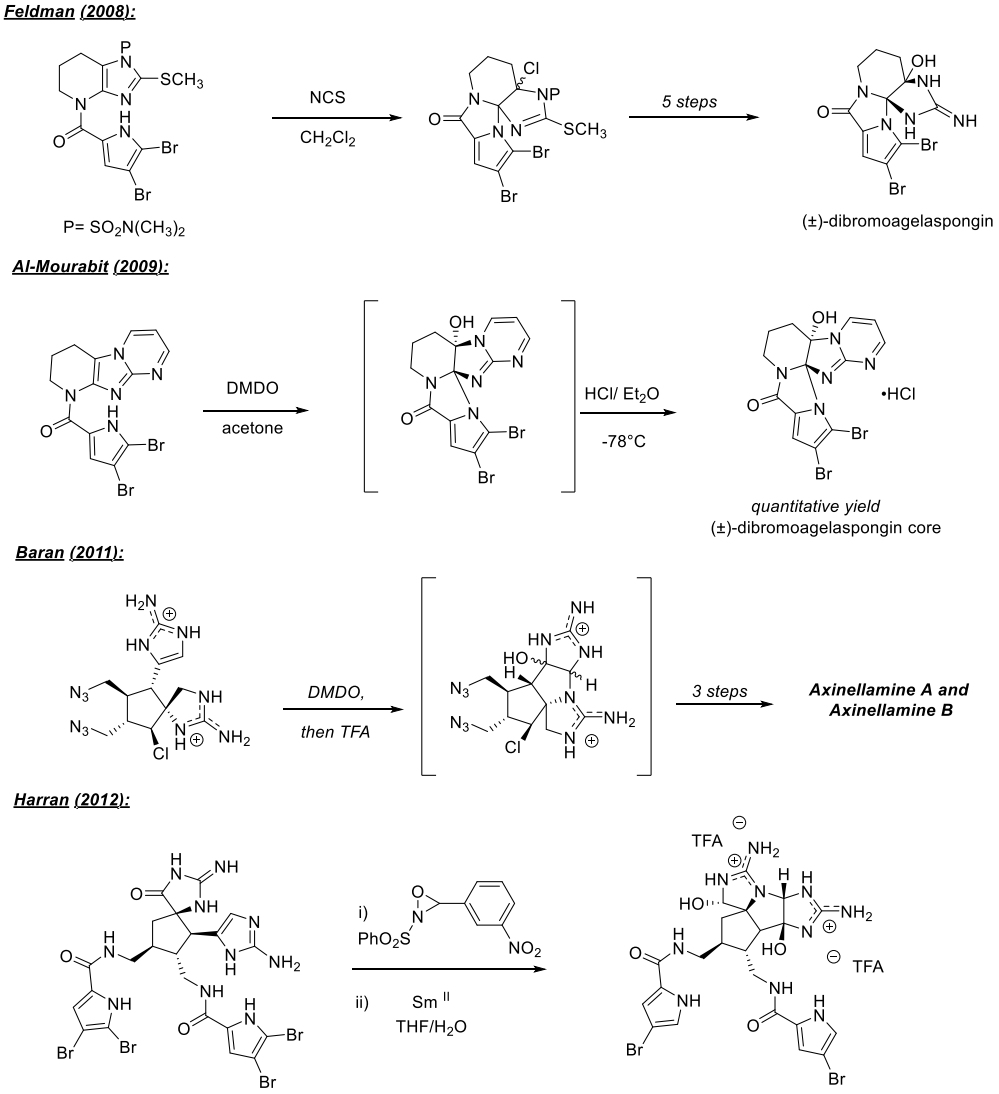

Nucleophilic attack of guanidine upon this intermediate and subsequent cyclization is proposed to afford the desired product, without elimination of the alcohol. The nucleophilic addition of the guanidine was predicted to occur in an *anti*-fashion relative to the pyrrolyl carboxamide substituent to afford the desired diastereomer. Prior to access to the α-ketoimine core, the molecule could be synthesized from two separate fragments: a dibromopyrrole carboxylic acid and pyrrolidine-containing core. Both fragments could be accessed easily from commercially available pyrrole and *trans*-4-hydroxy-*L*-proline.

Scheme 4.3 Initial retrosynthesis of nagelamide M

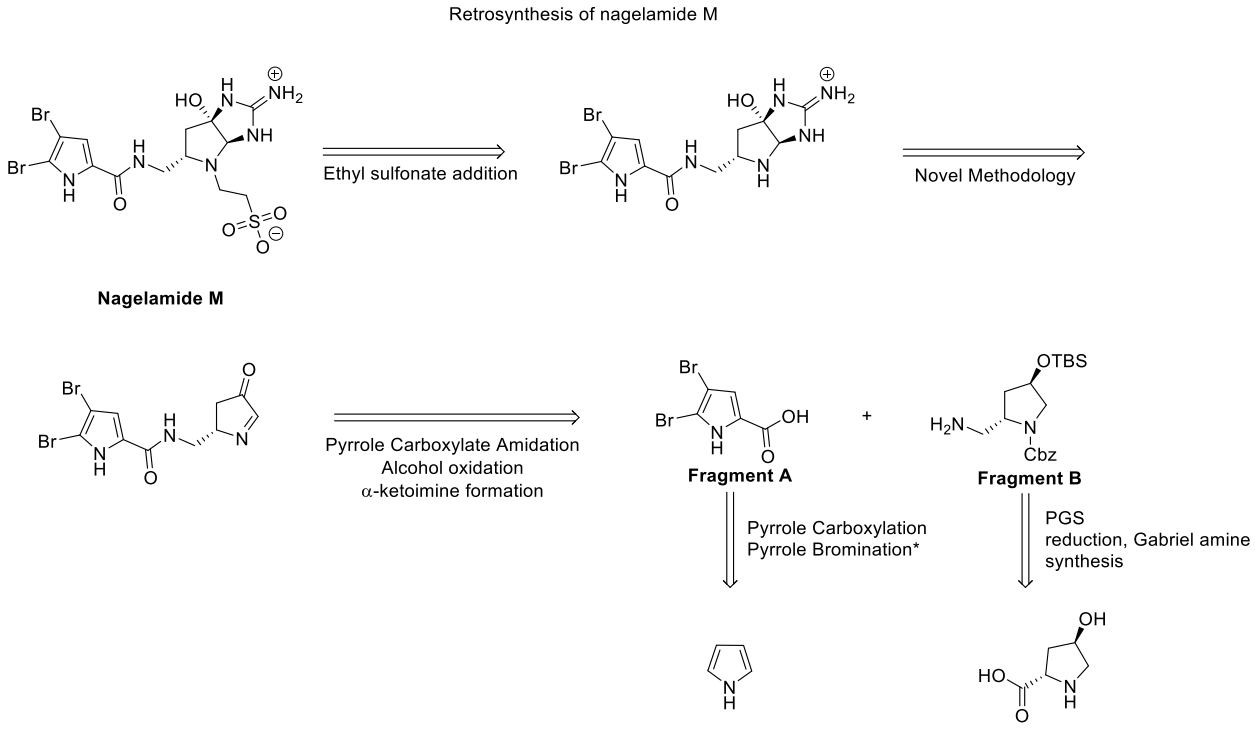

While no exact methodology is known which affords the 2-aminooctahydropyrrolo[2,3-*d*]imidazole core through this type of approach, there is literature precedence which demonstrates the utility of guanidines as nucleophiles towards α-keto electrophiles (**Scheme 4.4**). For example, Kitajima *et al.* reported the synthesis of 2-aminoimidazoles from α-diketones.[7] The use of cyclic α-keto electrophiles have additionally been reported to access more structurally similar [5.5]-fused scaffolds. The Webber group reported specifically that reaction of *N*-acylguanidine with 2-chlorocyclopentanone affords a bicyclic 2-aminooctahydrocyclopento[2,3-d]imidazole core[8] reminiscent of the bicyclic core of nagelamide M.

Scheme 4.4 Literature precedence upon α-keto electrophiles and guanidines

Kitajima (1979): *Synthesis of 2-aminoimidazoles from α-diketones*

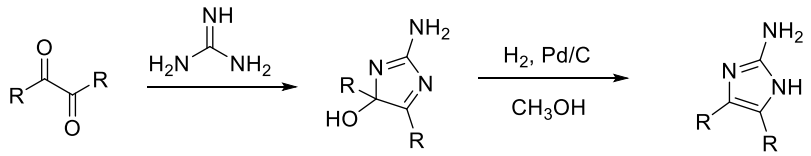

Webber (1994): *Synthesis of 2-aminoimidazoles from α-haloketones*

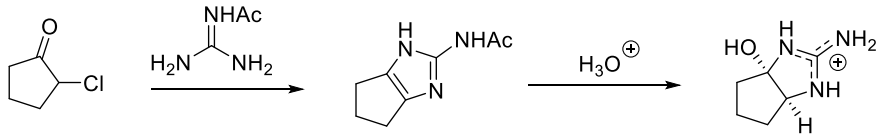

Proposed Synthesis: *Synthesis of tetrahydropyrrolo-imidazolol scaffold from cyclization of α-ketoimine and guanidine*

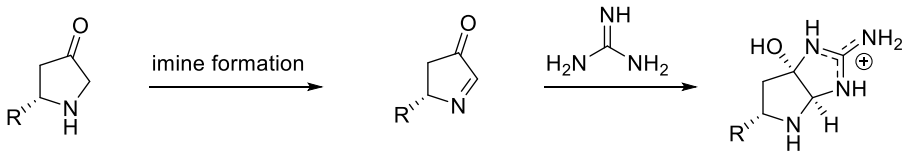

The proposed methodology to access the desired 2-aminooctahydropyrrolo[2,3-*d*]imidazole core is shown in **Scheme 4.4**. With this literature precedence in mind, efforts towards accessing the desired bicyclic core via model systems will be discussed in the following section.

4.1.2.1 Attempts to access [5.5] core using model systems

The first focus of this project was to explore the proposed methodology utilizing simplified model systems. A variety of methods exist to form imines from cyclic amine substrates including oxidative approaches as well as dehydrohalogenation.[9-11] This dehydrohalogenation pathway was first explored utilizing a simplified substrate in 3-pyrrolidinone hydrochloride, as it closely resembles the structure of the 3-pyrrolidinone product from the retrosynthesis of nagelamide M discussed previously.

Utilizing the dehydrohalogenation strategy to investigate formation of the desired alpha-keto imine, *t*-butyl hypochlorite was employed in the presence of several bases including DBU, triethylamine, and Hunig's base (**Table 4.1**). Unfortunately, these reactions did not appear to

afford the desired imine substrate. Instead, rapid formation of an insoluble black tar occurred in most cases following addition of two second equivalents of base. The crude NMR from these reactions did not indicate the formation of an imine, and instead the reaction is proposed to be potentially undergoing overoxidation to afford undesired byproducts in the system such as pyrrole species among other compounds. The reactivity of the α-imino ketone intermediate is credited for the formation of these byproducts. Lack of conclusive evidence regarding the product identity hampered further optimization of this process.

Table 4.1 Attempted dehydrohalogenation of 3-pyrrolidinone

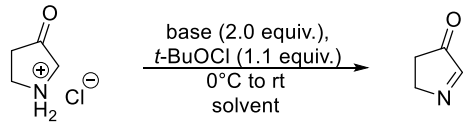

Base: DBU, DIPEA, TEA
Solvent: THF, DCM

Entry	Solvent	Conditions	Result
1	THF	DBU (2.0 equiv), *t*-BuOCl (1.1 equiv)	Failed
2	THF	DIPEA (2.0 equiv), *t*-BuOCl (1.1 equiv)	Failed
3	THF	TEA (2.0 equiv), *t*-BuOCl (1.1 equiv)	Failed
4	DCM	DBU (2.0 equiv), *t*-BuOCl (1.1 equiv)	Failed
5	DCM	DIPEA (2.0 equiv), *t*-BuOCl (1.1 equiv)	Failed
6	DCM	TEA (2.0 equiv), *t*-BuOCl (1.1 equiv)	Failed

At this time, it appeared more advantageous to move onwards to another substrate to investigate an analogous cyclization which may apply to the total synthesis of nagelamide M. The second substrate of interest was derived from the basis of known synthesis of a system which contains a reactive imine due to the presence of an ester at its alpha position. Substrate 2 (**Scheme 4.5**) was proposed as a potential analog for the use in methodology exploration. Ideally, a methodology focused on nucleophilic attack of guanidine or urea upon the imine and subsequent

cyclization upon the methyl ester would afford a novel *N*-spirohydantoin scaffold, which has not been previously reported.

Scheme 4.5 Proposed access to *N*-spirohydantoin through two-step approach

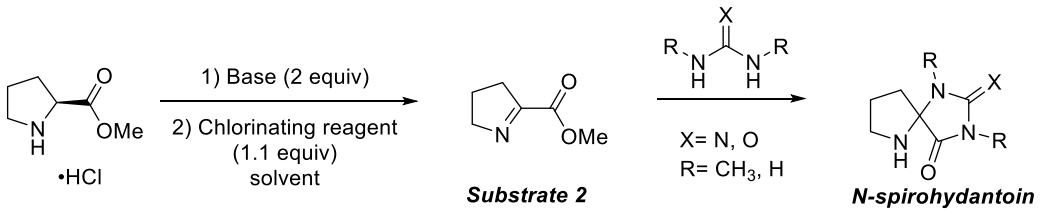

A variety of methods exist for the synthesis of the imino ester scaffold. Starting from L-proline methyl ester hydrochloride, dehydrohalogenation conditions were first explored to afford the desired imine. **Table 4.2** indicates the variety of dehydrohalogenative conditions utilized to afford the desired imine substrate. Imine formation was successful under a variety of conditions. Though this imine has been reported to be isolable, the volatility of the imine proved difficult in its isolation. Attempts to isolate this imine from a variety of solvents using vacuum distillation failed, and so it was decided that the best approach would be *in situ* imine formation of the imine, followed by addition of the desired nucleophile for use in cyclization.

Table 4.2 Synthesis of **substrate 2** by dehydrohalogenation

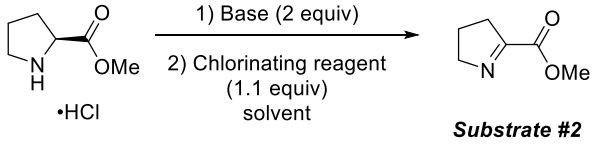

Trial	Solvent	Conditions	Results
1	DCM	TEA (2.3 equiv), NCS (1.1 equiv)	Imine formation successful
2	THF	TEA (2.0 equiv), t-BuOCl (1.1 equiv)	Imine formation successful
3	THF	K_2CO_3 (extraction), t-BuOCl (1.1 equiv), *t*-BuOK (1.0 equiv)	Imine formation successful

To investigate the nucleophilicity of a urea substrate towards the α-iminoester, *N,N'*-dimethylurea was first chosen for use. Because of the relatively poor nucleophilicity of the urea, it was envisioned that generation of a strong nucleophile in a urea anion could be generated via deprotonation from a strong base such as sodium hydride or sodium methoxide (**Table 4.3**). Following generation of this nucleophile, it was introduced into the mixture containing the imine. However, this led to the formation of products which were insoluble in most organic media and were also difficult to characterize. 2D NMR experiments failed to reveal the structure of these compounds.

Upon further reflection, it appears that one potential issue in this experimental setup is the generation of the basic urea anion. Due to this, along with the acidity of the α-proton of the imine, there is strong potential that acid-base chemistry instead led to the formation of the α,β-unsaturated ester and subsequent undesired reactions.

Next, to avoid the use of strong bases, neutral and acidic pathways were considered to facilitate nucleophilic attack and subsequent ring closure. Additionally, guanidine derivatives such as *N*-Boc-guanidine and Cbz-guanidine were employed as nucleophiles. Brønsted acids such as PTSA have been utilized previously to activate imines towards nucleophilic attack.[12] This cyclization under Lewis acidic conditions was also investigated using $BF_3 \cdot OEt_2$.

Table 4.3 Attempts at *N*-spirohydantoin synthesis from **substrate 2**

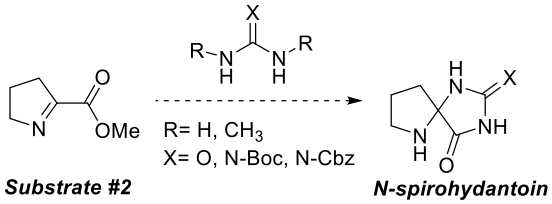

Trial	Conditions	Result
1	N,N'-dimethylurea (1.0 equiv), NaH (2.0 equiv)	Product formation unsuccessful
2	N,N'-dimethylurea (1.0 equiv), NaOMe (2.0 equiv)	Product formation unsuccessful
3	Boc-guanidine (1.0 equiv)	Product formation unsuccessful
4	Boc-guanidine (1.0 equiv), PTSA (1.0 equiv)	Product formation unsuccessful
5	Boc-guanidine (1.0 equiv), $BF_3{\cdot}OEt_2$ (1.0 equiv)	Product formation unsuccessful
6	Cbz-guanidine (1.0 equiv)	Product formation unsuccessful
7	Cbz-guanidine (1.0 equiv), PTSA (1.0 equiv)	Product formation unsuccessful
8	Cbz-guanidine (1.0 equiv), $BF_3{\cdot}OEt_2$ (1.0 equiv)	Product formation unsuccessful

Following previously established conditions for imine formation, the guanidine derivative was added under either neutral, Brønsted or Lewis acid conditions. Neutral conditions for either guanidine derivative did not yield cyclization products. Additionally, Bronsted acidic conditions did not afford the desired. Finally, Lewis acidic conditions failed to yield the desired cyclization. Neither thin-layer chromatography nor NMR spectroscopy indicated the formation of the desired cyclized product. Analysis of the crude reaction mixture by high-resolution mass spectrometry also indicated that this desired cyclized hydantoin product was not formed. In fact, of the many proposed potential substrates, only the imine was observed by high-resolution mass spectrometry for these reactions.

It appears that one of the greatest complications in this approach lies in the inherent Lewis basicity and Bronsted basicity of the guanidine substrate. In the presence of PTSA, guanidine

derivatives are preferentially protonated instead of the imine substrate, which would hinder nucleophilic attack. Additionally, in the presence of a Lewis acid, guanidine and its derivatives could potentially act as a Lewis base, which would again prevent any reaction between the imine substrate and Lewis acid, as well as prevent desired cyclization.

These early failures at access to the 2-aminooctahydropyrrolo[2,3-*d*]imidazole core highlighted several potential challenges associated with methodology development in this project. First and foremost, the reactivity of the α-iminoketone intermediate was of considerable concern. Future methodology development was planned once the accessible precursor could be obtained from the total synthesis route.

4.1.2.2 Synthesis of Fragment A (IV-4)

The desired pyrrole fragment A was synthesized from pyrrole in three steps (**Scheme 4.6**). Pyrrole was first acylated to afford 2,2,2-trichloroacetylpyrrole **IV-2** in 86% yield. Subsequent dibromination of the pyrrole at the C_4 and C_5 positions using molecular bromine under acidic conditions afforded the previously reported 4,5-dibromo-2,2,2-trichloroacetylpyrrole product **IV-3** in 87%. The desired pyrrole-2-carboxylic **IV-4** was accessed by careful heating of the substrate under dilute basic conditions to produce the carboxylate and subsequent acidification to access the substrate in 78% yield. With **IV-4** in hand, efforts were next turned towards the synthesis of the other fragment in this synthesis.

Scheme 4.6 Synthesis of Fragment A (**IV-4**)

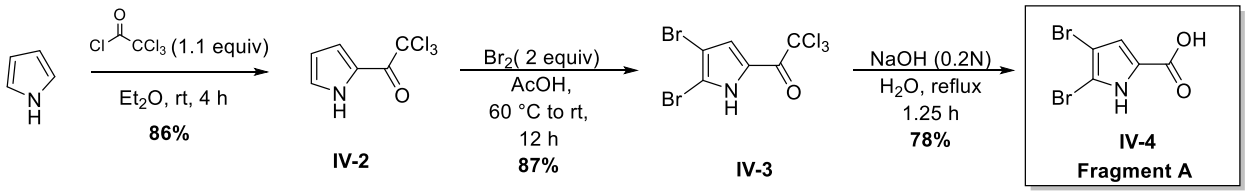

4.1.2.3 Synthesis of Fragment B (IV-12)

The initial synthetic pathway explored to access **Fragment B** was focused on formation of the desired fragment from *trans*-4-hydroxy-L-proline (**Scheme 4.7**). The amine was protected with a benzyloxycarbonyl (Cbz) group under standard conditions to access **IV-5** in 69% yield. Subsequent protection of the secondary alcohol using a silyl ether protecting strategy with the *tert*-butyl dimethyl silyl ether protecting group was next carried out to produce the desired product **IV-6** in 80% yield. The third step in this synthesis involved selective reduction of the carboxylic acid in the presence of the carbamate. This transformation was first attempted with BH_3·THF as the reducing agent but failed under the conditions attempted. Transformation to the desired primary alcohol **IV-7** was successfully achieved using BH_3·SMe_2 in a maximum of 61% yield. However, the transformation proved difficult to reproduce during scale-up conditions. Additionally, subjecting the compounds to prolonged refluxing conditions appeared to cause some loss of the carbamate protecting group and undesired decomposition, and so at this point an alternative pathway to access **IV-7** was explored (**Scheme 4.8**).

Scheme 4.7 Initial synthetic approach towards alcohol **IV-7**

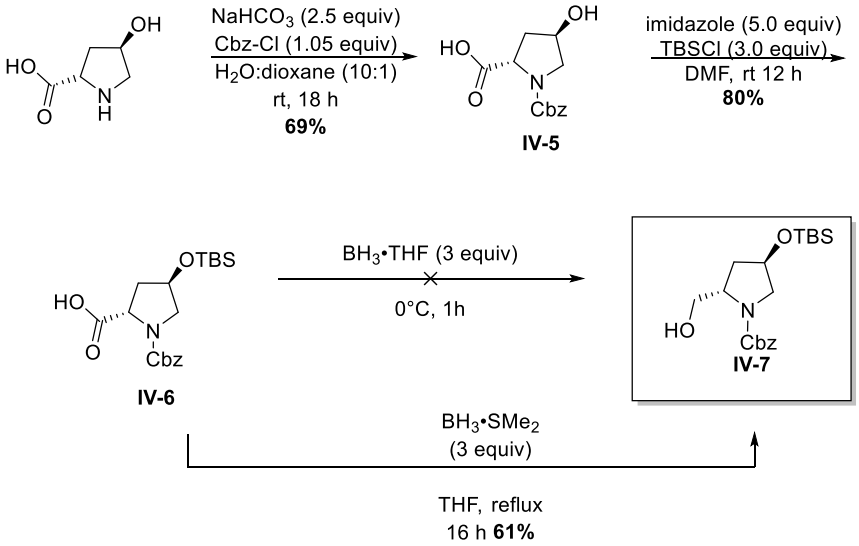

Instead of carrying forward the carboxylic acid, it was envisioned that conversion to an ester may afford more mild conditions for selective reduction. Thus, the first step in the second approach involved the conversion of *trans*-4-hydroxy-*L*-proline to its methyl ester hydrochloride salt **IV-8**. The transformation was achieved in high yield of 88%. Further transformations in this pathway followed the syntheses previously established in the initial approach including amine protection and alcohol protection to access **IV-9** and **IV-10** respectively.

Finally, the key step in the second approach was selective reduction of the methyl ester in the presence of the benzyloxy carbonyl amine protecting group. Two conditions were investigated for this reduction including selective reduction using sodium borohydride in a *tert*-butanol/methanol solvent mixture,[13] and selective reduction using lithium borohydride in THF.[14] Interestingly, although conversion of a similar substrate was reported to afford the desired product in high yield in only 1 hour,[13] the formation of the desired primary alcohol was highly unsuccessful under conditions using sodium borohydride as reductant. Following purification, 33% of **IV-10** was recovered, and only 17% of the desired product **IV-7** was isolated over a 2-hour period. Thankfully, reduction of the methyl ester using lithium borohydride afforded the desired primary alcohol in high yield (89%) under mild conditions.

Scheme 4.8 Second synthetic approach to access **IV-7**

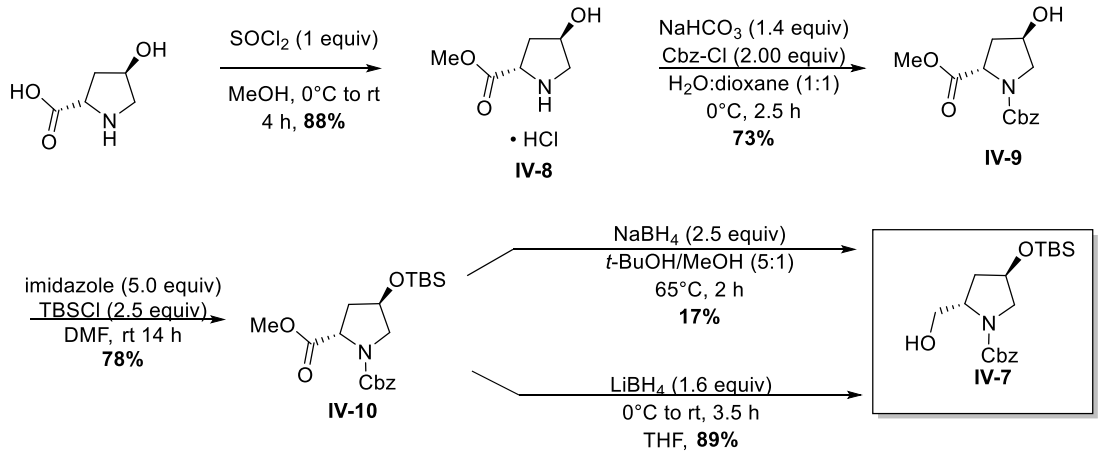

Based upon the comparative success of pathway 2 for the synthesis of **IV-7**, this pathway appears to be the more desirable for total synthesis of nagelamide M. Although it contains an additional step, the yields associated with this pathway are high and the conditions for reduction to yield the primary alcohol appear to be more desirable than in the initial synthetic approach.

With alcohol **IV-7** in hand, the next focus was completing the synthesis of Fragment B (**Scheme 4.9**). Subjecting the primary alcohol to Gabriel amine synthesis under Mitsunobu conditions afforded the desired phthalimide **IV-11** in 90% yield. The desired primary amine **IV-12** was accessible through subsequent phthalimide deprotection in the presence of excess hydrazine hydrate in 72%.

Scheme 4.9 Synthesis of **IV-12** via Gabriel amine synthesis

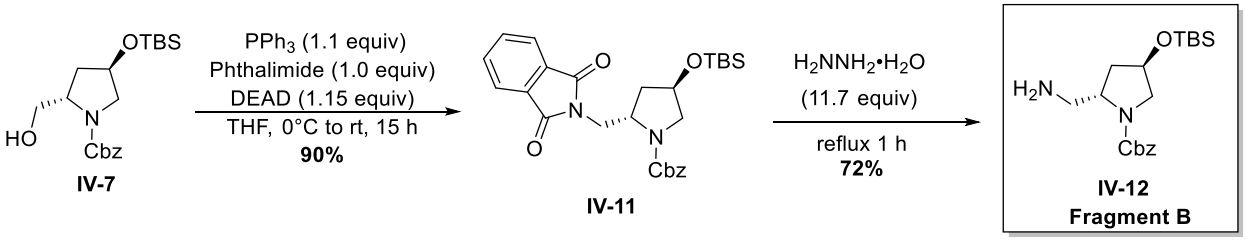

4.1.2.4 Access to pyrrole carboxamide IV-13

Following optimized synthesis of Fragments A and B, synthesis of the pyrrole carboxamide **IV-13** was explored using EDCI coupling conditions (**Table 4.4**). Often under these conditions excess amine nucleophile is used to facilitate amide formation. This approach was not possible however, based largely on the fact that the amine in this total synthesis takes several steps to synthesize. Only one equivalent of the amine was therefore used, and an additional nucleophile was needed to facilitate product formation. Dimethylaminopyridine (DMAP) is often used in EDCI conditions as a catalytic base and intermediate nucleophile to further enable the formation of the desired amide. Under catalytic conditions, the maximum isolated yield of the product was 29%

after 4 hours (**Table 4.4**, Entry 1). Extended reaction time showed little improvement; the yield after 23 hours is slightly depleted to 26% (Entry 2).

In order to facilitate product formation, the equivalents of the DMAP were increased from catalytic to stoichiometric amounts. Entry 3 from Table 4.4 was an encouraging result which suggested that increasing the equivalents of DMAP could potentially solve the problem at hand. Encouraged by these results, the equivalents of DMAP were further increased to 3 equivalents relative to the amine and carboxylic acid starting materials. Following this result, solvent effects were also investigated (Table 2, entries 4 to 7). Maximum yields after 16 hours of reaction time were achieved when THF and CH_2Cl_2 were used (45% and 43%, respectively). The use of more polar solvents like MeCN and DMF did not provide desirable product yields (entries 5 and 7). Allowing the reactions to run for an extended time period improved the yield marginally (entries 8 and 9).

Table 4.4 EDCI coupling attempts to access pyrrole carboxamide **IV-13**

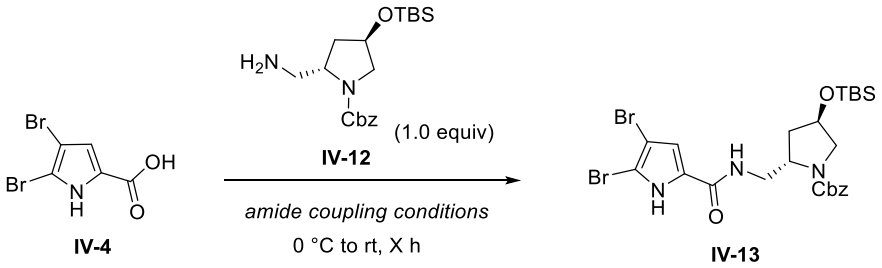

Entry	Reagents	Solvent	Time	Yield (%)
1	EDCI (2.0 equiv), DMAP (25 mol %)	CH_2Cl_2	4 h	29%
2	EDCI (2.0 equiv), DMAP (25 mol %)	CH_2Cl_2	23 h	26%
3	EDCI (1.4 equiv), DMAP (1.4 equiv)	CH_2Cl_2	12 h	42%
4	EDCI (2.0 equiv), DMAP (3.0 equiv)	CH_2Cl_2	16 h	43%
5	EDCI (2.0 equiv), DMAP (3.0 equiv)	MeCN	16 h	12%
6	EDCI (2.0 equiv), DMAP (3.0 equiv)	THF	16 h	45%
7	EDCI (2.0 equiv), DMAP (3.0 equiv)	DMF	16 h	25%
8	EDCI (2.0 equiv), DMAP (3.0 equiv)	THF	24 h	51%
9	EDCI (2.0 equiv), DMAP (3.0 equiv)	CH_2Cl_2	60 h	52%

With no further optimization in sight, a different synthetic approach to the desired pyrrole carboxamide **IV-13** appeared to be necessary. Literature research indicated that a separate route may be possible to access this product. In Horne's total synthesis of oroidin alkaloid natural product dibromophakellstatin, pyrrole carboxamide formation results from the reaction of 4,5-dibromo(2-trichloroacetyl)pyrrole with an amine nucleophile.[15] Thankfully, this pyrrole starting material is part of the synthetic pathway for access to Fragment A and was therefore available in abundance under established conditions. To avoid sacrificing **IV-12**, triethylamine was added to facilitate product formation. Using excess triethylamine (2.1 equiv), the reaction was carried out

in DMF at rt. After stirring for 48 hours, starting material was still visible by thin layer chromatography. An additional 2 equivalents of triethylamine were therefore added to the reaction mixture, and the reaction was run for a total of 96 hours. This first attempt provided a product yield of 74%, with 14% of the 4,5-dibromo(2-trichloroacetyl)-pyrrole recovered following purification. The reaction was repeated, this time using 4.1 equivalents of triethylamine at the outset to provide a maximum product yield of 80% (**Scheme 4.10**).

Scheme 4.10 Successful access to pyrrole carboxamide **IV-13** via **IV-3**

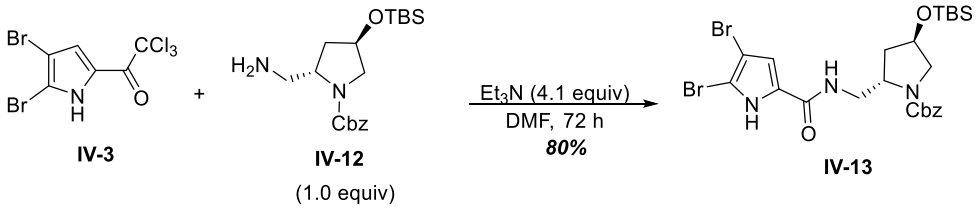

4.1.2.5 Access to ketone IV-15 & attempted Cbz deprotection

After optimization of the synthesis of pyrrole carboxamide **IV-13**, access to the α-ketoimine precursor was desired (**Scheme 4.11**). Alcohol deprotection was achieved under standard conditions to access alcohol **IV-14** in 86% yield. Attempt to access the ketone via Swern oxidation conditions failed. The alcohol starting material is not readily soluble in methylene chloride, especially at such low temperatures. Even after addition of THF as a co-solvent, the solubility of this starting material was negligible at -78 °C. This lack of solubility is believed to be the main contributor to failure under these oxidative conditions. While Swern oxidation failed, the desired ketone **IV-15** was accessible under IBX oxidation in DMSO in 64-67% yield.

Scheme 4.11 Synthesis of α-ketoimine precursor **IV-15**

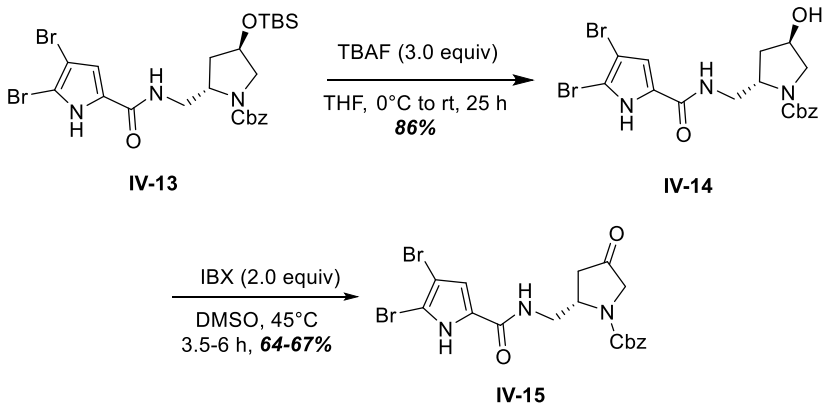

After access to the desired ketone **IV-15** was achieved, the next focus in synthesis became selective deprotection of the carboxybenzoyloxy group to access the free 3-pyrroldinone scaffold. Many attempts were made to deprotect the Cbz group including Pd-catalyzed hydrogenation, Lewis acid mediated deprotection in the presence of dimethyl sulfide, and triflouroacetic acid mediated deprotection under heating conditions (**Scheme 4.12**). These conditions suffered from poor conversion and degradation of the starting material in certain circumstances. The use of hydrogenative conditions towards dibrominated pyrrole alkaloids without effect towards the bromine atoms has previously been reported in literature.[3] While the hydrogenation did eventually facilitate loss of the Cbz group, debromination of the pyrrole ring took place under these conditions which made it an undesirable approach. It became evident that a slight alteration of the route would be necessary moving forward.

Scheme 4.12 Attempted deprotection of the Cbz group

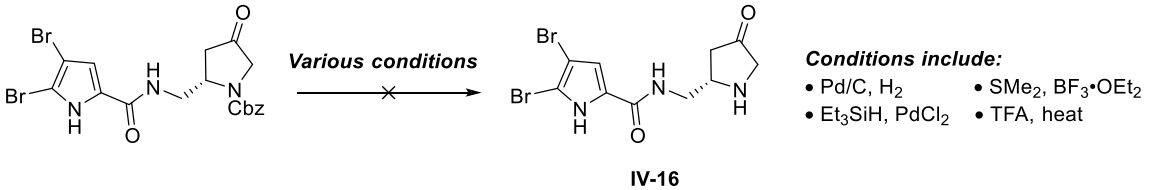

4.1.2.6 Access to the α-ketoimine precursor via Boc-protecting group

With these challenges in mind, the synthesis was slightly altered under the assumption that the use of a Boc-protecting group would allow more facile access to the desired product as an ammonium salt. The synthesis of the Boc-containing scaffold **IV-23** is shown in **Scheme 4.13**. Fortunately, the established synthetic approach was applicable to this scaffold. The desired scaffold was accessible in nine linear steps from *trans*-4-hydroxy-*L*-proline. Following access to **IV-23**, the desired ammonium salt **IV-24** was subsequently accessed by TFA-mediated Boc deprotection in nearly quantitative yield (97%).

In conclusion, access to the desired α-ketoimine precursor was finally successfully achieved following alteration of the synthetic route of nagelamide M using a Boc protecting group instead of the original Cbz protecting group. While the total synthesis of nagelamide M was not yet achieved at present time, these efforts led to the establishment of a robust route towards the synthesis of this natural product. Attempts to develop the proposed methodology were hindered by the apparent reactivity of the pyrrolidinone scaffold towards oxidative conditions; the presence of the ketone is proposed to contribute to the formation of undesired byproducts in the system. Subsequent steps in this synthesis involve the key proposed guanidine cyclization upon the reactive α-ketoimine scaffold and installation of the taurine moiety to access nagelamide M. Future work will focus on the completion of the total synthesis of this natural product.

Scheme 4.13 Access to Boc-protected ketone scaffold

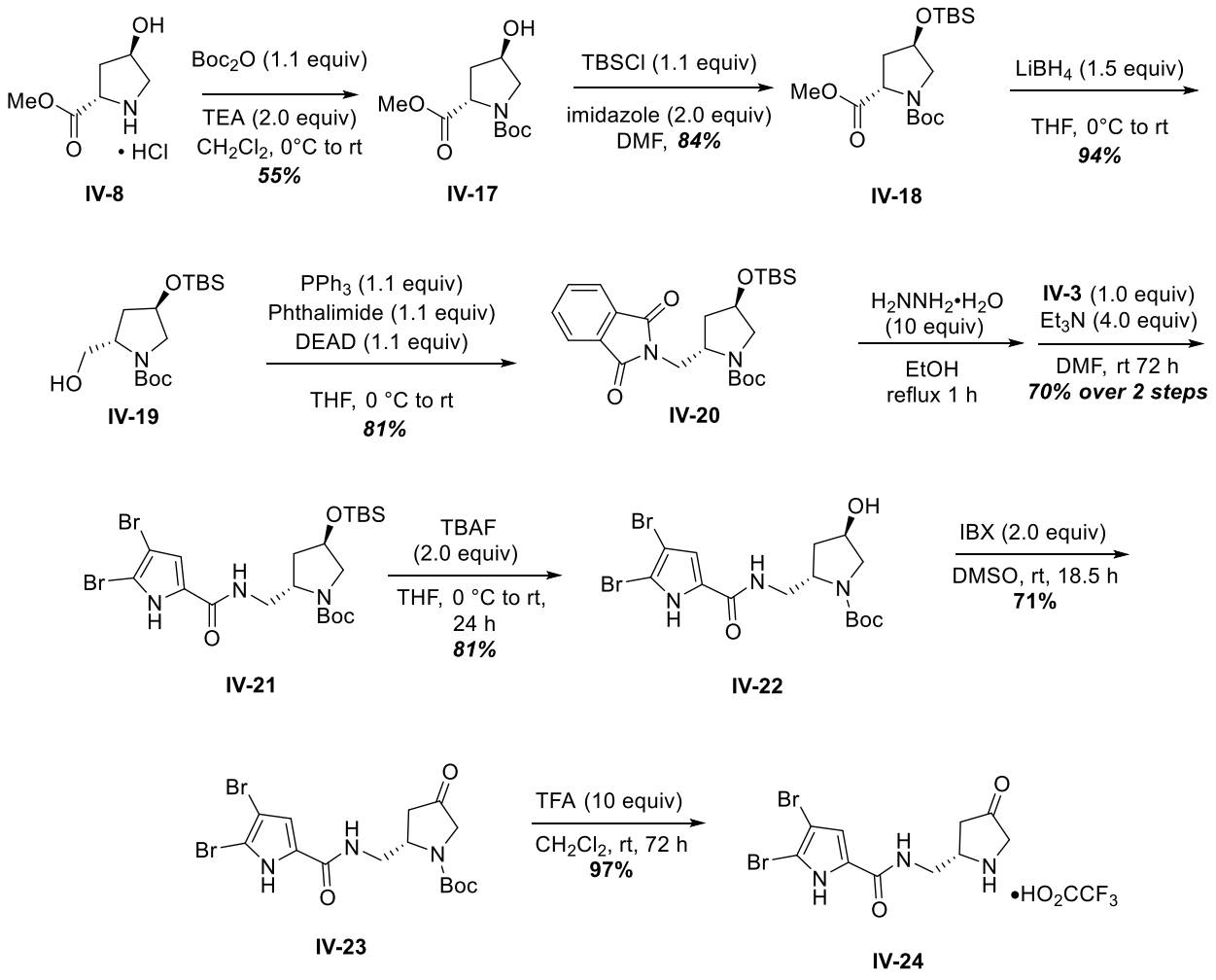

4.2 Ugibohlin and Debromougibohlins

4.2.1 Introduction

The natural product ugibohlin (**IV-25**) (**Figure 4.4**) is a tricyclic pyrrole imidazole alkaloid originally isolated as a metabolite of the marine sponge *Axinella carteri* in 2001.[16] At the time of its discovery, no analysis of its biological activities was reported. The *D*-ring *seco*-isomer of dibromoisophakellin, this natural product has only been achieved in the laboratory through transformation of dibromoisophakellin by the Lindel group.[17] The more recently discovered derivatives 4-debromougibohlin (**IV-26**) and 5-debromougobohlin (**IV-27**) were isolated in 2018

from a *Dictyonella* sp. marine sponge which was collected from the mouth of the Amazon River.[18] While **IV-26** and **IV-27** were inactive against the 20S proteasome when tested, the lack of biological activity of these molecules indicates a motivation for their synthesis. The bromine substitution pattern of **IV-27** is relatively unique among this natural product family; pyrroles monobrominated at the C-5 position are observed in 9.2% of pyrrole alkaloids.[18] Few examples exist for selective bromination at this position,[19-23] and this therefore represents an additional synthetic challenge. Our lab recently developed a C-5 selective monobromination method for C-2 pyrrole carboxamides,[23] and the application of this methodology towards the synthesis of **IV-27** was envisioned.

Figure 4.4 Ugibohlin natural products and *D*-ring isomers

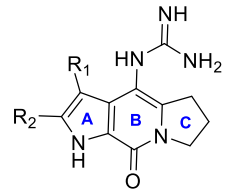

R_1,R_2=Br ***ugibohlin (IV-25)***
R_1,R_2=Br,H ***5-debromougibohlin (IV-26)***
R_1,R_2=H,Br ***4-debromougibohlin (IV-27)***

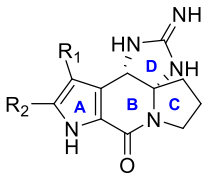

R_1,R_2=Br ***dibromoisophakellin***
R_1,R_2=Br, H ***monobromoisophakellin***

Several groups have attempted to access this molecule and molecules of similar structure, focusing on the construction and modification of the tricycle A, B, C ring system common to other pyrrole alkaloids such as cylindradrine, styloguanidine and dibromocantharelline. The Al-Mourabit group first focused on the development of regioselective synthesis strategies for the access of the two isomeric tricyclic systems (**Scheme 4.14**).[24] Following access to the desired tricycle, the group noted that halogenation of the tricycle takes place at C_4 of the pyrrole ring in addition to the C_6 of the pyridone ring. The use of additional bromine in DMSO finally brominated the least nucleophilic site of C_5 to afford a tribrominated species.

Scheme 4.14 Al-Mourabit's bromination of ugibohlin core

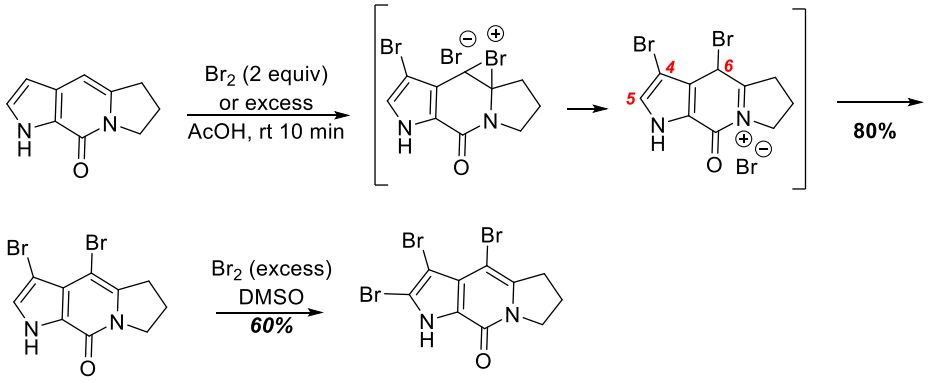

An attempt to access the desired tricycle containing a nitrogen substitution at C-6 of the pyridone was later published by Chien et al in 2013.[25] The work focused on the synthesis of the tricyclic core of ugibohlin, dibromoisophakellin and styloguanidine through a Vilsmeier-Haack cyclization to construct the B-ring of the tricycle without the protection of the pyrrole nitrogen (**Scheme 4.15**). Tertiary amides readily underwent cyclization under dehydrating conditions to afford the aminated tricycle. However, secondary amides underwent a subsequent auto-oxidative mechanism to form alpha-hydroxy ketones upon purification. The A,B-ring unit is especially oxidizable; the 6-amino substituted compounds undergo facile auto-oxidation through a Kornblum-DeLaMare type rearrangement to afford the alpha-hydroxy ketone product. A similar example was more recently reported by the Wipf group in 2019.[26] The electron-donating ability of the 6-amino substituents is considered responsible for this unexpected aerobic oxidation. The issues of regioselectivity coupled with the issues associated with the Vilsmeier-Haack approach suggest that perhaps introduction of the amino moiety through a separate strategy may be necessary. Careful choice of guanidine synthon is also important to avoid auto-oxidation of the pyridone core.

Scheme 4.15 Chien's Vilsmeier-Haack approach to aminated ugibohlin core

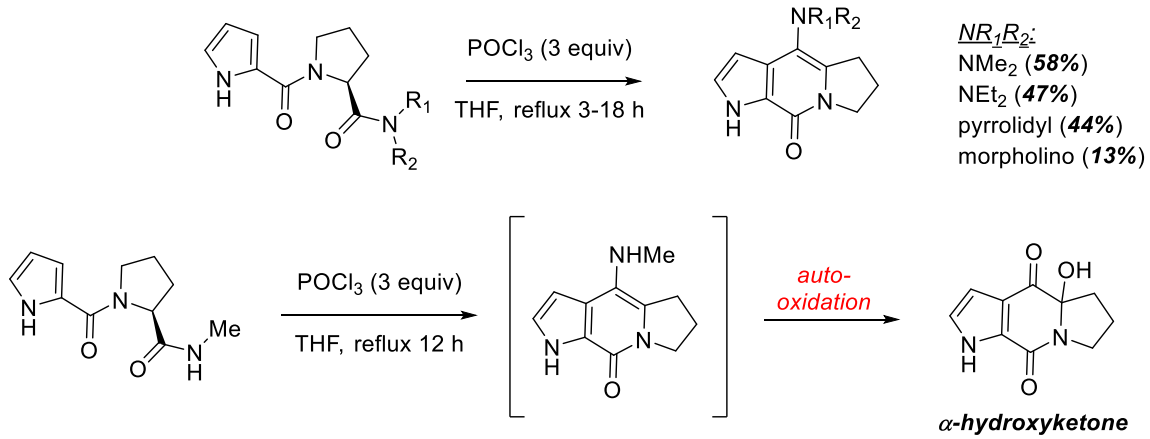

In an attempt to synthesize dibromoisophakellin, former lab member Nicole Hewlett explored the effects of modifying the electronics of this system through protection of the pyrrole nitrogen with an electron withdrawing group. Using a similar strategy to that of the Al-Mourabit group, Hewlett synthesized *N*-tosylated tricycle **IV-34**. Further functionalization of this tricycle was sought to access the desired natural product. The presence of the electron-withdrawing group removed electron density from the pyrrole ring, resulting in alteration of the most nucleophilic site to the enamine moiety of the pyridone ring. Hewlett attempted the total synthesis of dibromoisophakellin using an analogous strategy to that utilized in the total synthesis of dibromophakellin: an intermolecular cyclic guanidine formation through a bromonium intermediate (**Scheme 4.16**). However, unlike in the case of dibromophakellin the formation of the desired cyclic guanidine through this strategy did not occur. Instead, bromination of the pyridone ring (C_6) occurs, followed by rearomatization to afford a vinylic bromide.

Scheme 4.16 Hewlett's attempted synthesis of dibromoisophakellin

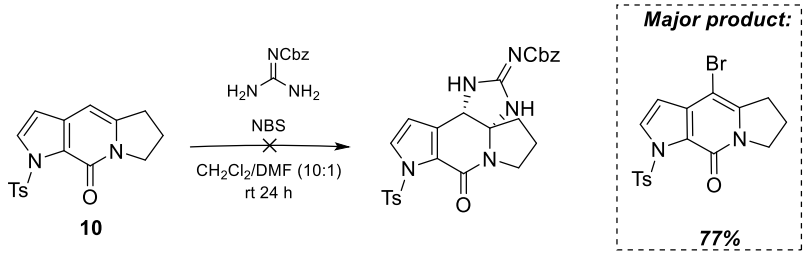

While this was not the desired result for that total synthesis, it posed an interesting starting point of the total synthesis of the ugibohlins. We envisioned that further exploration of the NBS-mediated approach with the appropriate synthon. Additionally, the *N*-tosylated halogenated tricycle could be a key intermediate in the synthesis of the ugibohlins: C-N bond formation using this molecule as hetaryl halide equivalent in an Ullmann-type or Buchwald-Hartwig-type coupling reaction with a suitable guanidine synthon. Following functionalization of the enamine moiety, a late-stage bromination may be explored within the pyrrole ring following removal of the tosyl protecting group.

The proposed retrosynthesis of the ugibohlins is shown below: late-stage regioselective brominations will allow for access to the natural products. The non-brominated precursor would arise following detosylation of the tricyclic core, which has been substituted at the pyridone core with a suitable guanidine synthon. The presence of the cyanamide functional group is proposed to prevent auto-oxidation of the tricycle due to the fact that electrons of the nitrogen bound to the pyridone ring are in resonance with the nitrile, therefore depleting potential for electron donation. Both a guanidine and cyanamide are proposed as possible substitutions at the pyridone core. This would be synthesized from regioselective amination of the tosylated tricycle. Regioselective functionalization to afford the desired hetaryl halide would be a direct result of the depletion of the electron density of the pyrrole ring due to the *N*-tosyl group. Access to the tricycle is shown within the retrosynthetic analysis below (**Scheme 4.17**).

Scheme 4.17 Retrosynthetic analysis of ugibohlins

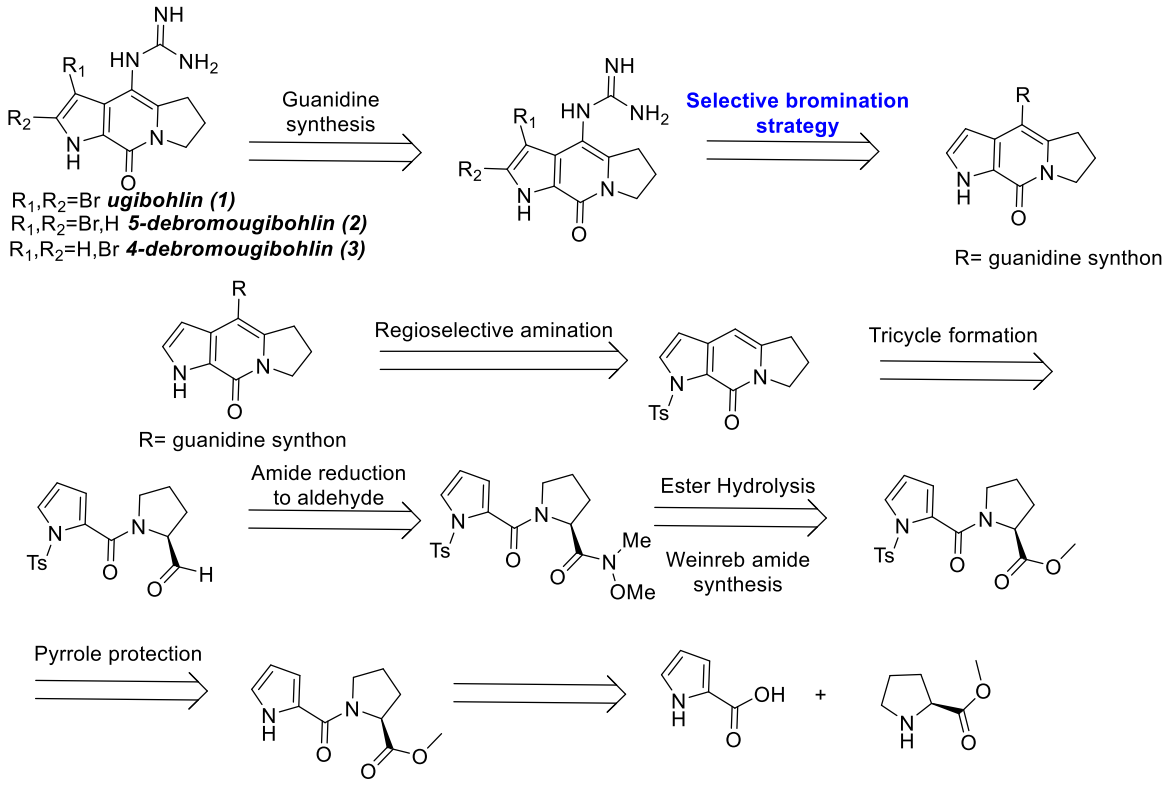

R_1,R_2=Br ***ugibohlin (1)***
R_1,R_2=Br,H ***5-debromougibohlin (2)***
R_1,R_2=H,Br ***4-debromougibohlin (3)***

4.2.2 Results & Discussion

4.2.2.1 Access to the tricyclic core

Optimization of the synthesis of the desired tricycle **IV-34** was successfully achieved starting from pyrrole and proline building blocks (**Scheme 4.18**). 2,2,2-trichloroacetylpyrrole **IV-2** was first hydrolyzed under basic conditions, and acidic workup afforded pyrrole-2-carboxylic acid **IV-28** in high yield (91%). This was then coupled with *L*-proline-methyl ester hydrochloride under EDCI conditions to afford the desired pyrrole carboxamide **IV-29** (87%). Using a stoichiometric amount of base (DMAP) yielded the product in short reaction times.

Hydrolysis of the ester under basic conditions produced the carboxylic acid **IV-30** (90%). The carboxylic acid underwent EDCI coupling identical to those used by Al-Mourabit[24] to afford the Weinreb amide **IV-31** in high yield (87%). Following synthesis of the desired carboxamide,

the next important step was introduction of the electron-withdrawing tosyl group on the pyrrole nitrogen. As mentioned previously, the presence of this electron-withdrawing group was proposed to bear a considerable effect electronically such that functionalization within the pyrrole becomes less favorable. The tosyl group was introduced easily using sodium hydride and tosyl chloride to afford **IV-32** in high yield (88%).

After pyrrole *N*-tosylation, the next focus in the synthesis was access to the desired tricycle through construction of the pyridone ring. Partial reduction of the Weinreb amide to aldehyde **IV-33** was carried out using DIBAL-H; it should be noted that the use of excess DIBAL-H and short reaction times afforded maximum product formation with less over-reduction. Prolonged reactions times resulted in lower product yields, however starting material recovery was routine. Optimal conditions included the use of three equivalents of DIBAL-H and a reaction time of 1.5 hours to afford the aldehyde in 56% yield.

Scheme 4.18 Synthesis of tricyclic core **IV-34**

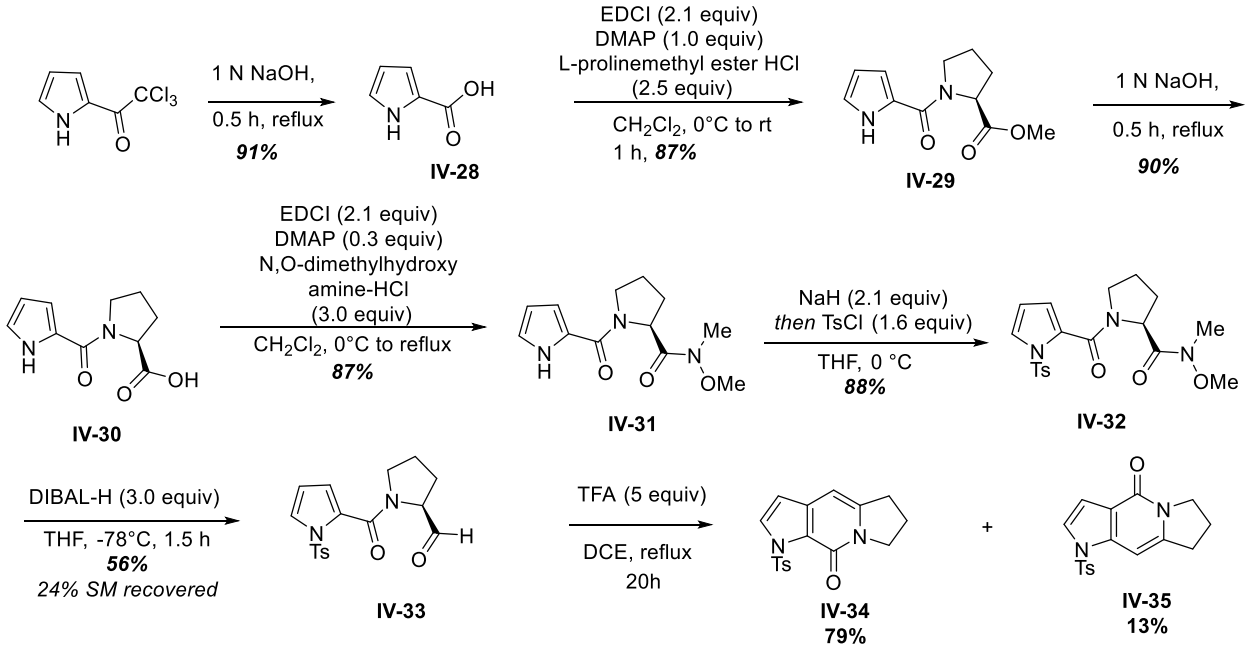

Acylation of the pyrrole at C-3 under acidic conditions followed by elimination affords the desired tricycle **IV-34**. Excess trifluoroacetic acid was utilized to activate the aldehyde towards nucleophilic attack by the electron depleted pyrrole. Initial attempts at this synthesis included the use of dichloromethane as solvent and long reaction times. However, the challenge of maintaining solvent levels without evaporation led to utilization of higher boiling solvent dichloroethane. Using dichloroethane allowed for heating overnight without concomitant solvent evaporation. The major tricycle was produced in 79% yield alongside a minor by-product identified as **IV-35.** This by-product is possibly forming through a Pictet-Spengler-type rearrangement.

Efforts were next focused on investigation of the regioselective functionalization of the core and attempted amination by several approaches.

4.2.2.2 Regioselective functionalization of tricyclic core

With the desired tricycle in hand, initial attempts at inclusion of the guanidine synthon were made via an NBS-mediated process. As mentioned previously, the presence of the tosyl group depletes electron density in the pyrrole ring; halogenation is thus predicted to occur preferentially through the enamine moiety of the pyridone ring. In the total synthesis of (±)-dibromophakellin by Hewlett and Tepe, NBS was utilized as bromine source to facilitate construction of a cyclic guanidine ring.[27] The proposed mechanism of product formation was proposed and is provided below (**Scheme 4.19**). The mechanism involves initial bromination of the guanidine to afford an electrophilic intermediate. Subsequent nucleophilic attack by the enamine in an S_N2'-type mechanism affords the intermediate **IV-36**. Intramolecular attack by the guanidine upon the iminium affords the cyclized intermediate **IV-37**, which can then tautomerize to the desired cyclic product **IV-38**.

Scheme 4.19 Proposed mechanisms for NBS-mediated guanidine cyclization

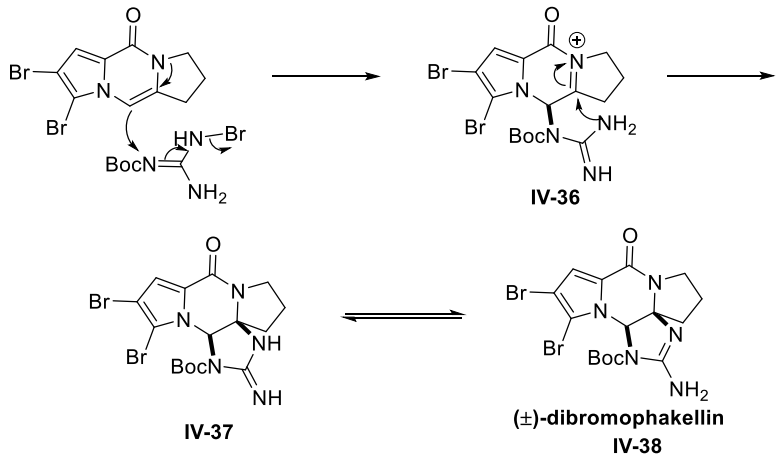

In the synthesis of the ugibohlins, an analogous possibility was envisioned (**Scheme 4.20**). The NBS-mediated process was attempted upon tricycle **IV-34** using cyanamide as guanidine synthon, but only yielded the vinylic bromide **IV-40**. None of the desired product was observed or isolated, regardless of addition order. These results suggest that in the case of the pyridone core, bromination and re-aromatization occurs more readily in this system than cyanamidation. Following this failure, focus turned towards C-N bond formation through transition metal-mediated means such as Ullmann coupling or Buchwald-Hartwig conditions.

Scheme 4.20 Attempted cyanamidation of tricycle **IV-34**

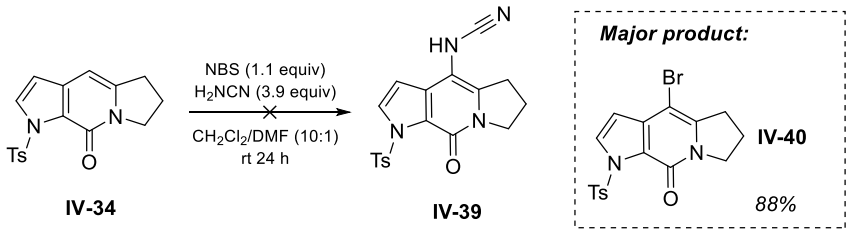

4.2.2.3 Attempt to Install Guanidine via Ullmann coupling

Recently, several groups have established methods for the synthesis of substituted aryl cyanamides and guanidine species through Cu- and Pd-catalyzed processes.[28-32] These approaches

bear similarity to the Goldberg coupling of amides to aryl halides. With this approach in mind, the vinylic bromide **IV-40** was deliberately synthesized from **IV-34** in 58% yield to act as heteroaryl halide equivalent (**Scheme 4.21**). Attempted coupling of this species with PMB-protected guanidine **IV-41** using Ullmann-type conditions established by Hammoud et al.[32] did not result in product formation. These results were suggestive instead of detosylation of the pyrrole nitrogen due to extensive heating. Similar attempts using cyanamide as nucleophile were made, but also resulted in formation of the detosylated product **IV-43** in 47% yield. Initially it was believed that cyanamide could be playing role as nucleophile to aid in detosylation in the system, and so 3 equivalents of cyanamide were utilized to facilitate a one-pot two-step sequence of deprotection/coupling to access **IV-46**. Unfortunately, this reaction also indicated primarily detosylation in the system. The desired detosylated coupled product was never isolated.

Scheme 4.21 Attempted functionalization of **IV-40** by Ullmann-coupling

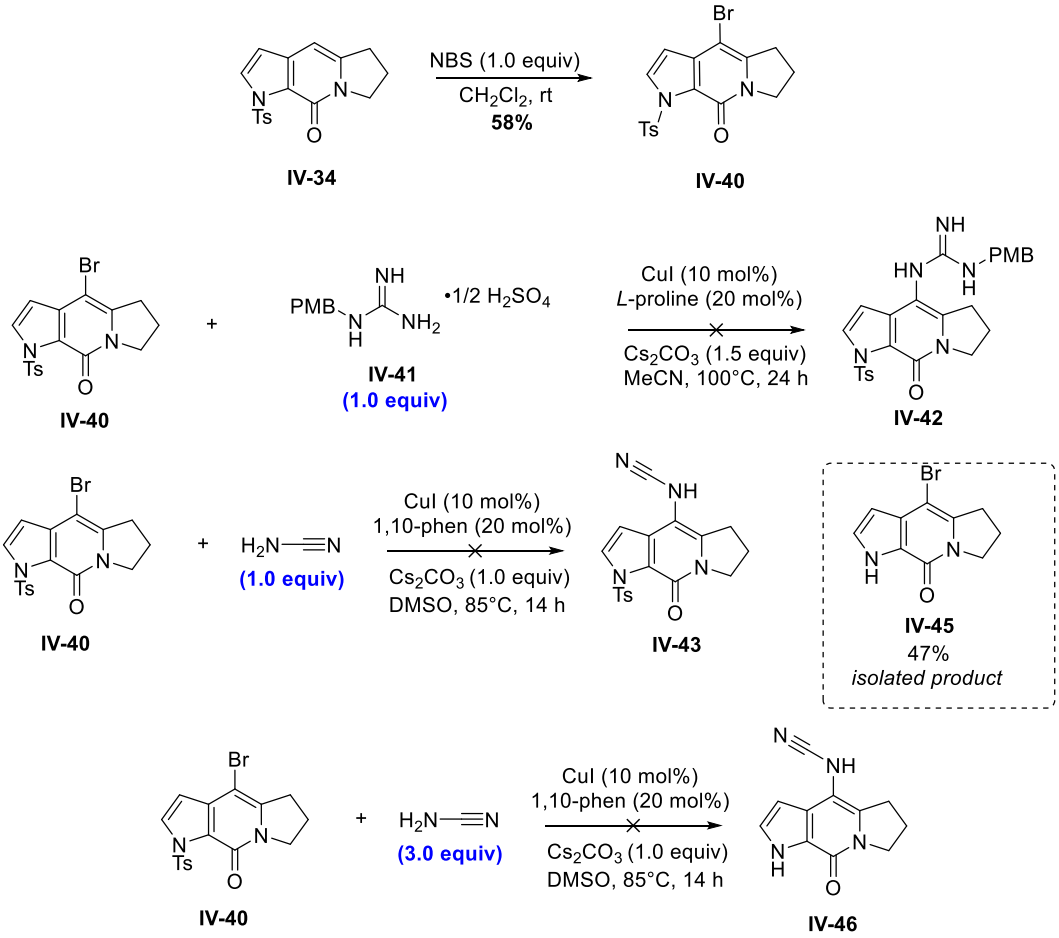

The initial failures in this system were suspected to be potentially caused by the lack of reactivity of the brominated tricycle. To overcome this lack of reactivity under the current conditions, the iodinated tricycle **IV-47** was synthesized for evaluation as a coupling partner. The iodinated tricycle was subjected to identical conditions as previously described, affording the detosylated starting material. Although crude mass spectrometry did suggest that the coupled/detosylated product may be present in the system, the main observed product in this system was the detosylated tricycle **IV-48**. Further attempts to optimize the reaction including higher temperatures, alteration of ligands, and varying catalyst loading all failed to afford any

improvement. Based upon these failures, it became apparent that even with the theoretically more reactive tricyclic halide **IV-47**, the reaction was not favored to occur.

Scheme 4.22 Efforts towards amination with iodinated tricycle **IV-47**

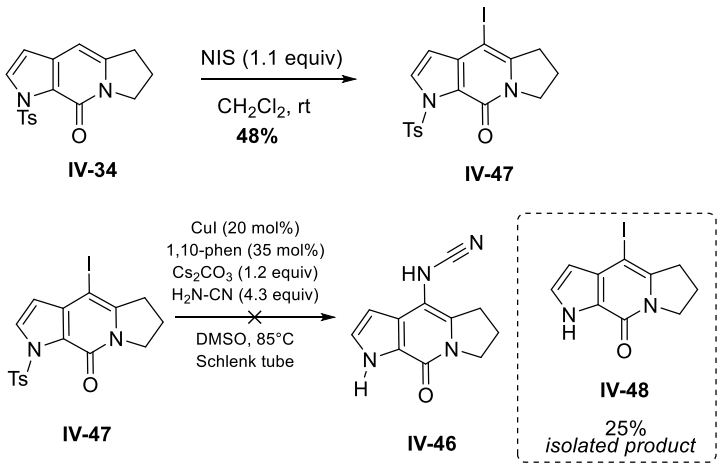

Further literature investigation revealed a possible cause for the failure to guanidylate or cyanamidate halogenated tricycles **IV-40** and **IV-47** using the Ullmann approach. When considering reaction scope for these types of methods, a scope limitation was identified: electron-dense hetaryl halides are noticeably absent. While mechanistic studies of the copper-catalyzed guanidylation of aryl halides are scarce, researchers have investigated the amidation and imidation of aryl halides under similar reaction conditions.

The general mechanism for a Goldberg reaction is provided below (**Scheme 4.23**). The first step in the reaction involves a ligand exchange whereby the amide nucleophile coordinates to the copper metal to afford the Cu(I) complex. Subsequent oxidative addition of the aryl halide affords the Cu(III) intermediate. Finally, reductive elimination affords the desired product and regenerates the Cu(I) active species.

Scheme 4.23 Mechanism of Goldberg reaction

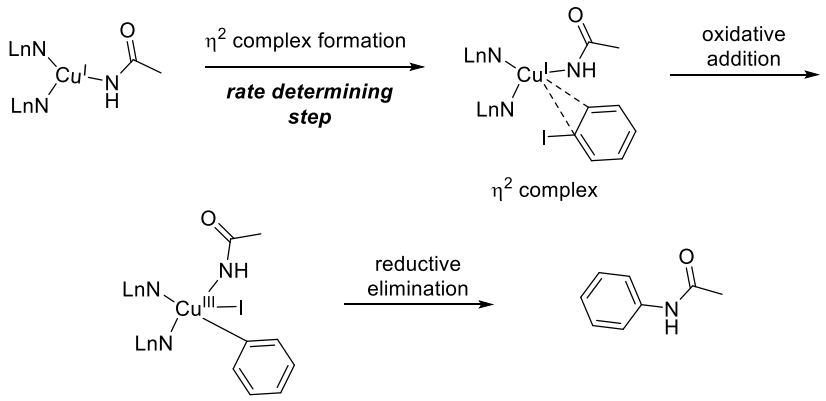

Theoretical studies associated with this reaction suggest that the rate-limiting step is the oxidative addition of the aryl halide.[33] The oxidative addition occurs through formation of an η^2-complex which is energetically favored in the presence of electron-deficient aryl halides. The electron-deficiency of these species is believed to lower the LUMO of the aromatic ring and thus provide a more favorable oxidative addition. Conversely, electron-dense scaffolds suffer from lower reaction rates. With these considerations in mind, the use of the Ullmann coupling approach was abandoned, and instead an indirect approach to guanidylation was next examined.

4.2.2.4 Attempt to install guanidine via Tiemann rearrangement

Following the failures associated with direct installation of the guanidine by Ullmann coupling conditions, the retrosynthesis of the ugibohlins was revised (**Scheme 4.24**). While there was little evidence for direct aminations of analogous hetaryl halides found in literature, an indirect approach to access the amination via Tiemann rearrangement was proposed. Access to the desired aminated product sought to install a cyanamide by a three-step process: cyanide synthesis, amidoxime formation, and finally a Tiemann rearrangement to afford the desired product, which could subsequently be transformed into the desired guanidine.

Scheme 4.24 Revised retrosynthesis of ugibohlin core via Tiemann rearrangement

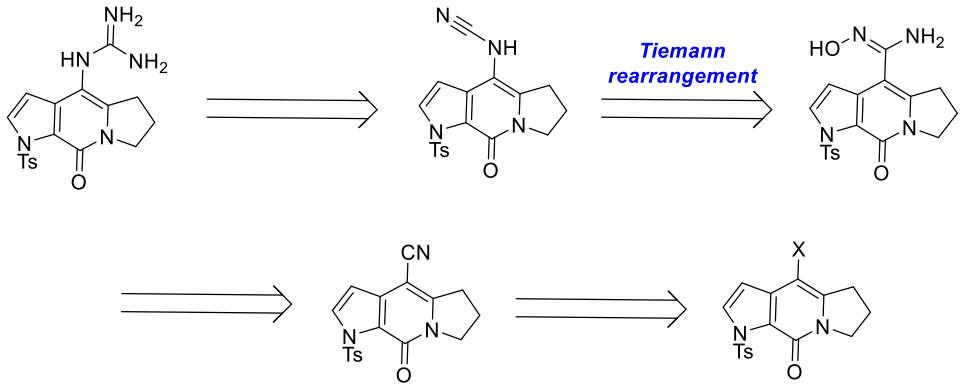

The Tiemann's rearrangement involves the *O*-sulfonylation of amidoximes to allow C-N bond formation. The reaction was first reported by Tiemann in 1891 when *N*-phenyl urea was observed from the reaction of benzamidoxime and *p*-toluenesulfonyl chloride (**Scheme 4.25**, Eqn 1).[34] Installation of the *O*-sulfonyl group weakens the N-O bond to facilitate rearrangement and in the presence of base or heat, leads to various products. Some recent explorations of this rearrangement report mild conditions for access to the desired cyanamide scaffold (**Scheme 4.25**, Eqn 2).[35] In this work, researchers observed that π-electron-rich aryl amidoximes underwent facile rearrangement to access the desired cyanamide product. Based upon these results, the electron-density of the tricyclic amidoxime was predicted to contribute to a favorable rearrangement in this synthesis.

Scheme 4.25 Previous examples of Tiemann rearrangement

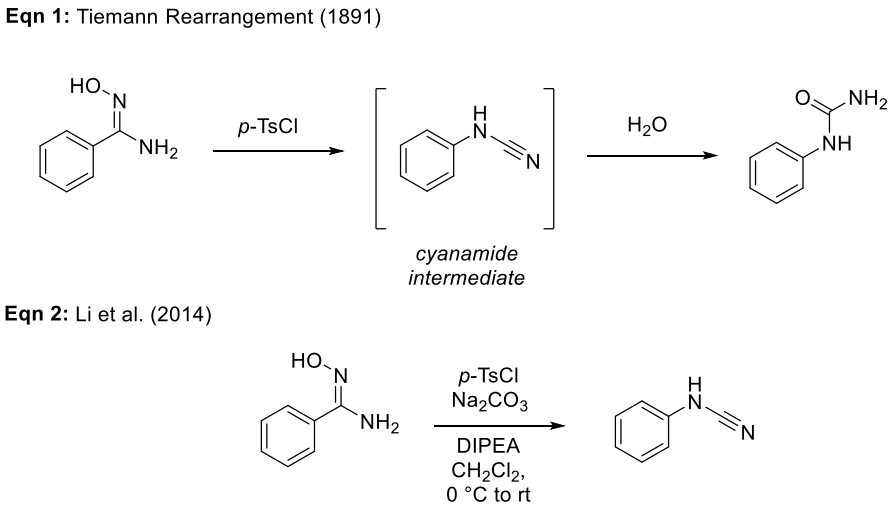

The first synthetic focus in this approach was access to the cyanated tricycle **IV-50** as an amidoxime precursor through Pd-catalysis. Pd(II)-catalyzed cyanation of aryl halides was first reported by Takagi *et al* in 1973.[36] The seminal paper demonstrated that aryl nitriles are accessible from aryl iodides and bromides in moderate to high yields in the presence of a Pd(II) source and KCN. Since this discovery, further optimization of the system has led to use of phosphine ligands and introduction of less toxic cyanide salts (i.e. $K_4[Fe(CN)_6]$ and $ZnCN_2$) which provide a milder and safer alternative to the original method.[37, 38] Electron-dense heteroaryl halides including C_3-iodinated indoles have been reported in patent literature to access nitriles by Pd(II)-catalyzed approaches.[39] The Pd(II)-catalyzed cyanation of tricycle **IV-47** was thus embarked upon utilizing conditions from patent literature in conjunction with the used of the mild cyanation reagent $Zn(CN)_2$.

The optimization of the synthesis of nitrile **IV-50** is shown below in **Scheme 4.26.** An initial attempt was made utilizing tris(dibenzylidene)dipalladium(0) and dppf as phosphine ligand at 85 °C, however conversion of the starting material was incomplete after 24 hours. Applying the same reaction conditions at higher temperatures afforded the optimized yield of 93%.

Scheme 4.26 Synthesis of nitrile **IV-50** by Pd(II)-catalyzed cyanation

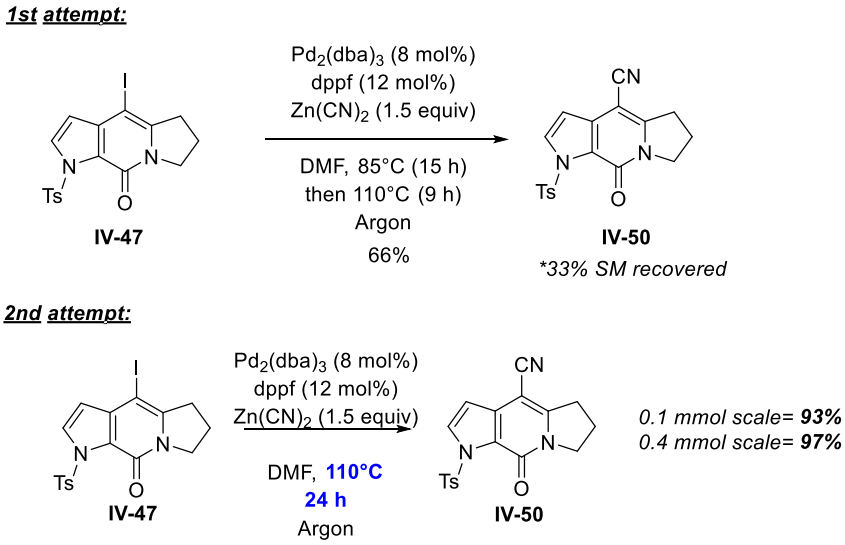

Following cyanation, the next focus was synthesis of the amidoxime substrate *en route* to the desired cyanamide through the Tiemann rearrangement. The proposed Tiemann rearrangement was inspired by a recent report of practical approaches to cyanamides using *O*-sulfonyl intermediates.[40, 41]

Unfortunately, synthesis of the amidoxime was more challenging than initially anticipated. Poor conversion resulted when attempts were made using the reported protocol by Lin et al.,[35] which utilized 1.5-2.0 equivalents of hydroxylamine. The lack of conversion for this step likely results from the fact that the enamine is capable of stabilizing the nitrile through resonance, thus decreasing electrophilicity of the carbon center towards the hydroxylamine nucleophile. To combat this issue, equivalents of hydroxylamine reagent were increased in an attempt to increase the rate of conversion. Conversion of the starting substrate was slow, and product formation was only ever achieved in a yield of 34% (**IV-51**) after several attempts of optimization and the use of high excess of hydroxylamine (**Scheme 4.27**). Attempts to improve conversion were also made by exploring higher-boiling alcoholic solvents. Disappointingly, while these changes did facilitate

conversion, they also led to the formation of a detrimental amide byproduct (**IV-52**). This byproduct was observed on several occasions.

Scheme 4.27 Synthesis of amidoxime **IV-51**

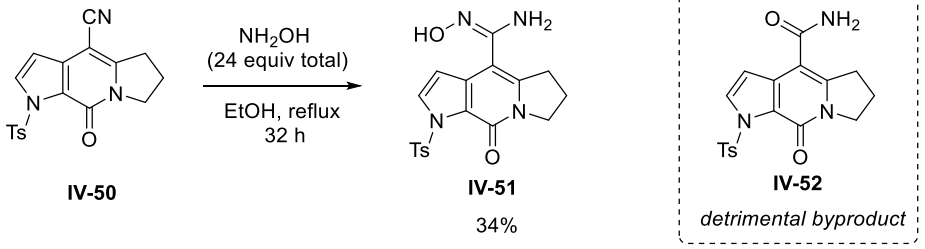

Formation of the amide byproduct in this type of transformation has been reported in literature,[42] and mechanistic studies suggest that the amide product arises from reaction of excess hydroxylamine with an undesired intermediate, which forms from the nitrile by "*O*-attack" of the hydroxylamine. Subsequent reaction with excess hydroxylamine affords the amide byproduct by reduction of the O-N bond in the undesired intermediate. The compounding factors associated with the lack of conversion of the starting material and byproduct formation were difficult to overcome. Despite several attempts to combat the issue of amide formation, there was never a successful solution found. Other approaches were thus sought to access the desired guanidylated product.

Based upon the failed results associated with the Ullmann condensation and the success associated with coupling the tricycle as a nucleophilic partner in the cyanation, it became clear that the tricycle must act as a nucleophilic partner in any approach to access direct C-N bond formation. An electrophilic nitrogen source was thus required in order to directly aminate the tricyclic core. With this in mind, studies towards direct amination by an Umpolung approach were next undertaken.

4.2.2.5 Attempts to Form C-N bond through Umpolung Approach

As a preliminary study, several reactions were explored between the tricycle and various electrophilic nitrogen species. These reactions are summarized below (**Schemes 4.28**). To explore the ability to aminate the tricycle, amination with DEAD was first attempted. Diazo-carboxylates are established electrophilic nitrogen species which have been used to install aminated species through multistep processes.[43] This reaction resulted in 72% starting material recovery, and trace amounts of product formation and functionalization of the tricycle. Direct installation of a carbamate was also attempted utilizing a nitrene electrophile. Nitrenes are well-established substrates utilized for the direct amination.[43] Nitrenes can be generated under basic conditions from N-O-tosylate precursors.[44] Following previously published conditions, this approach was carried out but resulted in quantitative recovery of the starting material.

Scheme 4.28 Initial studies towards direct amination with electrophilic *N*-species

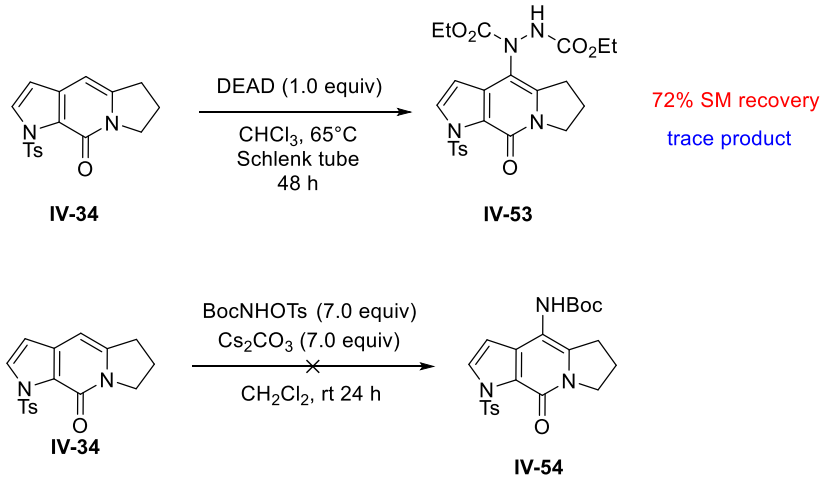

N-O-tosylates have also been utilized as nitrene coupling partners in Pd-catalyzed coupling reactions using amide directing groups through C-H activation.[45] Due to the lack of an inherent directing group in our system, a Pd-catalyzed approach was instead attempted using the iodinated tricycle (**Scheme 4.29**). First, oxidative addition of the iodinated tricycle to afford a Pd(II) intermediate would take place. Hypothetically, the nitrene species could subsequently insert to

afford a Pd(IV) intermediate. Reductive elimination would afford the desired aminated tricycle. Disappointingly, no product was isolated from this reaction, and instead 38% yield of the starting material was recovered.

Scheme 4.29 Attempted amination via Pd(II)/Pd(IV) catalysis

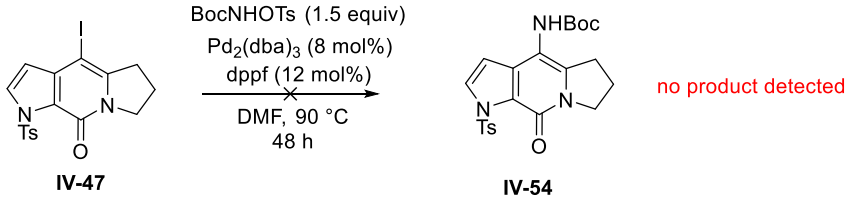

Access to the ugibohlin natural products through a variety of amination strategies has been explored. This amination was a considerable challenge to overcome and remains a hindrance in the successful completion of the total syntheses of the ugibohlin natural products. While direct guanidylation of the pyridone core has yet to be achieved, a clear necessity to install using an Umpolung strategy was identified.

4.3 Conclusion

Further exploration of literature revealed a possible novel approach to access the desired guanidylation in a direct manner. Direct guanidylation is proposed using a Rh(II)-nitrene synthetic approach inspired by early work by the Du Bois group[46] and more recent work reported by Paudyal et al (**Scheme 4.30**).[47] The Du Bois group first demonstrated the utility of $Rh_2(esp)_2$ as a catalyst in the intramolecular oxidative cyclizations of Tces-protected urea and guanidines through sp^3 C-H activation. Paudyal et al later demonstrated that further application of this catalyst and amines with an internal oxidant allows for intermolecular amination of arenes which is directed electronically to the most electron-dense site of the ring. With these reports in mind, a Rh(II)-nitrene approach is proposed which would allow for direct guanidylation of the pyridone core of ugibohlin. The guanidine equivalent could either contain an electron-withdrawing Tces group and

be utilized in the presence of PIDA per the Du Bois conditions or utilize an internal N-O bond to act as oxidant in the system.

Scheme 4.30 Proposed synthesis of guanidylated core by Rh(II)-catalysis

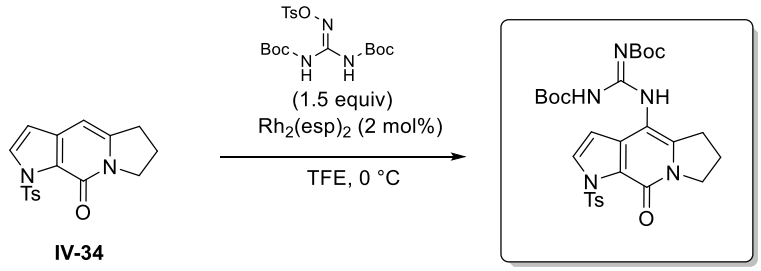

This chapter summarizes the synthetic efforts towards the total synthesis of several natural products belonging to the pyrrole alkaloid family. Key challenges in the syntheses of these compounds were identified which hindered their completion at the present time. While the total syntheses of nagelamide M and the ugibohlins have not be achieved, these studies provided valuable insights which we hope will lead to future achievement in their syntheses.

4.4 Experimental

2,2,2-trichloro-1-(1*H*-pyrrol-2-yl)ethan-1-one (IV-2)

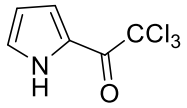

To an oven-dried round bottom flask was added a dry stir bar. The flask was flushed with nitrogen gas for 5 minutes and sealed under N_2 atm. To the flask was added 50 mL anhydrous diethyl ether, followed by trichloroacetylchloride (5.82 mL, 51.85 mmol). Pyrrole (3.27 mL, 47.13 mmol) was introduced to the reaction in 0.5 mL portions every 10 minutes for 70 minutes. The reaction was then allowed to proceed at rt under nitrogen atmosphere for 3.25 hours. The reaction was quenched with 8 mL water, followed by slow addition of 20 mL saturated aqueous K_2CO_3 solution until bubbles no longer evolved. The organic layer was then separated and stirred with activated charcoal in Erlenmeyer flask for 15 minutes. The mixture was then filtered by celite plug, and the resulting filtrate was concentrated *in vacuo* to afford the crude product. The product was recrystallized from hexanes to yield a white solid (8.62 g, 86 %). m.p = 72-73 °C (Lit=75-75.5°C).[2] ^{1}H NMR (500 MHz, $CDCl_3$) δ 9.44 (s, 1H), 7.40-7.38 (m, 1H), 7.19-7.16 (m, 1H), 6.40-6.38 (m, 1H). $^{13}C\{^1H\}$ NMR (126 MHz, $CDCl_3$) δ 173.3, 127.2, 123.1, 121.3, 112.0, 95.0. FTIR (cm^{-1}): 3316 (sh.), 1650, 1530, 1422, 1110. HRMS-ESI (m/z) calcd for $C_6H_3Cl_3NO$[M-H]- 209.9280. Mass not found.

2,2,2-trichloro-1-(4,5-dibromo-1*H*-pyrrol-2-yl)ethan-1-one (IV-3)

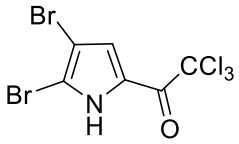

2,2,2-trichloro-1-(1*H*-pyrrol-2-yl)ethan-1-one (**IV-2**) (3.04 g, 14.3 mmol) was dissolved in acetic acid and stirred under nitrogen atmosphere. Bromine (1.48 mL, 28.71 mmol) was then introduced to the reaction flask slowly via syringe. The reaction was then heated at 60 ℃ for 2 hours, cooled to rt, and allowed to proceed overnight. The reaction was quenched with water. The pH of the reaction was adjusted to 5 with 2 N NaOH. The reaction mixture was then extracted with ethyl acetate (3x). The organic layers were pooled, dried over Na_2SO_4 and filtered. Volatiles were removed in vacuo to yield a crude solid. The pure beige solid was obtained via recrystallization with ethanol/water (4.96 g, 87% yield). mp= 137-139 ℃ (Lit=137 ℃).[3] ^{1}H NMR (500 MHz, DMSO-d_6) δ 13.74 (s, 1H), 7.38 (s, 1H). $^{13}C\{^1H\}$ NMR (126 MHz, DMSO-d_6) δ 171.4, 123.7, 122.9, 115.1, 101.3, 94.5. FTIR (cm^{-1}): 3282, 1530, 1654, 1365, 838. HRMS-ESI (m/z) calcd for $C_6H_1Cl_3Br_2NO[M-H]^-$ 365.7491. Found 365.7488.

4,5-dibromo-1*H*-pyrrole-2-carboxylic acid (IV-4)

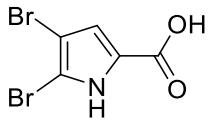

4,5-dibromo-2-(trichloroacetyl)-pyrrole (**IV-3**) (3.36 g, 9.17 mmol) was dissolved in 34 mL 2 N NaOH in a round-bottom flask. The flask was then heated under nitrogen atmosphere via oil bath for 1 hour. Following removal from heat, the reaction was cooled to rt. The pH of the solution was then adjusted by slow addition of 2 N HCl. The solid which formed was then isolated, dissolved in methanol, and stirred for 10 minutes with activated charcoal. The reaction was filtered through celite plug, and isolated filtrate was then concentrated in vacuo to yield a red solid (1.91 g, 78% yield). mp= 120 ℃ (decomposed). (Lit =179-183 ℃).[4] ^{1}H NMR (500 MHz, DMSO-d_6) δ 12.95 (s, 1H), 6.82 (s, 1H). $^{13}C\{^1H\}$ (126 MHz, DMSO-d_6) δ 160.3, 125.5, 122.5, 116.8, 106.7, 98.7. FTIR

(cm^{-1}): 3430, 3181, 1638, 1553, 1361, 832. HRMS-ESI (m/z) calcd for $C_5H_2Br_2NO_2$ [M-H]- 265.8452. Found 265.8453.

(2*S*,4*R*)-1-((benzyloxy)carbonyl)-4-hydroxypyrrolidine-2-carboxylic acid (IV-5)

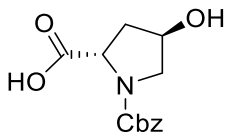

Trans-4-hydroxy-*L*-proline (2.00 g, 15.3 mmol) and $NaHCO_3$ (3.21 g, 38.2 mmol) were combined in a round bottom flask with stir bar and dissolved in 25 mL H_2O. Benzyl chloroformate (3.43 mL, 24.02 mmol) in 2.5 mL 1,4-dioxane was then added via syringe. The reaction was then allowed to proceed at rt for 18.5 h hours under nitrogen atmosphere. The reaction was then chilled to 0 ℃ and adjusted to pH 2 with 2 N HCl, and the aqueous layer was then washed three times with ethyl acetate. Organic layers were pooled, dried with Na_2SO_4, filtered, and concentrated *in vacuo*. The reaction was purified by automated CombiFlash chromatography (EtOAc/Hexane) to yield a clear viscous oil (2.79 g, 69%), the product as a mixture of rotamers. ^{1}H NMR (500 MHz, $CDCl_3$) δ 7.32 – 7.20 (m, 5H), 5.13-5.04 (m, 2H), 4.51 – 4.40 (m, 2H), 3.60 – 3.52 (m, 2H), 2.34 – 2.06 (m, 2H) *exchangeable protons missing*. ^{13}C{^{1}H} NMR (126 MHz, $CDCl_3$) δ 176.8/175.4, 156.1/155.1, 136.2/136.1, 128.7/128.6, 128.3/128.1, 128.0/127.7, 69.8/69.3, 67.9/67.6, 58.0/57.7, 55.0/54.6, 39.0/38.0. Spectra matches literature data.[48] FTIR (cm^{-1}): 3000 (br.), 1670 (br. st.) 1423, 1353, 1119, 1170, 1077. HRMS-ESI (m/z) calcd for $C_{13}H_{15}NO_5Na$ [M+Na]+ 288.0848. Found 288.0860.

(2*S*,4*R*)-1-((benzyloxy)carbonyl)-4-((tert-butyldimethylsilyl)oxy)pyrrolidine-2-carboxylic acid (IV-6)

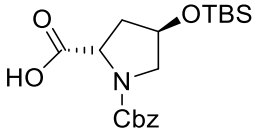

(2*S*,4*R*)-1-((benzyloxy)carbonyl)-4-hydroxypyrrolidine-2-carboxylic acid (**IV-5**) (0.511 g, 1.93 mmol) was dissolved in 15 mL DMF in round bottom flask with stir bar. Imidazole (0.655 g, 9.62 mmol) was next added to the reaction, followed by *tert*-butyl-dimethychlorosilane (0.883 g, 5.86 mmol). The reaction was then allowed to proceed at rt for 12 hours under nitrogen atmosphere. 10 mL methanol was then added to the reaction, and the reaction mixture was stirred for an additional 2 hours. Volatiles were then removed in vacuo. The crude mixture was diluted in ethyl acetate, and then washed once with 1 N HCl. The aqueous layer was then washed twice with ethyl acetate. Organic layers were pooled, dried with $MgSO_4$, filtered and concentrated. The reaction was purified by automated CombiFlash chromatography (EtOAc/Hexane) to yield an extremely viscous oil (0.584 g, 80%), a mixture of rotamers. ^{1}H NMR (500 MHz, $CDCl_3$): δ 10.97 (s, 1H), 7.36 – 7.24 (m, 5H), 5.23 – 5.12 (m, 2H), 4.56 – 4.43 (m, 2H), 3.68-3.61 (m, 1H), 3.54 – 3.44 (m, 1H), 2.30 – 2.08 (m, 2H), 0.87 (d, *J* = 2.8 Hz, 9H), 0.08 – 0.05 (m, 6H). ^{13}C{^{1}H} NMR (126 MHz, $CDCl_3$) δ 178.3/176.9, 155.9/154.7, 136.4/136.3, 128.6, 128.5, 128.2, 127.94, 127.92, 127.6, 70.3/69.7, 67.6/67.4, 58.2/57.7, 55.3/54.8, 39.9/38.6, 25.8/25.7, 18.02/17.98, -4.73, -4.78, -4.80, -4.85. FTIR (cm^{-1}): 3000 (b. st.), 1715, 1648, 1164. HRMS-ESI (m/z) calcd for $C_{19}H_{29}NO_5SiNa$ [M+Na]+ 402.1713. Found 402.1713.

methyl (2*S*,4*R*)-4-hydroxypyrrolidine-2-carboxylate hydrogen chloride (IV-8)

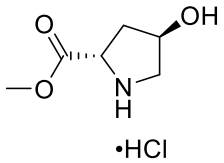

Trans-4-hydroxy-*L*-proline (6.24 g, 47.55 mmol) was dissolved in 160 mL methanol and chilled to 0°C via ice bath. Thionyl chloride (3.47 mL, 47.55 mmol) was added slowly to the reaction mixture via drop funnel. The reaction was then removed from ice bath and allowed to stir at rt for 4 hours. Then, solvent and volatiles were evaporated in vacuo to yield a crude white solid. This

solid was diluted several times with methylene chloride, and volatiles were evaporated in vacuo. The solid was then triturated with diethyl ether, and pure white solid was isolated via vacuum filtration (7.62 g, 88% yield). ^{1}H NMR (500 MHz, DMSO-d_6) δ 10.43 (s, 1H), 9.48 (s, 1H), 5.64 (s, 1H), 4.45 – 4.31 (m, 2H), 3.73 (s, 3H), 3.38 (dd, J = 12.0, 4.6 Hz, 1H), 3.05 (d, J = 12.1 Hz, 1H), 2.21 – 2.03 (m, 2H). ^{13}C{^{1}H} NMR (126 MHz, DMSO-d_6) δ 169.5, 68.8, 58.0, 57.84, 53.45, 37.39. FTIR (cm^{-1}): 3319, 3216 (br), 2956, 1738. HRMS-ESI (m/z) calcd for $C_6H_{12}NO_3$ [M+H]+ 146.0817. Found 146.0814.

1-benzyl 2-methyl (2*S*,4*R*)-4-hydroxypyrrolidine-1,2-dicarboxylate (IV-9)

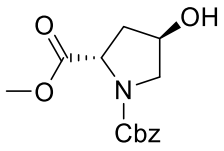

Sodium bicarbonate (3.61 g, 42.9 mmol) was dissolved in 60 mL of a 1:1 water/dioxane solvent mixture in a round-bottom flask with stir bar. The reaction flask was cooled to 0 ℃. methyl (2*S*,4*R*)-4-hydroxypyrrolidine-2-carboxylate hydrogen chloride (**IV-8**) (5.65 g, 31.09 mmol) was then added to the reaction flask, and the reaction was allowed to proceed at 0 ℃ while stirring for 30 minutes. Benzyl chloroformate (8.74 mL, 61.2 mmol) was then added to the reaction mixture via syringe, and the reaction was then allowed to proceed at 0℃ for 2 hours under nitrogen atmosphere. The reaction mixture was then removed from ice bath, and the solvent was concentrated in vacuo. The crude oil was then diluted in methylene chloride and transferred to a separatory funnel. 1 N HCl aqueous solution was next added to the separatory funnel (to pH 2), and the reaction mixture was extracted. The layers were separated, and the aqueous layer was next washed two subsequent times with equal volumes of methylene chloride. The organic layers were pooled, dried over anhydrous Na_2SO_4, and filtered. The filtrate was then concentrated in vacuo to yield a crude yellow oil. The reaction was purified by automated CombiFlash chromatography

(EtOAc/Hexane) to yield a pale yellow oil as a mixture of rotamers (6.30 g, 73% yield).The product matched literature data.[49] ^{1}H NMR (500 MHz, $CDCl_3$) δ 7.34 – 7.26 (m, 5H), 5.19 – 4.97 (m, 2H), 4.52- 4.43 (m, 2H), 3.74 – 3.53 (m, 5H), 2.33-2.24 (m, 1H), 2.09-2.02 (m, 1H). ^{13}C{^{1}H} NMR (126 MHz, $CDCl_3$) δ 173.4/173.2, 155.2/154.7, 136.5/136.3, 128.6/128.5, 128.2/128.1, 128.0/127.9 70.2/69.4, 67.41/67.38, 58.0/57.8, 55.3/54.7, 52.5/52.3, 39.2/38.5. FTIR (cm^{-1}): 3430 (br), 2946, 1744, 1675 (s), 1164. HRMS-ESI (m/z) calcd for $C_{14}H_{18}NO_5$ [M+H]+ 280.1185. Found 280.1175.

1-benzyl 2-methyl (2*S*,4*R*)-4-((tert-butyldimethylsilyl)oxy)pyrrolidine-1,2-dicarboxylate (IV-10)

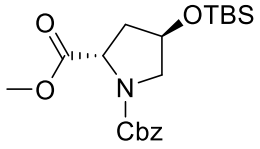

1-benzyl 2-methyl (2*S*,4*R*)-4-hydroxypyrrolidine-1,2-dicarboxylate (**IV-9**) (8.19 g, 29.3 mmol) was dissolved in 125 mL DMF in a round-bottom flask and stirred. *Tert*-butyl-dimethylchlorosilane (11.1 g, 73.3 mmol) was added to the reaction flask, followed by imidazole (9.97 g, 146.5 mmol). The reaction was then sealed and allowed to stir at rt under nitrogen atmosphere for 14 hours. Methanol (100 mL) was added to the reaction flask, and the reaction was stirred for an additional 2.5 hours. The reaction was then concentrated *in vacuo*, and the crude mixture was then transferred to a separatory funnel. Equal volume of aqueous 10% LiBr solution was next added. This aqueous layer was extracted twice with equal volume of ethyl acetate. The ethyl acetate layers were then collected, washed once with 10% aqueous LiBr solution, dried over anhydrous $MgSO_4$, and filtered. The filtrate was then collected and concentrated to yield a crude oil. The reaction was purified by automated CombiFlash chromatography (EtOAc/Hexane) to yield a clear oil as a mixture of rotamers (9.00 g, 78%). ^{1}H NMR (500 MHz, $CDCl_3$) δ 7.34 – 7.27 (m, 5H), 5.20 – 5.01 (m, 2H), 4.50 – 4.40 (m, 2H), 3.74– 3.40 (m, 5H), 2.23 – 2.16 (m, 1H), 2.06-

2.00 (m, 1H), 0.86-0.84 (m, 9H), 0.06–0.03 (m, 6H). $^{13}C\{^{1}H\}$ NMR (126 MHz, $CDCl_3$) δ 173.3/173.2, 155.1/154.4, 136.6/136.5, 128.5/128.4, 128.0/127.98, 129.9/127.8, 70.4/69.8, 67.1, 58.1/57.9, 55.3/54.8, 52.3/52.1, 39.9/39.0, 25.8/25.7, 18.01/17.96, -4.7, -4.8, -4.82, -4.86. FTIR (cm^{-1}): 3003, 2950, 1747 (s), 1708 (s). HRMS-ESI (m/z) calcd for $C_{20}H_{32}NO_5Si$ [M+H]+ 394.2050. Found 394.2050.

Benzyl (2*S*,4*R*)-4-((tert-butyldimethylsilyl)oxy)-2-(hydroxymethyl)pyrrolidine-1-carboxylate (IV-7)

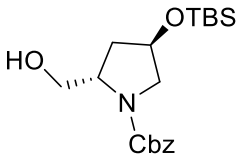

Preparation 1:

(2*S*,4*R*)-1-((benzyloxy)carbonyl)-4-((*tert*-butyldimethylsilyl)oxy)pyrrolidine-2-carboxylic acid (**IV-6**) (2.11 g, 5.57 mmol) was dissolved in 25 mL THF and transferred to round bottom flask containing stir bar. BH_3·DMS (8.35 mL, 16.71 mmol of a 2 M solution) was then added dropwise, and bubbling was observed. The reaction mixture was then refluxed via oil bath for 16 hours under nitrogen atmosphere. The reaction was quenched with water and washed with brine. The aqueous layer was then extracted three times with ethyl acetate. Organic layers were dried with Na_2SO_4, filtered, and concentrated in vacuo. The reaction was purified by automated CombiFlash chromatography (EtOAc/Hexane) to yield a clear oil (1.24 g, 61%). ^{1}H NMR (500 MHz, $CDCl_3$) δ 7.34-7.28 (m, 5H), 5.18 – 5.09 (m, 2H), 4.66 (s, 1H), 4.40 – 4.14 (m, 2H), 3.75 – 3.42 (m, 4H), 1.97-1.92 (m, 1H), 1.71-1.66 (m, 1H), 0.85 (s, 9H), 0.05-0.03 (m, 6H). $^{13}C\{^{1}H\}$ NMR (126 MHz, $CDCl_3$) δ 157.2, 136.5, 128.5, 128.0, 127.7, 69.8, 67.2/66.2, 59.5, 55.9, 37.8, 25.7, 17.9, -5.03, -4.8, -4.9. FTIR (cm^{-1}): 3400, 2948, 1254, 1108. HRMS-ESI (m/z) calcd for $C_{19}H_{32}NO_4Si$ [M+H]+ 366.2101. Found 366.2101.

Preparation 2:

1-benzyl 2-methyl (2*S*,4*R*)-4-((tert-butyldimethylsilyl)oxy)pyrrolidine-1,2-dicarboxylate (**IV-10**) (5.77 g, 14.7 mmol) was dissolved in dry THF and transferred to a round bottom flask. A total of 75 mL THF was added to the reaction flask, and the reaction was cooled to 0 ℃ via ice bath. Lithium borohydride (0.52 g, 23.49 mmol) was next added to the reaction mixture, and then the reaction was sealed and stirred at rt for 3 hours under nitrogen atmosphere. The reaction was quenched with 80 mL water, and then transferred to a separatory funnel for extraction. The aqueous layer was extracted three times (80 mL each) with ethyl acetate. The organic layers were then pooled and washed once with brine. The organic layer was then dried over anhydrous $MgSO_4$ and filtered. The filtrate was then concentrated *in vacuo* to yield a clear oil. The reaction was purified by automated CombiFlash chromatography (EtOAc/Hexane) to yield a clear oil as a mixture of rotamers (4.76 g, 89% yield). NMR matches spectra of previously obtained product in preparation 1.

Benzyl (2*S*,4*R*)-4-((tert-butyldimethylsilyl)oxy)-2-((1,3-dioxoisoindolin-2-yl)methyl)pyrrolidine-1-carboxylate (IV-11)

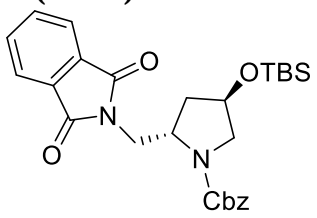

Benzyl (2*S*,4*R*)-4-((*tert*-butyldimethylsilyl)oxy)-2-(hydroxymethyl)pyrrolidine-1-carboxylate (**IV-7**) (5.97 g, 16.4 mmol), triphenyl phosphine (4.29 g, 16.4 mmol) and phthalimide (2.41 g, 16.4 mmol) were combined in a round bottom flask with stir bar and THF and cooled to 0 ℃. DEAD (7.12 g, 16.4 mmol; 40% w/w in toluene) was then added dropwise, and the reaction stirred at rt for 14 hours under nitrogen atmosphere. The solvent was then concentrated to yield a crude yellow oil. Recrystallization of triphenylphosphine oxide byproduct was conducted using cold

hexane/diethyl ether. After removal of the triphenylphosphine oxide by vacuum filtration, the filtrate was then concentrated *in vacuo* to yield a crude yellow oil. The reaction was purified by automated CombiFlash chromatography (EtOAc/Hexane) to yield the desired product (7.26 g, 90%) as a clear oil (mixture of rotamers). ^{1}H NMR (500 MHz, $CDCl_3$) δ 7.82 – 7.75 (m, 2H), 7.69-7.65 (m, 2H), 7.31 – 7.25 (m, 5H), 5.17 – 4.89 (m, 2H), 4.45 – 4.34 (m, 2H), 3.95 – 3.71 (m, 2H), 3.51 – 3.37 (m, 2H), 2.02 (m, 2H), 0.81 (s, 9H), 0.01— -0.015 (m, 6H). ^{13}C{^{1}H} NMR (126 MHz, $CDCl_3$) δ 168.4/168.3, 155.6/155.3, 136.9/136.5, 134.0/133.9, 132.1/131.9, 128.4, 127.8, 127.7, 123.3/123.25, 70.1/69.5, 67.1/66.7, 55.3/55.0, 54.8/54.3, 41.1/40.9, 38.9/38.1, 25.7, 17.9, -4.8, -4.87, -4.92, -4.98. FTIR (cm^{-1}): 3031, 2952, 1774, 1704. HRMS-ESI (m/z) calcd for $C_{27}H_{35}N_2O_5Si$ [M+H]+ 495.2315. Found 495.2307.

Benzyl (2*S*,4*R*)-2-(aminomethyl)-4-((tert-butyldimethylsilyl)oxy)pyrrolidine-1-carboxylate (IV-12)

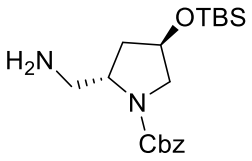

Benzyl (2*S*,4*R*)-4-((tert-butyldimethylsilyl)oxy)-2-((1,3-dioxoisoindolin-2-yl)methyl)pyrrolidine-1-carboxylate (2.55 g, 5.15 mmol) was dissolved in 100 mL ethanol and transferred to round bottom flask with stir bar. Hydrazine hydrate (2.75 mL, 56.7 mmol) was then added dropwise, and the reaction stirred at rt for 45 minutes under nitrogen atmosphere. The reaction was then heated to reflux for 1 hour via oil bath. The flask was then removed from heat and cooled via ice bath. A precipitate formed, and this was filtered and then rinsed several times with ethanol. The filtrate was then concentrated under vacuum, and The reaction was purified by automated CombiFlash chromatography (EtOAc/Hexane) to yield a pale oil as a mixture of rotamers (1.34 g, 72%).^{1}H-NMR (500 MHz, $CDCl_3$) δ 7.35-7.28 (m, 5 H), 5.17-5.07 (m, 2H), 4.37-4.35 (m, 1H), 4.04-3.98 (m, 1H), 3.58-3.40 (m, 2H), 2.94-2.77 (m, 2H), 2.00-1.84 (m, 4H), 0.85 (s, 9H), 0.05-0.03 (m,

6H). $^{13}C\{^{1}H\}$ NMR (126 MHz, $CDCl_3$) δ 155.9/155.7, 136.85/136.81, 128.5, 127.9, 127.7, 70.2/69.8, 66.9/66.7, 58.8/58.2, 55.8/55.4, 45.1/44.9, 38.7/38.2, 25.7, 17.9, -4.78, -4.84, -4.9. FTIR (cm^{-1}): 1697 (s), 1414, 832, 774, 697. HRMS-ESI (m/z) calcd for $C_{10}H_{33}N_2O_3Si$ [M+H]+ 365.2260. Found 365.2260.

Benzyl (2*S*,4*R*)-4-((tert-butyldimethylsilyl)oxy)-2-((4,5-dibromo-1*H*-pyrrole-2-carboxamido)methyl)pyrrolidine-1-carboxylate (IV-13)

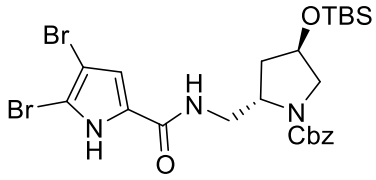

Benzyl (2*S*,4*R*)-2-(aminomethyl)-4-((tert-butyldimethylsilyl)oxy)pyrrolidine-1-carboxylate (**IV-12**) (0.491 g, 1.35 mmol) was combined in a round-bottom flask with stir-bar, and then dissolved in dimethylformamide (10 mL). 2,2,2-trichloro-1-(4,5-dibromo-1*H*-pyrrol-2-yl)ethan-1-one (**IV-3**) (0.495 g, 1.35 mmol) was then added to the stirring solution. Triethylamine (0.77 mL, 5.53 mmol) was then added to the reaction mixture dropwise via syringe. The reaction was then stirred at rt for 72 h under N_2 atmosphere. The reaction was concentrated to remove excess solvent and yield a brown residue. This was dissolved in methylene chloride and transferred to a separatory funnel. The organic layer was then extracted with water (equal volume). The organic layer was separated, and the aqueous layer was extracted twice more with methylene chloride. The organic layers were then pooled, dried over anhydrous sodium sulfate, filtered, and concentrated. The reaction was purified by automated CombiFlash chromatography (EtOAc/Hexane) to yield the desired pyrrole carboxamide as an amber oil (0.662 g, 80%). ^{1}H NMR (500 MHz, $CDCl_3$) δ 9.87 (s, 1H), 8.21 (s, 1H), 7.37-7.32 (m, 5H), 6.62 (s, 1H), 5.19 (s, 2H), 4.36-4.35 (m, 1H), 4.28 (q, *J* = 8.7 Hz, 1H), 3.73 (dd, *J*= 13.8, 4.7 Hz, 1H), 3.56 (d, *J*= 12.0 Hz, 1H), 3.44 (dd, *J*= 11.6, 4.4 Hz, 1H), 3.26-3.21 (m, 1H), 2.12-2.07 (m, 1H), 1.78-1.73 (m, 1H), 0.85 (s, 9H), 0.05-0.03 (m, 6H).

$^{13}C\{^{1}H\}$ NMR (126 MHz, $CDCl_3$) δ 159.8, 157.8, 136.3, 128.6, 128.2, 127.9, 127.2, 112.5, 105.2, 99.5, 69.8, 67.6, 56.2, 55.4, 45.8, 39.2, 25.7, 17.9, -4.8, 4.9. FTIR (cm^{-1}): 3310 (br) 3111 (br), 2950, 1676, 1631. HRMS-ESI (m/z) calcd for $C_{24}H_{34}Br_2N_3O_4Si$ [M+H]+ 616.0067. Found 616.0067.

Benzyl (2*S*,4*R*)-2-((4,5-dibromo-1*H*-pyrrole-2-carboxamido)methyl)-4-hydroxypyrrolidine-1-carboxylate (IV-14)

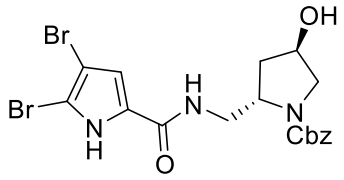

Benzyl (2*S*,4*R*)-4-((*tert*-butyldimethylsilyl)oxy)-2-((4,5-dibromo-*1H*-pyrrole-2-carboxamido)methyl)pyrrolidine-1-carboxylate (**IV-13**) (0.193 g, 0.31 mmol) was combined in a round bottom flask with stir bar, then dissolved in 5 mL dry THF. The reaction flask was sealed and cooled to 0 °C via ice bath. TBAF (0.94 mL, 0.94 mmol, 1 M solution in THF) was introduced dropwise via syringe. Following complete addition, the flask was removed from ice bath and allowed to warm spontaneously to rt. The reaction was then allowed to proceed at rt under N_2 atmosphere for 25 hours. After complete consumption of starting material was observed by TLC, the reaction mixture was transferred to a separatory funnel. The reaction was quenched with a saturated ammonium chloride solution (aqueous). The aqueous solution was then extracted three times with equal volume of methylene chloride. The organic layers were pooled, dried over anhydrous sodium sulfate, filtered, and concentrated to yield a pale-yellow oil. The reaction was purified by automated CombiFlash chromatography (EtOAc/Hexane) to afford a pale-yellow foam (0.158 g, 86% yield). ^{1}H NMR (500 MHz, DMSO-d_6) δ 12.69 (s, 1H), 8.19 (q, J = 6.6 Hz, 1H), 7.40 – 7.29 (m, 5H), 6.96-6.95 (m, 1H), 5.08 (p, J = 12.4 Hz, 2H), 4.97 (dd, J = 14.6, 3.6 Hz, 1H), 4.23-4.20 (m, 1H), 4.07 – 3.99 (m, 1H), 3.54 – 3.28 (m, 4H), 1.92-1.83 (m, 2H). $^{13}C\{^{1}H\}$ NMR

(126 MHz, DMSO-d_6) δ 159.3/159.2, 154.8/154.5, 137.0, 128.4, 128.1, 127.8/127.7, 127.52/127.50, 112.8/112.1, 104.7, 97.8, 68.1/67.7, 66.0/65.9, 56.5/55.8, 55.1/54.6, 41.3/40.8, 37.6/37.0. FTIR (cm^{-1}): 3316 (br), 3123 (br), 2938, 1673, 1631, 1184. HRMS-ESI (m/z) calcd for $C_{18}H_{20}Br_2N_3O_4$ [M+H]+ 499.9821. Found 499.9818.

Benzyl (*S*)-2-((4,5-dibromo-1*H*-pyrrole-2-carboxamido)methyl)-4-oxopyrrolidine-1-carboxylate (IV-15)

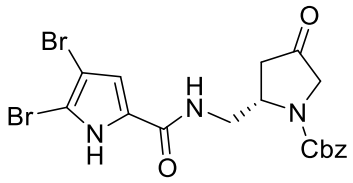

Benzyl (2*S*,4*R*)-2-((4,5-dibromo-1H-pyrrole-2-carboxamido)methyl)-4-hydroxypyrrolidine-1-carboxylate (0.100 g, 0.2 mmol) was dissolved in 1 mL dry DMSO in a round-bottom flask and combined with stir bar. IBX (0.110 g, 0.4 mmol) was then added to the reaction mixture, and the reaction was heated to 45 °C with oil bath. After 3.5 h, the flask was removed from heat and cooled to rt. Saturated sodium thiosulfate solution (1 mL) was added to the reaction flask along with 1 mL EtOAc, and the flask was stirred for 20 minutes. The reaction mixture was transferred to a separatory funnel and basified to pH 8 with a saturated sodium bicarbonate solution. The aqueous layer was then washed thrice with ethyl acetate. The organic layers were pooled, washed twice with saturate sodium bicarbonate solution, and then once with brine. The organic layer was dried with sodium sulfate, filtered and concentrated to yield a pale-yellow foam. The reaction was purified by automated CombiFlash chromatography (EtOAc/Hexane) to yield a pale-yellow foam (0.065 g, 64%). Mp: 110-112 ^{1}H NMR (500 MHz, $CDCl_3$) δ 11.39 (s, 1H), 7.51 (s, 1H), 7.32-7.28 (m, 5H), 6.62 (s, 1H), 5.17 (s, 2H), 4.67 – 4.62 (m, 1H), 4.02 (d, *J*= 19.0 Hz, 1H), 3.77 (d, *J* = 19.2 Hz, 1H), 3.62-3.56 (m, 2H), 2.83-2.77 (m, 1H), 2.53-2.40 (m, 1H). ^{13}C{^{1}H} NMR (126 MHz, $CDCl_3$) δ 209.0, 160.2, 156.3, 135.7, 128.6, 128.5, 128.1, 126.6, 113.0, 106.1, 99.6, 68.0, 54.2,

52.4, 44.6, 40.9. FTIR (cm^{-1}): 3324, 3117, 3067, 2925, 1757, 1688. HRMS-ESI (m/z) calcd for $C_{18}H_{18}Br_2N_3O_4$ [M+H]+ 497.9664, found 497.9662, 499.9654.

1-(*tert*-butyl) 2-methyl (2*S*,4*R*)-4-hydroxypyrrolidine-1,2-dicarboxylate (IV-17)

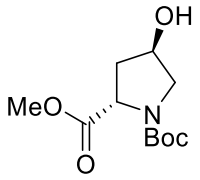

Methyl (2*S*,4*R*)-4-hydroxypyrrolidine-2-carboxylate hydrogen chloride (**IV-8**) (3.93 g, 21.6 mmol) was dissolved in 50 mL dry CH_2Cl_2 in a dry round-bottom flask equipped with stir bar. The reaction flask was cooled to 0 °C by ice bath. Triethylamine (6.03 mL, 43.3 mmol) was added by syringe, and the reaction stirred for 30 minutes in ice bath. Di-*tert*-butyl decarbonate (5.26 g, 24.1 mmol) was added to the reaction in one portion. The reaction mixture stirred for 30 minutes at 0 °C, and was allowed to stir at rt for an additional 18 h under N_2 atm. After 18 h, the reaction was transferred to a separatory funnel and was washed twice with a 10% $NaHSO_4$ aqueous solution. The organic layer was washed subsequently with 5% $NaHCO_3$ solution (2x 50 mL) and water (2 x 100 mL). The organic layer was dried over anhydrous Na_2SO_4, filtered and concentrated. The reaction was purified by automated CombiFlash chromatography (EtOAc/Hexane) to afford a clear oil (2.91 g, 55%). ^1H NMR (500 MHz, $CDCl_3$) δ 4.46-4.34 (m, 2H), 3.71 (s, 3H), 3.62-3.42 (m, 2H), 2.31-2.21 (m, 1H), 2.07-2.00 (m, 1H), 1.43-1.37 (m, 9H). $^{13}C\{^1H\}$ NMR (126 MHz, $CDCl_3$) (mixture of rotamers) δ 174.8/173.6, 154.7/154.1, 80.5/80.4, 70.2/69.4, 58.0/57.6, 54.8/54.7, 52.4/52.2, 39.2/38.5, 28.5/28.3. FTIR (cm^{-1}): 3418, 2977, 1744, 1671, 1398, 1157. HRMS-ESI (m/z) calcd for $C_{11}H_{19}NO_5Na$ [M+Na]+ 268.1161. Found: 268.1181.

1-(*tert*-butyl) 2-methyl (2*S*,4*R*)-4-((*tert*-butyldimethylsilyl)oxy)pyrrolidine-1,2-dicarboxylate (IV-18)

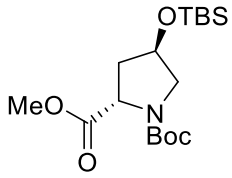

1-(*tert*-butyl) 2-methyl (2*S*,4*R*)-4-hydroxypyrrolidine-1,2-dicarboxylate (**IV-17**) (2.68 g, 10.9 mmol) was dissolved in DMF (35 mL) in dry round bottom flask equipped with stir bar. To the flask was added imidazole (1.49 g, 21.7 mmol), followed immediately by addition of TBSCl (1.81 g, 12.0 mmol). The reaction was stirred at rt under N_2 atm for 60 h. Following this, the reaction was transferred to separatory funnel. The organic layer was diluted with EtOAc and to the separatory funnel was added sat. NH_4Cl solution. The organic layer was extracted and separated, then washed once with brine. The organic layer was dried over Na_2SO_4, filtered and concentrated to afford the crude product. The reaction was purified by automated CombiFlash chromatography (EtOAc/Hexane) to afford a clear oil (3.29 g, 84%) as a mixture of rotamers. ^{1}H NMR (500 MHz, $CDCl_3$) δ 4.36-4.33 (m, 1H), 4.26 (t, *J*= 8.0 Hz, 1H), 3.66-3.66 (m, 3 H), 3.55-3.49 (m, 1H), 3.35-3.24 (m, 1H), 2.14-1.90 (m, 2H), 1.39-1.34 (m, 9H), 0.80 (s, 9H), 0.01— -0.11 (m, 6H). ^{13}C{^{1}H} NMR (126 MHz, $CDCl_3$) δ 173.7/173.5, 154.6/153.8, 80.0/79.9, 70.4/69.7, 58.0/57.6, 54.9/54.6, 52.1/51.9, 28.4/28.2, 25.7/25.6, 18.0/117.9, -0.484, -4.87. FTIR (cm^{-1}): 2952, 1749, 1699, 1394. HRMS-ESI (m/z) calcd for $C_{17}H_{33}NO_5SiNa$ [M+Na]+ 382.2020, found 382.2035.

***Tert*-butyl (2*S*,4*R*)-4-((*tert*-butyldimethylsilyl)oxy)-2-(hydroxymethyl)pyrrolidine-1-carboxylate (IV-19)**

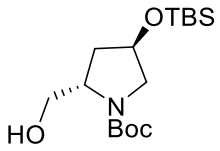

1-(*tert*-butyl) 2-methyl (2*S*,4*R*)-4-((*tert*-butyldimethylsilyl)oxy)pyrrolidine-1,2-dicarboxylate (**IV-18**) (2.98 g, 8.29 mmol) was dissolved in dry THF (60 mL) in a dry round-bottom flask

equipped with stir bar. The reaction mixture was cooled to 0 °C by ice bath. Lithium borohydride was added to the reaction flask in one portion; the reaction then stirred at rt under N_2 atm for 16 h. The reaction was then concentrated *in vacuo* to afford a crude residue, which was diluted in water. The aqueous layer was extracted three times with EtOAc, and the resulting organic layers were pooled, dried over Na_2SO_4, filtered and concentrated to afford the desired product as an oil (2.59 g, 94%). ^{1}H NMR (500 MHz, $CDCl_3$) δ 4.26 (br s, 1H), 4.07 (br s, 1H), 3.67 (d, *J* = 10.8 Hz, 1H), 3.54 (dd, *J* = 10.8, 7.3 Hz, 1H), 3.42 (d, *J* = 11.2 Hz, 1H), 3.33 (dd, *J* = 11.3, 4.0 Hz, 1H), 1.95-1.90 (m, 1H), 1.59-1.53 (m, 1H), 1.44 (s, 9H), 0.84 (s, 9H), 0.03 (s, 6H), missing exchangeable proton, spectrum matches literature data.[50] ^{13}C{^{1}H} NMR (126 MHz, $CDCl_3$) δ 157.5, 80.4, 69.9, 67.3, 59.1, 56.1, 38.0, 28.5, 25.8, 18.0, -4.7, -4.8. FTIR (cm^{-1}): 3422, 2952, 1669, 1367, 1252, 1109. HRMS-ESI (m/z) calcd for $C_{16}H_{33}NO_4SiNa$ [M+Na]+ 354.2076. Found: 354.2083.

Tert-butyl (2*S*,4*R*)-4-((_tert_-butyldimethylsilyl)oxy)-2-((1,3-dioxoisoindolin-2-yl)methyl)pyrrolidine-1-carboxylate (IV-20)

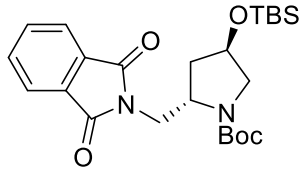

Tert-butyl (2*S*,4*R*)-4-((*tert*-butyldimethylsilyl)oxy)-2-(hydroxymethyl)pyrrolidine-1-carboxylate (**IV-19**), was dissolved in dry THF (30 mL) in a dry reaction flask equipped with stir bar. Phthalimide (0.67 g, 4.54 mmol) was added to the flask, followed immediately by addition of triphenylphosphine (1.19 g, 4.53 mmol). Lastly, DEAD (2.18 g, 5.02 mmol, 40 wt% in toluene) was finally added to the reaction by Pasteur pipette. The reaction mixture was stirred at rt overnight under N_2 atm. The following day, the reaction mixture was concentrated *in vacuo* to afford a crude residue. Recrystallization of triphenylphosphine oxide byproduct was conducted using cold hexane/diethyl ether. After removal of the triphenylphosphine oxide by vacuum filtration, the

filtrate was then concentrated *in vacuo* to yield a crude yellow oil. The reaction was purified by flash chromatography (CH_2Cl_2/MeOH) to yield the desired product as a white solid (1.54 g, 81%) as mixture of rotamers. Mp: 148-150 °C ^{1}H NMR (500 MHz, DMSO-d_6) δ 7.90-7.80 (m, 4H), 4.42-4.38 (m, 1H), 4.22-4.11 (m, 1H), 3.72 (dd, J= 14.0, 8.0 Hz, 1H), 3.61 (dt, *J*= 15.8, 4.3 Hz, 1H), 3.31-3.21 (m, 2H), 1.90-1.80 (m, 2H), 1.20-1.16 (m, 9H), 0.83-9.80 (m, 9H), 0.04-0.02 (m, 6H). ^{13}C{^{1}H} NMR (126 MHz, DMSO-d_6) δ 168.0/167.9, 154.5/153.9, 134.5/134.2, 131.8/131.7, 123.1/122.9, 78.5/78.4, 70.1/69.7, 54.6/54.1, 53.8/53.6, 38.5/37.6, 27.8/27.7, 25.6/25.5, 27.6, -4.9, -5.00, -5.03. FTIR (cm^{-1}): 3056, 2954, 1715, 1675, 1391, 1250. HRMS-ESI (m/z) calcd for $C_{24}H_{36}N_2O_5SiNa$ [M+Na]+ 483.2291. Found: 483.2291.

Tert-butyl (2*S*,4*R*)-4-((*tert*-butyldimethylsilyl)oxy)-2-((4,5-dibromo-1*H*-pyrrole-2-carboxamido)methyl)pyrrolidine-1-carboxylate (IV-21)

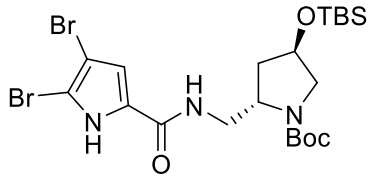

Tert-butyl (2*S*,4*R*)-4-((*tert*-butyldimethylsilyl)oxy)-2-((1,3-dioxoisoindolin-2-yl)methyl)pyrrolidine-1-carboxylate (**IV-20**) (0.900 g, 1.95 mmol) was dissolved in 25 mL EtOH in a round bottom flask equipped with stir bar. Hydrazine hydrate (0.95 mL, 19.5 mmol) was introduced to the reaction by syringe. Following complete addition of hydrazine hydrate, the reaction mixture stirred at rt for 10 minutes. The reaction flask was then refluxed by sand bath for 1 h. The reaction was cooled to rt, and the resulting crude mixture was filtered by celite plug and washed once with EtOH. The filtrate was concentrated *in vacuo* to afford the crude amine product, which was used in the next step without purification.

The crude amine was dissolved in 20 mL DMF and transferred to a round bottom flask equipped with stir bar. To the flask was added **IV-3** (0.724 g, 1.95 mmol) and triethylamine (1.12 mL, 8.04

mmol). The reaction was allowed to stir at rt for 72 h under N_2 atm. The reaction was concentrated to remove excess solvent and yield a crude residue. This was dissolved in methylene chloride and transferred to a separatory funnel. The organic layer was then extracted with water (equal volume). The organic layer was separated, and the aqueous layer was extracted twice more with methylene chloride. The organic layers were then pooled, dried over anhydrous sodium sulfate, filtered, and concentrated. The reaction was purified by automated CombiFlash chromatography (EtOAc/Hexane) to yield the desired pyrrole carboxamide as a white foam (0.798 g, 70% over two steps). Mp: 148-150 °C ^{1}H NMR (500 MHz, $CDCl_3$) δ 10.22, 6.69 (d, *J*= 2.6 Hz, 1H), 4.33 (p, *J*= 3.8 Hz, 1H), 4.24 (q, *J*= 7.5 Hz, 1H), 3.62 (dd, *J*= 13.8, 1.9 Hz, 1H), 3.49-3.46 (m, 1H), 3.37-3.26 (m, 2H), 2.10-2.06 (m, 1H), 1.76-1.71 (m, 1H), 1.49 (s, 9H), 0.86 (s, 9H), 0.06 (s, 6H). ^{13}C{^{1}H} NMR (126 MHz, $CDCl_3$) δ 159.9, 157.8, 127.4, 112.7, 105.1, 99.7, 80.9, 70.1, 54.5, 35.4, 46.7, 39.3, 28.6, 25.8, 18.0, -4.7- -4.8. FTIR (cm^{-1}): 3336, 3117, 2930, 1676, 1632. HRMS-ESI (m/z) calcd for $C_{21}H_{36}Br_2N_3O_4Si$ [M+H]+ 580.0842. Found: 580.0842.

Tert-butyl (2*S*,4*R*)-2-((4,5-dibromo-1*H*-pyrrole-2-carboxamido)methyl)-4-hydroxypyrrolidine-1-carboxylate (IV-22)

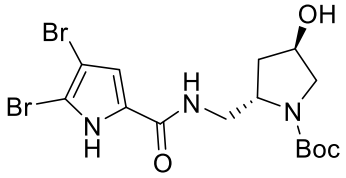

Tert-butyl (2*S*,4*R*)-4-((*tert*-butyldimethylsilyl)oxy)-2-((4,5-dibromo-1*H*-pyrrole-2-carboxamido)methyl)pyrrolidine-1-carboxylate (**IV-21**) (0.201 g, 0.35 mmol) was dissolved in 20 mL dry THF in a round-bottom flask equipped with stir bar. The reaction was cooled to 0 °C by ice bath. TBAF (0.72 mL, 0.72 mmol, 1M solution in THF) was added to by syringe. The reaction was removed from ice bath and stirred at rt under N2 atm for 20 hours. The reaction was quenched with sat. NH_4Cl solution, and then extracted three times with CH_2Cl_2. The organic layer was dried

over Na_2SO_4, dried, and filtered to afford a crude residue. The reaction was purified by automated CombiFlash chromatography (EtOAc/Hexane) was isolated as a pale-yellow solid (0.130 g, 81%). Mp: 166-168 °C ^{1}H NMR (500 MHz, DMSO-d_6) δ 12.69 (s, 1H), 8.15-8.09 (m, 1H), 6.98-6.92 (m, 1H), 4.91 (dd, *J*= 12.6, 3.0 Hz, 1H), 4.21-4.17 (m, 1H), 3.95-3.89 (m, 1H), 3.53-3.45 (m, 1H), 3.34-3.21 (m, 3H), 1.89-1.79 (m, 2H), 1.40 (s, 9H). ^{13}C{^{1}H} NMR (126 MHz, DMSO-d_6) δ 159.1, 154.5/153.9, 128.12, 112.7, 104.6, 97.8, 78.5/78.4, 68.1/67.6, 55.7/55.6, 54.7/54.3, 41.6/41.4, 37.7/37.1, 28.2/28.18. FTIR (cm^{-1}): 3276, 3109, 2932, 1663, 1628, 1402. HRMS-ESI (m/z) calcd for $C_{15}H_{22}Br_2N_3O_4$ [M+H]+ 465.9965. Found: 465.9977.

Tert-butyl (*S*)-2-((4,5-dibromo-1*H*-pyrrole-2-carboxamido)methyl)-4-oxopyrrolidine-1-carboxylate (IV-23)

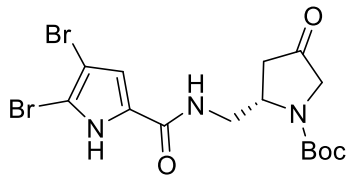

Tert-butyl (2*S*,4*R*)-2-((4,5-dibromo-1*H*-pyrrole-2-carboxamido)methyl)-4-hydroxypyrrolidine-1-carboxylate (**IV-22**) (0.131 g, 0.28 mmol) was dissolved in dry DMSO (2.0 mL) in a dry round bottom flask equipped with stir bar. IBX (0.157 g, 0.56 mmol) was next added, and the reaction mixture stirred at rt under N_2 atm for 42 h. After this time period, a 1:1 mixture of sat. $Na_2S_2O_3$ solution/EtOAc was added (4 mL total) to the reaction flask, and this stirred for 30 minutes. The reaction mixture was transferred to a separatory funnel. The aqueous layer was basified to a pH 8 with sat. $NaHCO_3$ solution, then extracted three times with EtOAc. The organic layers were pooled, dried over Na_2SO_4, filtered and concentrated to afford a crude reaction mixture. The reaction was purified by automated CombiFlash chromatography (EtOAc/Hexane) as a beige-yellow foam (0.093 g, 71%). Mp: 131-133 °C ^{1}H NMR (500 MHz, $CDCl_3$) δ 11.09 (s, 1H), 7.65 (s, 1H), 6.65 (s, 1H), 4.65-4.59 (m, 1H), 3.98 (d, *J*= 19.0 Hz, 1H), 3.71 (d, *J*= 19.0 Hz, 1H), 3.55-

3.49 (m, 2H), 2.88-2.82 (m, 1H), 2.51-2.34 (d, *J*= 18.1 Hz, 1H), 1.47 (s, 9H). $^{13}C\{^{1}H\}$ NMR (126 MHz, DMSO-d_6) δ 210.7, 159.5, 152.9, 127.8, 112.9, 104.9, 97.8, 79.2, 55.0, 54.4, 52.2, 40.5, 28.1. FTIR (cm^{-1}): 3305,3115, 2976, 2930, 1758, 1672, 1630. HRMS-ESI (m/z) calcd for $C_{15}H_{20}Br_2N_3O_4$ [M+H]+ 463.9821. Found: 465.9798.

(*S*)-4,5-dibromo-*N*-((4-oxopyrrolidin-2-yl)methyl)-1*H*-pyrrole-2-carboxamide trifluoroacetate (IV-24)

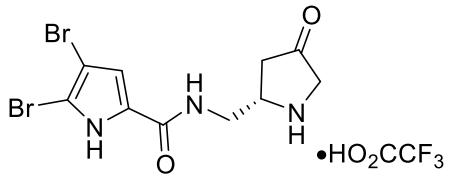

Tert-butyl (*S*)-2-((4,5-dibromo-1*H*-pyrrole-2-carboxamido)methyl)-4-oxopyrrolidine-1-carboxylate (**IV-23**) (0.047 g, 0.1 mmol) was dissolved int CH_2Cl_2 (1.0 mL) in a dry round bottom flask equipped with stir bar. Trifluoroacetic acid (0.08 mL, 1.0 mmol) was added via syringe, and the reaction was stirred at rt. The next morning, the reaction was diluted with 1.0 mL CH_2Cl_2, and an additional amount of trifluoroacetic acid (0.08 mL, 1.0 mmol) was added to the reaction, and it was stirred for an additional 24 hours. The following day, an additional 1.0 mL CH_2Cl_2 and trifluoroacetic acid (0.1 mL, 0.13 mmol) was added, and the reaction stirred for a total of 3 days under N_2 atm. After this time period, the reaction was concentrated to afford a crude oil. The excess trifluoroacetic acid was removed by azeotropic evaporation using toluene to afford a light green solid (0.047 g, 97%). ^{1}H NMR (500 MHz, $CDCl_3$) δ 12.82 (s, 1H), 9.92 (s, 1H), 8.75 (s, 1H), 8.53 (t, *J*= 5.8 Hz, 1H), 6.95 (d, *J*= 2.6 Hz, 1H), 4.10 (s, 1H), 3.76-3.63 (m, 4H), 2.70 (dd, *J*= 18.5 Hz, 7.6 Hz, 1H), 2.47 (dd, *J*= 18.5 Hz, 10.6 Hz, 1H). Mp: 200 °C (decomp) FTIR (cm^{-1}): 3125, 2952, 1711, 1671, 1391. HRMS-ESI (m/z) calcd for $C_{10}H_{12}Br_2N_3O_2$ [M+H]+ 363.9296. Found: 363.9298.

Pyrrole-2-carboxylic acid (IV-28)

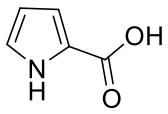

2-trichloroacetylpyrrole (**IV-2**) (9.572 g, 45.0 mmol) was dissolved in 75 mL of 1 N NaOH aqueous solution and heated to reflux for 30 minutes. The reaction flask was removed from heat and cooled to rt. The pH of the solution was adjusted from 11 to pH 2 with 1.2 M aqueous HCl solution, and a brown solid precipitated from the acidic solution. The reaction mixture was transferred to a separatory funnel and the aqueous layer was washed 3 times with ethyl acetate (200 mL ea.). The organic layers were pooled, dried over anhydrous Na_2SO_4, filtered and concentrated by rotary evaporator to afford a dark brown solid product (4.5718 g, 91%). m.p. 200°C (decomp). ^{1}H NMR (500 MHz, DMSO-d_6) δ 12.22 (s, 1H), 11.71 (s, 1H), 6.95 (s, 1H), 6.72 (s, 1H), 6.13 (s, 1H). ^{13}C{^{1}H} NMR (126 MHz, DMSO-d_6) δ 162.0, 123.5, 122.9, 114.7, 109.34. FTIR (cm^{-1}): 3347, 3120, 1649. HRMS-ESI (m/z) calcd for $C_5H_4NO_2$ [M-H]- 110.0242. Found: 110.0225.

methyl (1*H*-pyrrole-2-carbonyl)-*L*-prolinate (IV-29)

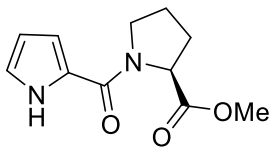

Pyrrole-2-carboxylic acid (**IV-28**) (1.51 g, 13.6 mmol) and *L*-proline methyl ester hydrochloride (5.83 g, 35.3 mmol) were combined in a dry round-bottom flask with dry dichloromethane (150 mL) and stir bar. The flask was cooled to 0 ̊C with ice bath, and 4-dimethylaminopyridine (DMAP) (1.69 g, 13.9 mmol) was added. EDCI-HCl (5.51 g, 28.7 mmol) was next added to the reaction, and the reaction mixture was stirred for 15 minutes at 0 ̊C. The ice bath was removed and reaction

stirred at rt for an additional 30 minutes. Following complete conversion of pyrrole-2-carboxylic acid, the reaction mixture was transferred to a separatory funnel. The organic layer was washed with H_2O (130 mL), then separated. The aqueous layer was washed twice with dichloromethane (2x150 mL). The organic layers were pooled, dried over Na_2SO_4, filtered and concentrated to afford a crude brown oil. The reaction was purified by automated CombiFlash chromatography (EtOAc/Hexane) to afford the product as an oily solid (2.62 g, 87%). mp: 75-77 °C ^{1}H NMR (500 MHz, $CDCl_3$) δ 10.9 (s, 1H), 6.95-6.94 (m, 1H), 6.65-6.63 (m, 1H), 6.23 – 6.21 (m, 1H), 4.67 (dd, *J* = 7.8, 4.6 Hz, 1H), 3.95 – 3.81 (m, 2H), 3.70 (s, 3H), 2.22 – 2.10 (m, 2H), 2.04-1.96 (m, 2H). ^{13}C{^{1}H} NMR (126 MHz, $CDCl_3$) δ 173.0, 160.7, 125.0, 122.2, 112.9, 109.6, 60.2, 52.1, 48.3, 28.7, 25.4. FTIR (cm^{-1}): 3210, 2950, 1746, 1578, 1166. HRMS-ESI (m/z), calcd for $C_{11}H_{14}N_2O_3$ $[M+Na]^+$: 245.0902. Found: 245.1028.

(1*H*-pyrrole-2-carbonyl)-*L*-proline (IV-30)

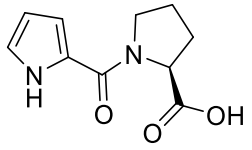

Ester **IV-29** (1.81 g, 8.1 mmol) was dissolved in 25 mL of 1 N NaOH aqueous solution and heated to reflux for 1 hour. The reaction flask was removed from heat and cooled to rt. The pH of the solution was adjusted from 11 to pH 2 with 1.2 M aqueous HCl solution, and a white solid precipitated from the acidic solution. The reaction mixture was transferred to a separatory funnel and the aqueous layer was washed 3 times with ethyl acetate (60 mL ea.). The organic layers were pooled, dried over anhydrous Na_2SO_4, filtered and concentrated by rotary evaporator to afford a white solid (1.53 g, 90%). m.p.: 169 °C (decomp). ^{1}H NMR (500 MHz, DMSO-d_6) δ 12.49 (s, 1H), 11.46 (s, 1H), 6.95-6.87 (m, 1H), 6.65 (s, 1H), 6.16 (d, *J* = 2.7 Hz, 1H), 4.41 (dd, *J* = 8.4, 4.4 Hz, 1H), 3.78 (t, *J* = 6.7 Hz, 2H), 2.22-2.14 (m, 1H), 2.00 – 1.96 (m, 2H), 1.89-1.83 (m, 1H).

$^{13}C\{^{1}H\}$ NMR (126 MHz, DMSO-d_6) δ 173.8, 159.8, 125.2, 121.8, 112.5, 109.1, 109.09, 59.7, 48.1, 28.3, 25.0. FTIR (cm^{-1}): 3345, 3246, 2959, 1711, 1693. HRMS-ESI (m/z), calcd for $C_{10}H_{13}N_2O_3$ $[M+H]^+$: 209.0926. Found: 209.0988.

(*S*)-*N*-methoxy-*N*-methyl-1-(*1H*-pyrrole-2-carbonyl)pyrrolidine-2-carboxamide (IV-31)

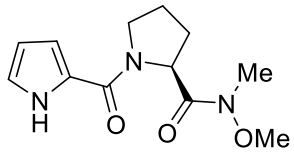

Carboxylic acid (**IV-30**) (1.33 g, 6.4 mmol), N,O-dimethoxyhydroxylamine hydrochloride (1.85 g, 18.9 mmol) and DMAP (0.237 g, 1.9 mmol) were combined in a round bottom flask with dry CH_2Cl_2 (70 mL). The reaction was cooled with ice bath, and EDCI (2.57 g, mmol) was added to the reaction. The reaction stirred at 0 °C for 15 minutes and was heated to reflux over sandbath for 2.5 hours. The flask was cooled to rt and transferred to a separatory funnel. The organic layer was extracted with saturated sodium bicarbonate solution (50 mL). The layers were separated and the aqueous layer washed two additional times with 70 mL CH_2Cl_2. The organic layers were pooled, dried over Na_2SO_4, filtered and concentrated in vacuo to yield a crude solid. The solid was triturated in hexanes and isolated by vacuum filtration to yield a beige solid (1.39 g, 87%). Mp: 164-165 °C. ^{1}H NMR (500 MHz, $CDCl_3$) δ 9.66 (s, 1H), 6.92-6.90 (m, 1H), 6.67 (s, 1H), 6.26 (q, *J* = 3.1 Hz, 1H), 5.11-5.09 (m, 1H), 4.03-3.98 (m, 1H), 3.90 – 3.86 (m, 4H), 3.23 (s, 3H), 2.27-2.17 (m, 2H), 2.07 – 1.93 (m, 2H). $^{13}C\{^{1}H\}$ NMR (126 MHz, $CDCl_3$) δ 172.8, 160.4, 125.7, 121.3, 112.7, 110.1, 61.4, 57.9, 48.7, 32.3, 28.6, 25.3. FTIR (cm^{-1}): 3208, 3091, 2966, 1658. HRMS-ESI (m/z) calcd for $C_{12}H_{17}N_3O_3Na$ $[M+Na]^+$: 274.1168. Found: 274.1183.

***(S)*-*N*-methoxy-*N*-methyl-1-(1-tosyl-1*H*-pyrrole-2-carbonyl)pyrrolidine-2-carboxamide (IV-32)**

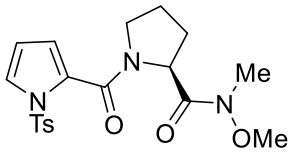

Weinreb amide (**IV-31**) (0.519 g, 2.07 mmol) was dissolved in dry THF (23 mL) in an oven-dried round-bottomed flask equipped with stir bar. The reaction flask was cooled to 0 °C with ice bath, and sodium hydride (0.173 g (60 wt% oil dispersion), 4.14 mmol) was added in one portion. The reaction stirred for 30 minutes, and *p*-tolylsulfonyl chloride (0.637 g, 3.34 mmol) was added to the flask. The flask was warmed to rt overnight. The reaction mixture was slowly quenched with 30 mL water, and this mixture was transferred to separatory funnel. The aqueous layer was extracted three times (3x50 mL) with ethyl acetate. Organic layers were pooled, dried over Na_2SO_4, filtered and concentrated to yield a white foam (0.7389 g, 88%) as a 1:1 mix of rotamers. Mp: 96-98 °C. ^{1}H NMR (500 MHz, $CDCl_3$) δ 7.96 (dd, *J* = 8.3, 2.9 Hz, 4H), 7.31 (d, *J* = 8.2 Hz, 2H), 7.27 (d, *J* = 8.3 Hz, 2H), 7.18 (dd, *J* = 3.1, 1.5 Hz, 1H), 7.16 (dd, *J* = 3.1, 1.6 Hz, 1H), 6.46 (dd, *J* = 3.3, 1.6 Hz, 1H), 6.24 (t, *J* = 3.2 Hz, 1H), 6.20 (dd, *J* = 3.3, 1.6 Hz, 1H), 6.16 (t, *J* = 3.2 Hz, 1H), 5.12 (t, *J* = 5.9 Hz, 1H), 4.66 (d, *J* = 8.5 Hz, 1H), 3.88 (s, 3H), 3.86-3.76 (m, 2H), 3.60-3.50 (m, 2H), 3.31 (s, 3H), 3.22 (s, 3H), 3.09 (s, 3H), 2.39 (s, 3H), 2.38 (s, 3H), 2.35 –2.26 (m, 2H), 2.09-1.87 (m, 6H). ^{13}C{^{1}H} NMR (126 MHz, $CDCl_3$) δ 172.9/171.7, 162.0/161.3, 145.5/145.0, 135.6/135.1, 129.78/ 129.6, 129.3/129.0, 128.1/128.0, 122.72/121.71, 114.8/114.1, 112.1/111.9, 61.3/61.0, 59.4/56.5, 49.6/46.9, 30.5/29.4, 24.8/22.8, 21.69/21.65. FTIR (cm^{-1}): 3127, 3062, 2979, 1683. HRMS-ESI (m/z) calcd for $C_{19}H_{23}N_3O_5SNa$ $[M+Na]^+$ 428.1256. Found: 428.1272.

(*S*)-1-(1-tosyl-1*H*-pyrrole-2-carbonyl)pyrrolidine-2-carbaldehyde (IV-33)

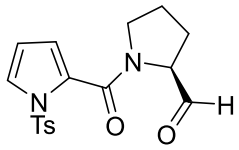

Compound **IV-32** (0.777 g, 1.9 mmol) was dissolved in dry THF (4 mL) in a round-bottom flask equipped with stir bar. The flask was cooled to -78 ˚C with cold bath, and DIBAL (1M in THF, 5.75 mL, 5.75 mmol) was added dropwise to the reaction mixture. The reaction was stirred at -78 °C for 1.5 h before slow quenching with 8 mL of MeOH/HCl (1:1, 1.2 N HCl). The cold bath was removed and the reaction flask warmed to rt before transfer to a separatory funnel. The aqueous layer was washed several times with CH_2Cl_2 (3x40 mL). The organic layers were pooled, dried over Na_2SO_4, filtered and concentrated to yield a crude oil. The reaction was purified by automated CombiFlash chromatography (EtOAc/Hexane) to afford the desired aldehyde (0.374 g, 56%) as a ~ 3:1 mixture of rotamers. Starting material was also recovered from the reaction (24%). Mp: 97-99 °C ^{1}H NMR (500 MHz, $CDCl_3$) δ 9.73 (d, *J* = 2.3 Hz, 1H), 9.44 (s, 0.3H), 7.93-7.89 (m, 2.6H), 7.32-7.29 (m, 2.6H), 7.25 (dd, *J* = 3.2, 1.5 Hz, 1H), 7.19-7.18 (m, 0.3H), 6.41 (dd, *J* = 3.3, 1.5 Hz, 1H), 6.26 (t, *J* = 3.3 Hz, 1H), 6.24-6.23 (m, 0.3H), 6.18 (t, *J* = 3.0 Hz, 0.3H), 4.57-4.54 (m, 1H), 4.38 (dd, *J* = 7.7, 2.7 Hz, 0.3 H), 3.87-3.69 (m, 0.6 H), 3.62-3.53 (m, 2H), 2.39 (s, 4H), 2.27-217 (m, 1.3H), 2.11-2.06 (m, 1.3H), 2.00-1.86 (m, 2.6H). ^{13}C{^{1}H} NMR (126 MHz, $CDCl_3$) (only major rotamer peaks reported) δ 200.2, 162.5, 145.4, 135.3, 129.8, 128.4, 128.0, 123.2, 114.5, 112.1, 65.0, 49.4, 26.8, 25.0, 21.7. FTIR (cm^{-1}): 3136, 2919, 1726, 1609, 1151. HRMS-ESI (m/z) calcd for $C_{17}H_{19}N_2O_4S$ $[M+H]^+$ 347.1066 Found: 347.1118.

1-tosyl-1,5,6,7-tetrahydro-9*H*-pyrrolo[2,3-f]indolizin-9-one *(*IV-34*)* and isomer (IV-35)

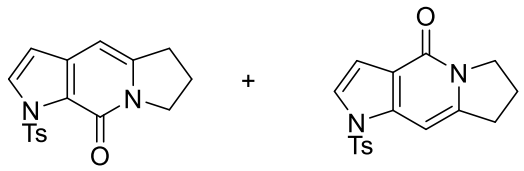

IV-34 **IV-35**

Aldehyde **IV-33** (1.01 g, 2.90 mmol) was dissolved in DCE (40 mL) in a dry round-bottom flask equipped with stir bar. To the reaction was added TFA (1.12 mL, 14.6 mmol) via syringe. The reaction flask was heated to reflux with sand bath for 20 hours. After complete consumption of the starting material, the reaction was removed from heat and cooled to rt. The reaction mixture was transferred to a separatory funnel and neutralized with saturated sodium bicarbonate solution (40 mL). The organic layer was separated, and the aqueous layer was washed two additional times with CH_2Cl_2 (80 mL ea). The organic layers were pooled and dried over Na_2SO_4, filtered and concentrated to yield a crude solid. The reaction was purified by automated CombiFlash chromatography (EtOAc/Hexane) to afford a beige solid **IV-34** as the major product (0.757 g, 79%). M.p: 221 °C (decomp). ^{1}H NMR (500 MHz, $CDCl_3$) δ 8.03 (d, *J* = 8.5 Hz, 2H), 7.83 (d, *J* = 3.4 Hz, 1H), 7.29 (d, *J* = 8.2 Hz, 2H), 6.37 (d, *J* = 3.5 H, 1H), 6.26 (t, *J* = 1.3 Hz, 1H), 4.09 (t, *J* = 7.2 Hz, 2H), 3.02 (td, *J* = 7.7, 1.2 Hz, 2H), 2.38 (s, 3H), 2.15 (p, *J* = 7.5 Hz, 2H). ^{13}C{^{1}H} NMR (126 MHz, $CDCl_3$) δ 152.6, 144.8, 144.7, 138.2, 136.3, 130.9, 129.6, 128.8, 121.8, 106.0, 95.1, 48.3, 31.3, 22.5, 21.8. FTIR (cm^{-1}): 3153, 2954, 1664. HRMS-ESI (m/z) calcd for $C_{17}H_{18}N_2O_3SNa$ $[M+Na]^+$: 351.0779 Found: 351.0798.

IV-35 was isolated as a minor byproduct in the above-described reaction as a brown solid (0.126 g, 13%).Mp: 184-186 °C ^{1}H NMR (500 MHz, $CDCl_3$) δ 7.75 (d, *J* = 8.3 Hz, 2H), 7.30-7.27 (m, 2H), 6.87 (s, 1H), 6.85 (d, *J*= 3.5 Hz, 1H), 4.14 (t, *J* = 7.1 Hz, 2H), 3.13 (t, *J* = 7.6 Hz, 2H), 2.39

(s, 3H), 2.23 (p, *J* = 7.5 Hz, 2H). $^{13}C\{^{1}H\}$ NMR (126 MHz, $CDCl_3$) δ 158.0, 146.6, 145.7, 140.4, 135.3, 130.3, 127.0, 123.3, 117.6, 109.2, 91.1, 48.2, 31.9, 22.3, 21.8. FTIR (cm^{-1}): 3144, 2952, 1660. HRMS-ESI (m/z), calcd for $C_{17}H_{19}N_2O_3S$ $[M+H]^+$: 329.0960, Found: 329.0969.

4-bromo-1-tosyl-1,5,6,7-tetrahydro-9*H*-pyrrolo[2,3-f]indolizin-9-one (IV-40)

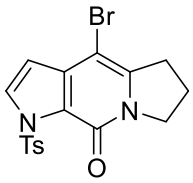

Tricycle **IV-34** (0.109 g, 0.33 mmol) was dissolved in dry CH_2Cl_2 (4 mL) in a dry round-bottom flask. To the flask was added *N*-bromosuccinimide (0.0652 g, 0.33 mmol) in one portion. The reaction was stirred at rt for 24 h before workup. The reaction mixture was transferred to separatory funnel and diluted with 12 mL CH_2Cl_2. The organic layer was washed once with brine (20 mL) and separated. The aqueous layer was extracted once more with CH_2Cl_2 (20 mL). The organic layers were pooled, dried over Na_2SO_4, filtered and concentrated to afford a crude solid. T The reaction was purified by automated CombiFlash chromatography (EtOAc/Hexane) to afford a solid. This solid was precipitated from a minimal amount of cold ethyl acetate (0.078 g, 58%). Mp: 178-180 °C. ^{1}H NMR (500 MHz, $CDCl_3$) δ 8.02 (d, *J* = 7.7 Hz, 2H), 7.90-7.89 (m, 1H), 7.31 (d, *J* = 8.0 Hz, 2H), 6.51- 6.49 (m, *J* = 3.5, 1H), 4.18 (t, *J* = 7.3 Hz, 2H), 3.08 (t, *J* = 7.6 Hz, 2H), 2.40 (s, 3H), 2.18 (p, *J* = 6.8 Hz, 2H). $^{13}C\{^{1}H\}$ NMR (126 MHz, $CDCl_3$) δ 151.8, 145.2, 143.1, 138.3, 135.9, 131.0, 129.7, 128.9, 121.5, 106.0, 88.6, 50.0, 32.5, 21.9, 21.8. FTIR (cm^{-1}): 3205, 3007, 2952, 1673. HRMS-ESI (m/z), calcd for $C_{17}H_{16}BrN_2O_3S$ $[M+H]^+$: 407.0065 Found: 407.0088.

1-(4-methoxybenzyl)guanidine hemisulfate (IV-41)

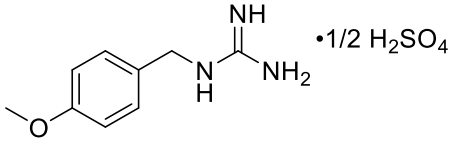

S-methylthiouronium sulfate (2.61 g, 9.4 mmol) was dissolved in water/ethanol (1:1, 50 mL) in a round bottom flask equipped with stir bar. 4-methoxybenzylamine (2.43 mL, 18.7 mmol) was added and the flask was stirred at reflux for 24 hours. The reaction was removed from heat and its volume reduced under vacuum evaporation. The product was recrystallized from ethanol/water. The resulting yellow solid was isolated by vacuum filtration and washed with a minimal amount of water, and then dried by vacuum filtration for several hours before storage. The desired product was isolated as a yellow solid (1.96 g, 48%) and matched literature data.[32] Mp: 212-125 °C. ^{1}H NMR (500 MHz, DMSO-d_6) δ 8.88 (br s, 1H), 7.78 (br s, 3H), 7.24 (d, J = 8.7 Hz, 2H), 6.87 (d, J = 8.7 Hz, 2H), 4.17 (d, J = 5.7 Hz, 2H), 3.71 (s, 3H). FTIR (cm^{-1}): 3462, 3323, 3007, 2952, 1609. HRMS-ESI (m/z), calcd for $C_9H_{14}N_3O$ $[M+H]^+$: 180.1137, Found: 180.1146.

4-bromo-1,5,6,7-tetrahydro-9*H*-pyrrolo[2,3-f]indolizin-9-one (IV-45)

Compound **IV-40** (0.167 g, 0.44 mmol), cyanamide (0.0182 g, 0.44 mmol), 1,10-phenanthroline (0.0149 g, 0.08 mmol), copper (I) iodide (0.0074 g, 0.04 mmol) and cesium carbonate (0.142 g, 0.44 mmol) were combined in a dry Schlenk tube with stir bar. The tube was flushed with nitrogen gas, and dry degassed DMSO (0.8 mL) was added via syringe. The tube was sealed and heated by oil bath to 80 °C for 14 hours. The tube was removed from heat and transferred to a separatory funnel. The solution was diluted in water (2 mL) and extracted with ethyl acetate (10 mL). The aqueous layer was additionally washed with dichloromethane (2 x 10mL). Organic layers were pooled, dried with Na_2SO_4 filtered and concentrated. The reaction was purified by automated CombiFlash chromatography (CH_2Cl_2/MeOH) to afford a crude mixture of starting material and

IV-45. The detosylated tricycle (**IV-45**) was afforded following precipitation from cold dichloromethane as a white solid (0.049 g, 47%). Mp: 225 °C (decomp). ^{1}H NMR (500 MHz, DMSO-d_6) δ 12.24 (s, 1H), 7.32 (t, J = 2.8 Hz, 1H), 6.22 (t, J = 2.4 Hz, 1H), 4.10 (t, J = 7.2 Hz, 2H), 3.05 (t, J = 7.6 Hz, 2H), 2.16 (p, J = 7.4 Hz, 2H). ^{13}C{^{1}H} NMR (126 MHz, DMSO-d_6) δ 152.6, 138.8, 131.3, 127.3, 122.3, 102.1, 88.6, 48.8, 31.5, 21.6. FTIR (cm^{-1}): 3122, 3016, 2920, 1642. HRMS-ESI (m/z) calcd for $C_{10}H_{11}BrN_2O$ [M+H]$^{+}$: 252.9977, Found: 252.9998.

4-iodo-1-tosyl-1,5,6,7-tetrahydro-9*H*-pyrrolo[2,3-f]indolizin-9-one (IV-47)

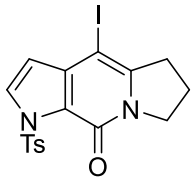

Tricycle **IV-34** (0.100 g, 0.33 mmol) was dissolved in dry CH_2Cl_2 (8 mL) in a dry round-bottom flask. To the flask was added *N*-iodosuccinimide (0.076 g, 0.36 mmol) in one portion. The reaction was stirred at rt for 24 h before workup. The reaction was quenched with saturated $Na_2S_2O_3$ (< 2mL), and the reaction was stirred for 10 minutes before transfer to separatory funnel. The reaction mixture was transferred to separatory funnel and diluted with 6 mL water. The layers were extracted and separated. The aqueous layer was extracted twice more with CH_2Cl_2 (8 mL ea). The organic layers were pooled, dried over Na_2SO_4, filtered and concentrated to afford a crude solid. The reaction was purified by automated CombiFlash chromatography (EtOAc/Hexane). This solid was precipitated from a minimal amount of cold ethyl acetate (0.066 g, 48%). Mp: 131-133 °C. ^{1}H NMR (500 MHz, $CDCl_3$) δ 8.01 (d, J = 8.4 Hz, 1H), 7.89 (d, J =3.5 Hz, 1H), 7.30 (d, J = 8.1 Hz, 2H), 6.40 (d, J = 3.5 Hz, 1H), 4.23 (t, J = 7.3 Hz, 2H), 3.07 (t, J = 7.7 Hz, 2H), 2.39 (s, 3H), 2.17 (p, J = 7.6 Hz, 2H). ^{13}C{^{1}H} NMR (126 MHz, $CDCl_3$) δ 152.0, 146.7, 145.1, 140.8, 135.9, 130.6,

129.7, 128.9, 120.7, 109.0, 57.6, 50.5, 35.7, 21.9, 21.5. FTIR (cm^{-1}): 3158, 2898, 1662, 1148. HRMS-ESI (m/z), calcd for $C_{17}H_{16}IN_2O_3S$ $[M+H]^+$: 484.9926 Found: 484.9968.

4-iodo-1,5,6,7-tetrahydro-9*H*-pyrrolo[2,3-f]indolizin-9-one (IV-49)

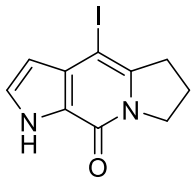

Compound **IV-47** (0.045 g, 0.1 mmol), cyanamide (0.018 g, 0.43 mmol), 1,10-phenanthroline (0.0063g, 0.035 mmol), copper (I) iodide (0.0074 g, 0.02 mmol) and cesium carbonate (0.0394g, 0.12 mmol) were combined in a dry Schlenk tube with stir bar. The tube was flushed with nitrogen gas, and dry degassed DMSO (1.0 mL) was added via syringe. The tube was sealed and heated by oil bath to 85 ℃ for 24 hours. The tube was removed from heat and transferred to a separatory funnel. The solution was diluted in water (2 mL) and extracted three times with ethyl acetate (3x15 mL). The aqueous layer was inundated with solid sodium chloride and washed two additional times with ethyl acetate (2x30 mL). Organic layers were pooled, dried with Na_2SO_4 filtered and concentrated. The detosylated tricycle (**IV-49**) was afforded following precipitation from cold dichloromethane as a white solid (7.6 mg, 25%). Mp: 194 °C (decomp). ^{1}H NMR (500 MHz, DMSO-d_6) δ 12.21 (s, 1H), 7.30 (d, J = 2.7 Hz, 1H), 6.09 (d, J = 2.7 Hz, 1H), 4.15 (t, J = 7.2 Hz, 2H), 3.04 (t, J = 7.6 Hz, 2H), 2.14 (p, J = 7.5 Hz, 2H). ^{13}C{^{1}H} NMR (126 MHz, DMSO-d_6) δ 152.9, 142.1, 134.3, 126.7, 121.4, 104.9, 59.3, 49.2, 34.7, 21.38. FTIR (cm^{-1}): 3100, 3044, 2908, 1643. HRMS-ESI (m/z) calcd for $C_{10}H_{11}IN_2O$ $[M+H]^+$: 330.9838, Found: 330.9761.

9-oxo-1-tosyl-5,6,7,9-tetrahydro-1*H*-pyrrolo[2,3-f]indolizine-4-carbonitrile (IV-50)

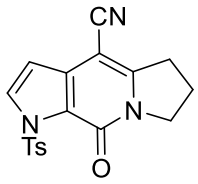

$Pd_2(dba)_3$ (0.033 g, 0.04 mmol), 1,1-Bis(diphenylphosphino)-ferrocene (0.030 g, 0.05 mmol), and zinc (II) cyanide (0.077 g, 0.65 mmol) were combined in a dry round-bottom flask equipped with stir bar. To the flask was added DMF (1.5 mL) and deionized water (0.02 mL). The heteroaryl iodide **IV-47** (0.197 g, 0.43 mmol, dissolved in 1 mL DMF) was introduced to the reaction at rt. The reaction was heated to 110 ° C and stirred for 22 hours under Argon atmosphere. Upon complete consumption of the starting material, the reaction mixture was removed from heat and cooled to rt. The mixture was diluted in 15 mL each of brine solution and ethyl acetate and transferred to a separatory funnel. The mixture was extracted and separated. The organic layer was filtered through a celite plug and then washed with ethyl acetate. The resulting filtrate was dried over sodium sulfate, filtered and concentrated *in vacuo* to yield a dark brown residue. The reaction was purified by automated CombiFlash chromatography (EtOAc/Hexane) to afford a light brown solid (0.149 g, 97%). ^{1}H NMR (500 MHz, $CDCl_3$) δ 8.01 (d, *J* = 8.0 Hz, 2H), 7.95 (d, *J* = 3.1 Hz, 1H), 7.32 (d, *J* = 8.0 Hz, 2H), 6.59 (d, *J* = 3.0 Hz, 1H), 4.16 (t, *J* = 7.3 Hz, 2H), 3.29 (t, *J* = 7.8 Hz, 2H), 2.41 (s, 3H), 2.26 (p, *J* = 7.4 Hz, 2H). $^{13}C\{^1H\}$ NMR (126 MHz, $CDCl_3$) δ 154.1, 151.7, 145.6, 135.8, 135.4, 132.1, 129.8, 129.0, 120.8, 115.6, 104.2, 81.3, 49.2, 32.0, 21.9, 21.3. FTIR (cm^{-1}): 3154, 3016, 2972, 2221, 1660. mp: 215-217 °C. HRMS-ESI (m/z) calcd for $C_{18}H_{17}N_3O_3S$ [M+H]+ 354.0912, found: 354.0913.

_N'_-hydroxy-9-oxo-1-tosyl-5,6,7,9-tetrahydro-1_H_-pyrrolo[2,3-f]indolizine-4-carboximidamide (IV-51)

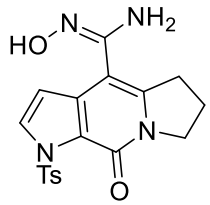

Nitrile **IV-50** (0.0278 g, 0.08 mmol) was suspended in EtOH (1.25 mL) in a round bottom flask equipped with stir bar. Hydroxylamine solution (0.033 g, 0.5 mmol, 50 wt% in H_2O) was added to the flask, and the reaction was heated to reflux by sandbath. The reaction was monitored by TLC. After 25 h, additional hydroxylamine solution (0.044 g, 0.67 mmol, 50 wt% in H_2O) was added to the solution. After 3 h, an additional amount of hydroxylamine solution (0.052 g, 0.078 mmol, 50 wt% in H_2O) was added to the reaction. After a total of 32 hours, the reaction mixture was removed from heat and concentrated to remove excess solvent. The reaction mixture was purified by flash chromatography (CH_2Cl_2/MeOH) to afford the desired product as a white solid (10.4 mg, 34%). ^{1}H NMR (500 MHz, DMSO-d_6) δ 9.45 (s, 1H), 7.98 – 7.89 (m, 3H), 7.41 (d, J = 8.0 Hz, 2H), 6.64 (d, J = 3.6 Hz, 1H), 5.72 (s, 2H), 3.93 (t, J = 7.1 Hz, 2H), 3.11 (t, J = 7.7 Hz, 2H), 2.37 (s, 3H), 2.04 (p, J = 7.4 Hz, 2H). HRMS-ESI (m/z) calcd for $C_{18}H_{19}N_4O_4S$ [M+H]+ 387.1127 found: 387.1133.

9-oxo-1-tosyl-5,6,7,9-tetrahydro-1_H_-pyrrolo[2,3-f]indolizine-4-carboxamide (IV-52)

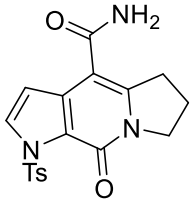

^{1}H NMR (500 MHz, DMSO-d_6) δ 7.95 (d, J = 3.5 Hz, 1H), 7.93 (d, J = 8.3 Hz, 2H), 7.42 – 7.40 (m, 4H), 6.75 (d, J = 3.5 Hz, 1H), 3.93 (t, J = 7.1 Hz, 2H), 3.23 (t, J = 7.4 Hz, 2H), 2.37 (s, 3H),

2.07 (p, *J* = 7.9 Hz, 2H). $^{13}C\{^{1}H\}$ NMR (126 MHz, DMSO-d_6) δ 166.8, 150.9, 146.5, 145.1, 136.0, 135.4, 131.0, 129.6, 128.3, 120.4, 106.8, 104.8, 48.3, 31.5, 21.5, 21.1. HRMS-ESI (m/z) calcd for $C_{18}H_{18}N_3O_4S$ [M+H]+ 372.1018, found: 372.1022.

REFERENCES

1. Chu, M.-J.; Li, M.; Ma, H.; Li, P.-L.; Li, G.-Q., *RSC Adv.,* **2022**, *12*, 7789-7820.

2. Kubota, T.; Araki, A.; Ito, J.; Mikami, Y.; Fromont, J.; Kobayashi, J., *Tetrahedron,* **2008**, *64*, 10810-10813.

3. Feldman, K. S.; Fodor, M. D., *J. Am. Chem. Soc.,* **2008**, *130*, 14964-14965.

4. Picon, S.; Dau, E. T. T.; Martin, M.-T.; Retallieau, P.; Zaparucha, A.; Al-Mourabit, A., *Org. Lett.,* **2009**, *11*, 2523-2526.

5. Su, S.; Rodriguez, R. A.; Baran, P. S., *J. Am. Chem. Soc.*, **2011**, *133*, 13922-13925.

6. Ding, H.; Roberts, A. G.; Harran, P. G., *Angew. Chem., Int. Ed. Engl.,* **2012**, *51*, 4340-4343.

7. Nishimura, T.; Kitajima, K., Reactions of guanidines with a-diketones. *J. Org. Chem.,* **1979**, *44*, 818-824.

8. Little, T. L.; Webber, S. E., *J. Org. Chem.,* **1994**, *59*, 7299-7305.

9. Kimpe, N. G.; Stevens, C. V.; Keppens, M. A.,. *Agric. Food. Chem.,* **1993**, 1458-1461.

10. Bowers, M. M.; Carroll, P.; Joullie, M. M., *J. Chem. Soc. Perkin Trans.,* **1989**, *1*, 857-865.

11. de Graaf, C.; Bensch, L.; van Lint, M. J.; Ruijter, E.; Orru, R. V. A., *Org. Biomol. Chem.,* **2015,** *13*, 10108-10112.

12. Naidu, P. S.; Kolita, S.; Sharma, M.; Bhuyan, P. J., *J. Org. Chem.,* **2015,** *80*, 6381-6390.

13. Kenso, S.; Hidekazu, O.; Masako, T., *Bull. Chem. Soc. Jpn.* **1984**, *57*, 2327-2328.

14. Friedemen, N.; Eustergerling, A.; Nubbemeyer, U., *Eur. J. Org. Chem.,* **2012**, *4*, 837-843.

15. Weise, K. J.; Yakushijin, K.; Horne, D. A., *Tetrahedron Lett.,* **2002**, *43*, 5135-5136.

16. Goetz, G. H.; Harrigan, G. C.; Likos, J., *J. Nat. Prod.,* **2001**, *64*, 1581-1582.

17. Moldovan, R.-P.; Lindel, T., *Z. Naturforsch,* **2009**, *64*, 1612-1616.

18. De Souza, R. T. M. P.; Freire, V. F.; Gubiani, J. R.; Ferreira, R. O.; Trivella, D. B. B.; Moraes, F. C.; Paradas, W. C.; Salgado, L. T.; Pereira, R. C.; Amado Filho, G. M.;

Ferreira, A. G.; Williams, D. E.; Andersen, R. J.; Molinski, T. F.; Berlinck, R. G. S., *J. Nat. Prod.,* **2018**, *81*, 2296-2300.

19. Feldman, K. S.; Saunders, J. C., *J. Am. Chem. Soc.*, **2002**, *124*, 9060-9061.

20. Domostoj, M. M.; Irving, E.; Scheinmann, F.; Hale, K. J., *Org. Lett.,* **2004**, *6*, 2615-2618.

21. Papeo, G.; Posteri, H.; Borghi, D.; Varasi, M., *Org. Lett.* **2005**, *7*, 5641-5644.

22. Zaib, R. S.; Tepe, J. J., *Tetrahedron Lett.* **2015**, 3011-3013.

23. Gao, S.; Bethel, T. K.; Kakeshpour, T.; Hubbell, G. E.; Jackson, J. E.; Tepe, J. J., *J. Org. Chem.,* **2018**, *83*, 9250-9255.

24. Travert, N.; Martin, M.-T.; Bourguet-Kondracki, M.-L.; Al-Mourabit, A., *Tetrahedron Lett.,* **2005**, *46*, 249-252.

25. Chang, C.-W.; Wu, C.-C.; Chang, Y.-Y.; Lin, C.-C.; Chien, T.-C., *J. Org. Chem.,* **2013**, *78*, 10459-10468.

26. Tasker, N. R.; Rastelli, E. J.; Blanco, I. K.; Burnett, J. C.; Sharlow, E. R.; Lazo, J. S.; Wipf, P., *Org. Biomol. Chem.,* **2019**, *17*, 2448-2466.

27. Hewlett, N. M.; Tepe, J. J., *Org. Lett.,* **2011**, *13*, 4550-4553.

28. Boddapati, S. N. M.; Polam, N.; Mutchu, B. R.; Bollikolla, H. B., *New J. Chem.,* **2018**, *48*, 918.

29. Kwak, J. P.; Dao, P. D. Q.; Cho, C. S., *Eur. J. Org. Chem.,* **2020**, 3468-3474.

30. Li, J.; Neuville, L., Org. Lett., **2013**, *15*, 6124-6127.

31. Deng, X.; McAllister, H.; Mani, N. S *J. Org. Chem.* **2009**, *74*, 5742-5745.

32. Hammoud, H.; Schmitt, M.; Bihel, F.; Antheaume, C.; Bourguignon, J.-J., *J. Org. Chem.* **2012**, *77*, 417-423.

33. Zhang, S.-L.; Liu, L.; Fu, Y.; Guo, Q.-X., *Organometallics,* **2007**, *26*, 4546-4554.

34. Tiemann, F., *Ber. Dtsch, Chem. Ges.* **1891,** *24*, 4162-4167.

35. Lin, C.-C.; Hsieh, T.-H.; Liao, P.-Y.; Liao, Z.-Y.; Chang, C.-W.; Shih, Y.-C.; Yeh, W.-H.; Chien, T.-C., *Org. Lett.,* **2014**, *16*, 892-895.

36. Takagi, K.; Okamoto, T.; Sakakibara, Y.; Oka, S., *Chem. Lett.,* **1973,** *2*, 471-474.

37. Anbarasan, P.; Schareina, T.; Beller, M., *Chem. Soc. Rev.*, **2011**, *40*, 5049-5067.

38. Neetha, M.; Afsina, C. M. A.; Aneeja, T.; Anilkumar, G., *RSC Adv.*, **2020**, *10*, 33683-33699.

39. Jakob, F.; Alen, J.; Lucas, S.; Craan, L.; Konetzki, I.; Kless, A.; Schunk, S.; Ratcliffe, P.; Wachten, S.; Cruwys, S. PCT/EP2019/06911. 2020.

40. Lin, C.-C.; Hsieh, T.-H.; Liao, P.-Y.; Liao, Z.-Y.; Chang, C.-W.; Shih, Y.-C.; Yeh, W.-H.; Chien, T.-C., *Org. Lett.*, **2014**, *16*, 892-895.

41. Zhang, G.; Zhao, Y.; Ding, C., *Org. Biomol. Chem.*, **2019**, *17*, 7684.

42. Voros, A.; Mucsi, Z.; Baan, Z.; Timari, G.; Hermecz, I.; Mizsey, P.; Finta, Z., *Org. Biomol. Chem.*, **2014,** *12*, 8036.

43. Zollinger, M.; Mayer, P.; Lindel, T., *J. Org. Chem.*, **2006**, *71*, 9431-9439.

44. Barani, M.; Fioravanti, S.; Pellacani, L.; Tardella, P. A., *Tetrahedron*, **1994**, *50*, 11235-11238.

45. Ng, K.-H.; Chan, A. S. C.; Yu, W.-Y., *J. Am. Chem. Soc.*, **2010**, *132*, 12862-12864.

46. Kim, M.; Mulcahy, J. V.; Espino, C. G.; Du Bois, J., *Org. Lett.* **2006**, *8*, 1073-1076.

47. Paudyal, M. P.; Adebesin, A. M.; Burt, S. R.; Ess, D. H.; Ma, Z.; Kurti, L.; Falck, J. R., *Science*, **2016**, *353*, 1144-1147.

48. Priem, C.; Wuttke, A.; Berditsch, M.; Ulrich, A.; Geyer, A., *J. Org. Chem.*, **2017**, *82*, 1 2366-12376.

49. Lai, W.; Zaho, S.; Lai, Q.; Zhou, W.; Wu, M.; Jiang, X.; Wang, X.; Peng, Y.; Wei, X.; Ouyang, L.; Gou, L.; Chen, H.; Wang, Y.; Yang, J., *J. Med. Chem.*, **2022**, *65*, 11679-11702.

50. Klapaneris, N.; Koutoulogenis, G.; Raftopoulou, M.; Kokotos, C.G. *J. Org. Chem.*, **2015**, *80*, 5464-54

APPENDIX

Figure 4.5 ^{1}H and $^{13}C\{^{1}H\}$ NMR spectra of compound **IV-2**

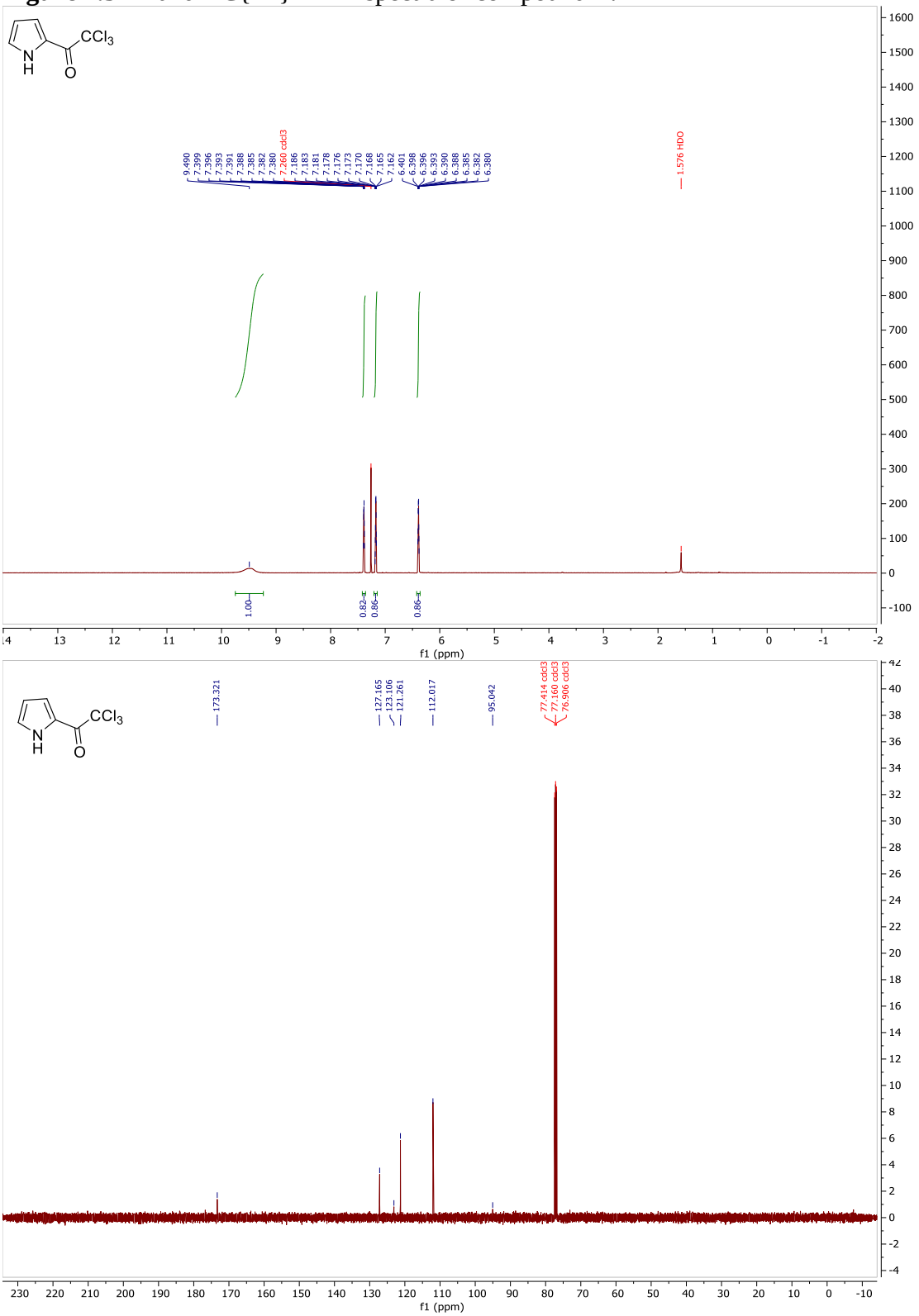

Figure 4.6 ^{1}H and $^{13}C\{^{1}H\}$ NMR spectra of compound **IV-3**

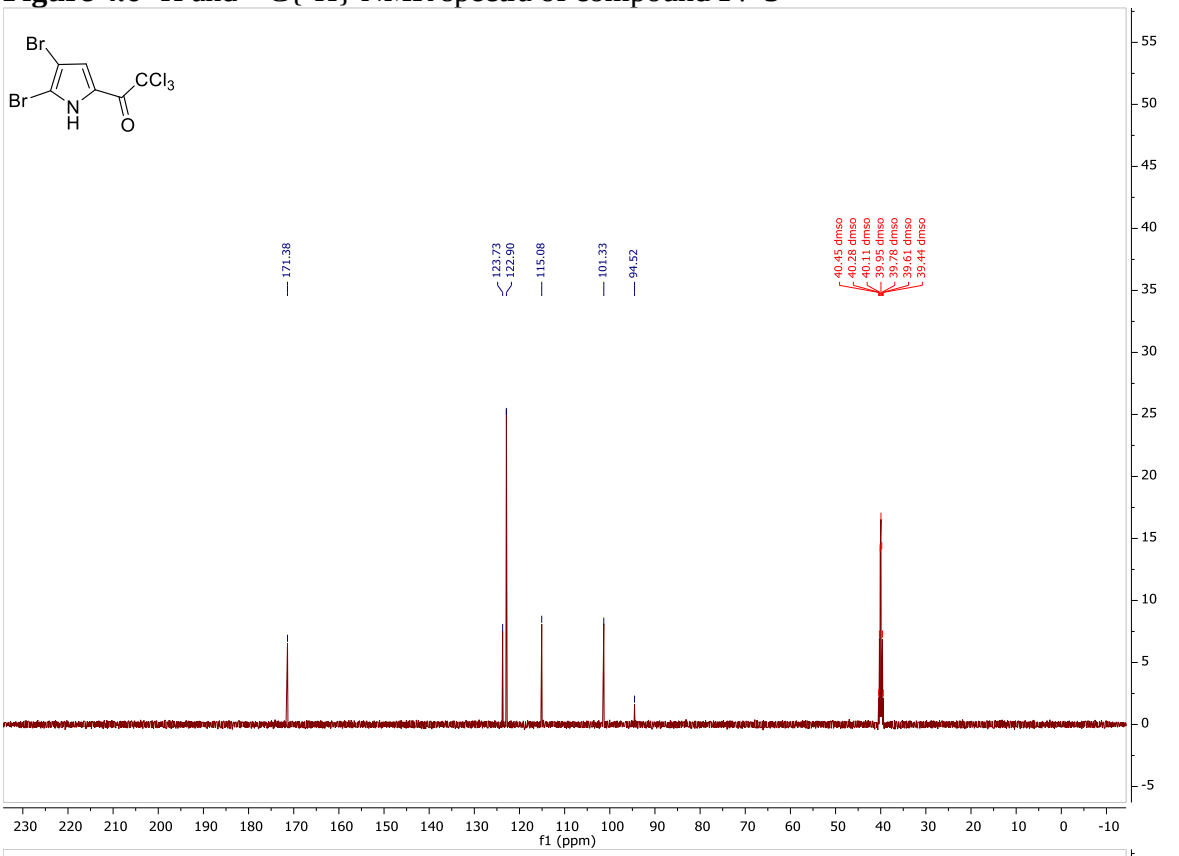

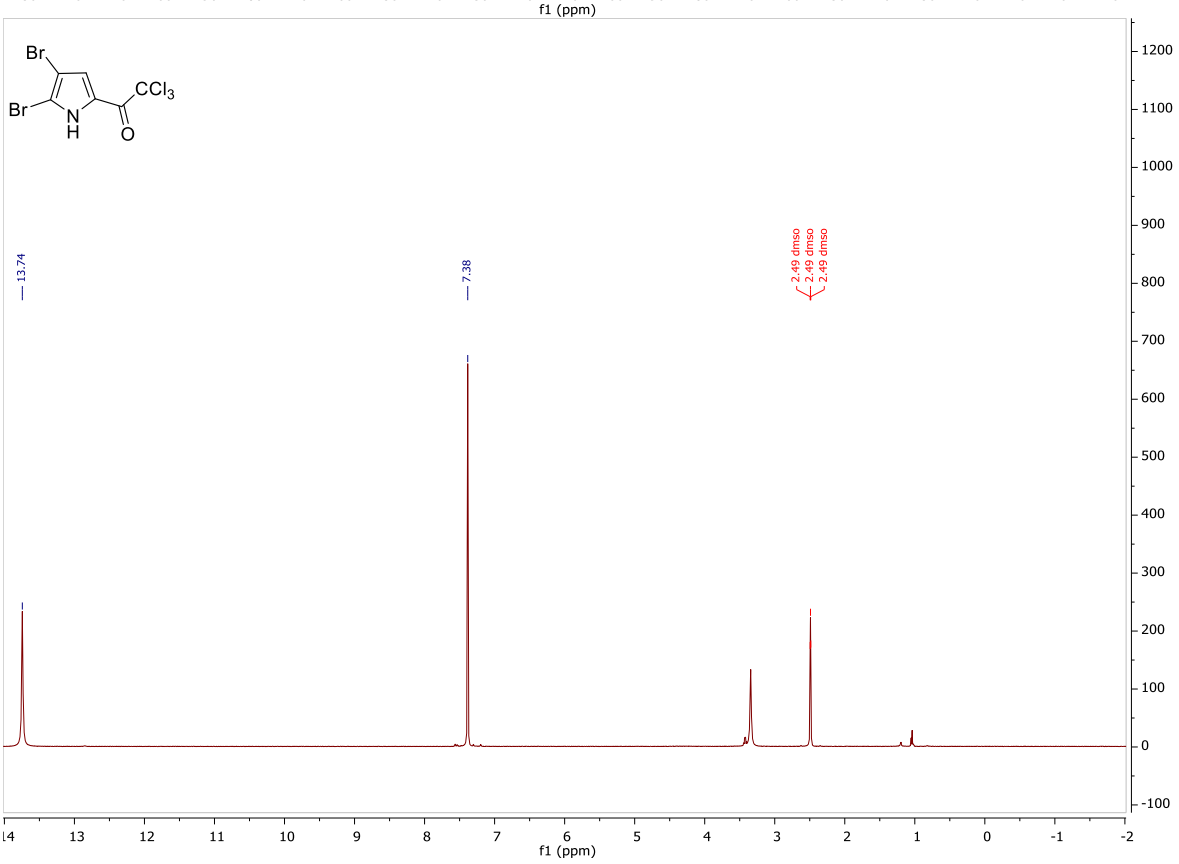

Figure 4.7 ^{1}H and $^{13}C\{^{1}H\}$ NMR spectra of compound **IV-4**

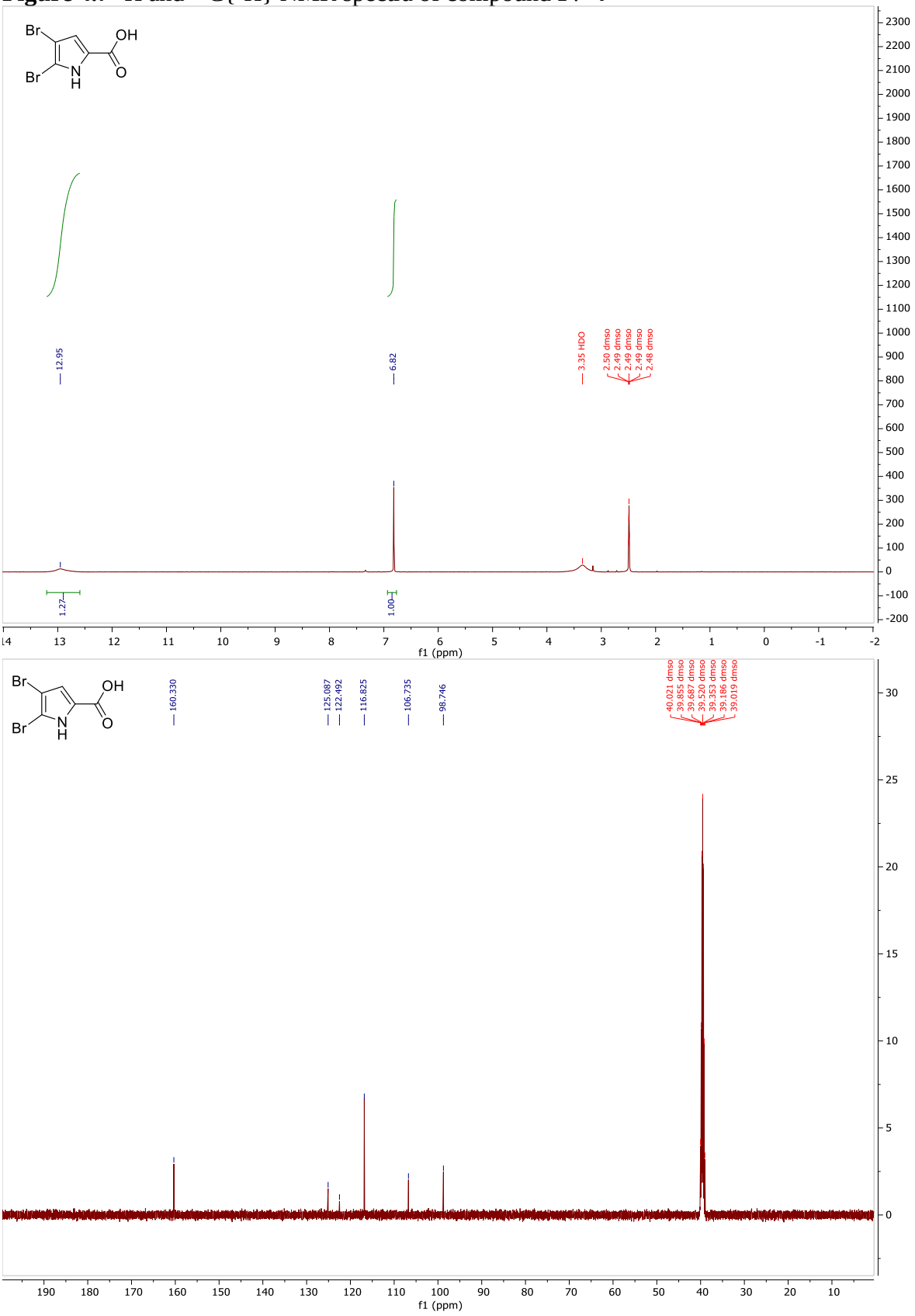

Figure 4.8 ^{1}H and $^{13}C\{^{1}H\}$ NMR spectra of compound **IV-5**

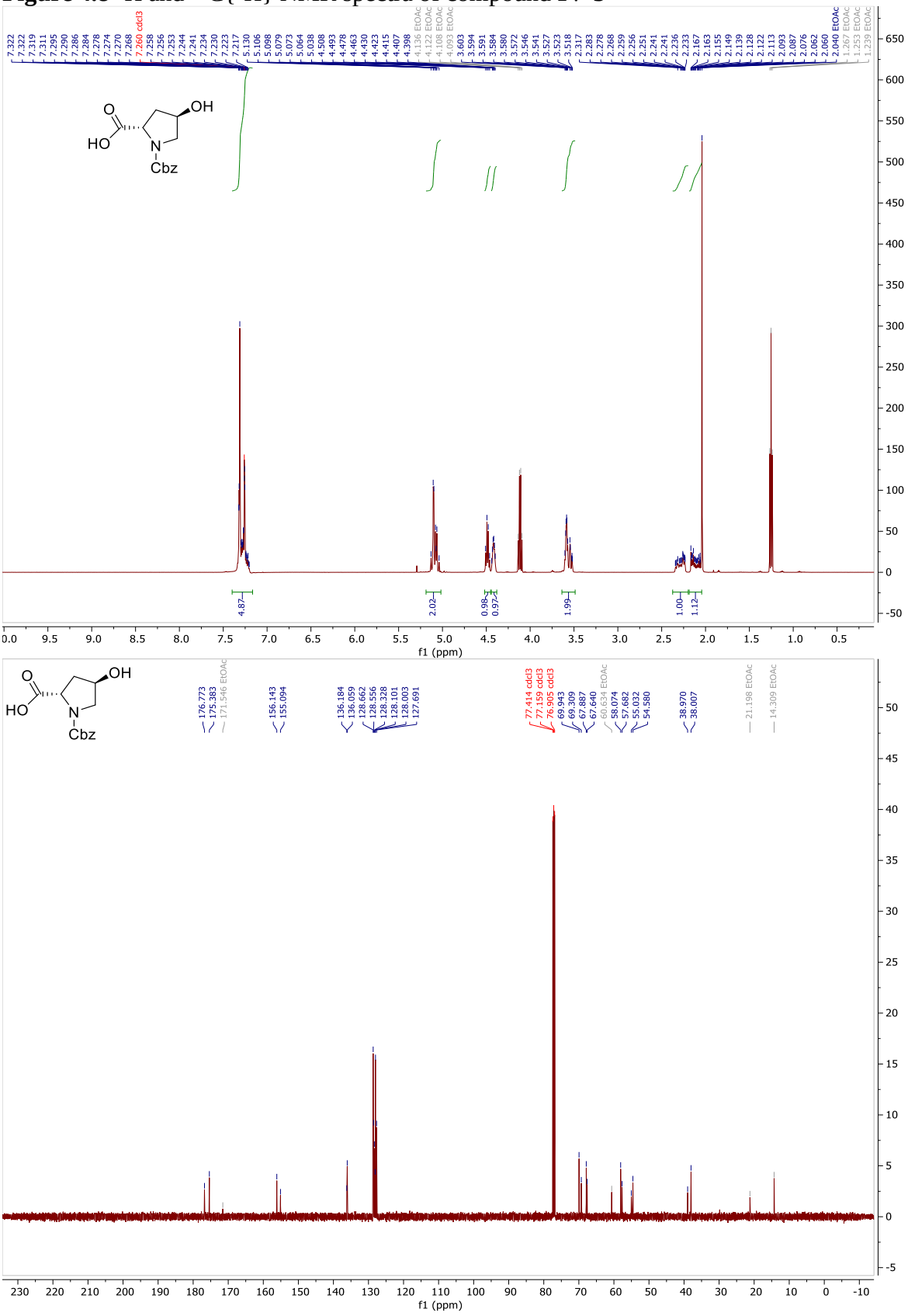

Figure 4.9 ^{1}H and $^{13}C\{^{1}H\}$ NMR spectra of compound **IV-6**

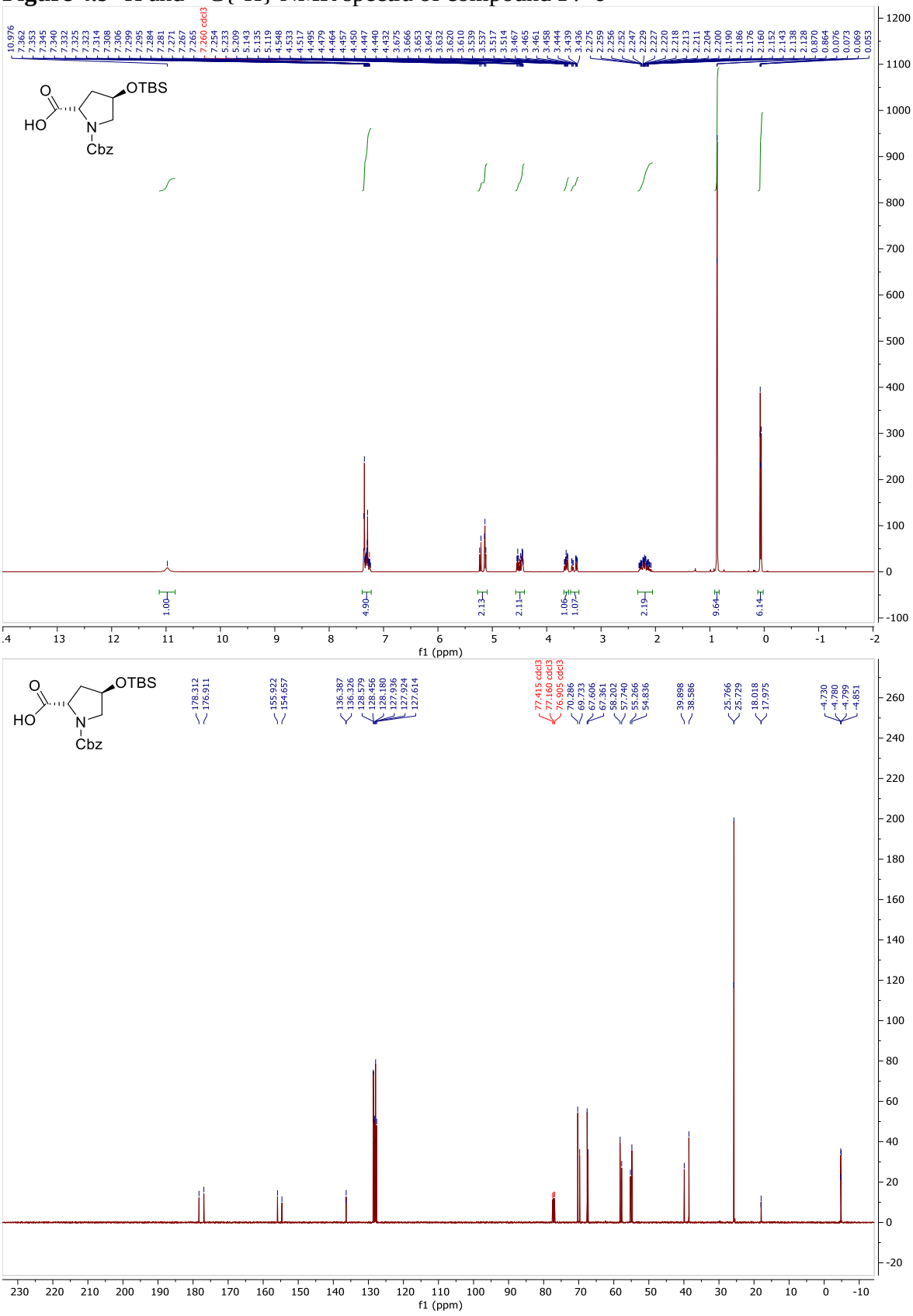

Figure 4.10 ^{1}H and $^{13}C\{^{1}H\}$ NMR spectra of compound **IV-7**

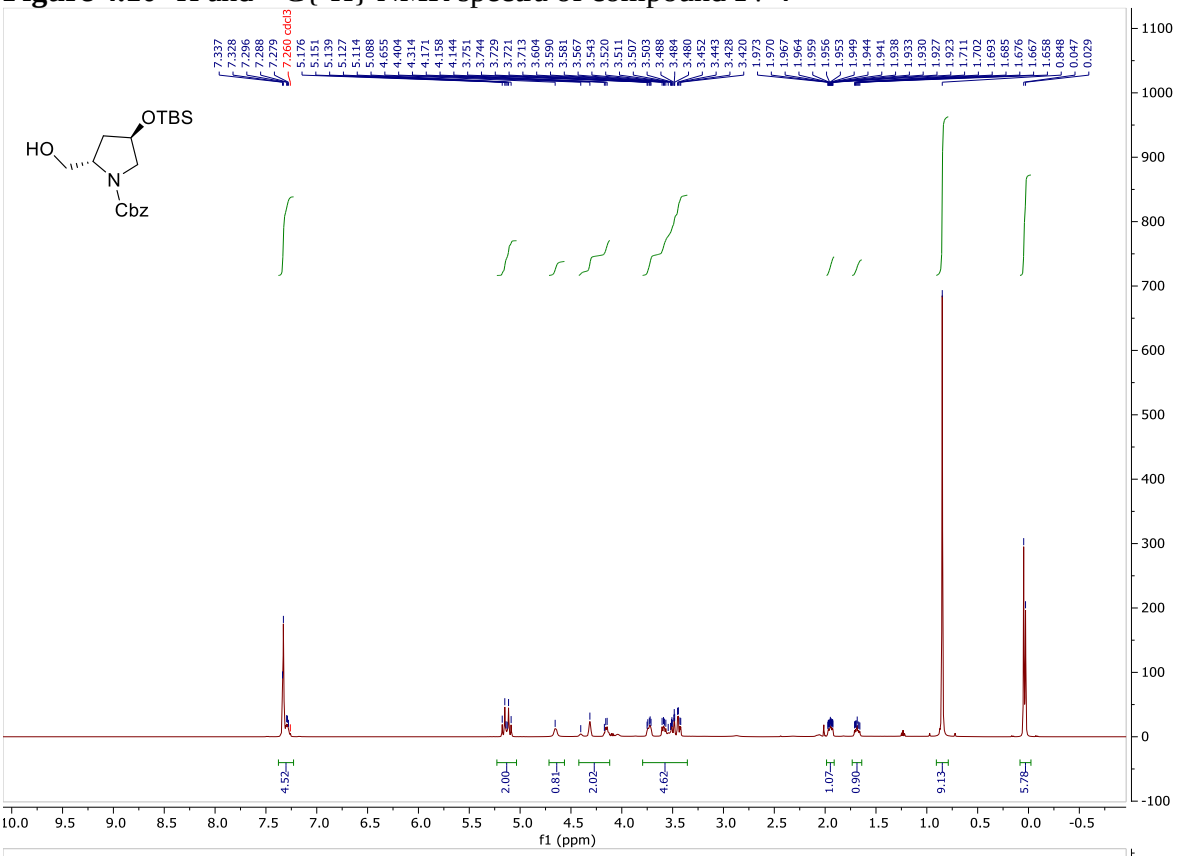

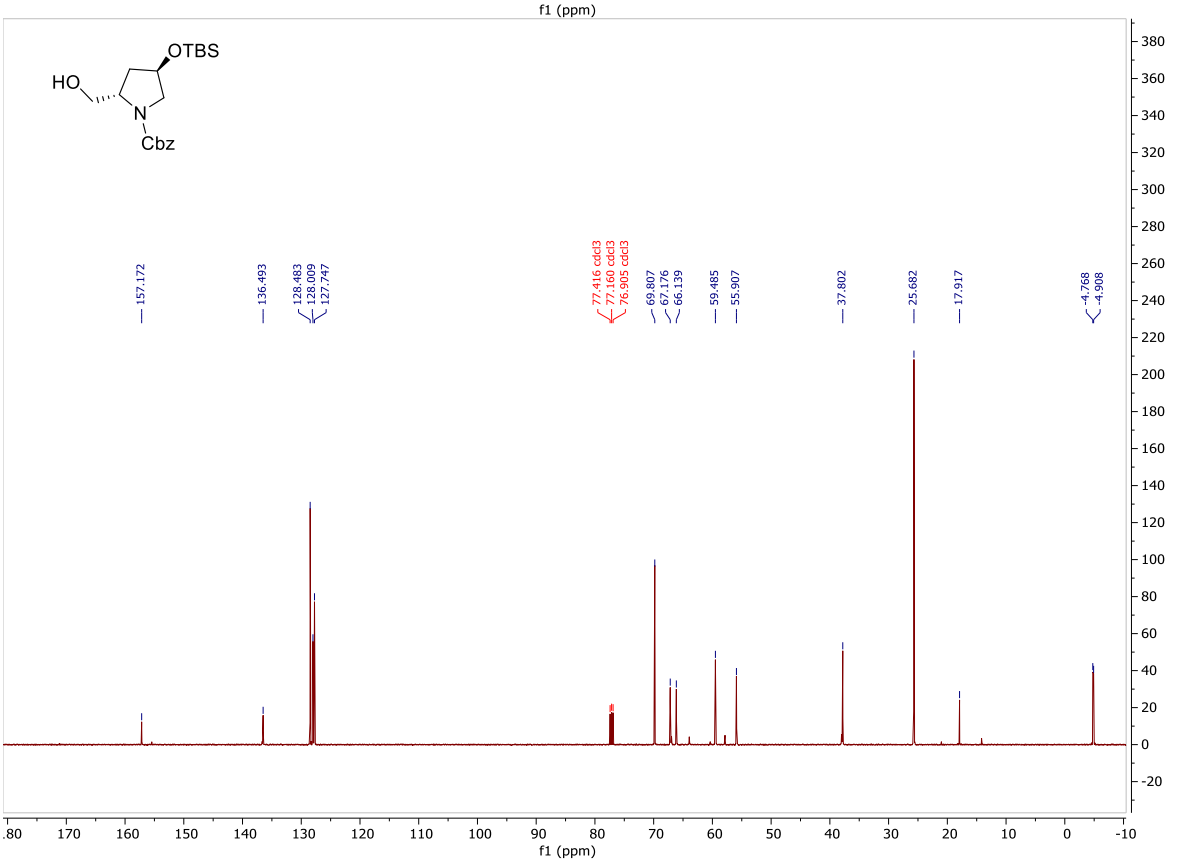

Figure 4.11 ^{1}H and $^{13}C\{^{1}H\}$ NMR spectra of compound **IV-8**

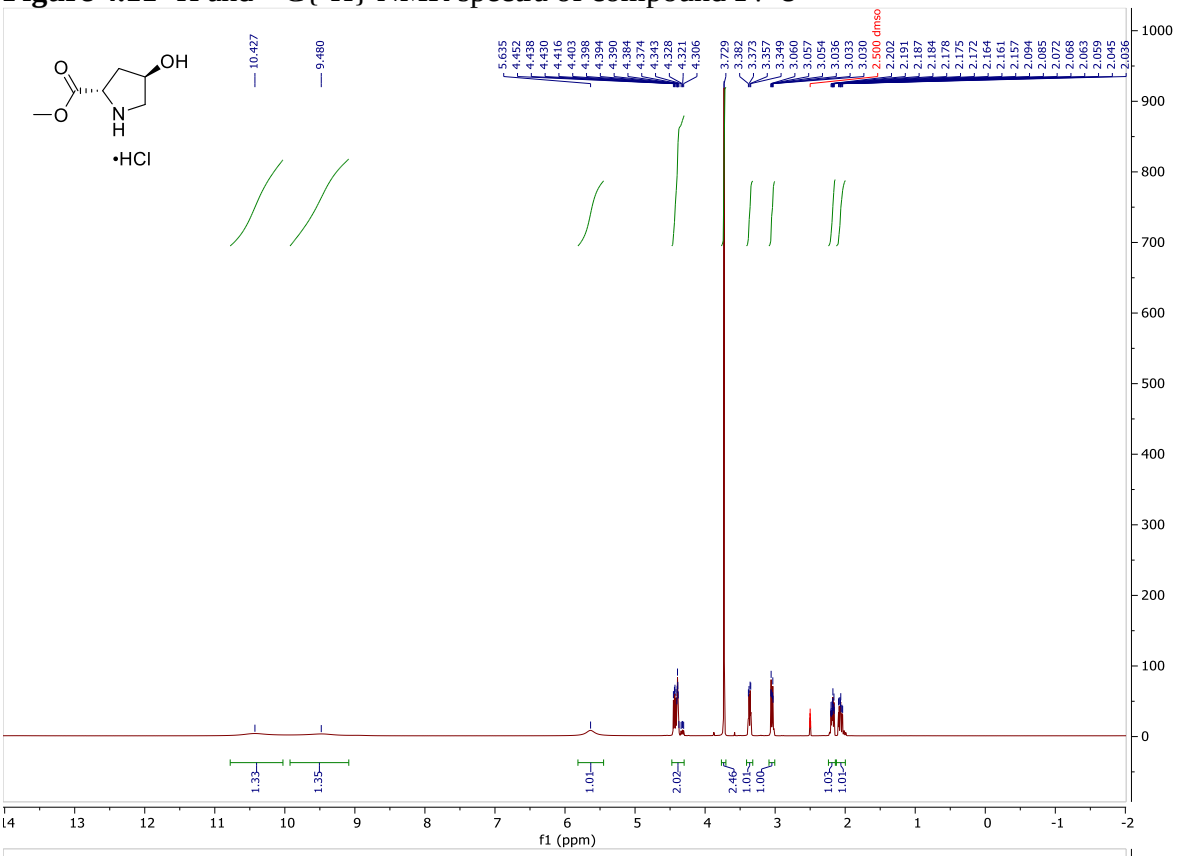

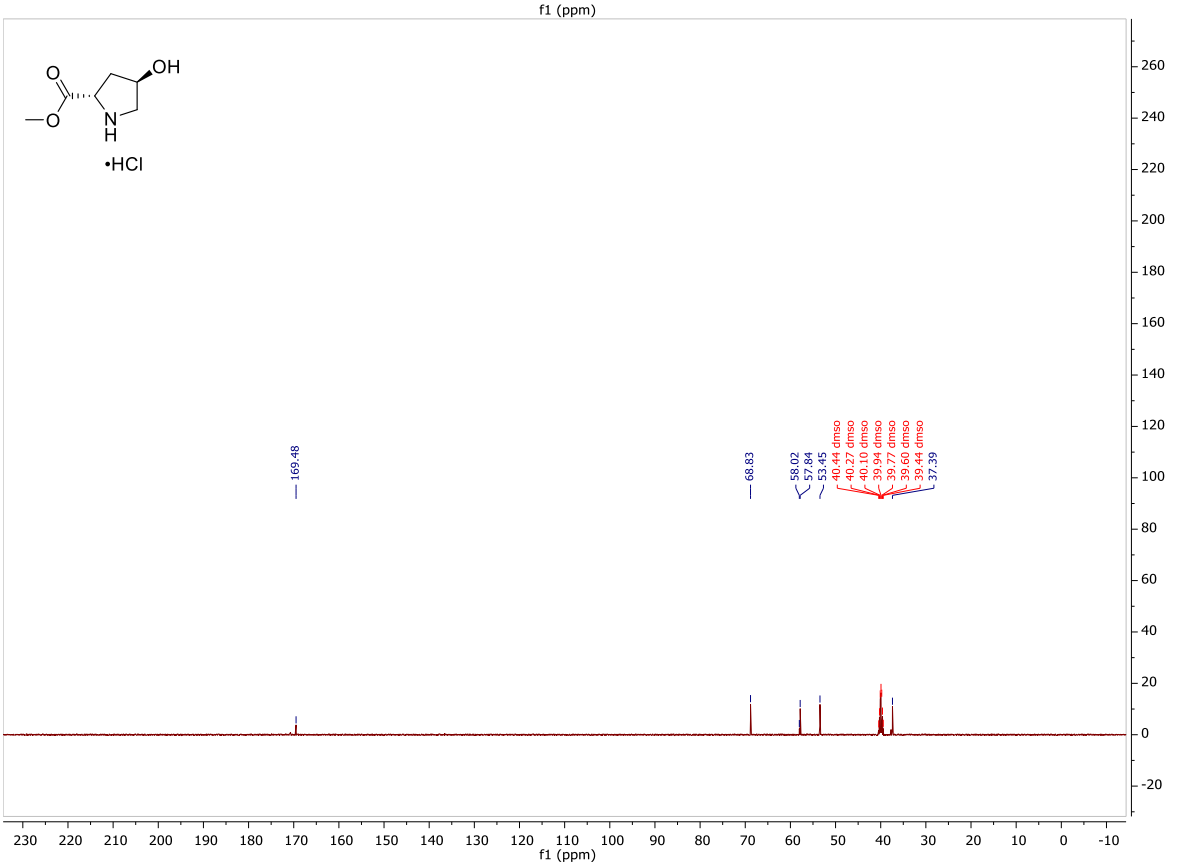

Figure 4.12 ^{1}H and $^{13}C\{^{1}H\}$ NMR spectra of compound **IV-9**

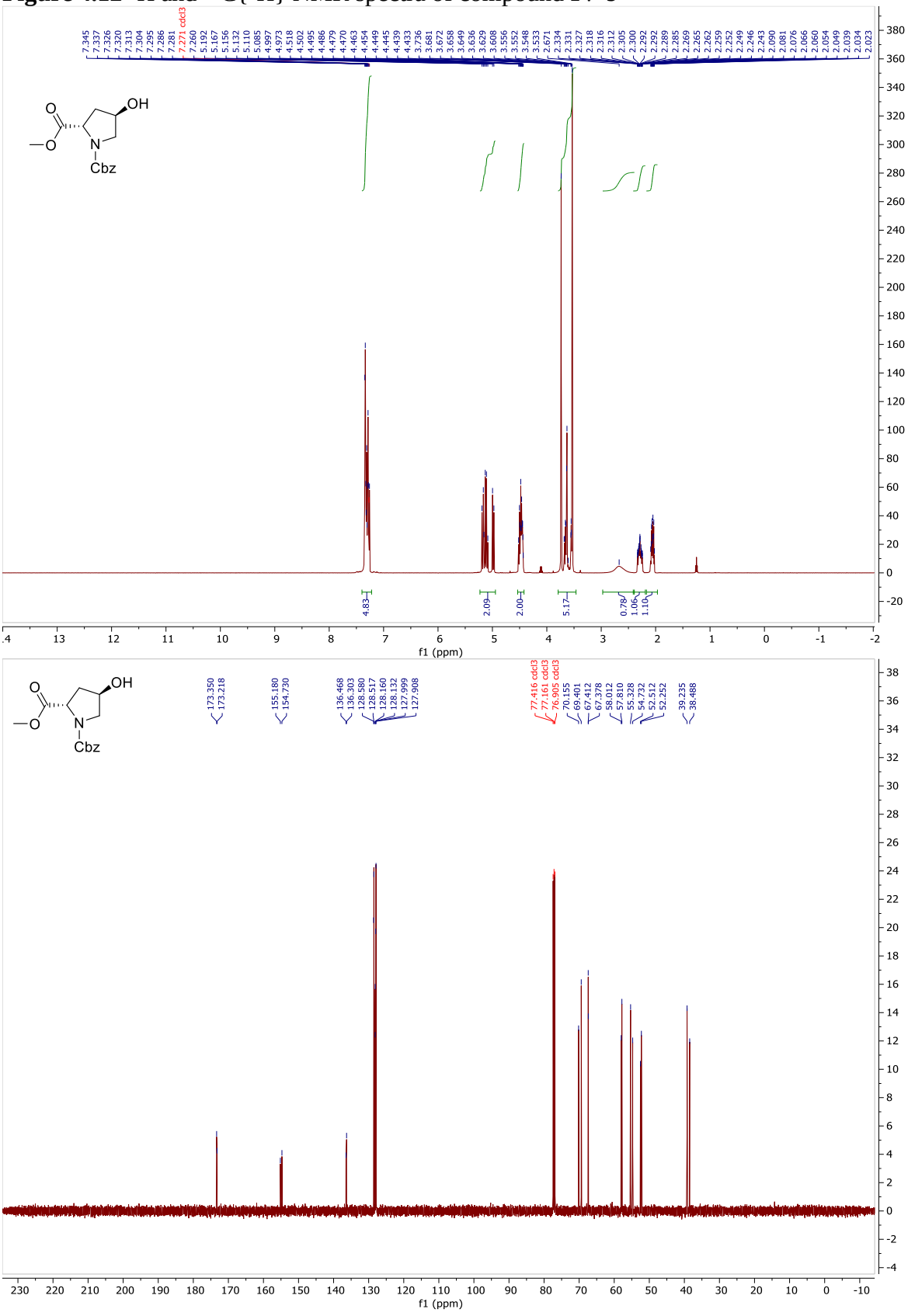

Figure 4.13 ^{1}H and $^{13}C\{^{1}H\}$ NMR spectra of compound **IV-10**

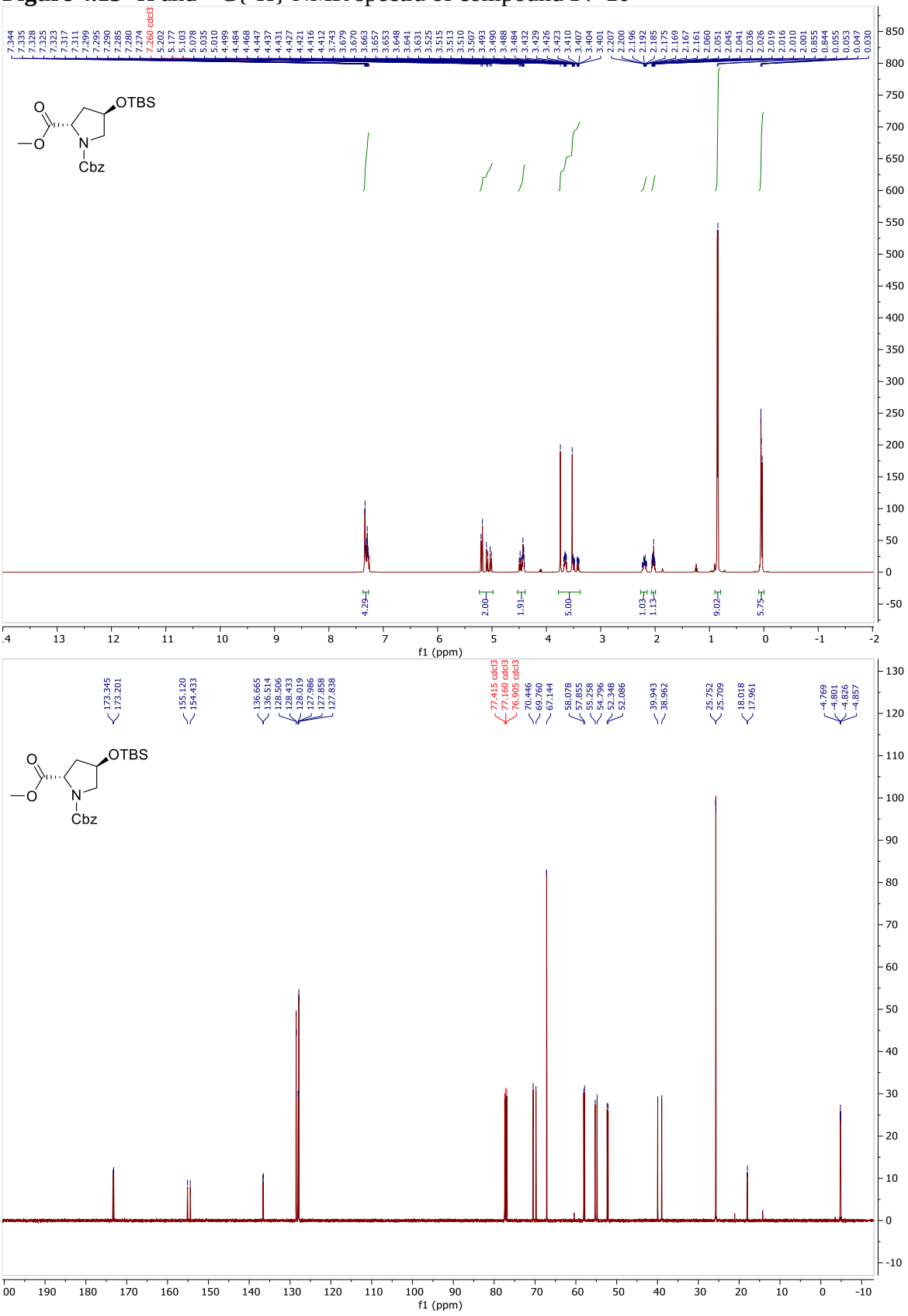

Figure 4.14 ^{1}H and $^{13}C\{^{1}H\}$ NMR spectra of compound **IV-11**

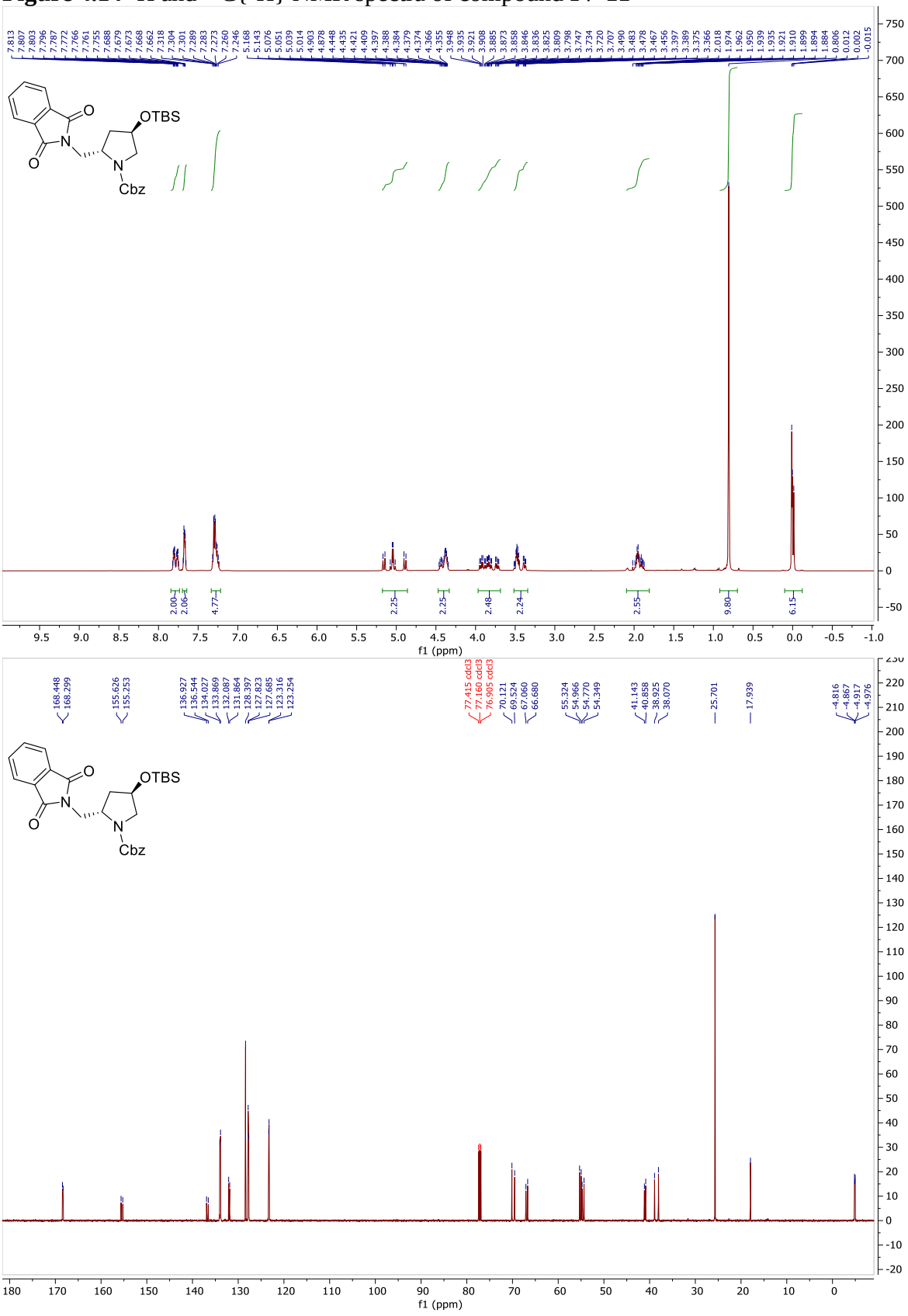

Figure 4.15 ^{1}H and $^{13}C\{^{1}H\}$ NMR spectra of compound **IV-12**

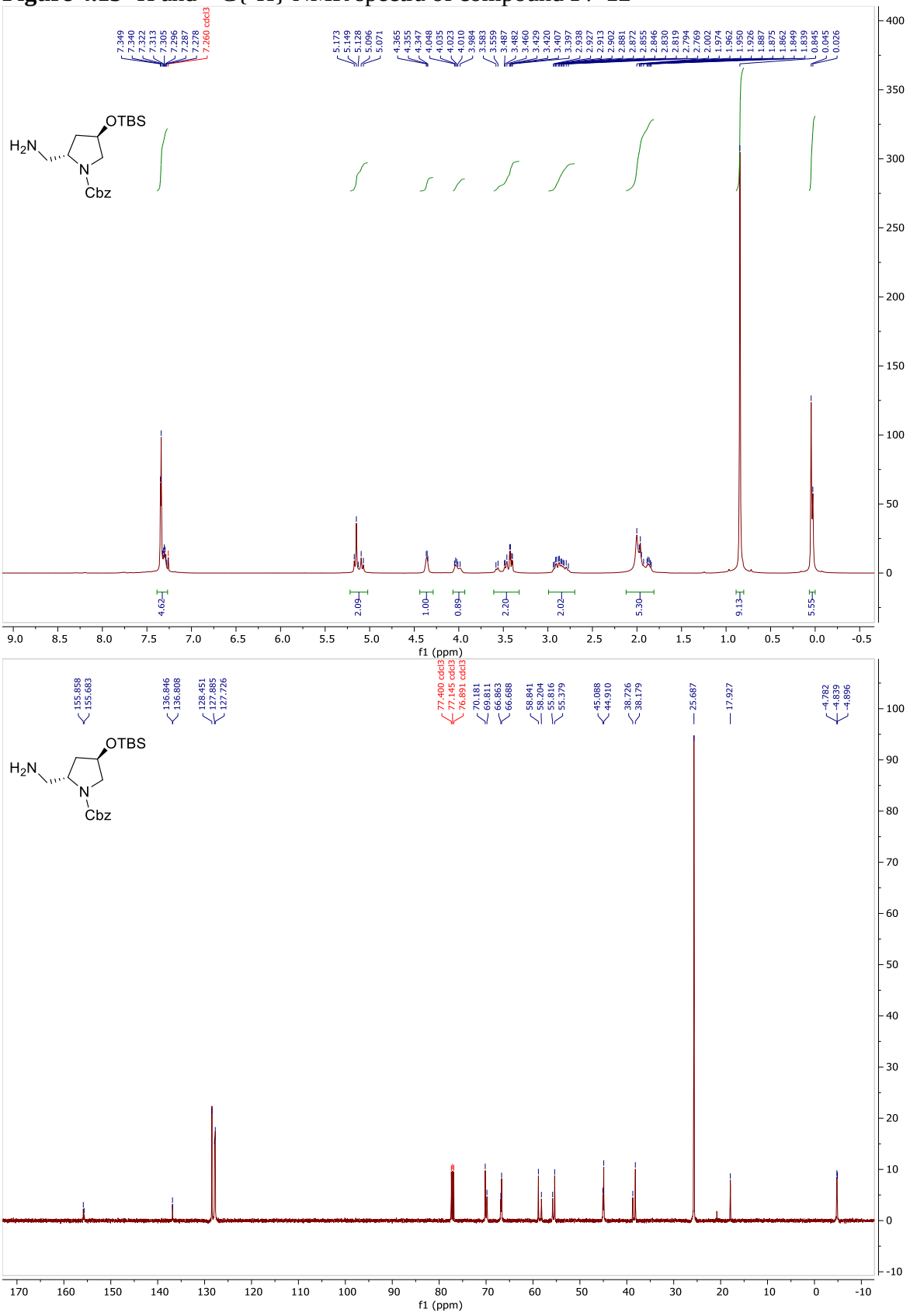

Figure 4.16 ^{1}H and $^{13}C\{^{1}H\}$ NMR spectra of compound **IV-13**

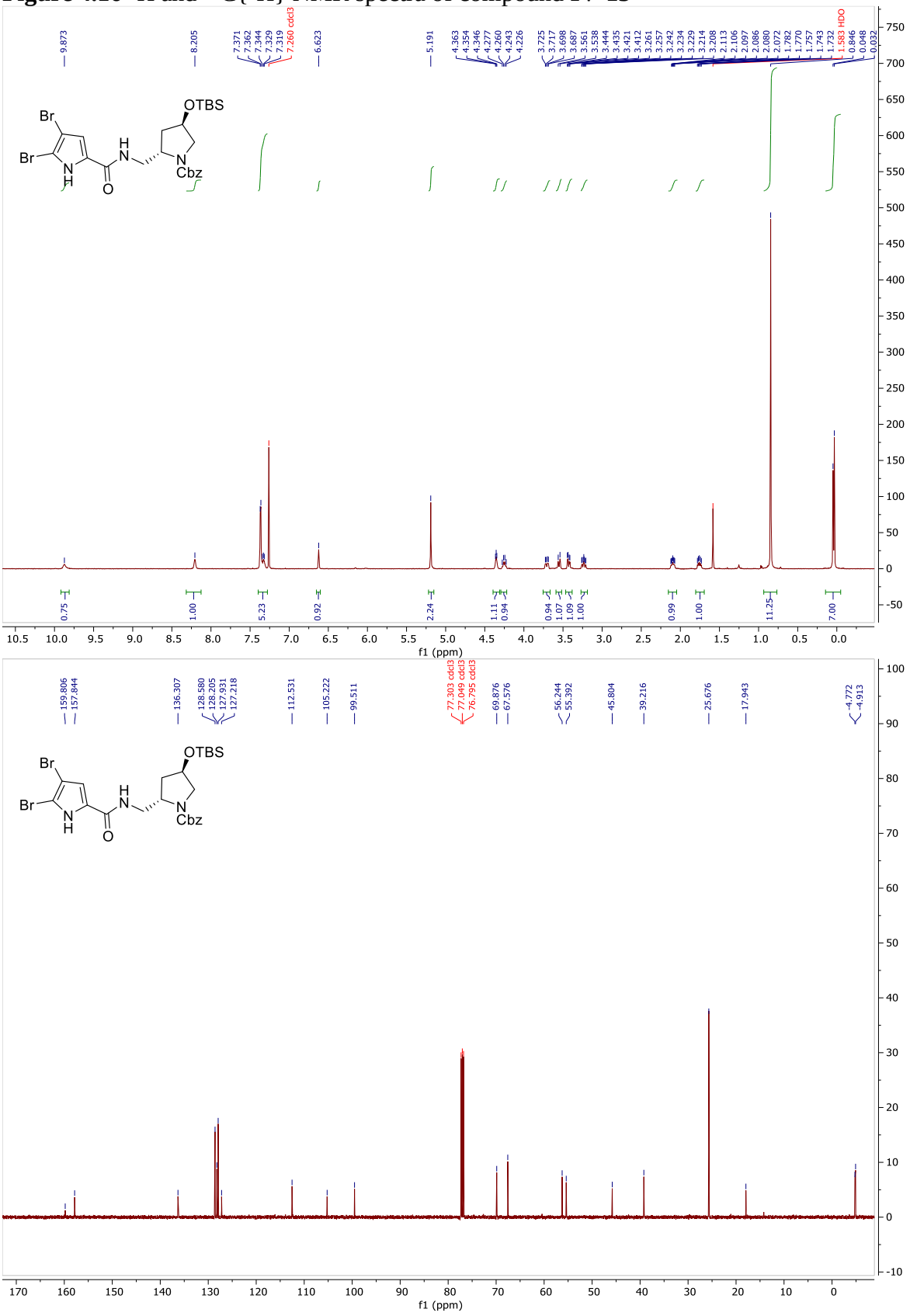

Figure 4.17 ^{1}H and $^{13}C\{^{1}H\}$ NMR spectra of compound **IV-14**

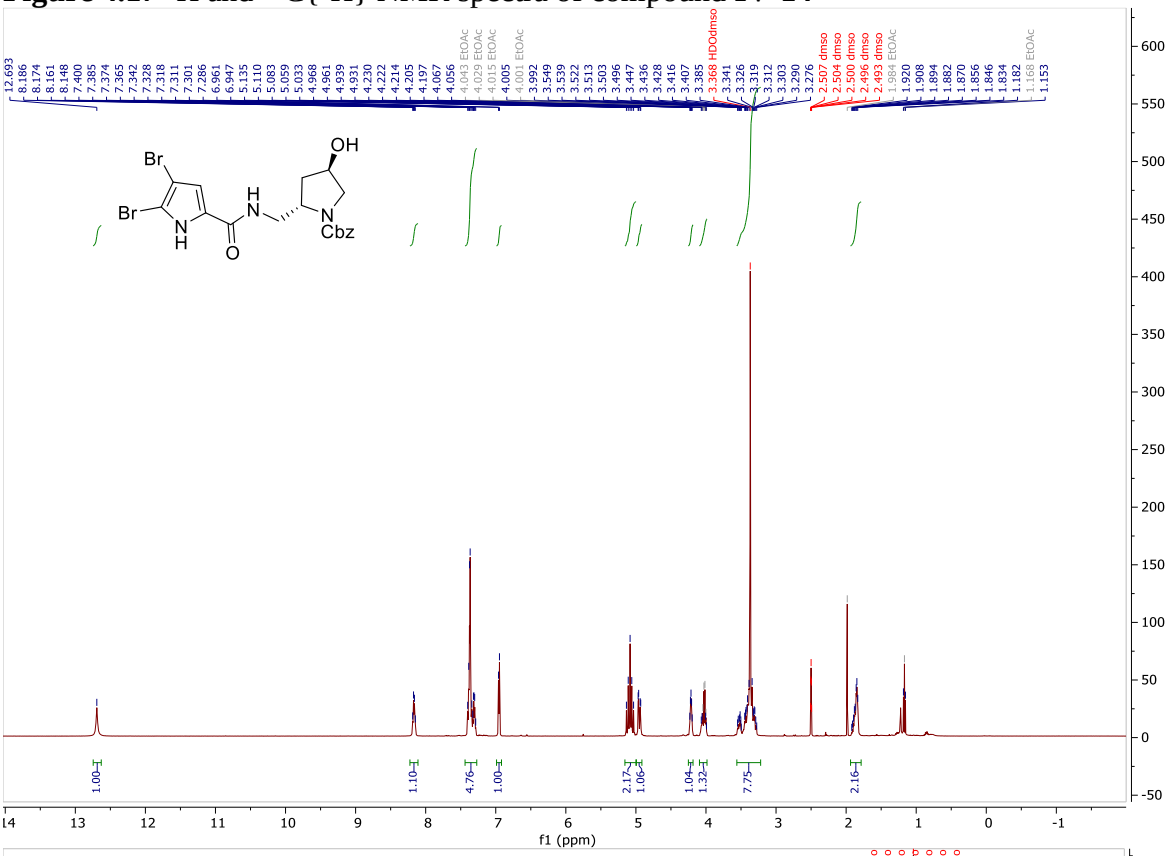

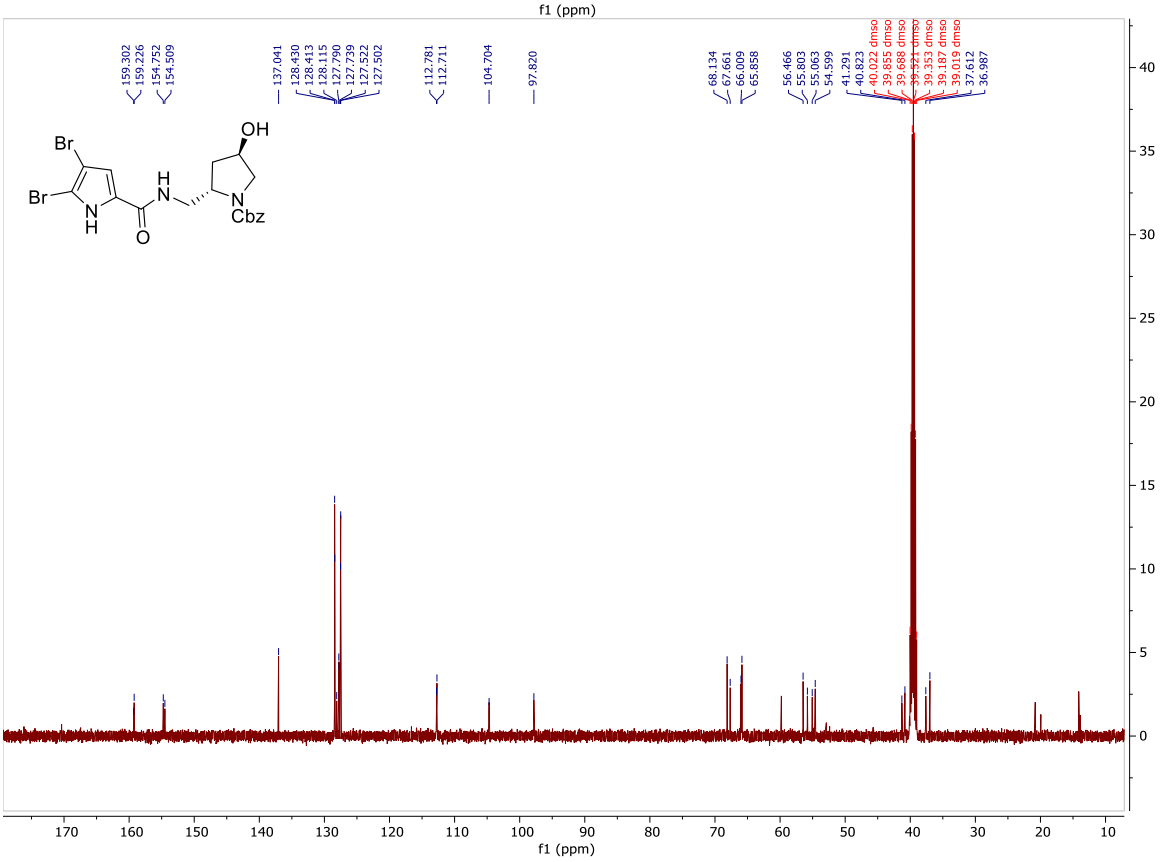

Figure 4.18 ^{1}H and $^{13}C\{^{1}H\}$ NMR spectra of compound **IV-15**

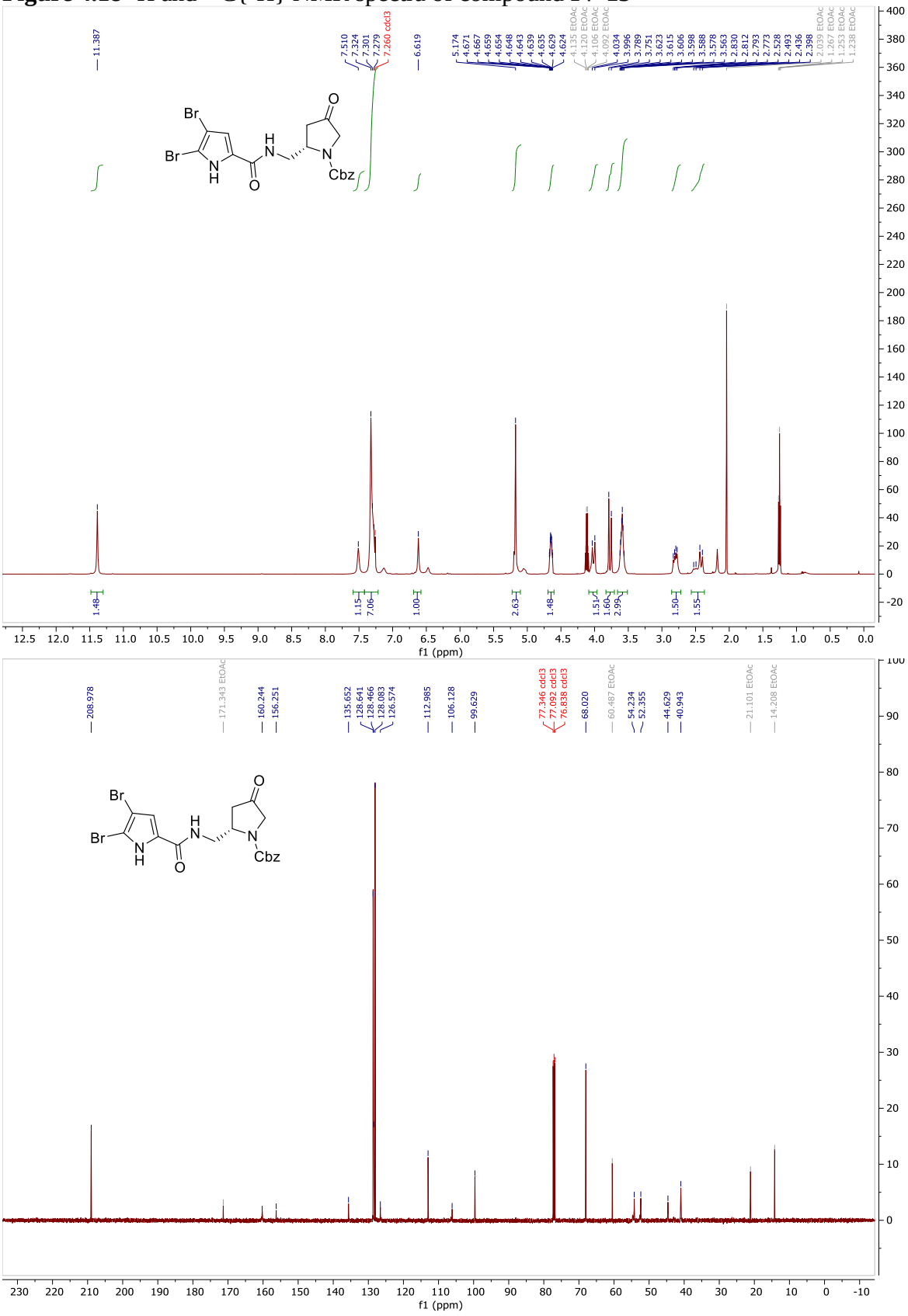

Figure 4.19 ^{1}H and $^{13}C\{^{1}H\}$ NMR spectra of compound **IV-17**

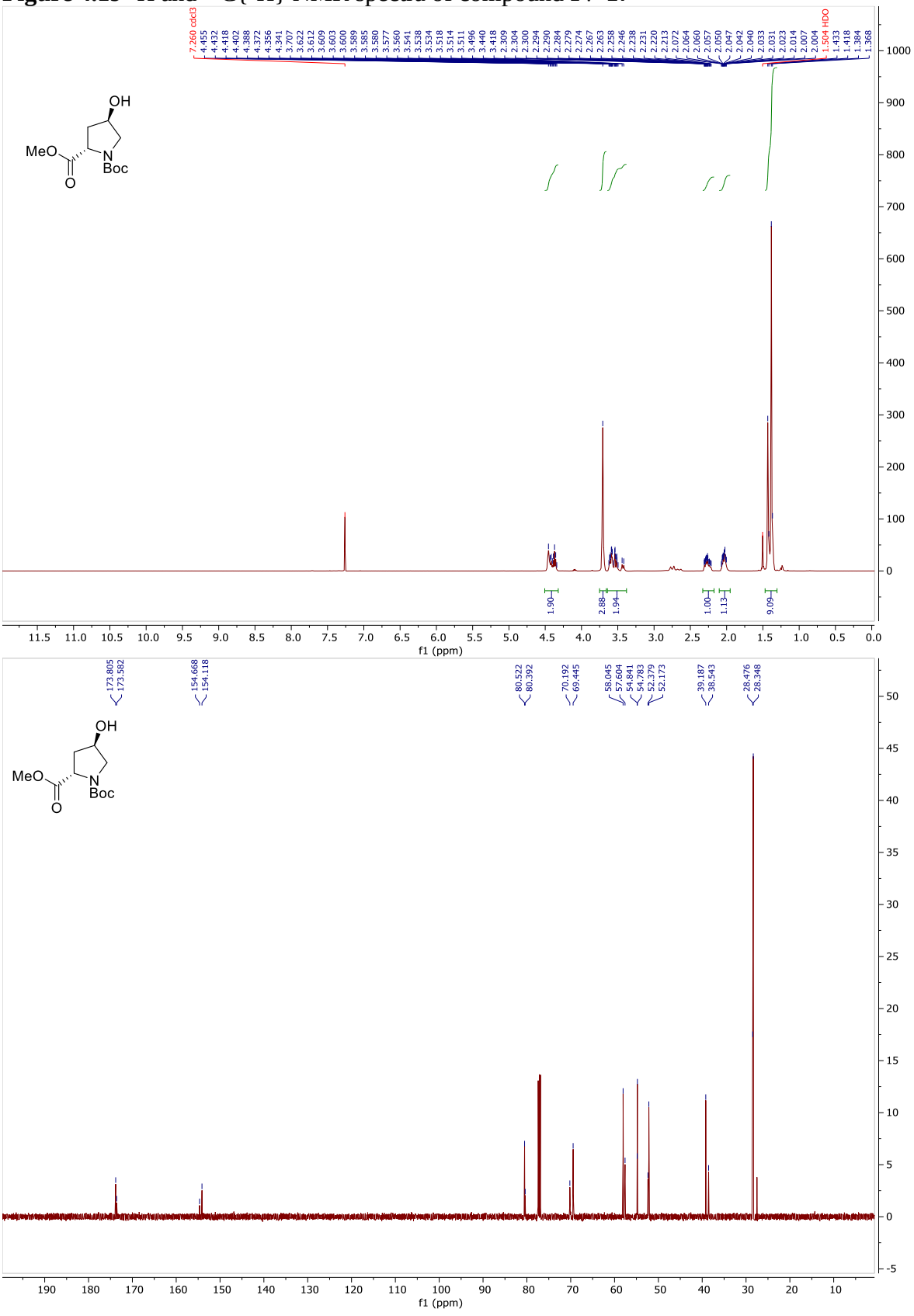

Figure 4.20 ^{1}H and $^{13}C\{^{1}H\}$ NMR spectra of compound **IV-18**

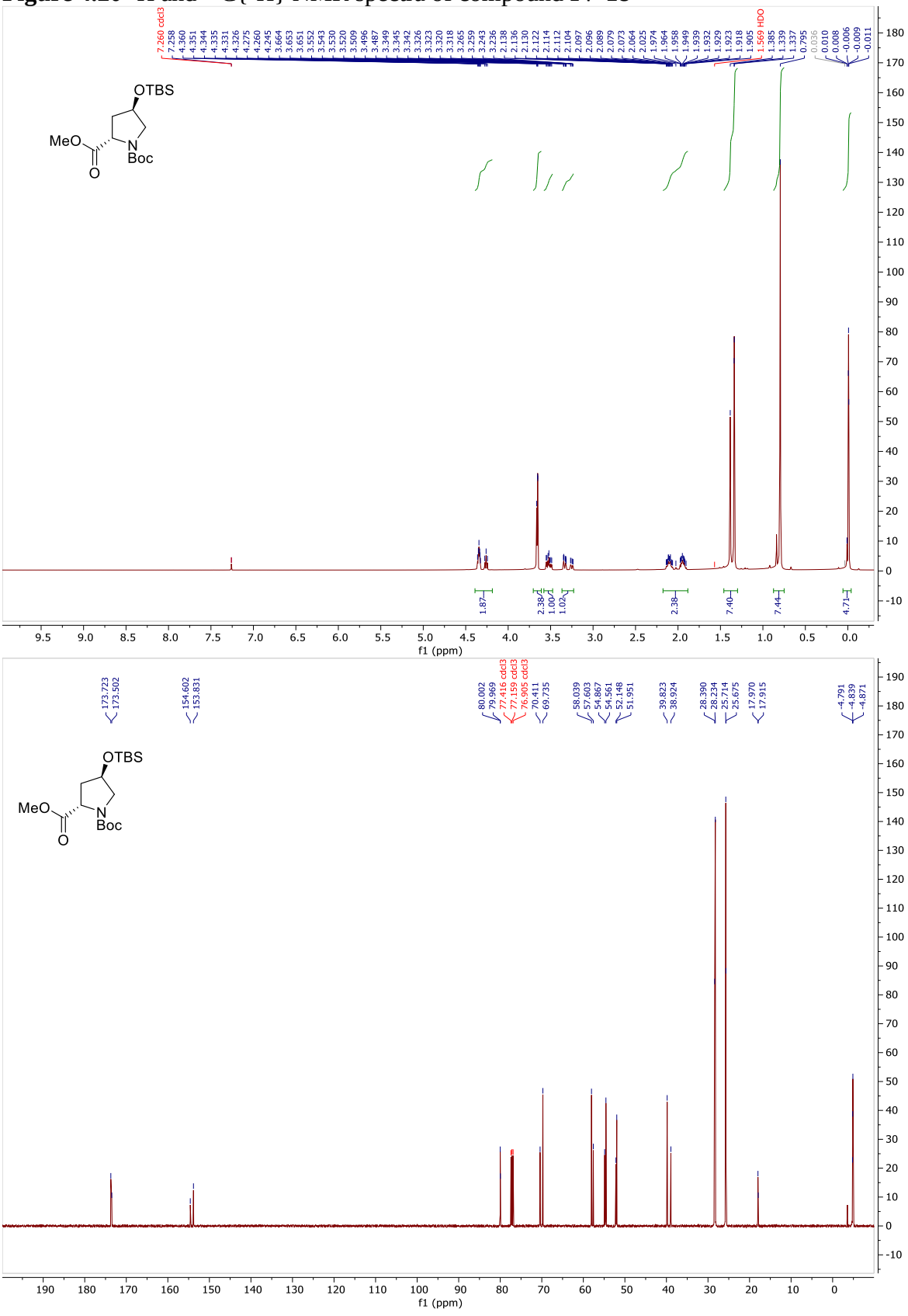

Figure 4.21 ^{1}H and $^{13}C\{^{1}H\}$ NMR spectra of compound **IV-19**

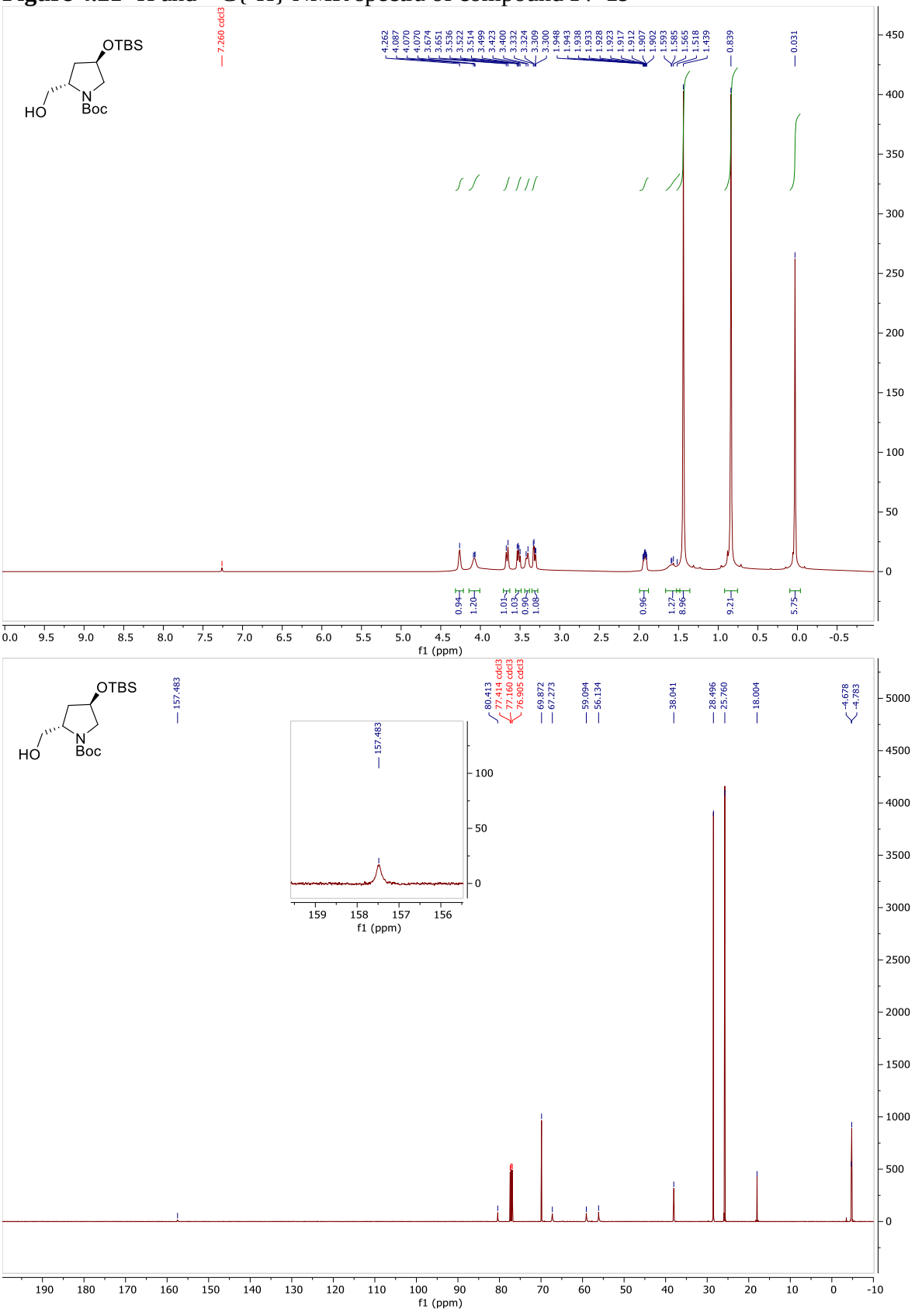

Figure 4.22 ^{1}H and $^{13}C\{^{1}H\}$ NMR spectra of compound **IV-20**

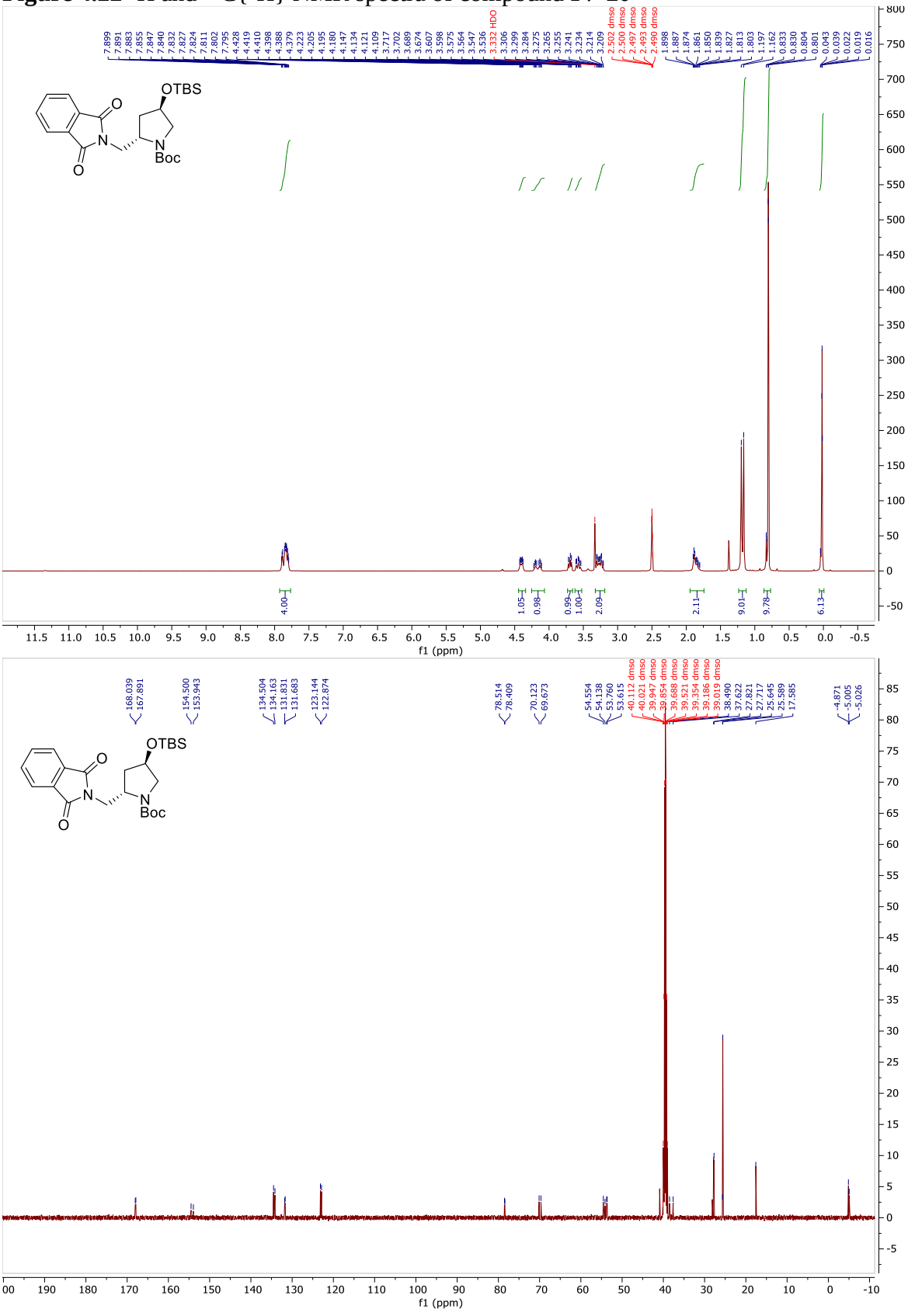

Figure 4.23 ^{1}H and $^{13}C\{^{1}H\}$ NMR spectra of compound **IV-21**

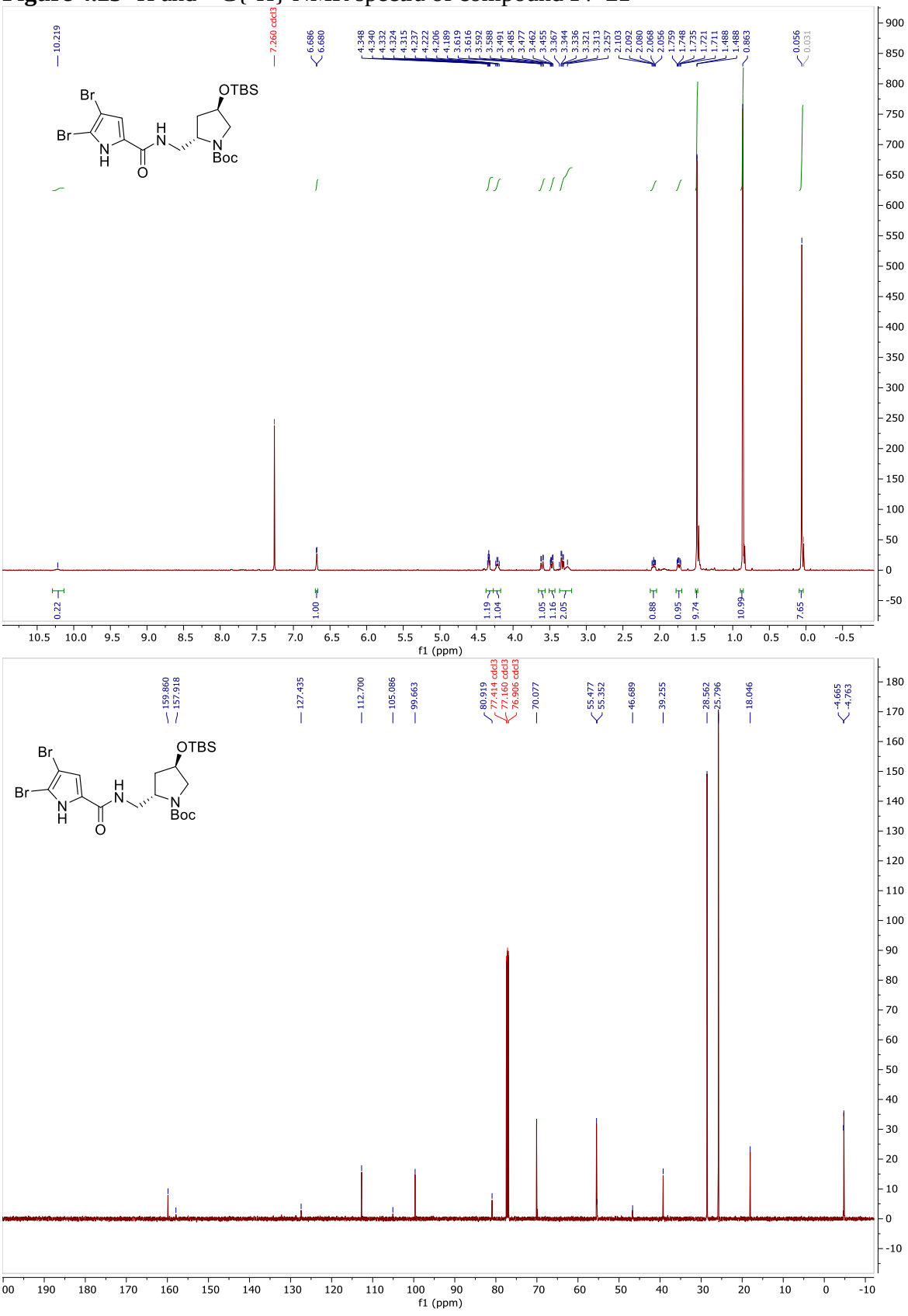

Figure 4.24 ^{1}H and $^{13}C\{^{1}H\}$ NMR spectra of compound **IV-22**

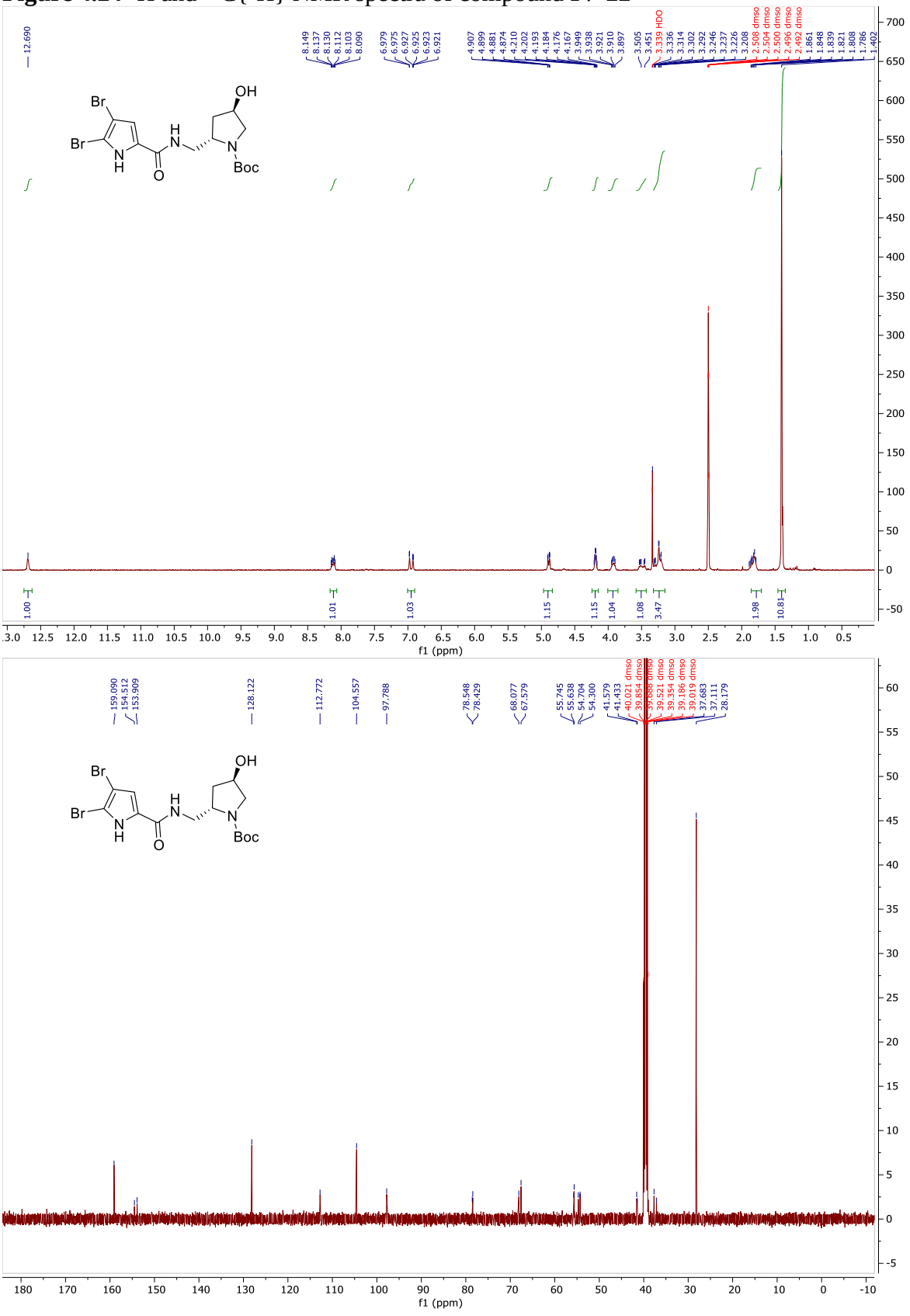

Figure 4.25 ^{1}H and $^{13}C\{^{1}H\}$ NMR spectra of compound **IV-23**

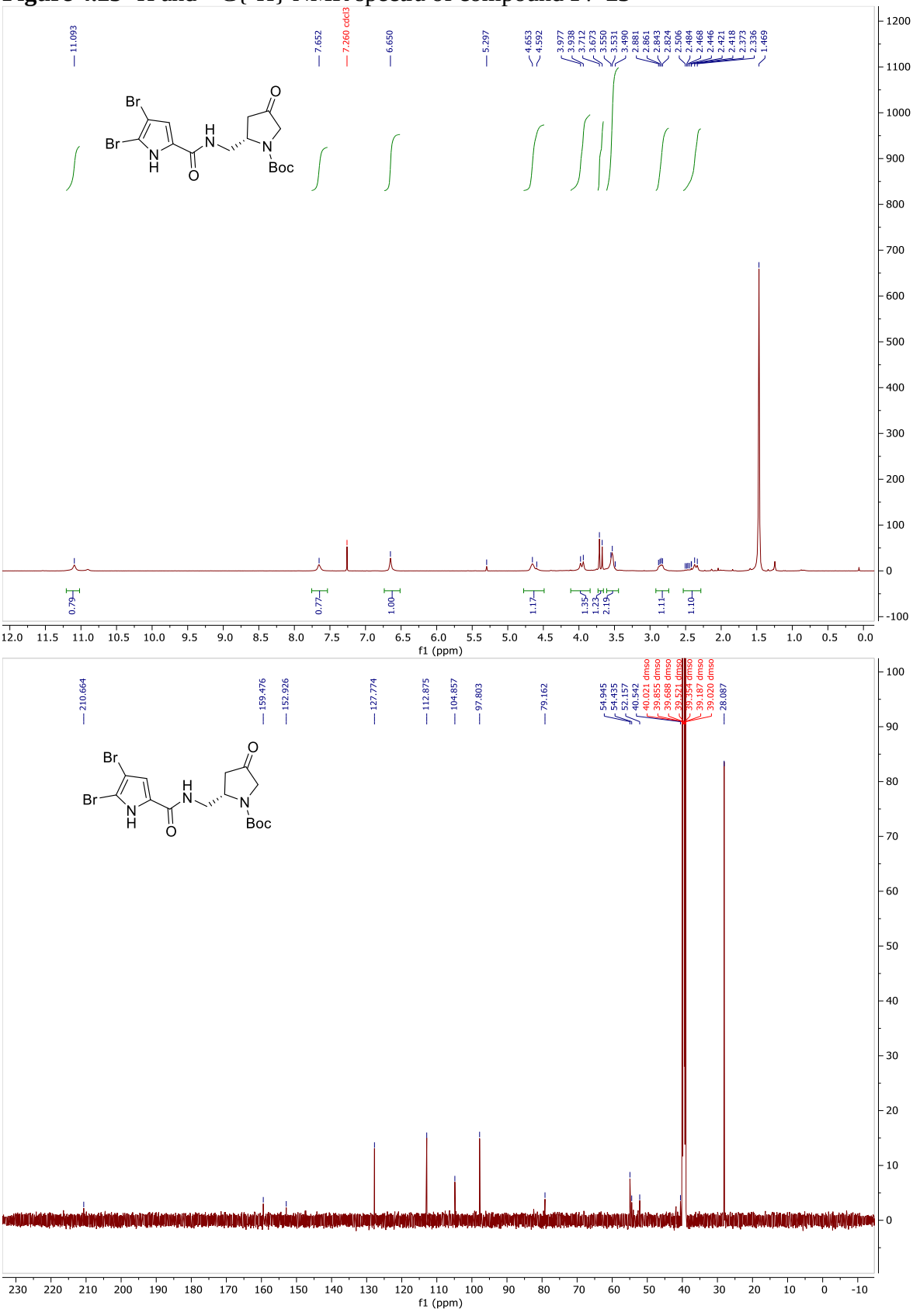

Figure 4.26 ^{1}H NMR spectrum of compound **IV-24**

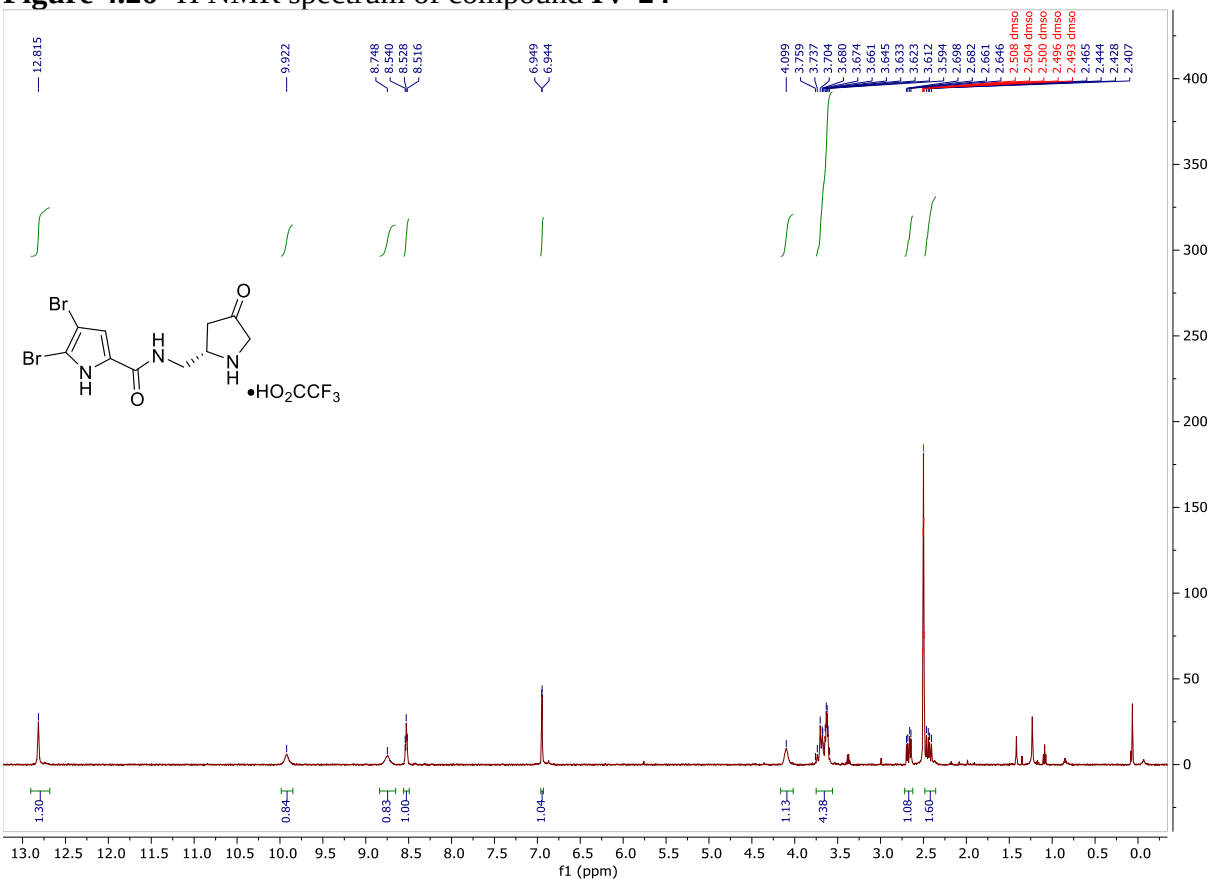

Figure 4.27 ^{1}H and $^{13}C\{^{1}H\}$ NMR spectra of compound **IV-28**

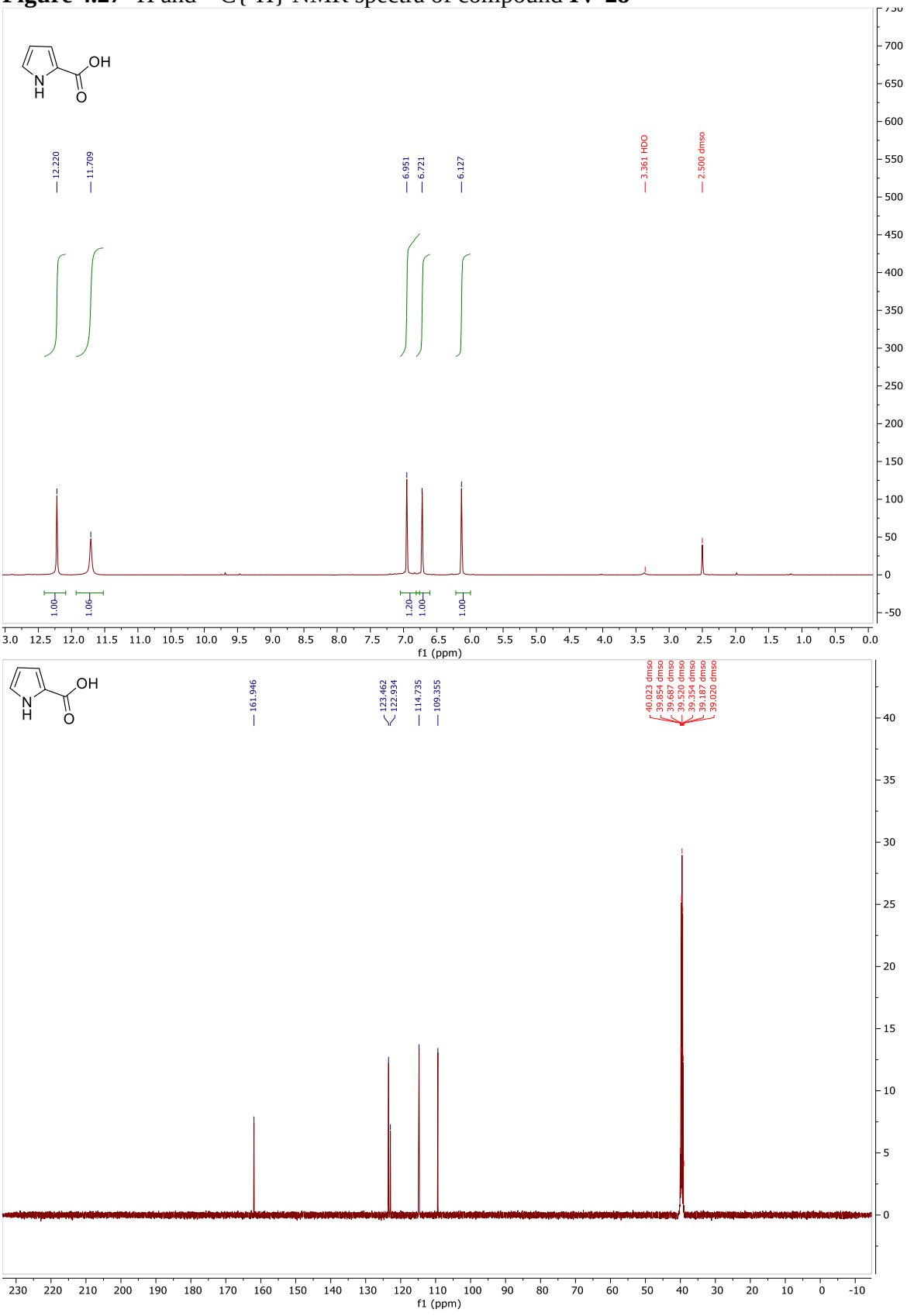

Figure 4.28 ^{1}H and $^{13}C\{^{1}H\}$ NMR spectra of compound **IV-29**

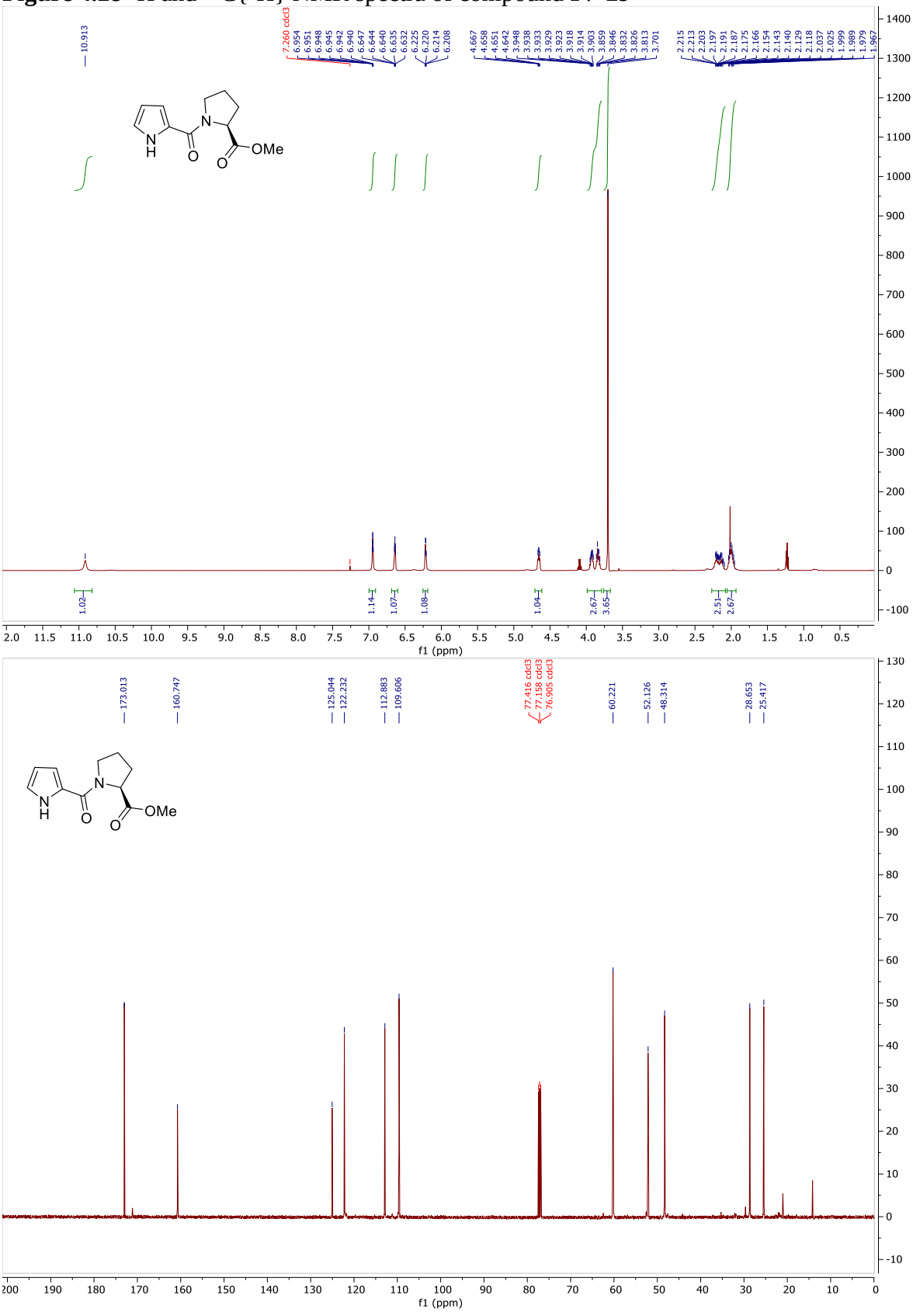

Figure 4.29 ^{1}H and $^{13}C\{^{1}H\}$ NMR spectra of compound **IV-30**

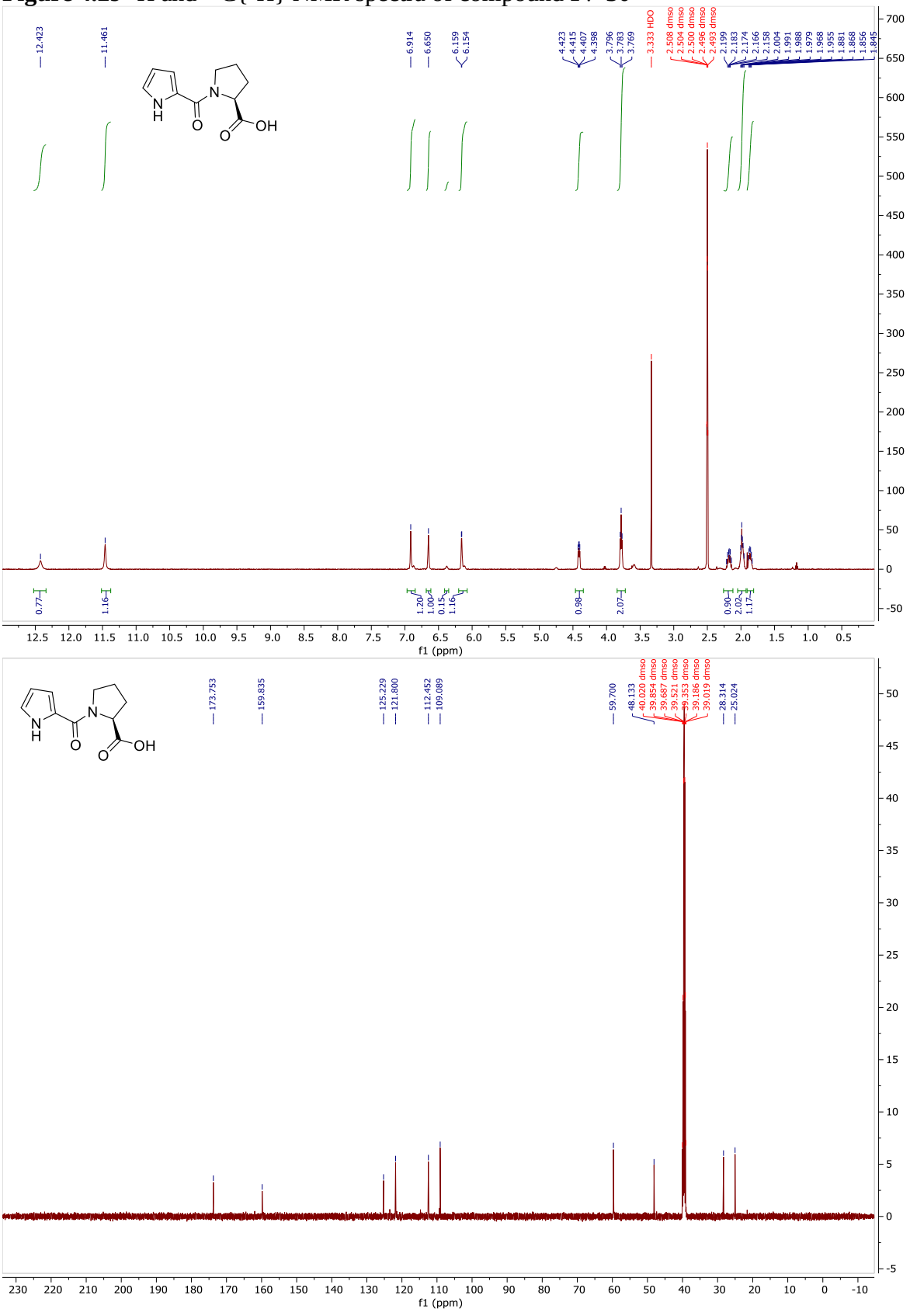

Figure 4.30 ^{1}H and $^{13}C\{^{1}H\}$ NMR spectra of compound **IV-31**

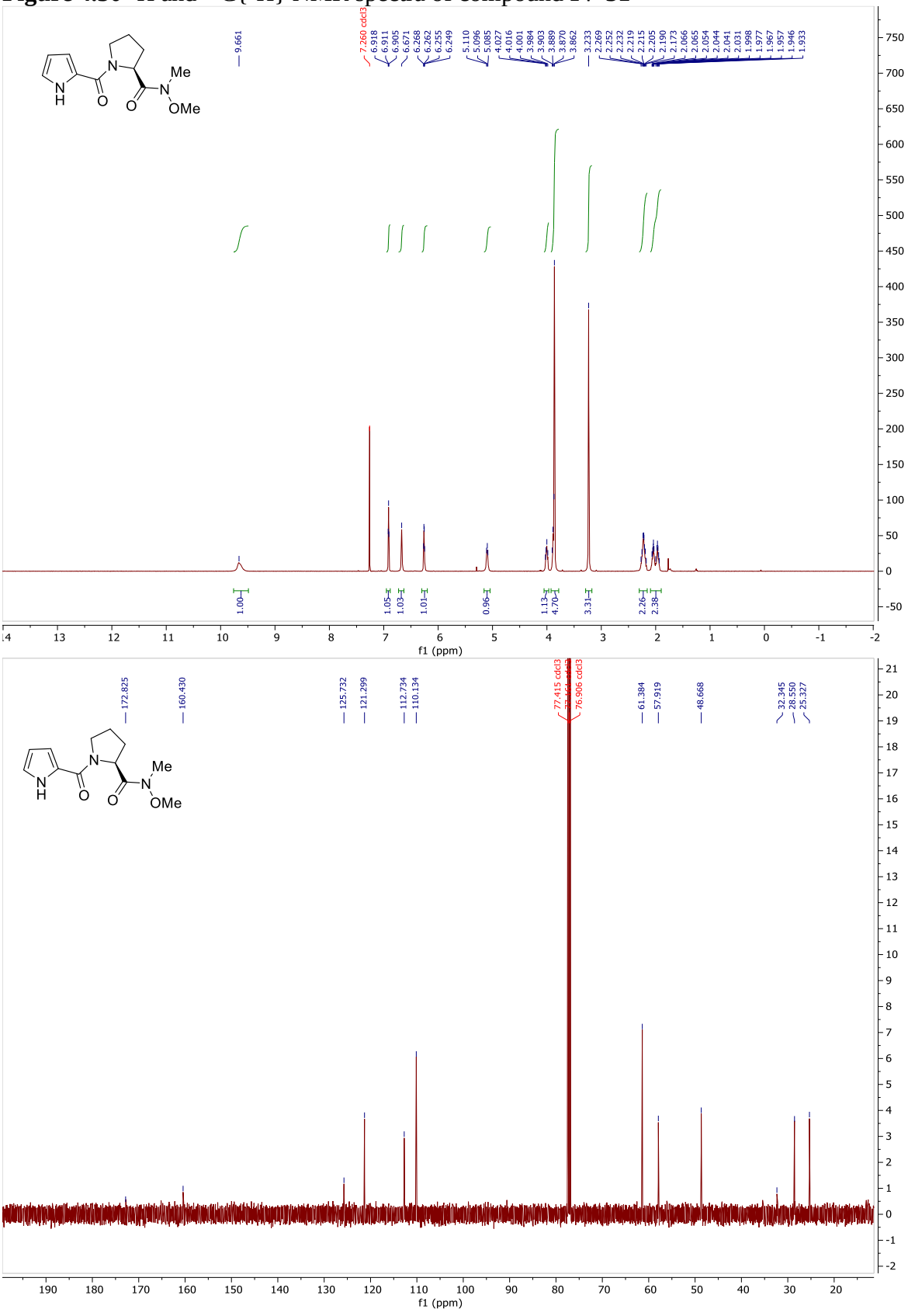

Figure 4.31 ^{1}H and $^{13}C\{^{1}H\}$ NMR spectra of compound **IV-32**

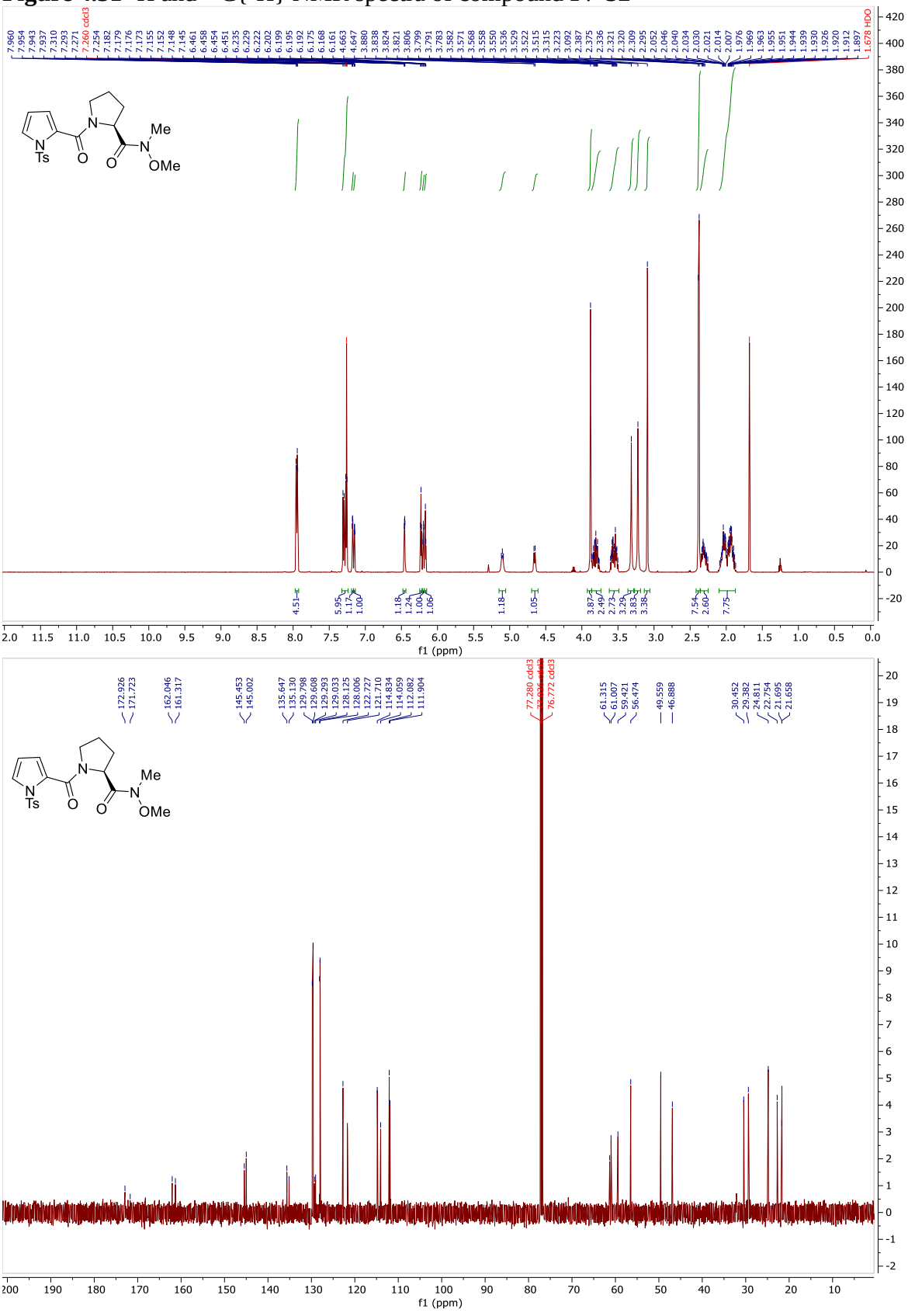

Figure 4.32 ^{1}H and $^{13}C\{^{1}H\}$ NMR spectra of compound **IV-33**

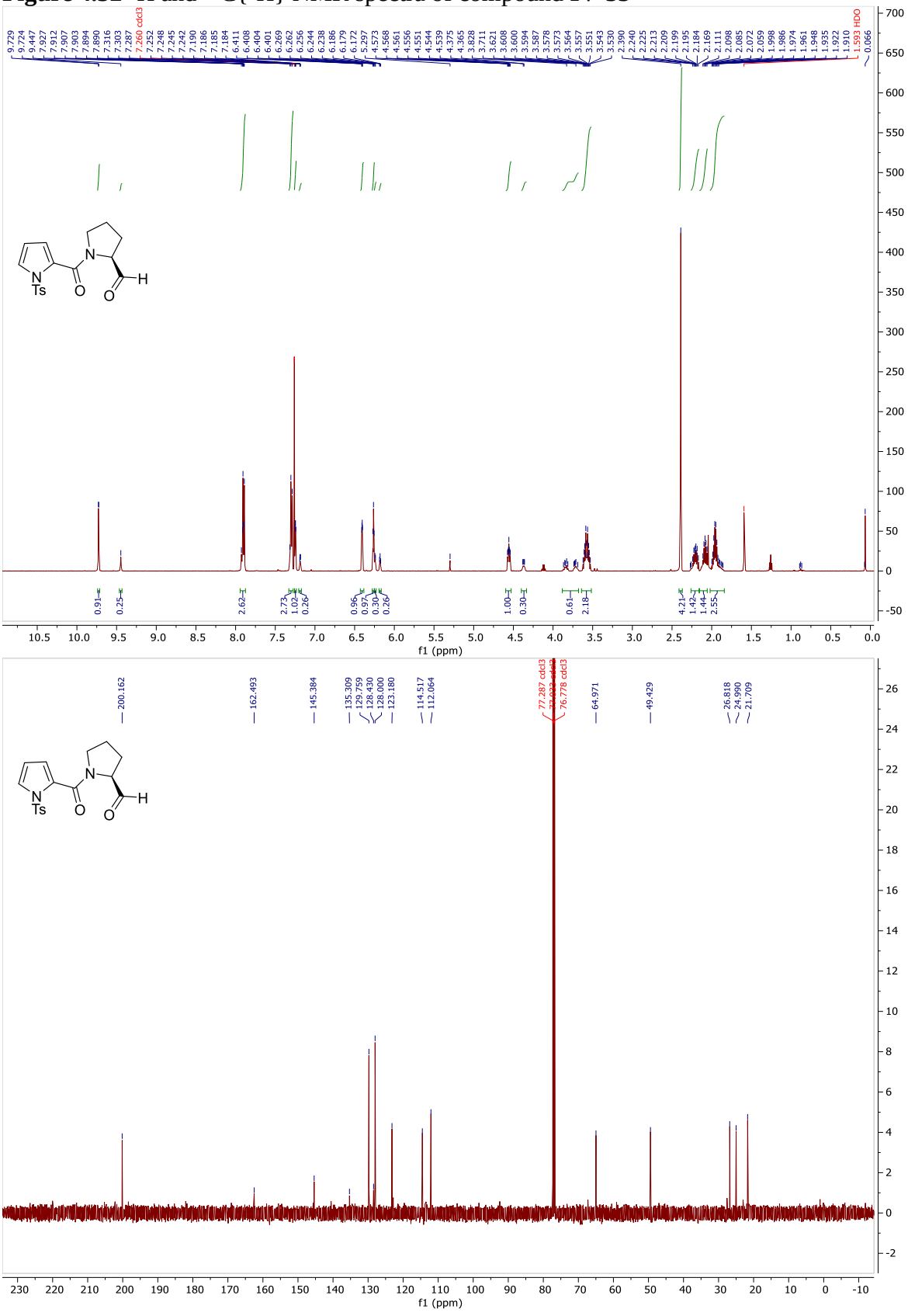

Figure 4.33 ^{1}H and $^{13}C\{^{1}H\}$ NMR spectra of compound **IV-34**

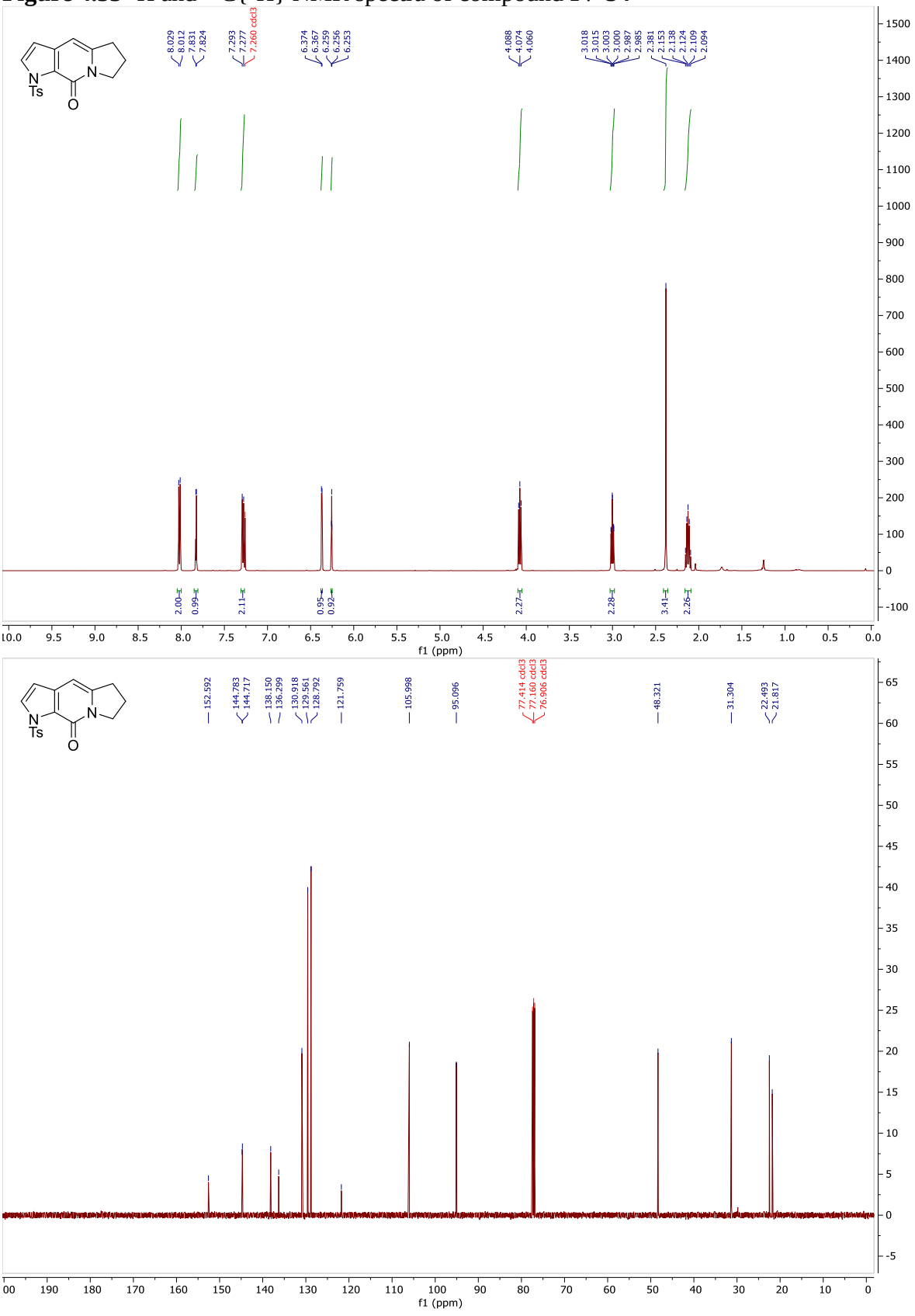

Figure 4.34 ^{1}H and $^{13}C\{^{1}H\}$ NMR spectra of compound **IV-35**

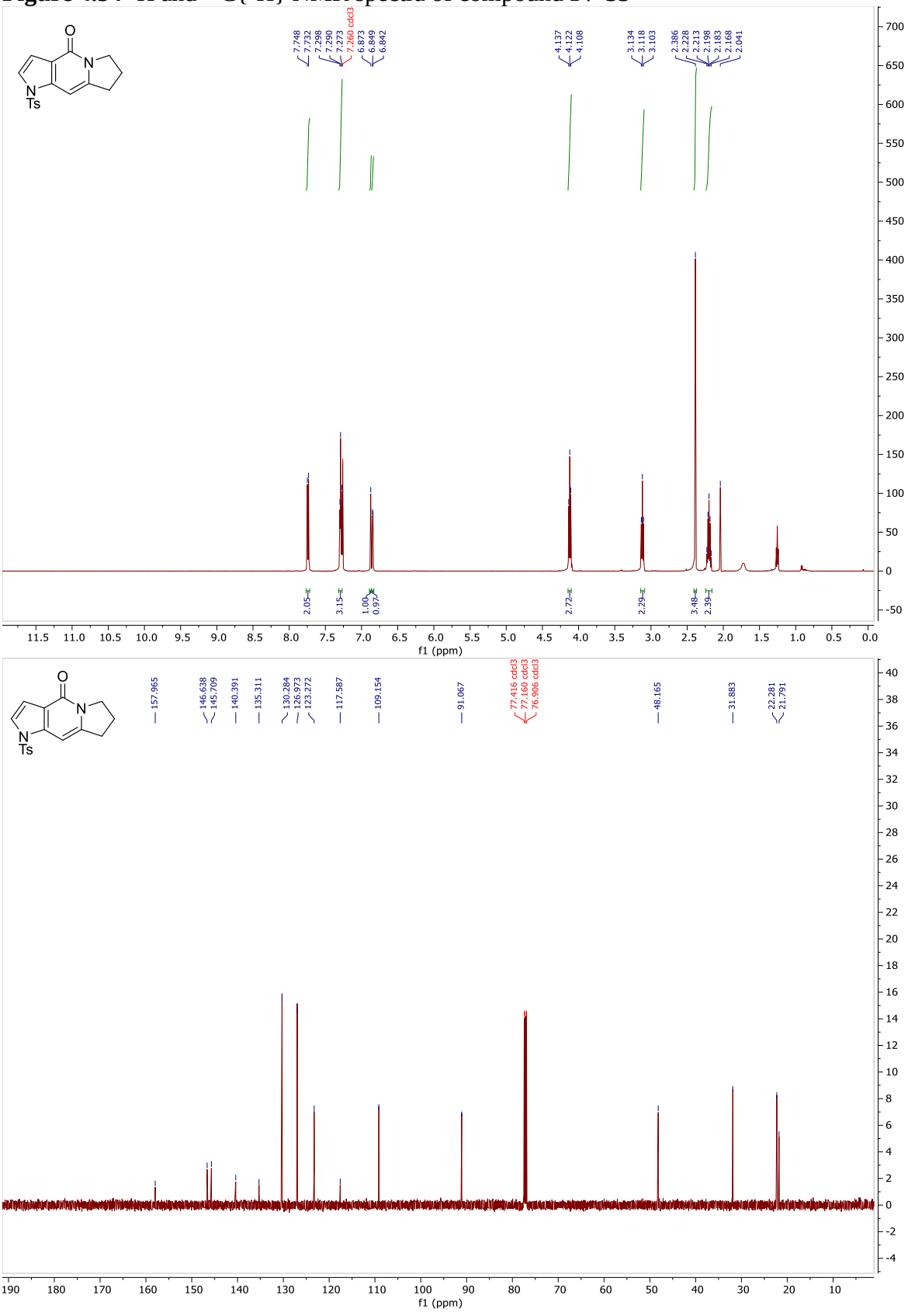

Figure 4.35 ^{1}H and $^{13}C\{^{1}H\}$ NMR spectra of compound **IV-40**

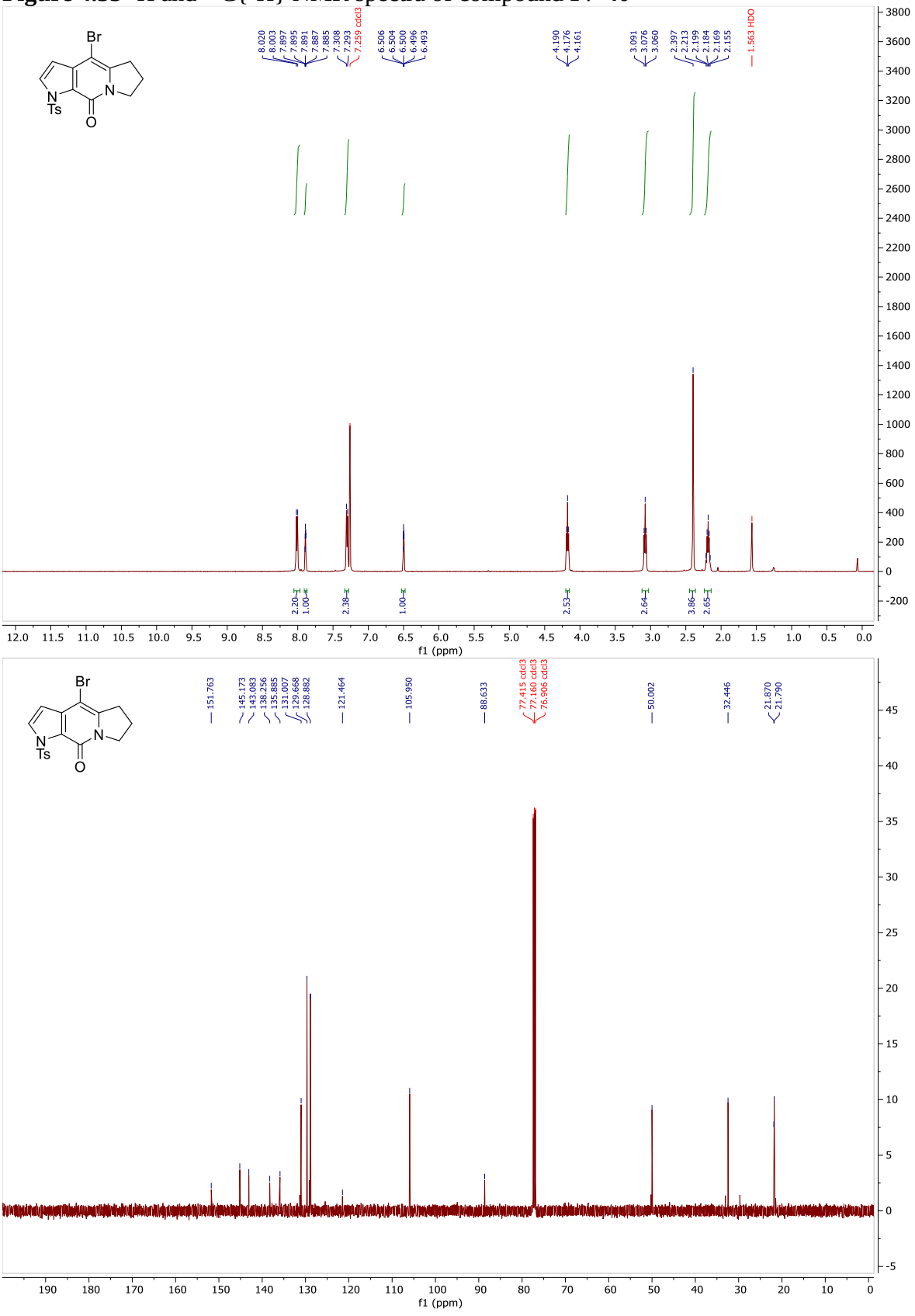

Figure 4.36 ^{1}H NMR spectrum of compound **IV-41**

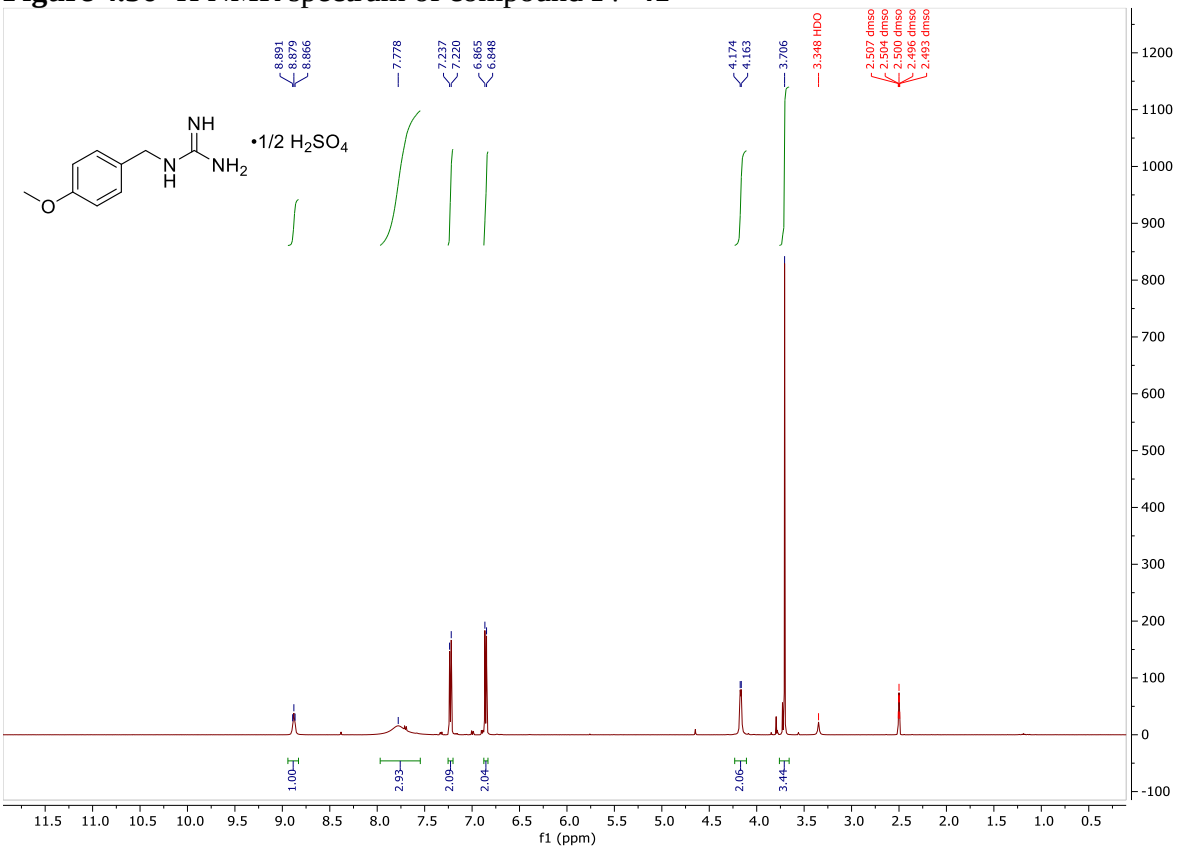

Figure 4.37 ^{1}H and $^{13}C\{^{1}H\}$ NMR spectra of compound **IV-45**

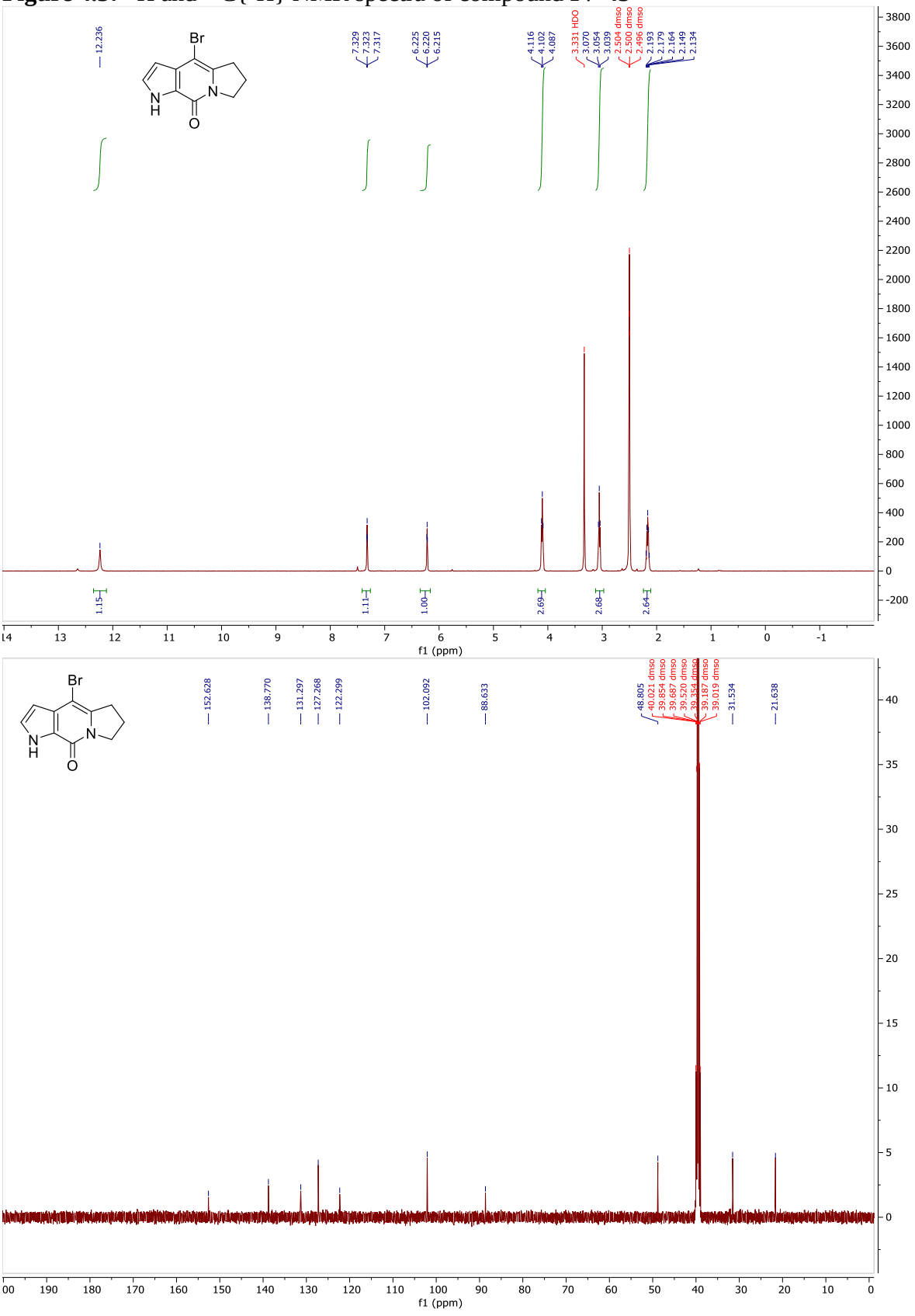

Figure 4.38 ^{1}H and $^{13}C\{^{1}H\}$ NMR spectra of compound **IV-47**

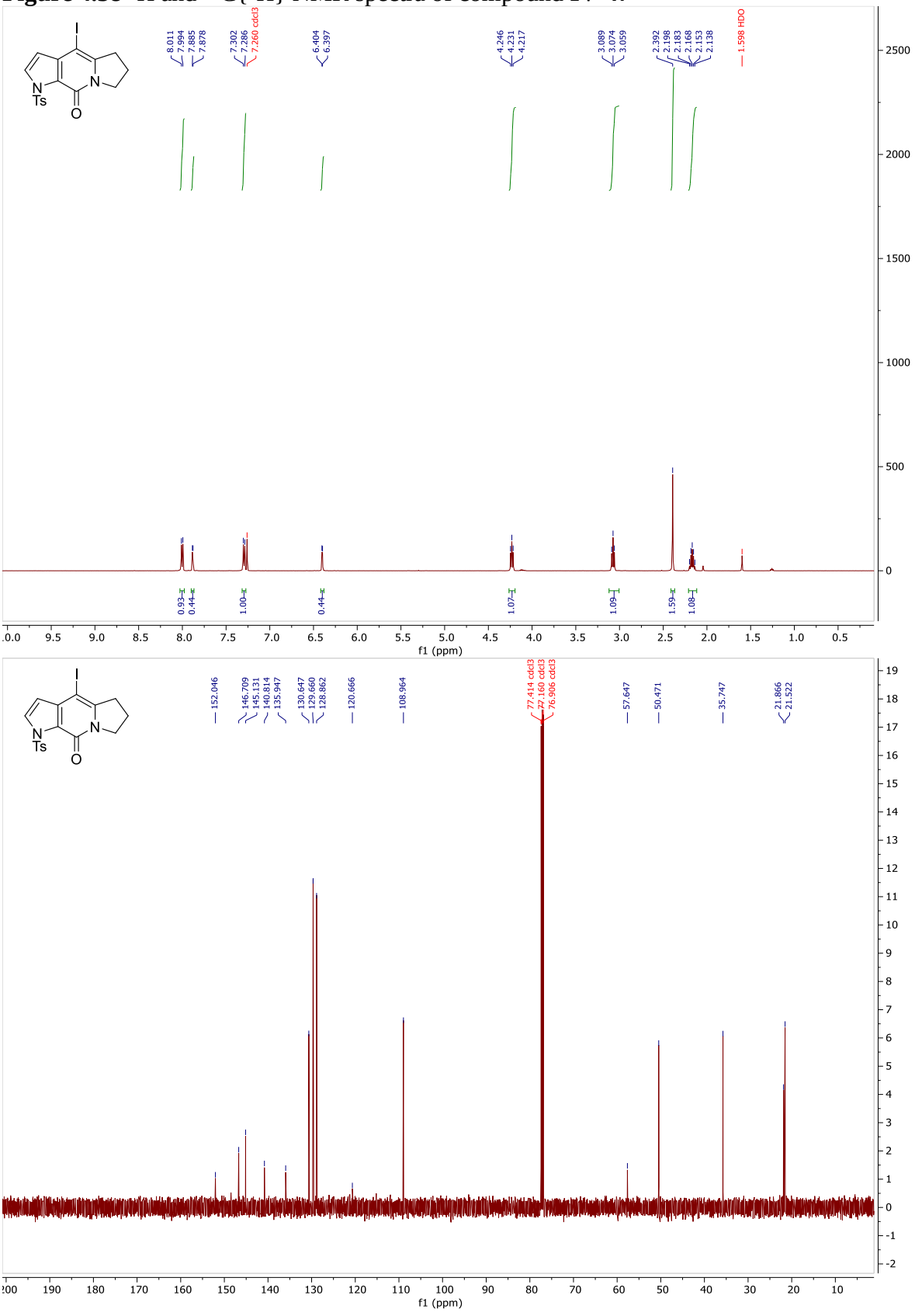

Figure 4.39 ^{1}H and $^{13}C\{^{1}H\}$ NMR spectra of compound **IV-49**

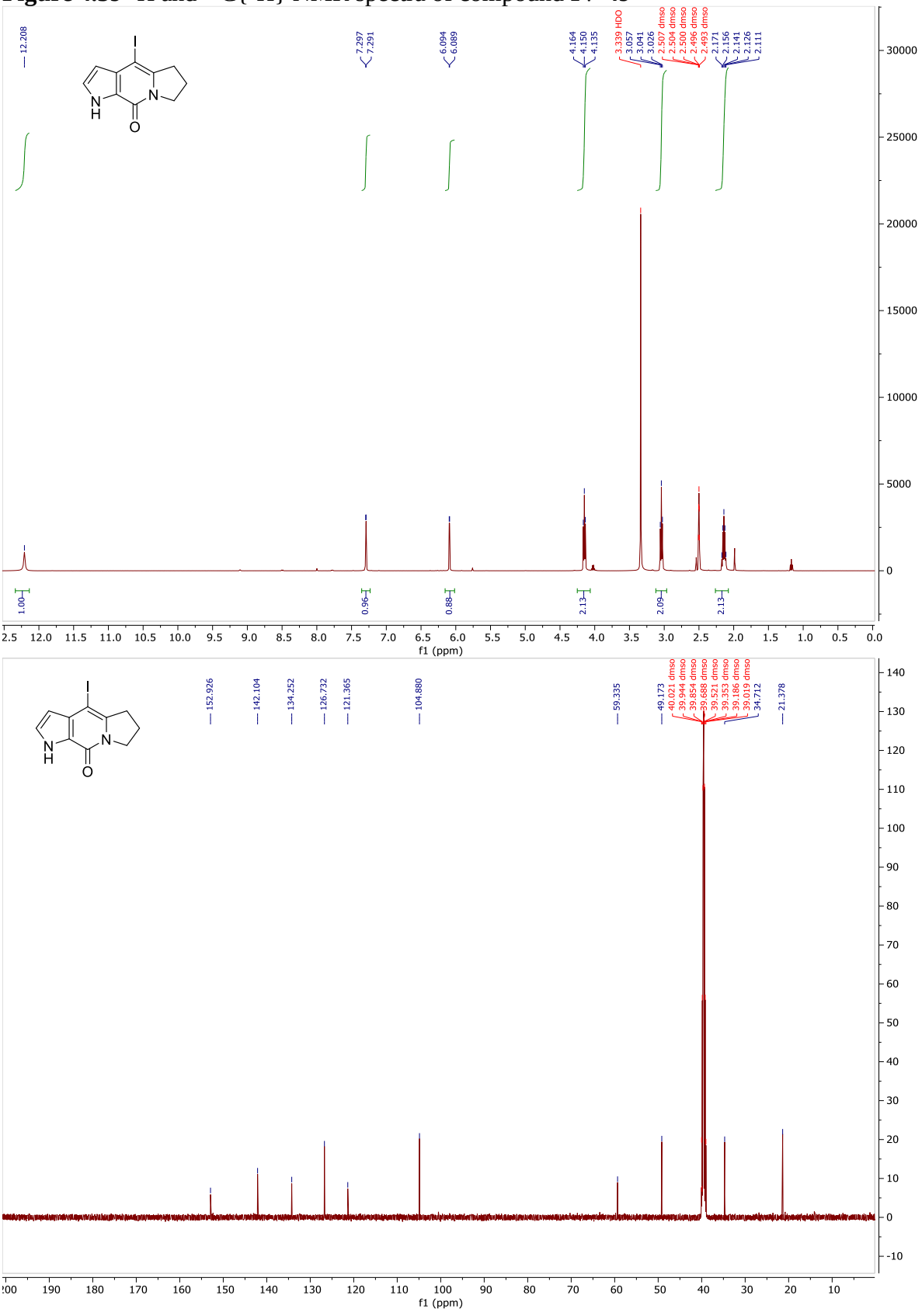

Figure 4.40 ^{1}H and $^{13}C\{^{1}H\}$ NMR spectra of compound **IV-50**

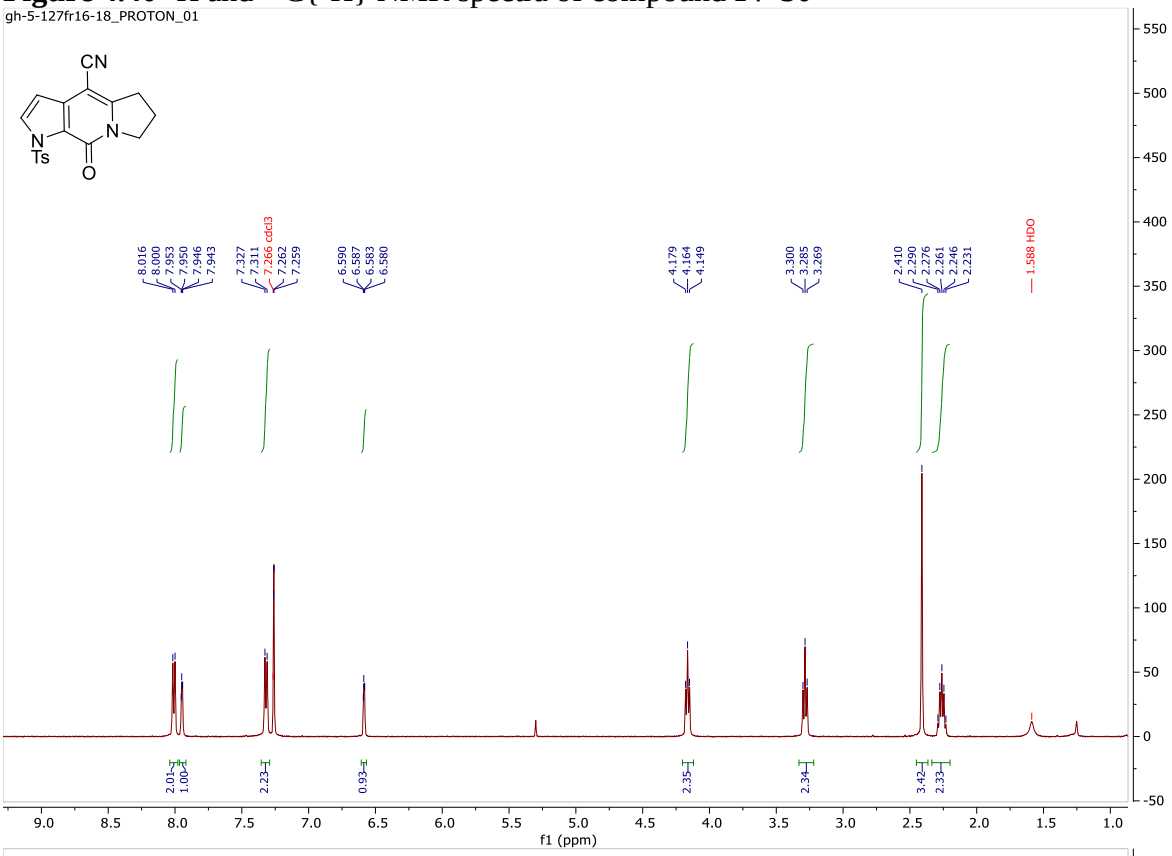

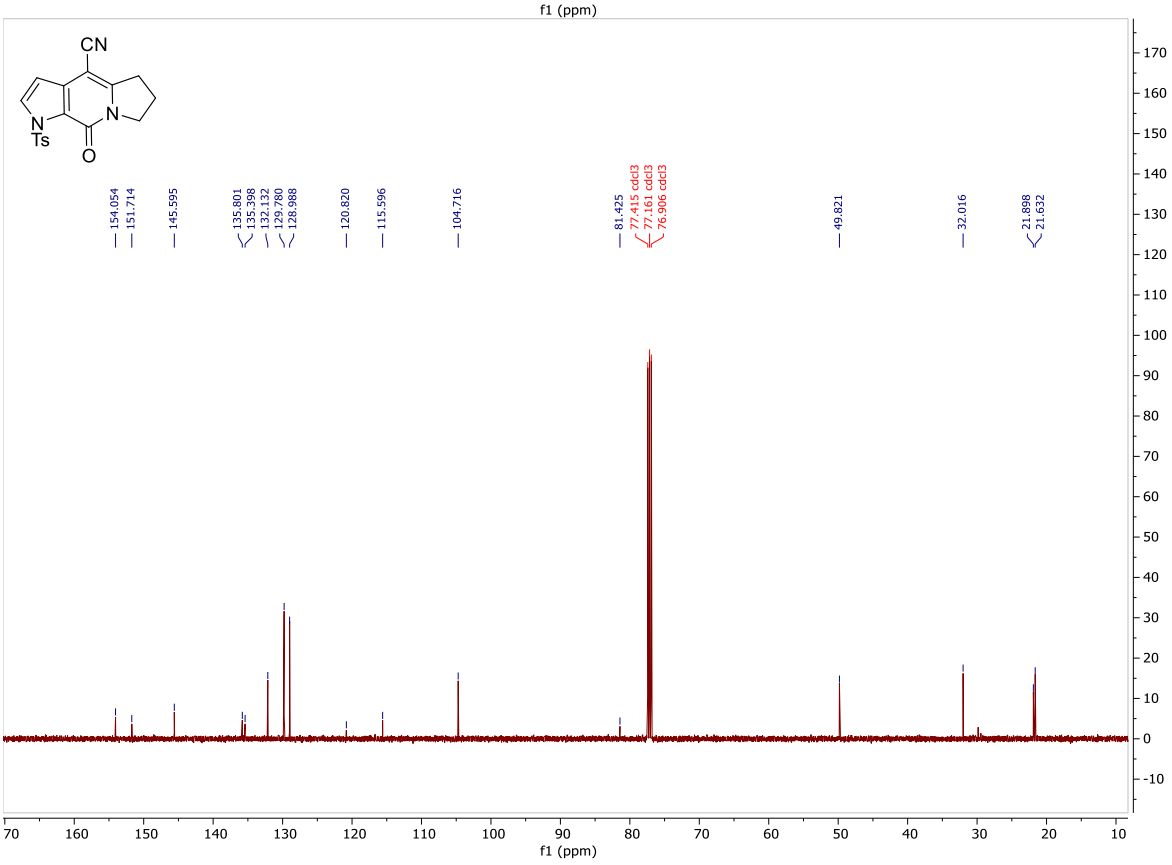

Figure 4.41 ^{1}H NMR spectrum of compound **IV-51**

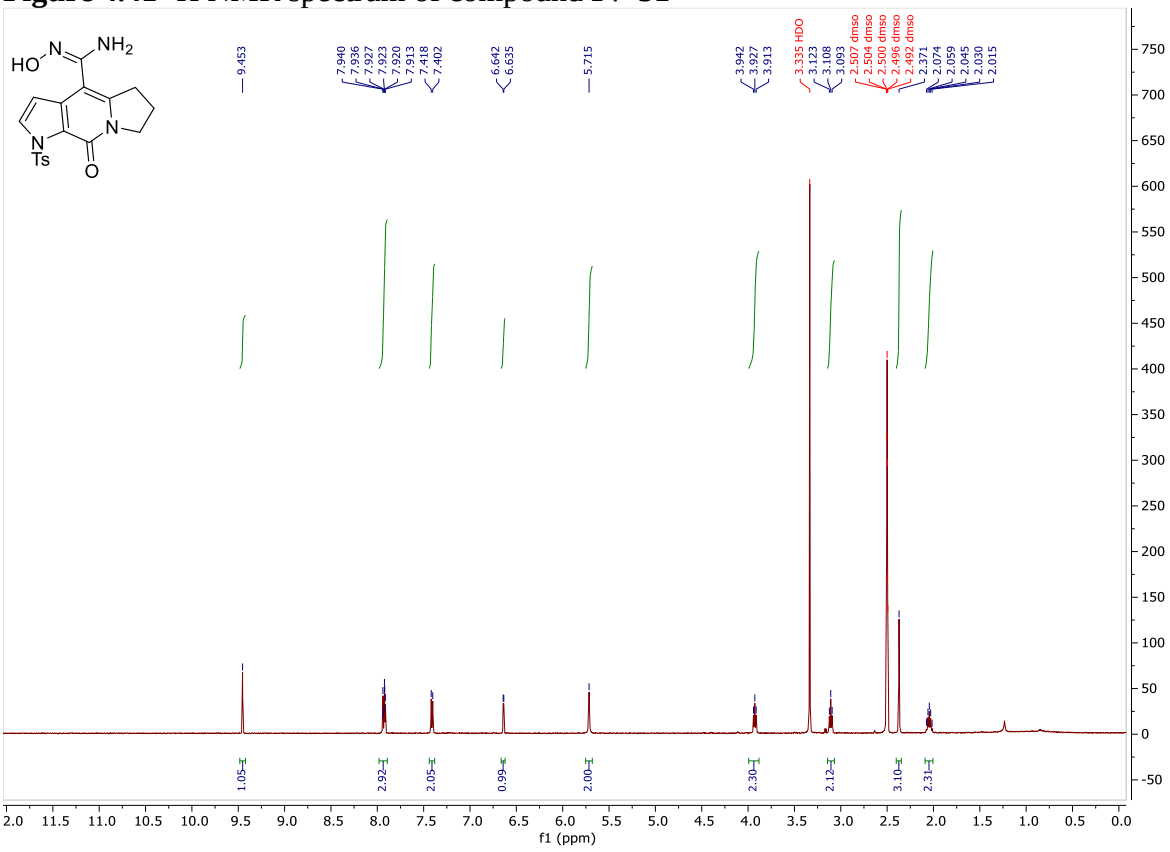

Figure 4.42 ^{1}H and $^{13}C\{^{1}H\}$ NMR spectra of compound **IV-52**

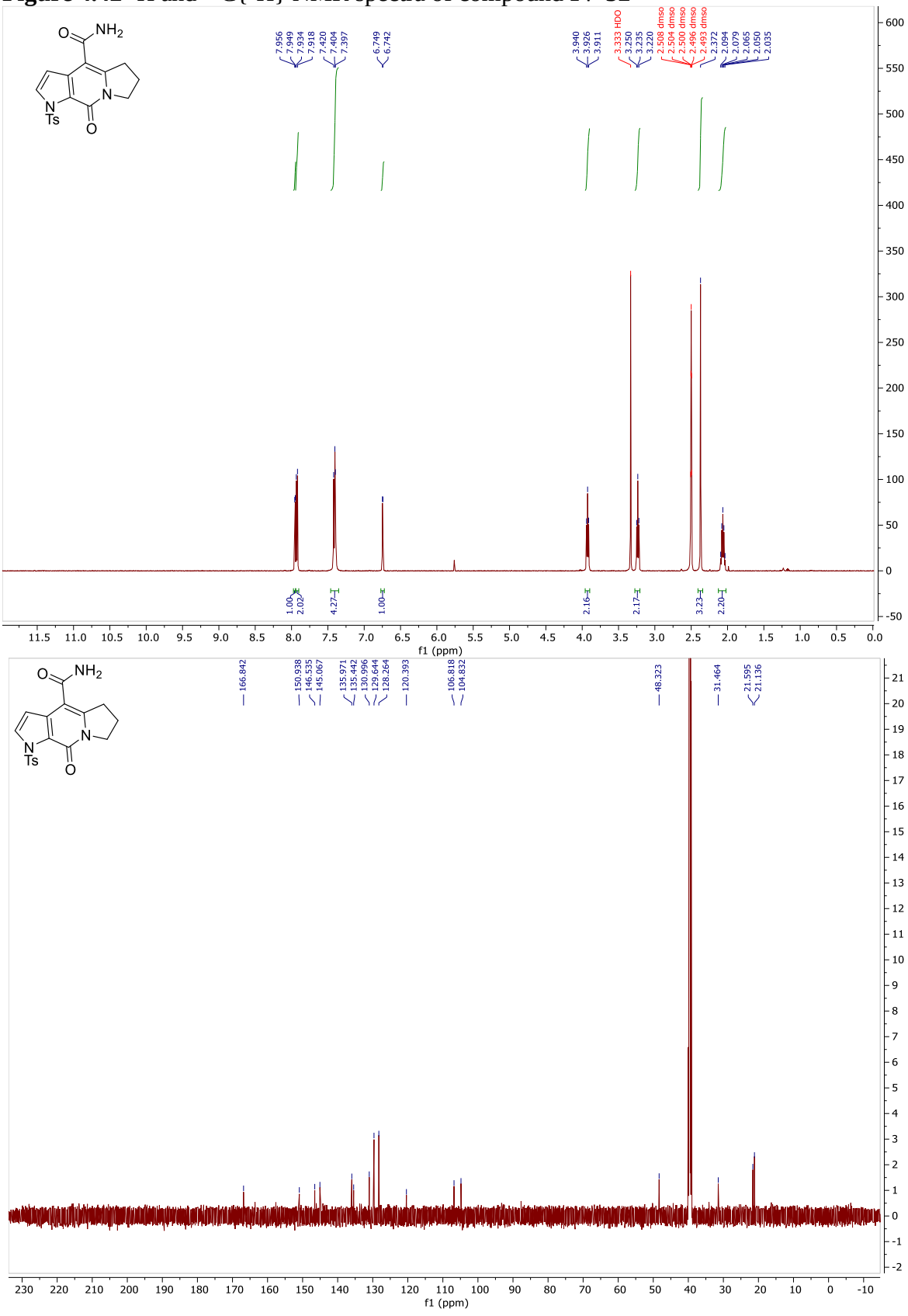

Chapter 5: Conclusions & Future Works

In conclusion, my work during my PhD career in the Tepe lab at Michigan State University has focused on the application of pyrrole-alkaloid natural products as inhibitors of the 20S proteasome. The work centered on the development of novel approaches to synthetically access pyrrole-alkaloid natural products and pyrrole-alkaloid-like scaffolds through total synthesis, small molecule synthesis, and methodology development for future evaluation for their inhibitory activity towards the 20S human proteasome. The efforts towards achieving the total syntheses of pyrrole alkaloid natural products nagelamide M and the ugibohlins along with the considerable challenges which arose from these approaches were discussed. While incomplete, the results from these studies provided insight and paths towards the completion of these projects if further explored. The challenges associated with multi-step synthesis of small molecule inhibitors inspired the development of an expeditious Rh(III)-catalyzed C-H activation/annulation methodology to access pyrrole-alkaloid-like scaffolds. Future work in this project will be focused on application of the method towards the synthesis of novel scaffolds for evaluation as 20S proteasome inhibitors. Adaptation of this method is also envisioned to provide access to several of the guanidine-fused pyrrolo-pyridone-containing pyrrole alkaloid natural products.